



HHS Public Access

Author manuscript

Chem Rev. Author manuscript; available in PMC 2019 June 22.

Author Manuscript

Author Manuscript

Author Manuscript

Author Manuscript

Published in final edited form as:

Chem Rev. 2019 April 24; 119(8): 5298–5415. doi:10.1021/acs.chemrev.8b00593.

Electrospinning and Electrospun Nanofibers: Methods, Materials, and Applications

Jiajia Xue^{†,||}, Tong Wu^{†,||}, Yunqian Dai^{‡,||}, and Younan Xia^{*,†,§}

[†]The Wallace H. Coulter Department of Biomedical Engineering, Georgia Institute of Technology and Emory University, Atlanta, Georgia 30332, United States

[‡]School of Chemistry and Chemical Engineering, Southeast University, Nanjing, Jiangsu 211189, People's Republic of China

[§]School of Chemistry and Biochemistry, School of Chemical and Biomolecular Engineering, Georgia Institute of Technology, Atlanta, Georgia 30332, United States

Abstract

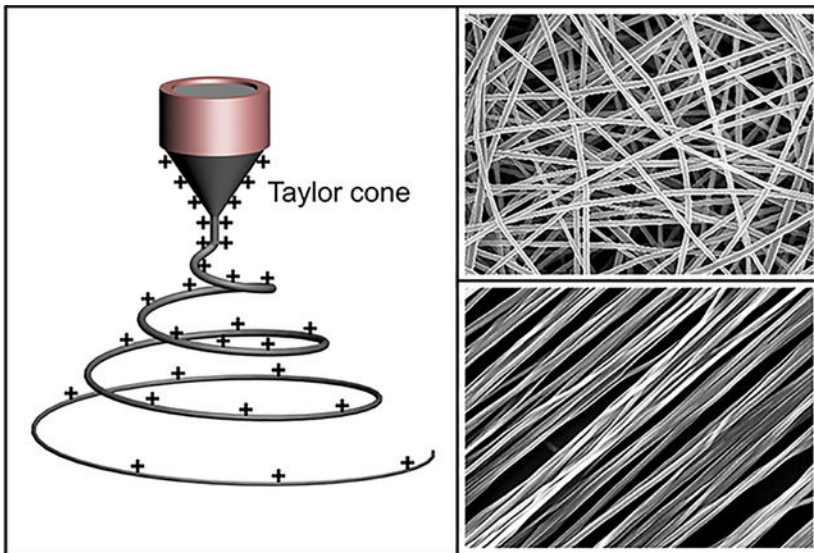
Electrospinning is a versatile and viable technique for generating ultrathin fibers. Remarkable progress has been made with regard to the development of electrospinning methods and engineering of electrospun nanofibers to suit or enable various applications. We aim to provide a comprehensive overview of electrospinning, including the principle, methods, materials, and applications. We begin with a brief introduction to the early history of electrospinning, followed by discussion of its principle and typical apparatus. We then discuss its renaissance over the past two decades as a powerful technology for the production of nanofibers with diversified compositions, structures, and properties. Afterward, we discuss the applications of electrospun nanofibers, including their use as “smart” mats, filtration membranes, catalytic supports, energy harvesting/conversion/storage components, and photonic and electronic devices, as well as biomedical scaffolds. We highlight the most relevant and recent advances related to the applications of electrospun nanofibers by focusing on the most representative examples. We also offer perspectives on the challenges, opportunities, and new directions for future development. At the end, we discuss approaches to the scale-up production of electrospun nanofibers and briefly discuss various types of commercial products based on electrospun nanofibers that have found widespread use in our everyday life.

Graphical Abstract

*Corresponding Author: younan.xia@bme.gatech.edu.

||J.X., T.W., and Y.D. contributed equally to the preparation of this review article.

The authors declare no competing financial interest.



1. INTRODUCTION

Fibers, in the form of either continuous filaments or elongated objects, are ubiquitous in nature. For more than 140 million years, spiders have relied on webs of fibers to capture prey. The webs are constructed from silk fibers with diameters ranging from 2 to 5 μm . Silkworms are also well-known for their remarkable ability to produce silk filaments for the construction of cocoons. These and many other natural systems have served as an important source of inspiration for the development of man-made fibers.^{1–3} As a matter of fact, fibers have been a fundamental part of human life since the dawn of civilization. The history of fiber production by mankind can be traced back to prehistoric times. Fragments of cotton articles dating back to 5000 BC have been excavated, and silkworm cultivation began in 2700 BC for the production of silk fibers and textiles. Around 1300, the spindle was invented to fabricate fibers from wool and cotton for the production of fabrics and clothes, and this practice slowly evolved into the textile industry in the 1880s. Rayon, made of cotton or wood cellulose fibers, represents the first man-made fabrics. Although it was reported in 1891, it was not commercially marketed until 1911.⁴ About 50 years later, synthetic fibers were produced along with the development of chemistry and polymer science. As the first commercially viable synthetic fiber, nylon was introduced by DuPont in 1938, and it immediately caught the public's attention.^{5,6} Thereafter, many different types of polyesters and other synthetic polymers have been developed one after another for the manufacturing of synthetic fibers.⁷ The synthetic fibers significantly reduce the public's demand for natural fibers while greatly expanding the scope of applications.

Many methods have been developed for producing fibers from synthetic polymers, most notably, those based on wet, dry, melt, and gel spinning.^{8,9} Wet spinning involves a spinneret submerged in a chemical bath. When a polymer solution is extruded from the spinneret into the chemical bath, the polymer is precipitated out because of the dilution effect or chemical reaction, generating fibers through solidification. For dry spinning, a polymer solution is extruded into air through a spinneret and fibers are obtained as a result of solvent

Author Manuscript
Author Manuscript
Author Manuscript
Author Manuscript

evaporation from the jets aided by a stream of hot air. During melt spinning, a polymer melt is extruded from a spinneret to generate fibers upon cooling. Gel spinning is used to produce fibers with high mechanical strength or other special properties by spinning a polymer in the “gel” state, followed by drying in air and then cooling in a liquid bath. During these spinning processes, jets are mainly formed under external shearing forces and/or mechanical drawing when passing through spinnerets, and fibers are formed upon solidification of the jets as a result of precipitation or drying. The jets are only stretched to a limited extent, corresponding to the formation of fibers with diameters typically in the range of 10–100 μm .^{8,9} Even with further mechanical drawing during the solidification process or after complete cooling of the jets, the resultant fibers still cannot reach the sub-micrometer scale.

In 1887, Charles V. Boys reported that fibers could be drawn from a viscoelastic liquid in the presence of an external electric field.¹⁰ He used an apparatus consisting of an insulated dish connected to an electrical supply. It was demonstrated that a viscous liquid (e.g., beeswax and collodion) could be drawn into fibers when it moved to the edge of the dish. Widely known as electrospinning now, this technique opens the door to the production of ultrathin fibers with diameters down to the nanometer scale. In general, electrospinning allows for the facile production of continuous fibers with diameters ranging from tens of nanometers to several micrometers.¹¹ Electrospun fibers with diameters down to 1 nm, and even below, have also been reported.¹² In literature, electrospun fibers are often referred to as nanofibers when their diameters are thinner than roughly 500 nm.

The concept of electrospinning was conceived in an earlier study conducted by William Gilbert in 1600, in which he observed the formation of a cone-shaped water droplet in the presence of an electric field.¹³ About one century later, Stephen Gray observed the electrohydrodynamic atomization of a water droplet from which a very fine stream was generated.¹⁴ In 1747, Abbé Nollet performed the earliest known electrospraying experiment, demonstrating that water could be sprayed as an aerosol when passing through an electrostatically charged vessel that was placed next to the ground.¹⁵ The behaviors of charged droplets were then systematically studied by Lord Rayleigh. In 1882, he theoretically estimated the maximum amount of charges that a liquid droplet could carry before liquid jets would be ejected from the surface.¹⁶ Electrospinning can be considered a variant of the electrospraying technique,¹⁷ both of which rely on the use of a high voltage to eject liquid jets. The major differences between electrospinning and electrospraying lie in the viscosity and viscoelasticity of the liquid involved and thus the behavior of the jet. During electrospinning, the jet can be kept in a continuous form to produce fibers instead of breaking into droplets (for the formation of particles) as with electrospraying.

In 1902, two patents on electrospinning were filed by John Cooley and William Morton, respectively,^{18,19} describing a prototype of the setup for electrospinning. Afterward, Anton Formhals filed a couple of additional patents in 1934 and 1944 to disclose the improvement in equipment, moving toward the commercialization of electrospinning for the fabrication of textile yarns.^{20,21} Electrospun nanofibers were first implemented in the Soviet Union in 1938 for the development of air filters, known as “Petryanov filters”, for capturing aerosol particles. By 1939, this work had led to the establishment of a factory in Tver for the manufacturing of smoke filters with nanofiber-based mats as gas masks. During this period

Author Manuscript

Author Manuscript

Author Manuscript

Author Manuscript

of time, a mechanistic understanding of electrospinning was slowly developed. Between 1964 and 1969, Geoffrey Taylor published a series of pioneering papers, showing how to mathematically describe and model the spherical to conical shape change of a polymer solution or melt droplet under the influence of a strong electric field.^{22–24} Specifically, as the strength of the electric field was increased beyond a critical level, the spherical droplet would gradually evolve into a cone (now commonly referred to as Taylor cone) and emanate a liquid jet. Afterward, the development of electrospinning technique experienced 20 years of stagnancy, as it did not receive much attention from academia or industry during this period of time. This stagnancy can be largely attributed to the lack of characterization tools capable of accurately measuring the sizes of fibers with diameters down to the sub-micrometer range. Nevertheless, a variety of applications were proposed for electrospun fibers during this period of time, including their potential use as wound dressing materials as described by a patent filed in 1977.²⁵ In the early 1980s, Donaldson Co. Inc. in the U.S. began to produce and sell filters comprised of electrospun fibers for air filtration. However, the company did not disclose the makeup of their products in order to gain advantages over its competitors.

It was not until the early 1990s that several research groups, notably those led by Darrell Reneker and Gregory Rutledge, began to reinvent this technique.^{26–32} This was made possible by the increased accessibility of electron microscopes capable of resolving features down to the nanometer scale. These groups demonstrated that many different organic polymers could be electrospun into nanofibers. The term “electrospinning” was popularized for describing this technique. Their studies brought new life to electrospinning, and this technique eventually became the method of choice for producing long and continuous fibers with diameters down to the nanometer scale. At the beginning of this century, electrospinning started to receive increasing attention when its capability was further expanded by switching to new materials and formulations for the fabrication of composite and ceramic nanofibers.^{33–35} The ability to electrospin new materials quickly enabled new applications in catalysis, as well as energy harvesting, conversion, and storage, which were traditionally dominated by inorganic nanoparticles. In parallel, new strategies were also developed to control the structure and alignment of electrospun nanofibers, opening a world of opportunities in energy-related and biomedical applications. Notably, several methods for aligning the nanofibers were developed, demonstrating the feasibility to combine different properties arising from the size, structure, composition, morphology, porosity, and assembly of nanofibers.^{35–38} At the same time, coaxial electrospinning was developed to produce continuous core–sheath and hollow nanofibers.³⁹ The fabrication of continuous yarns of electro-spun nanofibers was also reported.⁴⁰ Figure 1 shows a brief summary of the major milestones for the development of electrospinning. These achievements make electrospinning a versatile and viable technology for the production of nanofiber-based materials to target a broad range of applications.

Today, industrial production lines have been designed and implemented by a number of companies to manufacture electrospun nanofibers in large volumes, enabling downstream commercial products. At the moment, electrospun nanofibers are widely used for water and air filtration, ranging from industrial products (e.g., car filters) to civilian goods (e.g., facial masks and water filters). With the receipt of the Conformité Européene (CE) Mark for the

AVflo vascular access graft by Nicast, more and more biomedical products based on electrospun nanofibers are approved for clinical use. Meanwhile, in the laboratory setting, electrospun nanofibers have been further engineered with specific compositions and innovative structures, endowing them with special functions for advanced applications.

In preparing this review, we aim to provide a comprehensive overview of electrospinning, including the principle, methods, materials, and applications. We begin with a discussion on the principle and typical apparatus of electrospinning to give the readers a clear picture of this remarkably simple and versatile technique. We then extensively review the methods and materials typically involved in electrospinning. Afterward, we discuss how the compositions, structures, and properties of electrospun nanofibers can be engineered to target different types of applications. All these attributes make electrospun nanofibers a class of nanomaterials well-suited for a broad spectrum of applications, including their use as “smart” mats, filtration membranes, catalytic supports, energy harvesting/conversion/storage components, and photonic and electronic devices, as well as biomedical scaffolds. We concentrate on the most relevant examples to highlight the advances related to the development of electrospun nanofibers. At the end of each section, we also offer perspectives on the challenges, opportunities, and new directions for future development. Finally, after a brief summary, we discuss approaches to the scale-up production of electrospun nanofibers and showcase typical examples of commercial products based on electrospun nanofibers. We also briefly compare electrospinning with other techniques that have been developed in recent years for producing nanofibers.

2. ELECTROSPINNING

2.1. Principle of Electrospinning

Electrospinning involves an electrohydrodynamic process, during which a liquid droplet is electrified to generate a jet, followed by stretching and elongation to generate fiber(s). As illustrated in Figure 2A, the basic setup for electrospinning is rather simple, making it accessible to almost every laboratory.^{41,42} The major components include a high-voltage power supply, a syringe pump, a spinneret (usually, a hypodermic needle with blunt tip), and a conductive collector. The power supply can be either direct current (DC) or alternating current (AC). During electrospinning, the liquid is extruded from the spinneret to produce a pendant droplet as a result of surface tension. Upon electrification, the electrostatic repulsion among the surface charges that feature the same sign deforms the droplet into a Taylor cone, from which a charged jet is ejected. The jet initially extends in a straight line and then undergoes vigorous whipping motions because of bending instabilities. As the jet is stretched into finer diameters, it solidifies quickly, leading to the deposition of solid fiber(s) on the grounded collector. In general, the electrospinning process can be divided into four consecutive steps: (i) charging of the liquid droplet and formation of Taylor cone or cone-shaped jet; (ii) extension of the charged jet along a straight line; (iii) thinning of the jet in the presence of an electric field and growth of electrical bending instability (also known as whipping instability); and (iv) solidification and collection of the jet as solid fiber(s) on a grounded collector.^{41,43,44} A more detailed discussion of these four steps is provided in the following subsections.

2.1.1. Formation of Taylor Cone upon Charging a Liquid Droplet.—To

understand the formation of a Taylor cone from an electrically charged liquid droplet during electrospinning, it is necessary to grasp the electrohydrodynamic principles involved. A classic example can be found in the formation of Rayleigh jets from levitated droplets of ethylene glycol in an electric field (Figure 2B).⁴⁵ Upon injection into the levitator, the droplet took a spherical shape with a radius of 58 μm. The charge on the surface was about 3.3 pC. Due to the evaporation of neutral molecules, the droplet shrank in size over time, reaching the limit of Rayleigh stability at a radius of about 24 μm within 140 μs. At that point, the droplet deformed into an ellipsoidal shape, and two sharp tips were developed at the poles. Almost immediately after the formation of tips, two fine liquid jets were ejected from the tips along the opposite directions. The jets later broke into fine droplets that were repelled away from the parent droplet due to electrostatic repulsion. Upon the ejection of jets, the tips disappeared, and the barrel-shaped droplet contracted until it regained a spherical shape after about 210 μs. This experiment clearly shows the disintegration of a droplet charged to the limit of Rayleigh instability and the production of Rayleigh jets. When the ethylene glycol in the droplets was replaced by a sol–gel precursor solution, the Rayleigh jets could be fixed for characterization using electron microscopy.⁴⁶

During electrospinning, the liquid is typically fed through the spinneret at a constant and controllable rate using a syringe pump. When there is a potential difference between the spinneret and the collector, positive and negative charges will undergo separation within the liquid and charges in the same sign as the spinneret's polarity will migrate toward the surface of the droplet, producing excess charges. With the gradual increase of voltage, more charges will be accumulated, increasing the density of surface charges residing on the droplet. While the surface tension favors a spherical shape to minimize the total surface free energy of the droplet, electrostatic repulsion tends to deform the shape of the droplet, so its surface area will be increased to attenuate the repulsion.⁴⁷ The droplet is assumed to take a shape that minimizes the sum of the electrostatic energy and the surface free energy.

By assuming the liquid in the droplet as a perfect conductor,²² the electrostatic pressure (p_e) acting on the surface of the droplet by the external electric field can be calculated as $p_e = \epsilon E^2/2$, where ϵ is the dielectric constant of the medium surrounding the droplet and E is the intensity of the electric field. The capillary pressure (p_c) caused by the surface tension is defined by the Young–Laplace equation in the following form: $p_c = 2\gamma/r$, where γ is the surface tension and r is the mean radius of curvature of the surface, which can be represented by the inner radius of the spinneret.^{48,49} When the electric field reaches an adequate strength at a critical voltage of V_c , p_e will surpass p_c ; that is, the electrostatic repulsion will be strong enough to overcome the surface tension. In consequence, the droplet will deform into a conical shape.²² In this case, V_c can be calculated using the following equation:²⁴

$$V_c^2 = \frac{4H^2}{h^2} \left(\ln\left(\frac{2h}{R}\right) - 1.5 \right) (1.3\pi R\gamma)(0.09) \quad (1)$$

where H is the distance between the tip of the spinneret and the collector, h is the length of the spinneret, and R is the outer radius of the spinneret. The units of H , h , and R are all in

centimeters, while the unit of γ is dyn/cm and the unit of the voltage is kV. The factor 1.3 is derived from $2 \cos 49.3^\circ$ when considering that the cone has a semivertical angle close to a possible equilibrium value of 49.3° .²² During the electrospinning process, the critical voltage needed to generate a conical shape for the droplet is dependent on the properties of the liquid. When a viscous liquid is used, the voltage needs to reach a critical value capable of generating an electrostatic repulsion strong enough to overcome the surface tension plus the viscoelastic force of the liquid. As demonstrated by the photographs in Figure 2C, a pendent droplet of poly(ethylene oxide) (PEO) in water gradually deforms into a conical shape before a jet is ejected.⁵⁰ Figure 2D shows a photograph of the droplet at the critical point.⁵¹ The conical shape can be maintained as long as an adequate amount of liquid is supplied to replace the ejected amount during an electrospinning process.

2.1.2. Stretching of the Charged Jet.—From the apex of the Taylor cone, an electrically charged jet is ejected and then accelerated by the electric field. The jet will be extended in the direction of the electric field as it moves toward the collector.⁵² Based on both experimental observations and electrohydrodynamic theories, different models have been developed to describe the behavior of the charged jet. In one model, the jet was treated as a string of connected, viscoelastic dumbbells.²⁷ Using a linear Maxwell equation, the three-dimensional (3D) trajectory for the jet was calculated and the calculation results were in agreement with the experimental observations. In another model, the jet was treated as a long, slender object to account for the electrospinning phenomenon.³¹ In this case, the electrospinning process only involved whipping rather than splaying. This model was further extended to predict the saturation of whipping amplitude and the diameter of the resultant fiber(s).⁵³ A third model was also proposed, in which the role of nonlinear rheology in stretching the jet was included to describe its motion in an electric field.^{54,55} All these models help us achieve a deep understanding of the mechanism of electrospinning. More importantly, they also greatly assist experimentalists in designing new setups and controlling the parameters of electrospinning to obtain nanofibers with desirable diameters and structures.^{53,56}

As illustrated in Figure 3A,⁴⁷ the tapered jet initially follows a nearly straight line for a certain distance away from the tip of the spinneret, and this space is known as the near-field region. The viscoelastic properties of the fluid should be able to suppress the Rayleigh instability, which otherwise causes the jet to break into droplets.^{45,47} The surface charges move with the jet, generating a current passing through it. The velocity, length, and diameter of the jet in the straight segment can all be readily measured.^{57,58} The velocity of the jet at the end of the straight segment was estimated to be 1–15 m/s. The critical length (L) of the straight segment can be estimated using the following equation:^{56,59}

$$L = \frac{4kQ^3}{\pi\rho^2 I^2} \left(\frac{1}{R_0^2} - \frac{1}{r_0^2} \right) \quad (2)$$

where $R_0 = (2\sigma Q/\pi\kappa\rho E)^{1/3}$, σ is the surface charge, Q is the flow rate, κ is the electrical conductivity of the fluid, ρ is the density of the fluid, E is the strength of the electric field, I

is the current passing through the jet, and r_0 is the initial radius of the jet. Under some certain conditions (e.g., at a relatively slow flow rate), the straight segment can be very short. Figure 3B shows the characteristic interference colors observed in the straight segment of a jet of aqueous PEO.^{47,60} The illuminating light was produced by a Xenon arc lamp, and the image was recorded using a digital video camera. The observed color had a correlation with the diameter of the jet. The straight segment was about 30 mm in length. With the decrease of voltage, the straight segment was shortened. In another study involving a poly(ϵ -caprolactone) (PCL) solution in acetone, the straight segment was about 3 mm in length, together with a diameter of 5–10 μm at the midpoint. The jet tended to move downward at a velocity close to 1 m/s.⁵⁷

2.1.3. Thinning of the Jet.—During the acceleration of the jet as a straight line, the surface tension and viscoelastic force in the jet tend to prevent it from moving forward.⁵⁰ As a result, the acceleration is gradually attenuated. In the meantime, the diameter of the jet in the straight segment decreases monotonically with distance away from the tip as the jet is continuously stretched. When the acceleration drops to zero or a constant, any small perturbation is able to destroy the straight movement.⁵⁶ As such, instability can easily arise as a consequence of the electrostatic repulsion among the surface charges residing on the jet, entering the far-field regime.

In the far-field region, three different types of instabilities may occur to an electrically charged jet.^{27–29,31,32,61} The first type is axisymmetric, also known as Rayleigh instability, which may lead to the breakup of the jet into droplets. It is dominated by surface tension and can be suppressed at a strong electric field. The second type is also axisymmetric, which occurs at a stronger electric field than the first type. The third type, also known as whipping or bending instability, is non-axisymmetric. It describes long wave perturbations to the jet as driven by the aerodynamic instability and the “lateral electrostatic force” in a radial direction relative to the jet, resulting from the electrostatic repulsion among surface charges in a strong electric field.⁵⁰ As illustrated in Figure 3C, the jet is compelled to bend by the lateral force (F_R) resulting from the electrostatic repulsion among the surface charges.⁵⁰ The interactions among the charges residing on the jet and the external electric field coordinate these three different types of instabilities, which grow at different rates and are controlled by the physicochemical properties of the liquid and the electrospinning parameters.

To obtain ultrathin nanofibers by electrospinning, it is critical to achieve rapid growth of whipping instability and thereby bending or stretching of the jet.²⁷ The bending perturbation creates the lateral force of F_R perpendicular to the jet axis, further promoting the bending perturbation. The offaxis force generates a radial component for the velocity that is added vectorially to the downward velocity. As such, the jet quickly bends by an angle of about 90°, and the trajectory evolves into a series of loops, generating a coil with many turns around the original direction. The coil consists of one continuous, looping, spiraling, and gradually thinning jet that whips at a very high frequency. In space, the envelope of the coil takes a conical shape, known as “envelope cone”, with a well-defined half-angle at its vertex (Figure 3A). Most of the elongation takes place in the loops because of bending motion. The transverse velocity of a given loop is typically on the order of several tens m/s, whereas the downward velocity of the loop is much smaller, on the order of just 1 m/s.^{27,62} The jet

bends, elongates, and becomes thinner in diameter to maintain continuity of the path. With further elongation, the element in the jet elongates into a thinner segment along an arc to generate a much smaller coil, triggering the formation of another stage of bending instability, the second bending instability. If the jet solidifies before the second bending instability occurs, the diameter of the loops during the first bending instability no longer increases. As a result, the envelope cone becomes an “envelope cylinder”. Several phenomena may cause the shape of the envelope to become more complicated. For example, the evaporation of solvent constantly reduces the volume and changes the viscoelastic parameters of the jet in the path, making it difficult to further stretch the jet. As such, the loops will become smaller in diameter.

Whipping instability accounts for the substantial reduction in diameter for the jet by vastly increasing the path length, over which the jet is accelerated and stretched prior to solidification or deposition on the collector. During the whipping process, the length of the jet can be elongated by up to 10,000 times within a short period of 0.05 s or less. The elongation (drawing) rate is extremely large (up to 1,000,000 s⁻¹).⁶³ As a result, the diameter of the jet is reduced by several orders of magnitude, ultimately leading to the formation of fibers with diameters down to the sub-micrometer and even nanometer scale.³²

Figure 3D shows a stereographic picture captured using high-speed photography under the flash of an intense strobe light for 100 μs.⁴⁷ The experiment was done with a solution of PEO in a mixture of water and alcohol. While the straight segment is not included, the picture clearly shows the three stages of bending instabilities. The successive loops of the coil that passed through the region during the first bending instability were observed as an envelope cone. The onset of the second bending instability was observed to develop on the loop having the largest diameter from the first bending instability. The bottom part of the picture shows small glints from the more complicated path, which can be attributed to higher order bending instability.

For a charged liquid jet with bending instabilities in an electric field, the diameter of the terminal jet can be predicted using the following equation:⁵³

$$d_t = \left(\gamma \epsilon \frac{Q^2}{I^2} \frac{2}{\pi(2 \ln \chi - 3)} \right)^{1/3} \quad (3)$$

where d_t is the terminal diameter of the jet, γ is the surface tension of the liquid, ϵ is the dielectric constant of the medium surrounding the jet, Q is the flow rate of the liquid, I is the electric current through the jet, and χ corresponds to the dimensionless wavelength of the bending instability, which is positively correlated with the radius of the bending perturbation divided by the radius of the jet.

In addition to bending instabilities, other characteristic instabilities such as branching and capillary instability have also been observed.²⁶ When the number of charges per unit surface area is high enough, branches can grow outward from the primary jet.⁶⁴ When the density of

charges carried on the jet is reduced, capillary instability, which causes a cylindrical fluid jet to be disrupted into droplets, may occur, leading to the formation of beaded fibers.

2.1.4. Solidification of the Jet.—During the process of elongation, the jet solidifies to form fibers, which is caused by either the evaporation of solvent or the cooling of melt.

When the solidification process is slow, the elongation of the charged jet can last for a longer period of time to generate fibers with a thinner diameter. In one study, it was claimed that the cross-sectional radius of a dry fiber was only 1.3×10^{-3} times of that of the initial jet as a result of stretching and solvent evaporation.²⁸ After solidification, the charges can still be trapped on the surface of the dry fibers, but all the instabilities will cease.

2.1.5. Deposition of Fibers.—The final step in an electrospinning process is the deposition of fibers on a grounded collector. The morphologies of the fibers are mainly determined by the stage of bending instability in which the fibers are deposited. It is straightforward to collect the fibers in the loop region of the first bending instability as a nonwoven mat on a stationary or moving collector. However, the fibers in the small coiled region of the second and third bending instabilities may take a complex pattern, and the coils can be collected as fibers with a straight or wavy morphology, or even coils with many turns. After deposition, most of the charges on the fibers are quickly dissipated through the grounded collector. However, due to the low conductivity of most materials for the fibers, a measurable amount of residual charges still remain on the surface of the collected fibers.^{65,66} The buildup of residual charges on the collected fibers tends to repel the similarly charged jet, causing a pendulum-like motion for the electrified jet.⁶⁷ As a result, the achievable thickness of a nonwoven mat of electrospun fibers is often restricted by an upper limit of about 0.5–1 mm.⁶⁸

2.1.6. Control of an Electrospinning Process.—The formation of electrospun fibers and control of their diameters are largely determined by the processing parameters, including the applied voltage, the flow rate of the liquid, and the distance between the tip of the spinneret and the collector.

A static DC high voltage is usually applied to the spinneret to generate the electric field. The polarity of the voltage can be either positive or negative, which affects the distribution of charged molecules within the liquid and thus the type of charges accumulated on the surface of the jet. For some materials, especially electrolytes, their capacities for electrospinning are dependent on the polarity of the applied voltage.^{69,70} The applied voltage directly determines the amount of charges carried by the jet and the magnitude of electrostatic repulsion among the charges, as well as the strength of the interactions between the jet and the external electric field. A higher voltage usually favors the formation of thinner fibers,⁷¹ whereas it may also induce the ejection of more fluid, giving rise to fibers with thicker diameters.⁷² AC has also been used to electrospin fibers, but the jet shows significantly different behaviors relative to the case of DC.^{73–75} As illustrated in Figure 4A, the AC power supply introduces alternating segments of positive and negative charges to the jet, resulting in a decrease in electrostatic repulsion and thus the suppression of bending instability.⁷⁶ The length of the charged segments is determined by the frequency of the AC potential. If the frequency is too high, the transfer of charges may not be fast enough to

adequately electrify the liquid for electrospinning. When the frequency is too low, the jet may largely contain a single polarity instead of alternating segments with positive and negative charges. Only at an appropriate frequency, a whipping cloud will be formed from the spinneret, and a visible thread will emerge sometimes downstream, as shown in Figure 4B.⁷⁷ The thread does not display any significant attraction toward the grounded collector and consequently can be easily deflected away. Self-bundling of the jet during AC electrospinning has also been observed due to the presence of positively and negatively charged segments.⁷⁷ In addition, by applying AC high voltage, the amount of net charges on the generated fibers can be reduced, enabling long-term collection of fibers on a nonconductive substrate.⁷⁸

Regarding the flow rate of the liquid, any increase will typically result in the formation of fibers with enlarged diameters. The working distance between the tip of the spinneret and the collector determines the stage of instability at which the jet is deposited on the collector. A relatively long enough distance is required to ensure full extension and solidification of the jet, and thereby the formation of solid fibers. In general, thinner fibers will be formed as the distance is increased. When the distance between the tip of the spinneret and the collector is beyond a certain range, the fiber will not become thinner as the distance is increased because of solidification of the jet. In general, it is the intricate interplay of all the processing parameters that controls the morphology and diameter of the fibers. For example, with the increase of flow rate, one has to increase the critical voltage for generating the fiber, as well as the working distance between the tip of the spinneret and the collector to ensure full extension and solidification of the jet. As a result, it is necessary to optimize all the processing parameters in order to control an electrospinning process.

2.2. Materials for Electrospinning

Electrospinning has been utilized to generate nanofibers from various types of materials. The most commonly used materials are organic polymers in the form of either solution or melt. Small molecules can also be directly electrospun into nanofibers if they self-assemble and generate sufficient chain entanglement. When combined with sol–gel chemistry, a variety of composite materials have been directly electrospun into nanofibers. By introducing nanoscale components with different dimensions and/or morphologies (e.g., nanoparticles, nanorods, nanowires, nanotubes, and nanosheets) into polymer solutions, the as-obtained mixtures have also been used for electrospinning. The following subsections give a brief account of all these diversified materials in the context of electrospinning or electrospun nanofibers.

2.2.1. Organic Polymers.—Most of the organic polymers can be directly applied to electrospinning as long as they can be dissolved in appropriate solvents to obtain solutions or be melted without degradation. For simplicity, we call the corresponding methods solution electrospinning and melt electrospinning, respectively.

Solution Electrospinning: This method is more commonly used and better characterized than melt electrospinning. As the jet of a polymer solution is stretched, elongated, and thinned by whipping instability, the solvent is quickly evaporated, resulting in solidification

of the jet and deposition of solid nanofibers on the collector.⁴⁴ Figure 5A shows a scanning electron microscopy (SEM) image of poly(vinylpyrrolidone) (PVP) nanofibers electrospun from a 10 wt % ethanol solution of PVP with a molecular weight (M_w) of ca. 1,300,000, indicating that the nanofibers are deposited in the form of a nonwoven mat.

More than 100 different types of organic polymers, including both natural and synthetic polymers, have been successfully explored for solution electrospinning to directly produce nanofibers. Among them, synthetic polymers such as polystyrene (PS) and poly(vinyl chloride) (PVC) have been electrospun into nanofibers for commercial applications related to environmental protection. A large number of biocompatible and biodegradable synthetic polymers, such as PCL, poly(lactic acid) (PLA), and poly(lactic-*co*-glycolic acid) (PLGA), have been directly electrospun into nanofibers and further explored as scaffolds for biomedical applications. Natural biopolymers, such as DNA, silk fibroin, fibrinogens, dextran, chitin, chitosan, alginate, collagen, and gelatin, have also been electrospun into nanofibers from their solutions. Conductive polymers such as polyaniline (PANI) and polypyrrole (PPy) have been directly electrospun into nanofibers. Other types of functional polymers such as poly(vinylidene fluoride) (PVDF) have also been electrospun into nanofibers for piezoelectric and/or pyroelectric applications.

In general, the success of electrospinning a polymer solution, as well as the structure and morphology of the resultant polymer nanofibers, is determined by a set of parameters related to the polymer, solvent, polymer solution, processing parameters, and ambient conditions.^{41,42} There are two general requirements for a successful solution electrospinning: (i) sufficiently high molecular weight for the polymer and (ii) availability of a suitable solvent to dissolve the polymer. The molecular weight of a polymer has a major impact on the rheological behaviors and electrical properties of the solution. In general, lowering the molecular weight tends to generate beads rather than fibers because of the limited chain entanglement. The formation of a homogeneous polymer solution critically depends on the solubility parameter of the solvent,^{79,80} but the solvent with a high solubility parameter does not necessarily produce a solution suitable for electrospinning. The volatility or vapor pressure of the solvent determines its evaporation rate and thus the solidification rate of the jet. A very high volatility is not suitable for the spinning of fibers because the jet may solidify immediately upon exiting from the spinneret. If the volatility is too low, the fibers will still be wet when they are deposited on the collector. The dielectric constant of the solvent controls the magnitude of electrostatic repulsion among the surface charges residing on the jet. With increasing of the dielectric constant, the applied voltage required to achieve a stable jet will be increased.⁸⁰

The commonly used solvents include alcohols, dichloromethane, chloroform, dimethylformamide (DMF), tetrahydrofuran (THF), acetone, dimethyl sulfoxide (DMSO), hexafluoroisopropanol (HFIP), and trifluoroethanol, among others. Water is not a favorable solvent for electrospinning because of its high dielectric constant and thus the attenuation of electrostatic repulsion. Sometimes, it might be necessary to use a mixture of different solvents in order to achieve the optimal formulation for electrospinning.

In addition to the molecular weight of polymer and the type of solvent, the spinnability of a polymer solution critically depends on its concentration and electrical conductivity. In order to obtain fibers, a minimum concentration is required to achieve the chain entanglement critical to the transition from electrospraying to electrospinning.⁸¹ At a concentration below this limit, the interactions between the polymer chains are too weak to overcome the Rayleigh instability, the jet will break into droplet, and thus fine particles or polymer beads instead of continuous fibers will be obtained, in a process commonly referred to as electrospray. As the concentration increases, the jet will no longer break up and the shape of the beads will change from spherical to spindle-like, eventually leading to the formation of uniform fibers owing to the increase in chain entanglement and viscosity. If the concentration is too high, however, it will be extremely difficult to overcome the viscoelastic force and no jet will be formed. Within a suitable range, reducing the concentration favors the formation of thinner fibers. The polymer concentration, however, also affects the viscosity and surface tension of the solution, and both parameters can impact the morphology and size of the resultant fibers. In general, decreasing the viscosity and surface tension favors the production of thinner fibers, but this can also be realized by adding a surfactant rather than reducing the polymer concentration.^{71,82} When the viscosity is too low, no fiber will be produced. If the viscosity is too high, it will become difficult to eject the solution from the spinneret. With regard to electrical conductivity, it is difficult to electrospin a solution that is perfectly insulating because such a solution is unable to conduct charges from the interior of the solution to its surface. If the solution is too conductive, however, it will be difficult to generate Taylor cone or initiate bending instability as a result of the depleted electrostatic repulsion because surface charges cannot be accumulated on a conductive droplet or jet.^{83–85} It is only within a proper range that increase of electrical conductivity will favor the formation of thinner fibers because of extensive bending of the jet. One efficient strategy for increasing the conductivity of a polymer solution is to introduce ionic compounds such as salts or mineral acids.⁸⁶

The processing parameters (e.g., the applied voltage, flow rate of the polymer solution, and working distance between the spinneret and the collector) during solution electrospinning can affect the morphology and size of the fibers, as discussed in section 2.1.6. The ambient conditions, including relative humidity and temperature, also have an influence on solution electrospinning. The relative humidity influences the evaporation rate of the solvent and thus the solidification rate of the jet. A lower relative humidity favors the formation of thinner fibers with a more dried surface.⁸⁷ However, if the relative humidity is too low, the solvent evaporates quickly, hindering the extension of the jet. On the other hand, when the relative humidity reaches a sufficiently high level, the water vapor in the air may penetrate into the jet, causing morphological changes to the nanofibers. The ambient temperature is another crucial parameter for the formation of ultrafine fibers. At an elevated temperature, both the surface tension and viscosity of the polymer solution will be reduced, favoring the formation of thinner fibers. However, the evaporation of the solvent will also be accelerated at a higher temperature, limiting the extension of the jet. Taken together, the temperature has two opposite impacts on the diameter of the fibers, and it needs to be optimized carefully.⁸⁸

Some functional polymers (e.g., conductive polymers) and natural polymers may not be suitable for electrospinning from their solutions. Conductive polymers have rigid backbones

Author Manuscript
Author Manuscript
Author Manuscript
Author Manuscript

with low molecular weights, resulting in poor solubility in common solvents and thus inadequate chain entanglement in the solution phase. In addition, the high solution conductivity makes it difficult to form a stable jet.^{83–85} So far, only a limited number of conductive polymers have been successfully electrospun into nanofibers by modifying the polymer solutions and/or the electrospinning conditions.⁸⁹ In one study, PPy with an adequate molecular weight and high solubility in DMF was obtained by adding di(2-ethylhexyl) sulfosuccinate sodium salt during polymerization.⁹⁰ Upon electrospinning, PPy nanofibers with an average diameter of 70 nm were fabricated. In another study, Mg(NO₃)₂ (10 wt % Mg²⁺ relative to the polymer) was introduced into an aqueous mixture of poly(3,4-ethylenedioxythiophene) (PEDOT) and poly(styrenesulfonate) (PSS).⁹¹ Upon electrospinning, conductive nanofibers with diameters in the range of 70–100 nm were obtained (Figure 5B). The formation of nanofibers can be attributed to the introduced Mg²⁺ ions, which served as a physical cross-linker for the polymer chains (Figure 5C).

At a high relative humidity, “standing fibers” that stretch vertically between the spinneret and the grounded collector can be formed during electrospinning, as shown in Figure 5D for poly(phenylenevinylene) when electrospun at a relative humidity > 45%.⁹² The formation of standing fibers can be attributed to the strong electrostatic attraction between the fibers and the spinneret in the presence of a significant amount of water molecules.^{93–95} In order to achieve continuous formation and deposition of nanofibers on the grounded collector, the relative humidity should be controlled below a critical level. In addition, blowing air vertically downward can overcome the electrostatic attraction between the nanofibers and the spinneret, promoting the deposition of more fibers. Collecting the nanofibers in a liquid bath represents another way to manipulate the electric field for the facile collection of fibers.⁹⁶ For example, PANi nanofibers with an average diameter of around 139 nm were electrospun from a 20 wt % PANi solution in 98% formic acid with the use of a water bath as the collector.⁹⁷

Mixing a functional polymer with another electrospinnable polymer is an efficient way to obtain a suitable solution for electrospinning. To this end, a synthetic polymer can serve as a carrier phase to greatly assist the electrospinning process for the fabrication of nanofibers containing natural biopolymers. The nanofibers made of a polymer blend can also give rise to new applications due to the integration of functions originating from individual components. It should be pointed out that the different polymer components may separate into distinct phases in the jet as a result of solvent evaporation. The separation can be mitigated by improving the compatibility between the polymers and thus the entanglement of their chains.

Melt Electrospinning.: Some polymers are difficult to dissolve in suitable solvents for solution electrospinning; notable examples include polyethylene and polypropylene (PP). In these cases, fibers can be directly electrospun from their melts instead.⁹⁸ Figure 6A shows a schematic of the typical setup for melt electrospinning.⁹⁹ To keep the polymer in a molten state in the spinneret, it is necessary to add a heating device, such as an electrical heating tape, circulating fluid, and laser.^{100,101}

After ejection from the spinneret, the molten jet cools and solidifies to generate fiber(s) because of heat transfer between the jet and the surrounding medium (typically, air). The heat transfer rate can be greatly enhanced in the presence of an electric field due to the electrohydrodynamic effects.¹⁰² As shown in Figure 6B, when the tip of the spinneret and collector are applied to a positive potential separated by a dielectric component (molten jet and air in this case), the air close to the surface of the jet can be positively ionized, leading to a positive corona discharge.¹⁰³ It is critical to keep the applied voltage greater than the corona onset but below the air gap breakdown voltage. The resultant corona current is able to disturb the thermal boundary layer between the jet and the air, causing the heat transfer rate to increase by 1 order of magnitude. Figure 6C shows the images captured using an infrared camera, revealing the temperature profiles of the molten jets of nylon-6, PP, and PLA, respectively.¹⁰³ In all cases, the jets were thermally quenched rapidly along the ejection direction. The electrohydrodynamic quenching results in fast cooling and quick “freezing” of the jet, greatly reducing the degree of stretching for the jet.^{102,104–106}

Different from solution electrospinning, the whipping instability of the jet is largely suppressed in melt electrospinning.¹⁰⁰ This difference can be largely attributed to the unique properties of a polymer melt: (i) its electrical conductivity (typically less than 10^{-10} S/m) is much lower than that of a polymer solution, and (ii) its viscosity (typically between 40 and 200 Pa·s) is much higher than that of a polymer solution. As a result, the density of surface charges on the molten jet is lower, dampening the whipping instability. Moreover, when the temperature of the jet drops below the glass transition temperature (T_g) of the polymer, rapid solidification of the jet will further suppress the whipping instability and stronger electrostatic repulsion is required to overcome the viscoelastic force. Therefore, the electrostatic force provided by the external electric field contributes most to the thinning of the jet, and the jet usually travels in a straight line, as shown in Figure 6D.¹⁰⁷ Upon deposition onto a stationary collector, the jet buckles under compression, and the fiber(s) coil around the midline (see Figure 6E,F). The deposited fibers do not appear to repel the incoming fibers. Due to the lack of whipping instability and solvent evaporation, melt electrospinning produces thicker fibers (typically, on the micrometer scale) than solution electrospinning.

Only a small fraction of the commercially available polymers has been successfully explored for melt electrospinning.¹⁰⁰ As a prerequisite, the polymer must have a glass transition and melt at a temperature without involving thermal degradation. As such, melt electrospinning does not work for thermoset polymers, proteins, and thermally unstable polymers. The most commonly used polymers are thermoplastics such as PP and polyesters (e.g., polyurethane, PCL, PLA, and PLGA). Especially, polymers with low melting points (T_m), such as PCL, exhibit good thermal stability and favorable processability for melt electrospinning. Polyolefins and polyamides, which are only soluble in specific solvents, have also been processed into fibers using melt electrospinning. Other common industrial polymers that have been melt electrospun include nylon-6, polyethylene, poly(methyl methacrylate) (PMMA), and poly(ethylene terephthalate) (PET).

The electrospinnability of a polymer melt is critically dependent on its viscosity and electrical conductivity.¹⁰⁰ By adding viscosity-reducing additives into PP melt, the diameter

of the resultant fibers was significantly reduced from 35 ± 8 to $0.84 \pm 0.19 \mu\text{m}$. Increasing the electrical conductivity allows for more significant stretching of the jet, favoring the formation of thinner fibers. By adding 5 wt % NaCl, for example, the electrical conductivity of PP held at a processing temperature of 200 °C (above its T_m) could be increased from 10^{-12} to 10^{-8} S/m , leading to a substantial decrease in fiber diameter from 3.01 ± 1.07 to $0.31 \pm 0.10 \mu\text{m}$.¹⁰⁸

The processing parameters also have impacts on melt electrospinning. Specifically, the flow rate of a polymer melt is often low (typically, $<0.1 \text{ mL/h}$) to produce ultrathin fibers. The temperature of the melt in the spinneret is also important. By increasing the temperature to an appropriate range, both the viscosity of the melt and the cooling rate of the jet can be reduced to generate thinner fibers. An optimal combination of the applied voltage and spinneret-to-collector distance is also important to ensure adequate cooling for the jet. In addition, when a flat collector moves laterally below a stationary spinneret, the shape of the jet is greatly affected by the moving speed of the collector (S_C).¹⁰⁹ As illustrated in Figure 7A, as the ratio of S_C to the jet speed (S_J) is increased, the jet gradually transforms from a “compressive heel” ($S_C = S_J$) to a “catenary profile” ($S_C \gg S_J$), mainly due to the drag of the collector by the jet. Accordingly, the structure and diameter of the deposited fibers will be altered. Figure 7B shows an optical micrograph of PCL fibers produced by melt electrospinning at a flow rate of 0.05 mL/h and at 70 °C. By matching the S_C and S_J (in this case, 0.5 m/min), the coiling effect disappeared, leading to the formation of a straight, continuous fiber with a diameter of approximately $19 \mu\text{m}$.

The temperature of the surrounding air is another critical parameter. If the air is heated, the jet will be cooled at a slower rate, favoring the formation of a thinner jet. According to a modeling analysis, the heated air was able to contribute an additional 20-fold of thinning for the jet, downsizing the fibers to the nanometer scale.^{110,111} Through careful optimization of the aforementioned parameters, it is possible to produce nanofibers by melt electrospinning. The smallest diameter reported in literature is about $270 \pm 100 \text{ nm}$, which involved electrospinning of a blend of PEG-*b*-PCL and PCL.¹⁰⁷ Owing to its ability to precisely control the position of the deposited fiber, melt electrospinning has been explored as an additive manufacturing technique for the fabrication of 3D constructs with well-defined structures and feature sizes. For example, PCL fibers were assembled to form a multilayered construct with the orientations of fibers in adjacent layers rotated by 90° and 60°, respectively, as shown in Figure 7C,D.¹⁰⁹

In situ polymerization of oligomers in the flying jet is another interesting strategy for producing fibers through either solution or melt electrospinning. In one study, by carefully matching the rates of photopolymerization and jet flying, continuous fibers were obtained from a solution containing hexafunctional acrylic polyester (ca. 3700 in M_w).¹¹² Thermally induced polymerization has also been explored to produce fibers. For example, polyurethane prepolymer (1000–2000 in M_w) and PEG-400 chain extender were mixed and subjected to melt electrospinning, and the jet could be solidified quickly upon heating for the production of polyurethane fibers.¹¹³

In the case of solution electrospinning, the weight percentage of polymer in the solution is typically low and a large amount of solvent is involved, resulting in both economic and environmental concerns. The absence of solvent in melt electrospinning means no residue of toxic solvents, improving the safety and throughput of the process. In these regards, melt electrospinning has much higher productivity than solution electrospinning. Additionally, melt electrospinning enjoys the ability to precisely control the positions of fibers during their deposition. As a major limitation of melt electrospinning, it is difficult to produce fibers with diameters down to the nanometer scale. Extended heating can also lead to polymer degradation, and high processing temperatures may not be suitable for the processing of drugs or bioactive molecules. The number of polymers suitable for solution electrospinning is much greater than that for melt electrospinning. Therefore, it is necessary to fully analyze the polymer's properties and the target applications when choosing an electrospinning method (solution versus melt) for producing fibers from an organic polymer.

2.2.2. Small Molecules.—Small molecules can be directly electrospun into fibers when the chain entanglement is significant enough to stabilize the electrified jet and thus suppress the Rayleigh instability. The key factor is the presence of sufficient intramolecular interactions among the small molecules to form self-assembled structures in their highly concentrated solutions or pure melts.

The solution-phase electrospinnability of small molecules is mainly determined by their structures and concentrations, as well as the type of solvent. The reported small molecules mainly include amphiphiles and cyclodextrin derivatives.^{114,115}

Lecithin, a natural mixture of phospholipids and neutral lipids, is the first reported amphiphiles for electrospinning.^{116–118} It can self-assemble to form spherical micelles in a nonaqueous solution at a concentration above the critical micelle concentration (cmc). When the concentration is further increased, the morphology of the micelles undergoes transition from spherical to cylindrical, and eventually the cylindrical micelles can overlap and entangle to behave like polymer chains, as illustrated in Figure 8A.¹¹⁶ Upon electrospinning of a lecithin solution in a 70:30 (wt %) mixture of chloroform and DMF at a concentration of 43 wt % (higher than the cmc, 35 wt % in this case), continuous fibers with an average diameter of 2.8 μm were produced (Figure 8B). In comparison, particles were obtained from a solution at a concentration equal to cmc, as shown in Figure 8C. By further increasing the concentration to 50 wt %, the resultant fibers showed a thicker diameter of 5.9 μm . Similarly, gemini surfactants^{119,120} and bioactive peptide amphiphiles^{121–123} have also been directly electrospun into fibers with diameters on the micrometer scale.

As another example, cyclodextrin derivatives can form aggregates via hydrogen bonding to give a solution with high viscosity and thus a viscoelastic solid-like behavior owing to the doughnut-shaped glucopyranose rings in cyclodextrin (Figure 8D).¹²⁴ Upon electrospinning of a 120% (w/v) hydroxypropyl- β -cyclodextrin solution in dimethylacetamide, fibers with diameters in the range of 0.4–1.8 μm were produced, as shown in Figure 8E.

Some small molecules can also form entanglement in their melts. In these cases, continuous fibers can be readily obtained through melt electrospinning. For example, 1-palmitoyl-2-

oleoyl-*sn*-glycero-3-phosphoethanolamine, a phospholipid with a M_w of 718 g/mol, can form large aggregates in its melt.¹²⁵ Upon melt electrospinning at a temperature around 200 °C, fibers with an average diameter of $6.5 \pm 2.0 \mu\text{m}$ were produced. In another demonstration, both 1,3,5-benzene and 1,3,5-cyclohexanetrisamides were found to exhibit a distinguished self-assembly behavior in their melts due to strong hydrogen bonding, supporting their electrospinning into fibers. Perylene bisimides have also been processed into fibers by melt electrospinning, thanks to the strong π–π interactions.¹²⁶

2.2.3. Colloidal Particles.—A colloid, consisting of a dispersed phase (the suspended particles) and a continuous phase (the medium of suspension), has also been adapted for electrospinning when sufficient entanglement is formed among the particles to maintain the jet as a continuous structure. A typical example can be found in the electrospinning of aged inorganic sols with spinnable viscosities arising from the hydrolysis and condensation of metal alkoxides or metal salts. The colloidal particles need to have a certain size, in addition to cross-linking among them, in order to obtain a stable electrospinning process, with the viscosity being a critical parameter in determining the fiber's diameter. In a typical procedure, a silica sol was prepared from tetraethyl orthosilicate (TEOS), distilled water, ethanol, and HCl and then aged at 80 °C for 30 min.¹²⁷ Upon electrospinning, silica fibers with diameters in the range of 0.4–1 μm were produced. Similarly, silica nanofibers thinner than 400 nm in diameter were also produced by adjusting the properties of the aged sols.¹²⁸ In another study, an aged sol prepared from lithium acetate, cobalt acetate, distilled water, and citric acid was used for electrospinning.¹²⁹ Upon calcination of the as-spun composite fibers, LiCoO₂ fibers with diameters in the range of 0.5–2 μm (Figure 9A) were obtained. The transmission electron microscopy (TEM) image in Figure 9B indicates that the fiber was composed of uniform LiCoO₂ nanoparticles of 20–35 nm in diameter. Based on the sol–gel method, ceramic fibers made of oxides such as Co₃O₄, NiO, and a mixture of Al₂O₃ and ZnO have all been produced. However, the as-obtained fibers are typically more than several micrometers in diameter. In addition, the ability to control the size and uniformity of the fibers is quite limited because of the difficulty in precisely controlling the rheological properties of a sol.¹³⁰

When metal nanoparticles are dispersed in a solution at a high concentration, a spinnable mixture will be obtained for electrospinning. In a recent study, Ag nanoparticles ($40 \pm 5 \text{ nm}$) were dispersed in ethylene glycol at a concentration of 50 wt %.¹³¹ Upon electrospinning, followed by thermal annealing at 150 °C in air, the Ag nanoparticles were coalesced and converted to electrically conductive Ag nanofibers with an average diameter of $338 \pm 35 \text{ nm}$. In general, the capability of this method is limited due to the difficulty in preparing highly concentrated suspensions of metal nanoparticles.

2.2.4. Composites.—Composites, which are usually prepared by adding sol–gel precursors or nanoscale components into polymer solutions, have been extensively explored for solution electrospinning. In the case of a sol–gel precursor, one should avoid the occurrence of sol–gel reactions in the stock solution. The sol–gel reactions, including hydrolysis, condensation, and gelation of the precursor, should be initiated in the jet by contacting with the surrounding air.^{132,133} As such, a continuous network of the inorganic

Author Manuscript
Author Manuscript
Author Manuscript
Author Manuscript

phase will be formed in the polymer matrix, leading to the formation of nanofibers made of an inorganic–polymer composite. In an early demonstration, PVP and titanium tetraisopropoxide ($\text{Ti(O}i\text{Pr})_4$, a precursor to TiO_2) were dissolved in an alcohol to obtain a spinnable solution.¹³² Upon electrospinning, uniform nanofibers comprised of PVP and amorphous TiO_2 were produced, as shown in Figure 10A.

The electrospinnability of such a solution is mainly determined by the sol–gel precursor and the nature of the carrier polymer, as well as the viscosity and electrical conductivity of the solution. The carrier polymer should be spinnable, with either a high M_w or a significant degree of chain entanglement.¹³⁴ To this end, PVP represents one of the most popular carrier polymers owing to its high solubility in ethanol and water and its good compatibility with many sol–gel precursors. Other polymers, such as PEO, poly(vinyl alcohol) (PVA), and poly(acrylic acid), have also been successfully used as the carrier.^{132,133,135}

The type of precursor greatly affects the rates of sol–gel reactions in the jet.¹³² A rapid hydrolysis often causes the blockage to the spinneret, whereas a rapid gelation results in a less stretchable jet and thus thicker fibers. The commonly used precursors include metal salts, such as alkoxides, nitrates, acetates, chlorides, and sulfates. Sometimes, an additive (e.g., acetic acid, hydrochloric acid, or propionic acid) is needed in order to stabilize the precursor solution by adjusting both the hydrolysis and gelation rates to ensure a stable electrospinning process.^{127,136}

The viscosity of the solution plays a crucial role in stretching the jet, which can be controlled by varying the concentrations of the precursor and the polymer. The electrical conductivity of the solution can be increased by adding a salt (e.g., NaCl and $(\text{CH}_3)_4\text{NCl}$) to promote the formation of thinner fibers. Additionally, a well-controlled environment surrounding the jet is also of great importance. Typically, an atmosphere with a lower relative humidity and/or saturated with the solvent vapor can substantially reduce the rates of hydrolysis and gelation and therefore give rise to continuous electrospinning.¹³⁰ By optimizing these parameters, the diameter of the as-spun composite fibers can be reduced to several hundred nanometers.

The composites used for solution electrospinning have also been prepared by dispersing nanoscale components in a polymer solution through extensive stirring or ultrasonication. The commonly used nanoscale components include nanoparticles made of Ag, Au, and TiO_2 and even particles comprised of a metal–organic framework (MOF) compounds,^{137,138} one-dimensional (1D) nanostructures such as Au nanorods, Au or Ag nanowires, and carbon nanotubes, as well as two-dimensional (2D) nanostructures such as clay tablets and graphene nanosheets.¹³⁹

The electrospinnability of such a formulation critically depends on the type, size, and concentration of the added nanoscale components, which will also affect the morphology of the resultant composite nanofibers. A stable dispersion of the nanoscale components in the polymer solution is instrumental to the formation of nanofibers with a homogeneous distribution of the nanoscale components, whereas it is difficult to achieve stable electrospinning and obtain uniform fibers if the nanoscale components are inclined to

Author Manuscript
Author Manuscript
Author Manuscript
Author Manuscript

aggregate. The nanoscale components often need to be modified with a functional group to obtain a stable dispersion. The size and concentration of the nanoscale components also affect their dispersity and thus the morphology of resultant nanofibers.¹⁴⁰ In one study, composite nanofibers containing well-distributed Ag nanoparticles were produced, as shown in Figure 10B, by dispersing the Ag nanoparticles in an aqueous PVA solution at a Ag to PVA molar ratio of 2:530 (Ag in terms of atom and PVA in terms of repeat unit).¹⁴¹ By increasing the molar ratio to 4:530, more Ag nanoparticles were incorporated into the nanofibers (Figure 10C). When SiO₂ particles of 0.9 μm in diameter were used, necklace-like structures consisting of SiO₂ particles linked by PVA fibers were obtained, as shown in Figure 10D.¹⁴² In this case, the large particles may be exiled from some of the fibers during the electrospinning process.

When 1D nanostructures with anisotropy are used, they can be oriented along the fibers during electrospinning. The concentration of the nanostructures has a major impact on their orientation and the distance among them in an individual fiber. In one demonstration, composite fibers consisting of Ag nanowires and PVP were fabricated using magnetic-field-assisted solution electrospinning. As shown in Figure 10E, multiple (>10) Ag nanowires could be aligned in parallel, along an individual fiber.¹⁴³

2.3. Methods of Electrospinning

Electrospinning is typically conducted in the far-field mode with the use of a hollow needle as the spinneret and a piece of metal substrate (such as an aluminum foil) as the collector. This setup is mainly used for the production of nanofibers in small volumes in a laboratory setting, for evaluating the spinnability of new materials, or for optimizing the parameters for electrospinning before large-scale production. When whipping instability is involved, it will be difficult to precisely control the morphology of the deposited nanofibers. Built upon this general setup, modifications have been made to further increase the capability and versatility of electrospinning. By reducing the distance between the spinneret and the collector, for example, electrospinning can be conducted in the near field to collect fibers from the straight segment of the jet, making it possible to precisely control the position of the deposited fiber. In addition, an array of hollow needles (multiple-needle electrospinning) rather than a single needle has been used to increase the productivity of electrospinning. Instead of using a hollow needle, a 2D array of solid pins or a flat substrate with a large surface area (needleless electrospinning) has been used to increase the number of jets and thus the production volume, pushing electrospinning toward industrial production. The use of a coaxial needle further empowers electrospinning with the capability to produce nanofibers from unspinnable materials and/or to generate nanofibers with a core–sheath or other types of structures. As for the collector, it has been modified in multiple ways by combining with other techniques, such as lithography, to help organize the nanofibers into different patterns. Liquid bath has also been used as a collector, enabling the fabrication of novel fibrous structures (e.g., fiber yarns and filaments) rather than a nonwoven mat of nanofibers.

2.3.1. Far-Field versus Near-Field.—During electrospinning, the distance between the tip of the spinneret and the collector (H) determines the stages at which the fibers will be deposited on the collector. The conventional electrospinning is typically conducted in the

Author Manuscript
Author Manuscript
Author Manuscript
Author Manuscript

far-field mode ($H=5\text{--}15\text{ cm}$) with the application of a high voltage (10–20 kV). As such, a nonwoven mat of nanofibers is obtained, especially for solution electrospinning, due to the difficulty in precisely controlling the positions of the deposited fibers.

When the distance is reduced to $500\text{ }\mu\text{m}$ –5 cm, near-field electrospinning will be attained (Figure 11A),¹⁴⁴ by which the jet is impacted onto the collector within the straight segment. The distance can be predicted using the critical length (L) shown in eq 2.^{56,145} In this case, the electric field is highly concentrated between the spinneret and the collector (Figure 11B),¹⁴⁶ and the applied voltage can be lowered to several hundred volts (usually 0.6–3 kV). In addition, the flow rate of the liquid must be significantly reduced to 0.01–1 mL/h in order to support a stable jet. Figure 11C shows the result of a typical example of near-field electrospinning, which involved an 18 wt % PEO solution in a mixture of water and ethanol.¹⁴⁷ The charged jet followed a straight line for the deposition of fibers at well-defined positions on the collector when the distance and applied voltage were 1.0 mm and 1.7 kV, respectively.

Due to the lack of bending instability, near-field electrospinning allows for the deposition of fibers in high spatial definition by matching the average motion speed (S_J) of the jet with the relative speed (S_R) between the collector and the spinneret. However, the fibers take a large diameter, typically on the scale of several micrometers.^{148,149} Using a movable collector and a stationary spinneret, S_R can be controlled by varying the moving speed of the collector, enabling the collection of fibers shaped into coils, wavy lines, and straight lines. In the demonstration for near-field electrospinning with an 18 wt % PEO solution in a mixture of water and ethanol, fibers with a variety of shapes were produced.¹⁴⁷ As shown in Figure 11D, the fibers were deposited in a nonwoven pattern due to the oscillation motion of the jet caused by the repulsion from the already deposited fibers when the collector was moved at a speed of 0.03 m/s, slower than S_J (0.14 m/s in this case). With the increase of moving speed for the collector, the fibers were deposited onto a narrower area (Figure 11E). By increasing the moving speed of the collector to 0.36 m/s, the oscillation motion of the jet disappeared, and a straight fiber of $0.49\text{ }\mu\text{m}$ in diameter was obtained (Figure 11F). In addition, fibers with specific patterns could also be achieved by controlling the motion of the collector along both X and Y directions (Figure 11G).¹⁵⁰ A movable spinneret can also be used to adjust the S_R for the direct deposition of fibers in different patterns, such as the lattice structures shown in Figure 11H,I.¹⁵¹ Additionally, 3D architectures, such as grids, walls, and hollow cylinders, have all been fabricated using near-field electrospinning through layer-by-layer writing and assembly.^{152,153}

Compared with far-field electrospinning, near-field electrospinning offers a number of advantages: (i) substantial reduction in the applied voltage, (ii) the ability to precisely arrange the fibers over a relatively large area with minimum material consumption, and (iii) the ability to manipulate the spatial positions of the fibers along all three directions of X , Y , and Z for the printing of fibers.^{154–156} However, the flow rate of the liquid in a near-field electrospinning process is relatively low, leading to substantial reduction in the production volume. Moreover, the fibers are usually much thicker than those obtained through far-field electrospinning, and the complexity of the apparatus also limits its use for mass production.^{154–156}

2.3.2. Single Needle versus Multiple Needles.—The traditional setup for electrospinning uses a single needle, and the nanofibers are produced at a low throughput, typically 1–5 mL/h by flow rate or 0.1–1.0 g/h by fiber mass.¹⁵⁷ In order to increase the productivity, an auxiliary electrode can be introduced to increase the number of jets emanated from a single needle.¹⁵⁸ When a grounded electrode is placed near the needle, a strong gradient in electric field will be created between them, resulting in an asymmetrical distribution of the electric field and thus the initiation of multiple jets. In one study, 9–12 jets were ejected from the tip of the droplet by placing a grounded stainless-steel pin near the needle.¹⁵⁸ The capability of this method is limited by the poor stability of the jets and the potential safety issue.

Multiple-needle electrospinning offers another straightforward route to increase the productivity through the use of an array of hollow needles.^{159,160} The needles can be arranged into a linear array by organizing them in a straight line,¹⁶¹ or a 2D array by placing them in a special layout (e.g., a circular, elliptic, triangular, square, or hexagonal pattern),^{162–165} as illustrated in Figure 12A.¹⁶⁶ As such, multiple jets can be simultaneously ejected from the needles, and all of them then undergo bending instability.¹⁶⁴ The paths of the jets are often quite irregular due to the interplay of the external electric field, self-induced Coulombic interactions, and Coulombic repulsion among the jets (Figure 12B).¹⁶⁷ For example, the jets ejected from seven hexagonally arrayed needles were pushed away from each other, as shown in Figure 12C. In addition, the outer jets showed a longer length for the initial straight region and a larger size for the envelope cone than the central jet, due to the progressive weakening of electrical field from the edge to the center.¹⁶⁷

The distribution of the electric field and the Coulombic repulsion among the jets are dependent on the arrangements of the needles. Three key parameters should be considered to enable multiple-needle electrospinning: the spacing between the needles, the number of the needles, and the layout of the array.^{159,160} The spacing is mainly affected by the diameter of the needle and the properties of the solution for electrospinning. The smallest spacing is a distance at which the droplets suspended at the tips of neighboring needles do not fuse together. Increasing the interneedle distance decreases the repulsion among the jets, while pushing the jets closer is beneficial to concentrating the fibers. The number of the needles arranged over a certain area is dependent on both the spacing and the layout, and it ultimately determines the throughput of fiber production. The layout of the array controls the distribution of the electric field. In order to obtain uniform ejection of jets among all needles, the electric fields around the needles should be homogenized. Otherwise, some needles may not be able to reach the critical voltage for jetting, causing clogging to the needles. From one study involving six needles in triangular, square, and hexagonal layouts, the equilateral triangular pattern was shown to be an optimal setting for stable electrospinning.¹⁶¹ Additionally, by shortening the length of the needles at the edge sides, the discrepancies among the jets can also be effectively reduced.¹⁶⁸

Other parameters, such as the flow rate of the solution and the applied voltage, also need to be optimized. A same flow rate should be maintained among the different needles. By separately placing needles with different inner diameters in the central and peripheral locations, all needles have the same flow rates. The applied voltage has a major impact on

Author Manuscript
Author Manuscript
Author Manuscript
Author Manuscript

the densities of surface charges residing on the jets and thus the repulsion among the charged jets. By optimizing the arrangement of the needles and the processing parameters, fibers can be generated in high productivity. For example, with the use of 64 needles in an 8×8 array (Figure 12D), melt electrospinning was used to produce fibers with an average diameter of $0.55 \pm 0.26 \mu\text{m}$ and at a production rate of $18 \text{ m}^2/\text{h}$.¹⁰⁰ However, the clogging and cleaning of the needles and the difficulty in precisely controlling the morphology of the fibers remain to be addressed. Additionally, undesirable interactions, such as the generation of inhomogeneous fibers, fiber–fiber bonding, and/or poor fiber distribution in the collected mat, have also been observed, and they all deserve future attention.^{162,169,170}

In order to improve the stability of the multiple jets, an auxiliary electrode can be introduced nearby the needles to generate a secondary electric field between the needles and the electrode to neutralize the repulsion among the jets. As such, the multiple jets can be stabilized with high homogeneity among them, and the solidified fibers can be deposited in a highly concentrated region.^{169,170} In two studies, a ring¹⁶³ and a plate¹⁷¹ were introduced, respectively, to promote the production of uniform fibers. Another approach relies on the assistance of sheath gas to decrease the critical voltage required for jet emanation and thus the densities of surface charges residing on the jets. As such, the repulsion among the jets can be mitigated,¹⁷² leading to the even deposition of uniform fibers.^{173,174}

2.3.3. Hollow Spinneret versus Solid Spinneret.—Both hollow and solid spinnerets can be used for electrospinning as long as the strength of the external electric field can initiate the emanation of a jet. Hollow spinneret, such as a hollow needle or a tube with holes, is associated with an enclosure, through which the liquid is extruded. Solid spinneret, such as a solid pin, a 2D array of solid pins, and a flat substrate, allows multiple jets to emanate simultaneously from the surface for electrospinning.

In a laboratory setting, the most widely used hollow spinneret is a hypodermic needle with an inner diameter in the range of 0.3–1.0 mm, which usually produces nanofibers in low throughput. One way to increase the throughput is to use a tube or a flat electrode containing multiple holes. To this end, a cylindrical tube made of poly(tetrafluoroethylene) (PTFE) was used for electrospinning. On the wall of the tube, 20 holes (0.5 mm in diameter) were created as a two-row array (Figure 13A).¹⁷⁵ During electrospinning, multiple jets were ejected from the holes (Figure 13B), leading to the production of nanofibers in a larger volume. In another demonstration, a metallic flat substrate containing multiple (e.g., 3, 4, 7, 10, 13, or 19) holes was explored as the spinneret to significantly improve the throughput.^{176–178} With the use of a seven-hole system, seven jets were simultaneously ejected at a high voltage of 30–40 kV, as shown by the photograph in Figure 13C, which was taken at an exposure time of 33.33 ms.¹⁷⁸ As a major shortcoming, the hollow spinneret is susceptible to clogging.

A solid pin can serve as a spinneret for the ejection of a jet from the liquid droplet attached to the tip of the pin.¹⁷⁹ To increase the number of jets, a flat plate has also been explored as the spinneret.¹⁸⁰ In a typical process, the liquid flows from a reservoir to the edge of the plate, from which multiple jets can be simultaneously ejected. Other types of solid spinnerets have also been designed to further increase the number of jets, such as a stack of

Author Manuscript
Author Manuscript
Author Manuscript
Author Manuscript

multiple plates, a bowl with a curved edge,^{181,182} a conical wire coil,¹⁸³ a jagged metallic plate (Figure 13D),¹⁸⁴ a stepped pyramid (Figure 13E),^{185,186} and a 2D array of multiple solid pins, among others. In particular, metal wires with a diameter around 1 mm have been explored as spinnerets in the Nanospider equipment developed by Elmarco.¹⁸⁷ The polymer solution was continuously loaded onto the surface of the wire by moving the solution container in a reciprocating manner, and numerous jets were ejected from the wire to continuously produce nanofibers at a high throughput. When conducted in the stationary mode, how to continuously supply the electrospinning liquid remains one of the major problems in working with solid spinnerets.

Solid spinnerets have also been exploited for operation in a rotatory mode. In a typical example, a metal cylinder is partially immersed in an electrified liquid bath.¹⁸⁸ When the cylinder rotates and sweeps through the bath in a direction perpendicular to its radial axis, liquid is entrained and coated on the surface of the cylinder, resulting in the continuous formation of a large number of jets (Figure 13F).¹⁸⁹ A variety of different rotary spinnerets, such as rotary wire,¹⁹⁰ spiral wire coil,^{191,192} disc,¹⁸⁸ and ball,¹⁸⁸ have all been explored.

The rotatory solid spinneret offers several benefits, including the simplicity of design, robustness against clogging, and increased throughput through the simultaneous operation of numerous jets. However, undesired processes may also occur to the electrified liquid, such as water vapor absorption, solvent evaporation, and ignition as a result of corona discharge in extreme cases, because the open reservoir usually has a relatively large free liquid surface. To further improve the feasibility of the setup for industrial production, an enclosed container can be applied to avoid solvent evaporation, and the relative humidity can also be controlled to minimize the absorption of water vapor. However, it is difficult to precisely control the flow rate of the liquid and the emanation of uniform jets. These issues can be addressed by modifying the configuration of the spinneret. For example, a disc decorated with needles on the edge has been developed to concentrate the electric field at the tip of each needle for the ejection of uniform jets.¹⁹³

2.3.4. Simple Needle versus Coaxial Spinneret.—In the conventional setup, a simple hollow needle is usually used. A coaxial needle consisting of two concentric hollow needles has also been developed to generate a coaxially electrified jet for coaxial electrospinning (Figure 14A).^{194,195} The coaxial needle can be easily fabricated by inserting a small (inner) needle into a large (outer) needle in the coaxial configuration. Two syringe pumps are then used to drive two fluids into the outer and inner needles, respectively, at separately addressable flow rates. When the core and shell fluids meet at the exit end of the coaxial needle, the shell fluid will wrap around the core fluid to form a compound Taylor cone in the presence of an external electric field, followed by the ejection of a coaxial jet. Finally, core–sheath nanofibers with distinct compositions for the core and sheath will be obtained, as shown in Figure 14B.¹⁹⁶

The key to successful coaxial electrospinning is to ensure that the inner and outer fluids form a compound jet and stay together in a concentric manner.^{197,198} A high coaxiality of the coaxial needle is the preliminary request to ensure robust and reproducible generation of core–sheath nanofibers. With regard to the configuration, the end of the outer needle can be

Author Manuscript
Author Manuscript
Author Manuscript
Author Manuscript

equal to or over that of the inner needle or vice versa depending on the properties of the two fluids.¹⁹⁹ In generating core–sheath nanofibers, the properties of the inner and outer fluids, as well as the electrospinning parameters, all play important roles. Specifically, the inner and outer fluids should have sufficient viscosities to keep the jets continuous. The miscibility between the two fluids is also an important factor as it will be difficult to generate a coaxial jet from two fluids that are rapidly miscible. Only when the two fluids are immiscible, the inner and outer parts of the jet can be stretched simultaneously to generate core–sheath nanofibers by avoiding possible mixing or inversion of the two fluids. If the two fluids are partially miscible with each other, a blend of the two materials can be formed at the interface of the core–sheath nanofibers. The two fluids should also have similar dielectric properties to ensure a similar electrical force. In addition, the flow rates of the two fluids need to be carefully adjusted to ensure that the inner fluid will be fully wrapped by the outer fluid. The flow rates can also be tailored to change the diameter of the nanofibers and the thickness of the sheath.²⁰⁰

Coaxial electrospinning allows for the production of core–sheath nanofibers with a good control over the composition. Different types of materials, such as polymers, oligomers, metal salts, proteins, oils, liquid crystals, and even cells/bacteria/viruses have been incorporated into the core of a core–sheath nanofiber.^{201–205} Coaxial electrospinning also enables the facile fabrication of nanofibers from unspinnable liquids as they can be supplied as the inner fluid to produce nanofibers under the guidance of the outer fluid.^{196,206} For example, fibers made of thermoset polymers with a cross-linked network can be produced by coaxial electrospinning. In one study, PCL solution was used as the shell fluid while a liquid consisting of bisphenol A ethoxylate dimethacrylate and 2,2-dimethoxy-2-phenylacetophenone (photoinitiator) serving as the core fluid for coaxial electrospinning.²⁰⁷ Upon polymerization of the as-spun core–sheath fibers by UV radiation, followed by the selective removal of the sacrificial PCL sheath, fibers of thermoset polymer were obtained. Thermoset poly-(dimethylsiloxane) (PDMS),^{208,209} ethylene/propylene/diene terpolymer rubber,²¹⁰ and epoxy resin²¹¹ fibers have also been fabricated by thermally cross-linking the as-spun core–sheath fibers, followed by selectively removing the sacrificial sheath polymer. On the other hand, an unspinnable liquid (i.e., an organic solvent or a mixture of solvents) can be applied as the outer fluid to serve as a bridge for the mass transfer of solvent from the core to the atmosphere, favoring a longer period of stretching and slower solidification of the jet.^{212,213} In this case, thinner nanofibers will be generated.^{213,214} For example, by surrounding the inner polymer solution with an outer fluid (i.e., a mixture of acetone, ethanol, and *N,N*-dimethylacetamide at a volume ratio of 3:1:1), thinner PVP nanofibers were produced relative to the case without the use of the outer fluid.²¹⁵ In another study, ultrathin nanofibers could be produced from a highly concentrated PVP solution, which is unspinnable using a simple electrospinning, by applying *N,N*-dimethylacetamide as the outer fluid.²¹⁶

Coaxial electrospinning has also made it possible to fabricate hollow nanofibers with controllable thickness for the wall by selectively removing the core from the as-spun core–sheath nanofibers.^{194,217,218} By increasing the number of the inner needles, multiple cores could be formed in the core–sheath nanofibers. In one study, three metallic needles were inserted into an outer needle in the pattern of an equilateral triangle (Figure 14C).²¹⁹ By

Author Manuscript
Author Manuscript
Author Manuscript
Author Manuscript

feeding an ethanol solution of PVP and $\text{Ti}(\text{O}i\text{Pr})_4$ into the outer needle and paraffin oil into the three inner needles, respectively, core–sheath nanofibers containing three separated compartments were obtained. After removing the oil in the cores through calcination, multichannel tubes were created (Figure 14D).²¹⁹ The number of the concentric needles can also be increased to three to obtain a triaxial needle^{220,221} for the production of three-layer-structured (core@intermediate@sheath) fibers by separately feeding three different types of fluids (Figure 14E,F).^{222,223} However, when the feeding rate of the core liquid is not high enough, the fibers will be fragmented.

2.3.5. Conductive Solid Collector versus Liquid Bath Collector.—Electrospun nanofibers are usually deposited on a grounded solid collector (e.g., a piece of aluminum foil) to form a nonwoven mat. To better control the deposition of the nanofibers, various types of conductive solid collectors, as well as liquid bath collectors, have also been reported.

Conductive Solid Collectors.: Conductive solid collectors can be used in either stationary or movable mode. For a stationary collector, it can modulate the distribution of electric field and thus guide the deposition of nanofibers in two different ways: (*i*) patterning the surface of a conductive substrate with specific structures and (*ii*) combining different substrates with distinct conductivities to form the pattern.

Onto the surface of a conductive substrate, various types of structures (e.g., protrusions, microposts, and microwells) can be introduced to attract the highly charged nanofibers.^{224,225} In one example, nanofibers were preferentially deposited on the tips of Au-coated pyramidal microprotrusions patterned on a flat conductive substrate.²²⁴ Alloy substrates were patterned with topographical features (e.g., microposts or microwells) using imprint lithography to manipulate the collection of nanofibers.²²⁶ A human skin-mimic pattern was also produced on the surface of an Al-based alloy mold, enabling the fabrication of a biomimetic mat of nanofibers.²²⁷

For the collectors based on heterogeneous substrates with distinguishable conductivities (i.e., a metal and an insulator), they can induce a distorted electric field toward the surface of the metal. As such, the nanofibers will be preferentially deposited on the surface of the metal region and be extended across the insulating region, eventually leading to the formation of a patterned mat. For example, when a pair of conductive electrodes separated by an air gap (Figure 15A) are used as a collector, uniaxially aligned arrays of nanofibers will be deposited across the air gap by concentrating the electric field toward the conductive electrodes (Figure 15B).³⁵ The suspended nanofibers can be further transferred onto other substrates for specific applications.²²⁸ The paired electrodes can also be deposited on a highly insulating substrate in a configurable pattern and spacing (Figure 15C,D), leading to the extension of uniaxially aligned nanofibers across the insulating region.^{229,230} Based on this basic configuration, various types of collectors have been designed to guide and control the deposition of nanofibers. To this end, metal stencil plates framed into various configurations, such as woven wire fabric, stainless-steel mesh, and copper grid, can be used to direct the deposited nanofibers toward the conductive regions, enabling the fabrication of a nanofiber-based mat that replicates the pattern on the original collector.^{230,231} Free-

standing mats consisting of nanofibers in well-controlled patterns (e.g., parallel lines, woven lines, regular hexagons, and circular holes) have all been reported.^{231–233}

Other types of homemade collectors have also been designed to expand the capability of electrospinning.²³⁴ For example, a ring electrode (e.g., metal ring) with a point electrode (e.g., a sharp pin) in the center has been demonstrated for generating radially aligned nanofibers (see section 2.4.4).²³⁵ An assembly of stainless-steel beads was used to collect a mat of nanofibers containing an array of microwells.²³⁶ The nanofibers deposited on the surface of the stainless-steel beads were randomly oriented, whereas those deposited across the gap between adjacent beads were uniaxially aligned. On a star-shaped collector, the nanofibers were orientated diagonally to each arm of the star.²³⁷ The capability of this approach can be further improved by applying lithography to fabricate micropatterned templates.^{238–241} Furthermore, 3D conductive templates (e.g., a 3D tubular collector²⁴² or a wire spring²⁴³) have also been developed to manipulate the electric field, resulting in the formation of 3D-patterned tubes of nanofibers.

An insulating material can be used to mask a grounded conductive substrate and thus alter the distribution of electric field, helping direct the nanofibers toward the patterns of the insulating material. As such, the topographical feature of the insulating material can be faithfully duplicated by the nanofibers.²⁴⁴ For example, when a piece of paper with a pattern on the surface was employed to mask the conductive substrate, nanofibers could be directly deposited as a mat with surface feature close to the pattern on the paper.²²⁵ Generation of diversified patterns are feasible when other types of insulating substrates, such as nylon woven fabric, ping-pong paddle, gauze, and a letter “A”, are used as collectors.²⁴⁵ Using the stationary solid collector, the generated features in the nanofibers are supposed to be quickly lost with the increase of deposition time, resulting in the deposition of random nanofibers thereafter.

The collector can be programmed to move along the lateral directions, as we have described in sections 2.2.1 and 2.3.1 for melt electrospinning and near-field electrospinning. Rotating collectors (e.g., mandrel, wire, disc, drum, wheel, conveyor, and cone) are another class of movable collectors (Figure 15E),^{246,247} which offer a simple and straightforward method for generating aligned nanofibers. Increasing the rotation speed can lead to a significant decrease in diameter for the nanofibers due to the stretching force.²⁴⁸ The rotating collector can also be applied to directly fabricate tubular construct. For example, Inovenso Inc. has developed an electrospinning device (Model NS24), in which a rotating rod with a specific diameter is used to collect the nanofibers.²⁴⁹ The rotating rod is made of titanium to make it easy to remove the tubular coating, enabling the production of artificial blood vessels with a diameter around 3 mm. When two metallic tubes are placed in line along their axis and separated by an air gap, a seamless tube can be formed by setting the two tubes rotating at the same speed, while multifilament twisted yarn can be formed by rotating the tubes at different speeds.^{250,251} Other unique collectors, such as rotary funnel and rotary rings, have also been designed to generate nanofibers with specific structures.^{252–254} In a typical example, a continuous PVDF nanofiber yarn at tens of kilometers in length has been produced using a rotary metal funnel as the collector, followed by continuously withdrawing and twisting the newly formed yarn with a winder (Figure 15F).²⁵⁵ The collector can also be

arranged around the spinneret rather than above or below.^{256,257} In one example, a cylinder collector was placed around a rotating spinneret to conduct centrifugal electrospinning. The centrifugal force also contributes to the stretching of the jet to form nanofibers.^{258,259} In most cases, the procedures for manufacturing a patterned conductive collector with high resolution are often complicated. In addition, the currently reported conductive solid collectors are mostly limited to a stiff substrate with low flexibility, which may hamper the applications.

Liquid Bath Collectors.: Insulating liquid placed in a container below the spinneret has also been demonstrated as a collector. The liquid can act as a coagulation bath to improve the solidification of the jet to produce ultrafine nanofibers. For example, an ethanol bath was used to quickly remove the residual water in a jet of pullulan to prevent the fusion between the deposited nanofibers.²⁶⁰ Liquid bath also enables the generation of nanofibers with some special structures (Figure 15G).²⁶¹ For example, continuous nanofiber bundles were obtained by withdrawing the collected nanofibers in a water bath.²⁶² Nanofiber yarns have also been collected using a water vortex.^{263,264} Furthermore, flowing liquid was used for the continuous collection of nanofibers. In one study, a flowing water bath with recirculated water was used to collect bundled nanofibers.²⁶⁵ The nanofibers were first collected on the surface of the flowing water; thereafter, a continuous bundle composed of loosely aligned nanofibers was taken onto a rotatory roller, enabling continuous collection without interruption for hours.

In addition to insulating liquids, conductive liquids, such as an electrolyte solution, have been explored as collectors.²⁶⁶ The conductive liquid can generate an electric field distribution similar to the case of a metallic collector, enabling the selective deposition of nanofibers toward the surface of the conductive liquid. For example, with the use of an electrolyte solution, the deposition of nanofibers can be controlled by varying the salt concentration of the electrolyte solution.²⁶⁷ In one study, when a 3 M KCl solution was selectively placed on a substrate and then used as the collector (Figure 15H), random nanofibers were deposited on the surface of the KCl solution while aligned nanofibers were stretched across the air gap separating the solution, leading to the formation of a patterned mat (Figure 15I).²⁶⁷ However, when dielectric liquids, such as deionized water, ethylene glycol, or glycerol, were used to collect the nanofibers, the resultant mat would exhibit poor alignment. Although a liquid bath enables the deposition of a freestanding mat, the available configurations for the collector are kind of limited.

2.4. Engineering of Electrospun Nanofibers

By controlling the materials and methods of electrospinning, the composition, structure, and properties of the nanofibers can be engineered to target specific applications. From the electrospun nanofibers, new nanomaterials with a fibrous morphology can be obtained via suitable post-treatment. Typically, nanofibers made of carbon can be readily produced after stabilization and carbonization of polymer nanofibers. Nanofibers made of metal or ceramic are left behind by selectively removing the polymeric component in composite nanofibers. A variety of nanoparticles can also be incorporated into the nanofibers to bestow new functions. A nonwoven mat of electrospun nanofibers naturally possesses a high porosity

Author Manuscript
Author Manuscript
Author Manuscript
Author Manuscript

and large specific surface area. With the introduction of in-fiber pores, the porosity and specific surface area of the resultant mat can be further increased. In addition, the nanofibers can be fabricated with a beaded, core–sheath, or hollow morphology. By manipulating the alignment and/or patterning, electrospun nanofibers can be assembled into ordered arrays or hierarchical structures. If necessary, the nonwoven mat can be welded at the cross-points of the nanofibers to provide interfiber junctions. Different physical and/or chemical methods can be applied to modify the as-spun nanofibers for the purpose of adjusting the porosity and pore sizes, and/or introducing new functional groups and components. In addition, a thin mat of nanofibers can be expanded along the vertical direction to generate a 3D architecture.

2.4.1. Nanomaterials Derived from Electrospun Nanofibers.—New nanomaterials, including those made of carbon, metals, and ceramics, with a fibrous morphology have been derived through suitable post-treatment of the as-spun nanofibers.

Carbon Nanofibers: Carbon materials with a fibrous morphology (i.e., carbon nanofibers) can be derived through stabilization and carbonization of polymer nanofibers.²⁶⁸ The polymer nanofibers are first stabilized in air between 200 and 300 °C to convert the polymer into ladder compounds. This stabilization step is necessary for preventing the polymer from melting and thus loss of the fibrous morphology in the subsequent carbonization process.^{269–271} Afterward, upon carbonization at 400–1800 °C in an inert gas atmosphere (e.g., N₂ or Ar), carbon materials (>90 wt % in carbon content) are obtained without compromising the fibrous morphology by selectively eliminating the noncarbonized elements in a gaseous form.²⁶⁸ Sometimes, a graphitization process is also applied at an extremely high temperature up to 3000 °C to further eliminate heteroatoms, leading to the growth of graphitic layers and the improvement of stacking order.

Typically, carbon nanofibers can be derived from electrospun polyacrylonitrile (PAN) nanofibers by transforming the PAN from a linear structure into a graphite-like aromatic structure, as illustrated in Figure 16A.²⁷² In one study, PAN nanofibers (Figure 16B) were stabilized to minimize changes to both the morphology and diameter (330 nm) by heating at 280 °C in air for 3 h.²⁷³ After subsequent heating at 1000 °C under N₂ for 1 h, carbon nanofibers with partial graphitization were obtained (Figure 16C). The diameter of the resultant nanofibers was about 250 nm because of the evaporation of remaining solvents and the removal of heteroatoms. After further heating at 2200 °C under N₂ for 1 h, carbon nanofibers (220 nm in diameter) with ribbon-shaped, graphitic structures were formed.

In order to obtain ultrafine carbon nanofibers with desirable properties, it is important to control the type of the precursor polymer, which affects the carbon yield and thus the preservation of the fibrous morphology. PAN is the most widely used precursor polymer owing to its good spinnability and high carbon yield (>50%), as well as the superior mechanical properties of the resultant carbon nanofibers. However, it can only be dissolved in a limited number of solvents such as DMF. Polyimide can result in a high carbon yield (ca. 53%) after carbonization at 1000 °C, but the fabrication of polyimide nanofibers is relatively complicated.^{274,275} Lignin, one of the most abundant natural polymers, has been utilized to produce carbon nanofibers with diameter as thin as 200 nm, but its carbon yield is relatively low (20–40%).^{276,277} Many other types of precursor polymers, including pitch,²⁷⁸

PVDF,²⁷⁹ cellulose,²⁸⁰ PVA, and PVP^{281,282} have all been explored for the production of carbon nanofibers.

The properties of the derived carbon nanofibers are mainly affected by the diameter and morphology of the precursor nanofibers and the conditions used for the stabilization and carbonization processes. The diameter of carbon nanofibers usually increases with that of the precursor polymer nanofibers. If the precursor nanofibers have porous structures, the pores can be possibly retained in the resultant carbon nanofibers. The conditions for the stabilization and carbonization processes are both critically important in achieving ultrafine carbon nanofibers. During the stabilization process, a suitable temperature is required to ensure the formation of a thermoset polymer. For the carbonization process, a higher temperature usually leads to an increase in the graphitization degree of the carbon nanofibers which determines the physiochemical properties of the nanofibers. For example, the electrical conductivity of PAN-derived carbon nanofibers increased by 8 orders of magnitude with an increase of the carbonization temperature from 550 to 950 °C.²⁷² It is notable that a too high temperature may completely destroy the functional groups and/or heteroatoms, causing detrimental impacts to the versatility of the carbon nanofibers in practical applications.

In addition, it is of great importance to avoid shrinkage of the nanofibers during thermal treatment. Progressive and multistage heating procedures are preferred for both stabilization and carbonization steps. For example, much less planar dimensional shrinkage of a carbon nanofiber-based mat was realized by applying a progressive heating procedure (5 °C/min from 30 to 230 °C, 1 °C/min from 230 to 270 °C, and then 5 °C/min from 270 to 800 °C) for heating PAN nanofibers, relative to a one-step procedure (200 °C for 30 min, followed by 750 °C for 1 h).^{283,284} External tension can also be applied to the mat of nanofibers during thermal treatment, in an effort to avoid the shrinkage of the resultant mat.^{285,286}

Metallic Nanofibers.: Metals with a fibrous morphology (i.e., metallic nanofibers) can be derived from composite nanofibers through two different indirect methods. As illustrated in Figure 17A, the first method typically involves two steps of thermal treatment: (i) calcination in air to remove the polymer component in the as-spun composite nanofibers, obtaining metal oxide nanofibers; and then (ii) reduction in a reductive atmosphere to convert the metal oxides to metals.^{287,288} If the temperature for thermal treatment in the first step exceeds the decomposition temperature of the metal oxide, metallic nanofibers are directly formed. In a typical procedure, composite nanofibers comprising of PVA and copper acetate with a diameter of about 200 nm were first electrospun from an aqueous solution of PVA and copper acetate (1:1 (wt %)), as shown in Figure 17B.²⁸⁷ After calcination in air at 500 °C, the as-spun nanofibers were converted to CuO nanofibers. With a further thermal treatment in a hydrogen atmosphere at 300 °C, the CuO nanofibers were reduced to Cu nanofibers with a diameter of about 100 nm (Figure 17C,D). Each Cu nanofiber was comprised of compact Cu grains (Figure 17E) with no residual polymer component, but with detectable CuO on the surface. It is worth noting that the metallic nanofibers commonly present defective surfaces with high roughness. On the basis of this direct approach, various types of metals (e.g., Fe, Co, Ni, and Pt) with fibrous morphologies have been reported.
289–291

The structure of the metallic nanofibers is mainly determined by the concentration of the metal precursor, the type of the carrier polymer, and the thermal treatment conditions. A sufficient concentration of the metal precursor is required to prevent the nanofibers from breaking during thermal treatment. Within a suitable range, a lower concentration of the metal precursor favors the formation of thinner metallic nanofibers.²⁹² The carrier polymer is expected to have good miscibility with the metal precursor and be easily removed by thermal treatment for the generation of uniform metallic nanofibers. The thermal treatment conditions (e.g., temperature, time, and atmosphere) have influence on the removal of the polymer component and thus the diameter of the metallic nanofibers. Sometimes, UV irradiation is applied to decompose the polymer carrier (such as PMMA) and reduce the melt precursor (such as CF₃COOAg) for the fabrication of metallic nanofibers (e.g., Ag nanofibers) at room temperature.²⁹³ In this approach, however, some polymeric residuals may still be detectable in the resultant metallic nanofibers.

Metallic nanofibers can also be fabricated by depositing metals on the surface of as-spun polymer nanofibers, followed by selective removal of the polymer template (Figure 17F).²⁹⁴ As such, the as-obtained metallic nanofibers commonly have a hollow-shaped cross-section. Panels G–I of Figure 17 show SEM images of a network of intertwined Au nanofibers that was fabricated using this method. Each nanofiber showed a width of about 400 nm and thickness of about 80 nm. The dimensions of the fibers can be controlled by tuning the diameter of the polymer template and the deposition time for the metal. Using this method, a variety of metals, such as Au, Ag, Cu, Pt, Al, Cr, Ni, and their alloys, have been fabricated as networks of nanofibers.²⁹⁵

Ceramic Nanofibers.: Ceramics alone are usually considered to be non-electrospinnable, although, in principle, a ceramic melt can be electrospun as fibers at an extremely high temperature.^{26,53} By directly electrospinning an aged sol, highly dense ceramic fibers can be obtained, but the diameter of the fibers is usually in the range of micrometer, as we have discussed in section 2.2.3. For example, silica fibers were obtained by electrospinning an aged sol–gel solution with an optimal viscosity.¹²⁸ In another study, ZrP fibers were obtained using a reactive coaxial electrospinning approach,²⁹⁶ in which a zirconium precursor and a phosphorus source were electrospun together from separate solutions using a coaxial spinneret. The reaction between the zirconium and phosphorus sources was initiated at the interface in the core–sheath fibers to delay the formation of ZrP gel. After calcination and further treatment with H₃PO₄, ZrP fibers were obtained.

Ceramics with a fibrous morphology (i.e., ceramic nanofibers) can also be derived by removing the polymer component in composite nanofibers comprised of a polymer and an inorganic precursor through calcination.^{130,133,297,298} In a typical example, anatase TiO₂ nanofibers with an average diameter of 53 ± 8 nm were obtained by calcining composite nanofibers of PVP and amorphous TiO₂ (78 ± 9 nm) in air at 500 °C.¹³² The reduction of the diameter was attributed to the loss of PVP and the densification of TiO₂. The as-obtained anatase nanofibers consisted of fused TiO₂ nanoparticles that were ca. 10 nm in diameter and contained voids between adjacent nanoparticles (Figure 18A,B).¹³²

To produce continuous ceramic nanofibers, it is necessary to have a sufficient amount of the inorganic component in the composite nanofibers. The diameter of the ceramic nanofibers is mainly determined by the diameter and composition of the composite nanofibers and the calcination conditions. Taking the preparation of TiO_2 nanofibers as an example, thinner ceramic nanofibers were derived from the composite nanofibers with smaller diameters. A lower percentage of the amorphous TiO_2 in the composite nanofibers also led to the formation of thinner ceramic nanofibers, which could be achieved by adding a lower amount of the alkoxide precursor into the electrospinning solution.¹³² Additionally, a higher calcination temperature may lead to the formation of thinner ceramic nanofibers because a larger amount of polymer is removed.

The crystalline phase and composition of the ceramic nanofibers are highly dependent on both the calcination conditions (i.e., temperature, time, and atmosphere) and the components contained in the composite nanofibers. Calcination at an elevated temperature can cause a substantial increase in the grain size, leading to different surface textures. For example, a gradual increase in surface roughness was observed by converting amorphous TiO_2 to anatase and rutile after calcination in air at 500 and 1000 °C, respectively (Figure 18C,D).⁴² Carbonaceous residuals arising from the incomplete decomposition of the polymer matrix are often found in the ceramic nanofibers, resulting in the presence of impurities.²⁹⁹ Calcination in air usually leads to the formation of oxides, while thermal treatment under N_2 or NH_3 can lead to nitrides due to the nitridation of the ceramic particles. For example, TiN nanofibers were obtained by heating composite nanofibers made of PVP and TiO_2 at 900 °C under NH_3 .²⁹⁹ As such, ceramics of special compositions can be derived by sequentially heating the nanofibers in the presence of variable gases. In one study, WC nanofibers were derived by applying a two-step thermal treatment process: the composite nanofibers made of PVP and ammonium metatungstate were first oxidized with flowing O_2 at 500 °C and further heated at 780 °C under a mixture of CH_4 and H_2 .³⁰⁰ The composition of the ceramics can also be tailored by varying the type of the salt precursor. For example, Zr-doped TiO_2 ceramic nanofibers were fabricated by adding an appropriate amount of titanium(IV) isopropoxide and zirconium(IV) acetylacetone into the PVP solution.³⁰¹ Figure 18E shows the homogeneous distribution of Ti, Zr, and O elements in the as-obtained nanofibers at the nanoscale. Hierarchical nanostructure can also be produced. In one study, composite nanofibers were electrospun from a PVP solution containing $\text{Ti(O}i\text{Pr)}_4$ and vanadium(V) oxytriisopropoxide ($\text{VO(O}i\text{Pr)}_3$).³⁰² Upon calcination of the as-spun nanofibers, V_2O_5 nanorods were grown on the surfaces of TiO_2 nanofibers, generating a unique nanorod-on-nanofiber hierarchical nanostructure (see Figure 18F).

By carefully selecting the composite nanofibers and tailoring the calcination conditions, more than a hundred different types of ceramics (e.g., CeO_2 , SnO_2 , SiO_2 , VN, BaTiO_3 , LiCoO_2 , Codoped-ZnO, Sb-doped-SnO₂, and a blend of ZnO_2 and SiO_2) have been prepared as nanofibers.^{133,303–306} It is worth noting that the thermal treatment step may cause a shrinkage to the ceramic nanofibers and their mat due to the loss of the carrier polymer and the densification of nanocrystallites. This phenomenon may result in broken ceramic nanofibers and a brittle mat that tends to break into small pieces. In some cases, only small fragments are formed rather than freestanding mats, hindering their practical applications. The mechanical strength of ceramic nanofibers can be improved by integrating different

types of compounds together (e.g., integrating SiO_2 or CeO_2 with TiO_2)^{307,308} or by adding cations (e.g., Y^{3+} and Zr^{4+}) into the matrices.^{301,309} An additive with high thermal stability can also be incorporated to stabilize the nanofibers. In one study, 20 nm SiO_2 nanoparticles were added into a poly(acrylic acid) solution containing $\text{Ce}(\text{NO}_3)_3$ and then applied to electrospinning.³¹⁰ By calcining the as-spun nanofibers at 600 °C, the SiO_2 nanoparticles spontaneously cemented and formed continuous nanofibers.

Inorganic Hybrid Nanofibers.: Inorganic hybrids of carbon and metals or carbon and metal oxides can be derived from electrospun composite nanofibers through suitable thermal treatment. While the metal precursor is decomposed to generate metal or metal oxide(s), the polymer component is carbonized into carbon. The preferential growth of a certain metal or metal oxide on the carbon nanofibers are affected by the inclusion of a metal salt precursor and calcination conditions. In a typical example, titanium(IV) butoxide ($\text{Ti}(\text{OC}_4\text{H}_9)_4$) was mixed with PMMA and PAN in DMF for electrospinning.³¹¹ By stabilization in air at 280 °C and then carbonization in N_2 at 600 °C of the as-spun fibers, a hybrid structure consisting of nanometer-sized TiO_2 and carbon was obtained. By increasing the carbonization temperature to 1400 °C, a hybrid of TiC and carbon nanofibers was generated. Based on this approach, various types of metals or metal oxides have been incorporated into carbon nanofibers to generate different hybrid materials.^{312–314}

2.4.2. Incorporation of Nanoparticles.—Incorporating nanoparticles into electrospun nanofibers brings in additional functions and enhanced performance. The nanoparticles can be made of materials ranging from metals to metal oxides, carbon, and polymers. There are mainly two strategies for incorporating nanoparticles into electrospun nanofibers or attaching to the surface: (i) direct incorporation during electrospinning and (ii) post-treatment of the as-spun nanofibers.

For the direct approach, the nanoparticles are added into the solution for electrospinning, as discussed in section 2.2.4. Alternatively, nanoparticles are electrosprayed onto the surface of nanofibers during electrospinning.^{315,316} For the post-treatment approach, nanoparticles can be synthesized *in situ* inside nanofibers through thermal annealing of the composite nanofibers containing a suitable precursor.^{317,318} This method is mostly used to incorporate metallic or ceramic nanoparticles in carbon or ceramic nanofibers. The size of the resultant nanoparticles in the fibers can be varied by controlling the thermal treatment conditions. For example, Co–Ni alloy nanoparticles of 25–70 nm in diameter were synthesized *in situ* inside carbon nanofibers by stabilizing and carbonizing the composite nanofibers consisting of PAN, cobalt acetate, and nickel acetate.³¹⁹ In another example, Pt nanoparticles were grown *in situ* inside Nb-doped TiO_2 nanofibers via thermal treatment of the composite nanofibers containing Pt(II) 2,4-pentanedionate, a metal precursor, in air at 500 °C.³²⁰ At ramping rates of 2 and 10 °C min⁻¹, respectively, Pt nanoparticles of 3.5 and 10 nm in size were obtained. Nanoparticles with special morphologies can also be synthesized *in situ* by controlling the conditions for thermal treatment. In one study, Co_3O_4 hollow nanoparticles were synthesized in carbon nanofibers.³²¹ Specifically, nanofibers made of PAN and cobalt(II) acetylacetone were stabilized in air and then carbonized under N_2 at an elevated temperature. As such, the cobalt salt was decomposed and reduced to metallic Co nanoparticles within the carbon

Author Manuscript
Author Manuscript
Author Manuscript
Author Manuscript

nanofibers. Subsequently, the Co nanoparticles were oxidized in air at 400 °C to form Co_3O_4 hollow nanoparticles with nonuniform shell thicknesses, as shown in Figure 19A.³²¹ By exposing nanofibers to a specific gas atmosphere, such as H_2S , nanoparticles can also be synthesized *in situ* through a gas–solid reaction.³²² For instance, 5 nm PbS nanoparticles were formed and dispersed within PVP nanofibers by exposing composite nanofibers consisting of PVP and lead acetate to H_2S gas at room temperature.³²²

The nanoparticles can also be generated on the surface of electrospun nanofibers through surface deposition, *in situ* synthesis, or hydrothermal treatment. The simplest method is to immerse the as-spun nanofibers in a colloidal suspension of nanoparticles to catch the nanoparticles through chemical binding,^{323,324} electrostatic force,³²⁵ or hydrogen bonding. A requirement is that the nanofibers are not soluble in the colloidal suspension. In one study, cross-linked PVA nanofibers were functionalized with 3-mercaptopropyltrimethoxysilane and then immersed in an aqueous solution of Au nanoparticles.³²³ As a result, Au nanoparticles were tightly attached onto the surface of the PVA nanofibers due to the strong affinity between the thiol group and the Au surface (Figure 19B).³²³ In addition, multilayers of charged nanoparticles can be deposited on the nanofibers through a layer-by-layer technique.³²⁶ For instance, negatively charged Au nanoparticles and positively charged lysozyme were alternately deposited on negatively charged cellulose nanofibers.³²⁷ As a major drawback, the nanoparticles are often deposited nonuniformly on the surface of an individual nanofiber.

The deposited nanoparticles can be generated through an *in situ* synthesis to increase the uniformity of distribution on the surface of an individual nanofiber. A typical example is to generate nanoparticles of metal oxides on nanofibers through liquid-phase deposition.³²⁸ By immersing nanofibers in an aqueous solution of a metal precursor, nanoparticles of metal oxides can be readily produced on the nanofibers through the hydrolysis and condensation reactions of the metal precursor. For example, thin sheaths comprised of TiO_2 or SnO_2 nanoparticles were coated on PAN nanofibers using this method. Biomineralization has also been explored as a simple method to grow nanoparticles such as apatite, calcium phosphate, and CaCO_3 on the surface of nanofibers from specific salt solutions.^{329–332} For example, nanoparticles of $\text{Ca}_3(\text{PO}_4)_2$ could be grown on plasma-treated PLGA nanofibers, as shown in Figure 19C.³³⁰

In addition, nanoparticles can be synthesized *in situ* on the surface of nanofibers by reducing or annealing the absorbed precursor.³³³ This method is often used to incorporate nanoparticles made of metals or metal oxides on nanofibers. In a typical process, the as-spun nanofibers are first immersed in a precursor solution containing metal ion complex. The complex can interact with the functional groups on the nanofibers.³³⁴ Then, nanoparticles are produced by reducing the complex with a reducing agent or light irradiation. The structure of the nanoparticles is mainly determined by the conditions for the reduction reaction and the surface roughness of the nanofibers. For example, both Pt nanoparticles and nanorods (Figure 19D,E) were formed *in situ* on the surface of anatase TiO_2 nanofibers by fine-tuning the conditions of a polyol reduction reaction.³³⁵ The surface roughness of the nanofibers also has a major impact on the nucleation and thus the structure of the nanoparticles.³³⁶ Both homogeneous and heterogeneous nucleation of Pt nanostructures took

place when ZrO_2 nanofibers with a smooth surface were used, generating Pt nanoparticles deposited on the nanofibers and free Pt nanostars in the solution. In contrast, when the ZrO_2 nanofibers had a rough surface, only heterogeneous growth of Pt nanostructures was observed.³³⁶ Such a method has been explored to generate different metal/metal oxide nanostructures, including Au, Ag, Pd, Pt, Rh, TiO_2 , WO_3 , and SnO_2 , on various types of nanofibers made of carbon, ceramics, or polymers.^{302,306,335,337–339} Besides the outer surface, nanoparticles can also be incorporated in the inner surface of hollow nanofibers. In one study, Pt nanoparticles were embedded in the inner surface of hollow CeO_2 nanofibers, as shown in Figure 19F, by sequentially depositing Pt nanoparticles and CeO_2 sheaths on electrospun PS nanofibers, followed by calcination in air at 400 °C.³⁴⁰

Furthermore, the nanoparticles can be synthesized by simply annealing a precursor. In a very recent demonstration, multiple metal salt precursors MCl_xH_y (M is Pt, Pd, Ni, Fe, Co, Au, Cu, or Sn, among others) were mixed in a solution and then coated on the surface of carbon nanofibers that were derived from electrospun PAN nanofibers.³⁴¹ Through an electrically triggered Joule heating and rapid quenching, multimetallic nanoparticles made of immiscible elements were generated on the carbon nanofibers. As shown in Figure 20, up to eight dissimilar elements PtPdCoNiFeCuAuSn could be included as an alloy in single-phase nanoparticles deposited on the surface of carbon nanofibers.

When combined with hydrothermal treatment, nanoparticles with different morphologies (e.g., sphere, plate, and rod) can be readily synthesized on the surface of nanofibers.^{342–345} In this case, the nanofibers are sealed in an autoclave with the presence of a solution containing salt precursor(s) for the generation of nanoparticles via hydrothermal reactions. The structure of the nanoparticles is mainly determined by the hydrothermal conditions. Under a high pressure, the nanoparticles tend to be in close contact or even form covalent bonds with the nanofiber matrices. In addition, special structures can be generated on the nanofibers through hydrothermal synthesis. In one study, ZnO nanowires were grown on PS nanofibers coated with ZnO nanoparticles through a hydrothermal treatment, generating hybrid nanofibers with a “nanobrush-on-nanofiber” structure.³⁴⁶

Through the use of electrospinning, directly or indirectly, many types of materials ranging from organic polymers (i.e., thermoplastic, thermoset, and conjugated polymers) to inorganic solids (i.e., metals, metal oxides/carbides/nitrides), as well as carbon and doped-carbon, have all been processed as fibers. A summary is provided in Table 1.

2.4.3. Control of in-Fiber Porosity.—In general, nanofibers produced by electrospinning take a solid structure. When pores are introduced in the nanofibers, the specific surface area of the resultant nanofiber-based mat will be drastically increased.³⁸¹ There are mainly two strategies for generating pores on and/or in nanofibers: (i) inducing phase separation during electrospinning and (ii) selectively removing the sacrificial phase from the as-spun nanofibers via leaching or calcination. The in-fiber porosity can be controlled by manipulating the density, size, shape, and distribution of the pores.

Porous Structures Induced by Phase Separation.: Phase separation during electrospinning can be applied to introduce a porous structure by transforming one phase as

the pores while the other as the nanofiber matrix. In this case, phase separation can occur (i) between the polymer and solvent or (ii) between the polymer and a nonsolvent.

Phase separation between the polymer and solvent can be induced by rapidly cooling the incompletely solidified jet. The cooling effect is readily achieved either by rapidly evaporating a highly volatile solvent or by collecting the nanofibers in a cryogenic liquid. For example, electrospinning a polymer solution with a highly volatile solvent can generate pores both on the surface and in the bulk of each individual nanofiber.³⁸² Panels A and B of Figure 21 show typical SEM images of the surface and core of highly porous PLA nanofibers which were produced by electrospinning a 12.1 wt % PLA solution in dichloromethane.³⁸³ With the use of a highly volatile solvent such as dichloromethane, THF, chloroform, or acetone, porous nanofibers have been successfully prepared from a wide range of polymers, including PMMA,³⁸⁴ PS,³⁸⁵ cellulose acetate,³⁸⁶ poly(vinyl butyral),³⁸⁷ and PCL.³⁸⁸ Sometimes, due to the fast evaporation of the highly volatile solvent, the electrospinning process may be unstable and interrupted by needle clogging. The cooling effect can also be achieved by directly electrospinning the nanofibers into a cryogenic liquid bath to freeze the nanofibers for inducing phase separation between the polymer and residual solvent. For example, porous PS nanofibers were fabricated by electrospinning a 20% (w/v) PS solution in *N,N*-dimethylacetamide into a liquid nitrogen bath, followed by drying the as-spun nanofibers in *vacuo*.³⁸⁹ The nanofibers contained a high density of pores throughout the entire cross-section, as shown in Figure 21C,D. Using this simple method, porous nanofibers made of PAN, PVDF, and PCL have all been produced.³⁸⁹

Phase separation can also be induced between the polymer and a nonsolvent to generate porous structures, including both vapor-induced and liquid-induced phase separation. Vapor-induced phase separation is usually associated with electrospinning under a high relative humidity, during which water molecules in the air act as the nonsolvent.^{390,391} In this case, the temperature at the surface of the jet is rapidly decreased with the evaporation of solvent, resulting in the condensation of the surrounding water vapor into tiny water droplets. The water droplets are often distributed on the surface of the jet and may also penetrate into the jet.³⁸⁴ The demixing between the penetrated water and the jet promotes the formation of distinct polymer-depleted and polymer-enriched domains. After complete evaporation of the water and solvent, the polymer-enriched domains solidify to become the nanofiber's matrix, while the polymer-depleted domains are transformed to the pores on the surface of or inside the nanofiber.^{392–394} For example, by electrospinning a 20 wt % PS solution in THF under a relative humidity of 62%, a large number of pores were generated on the surface of the nanofibers (Figure 22A,B).³⁹¹ With the use of a mixture of DMF and THF at a weight ratio of 1:1 as the solvent, the water droplets could penetrate into the jet, resulting in the formation of internal pores and the formation of a yarn-like structure (Figure 22C,D).³⁹¹ Based on this method, porous nanofibers made of PVDF,³⁹⁴ poly(ether imide),³⁹⁵ and PET³⁹⁶ have also been reported.

Regarding liquid-induced phase separation, the porous structures can be generated by electrospinning a ternary system (i.e., polymer, solvent, and nonsolvent) or by collecting the nanofibers in a nonsolvent bath. When a polymer solution is premixed with a proper amount of a nonsolvent, a stable and homogeneous ternary system will be formed. Due to the

Author Manuscript
Author Manuscript
Author Manuscript
Author Manuscript

difference in volatility between the solvent and nonsolvent, the proportion of the ternary system in the jet will be changed, resulting in phase separation and thus the formation of porous structures. The generation of the pores is mainly governed by the relative rates of solvent/nonsolvent exchange, the dynamics of phase separation, and the spinnability of the ternary system.^{397–400} Based on this strategy, as shown in Figure 22E,F, highly porous PS nanofibers were produced by electrospinning of a 30 wt % PS solution in a mixture of chlorobenzene (solvent) and DMSO (nonsolvent) at a volume ratio of 70:30.⁴⁰¹ Liquid-induced phase separation can also occur when collecting nanofibers in a bath filled with a nonsolvent of the polymer. Once reaching the nonsolvent bath, the residual solvent in the nanofibers causes phase separation between the polymer and nonsolvent, resulting in the formation of porous structures.^{399,402} In this case, the miscibility between the solvent and nonsolvent affects the generation of pores. For example, porous PAN nanofibers were produced by electrospinning a PAN solution in DMF into a bath of ethanol, which is highly miscible with DMF.³⁹⁹ In comparison, nearly smooth and solid nanofibers were obtained when hexane, a solvent immiscible with DMF, was used as the bath.

Porous Structures Induced by Selective Removal of a Sacrificial Phase.: Porous structures can be readily generated by selectively removing a sacrificial phase from the nanofibers.⁴⁰³ The sacrificial phase can be small molecules (e.g., salt),⁴⁰⁴ block copolymers,⁴⁰⁵ polymers, or nanoparticles, which can be removed via a leaching or calcination process.^{406,407} In addition to polymer nanofibers, porous structures can also be introduced into carbon nanofibers by selectively leaching nanoparticles from the hybrid nanofibers. In one study, SiO₂ and Sb nanoparticles were formed in carbon fibers during the stabilization and carbonization of electrospun composite fibers made of PV, SbCl₃, and tetrathylorthosilicate.⁴⁰⁸ After etching the hybrid fibers with HF, the SiO₂ and Sb nanoparticles and their agglomerates were easily removed, resulting in the formation of pores in the carbon fibers, as shown in Figure 23A,B. Although viable, the generation of pores via solvent extraction is time-consuming due to the slow dissolution of most polymers, and complete removal of the sacrificial phase may not be always possible.

Thermal degradation of the sacrificial component offers another promising route. To this end, by heating nanofibers made of a blend of poly(3-hydroxybutyrate-*co*-3-hydroxyvalerate) and poly(ether imide) at 210 °C, porous poly(ether imide) nanofibers were fabricated via selective thermal degradation of poly(3-hydroxybutyrate-*co*-3-hydroxyvalerate).⁴⁰⁹ The porosity could be tuned by adjusting the ratio of the two components in the nanofibers. Thermal treatment is also often applied to create porous structures on carbon and ceramic nanofibers by selectively removing the sacrificial component.⁴¹⁰ In one study, after subjecting nanofibers made of a blend of PAN and Nafion to carbonization, pores were generated on the carbon nanofibers by converting the PAN component to carbon and decomposing the Nafion component.⁴¹⁰ In another study, porous TiO₂ nanofibers were fabricated using coaxial electrospinning, followed by calcination.¹⁹⁴ During electrospinning, the PS solution in a mixture of DMF and THF was used as the inner fluid, while a PVP solution in ethanol containing Ti(O*i*Pr)₄ was used as the outer fluid. Since the solvents were miscible, the two fluids were partially mixed in certain regions of the jet. With the rapid evaporation of solvents, the two polymers were separated, and the

nanoscale domains of PS were embedded in the continuous matrix made of PVP and TiO₂. After calcination, both PS and PVP were removed, leaving behind porous TiO₂ nanofibers, as shown in Figure 23C,D.¹⁹⁴ Because the calcination process is easy to operate, this strategy can be exploited to generate porous carbon and ceramic nanofibers in a controllable fashion.

2.4.4. Control of Morphology, Alignment, and Pattern.—Electrospun nanofibers are typically characterized by morphological features that include a uniform diameter, a circular cross-section, and a smooth surface. To meet the requirements from some applications, it is also desired to access electrospun nanofibers with other morphologies, such as beaded, core–sheath, and hollow. In addition, many studies have also demonstrated the capability to control the alignment and patterning of electrospun nanofibers.

Control of Morphology.: By carefully tuning the electrosinning parameters and exploring spinnerets and collectors with special configurations, nanofibers with exotic morphologies have been developed, including beaded, core–sheath, and hollow structures, as well as nanofibers with other unique structures.

Beaded nanofibers can be formed by tuning the surface tension and viscosity of the electrosinning liquid and the density of charges carried by the jet.^{26,30,31,411–413} In general, a lower viscosity and a lower density of surface charges both favor the formation of beaded nanofibers, whereas reduction of surface tension makes the beads disappear gradually.^{26,411,414} In general, the beads and nanofibers are made of the same material. By combining with other strategies, beads made of a material different from that of the nanofibers can also be produced, mimicking the structure of natural capture silk of a spider (Figure 24A,B).⁴¹⁵ In one study, upon coaxial electrosinning of a sprayable outer fluid with low viscosity and a spinnable inner fluid with high viscosity, hydrophilic beads were imprinted on a hydrophobic string (Figure 24C).⁴¹⁵ The key to the formation of beaded nanofibers is the use of an outer liquid with a high surface energy to prevent the sheath component from adhering to the core component and the spontaneous Rayleigh breakup of the outer fluid in the jet under an electric field. Beaded nanofibers can also be produced by electrosinning of an emulsion (emulsion electrosinning).⁴¹⁶ For instances, by electrosinning of an oil-in-water emulsion containing PS and PVA, PS beads could be generated on PVA nanofibers. Similarly, alginate beads could be formed on PLA nanofibers by electrosinning of their water-in-oil emulsion. The formation of beads can be attributed to the insufficient stretching of the jet and the phase separation between the two components in the emulsion during jet solidification. A colloidal suspension consisting of a polymer and beads has also been utilized to generate beaded nanofibers. With the incorporation of a large number of beads, necklace-like fibers were produced.^{142,417,418} As shown in Figure 24D, SiO₂ beads were strung together via a polyacrylamide fiber by electrosinning a suspension consisting of polyacrylamide and 1 μm SiO₂ beads.⁴¹⁹

Core–sheath nanofibers involve two different types of materials for the core and sheath, and a clear boundary between them can be identified. The core–sheath structures are usually generated via (i) coaxial electrosinning to physically separate the two materials or (ii) phase separation between the two materials. Coaxial electrosinning is the most commonly

used method for producing core–sheath nanofibers (see section 2.3.4 for a detailed discussion).³²⁴ However, its capability is limited by the requirement of a relatively complicated setup and the difficulty in achieving consistent concentricity for the jet due to the complex interplay between the properties of the two liquids.

By inducing phase separation between two components in a homogeneous solution or an emulsion, core–sheath nanofibers can also be produced using conventional electrospinning based on a single spinneret.^{420–422} In the case of a homogeneous solution, the phase separation is usually induced by the difference in solubility for the two polymers in the same solvent during the drying of the jet.^{423,424} For example, owing to the different solubilities of PEO and chitosan in water, PEO@chitosan core–sheath nanofibers were readily produced by electrospinning their homogeneous solution in water.⁴²⁵ Mixed solvents can also be used to induce incompatibility between the two polymers. In one study, PCL@poly(*N*-isopropylacrylamide) (PNIPAAm) core–sheath nanofibers were electrospun from a solution of PCL and PNIPAAm in a mixture of DMF and chloroform.⁴²⁶ Due to the higher boiling point of DMF (153 °C) relative to chloroform (61 °C), a higher ratio of DMF to chloroform was generated in the jet with the preferential evaporation of chloroform. Considering the difference in solubility for PNIPAAm and PCL in DMF, phase separation was favored thermodynamically. Kinetically, the relatively short molecular chains endowed PNIPAAm with a high mobility to move toward the surface of the jet, leading to the formation of core–sheath structures. In addition, water vapor can induce phase separation by altering the solubility of the polymeric component in the jet. For example, electrospinning of a homogeneous solution of PAN and PVP in DMF under a high relative humidity resulted in the generation of PAN@PVP core–sheath nanofibers.⁴²⁷ In most cases, however, the mobilities of the two polymers in the jet are significantly decreased with the rapid evaporation of solvent(s), preventing the large-scale phase separation needed for generating core–sheath nanofibers.

Regarding emulsion electrospinning, either oil-in-water or water-in-oil, phase separation can be induced in the jet by the de-emulsification caused by the evaporation of solvent, leading to the formation of core–sheath nanofibers, as illustrated in Figure 25A.⁴²⁸ In one study, a water-in-oil emulsion was prepared by mixing the aqueous phase of PEO in water and the oil phase of an amphiphilic PEG–PLA diblock copolymer in chloroform.⁴²⁸ Upon electrospinning, PEO@PEG–PLA core–sheath nanofibers were produced. In some cases, emulsion can also be formed by combining two polymers in one solvent to produce core–sheath nanofibers. One example was based on a mixture of PMMA and PAN in DMF, which decomposed into PMMA droplets (100 μm in diameter) dispersed in a PAN solution after storing for 1 day.⁴²⁹ A large amount of crosslinked polymeric, swollen colloids could also be dispersed in a polymer solution to prepare emulsion for generating core–sheath nanofibers. As illustrated in Figure 25B, core–sheath nanofibers were produced due to the phase separation between the colloids and the condensed polymer matrix.⁴³⁰ In a typical example, PNIPAAm microgel colloids lined up to form an array in the central region of PCL fibers (Figure 25C).⁴³⁰ The primary drawbacks associated with emulsion electrospinning are the instability of an emulsified solution and the presence of an emulsifier that may affect the applications of the nanofibers.^{431–433} Moreover, emulsion electrospinning can also result in

the production of nanofibers in which the dispersed phase is embedded as separate blobs instead of that with a core–sheath structures.

Hollow nanofibers can be produced using a number of methods, including coaxial electrospinning, emulsion electrospinning, controllable heating of preformed nanofibers, and the use of a sacrificial template.⁴³⁴ Coaxial electrospinning is the most versatile method for fabricating hollow nanofibers by selectively removing the core of core–sheath nanofibers.⁴³⁵ For example, anatase TiO₂ hollow nanofibers (Figure 26A,B) were fabricated by removing the core of mineral oil from the nanofibers made of PVP and TiO₂, followed by calcination to decompose the PVP.¹⁹⁴ The outer diameters and wall thicknesses of the hollow nanofibers could be conveniently tuned by adjusting the flow rates of the inner and outer fluids.³²⁴ Based on this method, hollow nanofibers containing multichannels or made of multicomponent materials have also been fabricated.²¹⁹ In one study, as we have described in section 2.3.4, three metallic capillaries were inserted in a larger capillary and used as the spinneret for electrospinning (Figure 14C).²¹⁹ A PVP solution in ethanol containing Ti(O*i*Pr)₄ was used as the outer fluid, with paraffin oil serving as the inner fluid. By removing the organics from the as-spun nanofibers through calcination, TiO₂ nanofibers with three channels were fabricated (Figure 14D). As shown in Figure 26C–E, nanofibers with two, four, and five channels were separately fabricated by adjusting the number of the inner capillaries.²¹⁹ In another study, with the use of a triaxial needle (Figure 14E), a layer termed as a fluid spacer (e.g., paraffin oil/water emulsion) was introduced to separate the outer and inner fluids.⁴³⁶ After selectively removing the spacer layer, a fiber-in-tube structure was generated (e.g., anatase nanofibers with nanowire-in-microtube structure, as shown in Figure 26F). In addition, the inner core and the outer surface of the hollow nanofibers can be further modified by simply adjusting the composition of the fluids to give heterogeneous structure and multifunction.³²⁴ For example, by adding tin isopropoxide to the oil-based inner fluid, SnO₂ nanoparticles were coated on the inner surfaces of the hollow TiO₂ nanofibers (Figure 26G).³²⁴ Based on this method, hollow nanofibers can be fabricated from various types of materials with controlled wall thicknesses. The limitation is the need of a coaxial spinneret and the complex procedure to remove the inner material.

Hollow nanofibers can be directly produced by inducing phase separation during emulsion electrospinning.⁴³⁷ In one typical example, a microemulsion was formed by adding PS into PAN solution.⁴³⁸ Upon electrospinning, the PS phase was stretched into nanowires in the PAN nanofibers. After carbonization of the as-spun nanofibers at 800 °C under Ar, the PS nanowires were decomposed, generating carbon nanofibers with interconnected channels. As shown in Figure 27A, the channel structure could be easily tuned by varying the ratio of PS to PAN in the range of 1:10–1:1. A larger amount of PS served to increase the number and diameter of the channels inside the fibers. In another study, phase separation was induced in a “gradient” electrospinning process to produce hollow nanofibers.⁴³⁹ The success of this method relied on the use of polymers with different molecular weights (low-, middle-, and high-molecular-weight PVA at a weight ratio of 3:2:1) in a solution containing metal salt precursors. During electrospinning, the low-, middle-, and high-molecular-weight PVA tended to be separated into the inner, middle, and outer layers of the fibers instead of being mixed together, as shown in Figure 27B. Upon calcination, the low-and middle-molecular-weight PVA were subjected to pyrolysis sequentially and moved to the outer layer together

Author Manuscript
Author Manuscript
Author Manuscript
Author Manuscript

with the generated inorganic materials, leading to the expansion of the inner region of the nanofibers. As a result, hollow inorganic nanofibers were produced once the organic components had been removed. Panels C and D of Figure 27 show representative TEM images of LiV_3O_8 and MnO_2 mesoporous hollow nanofibers, respectively, generated based on this method. Although the phase-separation method can produce hollow nanofibers, the fabrication process is hard to control and the available solution system for generating a uniform hollow interior is limited.

Hard templates have also been explored for the fabrication of hollow nanofibers.⁴⁴⁰ The most commonly used templates include SiO_2 particles. One study reported the fabrication of hollow carbon nanofibers through the use of hard templates, as shown in Figure 28A.⁴⁴¹ By heating the electrospun nanofibers made of a blend of PAN and tetraethyl orthosilicate at 1200 °C in an atmosphere of H_2 and Ar, SiO_2 particles were generated, aggregated, and uniformly lined in the core region within the resultant carbon nanofibers. After removing the hard templates through chemical etching with NaOH , HF, or NH_4HF_2 , hollow nanofibers were produced. As shown in Figure 28B,C, the bamboo-like carbon nanofibers showed hollow interiors, together with a graded and interconnected pore structure: small micro-and mesopores in the outer surface and larger mesopores in the inner region of the sheath.

Hollow nanofibers made of inorganic materials can be produced by thermally treating composite nanofibers under suitable conditions. In this case, the concentrations of the precursor salts that are located at the surface and in the interior of the nanofibers are usually different. As the heat treatment temperature is ramped up, the concentration gradient drives the salts to migrate from the interior to the surface of the nanofibers, eventually leading to the formation of hollow inorganic nanofibers. For example, Fe_2O_3 hollow nanofibers were produced by directly annealing as-spun composite nanofibers made of a blend of PVP and $\text{Fe}(\text{NO}_3)_3$.⁴⁴² The formation of hollow nanofibers was determined by the solvent composition, the contents of $\text{Fe}(\text{NO}_3)_3$ and PVP, and the heating rate. Furthermore, fiber-in-tube and tube-in-tube nanostructures have been fabricated by controlling the thermal treatment conditions. For example, SnO_2 (Figure 28D,E)⁴⁴³ hollow tube with a fiber inside was fabricated based on this approach.^{444,445} In another study, by heating the composite nanofibers that were electrospun from a solution containing PVP, PAN, and metal precursors in DMF, CoMn_2O_4 tube-in-tube nanostructures (Figure 28F,G) were fabricated.⁴⁴⁶

In addition to nanofibers with circular cross-sections, nanofibers with a variety of other cross-sectional shapes have also been fabricated, such as nanoribbons with an elliptical or flat cross-section.^{447,448} The nanoribbons can be generated from a polymer solution with strong intra-and/or interinteractions among the polymer chains. With the evaporation of solvent from the surface of the jet, a thin, mechanically distinct polymer skin will be formed due to the strong chain interactions. Subsequently, the solvent inside the jet escapes, and the jet further develops into a “tube”. With the further evaporation of solvent, the tube could collapse. As such, the cross-section of the jet transforms from a circular shape into an elliptic and then flattened one, corresponding to the formation of a ribbon with a cross-sectional perimeter nearly the same as that of the jet.⁴⁴⁷ By electrospinning a 30 wt % PS solution in DMF, ribbons with a flat cross-section were produced, as shown in Figure 29A.⁴⁴⁷ In another study, completely flat ribbons were produced by electrospinning a PVA

solution at a high concentration of 31 wt % (13,000–23,000 g/mol in M_w) or at a low concentration of 13 wt % but with a high M_w (50,000–89,000 g/mol).⁴⁴⁸ Ribbons can also be produced by electrospinning a solution in which polymers form anisotropic macromolecular structures.^{448,449} For example, in an aqueous solution of silk-elastin-like protein, even at a low concentration of 6 wt %, silk-like blocks could crystallize to form β -sheets surrounded by solvated elastin blocks.⁴⁵⁰ Upon electrospinning of an 18 wt % aqueous solution of the silk-elastin-like protein, ribbons were produced, as shown in Figure 29B.

Nanofibers with other unique structures have also been reported. For example, nanofibers with a hierarchical shish-kebab structure can be produced by controlling the crystallization of a polymer during electrospinning.^{451–453} In one study, solution electrospinning of PP at a high temperature produced PP nanofibers consisting of nanofibrils with a shish-kebab structure.⁴⁵² The shish-kebab structure can also be produced by inducing orientated crystal growth on the as-spun nanofibers through a post-treatment procedure. In a typical example, as-spun PEO nanofibers were incubated in a 0.3 wt % PEO solution in DMF to allow the PEO molecules in the solution to crystallize on the surface of the nanofibers.⁴⁵⁴ After incubation for a certain period of time (ca. 60 min), the PEO crystals formed a periodical decoration along the nanofibers, generating the shish-kebab structure (Figure 29C,D).^{454–456} Using a similar method, kebabs made of PCL-b-poly(acrylic acid) crystals were deposited on PCL nanofibers, as shown in Figure 29E.⁴⁵⁶ In terms of other structures, nanofibers with a high frequency of short branches, referred to as “barbed nanowires”, have also been produced via electrospinning of a 3 wt % aqueous PVA solution (Figure 29F).⁴⁵⁷

Control of Alignment: When a piece of conductive substrate is used as the collector, nanofibers with no orientation are produced in the form of a nonwoven mat. Modifications to the collector have to be made in order to fabricate nanofibers with controlled alignment.

The alignment of electrospun nanofibers can be controlled using three different forces: mechanical, electrostatic, and magnetic, through the use of a rotating mandrel, an array of electrodes, and a pair of permanent magnets, respectively. By collecting nanofibers on a rapidly rotating mandrel, the nanofibers orient along the rotating direction of the mandrel due to the mechanical stretching force, as we have described in section 2.3.5.²⁴⁷ By tuning the rotation speed of the mandrel, the degree of alignment of the deposited nanofibers can be controlled. Uniaxial alignment is often achieved for the nanofibers when the linear velocity of the rotating mandrel matches that of jet deposition.²⁴⁸ In general, it is a time-and energy-consuming method with the use of a rotating mandrel. Moreover, the as-obtained nanofibers cannot be conveniently transferred onto other substrates.

By manipulating the external electric field across a pair of electrodes separated by an air gap, uniaxially aligned nanofibers can be obtained (Figure 30A,B).^{35,458,459} A 3D grid was also fabricated by stacking the uniaxially aligned nanofibers in a layer-by-layer fashion with different stacking angles (Figure 30C,D).³⁵ It should be pointed out that only those nanofibers extended across the electrodes were aligned uniaxially, while those directly deposited on the electrodes showed no alignment. As a result, there was a random-to-aligned transition between the two regions.⁴⁵⁹ Similarly, radially aligned nanofibers have also been

produced by exploring a collector consisting of a ring with a sharp pin in the center (Figure 30E,F).²³⁵ In general, it is difficult to maintain the alignment when the deposition time is extended because the capability of the collector to manipulate the electric field would be inhibited by the deposited nanofibers.

Imposing an external magnetic field is another way for controlling the alignment of the nanofibers.⁴⁶⁰ In the presence of an external magnetic field created through two parallel permanent magnets, the nanofibers are driven to align in a parallel fashion along the magnetic field lines. Based on this method, both straight and wavy polymer nanofibers with uniaxial alignment were produced.⁴⁶¹

In addition, recent studies have also demonstrated the use of melt electrospinning⁹⁹ and near-field electrospinning¹⁵⁰ for tightly controlling the alignment of electrospun fibers by inhibiting the bending instability of the jet.

Patterning of Nanofibers.: Nanofiber-based mats with patterned micro-and/or nanostructures are interesting for their high specific surface areas and roughness. The nanofiber-based mats can be patterned using two different approaches: bottom-up and top-down.

For the bottom-up approach, micropatterned architectures can be readily generated in the mats by controlling the properties of the electrospinning liquid and parameters for electrospinning. One typical example is the formation of unique ultrafine nanonets comprised of interlinked ultrathin nanowires in the as-spun nanofiber-based mat.^{462–466} As shown in Figure 31A, nanonets of ultrathin nanowires (ca. 30 nm) are stacked layer-by-layer and distributed in the mat of poly(acrylic acid) nanofibers.^{465,466} The nanonets are only formed under certain conditions, for example, electrospinning of a solution containing salts or involvement of fast phase separation between the polymer and solvent. Electrospinning under a relatively high voltage or low relative humidity may also result in the formation of nanonets.^{86,467,468} In another typical example, PVA nanofiber-based mat with a honeycomb-patterned architecture was fabricated by inducing the self-assembly of wet nanofibers on a collector (Figure 31B).⁴⁶⁹ Micropatterned architectures can also be readily generated through the use of micropatterned conductive templates as collectors, as discussed in section 2.3.5. In this case, the electrical forces are the key factors in determining both the deposition and arrangement of nanofibers. The melt and near-field electrospinning techniques have also been demonstrated for patterning fibers through direct writing as discussed in sections 2.2.1 and 2.3.1, respectively.¹⁵⁰ The drawbacks are the complicated setups and relatively large feature sizes.

For the top-down approach, a few post-treatment strategies have been explored to pattern the as-spun nanofiber-based mats. One strategy is based on selective photo-cross-linking of electrospun nanofibers containing a photoinitiator to generate a patterned mat.⁴⁷⁰ Although various micropatterns have been achieved, this method is only available for the photo-cross-linkable materials. In an alternative way, patterning of the nanofiber-based mats can be achieved through localized removal of nanofibers using laser, UV, or solvent.^{471–473} For example, laser ablation shows great promise to generate patterns on nanofiber-based mats

due to the highly localized heat generated by the laser beam. In one study, femtosecond laser pulses could quickly create holes with controllable sizes in the mat, and the collateral damage to the neighboring nanofibers was sufficiently low to preserve the fibrous structure at the wall of the hole.^{474–476} In another study, groove patterns were produced on a nanofiber-based mat by laser ablation.⁴⁷¹ The width of the groove could be controlled in a range of 1–15 μm and the depth 15–110 μm . Panels C and D of Figure 31 show representative SEM images of the surface and cross-section of the nanofiber-based mat with groove, and Figure 31E shows corresponding atomic force microscopy (AFM) image of the patterned mat.

2.4.5. Welding of Nanofibers at Their Cross-Points.—Upon collection, the electrospun nanofibers are stacked in a layer-by-layer fashion, generating a weak contact only between the fibers at their cross-points. The nanofibers can be welded together at their cross-points through three different methods: thermal treatment, solvent (or vapor) exposure, and covalent cross-linking. The interfiber spacing and motion of macro-molecular chains in the fibers are two major parameters that affect the efficacy of welding. Welding at the cross-points of nanofibers offers interfiber connection, providing an effective way to improve the quality of the mat, especially the mechanical and electrical properties.

Thermal treatment is usually applied to weld a mat of polymer nanofibers. By heating to a temperature between the T_g and T_m of the polymer, the nanofibers at the cross-points can be fused together. For example, when a PCL ($T_m = 60^\circ\text{C}$) nanofiber-based mat was annealed between 54 and 60 $^\circ\text{C}$, the nanofibers were welded at their cross-points.⁴⁷⁶ For the nanofibers made of a polymer with a high melting point, an elevated temperature is usually needed for welding. In this case, polymers with low melting points (e.g., PEO, $T_m = 66\text{--}70^\circ\text{C}$) can be introduced into the nanofibers to serve as a welding solder and reduce the temperature. In one study, with the incorporation of PEO (10 wt %) into lignin nanofibers, fusion among the adjacent carbon nanofibers was observed after carbonization (Figure 32A).⁴⁷⁷ The welded mat of carbon nanofibers showed significantly higher mechanical strength and lower electrical resistance than the pristine mat.⁴⁷⁸ In addition to direct heating, photothermal heating has also been used to initiate the welding when photothermal dyes or nanoparticles (e.g., Au and Ag nanostructures) are doped in the nano-fibers.⁴⁷⁹ For example, upon laser irradiation at a power of 2–10 mW, the cross-points of PVDF nanofibers doping with Ag nanoparticles were successfully welded as the Ag nanoparticles absorbed photons and then transferred heat to the surrounding polymer matrix efficiently.^{480,481}

Exposing the nanofiber-based mat to the vapor of a suitable solvent is another effective way to weld the nanofibers at their cross-points. The vapor allows for the swelling, partial dissolution, and thus fusion of the nanofibers at their cross-points in a nonwoven mat. The degree of welding is mainly affected by the vapor pressure and the exposure time. The threshold time for welding at the cross-points without causing loss of fibrous morphology is dependent on the composition of the nanofibers and the type of solvent. For instance, saturated DMF vapor could be used to weld a mat of nanofibers made of a blend of PAN and polysulfone,⁴⁸² while dichloromethane vapor worked for the PCL nanofibers.⁴⁸³ As shown in Figure 32B, the two PCL nanofibers were welded at their cross-point.⁴⁸³ After welding, the tensile strength of the mat was significantly enhanced from 11.53 ± 0.89 to 21.4 ± 1.08

MPa. Using the vapor method, composite nanofibers made of PVP and In_2O_3 precursor were also welded at the cross-points.⁴⁸⁴ Upon calcination, the welded In_2O_3 nanofiber-based mat showed enhancement in both mechanical property and electrical conductivity. In addition to vapor, diluted solution can be used to weld the nanofibers at their cross-points.⁴⁸⁵

Covalent cross-linking through the use of either light or chemical agents can also weld the nanofibers at their cross-points. At a suitable degree of cross-linking, the cross-points can be welded together without significantly changing the fibrous morphology.^{486,487} However, the value of a cross-linking method is usually limited by the use of photo-cross-linking initiators or toxic chemical cross-linkers.

2.4.6. Physical and Chemical Modifications.—The as-spun nanofibers can be modified using a number of physical and/or chemical approaches to improve their performance in various applications. The commonly used physical approaches include mechanical drawing and thermal treatment. When mechanically drawn along one direction, the polymer chains in the nanofibers can be forced to align along the drawing direction. As a result, the crystallinity of polymer in the nanofibers is enhanced, and the tensile strength of the mat is thus improved.^{488,489} The postdrawing process can be combined with thermal or solution treatment to further control the crystallization of the polymer in the nano-fibers.^{488,490} For example, by mechanically drawing a mat of aligned PAN@PMMA core–sheath nanofibers to 200% of its original length along the direction of fiber alignment at 120 °C for 5 min, the tensile strength and modulus of the mat were significantly increased by 673.4% and 875.3%, respectively.⁴⁹⁰ It should be noted that overdrawing may cause nanofibers to break, leading to a worse mechanical strength.

Another effective strategy for physical modification of a nanofiber-based mat is thermal treatment, which can be used to improve the properties (e.g., compactness, mechanical strength, and chemical stability) of the mat by forming crystallized regions or by inducing diffusion to improve the homogeneity of the nanofibers. When annealing polymer nanofibers at an elevated temperature, a higher degree of crystallinity is obtained for the nanofibers.⁴⁸⁸ In addition, thermal treatment can encourage welding at the cross-points of the nanofibers.⁴⁹¹ However, the freestanding mat may shrink or wrap due to stress relaxation when no force is applied to the mat during thermal treatment. To maintain the dimensional stability, the perimeters of the mat need to be restrained. A compression pressure can also be co-applied to the mat during thermal treatment to improve the connectivity between the nanofibers at their cross-points and thus the compactness of the mat.^{492–494} In one study, the tensile strength of a PAN nanofiber-based mat was significantly increased from 8.7 to 63.0 MPa after hot-pressing at 220 °C.⁴⁹⁵ Hot-pressing can also be used to improve the adhesion of nanofibers to a backing substrate, preventing delamination between the two materials.⁴⁹⁶ Thermal treatment has also been employed for other nonconventional purposes. For example, a mat composed of PVA nanofibers and PTFE particles was treated at 380 °C for 30 min to remove the PVA component.⁴⁹⁷ In this way, the PTFE particles melted and fused together to form an interconnected nanofiber network, solving a difficult problem related to the fabrication of PTFE nanofibers.

A number of chemical approaches have been exploited to modify the nanofiber-based mat. Surface coating represents the simplest protocol for modifying the nanofibers with functional materials (e.g., fluorescent molecules, conducting polymers, and nanoparticles). Chemical vapor deposition has been used to coat or deposit metals or metal oxides on the surface of the as-spun nonwoven mat.⁴⁹⁸ In addition to single-layer deposition, multilayer coatings can be built-up through layer-by-layer self-assembly driven by the electrostatic attractions between oppositely charged constituents.⁴⁹⁹ Layer-by-layer assembly can incorporate different materials (e.g., polyelectrolytes, clay nanomaterials, and/or metal oxides) with opposite charges in multilayers, endowing nanofiber mats with multifunctions.^{500,501} In particular, spray-assisted layer-by-layer deposition is able to functionalize a nanofiber-based mat in a specific pattern.⁵⁰²

Another widely used surface modification strategy is to introduce chemically active groups to the surface of a nanofiber-based mat through plasma treatment or specific chemical reactions.^{503–505} Plasma treatment is one of the commonly used methods to introduce active groups to the surface of nanofibers. By manipulating the atmosphere and duration of plasma treatment, polar groups such as -COOH and -OH can be generated on the surface of nanofibers.⁵⁰⁶ For example, oxygen plasma was used to treat the PCL nanofibers to enhance the hydrophilicity and biological performance.⁵⁰⁷ Plasma treatment in CF₄ could produce a superhydrophobic surface for the nanofibers.⁵⁰⁸ Based on the active groups, secondary chemical modifications, such as graft copolymerization or grafting of small molecules, can be further realized.⁵⁰³ For example, living radical polymerization was initiated through the functional groups on the surface of nanofibers, leading to the production of thermoresponsive and solvent-resistant nanofibers.^{509,510} Cross-linking is another commonly used method to chemically modify a nanofiber-based mat. By cross-linking, the mechanical properties and the solvent resistance of the mat can be largely improved. For example, hydrophilic and water-soluble PVA nanofibers were modified to be superhydrophobic and water-resistant via cross-linking with glutaraldehyde and then modified with fluoroalkylsilane.⁵¹¹ Through suitable chemical modifications, the functionalized mats have been widely used in various applications. It is still a key issue to simplify the modification procedures to pave the way for commercialization.

2.4.7. Expansion along the Third Dimension.—As noted in section 2.1.5, a nonwoven mat of nanofibers usually takes a 2D morphology, hindering its application in some fields because of its limited porosity and thickness. Various means have been explored to expand the 2D mat along the third dimension for the production of a 3D foam. A straightforward method is to directly deposit nanofibers along the third dimension by engineering the collector. For example, a 3D cotton-ball-like foam with a highly porous structure was directly fabricated by collecting the PCL nanofibers in a nonconductive spherical dish embedded with an array of metal probes.⁵¹² Figure 33A shows the SEM image of the nanofibers as a foam. In another study, a similar collector was developed by embedding stainless-steel needles in a hemispherical PTFE dish.⁵¹³ During electrospinning, loosely stacked nanofibers were collected among the space between the stainless-steel needles, leading to the formation of a 3D foam with a thickness up to several centimeters.

A 3D foam can also be fabricated via post-treatment of the as-spun 2D mat. Typically, by cutting and homogenizing the mat in a liquid (usually water or ethanol according to the solubility of the nanofibers), a slurry of short nanofibers is obtained. After freeze-drying, a 3D foam is fabricated.^{514,515} Using this method, an ultralight 3D foam comprised of nanofibers made of a blend of PAN and SiO₂ with a hierarchical structure and superelasticity was developed, exhibiting a low density of 0.12 mg/cm³ and an ultrahigh porosity of 99.992%.^{514,515} Figure 33B shows the morphology of the nanofibers in the foam.⁵¹⁴ To enhance the interactions among the short nanofibers, a binder or cross-linker can be introduced.^{516–519} For instance, with the aid of PCL as a binder, self-agglomeration of the short nanofibers was induced thermally.⁵¹⁷ In an aqueous suspension at 55 °C, short nanofibers of PCL self-agglomerated due to the partial dissolution of PCL. After freeze-drying, a 3D foam was fabricated (Figure 33C).⁵¹⁷ Using this method, a 3D foam composed of a blend of PCL and PLA (mass ratio, 4:1) nanofibers was also developed, in which PCL served as a binder for the short nanofibers.⁵²⁰

Gas-foaming technique is another promising strategy for generating a 3D foam by expanding the physically stacked mat along the third dimension.⁵²¹ For instance, a 3D foam was constructed by immersing a 2D mat in an aqueous solution of NaBH₄. The rapid hydrolysis of NaBH₄ in water yielded H₂ in situ to exert pressure throughout the 2D mat and loosen the nanofibers to produce a multilayered 3D architecture.⁵²¹ In addition, dry ice was also applied to expand the mat into a 3D foam by generating CO₂, offering the possibility of encapsulating biological agents into the nanofibers without contacting a liquid before final use.^{522,523}

Using the aforementioned methods, the as-obtained 3D foams often take a disordered structure without topographic cues, and the approaches are restricted to certain materials. To overcome these limitations, a mat of uniaxially aligned nanofibers was treated with the gas-foaming technique involving NaBH₄ to generate a 3D foam containing a highly ordered structure.⁵²⁴ As shown in Figure 33D, the resultant foam showed a layered structure with controllable gap width and layer thickness on the order of micrometers, while maintaining the original alignment.⁵²⁵ By expanding the mat in a customized mold, scaffolds with controllable thickness ranging from 3 to 10 mm were obtained. Given the wide variety of materials that can be electrospun into nanofibers, the various types of 3D foams will enable the design of functional constructs for various applications.

2.5. New Directions for Future Development

Despite the large number of reports on the successful demonstration of electrospinning as a platform technique for the fabrication of (nano)fibers from a variety of materials, several issues are yet to be addressed. First of all, simulation models regarding the electrospinning process need to be further optimized by taking into consideration all the properties of a liquid for electrospinning and all the processing parameters to better elucidate the phenomenology of the electrified jets. If successful, one should be able to predict the behavior of the electrified jet for the deterministic fabrication of electrospun nanofibers with well-controlled size, structure, and morphology. Second, solution electrospinning is predominantly used for fabricating nanofibers from various types of materials. However, a

large amount of solvent is involved, resulting in both economic and environmental concerns. There is a critical need to develop methods based on “green” solvents or even solvent-free systems. While melt electrospinning involves no solvent and has much higher productivity than solution electrospinning, it is still limited to the production of fibers with relatively thick diameters. Third, it still remains a challenging task to generate nanofibers with diameters below 10 nm by electrospinning no matter which method is used. In this regard, computational modeling should offer insightful guidance for effectively downsizing the diameter of electrospun fibers.

In general, single-spinneret electrospinning is only suitable for laboratory use as it suffers from the intrinsic drawback of low throughput. To address this issue, innovative modifications to the conventional electrospinning setup have been made, including multiple-needle and needleless electrospinning. For multiple-needle electrospinning, future efforts should be concentrated on solving the problems related to clogging and cleaning of the multiple needles while addressing the challenges in precisely controlling the diameter and morphology of the fibers. Additionally, undesirable interactions, such as the generation of inhomogeneous fibers, fiber–fiber bonding, and/or poor fiber distribution in the collected mat, have also been observed, which all deserve future attention. For needleless electrospinning, one needs to address the stability issue associated with the electrospinning liquid and the safety concern related to the storage of a large volume of the liquid. It is still difficult to produce uniform fibers reproducibly and at a mass-production level, while ensuring the desired size, morphology, structure, and other properties. Although the fibers are supposed to be collected on the grounded target, they are actually deposited on every surface in the vicinity because they are highly charged. How to precisely control the deposition of nanofibers on a collector has also become increasingly important in order to fabricate highly ordered structures. To this end, there is a need to identify and further develop new materials, methods, and mechanisms for manipulating the collection of electrospun nanofibers.

3. ELECTROSPUN NANOFIBERS WITH “SMART” PROPERTIES

Over the past decade, electrospun nanofibers have been endowed with “smart” properties to enable a variety of new applications. For instance, stimuli-responsive nanofibers are able to undergo volume and/or wettability changes upon receiving an external stimulus. As a subset of the stimuli-responsive nanofibers, shape-memory nanofibers are able to assume different shapes. Self-cleaning surface can be constructed by controlling the structure and composition of the nanofibers. By mimicking the natural healing process of human skin, electrospun nanofibers can be utilized as a vehicle to deliver healing agents for fabricating self-healing materials. Live microorganisms such as microbes and cells can be incorporated to generate “living” nanofibers. Furthermore, nanofibers modified with special materials can sense changes in the surrounding environment. When combined with other outstanding features, such as large specific surface area, high porosity, flexibility, cost effectiveness, and portable nature, electrospun nanofibers have been actively explored for various applications, including controlled release, actuating, self-cleaning, self-healing, and sensing, among others.

3.1. Stimuli-Responsive

Stimuli-responsive polymers undertake conformational and/or chemical changes upon triggering by an external stimulus. The response time is inversely proportional to the rate at which the stimulus is able to reach the polymer chains, and this process is often dominated by diffusion.^{527–529} When stimuli-responsive polymers are electrospun into nanofibers, the transfer of stimulus is greatly accelerated, leading to a swifter response. The improvement can be mainly attributed to the highly porous structure and large surface-to-volume ratio of a nanofiber-based mat, as well as the small diameter of nanofibers and thereby a shortened distance of diffusion. Various types of stimuli-responsive nanofibers have been reported for applications such as cell-sheet harvest and controlled release. The external stimulus can be applied as a change in temperature or pH, as well as light, electric field, or magnetic field. In characterizing the performance of stimuli-responsive nanofibers, one should consider both the rate of stimuli-response and the reversibility of changes.⁵²⁶

Temperature represents one of the most commonly used stimuli. In response to variations in temperature, electrospun nanofibers made of thermoresponsive polymers undergo volume changes as reflected by variations in morphology and volume of the nanofiber-based mat, in addition to alteration in surface wettability. Typical examples of polymers include those characterized by low critical solution temperatures (LCSTs), such as PNIPAAm and its derivatives,^{530–533} hydroxybutyl chitosan,⁵³⁴ poly(N-vinylcaprolactam) cellulose,⁵³⁵ and amphiphilic polymers.⁵³⁶ For PNIPAAm, it has a LCST at 32 °C. It is soluble in aqueous solution and takes an extended conformation below 32 °C, whereas it becomes insoluble and exhibits a collapsed conformation above 32 °C.⁵³⁷ After cross-linking, a nonwoven mat of PNIPAAm nanofibers swiftly changed its volume in response to temperature variation due to reversible transition between the swollen and collapsed states. When tested as a nonwoven mat of nanofibers, the response rate of PNIPAAm could be enhanced by more than 100 times relative to that of a bulk gel.^{538,539}

The reversible changes in volume and/or surface hydrophobicity make the mats made of thermoresponsive nanofibers ideal for applications related to cell culture, drug delivery, and actuating.⁵⁴⁰ In one study, a mat of thermoresponsive nanofibers made of hydroxybutyl chitosan was seeded with cells.⁵³⁴ After cooling the cellular mat to a temperature below the LCST, the nanofibers were dissolved without disrupting the cell–cell interactions, leading to the harvest of an intact cell sheet. In another study, a mat of cross-linked thermoresponsive nanofibers made of NIPAAm copolymers was used to encapsulate and release cells, as illustrated in Figure 34A–C.⁵⁴¹ The mat had an LCST of approximately 18 °C. When a cell suspension was dropped on the mat at 37 °C, the mat immediately folded to encapsulate the cells (Figure 34A). After being transferred to 4 °C, the mat swelled and transformed into a hydrogel-like structure, as shown in Figure 34B. When heated again to 37 °C, the mat shrank from a swollen state to a collapsed state, resulting in the release of the cells (Figure 34C). Based on the volume change, various types of drugs and growth factors can also be triggered to leave the nanofibers, realizing on-demand release.^{542–544}

Thermoresponsive nanofibers can also be used for actuating.⁵³¹ When a thick layer of PNIPAAm nanofibers was sandwiched between two layers of PCL nanofibers with different thicknesses (<100 and 400 μm, respectively), a thermoresponsive, trilayer structure was

Author Manuscript
Author Manuscript
Author Manuscript
Author Manuscript

obtained, as shown in Figure 34D.⁵³¹ At 37 °C in an aqueous solution, PNIPAAm shrank significantly, forcing the mat to bend toward the side with the thinner PCL layer. As a result, the mat spontaneously rolled up into a tube, making the trilayer structure well-suited for the fabrication of actuators. Another typical example is the shape-recovery performance of thermoresponsive nanofibers in response to temperature changes, which will be discussed in detail in section 3.2.

In addition to volume changes, a “switching surface” can be obtained by grafting thermoresponsive polymers onto the surface of nanofibers. In one study, PNIPAAm was grafted to the surface of a mat of PS nanofibers. By reducing the temperature from 37 to 20 °C, the PNIPAAm transformed from an extended state to a collapsed state, and the water contact angle of the mat dropped significantly.⁵⁴⁵ With the introduction of this switching surface, cells were triggered to be released from the mat.⁵⁴⁰

The temperature changes can also be induced through photothermal heating. For example, near-infrared light (near-IR) is often used to increase the temperature for biomedical application due to its deep penetration into soft tissues and low risk of damage to healthy tissues. By incorporating near-IR-sensitive dyes (e.g., indocyanine green) or nanostructures (e.g., Au or Ag nanoparticles) into the thermoresponsive nanofibers, photothermal heating can be used to trigger the phase transition and volume changes.⁵⁴⁴ In one study, Au nanorods and bovine serum albumin (BSA) were incorporated into nanofibers of poly(N-isopropylacrylamide-co-poly(ethylene glycol acrylate)).⁵⁴⁶ The resultant composite nanofibers showed controlled delivery of BSA in response to the “on” and “off” of near-IR light. Upon exposure to near-IR light, the Au nanorods locally heated the polymer matrix, and the nanofibers subsequently experienced a major decrease in volume, leading to the acceleration of drug release. When the near-IR light was turned off, the nanofibers swelled and experienced an obvious increase in volume, resulting in drug release immediately. Photothermal heating allows for remote and spatial/temporal control as the optical irradiation can be readily focused onto a specific area of the mat of thermoresponsive nanofibers.

Variation in pH is another type of external stimulus that can be conveniently applied. The pH-responsive nanofibers are usually fabricated from polymers that contain either acidic groups (e.g., -COOH and -SO₃H) or basic groups (e.g., -NH₂).⁵⁴⁷ Notable examples include poly(acrylic acid), poly(allylamine hydrochloride), and chitosan.⁵⁴⁸ Variation in pH can result in changes to the water absorption capacity, swelling ratio, and the solubility of the pH-responsive nanofibers. The high surface-to-volume ratio facilitates the diffusion of ions from the surrounding solution to the nanofibers, ensuring a swift response. In one example, nanofibers made of cross-linked poly[styrene-co-(maleic sodium anhydride)] (PSMA) and SMA-cellulose acetate showed a substantial difference in the degree of water absorption as the pH was altered: 18.0 g/g at pH 2.5 and 28.0 g/g at pH 9, respectively.⁵²⁹ In another example, nanofibers made of poly(4-vinylbenzoic acid-*co*-(*ar*-vinylbenzyl)trimethylammonium chloride) ($pK_a = 7.65$) were able to reversibly swell and deswell between pH 5.4 and 8.8 due to the protonation and deprotonation, respectively, of 4-vinylbenzoic acid.⁵⁴⁹

The hydrolysis reaction is also kinetically dependent on pH. In general, nanofibers made of polymers containing acid/base-labile bonds (e.g., ester, acetal, and hydrazone groups) can be accelerated to degrade in response to pH variation. In one study, the degradation of PLGA nanofibers was accelerated when its hydrolysis reaction was catalyzed by a weak acid (through a reversible reaction that generated carboxylic acid and alcohol) or by a base (via a nonreversible reaction that produced carboxylate and alcohol).⁵⁵⁰ In another demonstration, electrospun nanofibers made of polymers containing ortho ester groups were stable in an aqueous solution at pH 7.4 but degraded in solutions at lower pH (5.6 or 4.0). Such pH-responsive nanofibers have been explored for pH-triggered drug release^{549,551} and are also promising as a pH sensor to monitor the pH value of a medium.⁵⁵² For example, luminescent pH-responsive nanofibers were used for continuously monitoring the pH of a culture medium to minimize the risk of contamination, providing a simple and sensitive platform superior to the conventional pH electrode.⁵⁵³

Light-responsive nanofibers are often based on the photo-induced isomerization of constituent groups or molecules that can undergo a large conformational change in response to light irradiation at different wavelengths. Typically, the trans–cis isomerization of azobenzene chromophore can cause the molecules reversibly interconvert between an extended, thermally relaxed trans isomer and a bent, higher energy cis isomer. In one study, a mat of nanofibers made of azobenzene-functionalized PCL nanofibers showed a light-responsive change in wettability.⁵⁵⁴ The contact angle of the mat could be reduced from 132.2° to 53.1° upon UV irradiation because the trans-to-cis isomerization caused an increase in dipole moment (μ) for the azobenzene molecules ($\mu \approx 5$ D for the cis form versus $\mu \approx 1$ D for the trans isomer).⁵⁵⁵ Then, the wettability was switched back by exposing the mat to visible light for 15 min for the recovery of the trans state.

The azobenzene-based nanofibers are attractive for light-triggered on-demand drug release. Driven by hydrophobic and van der Waals interactions, there is host–guest interaction between trans-azobenzene and α -cyclodextrin. The host–guest interaction can be hindered when azobenzene transforms from the trans to cis configuration under UV irradiation, leading to a light-responsive delivery of α -cyclodextrin-based prodrugs.⁵⁵⁶ In one study, azobenzene molecules were immobilized on the surface of nanofibers made of a block copolymer of vinyl–benzyl chloride and glycidyl methacrylate. Then, α -cyclodextrin-conjugated 5-fluorouracil, an anticancer drug, was loaded on the nanofibers in the dark.⁵⁵⁷ Upon exposing the nanofibers to UV light, a well-controllable release of the drug was observed whereas there was no drug release in the dark.

The external stimuli can also be applied as an electric field. The responsive capability of the nanofibers is usually realized through an electro-responsive material. For example, under an external electric field, ion transport usually takes place in an ion-doped conductive polymer (e.g., PEDOT), and the induced reversible movement of the ions can lead to a volume change to the conductive polymer. In one study, by applying a positive potential to the PEDOT-coated PLGA nanofibers, electrons were injected into the PEDOT chains to compensate the positive charges.⁵⁵⁸ To maintain overall charge neutrality, counterions were expelled toward the solution, leading to the contraction of the PEDOT chains and the nanofibers. By leveraging this electro-responsive volume change, controlled release of

Author Manuscript
Author Manuscript
Author Manuscript
Author Manuscript

dexamethasone was achieved using the drug-loaded nanofibers. The amount of the released drug was directly related to the contraction force and the duration of the contraction, both were controlled by the externally applied potential. In another example, a film of carbon nanotubes could expand and contract when placed in an electrochemical cell due to the electrochemical double-layer charging of carbon nanotubes.⁵⁵⁹ By incorporating multiwalled carbon nanotubes into nanofibers made of a blend of PVA and poly(acrylic acid), the resultant nanofibers swelled in response to the electric field.⁵⁶⁰ Both the swelling ratio and the swelling rate of the nanofibers were positively correlated to the applied voltage, which could be applied to trigger the release of a drug.

Superparamagnetic nanoparticles, such as Fe_3O_4 or Fe_2O_3 ,⁵⁶¹ have been incorporated into nanofibers with an aim to achieve magnetically responsive functions. In addition, nanofibers of pure Fe have also been fabricated to give superparamagnetic properties.⁵⁶² In one study, after introducing magnetite nanoparticles into PVA nanofibers, the resultant mat exhibited superparamagnetic properties and showed deflection toward an externally applied magnet.⁵⁶³

3.2. Shape Memory

Shape-memory nanofibers are able to transform from a deformed state (the temporary shape) to the original state (the permanent shape) in response to an external stimulus.^{564–566} Temperature is one of the most commonly used stimuli to induce the shape transition. In this case, shape-memory nanofibers are often fabricated by electrospinning polymers that can take two or multiple conformations at different temperatures.^{567,568} The polymers typically contain two different components: (i) soft segments that provide a low T_g or T_m and (ii) hard segments that ensure the formation of a stable network structure.⁵⁶⁴ A notable example of the polymer is thermoplastic polyurethane (TPU).

The simplest demonstration of shape memory involves a one-way mode, in which the nanofiber-based mat can exhibit two different shapes.⁵⁶⁵ At room temperature, the mat typically takes its permanent shape. Upon heating to a temperature above its shape-memory transition temperature (T_{trans} , mostly the T_g or T_m of the polymer), the mat becomes a soft elastomer due to the increased mobility of the polymer chains. As such, the mat is susceptible to deformation when an external force is applied. When the temperature drops below T_{trans} , the deformation is retained due to the freezing of the polymer chains, and the entropic energy is stored in the mat. When heating above T_{trans} again, the entropic energy will be released, forcing the mat to take its permanent shape. Two important quantities are usually used to describe the shape-memory effect, the shape fixity rate (R_f) and shape recovery rate (R_r). Specifically, R_f refers to the ability of a mat to fix the mechanical deformation, and R_r describes the ability of the mat to memorize the permanent shape.

Owing to the high porosity, a nanofiber-based mat offers much quicker and sharper shape recovery when benchmarked against a bulk film. Meanwhile, the quick recovery and fixing of shape can reduce the slipping of macromolecular chains under stress and thus weaken the stress relaxation. Therefore, electrospun nanofibers are superior for use in situations that require immediate control of the shape transition together with the capability for high strain recovery.⁵⁶⁹

The shape-memory effect and the transition temperature of a nanofiber-based mat are mainly determined by the structure of the polymers (i.e., the length of the soft segment and hard-to-soft segment content ratio) and the diameter and morphology of the nanofibers.⁵⁷⁰ For example, a higher hard-segment content in TPU contributed to a remarkably better shape recovery.⁵⁷¹ By exploring polymers with broadened transition temperatures, for example, a mat with quintuple-shape-memory effect which could memorize five different shapes was achieved by tailoring the diameter and morphology of the Nafion nanofibers.⁵⁷²

In addition to using direct heating, other remote means, such as an alternating magnetic or electric field, can also trigger the thermally induced shape-memory effect.⁵⁷³ For example, composite nanofibers containing PCL and multiwalled carbon nanotubes coated with Fe₃O₄ nanoparticles showed a shape-recovery effect in response to both hot water and an alternating magnetic field. The recovery process is clearly shown by a series of photographs in Figure 35A.⁵⁷³ While the Fe₃O₄ nanoparticles served as the magnetically responsive component, the carbon nanotubes acted as physical cross-linking points among the macromolecular chains. Electrically triggered shape recovery was also realized by incorporating conductive nanoparticles into thermally resistive nanofibers. In one study, with the application of a constant DC voltage, the mat of nanofibers made of Nafion and SiO₂ was heated to a temperature above its T_{trans} , leading to the shape recovery from its temporary shape.⁵⁷⁴ By increasing the applied electric current, the speed of the shape recovery was accelerated.

The nanofiber-based, shape-memory mat has been used in a variety of applications, such as tissue engineering and filtration. For example, a shape-memory mat can control the growth of cells via shape transition to mimic the dynamic environment in the human body.^{575,576} In one study, a mat consisting of randomly oriented nanofibers was uniaxially stretched to 100% in strain at 60 °C, and then by cooling to 0 °C (below T_g), it was fixed in a temporary shape consisting of uniaxially aligned nanofibers.⁵⁷⁵ After heating to 37 °C, the mat was recovered from the shape consisting of uniaxially aligned nanofibers back to the random nanofibers. Human adipose-derived stem cells cultured on the mat could change their orientations along with the transition of fiber alignment. Cells preferentially oriented along the direction of the aligned nanofibers and lost the orientation after the mat recovered the original shape. In another study, 3D shape-memory scaffolds were fabricated from nanofibers of poly(D,L-lactide-*co*-trimethylene carbonate).⁵⁷⁷ As shown in Figure 35B, the scaffold could recover from a temporary shape of a straight strip to take the permeant spiral shape within about 6 s upon heating to 39 °C in a water bath. Besides, heat-triggered shape recovery of samples in the shapes of “S”, “M”, and “P” were all completed within 12 s. The shape-memory nanofibers have also been used for *in vivo* study to fill complex defects using minimally invasive surgical implantation.⁵⁷⁸ For example, shape-memory grafts made of polyurethane nanofibers were explored to space-fill bone defects. The grafts showed rapid deployment within 60 s *in situ* upon irrigation with 45 °C saline (Figure 35C).⁵⁷⁸ After implantation, the grafts expanded to fill and conform to the 4 mm segmental defect. Stabilizing sleeves were also constructed from the shape-memory nanofibers to contract around the mouse femur after implantation upon thermal treatment.⁵⁷⁸

The capability of shape-memory nanofibers can be further extended to make composite materials. When the nanofibers are encapsulated within a polymer matrix, such as silicone rubber, the shape-memory function is transferred to the resultant composite. In this case, the nanofibers can act as a switching phase, while the rubber phase ensures the permanent shape. For instance, composites comprised of a poly(mannitol sebacate) matrix reinforced with PLA nanofibers showed an obvious shape-memory effect.⁵⁷⁹ By increasing the amount of the nanofibers in the composite from 4 to 10 and 15 wt %, R_f was increased from 72 to 87 and 91%, respectively. Such an approach is highly versatile because it allows for separate tuning of the two components and thus overall control of the shape-memory behavior.

3.3. Self-Cleaning

Self-cleaning coatings have been commercialized for various applications.^{580,581} Among the different types of coatings, nonwoven mats based upon electrospun nanofibers are advantageous for their breathable, flexible, and self-supporting properties. They can be applied to prevent contamination in medical devices and producing protective clothes.^{582,583} By controlling the surface structure and chemical composition of the nanofibers, the surface wettability of the mat can be manipulated to realize the self-cleaning ability.^{584,585} Two routes have been reported, including the formation of (i) a “film flow” on a superhydrophilic surface (Figure 36A), similar to the behavior of water on the fish scales in air⁵⁸⁶ or (ii) a “droplet flow” on a superhydrophobic surface (Figure 36B), similar to the behavior of water on the plant leaf.⁵⁸⁷

3.3.1. Superhydrophilic Surface.—When the nanofiber-based mat is superhydrophilic, water can completely spread out to generate a thin film on it. In this way, the flowing water film can wash away the dirt when the mat is inclined. The superhydrophilicity is mainly achieved by nanofibers containing photocatalytic TiO₂. Under exposure to UV light, the nanofiber-based mat containing TiO₂ exhibited an extremely small contact angle of less than 1°. The thickness of the mat also affects the formation of the water film. For a sufficiently thick mat (of the order of several hundred nanometers and above), the flowing of water film was a hydrodynamic process without beading of the water. For thinner mats, however, the flowing of water film involved rapid equilibration by surface diffusion.

The nanofiber-based mat with a superhydrophilic surface is often used as a coating layer to produce a self-cleaning glass. In this case, wettability is not the only desired function. The transparency or low scattering of the resultant glass is also essential, which is mainly determined by both the thickness of the mat and its adhesion to the glass. In one study, diethanolamine was added into the TiO₂ precursor solution for electrospinning.⁵⁸⁸ When the amount of diethanolamine was increased, the resultant coating layer changed from opaque nanofibers to transparent nanoparticles. In addition, the presence of diethanolamine allowed for stronger adhesion between the coating and the glass.

3.3.2. Superhydrophobic Surface.—Inspired by the superhydrophobic surfaces in nature, such as the lotus leaf, a nanofiber-based mat with a superhydrophobic surface has been fabricated to demonstrate the self-cleaning effect. The surface not only has a low surface energy but also exhibits a hierarchical roughness on at least two scales (i.e.,

micrometer and nanometer).⁵⁸⁹ In this case, the self-cleaning effect is achieved through rolling motion of water droplets on the surface of the mat. Three basic requirements are involved for the surface: (i) a high static water contact angle (WCA, >150°), (ii) a low adhesion to the water droplets such that the droplets can easily move even at low (<10°) inclination for the surface, and (iii) a lower adhesion to the dust than that to the water droplets so that the water droplets can actively pick up dust particles.⁵⁹⁰ Three approaches have been employed to produce mats with a superhydrophobic surface: (i) directly electrospinning a hydrophobic polymer, (ii) modifying the rough surface with a low-surface-energy material, and (iii) roughening the low-surface-energy material. The last two methods can be realized by manipulating the surface chemistry and topography of the nanofiber-based mat.

Nanofiber-based mats with a superhydrophobic surface can be produced by directly electrospinning a hydrophobic polymer. In this case, the superhydrophobicity of the resultant nanofibers is mainly determined by the macromolecular structures and the functional groups of the polymers. Among the different types of hydrophobic polymers, PS and PS-based copolymers are often used because of their low surface energy, low cost, and simplicity.⁵⁹¹ For example, a mat made of poly(styrene-*b*-dimethylsiloxane) block copolymer exhibited a contact angle of 163° and a hysteresis value of 15°, owing to the enrichment of the dimethylsiloxane components combined with the small diameters of the nanofibers (150–400 nm).⁵⁹² Other polymers, ranging from the conventional polymers (e.g., nylon-6 and cellulose acetate) to complicated copolymers, block polymers, and grafted polymers, are also commonly used. In particular, fluorinated polymers are highly hydrophobic due to the CF₃ groups. However, these polymers are difficult to dissolve in a solvent for electrospinning. As such, other spinnable polymers are often blended to proceed the electrospinning.⁵⁹³

Coating the surface of nanofibers with a low-surface-energy material is another effective way to fabricate a super-hydrophobic surface. For example, PTFE, one of the lowest-surface-energy materials, has been combined with PCL to generate core–sheath nanofibers via coaxial electrospinning.⁵⁹⁴ The resultant mat had a static WCA of 158° (Figure 36C) with a very small rolling angle of 7°, together with the observation of water bouncing behavior.

Electrospun nanofibers intrinsically provide at least one length scale of roughness due to their small diameter. By further incorporating the nanofibers with a second scale of roughness through the integration of nanoparticles or pores, the trapping of air between the water droplet and the nanofiber-based mat can be improved, and thus water is prevented from penetrating into the mat. In this way, a superhydrophobic mat can be obtained.⁵⁸⁴ For example, upon electrospinning of a PS solution in DMF (7 wt %), a mat consisting of nanofibers (50–70 nm) covered by micro-particles (2–7 μm) was directly generated, as shown in Figure 36D.⁵⁹⁵ The static WCA on such a mat was 162°, compared to 139° on a mat comprised of nanofibers only. A mat consisting of beaded nanofibers also showed better hydrophobicity than that of smooth nanofibers. In this case, the microparticles or beads are essentially mixed rather than hierarchically integrated. To address this issue, nanoparticles can be directly decorated on the surfaces of nanofibers to produce a hierarchically

Author Manuscript
Author Manuscript
Author Manuscript
Author Manuscript

roughened mat. For example, ZnO nanoparticles were integrated with PVDF nanofibers by direct electro-spinning of a PVDF solution containing 10 wt % ZnO nanoparticles.⁵⁹⁶ The resultant nanofibers showed a rough surface, together with a higher static WCA (171°) of the mat than that of PVDF nanofiber-based mat (146°) (Figure 36E). Nanometer-scale pores on the surface of nanofibers can also be considered as a second scale of roughness, which has the advantage of achieving hierarchically roughened mats in one single step.⁵⁹⁷

In general, the robustness of a self-cleaning coating is very important. However, the poor mechanical strength of nano-fiber-based mats greatly limits their utilization, which is probably the main reason why few products have been commercialized. Fabrication of self-cleaning mats with improved resistance to friction and wear are desirable to increase their viability in commercial applications.

3.4. Self-Healing

Engineering materials are often susceptible to damage in the form of cracks. It is often difficult to detect the location of a crack within a bulk material. Hence, repairing the crack is almost impossible. To this end, self-healing materials, which are able to self-repair damages and thus recover their pristine properties, are highly desirable. Particularly, self-healing is a key feature of the biological system that prolongs the lifespan of living organisms.⁵⁹⁸ The healing process is typically accomplished using a pervasive vascular network that supplies the necessary biochemical components. For example, a cut on human skin is able to heal spontaneously because the cut rapidly triggers blood flow through the capillary network in the dermal layer to the wound site, enabling the delivery of nutrients for the recovery (Figure 37A).⁵⁹⁸ By mimicking this natural phenomenon, self-healing composites have been developed using electrospun nanofibers with an interconnected network-like structure.⁵⁹⁹ Electrospun nanofibers are advantageous in introducing the self-healing property. Instead of using microcapsules as a vehicle for the delivery of healing agents, the use of electrospun nanofibers can simplify the fabrication process.⁶⁰⁰ As the nanofibers allow rapid diffusion of the healing agents along the boundary of the damaged cracks, a shortened healing time will be involved.

The nanofibers themselves often directly act as the healing agent. For example, PCL nanofiber ($T_m = 60^\circ\text{C}$) was randomly distributed in an epoxy matrix, and then a knife cut was made on the surface of the composite.⁶⁰¹ Upon heating at 80 °C for 10 min, the cut was completely closed with almost no detectable separation owing to the fact that the melted PCL nanofibers were able to bond the opposite sides of the crack together. In this case, however, an additional heat-treatment is required to trigger the self-healing process.

Alternative strategies are developed by encapsulating liquid healing agents in core–sheath nanofibers and then embedding the nanofibers in a polymer matrix. When a crack propagates through the nanofibers, the healing agents leave the broken nanofibers and flow to the surrounding matrix, generating healing materials (i.e., a polymer or a cross-linked product) to repair the crack.^{602–604} In general, two reagents (i.e., monomer and curing agent) are needed in order to generate the healing materials, and they are not supposed to encounter each other until the composite is damaged.⁶⁰⁵

Author Manuscript
Author Manuscript
Author Manuscript
Author Manuscript

A typical strategy for separating the two reagents is to have one of them encapsulated in the core of core–sheath nanofibers and the other distributed within the polymer matrix. In one study, the curing agent (dimethyl methylhydrogen siloxane) was encapsulated in the core of PAN nanofibers, and liquid droplets of the monomer (dimethylsiloxane) were loaded in the epoxy matrix.⁶⁰⁶ Once a cut was applied, the curing agent and monomer left the nanofiber core and the damaged matrix, respectively, initiating polymerization. After 2 days, self-healing was manifested to the damaged composite. Although the monomer encapsulated at a deep location of the matrix may not eventually participate in the polymerization, the self-healing process is still effective.

In a more elegant design, the monomer and curing agent can be separated by simultaneously co-electrospinning two types of core–sheath nanofibers that separately encapsulate the two liquid healing agents in their cores.^{603,607–609} For example, two types of nanofibers were simultaneously collected to form a mutually entangled mat by taking dimethylsiloxane and dimethyl methylhydrogen siloxane as the cores of PAN hollow fibers, respectively (Figure 37B).⁶⁰⁴ Afterward, the entangled mat was embedded in a PDMS matrix. When deformation was imposed on the composite via tensile stretching, the two healing agents were separately released from the cores of the nanofibers and polymerized inside the cracks, realizing self-healing of the composite. In this way, the Young’s modulus of the composite was completely recovered. In another study, two types of bead-on-string core–sheath nanofibers were fabricated to encapsulate the healing agents in the beads.⁶⁰⁷ Upon damage, the healing agents were released from the mechanically ruptured beads and flew into the scribed region for polymerization, as illustrated in Figure 37C.

The self-healing composites containing nanofibers have been explored as the “barrier” coatings of steel to prevent corrosion, which has long been a major concern in industries. Coated with a layer of self-healing composite, the steel can be kept from directly contacting with the corrosive environment. Because the microscale cracks in the coating layer are self-healable, the steel surface can be protected for a long period of time (Figure 37D).⁶¹⁰

3.5. “Living”

Live microorganisms such as microbes and cells can also be incorporated during electrospinning to produce “living” nanofibers. These living nanofibers are useful in a wide variety of biotechnological products such as microbial fuel cells, water decontamination membranes, food ingredients, and cellular constructs.⁶¹¹ From a suspension prepared by dispersing the live microorganisms in a polymer solution, a jet containing the organisms is projected. In general, the encapsulated microorganisms are not affected electrically because the excess charges are mainly distributed on the surface of the jet. However, several mechanical issues should be considered. First, the viscous forces acting on the microorganisms must be controlled because the biological structures of microorganisms can be destroyed by stress on the order of 10^3 N/m^2 .⁶¹¹ The viscous stress in a jet can reach a level of 10^5 N/m^2 , which may affect the viabilities of the encapsulated microorganisms. Second, drastic changes in the osmotic environment of the microorganisms are expected due to the evaporation of solvent, and rapid dehydration to the microorganisms needs to be

avoided as much as possible. Third, toxicity issues need to be considered with the goal of minimizing the exposure of the microorganisms to organic solvents.⁶¹²

Microbes, such as bacteria and viruses, can be encapsulated in nanofibers by directly electrospinning an aqueous suspension containing the microbes and a polymer. The microbes are usually dispersed in a dilute salt solution or nutrition medium and then mixed with an aqueous polymer solution. In one study, bacteria and viruses embedded in PVA nanofibers both could retain full viabilities for 3 months when held at both -20 and -55 °C.⁶¹³ To extend this method to water-insoluble polymers, one can use coaxial electrospinning to shield the microbes from the toxic solvent. For example, yeasts were encapsulated in the core of poly(vinylidene fluoride)-co-hexafluoropropylene nanofibers.⁶¹⁴ The bioactive mat was able to biodegrade 60% of phenols in a contaminated water sample in 72 h. The nanofibers could act as a protection layer for the encapsulated microbes to improve their viabilities during storage.⁶¹⁵ In addition, the living nanofibers can also be used for introducing beneficial microbes to a targeted site, which is useful in agricultural applications. For example, after being encapsulated in electrospun PVA nanofibers, rhizobia, a plant growth promoting bacterium, showed a significantly higher viability after 48 h of storage than that of the non-encapsulated rhizobia.⁶¹⁶ The PVA matrix protected the rhizobia from environmental stresses such as temperature and dehydration. After coating with the rhizobia-encapsulated living nanofibers for 30 days, soybean seeds showed significantly enhanced soybean production.⁶¹⁷

Living cells can also be encapsulated in electrospun nanofibers. The encapsulation allows for the protection of cells from harsh environments as well as a control over the physicomechanical properties of the cell's immediate surroundings (i.e., the chemical structure and permeability of the matrix).⁶¹¹ Different methods have been used to encapsulate cells in nanofibers, leading to variations in cell viability from less than 20%⁶¹⁸ to more than 60%.⁶¹⁹ The composition of the solution for loading the cells has a significant impact on the electrospinnability of the suspension and the viability of the cells encapsulated in the fibers.⁶²⁰ Electrospinning from a mixture of cells and polymer solution will subject the cells to the viscous force. In this case, a coaxial electrospinning setup is needed. The cells in the core solution are surrounded in a less viscous medium, which is beneficial to keeping the cells viable. The addition of cell neurites to create an isotonic environment can further improve the cell viability. For example, human umbilical vein endothelial cells were loaded into the core of PEO@PCL core-sheath nanofibers via coaxial electrospinning.⁶²¹ By introducing fetal bovine serum to the inner PEO solution, the viability of the cells was more than 95% in the first 2 h, whereas the viable cells were less than 3% when the core fluid was PEO solution alone.

3.6. Sensing

Owing to the highly porous structure and the large surface-to-volume ratio, electrospun nanofibers have been widely used in the area of sensing with a high sensitivity and rapid response rate. The nanofibers can be used to sense the changes in concentration for chemical species, including small molecules (e.g., water or glucose), biomolecules (e.g., enzymes or proteins), and even gaseous species. For example, 30 wt % LiCl-doped porous TiO₂

Author Manuscript
Author Manuscript
Author Manuscript
Author Manuscript

nanofibers showed good sensitivity toward humidity changes.⁶²² Sensitive detection of physiologically important molecules has also drawn much attention. Glucose represents one of the typical examples because of its importance in altering many biological processes.⁶²³ Various types of nanofibers have been integrated with glucose oxidase⁶²⁴ or functional nanomaterials (e.g., semiconducting oxides)⁶²⁵ to achieve sensitive detection of glucose, providing an efficient platform for glucose monitoring.⁶²⁶ The accurate and sensitive detection of proteins is also of importance in many applications.⁶²⁷ Quantitative protein analysis is mostly done using enzyme-linked immunosorbent assays (ELISA), in which the target protein is caught by an immobilized enzyme and then detected through a secondary antibody. As the sensitivity of detection correlates with the availability of the immobilized antibodies, a mat of nanofibers with a higher surface-to-volume ratio significantly boosts the detection limit. In one study, when the tissue culture plate used for the conventional ELISA assay was replaced by electrospun SiO₂ nanofibers, a 32-fold enhancement in sensitivity was obtained toward the detection of various proteins.⁶²⁸ In terms of time, the nanofiber-based assay could be completed in 1 h without any loss of the sensitivity, whereas the conventional assay often needs 24 h. Explosive or toxic gases (e.g., CO, NH₃, and NO₂) have also been detected using nanofiber-based mat by leveraging the chemical reaction between the gas molecules and the functional groups on the nanofibers.

Electrospun nanofibers can also serve as highly sensitive optical sensors.⁶²⁹ For example, long (up to 1 cm) and thin (40 nm in diameter) GaN nanofibers were produced by electrospinning.⁶³⁰ When exposed to UV light, the conductance of a GaN nanofiber was greatly increased by 830 times, which was over 10-fold greater than that of a single-crystal GaN nanowire (ca. 78 times) grown through chemical vapor deposition. The high sensitivity of electrospun GaN nanofibers was attributed to the polycrystalline structure and rough surface, which resulted in more photogenerated carriers relative to a smooth GaN nanowire.

3.7. New Directions for Future Development

The extremely large surface area of electrospun nanofibers and the high porosity of their nonwoven mats are instrumental to the incorporation of smart properties. To maximize the performance of stimuli-responsive nanofibers, one should consider both the rate of stimuli-response and the reversibility of changes. Future direction lies in the optimization of the structure and functionality of both the individual nanofibers and the nanofiber-based mats to accelerate the transfer of a stimulus and improve the accuracy of change to the nanofibers. Self-immolative electrospun nanofibers with a temporary lifetime that can be controlled through a triggered decomposition process have recently received significant interest, particularly with regard to the disposal of used products. For the nanofiber-based mats with a self-cleaning effect, their poor mechanical strength greatly limits the utilization. Fabrication of self-cleaning mats with improved resistance to friction and wear are desirable to increase their viability in commercial applications. In addition, how to preserve the self-cleaning capability needs future attention since the surface may be deteriorated after use for a certain period of time. When the nanofibers are used as a coating on a substrate such as a medical device, strong adhesion between the nanofibers and the substrate is highly desired, which is also an important aspect for future development.

Author Manuscript
Author Manuscript
Author Manuscript
Author Manuscript

Although electrospun nanofibers can be loaded with appropriate agents to fabricate self-healing materials, the types of healing agents that have been loaded into electrospun nanofibers are still limited to monomers and curing agents for the generation of silicone rubber or epoxy resin. Future efforts should be directed to the investigation of other healing agents for the development of composite materials. In addition, most of the reported systems require lengthy healing periods that often cannot be easily accommodated by commercial products. Regarding the living nanofibers, it is interesting to apply them to agricultural and food applications by introducing beneficial microbes into the targeted site. Electrospun nanofibers with active components for sensing can potentially provide capability for quick and even real-time response. To enhance the sensitivity, further investigation is required to increase the surface area and improve the pore structure of a nanofiber-based mat. Besides, integration of the nanofibers with devices such as microfluidic systems is still challenging because it requires nanofibers with the well-controlled diameter and orientation, as well as the reproducibility to place them at specific positions and with the right orientation.

4. ELECTROSPUN NANOFIBERS FOR ENVIRONMENT AND SUSTAINABILITY

Upon deposition on a collector, electrospun nanofibers naturally form a nonwoven mat with a large surface-to-volume ratio and high porosity, making it useful as a filtration membrane for various applications. The highly porous structure originating from the random entanglement of nanofibers greatly facilitates the mass transport of both gaseous and liquid samples. In fact, a gas stream or solution can flow through a nonwoven mat of electrospun nanofibers in high flux without experiencing much resistance. As a matter of fact, nanofiber-based mats, particularly those with alignment control and surface functionalization, have been actively explored as advanced filters for removing pollutants such as particulate matters (PMs), toxic ions, and organic molecules from both polluted air and wastewater. They have also been used to decompose harmful chemicals and recover precious metals. The reported data suggest that the membranes based on electrospun nanofibers are superior in quickly and effectively removing pollutants and recovering precious metals with high selectivity, good recyclability, and noticeable stability.

4.1. Purification of Air

Air pollution has long-lasting impacts on atmospheric environment and public health.⁶³¹ The major components of air pollutants include PMs in a liquid or solid form, CO_x, NO_x, SO₂, and ozone.⁶³¹ PMs refer to a mixture of small particles and liquid droplets suspended in air, consisting of various chemical components that include both inorganic (e.g., silicates, sulfates, and nitrates) and organic (organic compounds and elemental carbon) matters.⁶³² Specifically, PM_{2.5} and PM₁₀ (i.e., particles with aerodynamic equivalent diameters less than 2.5 and 10 μm , respectively) can easily infiltrate into the human body, causing lung cancer and pneumonia, congestive heart failure, and coronary artery blockage, among others.^{633,634} Particle pollutants are estimated to cause at least 500,000 deaths annually.⁶³⁵ Conventional air filters are plagued by three key issues: (i) low filtration efficiency, especially for PM_{1.0}; (ii) large air pressure drop across the filter; and (iii) safety hazards such as dust explosion and fire.⁶³⁶ In addition, the traditional air-filtration system is typically made of a multilayer

structure that needs a large amount of energy to maintain the large pressure difference between inlet and outlet and thus requires a high-power pump to push the air through.⁶³¹

The high porosity, good interconnectivity, micrometer-sized interstitial space, and large surface-to-volume ratio make nonwoven mats of electrospun nanofibers superior membranes for the purification of air. An ideal filter should possess a high filtration efficiency and a low pressure drop to maximize the quality factor (QF), which is defined as $-\ln[(1 - \eta)/\rho]$, where η and ρ represent the filtration efficiency and pressure drop, respectively.⁶³⁷ The higher the QF value is, the better the performance will be for filtration. The QF value is determined by three key parameters of the filter, including overall porosity, average pore size, and specific surface area. These parameters control the diffusion of gas molecules through the filter, the resistance of airflow, and the filtration efficiency.⁶³⁸ The mechanisms for removing PMs using a nanofiber-based membrane primarily involve Brownian diffusion, direct interception, inertial impaction, gravity, physisorption, chemisorption, and electrostatic attraction.⁶³⁷ Compared to the traditional filtration materials such as activated charcoal, nanofiber-based membranes are superior in filtration performance. Depending on the sizes of the particles in the air that are supposed to be filtered out, the sizes of void space in the mat and the pores in individual nanofibers can be optimized to attain notable filtration efficiency. The filtration efficiency can be further improved by reducing the fiber diameter and thereby increasing the specific surface area of the mat. Reducing the fiber diameter from micrometer to nanometer scale allows for the removal of PMs down to 300 nm in size.⁶³⁹ In recent years, nonwoven mats of nanofibers made of polymers, composites, and their derivatives have all been actively explored as advanced high-efficiency particulate air (HEPA) filters.

4.1.1. Membranes Based on Polymer Nanofibers.—Nonwoven mats made of polymer nanofibers are particularly well-suited for use as facial masks owing to the lightweight and breathable feature. For instance, a membrane based on silk nanofibers only weighs 3.4 g/m², but it has filtration performance similar to a commercial respirator of more than 60 times heavier.⁶³⁹ In one study, it was demonstrated that an ultralight membrane based on polymer nanofibers (ca. 0.63 g/m² in weight) could achieve a filtration efficiency above 99.97% while maintaining good mechanical robustness.⁶⁴⁰ Importantly, many spinnable polymers, such as PAN, PVP, PS, and PVA, are available in large quantities and at low costs, allowing for their use in the fabrication of disposable facial masks.

In general, the filtration efficiency will be improved when the polarity of the polymer is increased. The dipole–dipole or dipole–induced dipole force can greatly promote the binding of PMs to the surface of nanofibers, greatly enhancing the filtration efficiency. For example, the dipole moments of the repeating units of PAN, PVP, PVA, and PS are 3.6, 2.3, 1.2, and 0.7 D, respectively, as shown in Figure 38A.⁶⁴¹ By separately packing the nonwoven mats of these four types of nanofibers (with a similar diameter of ca. 200 nm and transmittance of ca. 70%) in the air filters, the PAN-based membrane gave the highest efficiency in removing both PM_{2.5} and PM_{10–2.5} (Figure 38B).⁶⁴¹ Clearly, by engineering the repeating units of the polymer and/or modifying the functional groups on the side chains, the interactions between the nanofibers and PMs can be maximized to obtain filtration membranes with the greatest efficiency for air purification.

The filtration efficiency can also be improved by increasing the electrostatic charges on the surface of nanofibers for capturing the targeted pollutants through long-range electrostatic interactions.^{631,642} Permanent surface charges can be generated either by co-electrospinning polymers with different triboelectric properties or by incorporating an electret into the nanofibers. In one report, the QF value of a nonwoven mat of PVDF nanofibers reached 0.14 Pa^{-1} by encapsulating PTFE nanoparticles.⁶⁴³ When applied to the removal of $\text{PM}_{2.5}$, such a mat exhibited a high filtration efficiency of 99.972% and a low pressure drop of 57 Pa.

The nonwoven mat of nanofibers can be deposited on a contoured surface to further enhance the filtration performance. In one study, a nonwoven mat of polyamide-6 nanofibers was deposited on a collector patterned with an array of relief structures to obtain an extremely small pore size, highly porous structure, and hugely extended frontal surface.⁶⁴⁴ Such a membrane allowed for the effective removal of $\text{PM}_{2.5}$ at a high efficiency of 99.996%, a low pressure drop of 95 Pa, and a high QF value above 0.11 Pa^{-1} .

There are major differences in terms of composition, structure, morphology, and capture mechanisms between $\text{PM}_{2.5}$ and PM_{10} , in addition to the dependence of these parameters on the source or location.^{632,645} As a result, the filtration membrane needs to be optimized individually to target specific PMs from an explicit source or location. In developing effective devices, it is also important to understand the evolution of PMs upon their capture by a nanofiber-based membrane. In a recent study, the dynamic nature involved in the capture of PMs by a nanofiber-based membrane was elucidated through *in situ* optical microscopy.⁶⁴⁶ The captured PMs tended to coalesce on the surface of nanofibers. Once captured, wetting droplets moved and grew into axisymmetric structures, while nonwetting droplets evolved into non-axisymmetric structures. For solid particles, they tended to grow into dendritic structures through aggregation or attachment.⁶⁴⁶ The membrane was eventually covered by large aggregates of PMs, with the joint points among nanofibers having more PMs accumulated, which tended to form spherical particles with substantially enlarged sizes relative to the original PMs.⁶⁴¹ These studies offer new insights with regard to the size and shape evolutions of different kinds of PMs once they are captured by the nanofiber-based membranes. These studies also suggest the importance to enhance the wettability and adhesion of the PMs and thus the filtration efficiency by tailoring the specific surface energy of the nanofibers. The *in situ* observations are very helpful in identifying the most effective membranes in terms of the type of polymer and pore structure prior to the manufacturing of large-area filters.

The high filtration efficiency of nanofiber-based membranes allows for the reduction of packing density and number of layers in a filtration device to provide promising features such as optical transparency. With the use of nanofibers made of a polar polymer such as PAN, or polyimide, the air filtration systems can serve as transparent and efficient PMs filters.^{641,647} For instance, nonwoven mats of 300 nm polyimide nanofibers could be made semitransparent (>40% transmittance in the visible region) while maintaining a high filtration efficiency of 99.97% and a high QF of 0.107 Pa^{-1} (Figure 38C–E).⁶⁴⁷ The semitransparent membranes showed a stable filtration efficiency, even when applied under different weather conditions. Such transparent membranes enable the exchange of air by natural ventilation through windows for ideal indoor air filtration.

In addition to the purification of polluted air, the nanofiber-based membranes can also be used to remove the pollutants from an exhaust line before the pollutants are discharged into the environment. The exhaust is often at an elevated temperature as it may come from a combustion engine or an industrial process. For example, many industrial dedusting processes are typically operated at temperatures in the range of 150–260 °C.⁶⁴⁸ In these cases, most of the polymer nanofibers would fail due to their poor thermal stability at temperature beyond 100 °C. To address this issue, polymers with high molecular weights and rigid backbones, such as poly(ether sulfone), polyimide, polybenzoxazole, poly(*m*-phenylene isophthalamide), and poly(ether imide), can be used to improve the thermal stability.⁶⁴⁸ In one study, nonwoven mats of 300 nm polyimide nanofibers were shown to maintain good filtration performance at a working temperature up to 370 °C.⁶⁴⁷ Field testing confirmed that the membranes could effectively remove all kinds of PMs from car exhaust at temperatures of 50–80 °C, bringing down the concentration of PMs to a level equivalent to that of clean air (Figure 38F,G).⁶⁴⁷ These mats can work independently or with other types of industrial dust collectors at both room and elevated temperatures.

To improve the comfort of facial mask users, the membrane can be deposited on proper substrates to introduce thermal management capability. In one demonstration, nylon-6 nanofibers were deposited on a porous polyethylene substrate to fabricate the filter.⁶⁴⁹ Due to strong adhesion between PMs and the nylon-6 nanofibers, the filter showed a high filtration efficiency of 99.6% toward PM_{2.5}. The porous polyethylene substrate is highly transparent in the infrared region, allowing for effective radiative cooling. By further sandwiching a Ag film between the substrate and the nanofiber-based mat, the trilayered membrane showed a high reflectance of 87.0% in the infrared region, making it useful for the purpose of warming. The multilayered facial masks can be applied to both outdoor and indoor conditions, protecting people from PMs while achieving personal thermal comfort.

Regarding safety issues (e.g., dust explosion and fire), nanofiber-based membranes with extraordinary flame retardation are highly desirable, especially for industrial applications. In a recent demonstration, flame-retardant mats were fabricated from core–sheath nanofibers, with the use of triphenyl phosphate (a flame retardant) for the core and nylon-6 for the sheath.⁶³⁶ At 80% of optical transmittance, the mats showed capture efficiencies of 99.00% for PM_{2.5} and >99.50% for PM_{10–2.5}, compatible to the mats made of nylon-6 nanofibers. During direct ignition tests, triphenyl phosphate was released from the core as the nylon-6 sheath melted, endowing the mat with an ability to extinguish the fire almost instantaneously. The self-extinguishing time of the filtrate-contaminated filter was nearly 0 s/g, compared to 150 s/g for the filter based on nanofibers of pure nylon-6.⁶³⁶

The nonwoven mat often has a long service lifetime, up to several hundred hours. For instance, the transparent mat made of 200 nm PAN nanofibers (with a transmittance of 75%) is estimated to be able to work for about 300 h under the hazardous PMs level.⁶⁴¹ The lifetime is long enough for disposable use in daily life but is still not sufficient to satisfy the long-term service in industry. The mats based on polymer nanofibers can be reused after removing the captured particles via mechanical shaking or air back-blown.⁶⁴⁰ At the end of their service life, the mats can be easily recycled by directly dissolving the polymer in a proper solvent, avoiding secondary pollution to the environment. After the removal of PMs

from the solution, the purified polymer can be processed for electrospinning to fabricate fresh nanofibers again, ensuring good sustainability.

4.1.2. Membranes Based on Composite Nanofibers.—Composite nanofibers have been extensively explored for the fabrication of filters to achieve high purification efficiency and introduce new functionalities by leveraging the synergistic effect between different components. In one study, by incorporating 7–40 nm SiO₂ nanoparticles in polyethylenimine nanofibers, the air purification performance of the resultant membrane was significantly improved due to the enhanced electrostatic interactions between the nanofibers and the pollutants.⁶⁵⁰ The permanent dipole orientation and the trap of adequate space charges, arising from the SiO₂ nanoparticles during electrospinning, contributed to the prominent filtration performance. The membrane was also lightweight, with a basis weight of about 0.71 g/m². After heat treatment at 200 °C for a short period of time, the mat could still serve as an effective air filter without sacrificing the filtration efficiency (99.992%) and pressure drop.⁶⁵⁰ However, it should be noted that excessive incorporation of SiO₂ nanoparticles (>6 wt %) would cause a decrease in filtration efficiency because of the decreased dipole orientations in the partially agglomerated SiO₂ in the composite nanofibers.

New functionalities (e.g., antibacterial activity, healthcare, and self-cleaning capability) can be readily added to produce multifunctional air filters by incorporating active components (e.g., metal, oxide, or organic molecules) into the nanofibers. For example, a lightweight silk nanofiber-based mat could serve as an air filter with filtration efficiencies of 98.8% for PM_{2.5} and 96.2% for 300 nm particles, respectively, at a lower pressure drop than the commercial membranes. When the nanofibers were loaded with Ag nanoparticles, the resultant mats showed antibacterial activities against both *Escherichia coli* (a typical Gram-negative bacterium) and *Staphylococcus aureus* (a typical Gram-positive bacterium).⁶³⁹ Beside inorganics, natural extracts from plants such as *Melaleuca alternifolia*, *Sophora flavescens*, and eucalyptus can also be directly introduced into the nanofibers as antibacterial fillers.⁶⁴⁸ Additionally, the nanofibers can be functionalized to release healthcare components at an almost constant rate over a relatively long period of time. In one recent study, 60 nm particles consisting mainly of Al₂O₃ and SiO₂ were introduced into PVDF nanofibers.⁶⁵¹ The mats could release negative ions at a constant rate, showing a well-maintained high PM_{2.5} removal efficiency at 99.99% in the event of haze and low air resistance in field tests in Shanghai.⁶⁵¹

The mats made of composite nanofibers can also have “smart” properties, for example, self-cleaning, to serve as air filters with longer lifetime in an energy-saving manner. With the integration of hydrophobic SiO₂ nanoparticles with polyethylenimine nanofibers, the mats showed a super-hydrophobic surface (a WCA of 152°), demonstrating a strong self-cleaning capability.⁶⁵⁰ The self-cleaning feature enables the mats to find an irreplaceable position in daily life or industrial community with virtue of prolonged service life and decreased cost. Combining the above unique characteristics with the easy fabrication procedure and low cost, nonwoven mats based on composite nanofibers have great potential for use as air filters, especially as comfortable and personal air purifiers in our daily life.

It is worth pointing out that the capture efficiency toward pollutants is very sensitive to the surface of the nanofibers. Introducing new component(s) into the nanofibers will cause changes to the surface properties and the binding affinity between pollutants and nanofibers accordingly. As such, in the multifunctional filters, one should optimize each component in the composite nanofibers without compromising the PM filtration efficiency. Meanwhile, the nanofiber-based mats can be readily damaged in a humid environment, especially when water-soluble components (e.g., PVP and PVA) are involved, causing the loss of filtration function. Besides, long-term irradiation of sunlight at a high intensity (e.g., in the summer) can accelerate the aging of the polymer component, shortening the lifetime. These issues may restrict their capability for long-term general use.

4.1.3. Membranes Based on Ceramic Nanofibers.—If endowed with good mechanical strength, ceramic nanofibers that have excellent thermal and chemical stabilities can also serve as efficient filters for air purification. For instance, the $\gamma\text{-Al}_2\text{O}_3$ nanofibers obtained at 700 °C exhibited a remarkable tensile stress of 2.98 MPa, mainly owing to the small grain size and dense packing of grains.⁶³⁷ The freestanding mat of $\gamma\text{-Al}_2\text{O}_3$ nanofibers can serve as a new line of promising air filters for air purification with a high filtration efficiency of >99.9%.⁶³⁷

Nonwoven mats made of thermal-and chemical-stable ceramic nanofibers can serve as superior air filters without any chemical modification, particularly in harsh environments such as in extremely humid weather or a high-temperature pollutant source, without the flammability issue. High purification efficiency has been achieved, although the QF value of mats based on ceramic nanofibers is often not as high as those of polymer-or composite-based systems. Still, their performance can be greater than several commercial products.⁶⁴⁷ By taking advantage of the (photo)catalytic activity of many ceramic nanofibers, the membranes can be potentially utilized to degrade or decompose the organic species in PMs, particularly with the aid of light irradiation. Currently, the main shortcoming of mats based on ceramic nanofibers as air filters is the requirement of heat treatment at high temperatures during their fabrication. This step makes the manufacturing procedure more complex and at a higher cost, compared with the mats based on polymer or composite nanofibers, significantly limiting their wide applications. On the other hand, this necessary manufacturing step enables the filter based on ceramic nanofibers to serve as a high-temperature-resistant filtration system. Another drawback of mats based on ceramic nanofibers lies in their intrinsic rigidity, fragility, and poor mechanical performance. To this end, filters based on the ceramic nanofibers are more suitable for applications in vehicle exhaust or other industrial filtration applications, where the mechanical strength or flexibility is less important and the environment is extremely harsh.

4.2. Treatment of Water

Nonwoven mats of electrospun nanofibers have been extensively explored as filters for the treatment of water, owing to their ability to simultaneously separate and degrade the pollutants in wastewater. Similar to the filtration of PMs from air, filters based on nanofibers can successfully remove particles of 3–10 μm in size (>95% rejection) from water without any significant drop in flow flux.⁶⁵² Electrospun nanofibers also offer an alternative

approach to the removal of toxic ions (e.g., heavy metal ions and phosphate) and organic pollutants (e.g., dyes, pesticides, and plasticizers) from wastewater via physisorption, chemisorption, electrostatic attraction, or a combination of these mechanisms.

4.2.1. Effective Adsorption at High Flux.—A large specific surface area for the nanofiber-based filter directly translates to a large number of adsorption sites and high adsorption capacity. The Brunauer–Emmett–Teller (BET) surface area is one of the most important parameters in determining the adsorption capacity of a nanofiber-based filter. In one study, a mat of nanofibers made of a blend of SiO_2 and TiO_2 exhibited high adsorption capacity and permeability in removing methylene blue from water (Figure 39A).⁶⁵³ By introducing hexadecyltrimethylammonium bromide (CTAB) as a pore generator, the BET surface area of the resultant mat reached $1032.6 \text{ m}^2/\text{g}$ with pores of $1.1\text{--}2.2 \text{ nm}$ in individual nanofibers. As such, the methylene blue molecules of $1.43 \times 0.61 \times 0.40 \text{ nm}^3$ in dimensions were predominantly captured in the mesopores of the nanofibers. Using such a porous mat, 45 mL of methylene blue solution was quickly purified with a removal efficiency of greater than 99% at a high flux of $1326 \text{ L}/(\text{m}^2\cdot\text{h})$ (Figure 39B). The high specific surface area, high diffusion speed through hydrophilic mesopores, and the electrostatic attractions between the nanofiber surface and the methylene blue molecules all contributed to the quick and effective purification. Remarkably, the nanofiber-based mats saturated with toxic organics can be readily recycled in a short period of time, avoiding secondary pollution to the environment. As shown in Figure 39C, the recycled mats of nanofibers made of a blend of SiO_2 and TiO_2 retained the same capability in removing methylene blue after calcination at 500°C for 4 h.
653

For the mats comprised of materials with inherently high chemical stability, such as those made of ceramic materials, they can be used under harsh conditions in the presence of acids, bases, and/or salts. For example, when a mat of SiO_2 nanofibers coated with flower-like MnO_2 particles was used in the presence of hydrogen peroxide, the oxidative degradation of methylene blue could be realized in a broad pH range of 0–14.⁶⁵⁴ The pores formed among nanofibers could effectively decrease the mass transfer resistance of liquid during the purification process. The mat with the flower-like MnO_2 particles on the SiO_2 nanofibers exhibited a much higher removal efficiency of 76% toward methylene blue at a much higher flux up to $490,000 \text{ L}/(\text{m}^2\cdot\text{h})$ relative to the conventional filters.^{653,654} This demonstration opens up a new avenue for water purification in a large-throughput, industrial setting.

4.2.2. Integration with New Active Adsorbents.—Superior purification capacity can be achieved for nanofiber-based mats when they are integrated with new active adsorbents. Active adsorbents, an important class of materials for water treatment, are commonly used in a powder form and thus are difficult to recycle. Upon immobilization, the adsorbents will be endowed with improved capacity, enhanced stability, and good recyclability. As a demonstration, a mat of TiO_2 nanofibers modified with hierarchically structured K_xMnO_2 nanoplates was explored as an effective filter to remove dyes such as Congo red in water. Upon deposition on the nanofibers, the K_xMnO_2 nanoplates were robust enough to survive from a relatively strong shear force caused by the flow of solution.³³⁸ The high specific surface area associated with the K_xMnO_2 nanoplates and the strong

electrostatic affinity between the K_xMnO_2 surface and Congo red molecules were responsible for the quick and efficient water purification. In contrast, the pristine TiO_2 nanofibers only exhibited a poor capacity under the same condition.³³⁸ In another example, water-stable MOF particles (e.g., $Zr_6O_4(OH)_4(COOH)_6\text{-}(BTC)_2$ or Zr-based MOF-808) were loaded into PAN nanofibers.^{137,138} The maximum adsorption capacities of Cd^{2+} and Zn^{2+} ions on the resultant mat reached 225.05 and 287.06 mg/g, respectively. The good compatibility between PAN and MOFs, arising from their organic moieties, prevented the MOFs in PAN nanofibers from leaking into the water, and the loading content of MOFs could reach a level as high as 20 wt %.¹³⁸ With the aid of nanofiber-based mats, numerous new active adsorbents can be easily constructed to obtain filters with easy recyclability and high flux filtration capability, significantly expanding the diversity of nanomaterials used in water purifications.

4.2.3. Selective Adsorption from a Mixture.—Selective removal of a targeted pollutant from water can be achieved either by immobilizing a specific capturing agent on the nanofiber's surface or tailoring the surface's wettability. For example, a mat of nanofibers with a low surface free energy and rough surface structure can selectively remove oil from polluted water, serving as an efficient means for oil–water separation during crude oil recycling.⁵⁸¹ In one demonstration, hydrophilic poly(*m*-phenylene isophthalamide) (PMIA) nano-fibers were functionalized to be superoleophilic by coating their surface with a layer of fluorinated polybenzoxazine- SiO_2 .⁶⁵⁵ While the octadecyl group provided by fluorinated polybenzoxazine at the side chain greatly lowered the surface free energy of the nanofibers, the hydrophobic SiO_2 nano-particles (7–30 nm) deposited on the surface greatly increased the roughness. The as-functionalized PMIA mats possessed an oil contact angle of 0° and exhibited an ability to selectively remove oil from an oil–water mixture, allowing for the fast removal of oil contaminant at a high flux of 3311 L/(m²·h).⁶⁵⁵

4.2.4. Degradation of Pollutants into Nontoxic Species.—When made of semiconductor oxides, the nanofibers can use sunlight to degrade organic molecules to nontoxic products (e.g., CO_2 and H_2O) or photocatalytically reduce toxic heavy metal ions to nontoxic products in water. For example, nonwoven mats of nanofibers made of a blend of TiO_2 and SiO_2 were demonstrated with superior photocatalytic activity for the degradation of rhodamine B. The mats showed performance comparable to that of commercial TiO_2 nano-particles (Degussa P25).⁶⁵⁶

Moreover, a control of intrafiber porosity in the nanofibers enabled the selective degradation of the targeted pollutants along with water filtration. In one study, core–sheath mesoporous $TiO_2@SiO_2$ nanofibers were fabricated by coaxial electrospinning to give 3–4 nm pores in the SiO_2 sheath and 6–8 nm pores in the TiO_2 core.⁶⁵⁷ In the presence of two different dyes, only methylene blue could selectively diffuse across the mesoporous SiO_2 sheath to react with TiO_2 in the core, whereas the Disperse Red S-3GFL molecules in a form of large aggregates were not photodegraded by TiO_2 . This merit allows the nanofiber-based mats to find use in practical applications, where the wastewater often has multiple components.

The mats of photocatalytic nanofibers can also be integrated with microfluidic devices for water purification in microreactors,⁶⁵⁸ by taking advantages of fine control over reaction

Author Manuscript
Author Manuscript
Author Manuscript
Author Manuscript

pathway and short diffusion distance.⁶⁵⁹ After sandwiching and sealing a mat of electrospun nanofibers between a glass slide and a PDMS substrate, a simple microreactor device was fabricated.⁶⁵⁹ With the interconnected pores and mesoporous structures, which contributed to a high specific surface area, the nanofiber-assisted microreactor exhibited greater water purification efficiency relative to that of the microreactor based on a conventional film. For instance, the microreactor based on a nonwoven mat of TiO₂ nanofibers allowed for enough contact with methylene blue to give superiority in photo-catalytic water purification. For a microreactor based on TiO₂ film, only a portion of the methylene blue could react with the limited TiO₂ surface, leading to a low degradation efficiency.⁶⁵⁹

4.3. Decontamination of Chemicals

Electrospun nanofibers have received great attention in the decontamination of harmful chemicals because of their high adsorption capacity.⁶⁶⁰ While serving the decontamination role, the nanofiber-based mats can also enhance the durability and tear strength of the protected textile. The decontamination performance can be greatly enhanced by incorporating active materials into the nanofibers through chemical modification. In one study, porous PAN nanofibers decorated with MOFs were prepared through the hydrothermal treatment of electrospun composite nanofibers made of a blend of PVP, PAN, and zinc acetylacetone in a 2-methylimidazole solution.⁶⁶¹ The nonwoven mat with an intrafiber porous structure exhibited a high adsorption capacity of 530.3 mg/g toward the U⁶⁺ ions in nuclear wastewater at pH = 3, owing to the surface complexation between the U⁶⁺ ions and the N atoms in 2-methylimidazole.⁶⁶¹

Filters with self-detoxification capability against lethal chemical warfare agents (CWAs) are highly desirable for the protection of human beings and the environment. Nanofiber-based mats play a critical role in the destructive decomposition of harmful chemicals during filtration. Preliminary tests using simulators of CWAs, such as paraoxon and dimethyl methyl phosphonate, immobilized on the nanofibers demonstrated effective decontamination.⁶⁵² In a recent work for catalytic hydrolysis of the simulators, flexible and self-standing mats of electrospun Zr-MOFs nanofibers were shown to exhibit fast and sustained degradation of organophosphate-based nerve agents.⁶⁶² This high performance can be attributed to the biomimetic phosphotriesterase activity endowed by Zr⁴⁺ ions, a Lewis acid, and the superior specificity and reactivity of MOFs toward the agents. A half-life as short as 2.4 min was obtained for the catalytic hydrolysis of dimethyl 4-nitrophenyl phosphate, and the decomposition efficiency remained at a level of above 90% over a long-term exposure of 2 h. Relative to Zr-MOF powders, the nonwoven mats made of Zr-MOF nanofibers were able to more quickly and effectively decontaminate the simulators of CWAs. The mats also enabled the efficient decontamination in a continuous-flow setting at a flux of 0.20 mL/min, showing good recyclability and structural stability.⁶⁶² The metal nanoparticles (e.g., Ag, Ni, and Ti) capable of catalyzing the decomposition of CWAs can also be incorporated into the nanofibers to further enhance the performance.⁶⁵²

4.4. Recovery of Precious Metals

The leaching of precious metal(s) from the catalyst during a catalytic process is a serious problem in both industrial catalysis and environmental remediation. There is a strong need to

keep the leached metal ions at a level below 1 ppm in the final products, as well as to recover the scarce and expensive metals for reuse. Nanofibers with proper functional groups on the surface can scavenge precious metal ions from a solution phase in high efficiency, owing to the strong binding between the functional groups and the metal ions and the large surface-to-volume ratio of a nonwoven mat. In one report, a freestanding mat made of TiO₂ nanofibers was demonstrated for removing precious metal ions from an aqueous solution to reduce their concentrations from 100 ppm to a level of parts per billion (ppb) (Figure 40A,B).⁵⁰³ The success relied on the use of an amino or thiol group conjugated to the surface of TiO₂ nanofibers through the siloxane chemistry. Both amino and thiol groups can rapidly form strong coordination bonds with precious metal ions (e.g., Pd²⁺, Pt⁴⁺, and Rh³⁺) and thus scavenge the ions from the aqueous solution. Specifically, when operated at room temperature in a continuous-flow setting at a flux of 1 mL/min, 99.95% of the Pd²⁺ ions were scavenged from an aqueous solution with an initial concentration of 100 ppm. Furthermore, the Pd²⁺ ions captured by the nanofibers could be chemically reduced to elemental Pd for the formation of Pd nanoparticles. The as-obtained nanoparticles exhibited a large number of active sites for use as an effective catalyst toward reactions such as Suzuki coupling in a continuous-flow reactor (Figure 40C). The Pd nanoparticles on the nanofibers showed good catalytic performance in terms of both activity and selectivity (Figure 40D).⁵⁰³ The good catalytic performance can be attributed to the ultrafine size (below 2 nm) of the nanoparticles and the possible synergy between the Pd nanoparticles and the TiO₂ nanofibers.

4.5. New Directions for Future Development

Recent studies have demonstrated that electrospinning offers a simple and versatile method for producing nonwoven mats with large surface-to-volume ratio and high porosity for niche applications related to environment and sustainability. Despite the tremendous progress toward the use of nanofiber-based membranes for water and air filtration, the efficiency and flux rate still need to be improved by further optimizing the composition, structure, and physiochemical properties of both individual nanofibers and their mats. Future work should be focused on the achievement of a comprehensive understanding of the molecular mechanisms responsible for the adsorption and desorption of ions/molecules at the active sites of the exposed surface and the transportation kinetics in the interconnected pores. A deep understanding of the mechanistic details will lead to the rational design and fabrication of nanofiber-based membranes.

Although surface functionalization of the mats can remarkably enhance their filtration performance, it often involves multiple steps, making it less desirable for the development of industrial products. Further efforts should be devoted to large-scale production of membranes through a single fabrication procedure with high reproducibility. Meanwhile, the toxicity of fibrous membranes, particularly those with the involvement of harmful organic solvents, for the handling and disposal of the nanofiber-based products still needs to be well-established. For commercial applications, understanding of the potential toxicity will contribute to the design of safe products. So far, little emphasis has been placed on the low-cost synthesis of high-performance filtration membranes. It is of key importance to explore environmentally friendly and facile routes while reducing the production cost. To this end, it

is an attractive idea to seek novel fibrous membranes that can harvest the power of sunlight for fast water treatment (e.g., decontamination, disinfection, and desalination) to directly produce potable water with high flux and at a low cost, particularly for the developing countries.

5. ELECTROSPUN NANOFIBERS FOR CATALYSIS, ENERGY, PHOTONICS, AND ELECTRONICS

Electrospun nanofibers have been extensively explored for applications related to catalysis, energy, photonics, and electronics. Owing to their large porosity, high specific surface area, and superb stability, electrospun nanofibers made of polymers, ceramics, and carbon are naturally good supports for various catalytic systems, especially those based on enzymes and metal nanoparticles. When fabricated with the right composition, nanofibers can support rapid conduction of electrons and/or intercalation of ions, opening the door to opportunities in energy harvesting, conversion, and storage. Notable examples include their use as electrodes or membranes for the fabrication of solar cells, rechargeable batteries, supercapacitors, and fuel cells, by which the energy harvested from various sources is converted to electricity or stored in the devices. Owing to the remarkable tolerance against mechanical deformations, the nanofiber-based devices can be made with flexibility and/or stretching capability. On the other hand, the ability to manipulate the composition, structure, morphology, and alignment of nanofibers has enabled their use in the fabrication of photonic and electronic devices, exemplified by both light-emitting diodes (LEDs) and field-effect transistors (FETs). In this section, we aim to showcase the promise of electrospun nanofibers in all these applications by highlighting a number of recent demonstrations.

5.1. Catalysis

Depending on the catalyst and reactant(s) involved, a catalytic process can be classified into three categories, that is, heterogeneous, homogeneous, and enzymatic catalysis.⁶⁶³ For heterogeneous catalysis, the catalyst and reactant(s) are in different phases (e.g., solid versus liquid or solid versus gas phases) and there exists a phase boundary. The catalyst is typically based on nanoparticles in an effort to increase the ratio of surface area to volume. Regarding homogeneous catalysis, the catalyst is molecularly dispersed in the same phase (almost always a liquid) that contains the reactant(s).⁶⁶³ Enzymatic catalysis usually occurs in an aqueous solution with the involvement of an enzyme, which can be either heterogeneous or homogeneous depending on the state of the reactants (or substrates), and whether the enzyme macromolecules are immobilized on a solid support or not. As a major advantage of heterogeneous catalysts, they can be readily separated from the reaction systems through centrifugation or other means. For homogeneous catalysts, it is more challenging to recover the catalysts, in particular, when a liquid medium is involved.

For heterogeneous catalysts, the nanoparticles (enzymes as well) are typically immobilized on solid supports. Nonwoven mats of electrospun nanofibers are attractive for use as catalytic supports because they offer a number of unique features, including (i) large specific surface areas; (ii) high porosity and fully accessible pores on/in individual nanofibers to effectively improve the transport kinetics; (iii) ability to protect the catalytic nanoparticles

Author Manuscript
Author Manuscript
Author Manuscript
Author Manuscript

from deactivation as caused by aggregation and/or leaching, particularly under harsh conditions; (iv) easy separation or recovery from the reaction medium; and (v) easy incorporation into a continuous-flow system. The nanofiber-based supports can endow the immobilized catalysts with enhanced activity, selectivity, durability, and thermal stability.

5.1.1. Immobilization of Enzymes.—Enzymes participate in many biochemical reactions that are necessary for life, including the biosynthesis of essential compounds and translation of genetic information, among others.⁶⁶⁴ Besides, enzyme-based catalysis is capable of transforming chemical manufacturing toward more sustainable and environmentally friendly processes, for example, the production of pharmaceuticals and value-added chemicals.^{665,666} However, enzymes are often unstable and sensitive to the surrounding environment. In particular, under harsh conditions (e.g., low or high pH value, elevated temperature, organic solvent, and UV irradiation), the enzymes can be autolyzed or damaged to lose the activities.⁶⁶⁴ To this end, enzymes can be immobilized in or on electrospun nanofibers to help preserve their configurations and thus the enzymatic activities and stabilities.⁶⁶⁷

Polymer nanofibers with porous, core–sheath, or hollow structures have been utilized as supports for immobilizing enzymes at a high loading level to produce biocatalytic nanofibers. The immobilized enzyme often exhibited half-life time increased by more than 100-fold when benchmarked against free enzymes in a solution.⁶⁶⁸ Compared with bulk films, the nanofibers also showed enhanced enzymatic activities by improving the mass transport of molecules to and/or from the active sites.⁶⁶⁹ Besides, when the nanofibers are used as nanoreactors, the local chemical and physical environments of the enzymes can be manipulated to further enhance the reaction kinetics, activity, and selectivity.

Immobilization of a Single Enzyme.: In general, a single type of enzyme can be immobilized (i) inside the nanofibers by directly electrospinning a polymer solution containing the enzyme or (ii) on the surface of electrospun nanofibers via physical adsorption or covalent grafting. Using the first method, the enzyme can be encapsulated with a high loading efficiency of nearly 100%. Since the activity of an enzyme will be drastically diminished when dissolved in an organic solvent,⁶⁷⁰ the enzyme is often dissolved in an aqueous polymer solution for electrospinning and thus immobilized on a water-soluble polymer (e.g., PVP and PVA). In this case, however, the enzyme can be easily leached out from the nanofibers in the presence of water. To address this issue, the enzyme-loaded nanofibers can be cross-linked. For instance, PVA nanofibers showed great resistance against water upon cross-linking with glutaraldehyde.⁶⁷¹ As a result, the α -galactosidase immobilized in cross-linked nanofibers could retain its hyperthermophilic nature with improved stability.⁶⁷¹ It should be pointed out that the chemical cross-linking agents may have potential adverse impacts on the performances of the enzyme, and residual chemicals can also be retained in the nanofibers as harmful impurities. Therefore, a purification step is often required.

The enzyme can also be immobilized inside nanofibers made of water-insoluble polymers. In one study, α -chymotrypsin was immobilized in nanofibers made of a blend of PS and poly(styrene-*co*-maleic anhydride) to significantly prolong its half-life time from 1 to 144 h.

⁶⁶⁹ By cross-linking the nanofibers with glutaraldehyde to achieve better leaching resistance, the stability of α -chymotrypsin was further enhanced. For this method, one remaining issue is the diminished enzymatic activity caused by the organic solvent. An alternative strategy is to immobilize the enzyme in the core of core–sheath nanofibers fabricated by coaxial electrospinning to help preserve the enzymatic activity. In this case, the diameter of the sheath must be optimized to allow for the diffusion of reactant molecules into the core of the nanofibers.

It is worth pointing out that the enzyme may irreversibly change its configuration due to the strong stretching force during electrospinning, resulting in poor performance relative to the pristine, support-free enzyme. When the stretching force is too strong, the enzyme can be denatured or damaged. This situation can be avoided by optimizing the strength of the electrical field.

Another straightforward method involves the immobilization of an enzyme on the surface of the as-spun nanofibers through physical adsorption or covalent grafting. In this case, the amount of the enzyme that can be immobilized on the nanofibers is often limited by the external surface area of the nanofibers, although the activity and stability of the enzyme are preserved. The amount and performance of the immobilized enzyme are mainly affected by their distribution and configuration.⁶⁶⁷

The enzyme-immobilized biocatalytic nanofibers can be applied as electrode materials to enhance the electrochemical performance and reduce the cost of biofuel cells or other types of energy conversion devices.⁶⁷² To achieve this goal, the polymer nanofibers are often converted into carbon nanofibers and then immobilized with an enzyme through the post-treatment method. In one study, porous carbon nanofibers immobilized with bilirubin oxidase showed remarkable performance in catalyzing the electroenzymatic oxygen reduction.⁶⁷³

Immobilization of Multiple Enzymes.: One of the most exciting developments in enzyme-carrying nanofibers is to immobilize multiple enzymes simultaneously in/on nanofibers for tandem reactions (also known as cascade reactions). In this case, the product of one enzymatic reaction serves as the substrate for the second reaction. As a result, the diffusion limitations can be bypassed owing to the close proximity of the substrate to the corresponding enzyme.⁶⁶⁸ To match the kinetics of the catalytic reactions and improve the overall enzymatic activity, the amount of each type of enzyme and the spatial distribution of the enzymes need to be precisely controlled. In one study, multiple enzymes, including 3 α -hydroxysteroid dehydrogenase, diaphorase, and nicotinamide adenine dinucleotide (a popular co-factor), were immobilized in the lumen of hollow polyurethane nanofibers (Figure 41A,B).⁶⁶⁸ By applying the hollow nanofibers as artificial cells for an assay to test the concentrations of bile acid, a good linearity was achieved in the concentration range of 0–200 μ M (Figure 41C). Compared with free enzymes, the nanofiber-based system demonstrated more than 170-fold enhancement in terms of half-life time for both the immobilized 3 α -hydroxysteroid dehydrogenase and diaphorase (Figure 41D).⁶⁶⁸

5.1.2. Immobilization of Catalytic Nanoparticles.—As another important class of catalysts, nanoparticles, with diversified compositions, sizes, and shapes, have been immobilized in and/or on electrospun nanofibers toward numerous heterogeneous catalytic reactions. In most cases, due to the favorable interactions between the catalysts and the solid supports, remarkable activity, selectivity, and long-term stability can be achieved.¹³³ Depending on the reactions, the catalytic nanoparticles can be immobilized on nanofibers made of polymers, ceramics, or carbon.

Polymer Nanofibers as Catalytic Supports.: Catalytic nanoparticles can be directly embedded in nanofibers by electrospinning a polymer solution containing well-dispersed nanoparticles. Notably, embedding the nanoparticles in porous nanofibers may allow certain reactants to reach the catalytic sites while excluding others, realizing selective catalysis toward a specific type of organic molecule.

Catalytic nanoparticles can also be immobilized on the surface of polymer nanofibers by simply immersing a mat of the nanofibers in a solution containing the corresponding precursors. For example, by immersing a mat of PAN nanofibers in ethylene glycol containing Na₂PdCl₄ and pyrrole, Pd nanoparticles were formed *in situ* and sandwiched between PAN core and PPy sheath.⁶⁷⁴ The resultant nanofibers exhibited superiority in catalytic performance toward the hydrolysis of ammonia borane for hydrogen generation. Such a simple procedure has potential for scaling up the production, moving toward practical applications in which large amounts of catalysts are often required.

It is also important to control the size, shape, and facet type of the catalytic nanoparticles immobilized on the nanofibers to achieve optimal catalytic performance. To this end, by atomic-layer-deposition, 2 nm Pd nanoparticles exposed with {111} active facets were immobilized on nylon nanofibers.⁶⁷⁵ Owing to the well-controlled size and facet of the Pd nanoparticles, the adsorption of negatively charged reactant and the hydrogen transfer could be facilitated during the reduction of *p*-nitrophenol. Even with a low immobilization amount of 20 µg/mg, the Pd nanoparticles could effectively catalyze the reduction of *p*-nitrophenol to generate *p*-aminophenol.⁶⁷⁵

In some cases, the metal can be leached out from the supported catalytic nanoparticles, leading to a decrease in catalytic activity. To avoid this situation, the structure or morphology of the nanofibers needs to be carefully engineered. In one study, poly(*p*-xylylene) was coated on the surface of composite nanofibers made of PLA and catalytic Au nano-particles (9 nm in size) through chemical vapor deposition.⁶⁷⁶ Upon pyrolysis, the PLA component was removed, leading to the formation of a semipermeable, tubular poly(*p*-xylylene) nanofibers (730 ± 83 nm in diameter) immobilized with Au nanoparticles on the inner surfaces. Toward the hydrolytic oxidation of dimethylphenylsilane and the alcoholysis of dimethylphenylsilane with *n*-butanol, the immobilized Au nanoparticles showed much higher activities than the case of free 3 nm Au nanoparticles. In addition, owing to the absence of metal leaching, the nanofibers could be reused for at least 18 rounds without any decrease in catalytic activity.

Carbon Nanofibers as Catalytic Supports.: Carbon nano-fibers are advantageous as supports for catalytic nanoparticles owing to their good chemical resistance, high electrical conductivity, and large specific surface area, as well as the remarkable mechanical strength. The composition, size, and distribution of the catalytic nanoparticles on the carbon nanofibers have all shown great influence on the catalytic performance, which can be controlled by varying the concentration of surface defects on carbon nanofibers. In a recent study, alloy nanoparticles were immobilized on carbon nanofibers via the carbothermal shock method, as described in section 2.4.2.³⁴¹ With the decrease of carbonization temperature, a higher concentration of surface defects was formed within the carbon nanofibers, leading to a more uniform distribution of the AuNi alloy nanoparticles on the nanofibers (Figure 42A). When the carbon nanofibers were coated with PtPdRhRuCe quinary nanoparticles for catalyzing the ammonia oxidation process, a conversion of ca. 100% was achieved for NH₃, together with an overall selectivity of 99% toward the generation of NO_x (NO and NO₂) versus N₂/N₂O (Figure 42B,C).³⁴¹ The pronounced performance can be attributed to a uniform distribution of the catalytic nano-particles on the carbon nanofibers.

The carbon nanofibers can also serve as a matrix to confine the nanoparticles, effectively preventing the nanoparticles from undesirable aggregation. In one study, Ni₂P nanoparticles (ca. 10 nm in diameter) were embedded in N-doped porous carbon nanofibers.⁶⁷⁷ Owing to the confinement effect provided by the nanofibers, the embedded Ni₂P nanoparticles could be prevented from irreversible fusion and aggregation, despite that the pyrolysis process was performed at a high temperature up to 700 °C. As a result, the Ni₂P nanoparticles still exhibited abundant exposed active sites toward the hydrogen evolution reaction.

Carbon nanofibers have been actively explored as solid supports for catalytic applications, in particular, electrocatalysis, where the support is often required to have a good electrical conductivity. The electrocatalytic performance is mainly determined by the exposed catalytic active sites, the channel, and distance for mass diffusion, as well as the pathway for electron transport. As such, the fiber-based catalytic systems, regardless of the types of materials for the supports, are expected to offer satisfactory performance in electrocatalysis.^{677,678} One should note that the carbon nanofibers have to be protected under inert atmosphere when applied to catalytic processes performed at high temperatures to prevent carbon from destruction by oxidation. In addition, the performance and lifetime of the applied catalytic nanoparticles are often limited by chemical and electrochemical corrosion of the carbon nanofibers. For instance, the Pt-immobilized carbon materials may undergo significant corrosion during an electrochemical reaction, leading to serious agglomeration and/or detachment of the supported catalysts, as well as the shortening of lifetime.

Ceramic Nanofibers as Catalytic Supports.: Ceramic nanofibers are another class of stable and robust solid supports for the immobilization of catalytic nanoparticles. Different from the carbon nanofibers, ceramic nanofibers can resist the corrosion for use in electrocatalysis, endowing the supported metal nanoparticles with better stability and activity via metal– support interaction.^{679,680} In one recent study, TiN hollow nanofibers were employed as a catalytic support for Pt nanoparticles toward oxygen reduction reaction (ORR) that is critical to the operation of a proton exchange membrane fuel cell (PEMFC).

⁶⁸¹ After accelerated durability tests (ADTs), the electrochemical surface area and mass activity of the nanofibers were only reduced by 6% and 14%, respectively, while those of the commercial Pt/C catalyst dropped by 44% and 46% (Figure 43A).⁶⁸¹

The ceramic nanofibers can also enhance the catalytic activity and durability of the catalytic nanoparticles. Notable examples include TiO₂ and ZrO₂ nanofibers that can serve as supports for Pt, Pd, Au, and Rh nanoparticles or nanorods. The as-obtained catalytic nanofibers exhibit good performance in a number of reactions, including the hydrogenation of azo bonds in methyl red (Figure 43B,C)^{42,335} with the use of Pt nanoparticles-immobilized TiO₂ nanofibers and the cross-coupling reactions.³⁰⁴ By taking advantage of the photocatalytic activity of some ceramic materials (e.g., TiO₂ and CeO₂), catalytic nanoparticles can be easily immobilized on the surface of nanofibers with a uniform distribution.^{306,333} In one study, Pt nanoparticles with an average diameter of 1.7 nm were photochemically deposited on porous CeO₂ nanofibers. When tested for the water gas shift reaction, the Pt-immobilized CeO₂ nanofibers exhibited high catalytic activity (with 95% CO conversion at 450 °C) and long-term stability (with CO conversion of 71% at 400 °C for 10 h), which could be attributed to the high porosity of CeO₂ nanofibers and the uniform distribution of Pt nanoparticles.³⁰⁶

It is feasible to regenerate and reactivate the catalytic nanoparticles immobilized on ceramic nanofibers for the purpose of recycling. For example, the Pd or Pt nanoparticles immobilized on TiO₂ nanofibers could be regenerated in an acidic solution, such as a diluted HNO₃ solution, at room temperature to obtain activity as high as a freshly prepared sample of the nanoparticles.^{304,335} From these demonstrations, ceramic nanofibers can be considered as an ideal catalyst support, especially for those reactions occurring under harsh conditions, allowing many important catalytic conversions to be performed with long-term durability.

Owing to the high porosity, regardless of the materials type for the solid supports, the nanofiber-based mat immobilized with catalytic nanoparticles also allows one to perform the catalytic reaction in a continuous-flow system without the need for product separation. In a typical setup, the catalytic mats can be placed in a column (e.g., a syringe) with a permeable plug at the bottom, and the reactants in a liquid solution or gas stream are allowed to pass through the mat at a constant rate to perform the catalytic reactions.^{304,335} In principle, the short diffusion distance within the mat and the high specific surface area of individual nanofibers allow the rapid diffusion of the reactants to the catalytic nanoparticles and of the products back into the reaction mixture efficiently.

5.1.3. Sinter-Resistant Heterogeneous Catalysts.—When a catalytic reaction is operated at an elevated temperature, the metal nanoparticles tend to sinter into larger structures in an effort to minimize the total surface energy, causing deactivation to the catalyst.⁶⁸² For example, the 3 nm Pt nanoparticles immobilized on TiO₂ nanofibers started to sinter at a temperature as low as 350 °C, eventually leading to a drastic loss of the catalytic activity.⁶⁸³ As a matter of fact, catalyst sintering is the main cause of deactivation for many important catalytic processes involving the use of elevated temperatures. There is an urgent need to develop catalysts resistant against sintering. Ceramic nanofibers can be carefully engineered or modified to make the catalytic nanoparticle sinter-resistant. In one

study, Pt nanoparticles were immobilized on TiO₂ nanofibers and then coated with a porous sheath of SiO₂.⁶⁸³ Even when calcined at a temperature as high as 750 °C, the Pt nanoparticles could maintain their original size without sintering (Figure 44A,B).⁶⁸³ When the nanofibers were applied to the hydrogenation of methyl red, the porous SiO₂ sheath could supply channels for the chemical species to reach the active sites on the Pt nanoparticles, allowing the catalytic reaction to proceed (Figure 44C).⁶⁸³

At the elevated temperature and pressure of a real application, however, the tiny pores in the porous protective sheath can be easily blocked by impurities (e.g., carbon) or simply collapse. To overcome this shortcoming, a sinter-resistant catalytic system was developed by selectively depositing SiO₂ only on the TiO₂ nanofibers while leaving the supported Pt nanoparticles mainly uncovered.⁶⁸⁴ As such, the Pt nanoparticles, with their surfaces exposed, were isolated from each other by the deposited SiO₂. The competitive interactions between Pt with the strongly interacting TiO₂ support and with the weakly interacting SiO₂ layer could lead to an effective energy barrier to inhibit the sintering of the Pt nanoparticles up to 700 °C, allowing the catalytic reaction to proceed effectively (Figure 44D–F).⁶⁸⁴

In retarding the sintering process, another strategy is to immobilize catalytic nanoparticles on the oxide nanofibers that can provide a strong chemical bonding with the metal. An example can be found in a highly reactive and sinter-resistant catalytic system, in which Pt nanoparticles were immobilized on the inner surfaces of porous CeO₂ hollow nanofibers (Figure 44G,H).³⁴⁰ The strong metal–support interaction in the Pt-immobilized CeO₂ catalysts could effectively stabilize the Pt nanoparticles against sintering up to 700 °C, enhancing the catalytic activities toward reactions involving rapid oxygen and/or electron transfer between the metal and the support. In addition, the porous walls, the hollow structures, and the open ends provided by the individual nanofibers also ensured high permeation and mass transfer rates for the chemical species involved in the catalytic reaction (Figure 44I).³⁴⁰ Enabled by the good sinter-resistance, the regeneration of a poisoned metal surface caused by, for instance, sulfur can be realized through a simple heat treatment, which is not possible for the traditional nanoparticles due to sintering.⁶⁸⁵ Most significantly, the achievement of sinter-resistant catalysts based on ceramic nanofibers allows one to make use of catalytic reactions or surface phenomena occurring at high temperatures.

5.2. Energy Harvesting, Conversion, and Storage

How to effectively harvest, convert, and store energy represents some of the persistent issues faced by our society. To address these issues, a wide variety of devices have been developed for use as solar cells, rechargeable batteries, and supercapacitors, as well as fuel cells. These devices are typically fabricated using two electrodes and an electrolyte, and conduction of electrons and/or ions plays a critical role in the operation of such devices. Naturally, nanostructured electrodes are excellent candidates for these applications because of their attractive properties such as high surface-to-volume ratio, large specific surface area, and short diffusion distance.⁶⁸⁶

Electrospun nanofibers, especially those made of metal oxides and/or carbon, have been actively explored for use as the electrode materials. Notably, a nanofiber-based electrode offers the desirable advantages such as a large electrode/electrolyte contact area, rapid

Author Manuscript
Author Manuscript
Author Manuscript
Author Manuscript

transfer of electrons and ions, and feasibility for functionalization to improve electroactivity. Furthermore, devices made of electrospun nanofibers have lightweight and good flexibility, making them attractive for energy applications. In this section, we will focus on the use of electrospun nanofibers for the fabrication of solar cells, rechargeable batteries, supercapacitors, and fuel cells, including a brief discussion on the remaining issues and challenges associated with the nanofibers.

5.2.1. Solar Cells.—Solar cells can be used to directly convert the energy of sunlight or an artificial light source into electricity, allowing for the generation of electrical power on a large scale. To realize a “low-carbon society”, solar cells, especially the third-generation solar cells (e.g., dye-sensitized solar cells (DSSCs) and perovskite solar cells (PSCs)) that can be fabricated using simple procedures and at low costs,⁶⁸⁷ will play a key role in energy harvesting.⁶⁸⁸

Dye-Sensitized Solar Cells.: Since the first report in 1991,⁶⁸⁹ DSSCs have been extensively explored because of their promising power conversion efficiency (PCE), low cost, and simple fabrication procedure. The PCE of DSSCs has been increased from 7% in 1991 to 14.3% in 2015 under the standard air mass 1.5 global conditions.⁶⁹⁰ Under indoor conditions with an artificial light source, DSSCs have been reported with an outstanding PCE over 20%.⁶⁹⁰

A DSSC is typically composed of an optically transparent film made of porous semiconductor (e.g., TiO₂) coated with a dye to harvest light as photoanode, an electrolyte containing the I⁻/I₃⁻ redox couples, and a piece of Pt foil as the counter electrode. Under light illumination, the dye molecules are photoexcited and oxidized to generate electrons, which are rapidly injected into the conduction band of the semiconductor. After randomly diffusing across the semiconductor film, electrons flow to the counter electrode via an external circuit. Meanwhile, the oxidized dyes are regenerated by accepting electrons from the reduced redox couples, and the oxidized redox couples are regenerated at the counter electrode by accepting electrons from the anode.^{689,691,692} The DSSC with good performance should provide enhanced light harvesting, fast electron transport, and reduced electron combination. Electrospun nanofibers have been explored as the photoanode, counter electrode, and electrolyte in either rigid or flexible DSSCs.

In general, the effective electron transfer in the porous oxide layer comprised of a semiconductor is often restricted by the random electron transport caused by electron scattering and by recombination at the grain boundaries.⁶⁸⁷ For the 1D oxide nanofibers, each nanofiber consists of fused or connected tiny (several to tens of nanometers) nanocrystals with fewer grain boundaries. This unique feature enables an effective diffusion of electrons along the axial direction of the individual nanofibers, avoiding the random electron transfer and significantly suppressing electron recombination. Moreover, the individual nanofibers with a high specific surface area and porosity can offer enriched sites for depositing a large amount of dyes while allowing for effective penetration of liquid or semi-solid electrolytes into the mesopores.

Metal oxide (e.g., TiO₂) nanofibers can be directly collected on conductive substrates to serve as the photoanode. It is crucial to ensure good adhesion and electrons transfer between the nanofiber-based porous mat and the substrate. To this end, a liquid oxide precursor can be filled between the mat and the substrate.⁶⁹³ During calcination, the precursor is converted to tiny nanoparticles to improve the adhesion. Alternatively, the mat and the substrate can also be bound together tightly by hot pressing.⁶⁹⁴ Another commonly used approach is to mix the fragile nanofibers with a polymer in the form of paste and then have the paste printed on a substrate using a doctor-blade method. After selective removal of the polymer matrix through calcination, the nanofibers will strongly adhere to the substrate. It is worth noting that when processed into a paste, the nanofibers, which are originally tens of micrometers long, tend to be broken into short segments of sub-micrometers to micrometers in length. The decrease in nanofiber length unavoidably impacts the electrical conductivity, which can be lowered by 1 order of magnitude (e.g., reduced from 1538 to 164 S/m in one typical case).⁶⁹⁵

The performance of the DSSCs critically depends not only on the materials used but also on the architecture of the photoanode. For example, the mats cross-aligned or vertically aligned relative to the conductive substrate are both featured with good performance. In one recent study, after post-treatment such as rolling up, stacking, and cutting, TiO₂ nanofibers aligned vertically to the substrate were explored as the photoanode.⁶⁹⁶ The vertical TiO₂ nanofiber arrays with a diameter of 90 ± 30 nm and a height up to 27 μm (Figure 45A) were attached on fluorine-doped tin oxide substrate by using TiO₂ nanoparticles as an adhesion layer (Figure 45B). The resultant DSSC showed a PCE of 2.87% (Figure 45C). Further improvement of the performance is expected upon optimization of the height of the vertical nanofibers, reduction of the diameter, and enhancement of the porosity.⁶⁹⁶

The thin layer of TiO₂ with high optical transparency can cause a large portion of sunlight to pass through the photoanode, limiting the performance of the resultant DSSC.⁶⁹⁷ To achieve a better light harvesting of the entire photoanode, a high level of dye loading and strong light scattering are two promising strategies. For instance, a larger interfacial area between the nanofibers and dyes can lead to a high absorbance of visible light from the numerous successive monolayers of dyes. In one study, porous TiO₂ hollow nanofibers with an average diameter of 130 nm and a wall thickness of 28 nm exhibited a specific surface area of 118 m^2/g , which was twice as high as that of solid TiO₂ nanofibers (59 m^2/g) with the same diameter.⁶⁹⁸ Arising from the enhancement of incident light absorption, the hollow nanofibers could double the amount of chemisorbed dyes (ruthenium dye, N719) and achieve a 33% increase in PCE relative to the case of TiO₂ solid nanofibers.⁶⁹⁸ Interestingly, the intrinsically porous structure usually endows the nanofiber-based mat with a strong light scattering ability to concentrate the incident light in the photoanode. The effect can be attributed to the matching between the pore size of the mat and the wavelength of sunlight, thus significantly enhancing the light harvesting efficiency via Mie scattering.⁶⁹⁷ For nanofibers with hollow interiors and/or hierarchical structures (e.g., with nanorods or nanoplates on the surface), they can effectively harvest the light through multiple reflections at a high photon efficiency. For example, owing to strong diffused reflectance, the DSSC based on nanorod-decorated TiO₂ nanofibers exhibited greatly enhanced PCE of 6.26%

relative to that (4.26%) of a device based on the conventional TiO₂ nanofibers (Figure 45D–F).⁶⁹³

In addition to photoanode, the nanofibers can also serve as the counter electrode materials owing to their key functions to collect electrons and catalyze the oxide/reduction reaction of I⁻/I₃⁻ redox couples. In general, Pt foil is the most effective counter electrode. However, it is too expensive and tends to degrade over time in a liquid electrolyte. To this end, carbon nanofibers of low cost, together with good charge transfer ability and stable corrosion resistance, have been demonstrated as a promising alternative to the commercial Pt electrode.^{687,699} The PCE can be significantly improved with the decrease of series resistance using thinner and highly porous carbon nanofibers to reduce the thickness of the counter electrodes. In one demonstration, the nanofibers comprised of a blend of carbon, graphene, and Ni were fabricated as novel counter electrode materials for efficient DSSCs. 700

In addition to electrode materials, nanofiber-based mats can also be utilized as solid or semi-solid electrolytes to replace the traditional liquid electrolytes and thus improve the durability and stability by avoiding the electrolyte leakage. For instance, quasi-solid-state DSSC with a mat of poly(vinylidenefluoride-*co*-hexafluoropropylene) nanofibers as the electrolyte exhibited excellent long-term durability.⁷⁰¹ It retained 96% of its initial PCE value after 13 days. Despite better durability, the PCE is often lower than those of DSSCs based on liquid electrolytes.

For satisfying the huge demand for flexible solar cells, electrospinning offers a promising approach toward device fabrication by offering an easy integration of electrode materials with plastic conducting substrates. In one study, TiO₂ nanoparticles were simply sprayed onto a mat of PVDF nanofibers.⁷⁰² Using the composite as a flexible photoanode, the resultant solar cell showed superior mechanical performance and high stability even after 1000 cycles of bending test, but exhibited a poor PCE (ca. 1%).⁷⁰² In another demonstration, Pt nanofibers were fabricated and then transferred and firmly attached to flexible substrates.⁷⁰³ Up to 94% transmittance could be obtained for the mat made of Pt nanofibers; see the left image in Figure 46A.⁷⁰³ Using the fiber-deposited substrate as a counter electrode, the DSSC could endure bending or twisting hundreds of times without peeling off the nanofibers from the substrate. In addition, the sheet resistance was over 170 Ω/sq, with a catalytic activity toward the reduction of I₃⁻ similar to the case of thermally evaporated Pt. By utilizing a mat of Pt nanofibers as a counter electrode (with a transmittance of ca. 85%) and TiO₂-nanotube arrays as a flexible photoanode, a high PCE of 3.82% of the resultant DSSC was achieved. Even after 200 bending cycles, the wearable DSSC could still maintain 90% of the original PCE (Figure 46B–D).⁷⁰³ Despite the low efficiency for these flexible DSSCs, they will have great potential applications in lightweight photovoltaic fields and other smart and portable electronic product areas.

Perovskite Solar Cells: The solar cells based on perovskite materials as light absorbers are termed as PSCs.^{704–706} Electrospun nanofibers also serve as promising building blocks in PSCs, which have recently achieved a remarkable PCE greater than 22%.⁷⁰⁴ Owing to the high porosity of the nanofiber-based mat, liquid perovskite precursors can easily penetrate

Author Manuscript
Author Manuscript
Author Manuscript
Author Manuscript

into the mat for quick crystallization of perovskite crystals on the surface of the nanofibers. For example, highly porous mats based on Zn_2SnO_4 nanofibers provided easy penetration of the $CH_3NH_3PbI_3$ solution in γ -butyrolactone for the quick crystallization of CH_3NH
 PbI_3 .⁷⁰⁷ The resultant PSCs exhibited remarkable performance with a PCE of 7.38%, higher than the case of PSC based on Zn_2SnO_4 nanoparticles (with a PCE of only 2.52%).⁷⁰⁷ By incorporating reduced graphene oxide sheets into porous Zn_2SnO_4 nanofibers, the PCE could be further improved to 13%.⁷⁰⁸ In another study, electrospun rutile SnO_2 nanofibers with flat cross-sections were used to provide better pathways and lower grain boundaries for charge transport, enabling the fabrication of a PSC with a high PCE over 16% and high stability.⁷⁰⁹

5.2.2. Rechargeable Batteries.—As a class of energy storage devices, rechargeable batteries have become an indispensable component of everyday life.^{710–712} Especially, lithium ion batteries (LIBs), one of the most explored rechargeable batteries, are playing a critical role in enabling the widespread use of home electronics and electric vehicles.⁷¹³ In the conventional LIB, the positive electrode is often based on a Li-intercalation compound (e.g., $LiMPO_4$, M = Fe, Co, or Ni),^{434,712} while the negative electrode is usually based on graphitic carbon. The two electrodes are separated by a solid separator. The sandwiched separator is soaked with a liquid electrolyte to transport lithium ions between the two electrodes. Upon charging, lithium ions are deintercalated from the positive electrode and intercalated into the negative electrode. This process is reversed during discharging.^{434,712} For an ideal rechargeable battery, it should have high energy density, long cycle lifetime, and good safety.

For electrode materials based on electrospun nanofibers, the ionic conductivity is markedly enhanced due to the shortening in ion diffusion pathway in LIBs and new generation batteries based on Na and Mg ions.^{714,715} In addition, the extremely long length of individual nanofibers can prevent themselves from aggregation during the charging/discharging process. To this end, electrospun nanofibers can serve as advanced electrode materials of high-performance rechargeable batteries featured with superb electrochemical performance, flexibility, and/or stretching capability, as well as good safety.

Strategies for Better Electrochemical Performance.: To achieve better electrochemical performance, one can optimize the composition and structure of the nanofibers used for the electrodes. When multiple components are incorporated into electrospun nanofibers in a controllable manner, the electrochemical kinetics and structural stability of the nanofiber-based electrode materials can be improved, when compared with the counterparts based on a single component. For instance, using the “gradient electrospinning” method described in section 2.4.4 and Figure 27, mesoporous $Li_3V_2(PO_4)_3$ hollow nanofibers (ca. 200 nm in outer diameter) were fabricated.⁴³⁹ By employing the nanofibers as the positive electrode, the resultant battery exhibited a high gravimetric capacity of 118 mA·h/g. Another efficient route to improve the electrochemical performance of the battery is to integrate ionic/electrical conductive materials in the nanofibers.^{711,716,717} For example, by applying the Si@carbon core–sheath nanofibers as the negative electrode, the LIB exhibited an outstanding electrochemical performance with a gravimetric capacity as high as 1384

mA·h/g at 0.1 C rate (where a 1 C rate represents a 1 h complete charging or discharging^{718,711}).

Owing to the ultralong structure, electrospun nanofibers have superb structural stability to resist the stress-induced cracking caused by volume expansion during the charging and discharging processes.⁷¹⁰ By engineering the secondary structures (e.g., porous and hollow) in each individual nanofiber, the enriched void spaces can effectively buffer the mechanical stress for restraining the structural deterioration. For example, batteries based on the above-mentioned mesoporous $\text{Li}_3\text{V}_2(\text{PO}_4)_3$ hollow nanofibers could be operated stably without cracking.⁴³⁹ Even performed after 9500 cycles at a high rate of 10 C, the LIB could retain a capacity 80% of its original value (Figure 47A), superior to the case of solid nanofibers.⁴³⁹

Strategies for Flexibility and/or Stretching Capability.: To achieve flexible and/or stretchable batteries, two key bottle-necks need to be addressed: (i) availability of flexible and/or stretchable electrode materials and (ii) achievement of good stability in terms of electrochemical performance at dynamic status.⁷¹⁹

Electrospun nanofibers usually exhibit exceptionally low flexural rigidities and remarkable tolerance against repeatedly mechanical deformations, holding great promise toward flexible batteries. Besides, the assemblies of nanofibers featured with free-standing and lightweight can directly serve as new binder-free flexible electrodes. In a recent study, a flexible electrode was fabricated by simultaneously electrospinning PAN nanofibers and electrospraying macroparticles made of Si and PAN (1–2 μm in size), followed by carbonization.⁷²⁰ This flexible negative electrode showed a high capacity of 1600 mA·h/g with capacity loss < 0.079% per cycle for 600 cycles.⁷²⁰

Well-aligned nanofibers have also been utilized to fabricate batteries with flexibility and excellent mechanical strength. Besides, owing to the parallel void space between the nanofibers, the individual nanofibers can be expanded without deforming the overall morphology of the electrodes during the charging and discharging cycles. For example, owing to excellent bending endurance, a flexible mat composed of aligned carbon nanofibers containing In_2O_3 nanoparticles was explored as a new negative electrode to produce flexible LIBs (Figure 47B).⁷²¹ When folded into different shapes, the flexible LIB (when using $\text{LiMn}_2\text{O}_4/\text{Al}$ foil as the positive electrode) could still serve as a stable energy source. Specifically, the flexible LIB showed negligible capacity loss after 120 times folding cycles (one cycle includes a horizontal fold and a vertical fold) (Figure 47C).⁷²¹

In some applications (e.g., wearable electronics), the batteries should be stretchable while maintaining their electrochemical functions under deformation. In a recent demonstration, an electrode based on PVDF@Ni@Si core–sheath nanofibers was fabricated by coating the stretchable PVDF nanofibers with Ni and Si layer by layer (Figure 47D). With the use of this stretchable mat as the negative electrode, the LIB showed ca. 20% stretching capability with a high capacity (1821 mA·h/g at 0.2 C) and long cycle life (56.9% capacity retention after 1000 cycles) (Figure 47E).⁷²² However, the 20% stretching capability is still not enough to be applied for most stretchable devices.

Strategies for Safety: In recent years, accidents related to fires and explosions of LIBs occur frequently worldwide, especially involving cell phones, laptops, and electric vehicles.⁷¹³ There is an urgent need to explore safer batteries. With the use of nanofiber-based materials, the safety issues of batteries can be addressed to a certain extent.

Lithium dendrite growth is one of the crucial reasons that cause serious safety hazards of LIBs. The lithium dendrite can pierce through the separator and provoke direct contact between the electrodes,⁷¹³ causing internal short-circuit in the battery.⁷²³ To retard the lithium dendrite growth, capturing the lithium ions by nanofibers based on polar polymers can guide the lithium ions to form uniform deposition.⁷²⁴ For example, when oxidized PAN nanofibers were deposited on top of the negative electrode, lithium dendrite growth could be inhibited significantly, leading to stable cycling with an average Coulombic efficiency of 97.4% over 120 cycles.⁷²⁴

Flammable liquid electrolyte is another crucial issue for safety concern.^{713,725} To address this issue, one promising strategy is to replace the flammable liquid electrolytes with nonflammable electrolytes, such as solid electrolytes. However, solid electrolytes commonly have low ionic conductivity.⁷²⁶ Using aligned ceramic nanofibers as ion-conductive fillers can enable the solid electrolyte with better ion transport. When integrated with well-aligned Li_{0.33}La_{0.557}TiO₃ nanofibers, for example, the solid electrolyte showed an ionic conductivity of 6.05×10^{-5} S/cm at 30 °C, which was 1 order of magnitude higher than the case using random nanofibers.⁷²⁷ Another strategy is to employ flame-retardant mat made of core–sheath nanofibers as a separator (as described in section 4.1.1), preventing sacrifice of the electrochemical performance. Once exothermic reaction goes out of control, the polymer sheath melts, and the flame retardant (in the core) will be released simultaneously, effectively avoiding the ignition of the electrolyte.⁷²⁵ For instance, owing to triphenyl phosphate@ poly(vinylidene fluoride–hexafluoropropylene) core–sheath fibers, the LIB showed nonflammability and similar electrochemical performance relative to the case based on a commercial polyethylene separator.⁷²⁵

5.2.3. Supercapacitors.—Supercapacitors, also known as electrochemical capacitors, are mainly used for energy storage. They offer a number of attractive features, including superior power densities, fast charging and discharging kinetics, excellent reversibility, and superb cycle lifetimes, as well as safe operation.^{728,729} A supercapacitor consists of a negative electrode, a positive electrode, and an ion-permeable separator soaked in an electrolyte that can dissociate into cations and anions.⁷³⁰ The two electrodes are usually made of capacitive materials (e.g., carbon, transition metal oxides or hydroxides, and conducting polymers). Basically, energy storage occurs at the interface of electrode and electrolyte. During the charging process, positive charges gradually accumulate on negative electrode while negative charges accumulate on the positive electrode. When these two electrodes are connected using a conductive wire with or without a load, a discharging process occurs.⁷³⁰ Until now, supercapacitors have still been plagued by their insufficient energy density, hindering their scope of applications, especially when a high-energy output is required.

As a novel class of electrode, the assembly of nanofibers made of capacitive materials can provide a large surface area accessible to the electrolyte, efficient electron and ion transport, and structural stability to prevent the electrode from destruction due to swelling and shrinkage. These attributes can contribute significantly to the high performance of a supercapacitor.

Strategies for Enhancing the Performance of a Supercapacitor: In principle, the energy density of a supercapacitor is in proportion to the capacitance and the square of cell potential.⁷²⁸ A high cell potential can be generally achieved by engineering the electrolyte (e.g., use of an organic electrolyte) and/or using an asymmetric electrode configuration.⁷²⁸ To increase the capacitance, porous nanofibers made of capacitive materials with high capacitances are advantageous. Higher capacitances can be readily obtained by engineering the distribution of pore size and increasing both ion conductivity and surface area of the nanofibers.⁷³¹ Notably, the interconnective pore structures within individual nanofibers are capable of introducing new electroactive sites and diffusion pathway to accelerate the kinetics of ion transport.⁷³² In one demonstration, featured with a continuous pore-size distribution from 0.64 nm to over 100 nm and high specific surface area up to 1912 m²/g, the carbon nanofibers showed an outstanding specific capacitance as high as 236 F/g at a current density of 5 A/g.⁴⁴¹ Meanwhile, the corresponding supercapacitors presented volumetric energy and power densities as high as 2.4×10^{-4} W·h/cm³ and 6.1 W/cm³, respectively, much larger than those based on graphene sheets or carbon nanotubes.⁴⁴¹

In addition, the pores naturally formed among the entangled nanofibers can provide void space for the enhanced loading of an active material. Meanwhile, the resulting denser architecture also provides a significantly larger contact area with the electrolyte and restricts swelling and shrinkage of electrode, contributing to superior electrochemical performance. For example, by simultaneously electrospinning and electrospraying, a nonwoven mat of polyindole nanofibers was filled with nanoparticles made of carbon nanotubes and polyindole.⁷³³ The mat showed a specific capacitance about 550 F/g and an excellent long-term cycling life with capacitance retention of 97.8% after 20,000 cycles.

Flexible Supercapacitors.: The key obstacle to the fabrication of flexible supercapacitors is the brittleness of carbon and most inorganic materials that cannot sustain repeated mechanical deformation. To address this issue, the assemblies of entangled nanofibers can serve as flexible, binder-free electrodes to achieve bendable, foldable, and wearable supercapacitors. With a proper design, the nanofibers with advanced architecture can significantly improve structural stability under different mechanical deformations, making it easy to recover their initial state after folding. For instance, inspired by the natural structure of bamboos, new bamboo-like carbon nanofibers with a periodic distribution of interior holes along the length and graded pore structure along the cross-section were fabricated, as discussed in section 2.4.4.⁴⁴¹ Strikingly, even under continuous dynamic operations of forceful bending (90°) and twisting (180°), the supercapacitor still exhibited stable electrochemical performances with 100% retention in capacitance (Figure 48A–C).⁴⁴¹ Such a supercapacitor holds great promise for the construction of high-performance flexible electronics.

Textile Format.: The nanofibers can be deposited on various supports to produce textile-type supercapacitors, holding great promise in integration with textile-based smart electronics. As the collector, electrically conductive textile (e.g., metal-coated cotton) can offer a robust support for nanofibers, avoiding the generation of brittle mats. In one study, PAN nanofibers containing carbon nanotubes were directly deposited on a Ni-coated cotton surface.⁷³⁴ The resultant supercapacitor showed a high areal capacitance of 973.5 mF/cm² (Figure 48D) and excellent electrochemical stability upon bending for 1000 cycles at a radius of 5 or 2 mm (Figure 48E). Notably, the supercapacitor can be readily tailored via conventional textile processing (e.g., sewing technology). For instance, three types of supercapacitor fabrics could be easily integrated into commercial textiles in desirable forms (Figure 48F,G).⁷³⁴ Still, the supercapacitors in the textile format often show low capacitance. Further improvement is expected by employing the nanofibers made of active materials with high capacitance and/or by using an asymmetric electrode configuration.

5.2.4. Fuel Cells.—Fuel cells represent another important class of electrochemical devices for energy conversion. They are able to convert chemical energy stored in compounds (fuels such as H₂, methanol, and ethanol) to electricity in the presence of electrocatalysts. Typically, a fuel cell has a sandwich structure, consisting of a cathode, an anode, and a layer of membrane and electrolyte between them. When the fuel is oxidized on the anode and oxygen is reduced on the cathode with the aid of electrocatalysts, electrons are transferred from the anode to the cathode while protons are transported through the layer of membrane and electrolyte, generating electricity. As long as fuel and oxygen are supplied, electricity can be continuously produced. Fuel cells represent one of the cleanest routes of energy conversion. When H₂ is used as the fuel, for example, the only byproduct to electricity is pure water.

The high porosity of a nonwoven mat of nanofibers and the interconnection among the pores can facilitate the mass transport of reactants, provide extensive contact between reactants and active sites on electrocatalysts, and promote electron and proton conduction. For the mats consisting of Pt-covered nanofibers, they can directly serve as electrodes.^{735,736} Additionally, a uniform distribution can be readily achieved for the Pt/C powder in a fibrous cathode by directly electrospinning the catalyst ink, enabling efficient proton transport and oxygen diffusion to the catalytic sites during the operation of a fuel cell.^{737,738} Over the past 2 decades, nanofibers made of polymers, metals, ceramics, and carbon have all been extensively explored for the fabrication of fuel cells in an effort to improve their efficiency and durability while reducing the cost.^{731,739,740}

Membranes Based on Polymer Nanofibers.: The semi-permeable membrane between two electrodes is a key component of a fuel cell, and it is typically made of an ionic conductive polymer such as Nafion. It can selectively transport protons through functional groups of the polymer while preventing fuel and oxidants from permeation.⁷⁴¹ By utilizing nonwoven mats of nanofibers made of Nafion (when blended with a carrier component such as PVDF) and related polymers as the semipermeable membranes, high proton conductivities were obtained, which could be optimized by adjusting the composition, diameter, and volume fraction of the nanofibers. Besides, the nanofiber-based membrane can achieve

Author Manuscript
Author Manuscript
Author Manuscript
Author Manuscript

reinforcement in terms of restricting water swelling and enhancing mechanical properties (i.e., strength and durability). Two commonly used approaches include filling the void space among nanofibers with an inert or uncharged polymer and creating a heterogeneous polymer blend and/or polymer/inorganic composite within individual nanofibers.^{742–744} In one study, the fuel cell involving a membrane based on nanofibers made of a blend of PVDF (a reinforcing polymer) and Nafion exhibited a high power output (1.31 W/cm^2), which was much greater than that with a commercial Nafion membrane (0.90 W/cm^2).⁷⁴⁵ In addition, the nanofiber-based membranes also consume less material than the conventional membranes, helping reduce the material cost of a fuel cell.

Electrodes and Electrocatalysts Based on Metallic Nano-fibers.: One of the current barriers to the commercialization of fuel cells lies in the sluggish kinetics of the ORR on the cathode. To meet the requirement on current output, a large amount of catalyst is often required. Currently, Pt and its alloys are the best-known ORR catalysts. Compared with the commercial Pt/C catalyst, self-standing Pt nanofibers can mitigate deactivation by hindering two main pathways: carbon corrosion and migration or agglomeration of Pt nanoparticles. In the Pt nanofibers, the Pt atoms cannot migrate as easily as in the tiny Pt nanoparticles of a commercial Pt/C catalyst. For instance, long, thin, and porous Pt–Fe alloy nanofibers showed a specific activity of 2.3 times higher than that of the commercial Pt/C catalyst.⁷⁴⁶ Remarkably, even under an extremely harsh condition, the porous Pt–Fe alloy nanofibers were stable, whereas the Pt/C catalyst degraded drastically.

Harvesting sunlight by plasmonic metal nanofibers is a promising strategy for enhancing the performance of fuel cells in terms of energy conversion. Plasmon-mediated electro-catalysis facilitates more efficient oxidation of fuels at the anode side. The generated hot electrons are responsible for preventing the metal catalyst from poisoning caused by covering the catalytic sites with byproducts such as CO.⁷⁴⁷ Under the irradiation of a halogen light bulb, for example, the Au nanofibers with a diameter of about 250 nm were demonstrated to break down the fuel into electrons and ions effectively. The electrocatalytic activity was increased by 1.61 times for methanol oxidation reaction and 2.07 times for ethanol oxidation reaction, respectively.⁷⁴⁷

Electrocatalysts Based on Doped-Carbon Nanofibers.: Owing to the high cost and declining activity of Pt, alternative catalysts based on nonprecious metals or metal-free materials are actively pursued. Carbon nanofibers are especially attractive as low-cost, metal-free electrocatalysts for fuel cells. However, the conventional pure carbon nanofibers generally exhibit an insufficient catalytic activity. With the activation of heteroatom dopants, the doped-carbon nanofibers are more active toward electrochemical reactions. Dopants such as N, B, S, and P have all been explored for adjusting the surface polarity, hydrophilicity, and electronic properties of carbon nanofibers. For instance, the electronegative N-dopants can induce the redistribution of both atomic charge density and spin density, consequently promoting the adsorption and reduction of O_2 .⁷⁴⁸ In one study, the high pyrrolic-N content was found to provide a high catalytic activity toward ORR for the N-doped carbon nanofibers, which was comparable to a commercial Pt/C catalyst in an alkaline medium.⁷⁴⁹ At 10,000 s post-ch chronoamperometric response, the current density of N-doped carbon

Author Manuscript
Author Manuscript
Author Manuscript
Author Manuscript

nanofibers only dropped by 6.6%, confirming good durability. There is no doubt that better catalytic activity and durability have been achieved for the low-cost, doped-carbon nanofibers when benchmarked against a commercial Pt/C catalyst. In general, the service lifetime of such a catalyst is mainly determined by the electrochemical corrosion of carbon nanofibers. Although multi-heteroatomic doping can provide a synergistic effect to facilitate O₂ reduction and electron transfer,⁷⁵⁰ it is still hard to precisely control the formation of multiple heteroatoms in carbon nanofibers.

Electrodes Based on Ceramic Nanofibers.: Solid oxide fuel cells (SOFCs) feature a high efficiency without the use of precious metals, but they are typically operated at a high temperature in the range of 700–1000 °C.^{751,752} The performance is mainly limited by the kinetics of ORR at the cathode side.⁷⁵³ The electrodes based on ceramic nanofibers offer several advantages: (i) high percolation; (ii) increased number of triple-phase interface where O₂ molecules, electrons, and protons react at catalytic sites;⁷⁵⁴ (iii) continuous pathway for electron and ion transport; (iv) good thermal stability at the operating temperature; and (v) easy infiltration by the electrolyte.⁷⁵⁵ As a result, these attributes enable the SOFCs to be operated at a reduced temperature. Compared with commercial powders and crushed nanofibers, longer and thinner nanofibers can provide a smaller tortuosity factor (Figure 49A), contributing to more efficient charge and mass transfer pathways.⁷⁵⁶ For example, when an assembly of PrBa_{0.5}Sr_{0.5}Co₂O_{5+δ} hollow nanofibers was used as the cathode, the SOFC had a power density of 1.11 W/cm² at 550 °C when humidified H₂ and ambient air were used as fuel and oxidant, respectively (Figure 49B,C).⁷⁵⁷ This power density was much higher than that of the SOFC involving a cathode derived from nanosized powders with a similar composition. The fibrous architecture also contributed to the excellent stability under the operating conditions. Specifically, when operated at a constant voltage of 0.6 V at 550 °C for more than 260 h, the fuel cell still showed a stable and high power output at 0.95 W/cm².⁷⁵⁷

5.3. Light-Emitting Devices

Light-emitting devices can produce light in a variety of colors on the basis of electroluminescence or photoluminescence.⁷⁵⁸ As a representative light-emitting device, a LED is typically constructed by sandwiching the p-type and n-type semi-conductors layer(s) made of inorganic or organic materials, between the anode and cathode.⁷⁵⁹ When a suitable voltage is applied between the two electrodes, the electrons recombine with holes at the p–n junction, releasing the energy in the form of photons. Until now, how to further improve the efficiency of LEDs still remains a major challenge. Remarkably, the characteristics of nanofibers, including ultrafast charge carrier transfer and good molecular alignment along the fiber axis, make them attractive in exploiting new LEDs with high efficiency, good stability, and flexibility.⁷⁶⁰

In general, the semiconducting nanofibers in a cylindrical shape contact the substrate tangentially, causing insufficient injection and extraction of the charge carriers. Upon a mild thermal treatment below the melting point, polymer nanofibers can be easily flattened, forming adequate electrical contact. For instance, ribbon-like poly[(9,9-dioctylfluorenyl-2,7-diyl)-alt-co-(1,4-benzo-{2,10,3}-thiadiazole)] nanofibers displayed a strong

electroluminescence in an organic LED.⁷⁶¹ Besides, light-emitting nanofibers can be precisely positioned on the substrate by near-field electrospinning (Figure 50A).⁷⁶²

Regarding durability, unstable semiconductors can be stabilized when encapsulated in nanofibers. For example, perovskite quantum dots made of cesium lead halide (CsPbX_3 , X = Cl, Br, and I) often undergo hydrolysis even when exposed to atmospheric moisture for only 10 min.⁷⁶⁰ By contrast, when encapsulated in hydrophobic poly(styrene-butadiene-styrene) nanofibers, the $\text{CsPb}(\text{Br}_{0.8}\text{I}_{0.2})_3$ nanocrystals could maintain bright photoluminescence in water for up to 1 h (Figure 50B).⁷⁶⁰ Better stability was also achieved by embedding the same nanocrystals in PS nanofibers, which could protect the $\text{CsPb}(\text{Br}_{0.8}\text{I}_{0.2})_3$ from damage in water for up to 192 h at room temperature or even for 2 h when heated at 80 °C.⁷⁶³ By directly covering two of these green and red mats onto a blue LED chip to mix the three basic colors together, the device was able to emit bright light close to sunlight.⁷⁶⁰

Flexible and/or stretchable light-emitting devices are crucial in wearable optoelectronics. When the luminescent components are encapsulated in elastic nanofibers, the light-emitting devices can be made with excellent stretching capability.⁷⁶⁰ As shown in Figure 50C, a high strain of 170% was achieved for the above-mentioned $\text{CsPb}(\text{Br}_{0.8}\text{I}_{0.2})_3$ nanocrystals-encapsulated poly(styrene-butadiene-styrene) nanofibers.⁷⁶⁰ Furthermore, the transparent, flexible, and conductive (e.g., Ag⁷⁶⁴ and Cu²⁸⁷) nanofiber-based substrates hold great promise in fabricating flexible light-emitting devices. For example, flexible organic LEDs based on Ag nanofibers showed greater bending endurance, together with higher luminance and stronger brightness relative to that based on commercially rigid indium tin oxide (ITO) (Figure 50D,E).⁷⁶⁴ Besides, by direct coating an electrode layer on core–sheath nanofibers, flexible light-emitting device can be easily constructed. For instance, in a typical core–sheath nanofiber, a core made of Galinstan liquid metal could serve as the cathode, and a sheath made of a blend of $[\text{Ru}(\text{bpy})_3]^{2+}(\text{PF}_6)^{-} \cdot 2$ and PEO could act as the electroluminescent layer. By further vapor-evaporating a layer of ITO on the outer surface of the core–sheath nanofiber to serve as the anode, strong light emitting was obtained.⁷⁶⁵ These light sources can be easily integrated into micro-/nanofluidic devices for on-chip illumination.

5.4. Field-Effect Transistors

FET utilizes an external electric field to control the charge transport behaviors of the device. A classic FET normally includes three key components: (i) three terminal electrodes termed as source, drain, and gate; (ii) an active channel; and (iii) a dielectric (typically, oxide) separating the gate electrode from the channel.^{766,767} When charge carriers flow from source to drain through the channel, a drain-source current will be generated. The current can be manipulated by applying a voltage bias at gate electrode with respect to drain or source electrode. The performance of a FET is mainly characterized by the field-effect mobility (μ_{FE}) and on/off current ratio ($I_{\text{on}}/I_{\text{off}}$).⁷⁶⁸ I_{off} is the drain-source current through the channel whenever the device is turned off, and I_{on} is the drain-source current once the device is turned on. Achieving high μ_{FE} and large $I_{\text{on}}/I_{\text{off}}$ are two major requirements for the development of FETs. When a nanofiber-based mat is utilized as the channel, the charge carriers can move through it at a rate several orders of magnitude higher than that through a

thin film.^{769,770} The enhancement in mobility can be attributed to the preferential orientation of polymer chains, enhanced $\pi-\pi$ stacking along the fiber axis, and the geometrical confinement provided by the nanofibers.

The coverage density of nanofibers on the substrate of an FET is a critical parameter that can affect the charge carrier mobility in the channel and thus the performance of the FET. In general, a low fiber density can cause an inadequate number of pathways for electrons, whereas excessive fiber density can weaken the ability for current modulation due to the uneven morphology and overlapping among the nanofibers.⁷⁷¹ Both μ_{FE} and I_{on} can be optimized by tightly controlling the fiber density. For example, by varying the deposition density of Gd-doped In_2O_3 nanofibers (60.2 ± 5.2 nm in diameter) on a substrate, optimal performance was achieved for the FET with a μ_{FE} value of $2.83\text{ cm}^2/(\text{V}\cdot\text{s})$ and an I_{on}/I_{off} value of 4×10^8 .⁷⁷¹

Welding at the cross-points of a nonwoven mat is another effective strategy to decrease the high contact resistance among the nanofibers and thus improve the performance of the FET. For example, by welding the cross-points among Hf-doped In_2O_3 nanofibers and utilizing the resultant mat as the channel, the μ_{FE} value was increased from 4.4 to $25\text{ cm}^2/(\text{V}\cdot\text{s})$ with reference to the device based on nanofibers without welding.⁷⁷²

The alignment of nanofibers has also been demonstrated to contribute to the performance of an FET. Upon deposition of aligned poly(3-hexylthiophene) nanofibers on a flexible polymer substrate for use as the channel, the as-obtained flexible FET had a μ_{FE} value of $\sim 2\text{ cm}^2/(\text{V}\cdot\text{s})$, which was calculated from the transfer characteristic curves in Figure 51A.⁷⁷³ The FET device also exhibited a good linear relationship between the maximum I_{on} and the number of the deposited nanofibers ranging from 1 to 10 (Figure 51B).⁷⁷³ Such deformable FETs are well-suited for the fabrication of highly sensitive sensors to be integrated with other flexible electronics, for example, embedded in electronic skin for application in soft robotics.

5.5. New Directions for Future Development

Rapid progress has been made in expanding electrospun nanofibers to applications in catalysis, energy, photonics, and electronics. As a platform technique, electrospinning can be directly applied to produce catalytic supports for either metal nanoparticles or enzymes in a continuous and scalable fashion. One of the existing hurdles that restrict the development of nanofiber-based catalytic systems is the poor mechanical strength of the nanofibers, especially for those based on ceramics due to their intrinsic brittleness. Despite a few demonstrations, it is still challenging to fabricate nanofiber-based catalytic systems with the desired mechanical properties. In addition, the irregular size and shape associated with the metal nanoparticles fabricated *in situ* on the surface of nanofibers make it difficult to uncover the structure–property relationship and further improve the catalytic performance. Future efforts should be directed to the use of catalytic nanoparticles with well-defined and controllable size, shape, and facet type. Meanwhile, a comprehensive understanding of the electrochemical processes taking place on the surface of a nanofiber-based system is also critically needed due to the unique feature size and pore structure of a nonwoven mat of

nanofibers. It will also be interesting to elucidate the possible synergistic effect arising from the multiple components of a nanofiber-based system.

Owing to the intrinsic flexibility of nanofibers, they are anticipated to find widespread use in the next-generation smart textiles. Despite recent demonstration of flexible devices related to energy, photonics, and electronics, it is still necessary to further enhance the flexibility and elasticity of the active materials while maintaining the high efficiency. Moreover, it is also important to precisely control the deposition of nanofibers in terms of the amount, pattern, and coverage density on a given substrate, in an effort to reduce the size of a device while retaining its functionality and performance. To this end, combining electrospinning with new techniques such as 3D printing represents an attractive direction for future development.

New opportunities have also been created by advanced characterization techniques, such as confocal Raman spectroscopy, that can provide information about the molecular structures of individual nanofibers such as the orientation of polymer chains. The application of these techniques has provided a wealth of new knowledge and propelled the research field into new directions. Based on the new knowledge, exciting applications of electrospun nanofibers can be extended to new frontiers, including the design and fabrication of micro-/nanoscale devices. At the moment, a detailed understanding of the catalytic and electrochemical mechanisms involved in a nanofiber-based system is still missing due to the complexity of such a catalytic system. With the help of advanced in situ tools, such as electron microscopy, it will be helpful to directly observe the dynamical changes occurring in a nanofiber-based system under the working conditions. These new directions will enable the researchers to develop new strategies and formulate design rules for the development of more effective catalysts, as well as next-generation devices for energy harvesting, conversion, and storage.

6. ELECTROSPUN NANOFIBERS FOR BIOMEDICAL APPLICATIONS

Over the past two decades, electrospun nanofibers have found widespread use in a variety of biomedical applications. By engineering their structures and properties, including diameter, porosity, alignment, stacking, patterning, surface functional groups, mechanical properties, and biodegradability, both 2D and 3D scaffolds have been designed and fabricated to control cell migration and/or stem cell differentiation for enhancing the repair or regeneration of various types of tissues (e.g., nerve, skin, heart, blood vessel, and musculoskeletal system) and tissue interfaces. Besides, electrospun nanofibers have been actively explored for cancer diagnosis and construction of *in vitro* 3D tumor models for cancer research. Cancer treatment has also been reported by manipulating the migration of cancer cells using uniaxially aligned nanofibers and/or by incorporating drugs into nanofibers for controlled release. Furthermore, electrospun nanofibers have been applied as implant coatings, barrier membranes, and filtration membranes, among others, for the improvement or development of biomedical devices.

6.1. Tissue Repair or Regeneration

Tissue repair or regeneration involves the integration of scaffolding materials, cells, and/or biological factors to promote tissue growth by providing a suitable combination of mechanical support, topographic guidance, and biochemical instruction to the cells. In

developing the scaffold, it is of critical importance to mimic the native extracellular matrix (ECM) as close as possible in terms of composition, architecture, and other properties.

In native tissues, cells are typically surrounded by a large amount of ECM, a collection of extracellular molecules secreted by the cells. The composition of ECM varies across tissues, all of which, however, provide the cells with a structural support, signaling cues, and a medium for the diffusion and convection of oxygen and nutrients. The ECM of most tissues contains three major classes of macromolecules: (i) structural proteins (e.g., collagen and elastin), (ii) complexes of proteins and polysaccharides (e.g., proteoglycans) for entrenching the structural proteins, and (iii) adhesive glycoproteins (e.g., fibronectin and laminin) for attaching cells to the matrix.⁷⁷⁴ The ECM of bone also contains inorganic substances derived from calcium phosphate, with a significant amount of >70% in dry weight, to account for its high mechanical strength.⁷⁷⁵ In addition, native ECM contains intrinsic biochemical cues, including growth factors and other soluble biomolecules, which play vital roles in regulating the phenotype and function of cells during development, homeostasis, and response to injury.⁷⁷⁶

In terms of architecture, native ECM can be considered as a 3D network assembled from fibrous structures. Collagen represents the most abundant ECM structural proteins, existing as nanofibers with diameters in the range of 50–500 nm. Each collagen nanofiber is comprised of multiple fibrils (10–300 nm in diameters) which are made of collagen triple helices.⁷⁷⁷ The orientation of collagen nanofibers can be either random or highly ordered depending on the type of tissue. For example, the collagen nanofibers in normal skin do not have any ordering, whereas those in tendon, ligament, and skeletal muscle are organized into highly oriented bundles.

To mimic the functions of ECM, electrospun nanofibers have been extensively explored as a class of scaffolding materials, owing to their unique ability to recapitulate the composition, length scale, and architecture typically of native ECM.⁷⁷⁸ From the viewpoint of composition, a wide variety of synthetic and natural polymers can be directly electrospun into nanofibers, and nanoparticles can also be readily integrated with the nanofibers.⁷⁷⁹ In particular, collagen, elastin, and some proteoglycans in ECM can be either used separately or blended together, as well as mixed with synthetic polymers, to fabricate electrospun nanofibers with diameters in the range of 50–500 nm. When blending synthetic and natural polymers at an optimal ratio, one can produce a ECM substitute with the desirable mechanical strength and biodegradability.^{243,780,781} Furthermore, the adhesive glycoproteins in ECM can be simply coated onto the surface of the as-spun nanofibers via electrostatic interaction, physical adsorption, and/or covalent grafting. To accelerate the establishment of a microenvironment that replicates the native tissue, the growth factors and other soluble biomolecules existing in ECM can be readily incorporated into the core of nanofibers during coaxial or emulsion electrospraying, and then sustainably released into the surrounding.⁷⁸² Biological effectors can also be loaded in nanoparticles and then integrated with nanofibers via encapsulation and/or surface coating. In general, it is easier to engineer a scaffold based on nanofibers to mimic the architecture of native ECM when benchmarked against other techniques. At the microscopic level, it is straightforward to engineer the surface topography of a scaffold. Topographical cues, including the diameter, alignment, and porosity of

Author Manuscript
Author Manuscript
Author Manuscript
Author Manuscript

individual nanofibers, as well as their assembled structure or pattern, can all be tailored to manipulate the behavior and fate of cells, controlling the outcome of tissue repair or regeneration. At the macroscopic level, it is possible to engineer the bulk structure of a scaffold, such as changing from a single layer to multiple layers or from 2D to 3D architectures, to match the shape or morphology of the target tissue.

In addition to replicating the composition and architecture of ECM, other requirements also need to be met in order to fully recover the function of the target tissue. During tissue regeneration, for example, the scaffold should only serve as a temporary ECM to promote the recruitment and proliferation of cells that are supposed to secret biomolecules and growth factors into the surrounding microenvironment for the construction of permanent ECM. As a result, the scaffold is supposed to degrade and eventually disappear during tissue neogenesis, and it is of critical importance for the inward growth of cells to exactly fill the space left behind by the degradation of the scaffold. Ideally, one should avoid the use of polymers, such as PLA and PLGA, that will release acidic compounds upon degradation. This issue can be addressed either by modifying the polymer with basic groups or mixing the polymer with a material that will release alkaline compounds upon degradation, such as alkaline polysaccharide (e.g., chitosan).

A variety of nanofiber-based scaffolds have been developed for regulating cell behaviors, such as the migration of cells and the differentiation of stem cells. By combining structural guidance with cellular components and/or bioactive molecules, electrospun nanofibers can improve the repair or regeneration of various types of tissues, including the repair of nerve injury, healing of wound, patching of myocardium defect, bridging of vascular rupture, remodeling of musculoskeletal tissue, and construction of interfaces between different tissues, etc. In this section, we start with a discussion on the progress in using electrospun nanofibers to regulate cell migration and stem cell differentiation. We then focus on the repair or regeneration of various types of tissues by briefly introducing the native anatomy and function of a tissue, highlighting the challenges for its regeneration, and then showing examples to illustrate how to engineer electrospun nanofibers to match the architecture of native tissue for optimal repair or regeneration.

6.1.1. Cell Migration.—Cell migration plays a central role in a wide variety of biological phenomena, ranging from embryogenesis to wound healing, tissue regeneration, and cancer spreading.⁷⁸³ Skin regeneration, for example, involves the re-establishment of the dermis, which can be accelerated by promoting the migration of fibroblasts to the wounded area.⁷⁸⁴ As such, a solid understanding of the factors that control cell migration is essential to the design of scaffolds with all features necessary for a seamless integration between the regenerated and native tissues. Starting from the mechanism of cell migration, we will discuss how this process can be accelerated by engineering the parameters and properties of electrospun nanofibers.

Mechanism of Cell Migration.: Cell migration is a complex process comprising multiple, sequential steps such as adhesion, polarization, and forward movement.^{785–787} The migration of a single cell is based on the establishment of a polarized cytoskeletal arrangement, the polarized organization of membrane trafficking, and the polarization of

Author Manuscript
Author Manuscript
Author Manuscript
Author Manuscript

signaling cascades (Figure 52A).⁷⁸⁷ At the front of the cell, cytoskeletal reconstruction leads to the formation of membrane protrusions such as filopodia and lamellipodia, offering a driving force for movement. The rear portion of the cell also actively participates in cell displacement via actomyosin contraction. The microtubule network and the intracellular membranes are also organized in a polarized manner along the direction of migration. As for the migration of collective cells, the molecular mechanism is similar to the case of single-cell migration, as shown in Figure 52B,C. In this case, the leader cells are clearly polarized under the stimulation arising from interactions with ECM and soluble factors (e.g., growth factors and chemokines) to initiate the migration. Afterward, the cell–cell communication between the follower and the leader cells will also play an important role in promoting the collective movement of cells.

Parameters Affecting Cell Migration.: Cell migration can be directed using various types of signals, including topographical, chemical, and mechanical cues.⁷⁸⁸ When prepared with the right diameter, alignment, surface chemistry, and mechanical properties, nanofibers can serve as effective substrates or scaffolds to control the migration of cells. The research activities include engineering the parameters and properties of nanofibers to investigate the migration of both normal or cancer cells *in vitro* and *ex vivo*, as well as exploration of tissue repair or tumor elimination *in vivo*. In this section, we focus on a set of cues provided by electrospun nanofibers for controlling the migration of cells *in vitro* and *ex vivo*. Detailed discussions on manipulating the migration of cells in wound healing and cancer treatment can be found in sections 6.1.4 and 6.2.3, respectively.

Through the contact guidance exerted on cells, electrospun nanofibers have been aligned into different patterns to manipulate the migration direction and speed of cells. On random nanofibers, cells tend to migrate along all possible directions without directionality, resulting in a short distance of translocation.⁷⁸⁹ On uniaxially aligned nanofibers, cells are directed to migrate along the nanofibers, together with a greatly increased migration speed.^{790,791} Taking the migration of astrocytes on scaffolds made of random and uniaxially aligned PLA fibers as an example, the cells cultured on uniaxially aligned PLA fibers were able to partially close a gap of 2.25 mm wide in 2 days, whereas the cells cultured on random PLA fibers remained relatively static even after 5 days (see Figure 53A,B).⁷⁹² The regulation of cell migration by fiber alignment also works for stem cells. For nanofibers with a similar diameter, both human neural progenitor cells and bone marrow-derived mesenchymal stem cells (MSCs) migrated at faster rates on uniaxially aligned nanofibers relative to the case of random nanofibers.^{793,794}

In some applications, for example, the regeneration of dural tissue, the cells are required to migrate from the periphery toward the center, and this can be achieved using a scaffold made of radially aligned nanofibers. In an *ex vivo* study, dural tissues were separately cultured on scaffolds comprised of random and radially aligned nanofibers.²³⁵ Panels C and D of Figure 53 show snapshots of the dural fibroblasts migrating from the surrounding tissue to the center of the corresponding scaffold after incubation for 4 days. On the scaffold comprised of radially aligned nanofibers, the entire surface was covered by the cells, whereas a void remained on the scaffold made of random nanofibers. Upon implantation, the scaffold

comprised of radially aligned nanofibers is expected to provide an interface to interact with the natural dura and thus promote migration of host cells from the periphery to the center.

In addition to the alignment, the diameter of nanofibers is another critical parameter that affects cell migration. In one study, people studied the migration of Schwann cells on uniaxially aligned PLA fibers with three different diameters: large (1325 ± 383 nm), intermediate (759 ± 179 nm), and small (293 ± 65 nm).⁷⁹⁵ The cells migrated the furthest on the fibers with the largest diameter among the three groups. The authors argued that the fibers with a larger diameter were more densely packed, impeding the Schwann cells from crossing onto nearby fibers. However, the effect of fiber diameter on cell migration also depends on the composition of the polymer and the cell type. For example, when aligned tussah silk fibroin fibers of 400, 800, and 1200 nm, respectively, in diameter were compared, the 400 nm fibers showed the best performance in promoting the migration of bone marrow-derived MSCs.⁷⁹³ Depending on the type of cells involved, the diameter of the nanofibers should be optimized case by case.

The functional groups on the surface of nanofibers also affect cell migration by regulating the interaction between the cells and nanofibers. Since cell migration is a process involving the adhesion and subsequently forward movement of cells, the strength at which the cells adhere to the nanofibers is of great importance in controlling the migration of cells. When the adhesion strength is too strong, the cells will lose mobility because of their confinement to the surface. At a very weak strength, the focal adhesion will not be formed, and thus the cells cannot move forward either. Many efforts have been made to improve the migration of cells by modifying the surface of nanofibers with biochemical cues through encapsulation, electrostatic attraction, adsorption, and covalent conjugation. The easiest way is to coat the surface of nanofibers with bioactive agents such as proteins and growth factors to adjust the interaction between the cells and the underneath fibers. One study compared the migration of primary dural fibroblasts on scaffolds made of radially aligned nanofibers with or without fibronectin coating.²³⁵ The fibronectin coating was found to greatly enhance cell adhesion, improve the uniformity of cell distribution, and increase the speed of cell migration.

To better guide the migration of cells along a specific direction, the bioactive agents can be applied as a gradient on the nanofibers. In this case, the cells prefer to migrate upward along the concentration gradient of the bioactive agent. The gradient can be produced by modifying the protocols for physical adsorption, chemical conjugation, and electrical deposition, as well as through the use of microfluidic mixing. A commonly used method is to vary the immersion time of a nanofiber-based mat in a solution of a bioactive agent along a particular axis. With the gradual addition of the bioactive agent solution, the amount of the agent deposited on the surface of the mat increases along the axis. As a result, a gradient of the bioactive agent will be formed. This approach has been successfully applied to generate a gradient of fibronectin on uniaxially aligned nanofibers, leading to the observation of a clear dependence of the number of NIH-3T3 cells on the protein content.⁷⁹⁶ As a major drawback, this approach requires the use of a large amount of expensive bioactive agents in a considerable volume of solution to generate the gradient. A more effective strategy is to generate a gradient of BSA on the surface of nanofibers and then fill the bare regions left behind by the bioactive agent to generate a gradient that runs countercurrent to the BSA

Author Manuscript
Author Manuscript
Author Manuscript
Author Manuscript

gradient.⁷⁹⁷ This strategy can also be used to generate a circular gradient of an active protein along radially aligned nanofibers.⁷⁹⁸ In a typical procedure, the central portion of a scaffold was raised by a copper wire to take a cone shape. Then, the scaffold was placed in a container (upright or upside-down), followed by dropwise addition of a BSA solution into the container. A gradient in BSA amount was generated along each nanofiber. The bare regions uncovered by BSA were then filled with an active protein of interest. Compared to the case of a uniform coating of laminin or epidermal growth factor on the surface of radially aligned PCL nanofibers, the gradient significantly promoted the migration of fibroblasts or keratinocytes from the periphery to the center.

Bioactive agents can be immobilized on the surface of nanofibers by leveraging either the electrostatic attraction or covalent bonding between the bioactive agents and the functional groups on the nanofibers. This approach offers another efficient route to the generation of a gradient of biochemical cue by controlling the density of functional groups on the nanofibers. In one study, nanofibers made of a blend of PCL and collagen were collected in a radially aligned fashion to generate a gradual increase in fiber density from the periphery to the center.⁷⁹⁹ When the collagen regions of the nanofibers were conjugated with the collagen-binding domain-fused stromal cell-derived factor-1 α , a circular gradient of the bioactive agents was produced along the nanofibers. This gradient could induce neural stem cells to migrate from the periphery to the center of the nanofiber mat. Other techniques, such as electrospraying, microfluidic mixing, and electrohydrodynamic jet printing, have also been combined with electrospun nanofibers to generate gradients of bioactive agents. When a microfluidic gradient generator was overlaid on nanofibers made of hyaluronic acid, a gradient of vascular endothelial growth factor along the direction of fiber alignment was produced.⁷⁸⁸

The migration of cells is also sensitive to the mechanical properties of the nanofibers. On the nanofibers with different moduli, the migration speed of cells can vary significantly. In a study related to the migration of cancer cells on core–sheath nanofibers, PCL served as the “sheath” to conserve the surface chemistry of the nanofibers while different types of polymers, including gelatin, poly(ethersulfone), and PDMS, were used for the “core” to modulate the mechanical properties of the nanofibers.⁸⁰⁰ The fastest migration speed (ca. 11 $\mu\text{m}/\text{h}$) was achieved for a single glioblastoma multiforme cell cultured on the nanofibers with an intermediate modulus (ca. 8 MPa, pure PCL). In comparison, slower migration speeds were observed for the nanofibers with both lower and higher moduli, that is, ca. 3.5 $\mu\text{m}/\text{h}$ for ca. 2 MPa (gelatin@PCL), ca. 6.3 $\mu\text{m}/\text{h}$ for ca. 30 MPa (PDMS@PCL), and ca. 5.8 $\mu\text{m}/\text{h}$ for ca. 30 MPa (poly(ethersulfone)@PCL). By varying the mechanical properties, electrospun nanofibers can be employed to examine the migration behavior of cancer cells and thus obtain a unique high-throughput, *in vitro* culture substrate to develop antimigration therapies for cancer treatment.

6.1.2. Stem Cell Differentiation.—Stem cells have the remarkable ability to perpetuate themselves through self-renewal and to generate mature cells of a particular tissue through differentiation.⁸⁰¹ They are emerging as one of the fundamental underpinnings of tissue biology, which allow the tissues to be replenished with fresh cells throughout life.⁸⁰² With the control of local tissue microenvironments, known as “niches”, the pluripotency of stem

Author Manuscript
Author Manuscript
Author Manuscript
Author Manuscript

cells can be maintained or regulated. Until recently, scientists primarily worked with embryonic stem cells and nonembryonic “somatic” or “adult” stem cells. Induced pluripotent stem cells (iPSCs) represent another type of widely studied stem cells, which are obtained by genetically reprogramming adult cells to an embryonic stem-cell-like state.

To regulate the proliferation and differentiation of stem cells for tissue engineering, scaffolds are normally designed to imitate the physical, chemical, and biological features of the stem cell niches.⁸⁰³ Electrospun nanofibers can be engineered to control the fate of stem cells by providing a right combination of topographic cues, physical characteristics, and biochemical niches.^{804,805} With the use of functional polymers and/or biochemical agents, the nanofibers can offer a progressive microenvironment to control stem cell proliferation and specific differentiation. In terms of the physical, chemical, and biological features provided by electrospun nanofibers, here we only discuss how they can be engineered to control the differentiation of stem cells.

One can regulate the fate of stem cells by altering the physical parameters of a nanofiber-based scaffold, including surface topography, dimensionality, and mechanical properties. Surface topography, such as fiber orientation and surface roughness, has been found to strongly affect stem cell differentiation. For example, by switching from a nonwoven mat of random nanofibers to an array of uniaxially aligned nanofibers, adipose-derived MSCs and human iPSCs-derived MSCs were both encouraged for tenogenic differentiation (Figure 54A,B).^{806,807} In addition, a blend of PLGA, graphene oxide, and silk was used to fabricate scaffolds consisting of multiple layers of orthogonally oriented nanofibers.⁸⁰⁸ An interplay of the orthogonal architecture and the mineralization of nanofibers promoted the differentiation of bone marrow-derived MSCs into osteoblasts.

In addition to straight nanofibers, those with a complex structure were shown to present a stronger influence on inducing stem cell differentiation. For example, coiled PCL fibers, which were collected in a coagulation bath containing ethanol, triggered mild myofibroblastic differentiation of bone marrow-derived MSCs (Figure 54C,D).⁸⁰⁹ Aligned nanofiber yarns, braided/woven/knitted yarn networks, and composites made of nanofiber yarns and hydrogels also show promise in inducing the differentiation of adipose-derived MSCs to anisotropic soft tissues.⁸¹⁰

The surface roughness of nanofibers also affects the generation of specific cell types from stem cells. Pores and protrusions can be created on nanofibers to increase the surface roughness. By varying the relative humidity during electrospinning, porous fibers made of a blend of poly(ethylene oxide terephthalate) and poly(butylene terephthalate) were fabricated with different degrees of surface roughness (Figure 54E).⁸¹¹ It was demonstrated that a higher degree of roughness enhanced the expression of osteogenic genes, whereas a lower degree of roughness enhanced the chondrogenic differentiation of human mesenchymal stromal cells. In another study, island-like chitosan protrusions were generated on PLA nanofibers (Figure 54F).⁸¹² The chitosan protrusions provided rough topography on the nanoscale, accelerating the mineralization of hydroxyapatite and increasing the alkaline phosphatase activity of the preosteoblast cells.

Scaffolds with surface patterns have also been designed to promote a specific phenotype of stem cell differentiation. For example, the differentiation of human iPSCs toward cardiac cells was achieved using a honeycomb-compartmented monolayer of gelatin nanofibers.⁸¹³ A net-like mat made of PLA and gelatin nanofibers, displaying both random and parallel arrangements, promoted the osteogenic differentiation of bone marrow-derived MSCs.⁸¹⁴ Compared with a traditional 2D-patterned surface, 3D scaffolds with patterned topography are advantageous in enhancing the infiltration as well as the specific differentiation of stem cells, especially for the potential use in hierarchical tissue regeneration. As a simple example, a 3D scaffold possessing interconnected micro-and macropores was fabricated through layer-by-layer assembly of aligned nanofibers made of PCL and hydroxyapatite.⁸¹⁵ The scaffold significantly promoted the osteogenesis-related gene expression of human fetal osteoblasts. In another example, a 3D nanofiber-based scaffold was fabricated to mimic the zonal organization of articular cartilage, and it could significantly promote the chondrogenic differentiation of human mesenchymal stromal cells relative to a nonwoven mat of the same nanofibers.⁸¹⁶

The mechanical properties of nanofibers and the mechanical stimulation conditions also affect the fate of stem cells. Manipulating the local mechanical properties of a scaffold is crucial in designing a scaffold for driving the differentiation of stem cells.⁸¹⁷ To this end, nanofibers with variable mechanical and biochemical properties were fabricated by altering the weight ratios of Tecophilic and gelatin in the nanofibers.⁸¹⁸ The differences in gelatin content and thus scaffold stiffness contributed to the observation of changeable phenotypes of smooth muscle cells (SMCs). Scaffolds with a higher gelatin content and weaker stiffness could guide the differentiation of SMCs into contractile phenotype and reduce the proliferation of SMCs. In this case, the stiffness seemed to play a more important role than the biochemical cue.

Electrochemical cue has also been integrated with nanofibers to regulate the differentiation of stem cells. In one study, cardiovascular disease-specific iPSCs were cultured on uniaxially aligned nanofibers made of PANi and polyetersulfone.⁸¹⁹ By applying electrical pulses to the cellular mat in a unidirectional manner to mimic the unidirectional wave of electrical stimulation in heart, the iPSCs were induced to differentiate into cardiomyocytes. Using a fiber-based scaffold made of piezoelectric materials such as poly(vinylidene fluoride-trifluoroethylene), an electrically active microenvironment was generated without the use of an external power source.⁸²⁰ Under dynamic loading, the piezoelectric scaffold under the influence of a low voltage promoted the chondrogenic differentiation of bone marrow-derived MSCs, whereas that under a high voltage promoted the osteogenic differentiation.

Biological cues involving growth factors, peptides, proteins, signal inhibitors, and even cells have been incorporated into nanofiber-based scaffolds to direct the differentiation and lineage commitment of stem cells.^{821–823} In one study, the local mechanical property was integrated with biological cues to control stem cell differentiation.⁸²⁴ Electrospun PCL nanofiber yarns were processed into plain-weaving fabrics interlaced with multiple PLA filaments, leading to a better mechanical property compared with the traditional PCL nanofibers. After co-culturing adipose-derived MSCs with human tenocytes and human

umbilical vein endothelial cells on the woven fabrics, the cells expressed higher upregulation of tendon-associated markers than that in the case of nonwoven mats made of PCL nanofibers. When incubating the tricultured constructs under a dynamic mechanical stimulation, it was demonstrated that dynamic stretch could further promote the total collagen secretion and tenogenic differentiation.

Integrating the physical, electrochemical, and biological cues together into the same scaffold shows a high synergistic effect on the control of stem cell differentiation. To this end, an all-inclusive scaffold was fabricated by electrospinning serum albumin into nanofibers and subsequently doping with hemin to confer conductivity.⁸²⁵ The scaffold was then functionalized with different recombinant proteins and growth factors. This scaffold actively provided a supportive microenvironment and presented topographical guidance, bioactive molecule incorporation, and electrical stimulation to substantially promote neuronal differentiation of the human iPSC-derived neural stem cells.

6.1.3. Peripheral Nerve Repair.—As illustrated in Figure 55A, peripheral nerve can be considered as an enclosed, cable-like bundle of nerve fibers or axons.⁸³⁶ An axon refers to the long, slender projection of a neuron, and the axon is typically wrapped in the myelin sheath comprised of Schwann cells and then surrounded by a layer of connective tissue known as the endoneurium. The axons are grouped into fascicles, with each fascicle coated by a layer of connective tissue called the perineurium. Finally, the entire nerve is wrapped by a layer of connective tissue referred to as the epineurium.⁸²⁷

Although the peripheral nervous system has a greater capacity for axonal regeneration after injury relative to the central nervous system, spontaneous nerve repair is always incomplete in terms of function recovery.⁸²⁸ In particular, spontaneous nerve regeneration can only occur for defects smaller than a few millimeters, and the repair of gaps greater than 10 mm still remains a major challenge in the clinic.⁸²⁶ For a large nerve gap, it is impossible to achieve tension-free neurorrhaphy by simply suturing together the nerve stumps. In this case, the interposition of a nerve guidance conduit (NGC) between the nerve stumps is required in order to bridge the gap and support axonal regrowth.⁸²⁸ In designing and fabricating the NGC, it is critical to include all the topographic and biochemical features of a native nerve in an effort to maximize neurite extension and Schwann cell growth, improving the outcome of nerve repair.

The research in this area has focused on the control of topographic cues, together with the integration with electrochemical cues and incorporation of biochemical cues in some cases.^{828,829} For *in vitro* studies, planar scaffolds are usually utilized to investigate the extension of neurites by taking rat pheochromocytoma (PC12 cells) and dorsal root ganglia (DRG) bodies as neuron models, as well as to examine the growth of Schwann cells. For *in vivo* studies, the scaffolds are often presented as NGCs with a tubular structure. Rat sciatic nerve injury models are most commonly used to evaluate the repair performance of NGCs in terms of small nerve gaps below 10 mm in length. For nerve gaps of 2–50 mm in length, rabbits and large mammals such as sheep, pigs, and monkeys are used to evaluate the performance of NGCs, and animal models for nerve gaps up to 60 mm have also been reported.⁸³⁰

Promoting Neurite Extension and Schwann Cell Growth in Vitro.: Electrospun nanofibers with uniaxial alignment have been extensively explored for neural tissue engineering.^{831,832} In particular, uniaxially aligned nanofibers can provide ECM-like microenvironment to direct cell alignment and neurite extension (Figure 55B).^{833,834} The nanofibers can be further modified with pores, grooves, or other secondary structures as additional topographic cues to promote neurite extension and/or Schwann cell growth (Figure 55C).^{389,835,836} When increasing the surface roughness by coating PLA nanofibers with graphene oxide nanosheets, the extension of neurites from PC12 cells along the fiber alignment and the proliferation of Schwann cells were significantly promoted.⁸³⁷ The surface roughness of the nanofibers can also be adjusted using electrosprayed particles. To this end, a continuous or discrete density gradient of biodegradable microparticles was electrosprayed on a glass slide through a mask to control the durations of deposition at different positions, showing impact on the extension of neurites from the body of DRG.⁸³⁸ This method can be further extended to vary the surface roughness of a nanofiber-based scaffold, offering a unique system for investigating the effects of two different types of physical cues on neurite extension.

In addition to the physical cues provided by the nanofibers, electrochemical cues derived from electroactivation also affect neurite extension and/or Schwann cell growth. Electroactive materials, including piezoelectric and conductive polymers, allow for the direct delivery of electrical, electrochemical, and/or electromechanical stimulation to cells in nerve repair.^{839,840} For example, piezoelectric nanofibers made of poly(vinylidene fluoride-trifluoroethylene) have been explored to promote neurite extension.⁸⁴¹ Due to their piezoelectric nature, the electrical stimulus can be delivered to cells without an external power source. However, the control over this type of stimulus is limited due to the requirement of mechanical strain. Different from the piezoelectric materials, conductive polymers allow for excellent control of the electrical stimulus through the external application of a potential drop. By taking advantage of the high conductivity, nanofibers made of conductive polymers have been used to promote neurite extension and/or Schwann cell growth.^{839,842} In one study, PPy was coated on the surface of PCL nanofibers to form conductive core–sheath nanofibers by combining electrospinning with aqueous polymerization.^{843,844} Under electrical stimulation, the neurite extension from DRG on the nanofibers was promoted regardless of the orientation of nanofibers (Figure 55D,E).^{843,844} PPy has also been coated on nanofibers made of a blend of poly(L-lactide-*co*- ϵ -caprolactone) (PLCL) and silk fibroin to demonstrate augmented neurites extension from PC12 cells and enhanced proliferation of Schwann cells under electrical stimulation.⁸⁴⁵

Biological cues are often integrated with the topographic and electrochemical guidance provided by nanofibers to promote neurite extension and/or Schwann cell proliferation. For example, by incorporating nerve growth factor into the core of nanofibers made of a blend of PANi, PLCL, and silk fibroin, the synergistic effect of electrical stimulation and nerve growth factor promoted both neurite extension from PC12 cells and Schwann cell growth.⁸⁴⁶ In addition, uniaxially aligned nanofibers functionalized with bioactive agents (e.g., laminin and nerve growth factor) were found to be effective in enhancing the guidance for neurite extension along the fiber alignment.^{797,847} In particular, by modifying uniaxially aligned

nanofibers with a gradient of nerve growth factor, the neurites extending from DRG along the increasing gradient were significantly longer than those extending against the gradient, indicating the synergistic effect of the topographic cue provided by the nanofibers and the chemotaxis offered by the gradient of nerve growth factor.^{797,798}

In addition, uniaxially aligned PCL nanofibers have been utilized as substrates to direct the differentiation of bone marrow-derived MSCs toward Schwann cells under in vitro chemical induction.⁸⁴⁸ The as-derived Schwann cells were used to promote the extension of neurites from both PC12 cells and DRG along the orientation of fibers (Figure 55F,G).

Design of NGCs for in Vivo Assessment.: For in vivo studies, the NGCs were initially made of a porous foam rod or a single hollow tube.^{849,850} Unfortunately, using a single hollow guide is not adequate to mimic the spatial arrangement of ECM and cells in a native nerve.^{825,850} As such, scaffolds designed to bridge peripheral nerve defects have evolved from a single hollow tube to more complex, multitubular conduits.^{826,851} The conduits can be further combined with physical, chemical, and biological cues that are important for Schwann cell migration and proliferation, and for axonal elongation. Intraluminal channels can be introduced into the NGC to construct a multichannel conduit.^{828,851–854} For example, PTFE sticks or other removable club-shaped templates and expendable sucrose fibers were used to generate channels with a controllable size within the lumen of NGCs by removing the templates or dissolving the sucrose fibers after the NGCs had been shaped (Figure 56A,B).^{826,851,855} In addition, NGCs incorporated with physical fillers (e.g., fibers, filaments, gels, and sponges) in the lumen have also been reported to offer topological cues for improving nerve regeneration.^{828,856–859} For example, nanofiber sponges with abundant macropores and high porosity made of a blend of PLCL and silk fibroin could serve as the filler inside a fibrous tube made of the same materials (Figure 56C).⁸⁵⁷ An array of electrospun PLA or laminin-coated PLGA nanofiber yarns with longitudinally aligned orientation have been explored as the biodegradable fillers within the NGC lumen as well (Figure 56D).^{859,860} Overall, compared with the NGCs made of a single tube, NGCs with multichannels or biomaterial-based fillers can better mimic the architecture of nerve fascicles and are able to, therefore, reduce the dispersion of regenerated axons within the NGC lumen, greatly enhancing the recovery of function.⁸²⁸

6.1.4. Wound Healing.—Wounds refer to injuries, usually restricted to those caused by physical means, to living tissues. Owing to its unique location, skin is particularly susceptible to injuries. As a multilayered structure, mammalian skin is primarily comprised of epidermis and dermis, which are located above the subcutaneous tissue that is abundant in fat.⁸⁶¹ The epidermis and dermis encompass keratinocytes and fibroblasts, respectively, embedded in ECM. During the continuous renewal of skin, keratinocytes are accumulated in the basal part of the epidermis, followed by their gradual migration toward the top layer of epidermis. Upon reaching the outermost layer, the keratinocytes undergo a specialized form of programmed cell death (commonly known as cornification) to generate the so-called stratum corneum composed of dead cells embedded in a lipid matrix.

Skin wounds are typically trauma-induced defects, which involve a number of cellular reactions from different types of cells, including immune cells and repairable cells. The

Author Manuscript
Author Manuscript
Author Manuscript
Author Manuscript

healing of such a wound normally experiences four consecutive phases: hemostasis, inflammation, migration/proliferation, and maturation/remolding.^{862,863} Minor wounds can heal through the body's intrinsic repair process, whereas the healing of large-scale or full-thickness wounds, such as extensive burns or chronic wounds of diabetic patients, requires the assistance of scaffolding materials to promote the migration and infiltration of repairable cells.⁸⁶³ A number of other processes or issues also need to be taken into consideration during wound healing, including anti-infection and anti-inflammation, reduction of scar formation, wound healing in diabetic patient, and prevention from skin cancer.

Electrospun nanofibers have been actively explored as a dressing material for wound healing. By engineering the nanofibers to provide topographical and biological cues, the migration and infiltration of repairable cells can be enhanced as expected. Once the nanofiber-based scaffolds have been optimized *in vitro* for the promotion of cell migration and/or delivery of biomolecules, they are subjected to evaluation for wound healing *in vivo* using a mouse, rat, or rabbit model.

Migration and Infiltration of Repairable Cells.: Collective cell migration is essential in the wound healing process.⁸⁶⁴ The topography of nanofibers has a major impact on the migration and growth of cells involved in the wound healing process, including both keratinocytes and fibroblasts. Inspired by the basketweave-like pattern of collagen fibrils in the native skin, scaffolds made of crossed nanofibers were fabricated.⁸⁶⁵ Compared with either random or uniaxially aligned nanofibers, the crossed nanofibers exhibited the best healing performance in terms of accelerating the migration of fibroblasts and keratinocytes *in vivo*. In another study, scaffolds made of chitosan@PCL core–sheath fibers with a cotton-wool-like and fluffy architecture were fabricated using emulsion electrospinning.⁸⁶⁶ The scaffolds promoted efficient infiltration and growth of fibroblasts and keratinocytes *in vitro*, achieving full-thickness wound healing within 3 weeks in a rat model.

The infiltration of fibroblasts from surrounding tissues into the interior of a 3D scaffold is critical to the regeneration of dermal ECM. To this end, a sandwich-type scaffold was designed for skin regeneration.⁸⁶⁷ The scaffold consisted of a mat of radially aligned nanofibers at the bottom, a mat of nanofibers with square-arrayed microwells at the top, and microskin tissues in between. Such a 3D scaffold could serve as a wound dressing by enhancing cell infiltration and excluding drainage at the wound site. In another study, a 3D scaffold comprised of PCL nanofibers and silk fibroin nanoparticles was fabricated to combine the desirable spatial cues with surface topography and chemistry.⁸⁶⁸ Using a temperature-controllable cold plate as the collector, the accumulation of ice crystals and deposition of nanofibers simultaneously occurred on the plate. As such, the electrical conductivity of the collector was continuously increased, enabling the collection of nanofibers as a relatively thick mat. When evaluated *in vivo* using a rat model, this scaffold supported the infiltration of native cells and showed the promise for wound healing with an efficacy comparable to the commercial Matriderm artificial dermis.

Biological cues, which are usually combined with scaffolds by immobilization on the surface or incorporation into the core of the nanofibers, are able to actively aid the healing and tissue regeneration at local wound sites *in vivo*. A variety of bioactive agents such as

Author Manuscript
Author Manuscript
Author Manuscript
Author Manuscript

active proteins, growth factors, genes, and herbal medicines have been incorporated into the nanofibers for enhancing wound healing.^{869,870} For example, as we discussed in section 6.1.1, scaffolds comprised of radially aligned PCL nanofibers coated with circular gradients of laminin or epidermal growth factor could accelerate the migration of fibroblasts and keratinocytes, respectively, from the periphery toward the center of the scaffolds *in vitro*, showing the potential for large-area wound healing.⁷⁹⁸ In another study, a collagen-coated bilayer scaffold comprised of a porous cotton-wool-like 3D layer and a mat made of chitosan@PCL core–sheath nanofibers was designed for burn wound healing.⁸⁷¹ The architecture and composition of the scaffold, as well as the coating of collagen, effectively accelerated the healing of third-degree burn wounds created in a rat model, in comparison with the Tegaderm dressing.

Different types of growth factors can also be released controllably from the nanofiber-based scaffold at different stages. In one study, a scaffold made of collagen and hyaluronic acid fibers was fabricated to realize re-epithelialization, dermal reconstruction, and formation of mature vasculature for the chronic wound healing in diabetic rats.⁸⁷² In this case, the stage-wise delivery of multiple angiogenic growth factors was achieved either by directly loading them into the nanofibers or encapsulating them in gelatin nanoparticles and then incorporating the nanoparticles into the nanofibers. As such, the initial delivery of basic fibroblast growth factor and epidermal growth factor was able to simulate the early stage of a wound healing process, whereas the slow release of vascular endothelial growth factor and platelet-derived growth factor could dictate the late-stage of skin reconstruction.

Anti-infection and Anti-inflammation: Even with proper treatments, infection and abnormal inflammation can still occur in the early stage of wound healing.⁸⁷³ As such, the development of wound dressings coupled with localized drug delivery for anti-infection and anti-inflammation represents an avenue for healing large wounds and promoting effective repair. To this end, commonly used antibiotics, such as amoxicillin, tetracycline, ciprofloxacin, levofloxacin, moxifloxacin, cefazolin, and fusidic acid, have all been integrated into nanofibers to provide an antimicrobial capability.^{873,874} In particular, scaffolds integrated with both antibacterial and antifungal drugs showed a broad spectrum of activities.⁸⁷⁵ Electrospun nanofibers containing Ag nanoparticles also showed antibacterial activity.⁸⁷⁶ In addition, Au nanoparticles coated with small molecules such as 6-aminopenicillanic acid showed a long-lasting and remarkable antibacterial activity against the multidrug-resistant bacteria. With the incorporation of the surface-modified Au nanoparticles, electrospun nanofibers made of a blend of PCL and gelatin showed a striking capability to remedy the wound infection caused by multidrug-resistant bacteria in a rat model.⁸⁷⁷ Furthermore, the delivery of anti-inflammatory drugs has been utilized to improve wound healing. The typical drugs include dexamethasone, prednisone, acetaminophen, ibuprofen, naproxen, and ketoprofen.⁸⁷³

Inhibiting Scar Formation: Inhibiting scar formation in the late stage of a wound healing process is a long-lasting difficulty in the clinic. Scar formation normally results from the abnormal fibroblast proliferation and collagen deposition.⁸⁷³ Hypertrophic scarring is a dermal disorder that usually occurs during wound healing post deep burns. Several cell

Author Manuscript
Author Manuscript
Author Manuscript
Author Manuscript

signaling molecules or pathways can be leveraged to inhibit scar formation, including matrix metalloproteinase, basic fibroblast growth factor, mitsugumin 53 protein, transforming growth factor- β 1, and 20(R)-ginsenoside Rg3.⁸⁷⁸ For example, inhibition of the transforming growth factor- β 1 signaling was found to be effective in preventing scar formation.⁸⁷⁸ The inclusion of transforming growth factor- β 1 inhibitors in the nanofibers made of a blend of PCL and gelatin effectively inhibited the proliferation of fibroblast in vitro and prevented the formation of hypertrophic scar during the healing of full-thickness wounds in a rabbit ear model. In another study, PLGA fibers were loaded with ginsenoside-Rg3 and then surface-immobilized with basic fibroblast growth factor to promote the early stage wound healing and inhibit late-stage hypertrophic scarring in rabbit ear wounds.⁸⁷⁹

Wound Healing in Diabetic Patients.: Wound healing in diabetic patients is unique owing to the alternation in inflammatory response, poor angiogenesis, ECM imbalance, and peripheral neuropathy.⁸⁸⁰ For example, the healing of diabetic foot ulcers is different from the normal process. Diabetic ulcers do not progress to the next phase in wound healing beyond the inflammatory and/or proliferation phase, leading to infection, inflammation, and delayed healing.⁸⁶³ Moreover, ECM balance, cell-cell communication, and the growth factors involved in normal wound healing are all absent in chronic diabetic wounds.⁸⁶³ In one study, nanofibers integrated with SiO₂ or SiO₂-based nanoparticles were found to be effective in promoting diabetic wound closure by activating the related pathways. By including the SiO₂-based bioceramic particles into the nanofibers made of a blend of PCL and gelatin, the hybrid scaffold synergistically induced angiogenesis, collagen deposition, and re-epithelialization, while inhibiting the inflammation reaction, at the wound site of a diabetic mouse model.⁸⁸¹ In addition, by coating the surface of a patterned nanofiber-based scaffold made of a blend of PLA and PCL with a layer of bioactive glass via pulsed laser deposition, a scaffolding system was developed for diabetic wound healing.⁸⁸² At 13 days postapplication, the scaffolding material promoted the closure of wound in a diabetic mouse by nearly 80%, in addition to the stimulation of angiogenesis and re-epithelialization. Furthermore, scaffolds made of aligned PLA porous nanofibers containing dimethyloxalylglycine-loaded mesoporous SiO₂ nanoparticles were designed for diabetic wound healing.⁸⁸³ By integrating the aligned nanofibers with the controlled release of dimethyloxalylglycine, the scaffolds were able to stimulate the healing of a diabetic wound by significantly improving neo-vascularization, re-epithelialization, and collagen formation, while inhibiting the inflammatory reaction.

Wound Healing and Prevention from Skin Cancer.: Although surgical excision can remove the skin tumor tissues completely, it simultaneously leads to cutaneous defects. As a new trend, wound dressing has been developed to enhance not only the antitumor function but also healing of the skin defect. To this end, bifunctional scaffolds with capabilities for localized skin tumor therapy and skin tissue regeneration showed great promise to avoid tumor recurrence while healing the tumor-induced wounds (Figure 57A).²³³ For example, Cu₂S nanoscale flowers were incorporated into a micro-patterned nanofiber-based scaffold made of a blend of PLA and PCL (Figure 57B,C).²³³ The photothermal heating effect of the embedded Cu₂S nanoparticles under near-infrared irradiation contributed to the high mortality (>90%) of skin tumor cells and effective inhibition of tumor growth. Meanwhile,

the patterned scaffold promoted *in vivo* healing of full-thickness skin defects by accelerating the proliferation and migration of skin cells, in addition to angiogenesis during wound healing.

6.1.5. Cardiac Tissue Regeneration.—The heart wall is made up of three layers, with the cardiac muscle tissue (myocardium) forming a thick, middle layer between the outer layer (epicardium) and the inner layer (endocardium). Specifically, the myocardium shows a gradual transition of aligned heart muscle cells (cardiomyocytes) from endocardium to epicardium (Figure 58).⁸⁸⁴ In addition, the myocardium exhibits an interwoven architecture, in which coiled perimysial fibers provide the cardiac muscle tissue with the mechanical properties for efficient contraction and relaxation through stretching and recoiling of the fibers.⁸⁸⁵

Cardiac failure has become a major health issue worldwide, and myocardial infarction is one of the main causes of death associated with cardiovascular disease.⁸⁸⁴ Myocardial infarction is typically caused by the lack of oxygen and nutrients supplied to the cardiac muscle, resulting in excessive cell death. The myocardial tissue damaged during infarction lacks regeneration ability, and ischemic cardiac tissues cannot self-renew and restore the normal functions.⁸⁸⁶ Current limitations in myocardial tissue regeneration include the inability to fully recapitulate the structural organization and mechanical environment of the native cardiac tissue.⁸⁸⁷ Implanting a tissue-engineered myocardium into the diseased heart seems to be the simplest approach to the repair of infarcted myocardium.

Scaffolds made of electrospun nanofibers have been actively explored for myocardial tissue regeneration.⁸⁸⁶ Researchers initially focus on engineering the planar cardiac scaffolds to provide topographic features. Subsequently, 3D cardiac scaffolds are developed to replicate the specific 3D architecture of the myocardium as shown in Figure 58. In these cases, the proliferation and contractility of cardiomyocytes, as well as the differentiation of stem cells, including cardiac stem cells and iPSCs, into cardiomyocytes, are often investigated *in vitro*. The overarching goal is to engineer 3D cellular scaffolds to regenerate myocardial tissues and restore their function and then investigate the *in vivo* performance.

Planar Cardiac Scaffolds with Topographic Cues: Electro-spinning has been used to fabricate cardiac scaffolds from completely decellularized porcine cardiac ECM.⁸⁸⁸ In this study, nanofibers made of a blend of the ECM and PEO were obtained, and then PEO was removed by washing in a water-based solution. The as-obtained scaffold was able to preserve the ECM composition, self-assemble into the same micro-structure of native cardiac ECM, and retain key mechanical properties. However, the decellularized ECM is limited in terms of supply, and its production involves complex processing. As such, electrospun nanofibers made of a blend of synthetic and natural polymers are mostly used to fabricate cardiac scaffolds, which can be engineered to provide topographic cues in a controlled fashion to mimic the environment in native tissue for regenerating the intrinsically anisotropic myocardium.⁸⁸⁹ Scaffolds made of uniaxially aligned PCL fibers were seeded with human iPSCs-derived cardiomyocytes.⁸⁹⁰ It was demonstrated that the derived cardiomyocytes were aligned along the direction of fiber alignment, showing greater maturation of myocardium and significantly higher velocity of maximum contraction than

Author Manuscript
Author Manuscript
Author Manuscript
Author Manuscript

those on scaffolds made of random fibers. In order to simulate the anisotropic architecture of myocardium, nanofiber-based scaffolds with a square, rectangle, or honeycomb pattern were fabricated for comparison.⁸⁹¹ The honeycomb-patterned scaffolds showed the highest cardiomyocyte viability, the deepest penetration of cells, and the strongest expression of cardiac-related genes among the three different types of patterned scaffolds. In particular, the cardiomyocytes on honeycomb-patterned scaffolds displayed a spontaneous beating rate of 101 ± 12 times/min after co-culture for 5 days, and the synchronous beating could remain at 94 ± 8 times/min after 15 days; both rates were close to those of adult and neonatal rats.

In addition to straight nanofibers, coiled, helical, or spring-like fibers are desired to recapitulate the morphology of the perimysial fibers in the native heart wall (Figure 59A–D).^{885,892} In one study, the scaffolds made of such fibers exhibited increased elasticity and extensibility relative to the scaffold made of straight nanofibers.⁸⁹² It was demonstrated that the scaffolds made of coiled fibers were able to support the assembly of functional cardiac tissue with strong contraction forces. In another study, Au nanoparticles were embedded in the coiled fibers of a scaffold.⁸⁸⁵ When cultured with the cardiac cells, the hybrid scaffolds promoted cells to organize into elongated and aligned shapes with massive actinin striation, generating a strong contraction force, a high contraction rate, and a low excitation threshold relative to the scaffold without Au nanoparticles. In addition, sinusoidal fibers fabricated using melt electrospinning showed great potential in cardiac tissue regeneration.⁸⁸⁷

Design of 3D Cardiac Scaffolds.: Despite the progress in engineering the topographic cues of planar cardiac scaffolds, the scaffold itself has limited effect on improving the maturation of myocardium.⁸⁹³ To achieve a better guidance for the maturation and strong contractility of cardiomyocytes, 3D cardiac scaffolds, which emulate the structural organization, mechanical properties, and the function of healthy native tissues, are desired.⁸⁹⁴ To mimic the native architecture of myocardium as shown in Figure 58, multiple mats or nanofiber yarn networks were stacked together layer-by-layer with a slight angle shift between adjacent layers for the fabrication of a 3D cardiac scaffold. This strategy makes it possible to individually control cellular orientation and organization in each layer. In one study, a woven fabric was fabricated using surgical suturing threads as the warp and uniaxially aligned nanofiber yarns made of a blend of PCL, silk, and carbon nanotubes as the weft.⁸⁸⁴ Then, the network of nanofiber yarns was enclosed in a hydrogel matrix, achieving a hybrid scaffold. Within the anisotropic interwoven layers and hydrogel structure, cardiomyocytes were aligned and elongated, and endothelialized myocardium was obtained.

To further promote the functional recovery of the myocardium, 3D cellular scaffolds have been developed. For example, conductive nanofibers made of a blend of PLA and PANi were developed to promote the differentiation of rat cardiomyoblasts and the maturation and spontaneous beating of primary cardiomyocytes.⁸⁹⁵ In a typical process, cardiomyocytes were loaded into the nanofiber mat to obtain bioactuators in a tubular or folded shape. The tubular bioactuator was fabricated by simply rolling up the mat, while the bioactuator with a folded shape was obtained by folding up the mat with a round shape into a semicircle along the diameter and then folding it again into a quarter circle. On these two types of scaffolds, the cardiomyocytes were able to spontaneously beat at a much higher frequency than those cultured on planar scaffolds made of PLA nanofibers.

The cardiac scaffolds with a 3D architecture have also been applied to in vivo evaluation. In one study, a modular and thick cardiac patch containing multilayers was developed for regenerating vasculature and myocardium.⁸⁹⁶ Laser was used to create microscale grooves and holes, or cage-like structures, respectively, on the scaffolds consisting of electrospun albumin nanofibers. Then, a bottom-up approach was used to assemble a modular cardiac scaffold that consists of various layers, each performing a different function. One layer with grooved structures was used to accommodate cardiac cells and promote their organization into a contracting tissue. Another layer was designed with channels and cage-like structures to accommodate vascular endothelial growth factor-loaded PLGA microparticles, enabling the organization of endothelial cells into vasculatures. The third layer with cage-like structures was used for the entrapment of dexamethasone-loaded PLGA microparticles, thus controlling the release of anti-inflammatory drugs into the exterior microenvironment. Each tissue layer was grown separately under the optimal conditions and integrated with an ECM-based biological glue to form vascularized and thick 3D cardiac tissues just before transplantation in vivo. After implantation into a rat model for 2 weeks, it was observed that a host blood vessel containing red blood cells infiltrated into the vascularized scaffold, demonstrating the potential of the cardiac scaffold to integrate properly with the native heart muscle.

6.1.6. Vascular Tissue Regeneration.—Blood vessel is comprised of three concentric layers known as intima, media, and adventitia (Figure 60A).⁸⁹⁷ In terms of cellular structure, intima is made of a continuous monolayer of endothelial cells for lumen patency; media contains a dense population of circumferentially aligned SMCs in an elastic tissue to ensure mechanical strength; and adventitia is mainly consisted of fibroblasts and perivascular nerve cells embedded in collagenous ECM.⁸⁹⁸ In contrast to the case of large-diameter arteries, where there are already practical non-tissue-engineered grafts, there is an urgent need to develop biomimetic scaffolds for clinically regenerating blood vessels of small sizes (typically, <6 mm).⁸⁹⁹ The currently used grafts are plagued by thrombosis and unsatisfactory long-term patency because of the poor blood compatibility, mismatch in biodegradability between the implanted graft and the progressively regenerating tissue, and poor mechanical strength incapable of supporting the dynamics of blood flow.

A promising approach is based on *in situ* tissue engineering, whereby an acellular tubular scaffold is implanted to provide structural and biological cues and thus guide *in situ* remodeling for the regeneration of a functional blood vessel. Vascular scaffolds have been fabricated from many types of materials in different structures. Among them, the tubular design with a multilayered wall is most attractive in mimicking the architecture of a native blood vessel (Figure 60B,C).^{898,900–903} From the perspective of function, intima plays the most important role in preventing thrombus and accelerating endothelialization, whereas media provides mechanical support to avoid unfavorable remodeling at the anastomotic sites. As a result, the research in this area has mainly focused on the functionalization of the inner and middle layers when constructing a vascular scaffold. Prior to *in vivo* evaluation, the scaffold must be tested to ensure that the tubular structure is able to support blood flow in the lumen without leakage, and the scaffolding material has anticoagulation ability to prevent stenosis and occlusion, which is critical to the lumen patency. To this end, the

scaffold is usually presented in a planar structure to investigate the reconstruction of intimal endothelium and regeneration of SMCs layer in vitro. Afterward, the scaffold is folded into a tubular structure, by changing the collector from a static plate to a rolling rod, for the investigation of *in situ* tissue regeneration. Animal models, including rat abdominal aorta, rabbit coronary artery, and canine femoral artery, are commonly used for testing vascular scaffolds in a period of time ranging from several weeks to one and a half years.

Lumen Patency without Leakage.: To maintain blood flow in the lumen of a vascular scaffold without leakage, an important parameter to consider is the pore size. Pores of too small will inhibit cell infiltration, whereas pores of too large can lead to blood leakage. Researchers have investigated the *in vitro* and *in vivo* performance of bilayer scaffolds, with one layer featuring low porosity and another layer exhibiting high porosity either on the luminal or adventitial side (Figure 61A–E).⁹⁰⁴ Compared with the vascular scaffolds made of a single layer of nanofibers with high porosity, the bilayer scaffolds significantly reduced blood leakage, indicating that a low-porosity layer is needed when constructing a multilayered vascular scaffold to achieve both good cell infiltration and low blood leakage. It was also found that most of the cellular infiltration came from the tissues surrounding the scaffold rather than the flowing blood (Figure 61F,G).

Anticoagulation and Rapid Endothelialization in the Lumen.: The critical roles of the inner layer of a vascular scaffold include anticoagulation and rapid endothelialization. Nanofibers coated with heparin^{905,906} or arginine-glycine-aspartic acid,^{907,908} and nanofibers loaded with heparin^{909,910} have been explored as the lumen surface to circumvent early thrombosis. Long-term patency, however, mainly relies on the formation of endothelium. A confluent monolayer of endothelia cells on the lumen surface is critical to the prevention of blood clotting.⁹⁰¹ Several strategies have been explored to accelerate the formation of endothelium. Vascular endothelial growth factor and stromal cell-derived factor-1α, which are two commonly used biological factors, can be incorporated in the scaffold either through grafting to the surface of nanofibers or encapsulation into the core of nanofibers, to promote the recruitment, migration, and proliferation of endothelia progenitor cells and endothelia cells.^{911–915} Another attractive approach involves the use of a target-delivery system for local delivery of miRNA to modulate the proliferation of endothelia cells by separately down-regulating and up-regulating the expression of relevant genes.⁹⁰³

Recovery of Smooth Muscle Tissues.: The unique contractile function of SMCs in the media of a blood vessel is instrumental in providing a mechanical support to match the dynamics of blood flow. The regulation of SMCs phenotype, alignment, and infiltration plays a critical role in determining the success of long-term vascular repair. Circumferentially aligned nanofibers have been explored to induce a spindle shape for the SMCs and align them along the nanofiber alignment.⁹¹⁶ In achieving the alignment and infiltration of SMCs, nanofiber yarns show great potential, as the aligned, porous, and puffed nanofiber yarns can provide contact guidance and space for SMCs growth.⁹¹⁷ When a biochemical

guidance is combined with the topographical cue, the phenotypes of SMCs can be further controlled. In one study, SMCs were shown to express higher contractile genes on uniaxially

aligned PLA@hyaluronan core–sheath nanofibers relative to the case of PLA nanofibers.⁹¹⁸ Interestingly, biochemical and mechanical features provided by random nanofibers also showed influence on the phenotypes of SMCs.⁸¹⁸ It was demonstrated that vascular scaffolds with a higher gelatin content and lower stiffness encouraged the contractility of SMCs. In addition, targeted, local delivery of miRNA was also able to modulate the phenotypes of SMCs, providing a viable approach to prevent intimal hyperplasia.⁹¹⁹

In Situ Vascular Tissue Engineering.: Tubular scaffolds made of multiple layers of nanofibers and loaded with various growth factors (e.g., vascular endothelial growth factor and platelet-derived growth factor) have been explored for in situ regeneration of vascular tissues.^{920,921} While rapid endothelialization can be achieved in most cases, the infiltration of SMCs into the void space among the nanofibers is insufficient due to the small pore size and slow biodegradation of the scaffold. To address this issue, tubular scaffolds with tunable biodegradability were developed to improve the regeneration of vascular tissues by matching the degradation rate of the scaffold with the remodeling speed of the tissue. In one study, tubular scaffold comprised of PCL and polydioxanone fibers was fabricated by co-electrospinning.⁹²² Owing to the hydrophilicity of polydioxanone, the scaffold possessed good patency and was able to enhance the coverage of endothelia cells relative to scaffold made of PCL fibers only. Significantly, the polydioxanone fibers could be completely degraded in 12 weeks to constantly provide additional space for cell infiltration. In a rat abdominal aorta model, vascular smooth muscle could be generated in the scaffold after implantation for 3 months. Despite this successful demonstration, it remains a challenge to synchronize the rates of scaffold degradation and new-tissue formation over a long period of time.^{922–924}

6.1.7. Musculoskeletal Tissue Regeneration.—The musculoskeletal system is comprised of skeleton, muscles, cartilages, tendons, ligaments, joints, and connective tissues.⁸⁰⁵ The primary function of the musculoskeletal system is to provide support, stability, protection, and movement to the body.⁹²⁵ A musculoskeletal injury refers to damage to the muscular or skeletal tissue caused by trauma, congenital defect, or tumor ablation.⁹²⁶ In general, nonwoven mats of nanofibers are used as patches to induce the specific differentiation of stem cells into osteogenic, chondrogenic, or tenogenic tissues. On the other hand, 3D scaffolds have also been developed from nanofibers to provide space for cell infiltration and tissue remodeling.

Bone Tissue Regeneration.: As a hard tissue, bone is primarily composed of type I collagen fibrils and hydroxyapatite nanoparticles. In addition to their critical roles in protecting and supporting various organs of the body, bones are also responsible for the storage of calcium, phosphorus, and other critical components of the hematopoietic system. Because of the strong mechanical strength and high mineral content, scaffolds used for bone regeneration are often designed by reinforcing the biodegradable polymers with a biocompatible inorganic phase (e.g., hydroxyapatite, bioactive glass, silica, and ZnO nanoparticles).^{927–931} An ideal 3D scaffold should not only structurally mimic the bulk tissue but also mechanically support the bone healing process and provide biochemical cues to induce osteogenesis.⁹³² In one study, a sponge-like 3D nanofiber-based scaffold made of a blend of

Author Manuscript
Author Manuscript
Author Manuscript
Author Manuscript

PLA, PCL, and PEO was fabricated.⁹³³ It possessed highly interconnected pores, intertwined sub-micrometer fibrous morphology, large pore sizes, and controlled release of dexamethasone. The scaffold could direct the osteogenic differentiation of human MSCs without the use of any differentiation medium. In addition, minerals and bioactive agents can also be introduced into the scaffold to further improve its performance. To this end, a 3D, nanofiber-based scaffold containing interconnected nanoscale and microscale pores was functionalized with minerals and bone morphogenic protein-2 peptide.⁹³² The functionalization not only gave a superior compressive modulus relative to the pristine scaffold but also upregulated the osteogenic differentiation of adipose-derived MSCs in the scaffold. Nanofiber-based scaffolds made of a shape-memory polymer also showed the potential to support bone tissue regeneration. A 2D planar or 3D cylindrical scaffold made of poly(D,L-lactide-*co*-trimethylene carbonate) showed excellent shape-memory properties with a high shape recovery ratio of more than 94% and a fast shape recovery of ca. 10 s at 39 °C.⁵⁷⁷ Such a scaffold can be fabricated in any expected shape to support osteogenesis, alkaline phosphatase expression, and mineral deposition, showing potential in repairing various types of bone defects, including the use as barrier membranes for guiding bone regeneration or as implants for healing bone screw holes.

Cartilage Tissue Regeneration.: Cartilage is a resilient and smooth elastic tissue that covers and protects the ends of long bones at the joints.⁹³⁴ Highly specialized chondrocytes are responsible for the production of collagen and proteoglycans in the cartilaginous ECM. From the superficial zone to the deep zone of cartilage, the content of type-II collagen decreases while that of proteoglycan increases.⁹³⁵ For the repair of cartilage defects, electrospun nanofibers have shown promise as a basis for chondrogenesis or chondrogenic differentiation. However, it is an ongoing challenge to achieve completely cellular infiltration throughout the full thickness of the defect site when 2D mats are used.⁹³⁶ To this end, a 3D, nanofiber-based scaffold with a hierarchical architecture and interconnected pores, possessing compressive strength and capable of promoting chondrogenesis, is desirable for the regeneration of thick cartilage tissues.⁵¹⁷ As discussed in section 2.4.7, a 3D scaffold made of PCL nanofibers provided interconnected and hierarchically structured pores with a high porosity of 96.4% (Figure 33C).⁵¹⁷ The scaffold could promote bone morphogenic protein-2-induced chondrogenic differentiation of bone marrow-derived MSCs. In another study, a hyaluronic acid-modified 3D, nanofiber-based scaffold made of a blend of gelatin and PLA effectively repaired the cartilage defects in a rabbit model.⁵¹⁹ The scaffold featured porous and fibrous structures, high compressive strength, and superabsorbent and shape recovery properties. Furthermore, as a native component of ECM in cartilage, the incorporation of hyaluronic acid enhanced the hydrophilicity of the scaffold and introduced more cell recognition sites. As such, the scaffold supported the chondrocyte growth, realized the regeneration of bulk cartilage tissue and filled up the defect site at 12 weeks postsurgery in a rabbit model.

Tendon/Ligament Tissue Regeneration.: Tendon is a dense and fibrous connective tissue that attaches a muscle to a bone and is capable of withstanding tension.⁹³⁷ Similarly, ligament is the fibrous connective tissue that connects bone to another bone. Histologically, both tendon and ligament comprise parallel arrays of dense regular connective tissue

bundles, that is, closely packed collagen fibers, and the bundles are encased in sheaths made of dense irregular connective tissues.⁹³⁷

Various 2D mats composed of uniaxially aligned nanofibers have been used in tendon and ligament tissue engineering as they can mimic the alignment of native tissues. However, the healthy tendon/ligament tissues are normally in bulk volume, together with highly anisotropic architectures and mechanical properties.⁹³⁵ To this end, biomimetic 3D scaffolds are required to provide the structural, physical, and biochemical features to simulate native tissues.⁹³⁸ For example, a reversibly expandable tube made of polyester urethane fibers, with a rough inner surface conjugated with platelet-derived growth factor, was applied to heal the ruptured site of a tendon.⁹³⁹ In addition, nanofiber yarns and the braided, woven, or knitted yarn networks are attractive for tendon and ligament tissue regeneration, due to their high mechanical strength, anisotropic architecture, and enlarged porosity for cell infiltration. For example, two cord yarns (20 mm in length) were tied to each other by a single filament for tendon repair by fixing the resultant cord yarn to tendon with sutures.⁹⁴⁰ In another study, a woven fabric was fabricated by plain-weaving with PCL nanofiber yarns as weft and multiple PLA filaments as warp (Figure 62A–E).⁸²⁴ The fabric showed a 3D aligned architecture, enlarged pore size, and enhanced tensile mechanical properties, promoting the regeneration of tendon. When the woven fabric was co-cultured with adipose-derived MSCs, human tenocytes, and human umbilical vein endothelial cells under a mechanical stimulation condition, both the collagen secretion and tenogenic differentiation were upregulated. Another strategy involves the application of composites containing fibers and hydrogel for ligament regeneration. The composites are advantageous in engineering 3D architecture and encapsulating cells and biological factors. As an example, a rolled mat of PLGA or poly(ester-urethane urea) fibers was enclosed within PEG hydrogel.⁹⁴¹ In another example, bilayer scaffolds fabricated by coating a hydrogel made of a blend of chitosan and hyaluronic acid on uniaxially aligned PCL fibers were used to promote ligament regeneration.⁹⁴²

Skeletal Muscle Regeneration: Skeletal muscles, consisting of bundles of highly oriented, densely packed myofibers derived from the multinucleated muscle cells, are connected to bone through tendons.⁹³⁵ Without proper alignment of myofibers, it is impossible to impose effective force transmission and contractility in the regeneration of functional muscle fibers.⁹⁴³ Hence, scaffolds capable of guiding muscle cell alignment and allowing for the formation of myotubes via topographical, chemical, and/or biological cues are believed to be critical in myogenesis.⁹³⁵ In recent studies, anisotropic nanofibrous materials, with their morphologies and functions closely resembling the native tissue, have been explored to develop scaffolds for skeletal muscle regeneration.⁹⁴⁴ Several planar mats with microscale or nanoscale patterns showed the potential in mediating myogenic differentiation *in vitro*. However, they cannot be applied to construct the 3D volumetric defects *in vivo*. As such, 3D porous scaffolds with uniaxial fiber alignment are advantageous in prealigning muscle cells, and thereby facilitating the early stage myogenic differentiation and the formation of long and thick myotubes.⁹⁴³

Among various designs, the fibrous bundle structures show feasibility in skeletal muscle regeneration. Electrospun fiber bundles made of silk fibroin have been used to mimic the

Author Manuscript
Author Manuscript
Author Manuscript
Author Manuscript

hierarchical assembly of uniaxially aligned fibrils of skeletal muscles.⁹⁴⁵ After further modification with PPy, the electroactive fiber bundles underwent electromechanical actuation in biologically relevant electrolyte solutions under the application of low potentials, mimicking the contractile function of native muscles. In addition, the nanofibers can be combined with other types of materials such as hydrogel to construct a 3D composite scaffold. Using nanofiber yarns as the core and photocurable hydrogel as the sheath, 3D cellular alignment and elongation of myoblasts were induced when a suitable 3D environment was provided.²⁶⁴

6.1.8. Tissue-to-Tissue Interface Engineering.—The tissue-to-tissue interfaces, including the transition either from a soft matrix to a hard matrix or from a soft matrix to another soft matrix, in the musculoskeletal system are responsible for tension or bear compression.⁹⁴⁶ It has been challenging to regenerate the interface between two different musculoskeletal tissues because of the low self-healing capacity after injury and the complicated architecture. In terms of the graded components and features commonly involved in native tissue-to-tissue interfaces, scaffolds capable of enabling the transition of composition, structure, and function between the two dissimilar tissues are most beneficial to the regeneration of interfaces.

The soft-to-hard interfaces in the musculoskeletal system include tendon-to-bone, ligament-to-bone, and cartilage-to-bone, which all involve changes in material architecture and mechanical properties. These junctions connect tissues that differ by 2 orders of magnitude in mechanical strength via gradual variations in mineral content and matrix composition.⁹⁴⁶ As such, the regeneration of such interfaces requires specialized scaffolds integrated with spatially organized material composition, cell types, signaling molecules, as well as a gradual transfer in mechanical stress between the two tissues.⁹⁴⁷

Interfaces between Tendon or Ligament and Bone.: These interfaces, known as entheses, are highly specialized tissues, allowing for a smooth transmission in spatial architectures and forces between mechanically dissimilar tissues.^{948,949} The transition zone from tendon or ligament to bone is a complex fibrocartilage region that includes nonmineralized and graded mineralized subregions (Figure 63A).^{950,951} The mineral content increases monotonically from tendon (or ligament) to bone, resulting in a gradation in mechanical strength to mediate load transfer between tendon (or ligament) and bone.⁹⁵²

Nanofiber-based mats with a transmission zone of gradient structure, mineral content, and mechanical strength have been explored to repair the tendon or ligament-to-bone interface. In an attempt to develop a suitable tendon or ligament-to-bone transition with a graded structure, a mat was fabricated from “aligned-to-random” nanofibers (Figure 63B,C).⁴⁵⁹ While the aligned portion mimicked the high level of alignment for collagen fibers in tendon, the random portion recapitulated the less ordered organization of collagen fibers in bone. In addition to the change in fiber orientation, a spatial gradient in modulus across the scaffold has been developed to mimic the load transfer between tendon (or ligament) and bone.⁹⁵³ Furthermore, scaffolds with a transmission zone in three dimensions have been explored to regenerate the gradually changing interfaces. For example, a bilayer nanofiber-based scaffold made of organic and inorganic materials has been fabricated.⁹⁵⁴ With the

PLA nanofiber mat serving as the upper layer, the mat of nanohydroxyapatite and PLA composites was used as the lower layer, separately simulating the non-mineralized fibrocartilage and mineralized fibrocartilage in tendon-to-bone integration.

Interface between Cartilage and Bone.: Another essential soft-to-hard interface in the musculoskeletal system is the cartilage–bone junction. As an osteochondral tissue, it is comprised of cartilage, intermediate calcified cartilage, and bone.⁹⁵⁵ Due to the spatially graded matrix components and the mechanically mismatched tissues at the cartilage–bone junction, scaffolds with graded properties are usually combined with hydrogels for regenerating the osteochondral tissue in three dimension.⁹⁵⁶ For example, multilayers of PCL nanofiber-based mats, incorporating with countercurrent gradients of chondroitin sulfate and bioactive glass, were assembled in an agarose–gelatin hydrogel.⁹⁵⁷ While the chondroitin sulfate promoted the regeneration of hyaline cartilage, the bioactive glass enhanced the remodeling of mineralized ECM. When encapsulated in the hybrid scaffold, the chondrocytes responded to the physical gradients of raw materials and thus generated an opposing gradient of sulfated glycosaminoglycan-enriched ECM (cartilage) and mineralized ECM (bone). This specific architecture was able to mimic the native osteochondral interface, showing the potential of combining a tissue-engineered cartilage with a mineralized ECM as the interface for better integration with the subchondral bone.

In addition to the soft-to-hard interfaces, the musculoskeletal system also contains the soft-to-soft interfaces, such as myotendinous junction and neuromuscular junction. These interfaces, however, have not been extensively studied.

Interface between Muscle and Tendon.: The myotendinous junction is an important interface, acting as the connection between skeletal muscle and tendon. The myotendinous junction contains fibroblasts that link the dense collagen fibers of tendon to muscle fibers at an oblique direction.⁹⁵² The force generated by muscle contraction is transmitted from intracellular contractile muscle proteins to the extracellular connective tissue proteins of tendon. Desirable scaffolds should bridge the gap between muscle and tendon, promoting the regeneration of entire muscle tissue units. In one study to mimic the pattern of a native myotendinous junction, a dual component scaffold with a mechanical gradient was developed.⁹⁵⁸ While the PCL fibers resembled the muscle with low stiffness and strength (4.49 MPa of Young's modulus and 1.07 MPa of ultimate tensile strength), the PLA fibers simulated the tendon and exhibited the highest stiffness and strength (27.62 MPa of Young's modulus and 3.74 MPa of ultimate tensile strength) in the scaffold. In the central region serving as the myotendinous junction, the mechanical properties showed a value between those of the two ends (20.06 MPa of Young's modulus and 2.38 MPa of ultimate tensile strength). This scaffold followed a mechanical trend similar to that of the native myotendinous junction. However, there is only 6-fold difference in stiffness between the tendon side and the muscle side in this study, which is far away from that between the natural tendon and muscle with a ratio ranging from 179 to 370,000.⁹⁵⁰ Therefore, the main issue in regenerating myotendinous junction tissue remains the lack of stiffness transition in comparison to the native tissues.

Interface at the Neuromuscular Junction.: The neuromuscular junction is critical to the functions and survival of motor neurons and skeletal muscles.⁹⁵⁹ It has a highly specialized synapse in the peripheral nervous system with primary functions to regulate the contraction and relaxation of muscles.^{805,960} The movements of limbs are driven by the contraction of skeletal muscles through the connection of neurotransmitters (acetylcholine) with a cluster of acetylcholine receptors.⁹⁵⁰ Without neuromuscular junction, the primary myotubes will be unable to mature, which may result in muscle atrophy. The innervation is of critical importance in the maturation of myofibers and generation of contractile force in muscles. In a preliminary study, researchers succeeded in utilizing an adjacent uninjured nerve as a source of axonal regeneration through a nanofiber conduit made of a blend of PCL and collagen to restore muscle function.⁹⁶¹ However, there are only a limited number of studies in the area of neuromuscular junction tissue engineering. Remaining issues include the construction of 3D engineered scaffolds to realize innervation on highly oriented muscle fibers and accelerate the response between the acetylcholine and the receptors for muscle contraction.

6.1.9. Repair or Regeneration of Other Tissues.—Scaffolds made of electrospun nanofibers can also be explored for potential use in the repair or regeneration of other tissues, such as bile duct, ureter, bladder, and trachea. However, the repair or regeneration of these tissues was far away from being well-studied because of their complex structures and/or complications postsurgery. For example, a bile duct can be considered as a long, tube-like structure, connecting the common hepatic to the cystic duct. Following biliary surgery, patients often suffer from various complications, such as biliary tract injury, biliary stenoses, and biliary leaks.⁹⁶² Clinically, metal or plastic stents are explored to repair injured bile ducts. However, these stents usually cause occlusions and infections due to the weak biocompatibility and histocompatibility. To solve this problem, a mat made of PLCL nanofibers loaded with ethylene diamine tetraacetic acid and sodium cholate in the core of each nanofiber has been used to coat the surface of a metal stent.⁹⁶³ The PLCL nanofibers are biocompatible, and the sustainable release of the drugs offered effectiveness in dissolving gallstone and thus inhibiting occlusions in the bile duct. Furthermore, as the main function of a bile duct is to carry bile, a prosthesis that mimics the common bile duct should have a considerable compliance to resist the dynamics. So far, only a limited number of studies have been carried out in terms of the compliance of a nanofiber-based scaffold for potential use in the repair of common bile duct, except for the test of a set of tubes made of polyurethane nanofibers fabricated under different electrospinning conditions.⁹⁶⁴

Inspired by the blood vessel, which is also as a tubular structure capable of transferring blood surrounding the body, we expect a comparable, tissue-engineered tubular scaffold could be developed to support bile flow through the lumen while improving the formation of new tissue surrounding the wall of the scaffold.

A ureter is a tube made of smooth muscle fibers that propel urine from the kidney to the urinary bladder. Similar to the repair of an injured bile duct using a stent, a ureter also has a high risk of obstruction and infection. Additionally, some other complications persist, including a second procedure for removal, pain, hematuria, and encrustation.⁹⁶⁵ To avoid these problems, nanofiber-based tubular scaffolds, together with biocompatibility and

biodegradability, have been explored to repair ureteral tissues. In one attempt, a tubular, ureteral scaffold with gradient degradation was developed and investigated in a porcine model, with commercial polyurethane Shagong stent as a control.⁹⁶⁵ The ureteral scaffold was composed of nanofibers made of a blend of PCL and PLGA. The proportion of PLGA decreased from the distal end to proximal terminal, leading to the gradual degradation along the same direction in the PCL/PLGA scaffold over 10 weeks, with no ureteral obstruction in any porcine model. According to the in vivo results, the PCL/PLGA also showed better biocompatibility than the commercial Shagong stent in terms of foreign-body reactions, tissue inflammation, and edema.

In addition to ureter, bladder also plays a critical role in the urinary system to eliminate waste from the body. A bladder is a hollow muscular organ that collects and stores urine from the kidneys before disposal by urination. Many clinical conditions can cause poor bladder compliance, reduced capacity, and incontinence, requiring bladder expansion or the use of regenerative techniques and scaffolds.⁹⁶⁶ An ideal scaffold for bladder tissue engineering is expected to provide the specific hollow architecture, a smooth surface for the urothelium, and a porous outer compartment for the SMCs.⁹⁶⁷ Furthermore, as a bladder needs to expand and contract for the purpose of storing and expelling urine, the tensile mechanical properties and compliance of the scaffold should also be taken into consideration. In one study for bladder tissue expansion, a layer of electrospun PLGA nanofibers was sandwiched between two layers of plastic-compressed collagen nanofibers to produce a 3D scaffold.⁹⁶⁸ Then, the scaffold was used to expand autologous minced urothelium by distributing the minced tissues either on top or both on top and inside the scaffold. The results showed that the cells from minced tissues migrated and reorganized to a confluent cell layer on the top of the scaffold after 2 weeks and formed a multilayered urothelium after 4 weeks, together with the typical cell morphology and phenotype for urothelial mucosa during tissue culture. In another attempt, degradable polyesterurethane was electrospun to produce fibers and collected on the external side of a wet bladder acellular matrix, forming a bilayer hybrid bladder scaffold. Due to the biocompatibility, mechanical property, and biodegradability of polyesterurethane fibers, bladder wall was reconstructed with particularly improved smooth muscle and urothelial regeneration, while reduced inflammatory reaction, compared with the hybrid scaffold made of PLGA fibers and the bladder acellular matrix.

Researchers have also made preliminary trials to regenerate tracheal tissues. A trachea is a cartilaginous tube that connects the pharynx and larynx to the lung, allowing for the passage of air. In a typical study to develop a suitable scaffold to regenerate tracheal tissues, a bilayer scaffold was produced using dense nanofibers as the inner layer and porous nanofiber yarns as the out layer, both of which were made from a blend of PLCL and collagen.⁹⁶⁹ Then, autologous tracheal epithelial cells and chondrocytes were separately seeded onto the inner and outer layers of the scaffold, followed by incubation *in vitro* for 7 days. After wrapping the cell-scaffold construct with rat tracheal fascia for prevascularization, it showed enhanced production of epithelium, cartilage maturation, and capillary neogenesis after implantation in a rat trachea injury model for 4 weeks when compared with the case of a blank scaffold. This study shows a synergistic effect between the topographic cues provided by the nanofiber-based scaffold and the biological cues generated by the autologous cells.

6.2. Cancer Research

Relative to a solid substrate with a smooth surface, a mat of electrospun nanofibers offers a much higher surface area-to-volume ratio, contributing to a larger contact area with analytes and cancer cells.⁹⁷⁰ In addition, electrospun nanofibers can be readily loaded with drugs for their controlled release and localized delivery, achieving more effective chemotherapy. As such, electrospun nanofibers, including those made of inorganic and organic materials, as well as inorganic and organic hybrid materials, have been applied to cancer research in the context of diagnosis, construction of 3D tumor models, and treatment.

6.2.1. Cancer Diagnosis.—Cancer cells usually overexpress specific protein biomarkers, providing an opportunity for early diagnosis.⁹⁷¹ Electrospun nanofibers have been employed to detect tumor markers or circulating tumor cells in the blood or body fluid in the early stage of cancer development. In an example of detecting tumor markers, ZnO nanofibers containing multiwall carbon nanotubes were covalently conjugated with the anticarcinoma antigen-125 antibody.⁹⁷²

The composite nanofibers showed a broad detection range for carcinoma antigen-125, a specific marker for ovarian cancer. Nanofibers can also be combined with microfluidic techniques to improve the sensitivity and selectivity toward specific cancer cells. For example, a microfluidic immune-biochip made of porous graphene foam and modified by carbon-doped TiO₂ nanofibers was used to detect the breast cancer biomarker.⁹⁷³

By serving as an immune-electrode biosensor, the biochip could detect the target antigens over a wide range of concentration, together with a high sensitivity at the femtomolar level.

In addition to specific biomarkers, oxygen is an important index in cancer cell biology. A number of oxygen sensors made of electrospun nanofibers have been designed. In one study, PCL nanofibers were combined with an oxygen-sensitive ruthenium compound to develop a sensor possessing a rapid response time of 0.90 ± 0.12 s to oxygen.⁹⁷⁴ In another study, Pt(II) or Pd(II) meso-tetra(pentafluorophenyl)porphine, oxygen-sensitive luminescent probes, were incorporated into the cores of poly (ether sulfone) @PCL or polysulfone @PCL core-sheath nanofibers.⁹⁷⁵ The nanofibers exhibited a rapid response to oxygen, typically within 0.5 s.

Circulating tumor cells (CTCs) offer another avenue to early cancer diagnosis.⁹⁷⁶ CTCs are often shed into the vasculature or lymphatics from the primary tumor and circulated into the bloodstream, resulting in metastasis to other organs.⁹⁷⁷ The capture of CTCs may slow down or prevent the metastasis of cancer.^{971,977} Electrospun nanofibers have been used to capture CTCs by modifying the surface of nanofibers with specific functional groups to target the tumor cells. The capture efficiency depends on both the size and morphology of the nanofibers. In one study, the surface of PS nanofibers with a beaded morphology was conjugated with an antibody of the epithelial-cell adhesion molecule to give a higher capture efficiency to human breast adenocarcinoma cells relative to PS microfibers and nanofibers with a smooth surface (Figure 64A,B).⁹⁷⁸ In addition, nanofibers can be combined with microfluidic techniques to improve the capture efficiency.⁹⁷⁹ To this end, PLGA nanofibers conjugated with biotinylated anti-epithelial-cell adhesion molecule were integrated with a

Author Manuscript
Author Manuscript
Author Manuscript
Author Manuscript

microfluidic device for the effective capture of human breast cancer cells.⁹⁸⁰ In another study, PLGA nanofibers modified with anti-146 antibody (a capture agent for melanoma) were integrated with a microfluidic chip to capture melanoma CTCs with a high efficiency.^{970,981}

Increasing the purity and enriching the population of the rare cancer cells is highly desired in cancer research. To this end, a bioelectronic device was designed to simultaneously achieve dynamic capture and release of CTCs.⁹⁸² Specifically, PEO-PEDOT@PSS core-sheath nanofibers were modified with bioactive agents in the order of poly-L-lysine-g-PEG-biotin, streptavidin, and anti-epithelial-cell adhesion molecule. The nanofibers were then deposited on a parallel array of individually addressable electrodes made of ITO and integrated with a PDMS chamber containing microfluidic channels. The device could serve as a bioelectronic interface for the isolation, detection, sequential collection, and enrichment of rare CTCs through the electrical activation of each single electrode (Figure 64C). Using a mat of nanofibers collected for 10 min, more than 90% of the targeted cancer cells were captured by the device. In addition, due to the electrochemical doping and dedoping characteristics of PEDOT, over 87% of the captured cancer cells could be electrically triggered to release from the electrode by desorbing poly-L-lysine-g-PEG-biotin. This type of device can be further explored for the detection, capture, and release of multiple types of cancer cells when modified with additional tumor-specific ligands.

6.2.2. In Vitro 3D Tumor Models.—Engineering in vitro 3D tumor models offers a viable and cost-effective way for identifying carcinogens, testing new medicines, screening drugs, and studying the mechanisms of tumor growth and metastasis.^{977,983} The major requirement is to design a specific 3D matrix similar to the tumor extracellular environment, supporting the cell–cell and cell–ECM communications, and enabling biochemical signaling during tumor metastasis. Electrospun nanofibers can mimic the composition and architecture of the native tumor ECM and realize biochemical functionalization via surface modification or drug encapsulation, providing an attractive platform for constructing in vitro 3D tumor models. To this end, an in vitro 3D model was constructed using collagen-coated gelatin nanofibers to investigate the metastasis of breast cancer.⁹⁸⁴ This tumor model mimicked the extracellular composition, surface complexity, and mechanical properties of connective tissues, achieving an obvious cellular invasion. In addition, the cellular microenvironment, in particular the component of ECM, was found to play an important role in regulating the metastasis of cancer cells. For example, laminin isoform could be coated on PS nanofibers to create a 3D model for U251 glioblastoma cell culture.⁹⁸⁵ In this case, a combination of the 3D architecture and laminin modification led to the development of glioma stemness.

6.2.3. Cancer Treatment.—Electrospun nanofibers have also been explored for cancer treatment by manipulating the migration of cancer cells, controlling the release of antitumor drugs, and/or offering a synergistic platform for the simultaneous suppression of cancer cell proliferation, angiogenesis, and invasion.

Manipulating the Migration of Cancer Cells: With the control of morphology and alignment, electrospun nanofibers can be applied to cancer treatment by regulating the migration of cancer cells and inducing cell apoptosis, offering a new strategy for inhibiting

Author Manuscript
Author Manuscript
Author Manuscript
Author Manuscript

the growth of primary tumors.⁹⁸⁶ For example, a nonwoven mat of uniaxially aligned PCL nanofibers was inserted into a conduit to guide glioblastoma tumor cells to migrate away from the initial tumor site to an extracortical cytotoxic hydrogel, in which the cancer cells were killed through apoptosis (Figure 65A,B).⁹⁸⁷ In vivo results demonstrated that the total volume of the tumor in the animal brain was drastically reduced after treatment with the conduit containing the nanofibers, in comparison with a conduit containing smooth PCL film and a blank control group.

Chemotherapy through the Release of Antitumor Drugs.: Electrospun nanofibers can also be used in cancer chemotherapy by leveraging their capability to encapsulate and release antitumor drugs in a controllable fashion. In one demonstration, coaxial electrospinning was used to develop gallic acid-loaded PEO@zein core–sheath nanofibers to improve the chemopreventive action of gallic acid on human gallbladder cancer cells.⁹⁸⁸ Compared with the nanofibers loaded with a single drug, those containing multiple drugs are beneficial to overcoming the chemoresistance against a single drug.⁹⁷⁷ For example, camptothecin-11 and 7-ethyl-10-hydroxycamptothecin, two antitumor drugs, were encapsulated in nanofibers made of a blend of poly(glycerol monostearate-co-e-caprolactone) and PCL for local delivery.⁹⁸⁹ Through the release of multiple antitumor drugs, chemotherapy over a prolonged period of time (>90 days) was achieved, contributing to significant tumor cytotoxicity against a human colorectal cell line.

Electrospun nanofibers are usually combined with multifunctional nanoparticles to offer an implantable device with a long-term release locally. In one study, an intratumorally injectable composite was fabricated to realize sustained release of drug-loaded micelles from fragments of electrospun fibers in response to tumor microenvironment.⁹⁹⁰ Specifically, camptothecin was conjugated to hyaluronic acid, and the conjugate was then grafted to PLA nanofibers via an acid-labile linker to produce injectable fiber fragments. It was demonstrated that the intratumoral injection of fiber fragments ensured micelle accumulation inside the tumor tissue for over 3 weeks. Furthermore, sustained release of micelles from the fiber fragments contributed to a significantly higher antitumor efficacy relative to the intratumoral injection of free micelles, offering a new way for target cancer chemotherapy. In another study, a smart system involving the tumor-triggered release of doxorubicin was developed using a composite material to inhibit cancer relapse.⁹⁹¹ The system was constructed from electrospun PLA fibers and CaCO₃-capped mesoporous SiO₂ nanoparticles (Figure 65C–E). This system was then demonstrated for the sustained release of doxorubicin to kill cancer cells in the acidic environment of cancerous tissue by leveraging the reaction between CaCO₃ and an acid. In contrast, the antitumor drug was only released at a minor level in normal tissues held at the physiological pH. This smart delivery system exhibited pH-triggered antitumor efficacy that could last over a period of 40 days.

Synergistic Cancer Therapy.: A synergistic therapy can simultaneously suppress cancer cell proliferation, angiogenesis, and invasion.⁹⁷⁷ In one demonstration, a dual delivery system was developed to combine RNA interference (RNAi) and chemotherapy for brain tumor therapy.⁹⁹² In this case, a designed RNAi plasmid complex was complexed with polyethylenimine, a gene carrier, in an effort to specifically suppress the expression of

matrix metalloproteinase-2 in the glioma signal pathway. The RNAi plasmid was then co-encapsulated with paclitaxel (a cytotoxic drug) in PLGA fibers to achieve sustained release for both agents. While the suppressed expression of matrix metalloproteinase-2 inhibited brain tumor invasion and angiogenesis, the cytotoxic paclitaxel was able to block the growth and proliferation of cancer cells. Compared with the single function provided by one type of agent, this study demonstrated a significantly improved efficacy due to the involvement of synergistic therapy.

6.3. Other Biomedical Applications

6.3.1. Implant Coatings.—As a functional material, electrospun nanofibers can be directly deposited on an implant to improve its biocompatibility and provide additional topographic features and/or biological cues. As an example, PK Papyrus, a commercial coronary balloon-expandable stent system developed by Biotronik, was fabricated by coating the surface of a single stent with elastic polyurethane nanofibers to provide high bending flexibility.⁹⁹³ The nanofibers could also be loaded with active proteins. In one demonstration, PLCL nanofibers loaded with heparin and vascular endothelial growth factor were deposited on an expandable stent for aneurysm treatment.⁹⁹⁴ While the high elasticity of PLCL nanofibers improved the expansion range of the stent, the encapsulated biological effectors were able to inhibit thrombus and promote rapid endothelialization after implantation into a rabbit model. The nanofiber-covered stent obliterated the aneurysm by separating the aneurysm dome from the blood circulation to keep a long-term patency for the parent artery.

6.3.2. Barrier Membranes.—Nonwoven mats of electrospun nanofibers can serve as barrier membranes to prevent postsurgery adhesion, enhance osteogenesis, and fight against bacteria. To this end, commercial ReDura made of PLA nanofibers was developed to repair defective dura and avoid adhesion with the surrounding tissues after dural repair.⁹⁹⁵

Similarly, NeoDura was also developed from nanofibers made of a blend of a synthetic polymer and porcine gelatin for antidual adhesion.⁹⁹⁶

A barrier membrane is also needed for tendon surgery. Chemotaxis of extrinsic fibroblastic precursor cells often causes postsurgery adhesion between tendon and surrounding tissues.⁹⁹⁷ It is highly desirable to create an antiadhesion membrane by endowing the nanofiber-based mat with multiple functions, including lubrication, prevention of fibroblast attachment, anti-infection, and anti-inflammation.⁹⁹⁷ In one study, membranes were fabricated from core–sheath nanofibers, where a mixture of hyaluronic acid and ibuprofen was contained in the core while Ag nanoparticles were loaded in the sheath made of a blend of PEG and PCL.⁹⁹⁷ The lubricating effect offered by hyaluronic acid was able to ensure smooth tendon gliding and reduce fibroblast attachment, while the Ag nanoparticles and ibuprofen could serve as anti-infection and anti-inflammation agents, respectively. The results from an *in vivo* study on a rabbit model for flexor tendon repair demonstrated that the multifunctional membrane was more effective in reducing inflammation and preventing peritendinous adhesion when benchmarked against the commercial SurgiWrap.

In guiding tissue regeneration for the treatment of periodontal defects, a barrier membrane is also required to prevent the apical migration of gingival epithelium, allowing the periodontal ligament and bone tissue to selectively repopulate the root surface.⁹³⁰ To this end, a PCL nanofiber mat containing ZnO nanoparticles was developed.⁹³⁰ Using a rat periodontal defect model, even the incorporation of ZnO nanoparticles at a level as low as 0.5 wt % endowed the mat with antibacterial and osteoconductive responses, enhancing the treatment of periodontitis-related bone loss.

6.3.3. Filtration Membranes.—Electrospun nanofibers are well-developed as filtration membranes for biomedical applications, such as the separation of bacteria and white blood cells. For example, an antibacterial filter was developed from PAN nanofibers containing Ag nanoparticles, exhibiting both bacterial filtration capability and antibacterial activity.⁹⁹⁸ When tested for Gram-positive *S. aureus* and Gram-negative *E. coli* bacteria, the filter showed 99% filtration efficiency in addition to marked antibacterial activity. In another study, electrospun nanofibers made of poly(butylene terephthalate) were coated on a traditional poly(butylene terephthalate) nonwoven fabric to improve the filtration of white blood cells.⁹⁹⁹ Compared with the pristine fabric that reduced the number of white blood cells from 10^9 to 10^5 L^{-1} , the fabric coated with electrospun nanofibers was able to reduce the number down to 10^4 L^{-1} .

6.4. New Directions for Future Development

Electrospinning is a simple and versatile technique capable of producing nanofibers to suit various biomedical applications. By optimizing the parameters for electrospinning and/or combining with other methods, one can readily generate physical, biological, and chemical cues on electrospun nanofibers in a controllable and reproducible manner. Hence, prior to designing a nanofiber-based scaffold, it is necessary to take a full consideration of the typical cues needed, the properties of the nanofiber-based scaffold, and the specific requirements from different applications. At the current stage of development, the main challenge comes from the difficulty in directly generating nanofiber-based 3D scaffolds with diversified structures by electrospinning. In addition, a robust and flexible 3D scaffold is also needed in order to mimic the natural microenvironment of tumor ECM for cancer research. However, only a limited number of studies have been conducted with regard to the design and fabrication of nanofiber-based, 3D scaffolds, let alone the generation of topographic, physicochemical, and biological cues in the same scaffold. As such, there is an urgent need to find a simple and versatile strategy for tailoring the 3D architecture of a scaffold and thus optimizing the cell patterns.

Electrospun nanofibers also allow for the versatile fabrication of cell–material composites. By integrating stem cells with a nanofiber-based scaffold and/or other cues (e.g., biochemical and electrical), one can further enhance the guidance provided by the scaffold and associated cues. As a result, it will be easier to provide a microenvironment similar to the native tissue, offering a desirable alternative for tissue regeneration. There is also a new trend in developing multifunctional scaffolds comprised of nanofibers and/or other bioactive components for localized tumor therapy and simultaneous tissue regeneration. To this end, the electrospun nanofibers are often integrated with topographic and biochemical cues

during electrospinning, together with the functionalization of nanoparticles post electrospinning.

It should be pointed out that past and current studies related to tissue regeneration are mostly conducted with healthy animals, which are not representative of actual clinical demands. For example, patients who require artificial vascular graft implantation are often accompanied by other comorbidities, such as hyperlipidaemia, hypertension, and diabetes, which should also be considered when assessing the potential of vascular grafts that are intended for clinical applications.¹⁰⁰⁰

To this end, developing appropriate animal models should also be taken into account when investigating tissue regeneration, as well as for cancer treatment and other related biomedical applications.

7. CONCLUDING REMARKS

Over the past two decades or so, remarkable progress has been made with regard to the development of electrospinning methods and engineering of electrospun nanofibers to suit or enable various applications. Most of the advances were made possible through the achievement of a better understanding of the electrospinning mechanism and a better control of the materials. A wide variety of materials, including polymers, small molecules, and colloidal particles, as well as composites, have been successfully electrospun into nanofibers. In terms of methods, electrospinning has been performed in both far-and near-field configurations. The spinneret has been designed with a hollow, solid, or coaxial structure and utilized as a single unit or in an array. In addition to conductive solid collectors with different surface patterns, liquid bath has been explored as a collector to enable the fabrication of nanofibers with novel structures and morphologies, in addition to the extension of dimensionality. During or post-electrospinning, it is also feasible to expand the diversity, scope, and functionality of electrospun nanofibers by engineering their composition, structure, morphology, and assembly. Notable examples include the fabrication of nanofibers made of carbon, ceramics, or metals; incorporation of enzymes, biological effectors, or nanoparticles into nanofibers; creation of pores and/or hollow interiors in the nanofibers; conjugation of specific functional groups or biological effectors to the surface of nanofibers; alignment of nanofibers into uniaxial or radial arrays; stacking of nanofibers into patterned architectures; and fabrication of 3D scaffolds by expanding a thin mat of nanofibers along the vertical direction.

As a result of their remarkable properties, electrospun nanofibers have found widespread use in a variety of applications ranging from catalysis to environmental protection, energy harvesting/conversion/storage, and biomedicine. Specifically, owing to their high porosity and large specific surface areas, nonwoven mats of electrospun nanofibers have been applied as advanced filters for the removal of pollutants from both polluted air and wastewater. Upon optimization in terms of diameter, porosity, alignment, stacking, surface functional groups, mechanical properties, and biodegradability, nanofiber-based scaffolds have been explored to enhance the repair or regeneration of various types of tissues, including nerve, skin, heart, blood vessel, musculoskeletal system, and tissue interfaces. Recent clinical trials on

electrospun nanofibers have begun to pave the way for their ultimate implementation in regenerative medicine, especially for use as barrier membranes to prevent the adhesion between tissues after surgery.

New applications are also reported from time to time by integrating electrospun nanofibers with other types of functional (nano)materials. When this review was prepared, for example, it was reported that plasmonic nanostructures such as Au nanoparticles and nanocages could be readily incorporated into PVDF nanofibers by directly introducing them into the solution for electrospinning.^{1001–1003} The incorporation of plasmonic nanostructures facilitated the PVDF polymer chains to pack in the ferroelectric β phase for maximal piezoelectric and pyroelectric conversions. The strong and tunable optical absorption associated with Au nanostructures also made the composite nanofibers an effective transducer for converting light to heat and then electrical signal. With the incorporation of Au nanocages, the electrospun PVDF nanofibers were found to exhibit greatly enhanced capabilities for tactile and near-infrared sensing.¹⁰⁰² In another report, the nonwoven mat of PVDF nanofibers loaded with Au nanocages was applied to highly effective evaporation of water via photothermal heating.¹⁰⁰³ Because PVDF is highly hydrophobic, its nonwoven mat naturally floats on the surface of water without sinking. Upon irradiation with photons whose wavelengths match the absorption peaks of the Au nanocages, the water at the surface will be heated for evaporation while the bulk will stay at the ambient temperature (Figure 66). As a result, the efficiency for water evaporation can be substantially increased relative to the conventional techniques. Under natural solar irradiation (1000 W/m^2), water evaporation efficiencies as high as 67.0% and 79.8% were achieved for nonwoven mats of PVDF nanofibers loaded with Au nanocages at weight percentages of 0.05% and 0.10%, respectively. This new class of sustainable and scalable floating membranes opens the door to a new application for electrospun nanofibers regarding water desalination and purification.

Despite the large number of reports on the successful use of electrospun nanofibers in various applications, several key issues, in particular, those related to scale-up production and safety, are yet to be fully addressed in the setting of both research and commercialization. The low yield of the product is still one of the major drawbacks of electrospinning.⁹ On the other hand, the electrospinning process requires the use of a high voltage, which may cause danger to the workers, and it is not well applicable to some electric-sensitive materials, especially biomolecules. At the same time, people are constantly searching for alternative methods capable of producing nanofibers without involving an electric field and electrostatic interactions.

7.1. Scale-up Production

According to the data released by “Research and Markets”, the global market for nanofibers can reach 1 billion U.S. dollars by the end of 2021.¹⁰⁰⁴ To meet the market demand, there is an urgent need to scale-up the production of electrospun nanofibers by developing and/or implementing new techniques. To transfer electrospinning technology from laboratory to industrial production, the main difficulties and challenges include the following: (i) large-

volume production, (ii) precision in controlling the products, (iii) increase of the diversity and functionality of the nanofibers, and (iv) environmental concern.^{166,246}

To achieve large-volume production, both high throughput (i.e., the mass of the collected fibers over a certain period of time) and large area are required for the produced mats. To this end, multiple-needle electrospinning and needleless electrospinning hold great promise in increasing the volume of production. A notable example of multiple-needle electrospinning is the Nanospinner Industrial Electrospinning Line developed by Inovenso Inc.,¹⁰⁰⁵ which involves 110 needles (Figure 67A) and has been redeemed to commercial use for the production of filtration membranes and medical devices. This system is able to produce nonwoven mats of 1.0 m in width (Figure 67B) at a net nanofiber production capacity of 5 kg/day when a 13 wt % solution of TPU is used.¹⁰⁰⁵ Several issues, including the repulsion among the different jets and clogging of the needles, remain to be addressed. A typical example of needleless electrospinning is the Nanospider Production Line developed by Elmarco Inc.,^{1006,1007} which uses a wire electrode to eject multiple jets (Figure 67C). Specifically, Nanospider NS 8S1600U is able to produce up to 20,000,000 m² of nonwoven mats annually, together with a maximum width of 1.6 m (Figure 67D). In addition, by coupling with a screw extruder, this needleless system can be applied to the continuous production of nanofibers from a polymer melt. Using a so-called umbellate spinneret, up to 60 jets could be simultaneously ejected, achieving a productivity of 0.86 kg/day.¹⁰⁰⁸ By further increasing the number of the umbellate spinnerets, the productivity was increased to 7.2–14.4 kg/day for the production of nonwoven mats with a width of 0.8 m. Because of its simple configuration and uniform electric field, needleless electrospinning is anticipated to become the workhorse for the commercial production of nanofibers. As a major limitation, it is still difficult to use this system to produce nanofibers with unconventional structures or morphologies, such as core-sheath nanofibers. In both cases, the production of the nanofiber-based mat is usually limited to several tens of kilograms per day, which cannot satisfy the industrial demand.

The reproducible manufacturing of high-quality products critically depends on both the accuracy and reproducibility of a production process.²⁴⁶ An integration of theoretical modeling and real-time manipulation of the parameters for electrospinning plays an important role in improving the reproducibility. A climate-controlled electrospinning system is also beneficial in terms of keeping the temperature and relative humidity within suitable ranges to maintain the reproducibility. In this regard, the laboratory-scale system developed by a Dutch company (IME Technologies) contains a chamber and a control cabinet to house the air conditioner, water filtration unit, and the control system for both temperature and relative humidity. The temperature can be controlled with an accuracy of ± 0.5 °C in the range of 20–45 °C $\pm 1\%$ while the relative humidity can be adjusted to any level in the range of 10–90%. Nanospider NS 8S1600U also has a mechanism for controlling the temperature and relative humidity.

Another important perspective in the scale-up production of nanofibers is to ensure the generation and/or retention of functions because nanofibers with unconventional structures (e.g., core-sheath or hollow) or assembled into ordered arrays could be of greater value when compared with the conventional nonwoven mats of solid nanofibers. To this end, specially

designed spinnerets or collectors have to be employed. For example, a conveyor belt sliding on a grounded conductive substrate has been demonstrated for use as a collector to continuously generate and collect uniaxially aligned nanofibers.²⁴⁶

The last but not the least, environmental issues, such as pollution and safety concern, have to be fully considered when scaling up a spinning technique. During solution electrospinning, for example, solvent typically occupies 70–90 wt % of the solution. Evaporation of the solvent into the environment will result in environmental burden and safety concern, as well as waste of chemicals. When flammable organic solvents are used, a large amount of combustible gas will be created, leading to a hidden fire hazard. The residual solvents in the products may also impact the properties of the products and raise safety concern, especially for those used in biomedical and pharmaceutical applications. When operated on a large scale, it is necessary to develop a solvent recovery system for collecting and recycling the evaporated solvent or to apply a “green” technique such as melt electrospinning to avoid the use of any solvent.

Recently, a number of entrepreneurs have taken electrospun nanofibers from academic research to commercial applications. To this end, although a wide variety of industrial-scale electrospinning equipment with different types of spinning/collecting devices and accessories are available, a number of issues still need to be addressed: (i) the throughput is often below what is needed for most industrial applications; (ii) a reliable system for monitoring and controlling the properties of the electrospinning liquid and the processing parameters is yet to be introduced; and (iii) an online system for real-time examination of the nanofibers and quality control is missing. Despite these and other issues, there are at least 20 companies in the world that manufacture a bunch of upstream nanofibers for over 50 different types of downstream products. As shown in Table 2, the products are predominantly used for gas and liquid filtration, including the following: (i) the removal of dust, diesel particulate, smoke, and aerosol particles from an air intake system and (ii) the separation of oil from wastewater. Filtration and purification constitute the most developed applications, in which the peculiarities of nanofibers have been fruitfully translated into commercial success. Emerging products include reverse osmosis membranes for water purification, membranes for fuel cells, separators for batteries, smart coatings, and biomedical scaffolds.^{166,246} In the near future, commercial products ready to debut are likely those related to energy storage (e.g., separators for batteries) and smart coatings. For biomedical applications, new products keep entering into clinical trials in recent years. Most of the companies in the biomedical field, however, are academic spinoffs or pharmaceutical companies that only develop proprietary products. Considering the tremendous time and efforts needed to get international validation and authorization, products for biomedical use are not expected in the near future.

7.2. Safety Concern of Nanofibers

As a class of 1D nanomaterials, the safety concern of nanofibers originates not only from the production process but also from their potential harm to human beings and other living species. The safety concern during the production process is mainly related to the toxicity and environmental burden of the polymers and solvents as discussed above. Although

electrospinning has been used to process recycled common plastics (e.g., PS, polyethylene terephthalate, polycarbonate, and their blends) into high-value and high-performance products by eliminating the step of purifying the recycled raw materials, the use of organic solvents still makes this technology less environmentally benign.^{1009,1010}

When assessing the impacts of electrospun nanofibers on human beings and other living species, the diameter, length, and composition of the nanofibers all need to be considered. It was reported that electrospun Ag nanofibers of 5–20 μm in length were lodged in the lungs of mice and caused respiratory problems when they were intrapleurally injected into the lungs.¹⁰¹¹ Other studies also suggested the harmful effects of inorganic nanofibers that were relatively short, with diameters in the range of tens of nanometers or below.¹⁰¹² Such short nanofibers may be easily inhaled to cause inflammatory reactions in lungs.¹⁰¹³ To this end, we should take lesson from the case of asbestos, a class of natural nanofibers that were very popular for use as building materials but later found to be carcinogenic.¹⁰¹⁴ In general, electrospun nanofibers have a length more than a few centimeters. At such a length scale, the chance for electrospun nanofibers to reach the lung is quite small. As shown in a study involving rat silicosis model, biodegradable and biocompatible electrospun cellulose nanofibers (20 μm in length) inhaled into the lung could even facilitate the clearance of silica particles.¹⁰¹⁵ Nevertheless, only a very limited number of studies have been conducted so far in addressing the inhalation safety of electrospun nanofibers; no conclusion can be drawn yet.

7.3. Other Techniques for Producing Nanofibers

In addition to electrospinning, other techniques have also been developed to generate (nano)fibers in recent years.^{9,1016} In these new variants, the electrostatic force needed to produce nanofibers in the electrospinning process is replaced with other forces such as centrifugal and shear forces. For example, a nozzle-free centrifugal spinning method was reported, by which polymer nanofibers with diameter as thin as 25 nm could be produced.¹⁰¹⁷ The method involves the application of drops of a polymer solution onto a standard spin coater, followed by fast rotation of the chuck of the spin coater. The fiber formation relies on the instability of the spin-coated liquid film, which arises as a result of the competition between the centrifugal force and the Laplace force induced by the surface curvature. On the basis of this design, a rotary jet-spinning technique was developed to further improve the production throughput.¹⁰¹⁸ In this process, polymer solution is fed into a rotating reservoir in the middle of the system. Rotation causes ejection of a jet of polymer solution from the orifices on the side wall of the rotating reservoir. To initiate jetting, it is necessary that the centrifugal force is greater than the capillary force exerted by the polymer solution in the orifices. The jet experiences an extension based on its inherent viscosity and the centrifugal force. Once the jets are solidified, fibers are formed and deposited on a cylindrical collector placed around the reservoir. Polymer nanofibers with diameters thinner than 100 nm can be produced using this technique.¹⁰¹⁹ Variants of this technique have also been reported and even commercialized, including Forcespinning,¹⁰²⁰ liquid shearing spinning,¹⁰²¹ magnetospinning,¹⁰²² and brush spinning,¹⁰²³ among others. Furthermore, a pressurized gyration process was developed by integrating centrifugal spinning with solution blowing to produce polymer nanofibers.^{1024,1025} In a typical process, a gas stream is connected to the

rotating reservoir to enhance the stretching of the jet by blowing a gas. This technique can produce nanofibers at a throughput of 6 kg/h, offering capability for mass production. Although these techniques are able to improve the throughput of nanofiber production, they tend to suffer from problems such as the difficulties in producing core-sheath, aligned, and/or patterned nanofibers. Therefore, it is still necessary to develop a new technique capable of producing nanofibers with diversified properties and at a high throughout.

ACKNOWLEDGMENTS

This work was supported in part by two grants from NIH (R01 AR060820 and R01 EB020050) and startup funds from the Georgia Institute of Technology. Y.D. was also partially supported by the National Natural Science Foundation of China (Grant 21201034) and the Natural Science Foundation of Jiangsu Province (Grant BK20171153).

Biographies

Jiajia Xue received her Ph.D. in Materials Science and Engineering from Beijing University of Chemical Technology in 2015 with Professor Liqun Zhang. She joined the Xia group as a postdoctoral fellow in August 2015. Her research interests include the fabrication of nanomaterials and scaffolds for tissue engineering and drug delivery.

Tong Wu received her Ph.D. in Biomaterials Science from Donghua University in 2018 with Professor Xiumei Mo. She joined the Xia group as a visiting graduate student in October 2016 and then started as a postdoctoral fellow in December 2018. Her research interests include the synthesis of nanostructured materials for biomedical, environmental, and energy-related applications.

Yunqian Dai received her Ph.D. in Materials Physics and Chemistry from Southeast University in 2011 with Professor Yueming Sun. She spent two years in the Xia group as a visiting graduate student at Washington University in St. Louis from 2008 to 2010. She started as an Assistant Professor in the School of Chemistry and Chemical Engineering in Southeast University in 2011 and then promoted to Associate Professor in 2015.

Younan Xia received his Ph.D. in Physical Chemistry from Harvard University in 1996 with Professor George M. Whitesides. He started as an Assistant Professor of Chemistry at the University of Washington (Seattle) in 1997 and then joined the Department of Biomedical Engineering at Washington University in St. Louis in 2007 as the James M. McKelvey Professor. Since 2012, he has held the position of Brock Family Chair and GRA Eminent Scholar in Nanomedicine at the Georgia Institute of Technology. He has served as an Associate Editor of *Nano Letters* since 2002.

LIST OF ABBREVIATIONS

η	filtration efficiency
μ	dipole moment
μ_{FE}	field-effect mobility

1D	one-dimensional
2D	two-dimensional
3D	three-dimensional
AC	alternating current
ADT	accelerated durability test
AFM	atomic force microscopy
Alq₃	tris(8-hydroxyquinolinato)aluminum
BET	Brunauer–Emmett–Teller
BSA	bovine serum albumin
CE	Conformité Européene
cmc	critical micelle concentration
CTAB	hexadecyltrimethylammonium bromide
CTCs	circulating tumor cells
CWAs	chemical warfare agents
DC	direct current
DMF	dimethylformamide
DMSO	dimethyl sulfoxide
D_p	pressure drop
DRG	dorsal root ganglia
DSSCs	dye-sensitized solar cells
ECM	extracellular matrix
ELISA	enzyme-linked immunosorbent assays FETs field-effect transistors
F_R	lateral force
HEPA	high-efficiency particulate air
HFIP	hexafluoroisopropanol
I_{on}/I_{off}	on/off current ratio
iPSCs	induced pluripotent stem cells
IR	infrared light
ITO	indium tin oxide

L	critical length
LCSTs	low critical solution temperatures LEDs light-emitting diodes
LIBs	lithium ion batteries
MOF	metal–organic framework
MSCs	mesenchymal stem cells
M_w	molecular weight
NGC	nerve guidance conduit
NPB	N,N'-di(1-naphthyl)-N,N'-diphenyl-(1,1'-biphenyl)-4,4'-diamine
ORR	oxygen reduction reaction
PAN	polyacrylonitrile
PANI	polyaniline
p_c	capillary pressure
PC12	cells rat pheochromocytoma
PCE	power conversion efficiency
PCL	poly(ϵ -caprolactone)
PDMS	poly(dimethylsiloxane)
p_e	electrostatic pressure
PEDOT	poly(3,4-ethylenedioxythiophene)
PEG	poly(ethylene glycol)
PEMFCs	proton exchange membrane fuel cells
PEO	poly(ethylene oxide)
PET	poly(ethylene terephthalate)
PLA	poly(lactic acid)
PLCL	poly(L-lactide- <i>co</i> - ϵ -caprolactone)
PLGA	poly(lactic- <i>co</i> -glycolic acid)
PMIA	poly(<i>m</i> -phenylene isophthalamide)
PMMA	poly(methyl methacrylate)
PMs	particulate matters
PNIPAAm	poly(<i>N</i> -isopropylacrylamide)

PP	polypropylene
ppb	parts per billion
ppm	parts per million
PPy	polypyrrole
PS	polystyrene
PSCs	perovskite solar cells
PSMA	poly[styrene- <i>co</i> -(maleic sodium anhydride)] PSS poly(styrenesulfonate)
PTFE	poly (tetrafluoroethylene)
PVA	poly(vinyl alcohol)
PVC	poly(vinyl chloride)
PVDF	poly(vinylidene fluoride)
PVP	poly(vinylpyrrolidone)
QF	quality factor
R_f	shape fixity rate
RNAi	RNA interference
R_r	shape recovery rate
SEM	scanning electron microscopy
SMCs	smooth muscle cells
SOFCs	solid oxide fuel cells
TEM	transmission electron microscopy
TEOS	tetraethyl orthosilicate
T_g	glass transition temperature
THF	tetrahydrofuran
Ti(O<i>i</i>Pr)₄	titanium tetraisopropoxide
T_m	melting point TOFs turnover frequencies
TPU	thermoplastic polyurethane Ttrans transition temperature
V_c	critical voltage
WCA	water contact angle

REFERENCES

- (1). Vollrath F; Knight DP Liquid Crystalline Spinning of Spider Silk. *Nature* 2001, 410, 541–548. [PubMed: 11279484]
- (2). Heim M; Keerl D; Scheibel T Spider Silk: From Soluble Protein to Extraordinary Fiber. *Angew. Chem., Int. Ed* 2009, 48, 3584–3596.
- (3). Andersson M; Jia Q; Abella A; Lee X-Y; Landreh M; Purhonen P; Hebert H; Tenje M; Robinson CV; Meng Q; et al. Biomimetic Spinning of Artificial Spider Silk from a Chimeric Minispidroin. *Nat. Chem. Biol* 2017, 13, 262–264. [PubMed: 28068309]
- (4). Woodings C, Ed. Regenerated Cellulose Fibres; Woodhead: Cambridge, U.K., 2001; Chapter 5.
- (5). Carothers WH Alkylene Ester of Polybasic Acids U.S. Pat. 2,012,267, 1935.
- (6). Carothers WH Linear Condensation Polymers U.S. Pat. 2,071,250, 1937.
- (7). McIntyre JE Synthetic Fibres: Nylon, Polyester, Acrylic, Polyolefin; Woodhead: Cambridge, U.K., 2005; Chapter 1.
- (8). Gupta V, Kothari V, Eds. Manufactured Fibre Technology; Chapman & Hall: London, 1997; Chapter 1.
- (9). Luo C; Stoyanov SD; Stride E; Pelan E; Edirisinghe M Electrospinning Versus Fibre Production Methods: From Specifics to Technological Convergence. *Chem. Soc. Rev* 2012, 41, 4708–4735. [PubMed: 22618026]
- (10). Boys CV On the Production, Properties, and Some Suggested Uses of the Finest Threads. *Proc. Phys. Soc. London* 1887, 9, 8201319.
- (11). Dzenis Y Spinning Continuous Fibers for Nanotechnology. *Science* 2004, 304, 1917–1919. [PubMed: 15218134]
- (12). Jian S; Zhu J; Jiang S; Chen S; Fang H; Song Y; Duan G; Zhang Y; Hou H Nanofibers with Diameter Below One Nanometer from Electrospinning. *RSC Adv* 2018, 8, 4794–4802.
- (13). Gilbert W De Magnete; Courier: New York, 1958.
- (14). Gray SA Letter Concerning the Electricity of Water, from Mr. Stephen Gray to Cromwell Mortimer. *Philos. Trans. R. Soc. London* 1731, 37, 227–260.
- (15). Nollet JAX Part of a Letter from Abbé Nollet, of the Royal Academy of Sciences at Paris, to Martin Folkes, Concerning Electricity. *Philos. Trans* 1748, 45, 187–194.
- (16). Rayleigh L XX. On the Equilibrium of Liquid Conducting Masses Charged with Electricity. *Philos. Mag* 1882, 14, 184–186.
- (17). Bailey AG Electrostatic Spraying of Liquids; John Wiley & Sons: New York, 1988.
- (18). Cooley JF Apparatus for Electrically Dispersing Fluids U.S. Pat. 692,631, 1902.
- (19). Morton WJ Method of Dispersing Fluid U.S. Pat. 705,691, 1902.
- (20). Formhals A Process and Apparatus for Preparing Artificial Threads U.S. Pat. 1,975,504, 1934.
- (21). Formhals A Method and Apparatus for Spinning U.S. Pat. 2,349,950, 1944.
- (22). Taylor GI Disintegration of Water Drops in an Electric Field. *Proc. R. Soc. London A* 1964, 280, 383–397.
- (23). Taylor GI The Force Exerted by an Electric Field on a Long Cylindrical Conductor. *Proc. R. Soc. London, Ser. A* 1966, 291, 145–158.
- (24). Taylor G Electrically Driven Jets. *Proc. R. Soc. London, Ser. A* 1969, 313, 453–475.
- (25). Martin GE; Cockshott ID Fibrillar Lining for Prosthetic Device U.S. Pat. 4,044,404, 1977.
- (26). Fong H; Chun I; Reneker DH Beaded Nanofibers Formed During Electrospinning. *Polymer* 1999, 40, 4585–4592.
- (27). Reneker DH; Yarin AL; Fong H; Koombhongse S Bending Instability of Electrically Charged Liquid Jets of Polymer Solutions in Electrospinning. *J. Appl. Phys* 2000, 87, 4531–4547.
- (28). Shin YM; Hohman MM; Brenner MP; Rutledge GC Experimental Characterization of Electrospinning: The Electrically Forced Jet and Instabilities. *Polymer* 2001, 42, 09955–09967.
- (29). Yarin AL; Koombhongse S; Reneker DH Bending Instability in Electrospinning of Nanofibers. *J. Appl. Phys* 2001, 89, 3018–3026.

- (30). Hohman MM; Shin M; Rutledge GC; Brenner MP Electrospinning and Electrically Forced Jets. I. Stability Theory. *Phys. Fluids* 2001, 13, 2201–2220.
- (31). Hohman MM; Shin M; Rutledge GC; Brenner MP Electrospinning and Electrically Forced Jets. II. Applications. *Phys. Fluids* 2001, 13, 2221–2236.
- (32). Shin YM; Hohman MM; Brenner MP; Rutledge GC Electrospinning: A Whipping Fluid Jet Generates Submicron Polymer Fibers. *Appl. Phys. Lett* 2001, 78, 1149–1151.
- (33). Dai H; Gong J; Kim H; Lee D A Novel Method for Preparing Ultra–Fine Alumina–Borate Oxide Fibres via an Electrospinning Technique. *Nanotechnol* 2002, 13, 674–677.
- (34). Larsen G; Velarde-Ortiz R; Minchow K; Barrero A; Loscertales IG A Method for Making Inorganic and Hybrid (Organic/Inorganic) Fibers and Vesicles with Diameters in the Submicrometer and Micrometer Range via Sol–Gel Chemistry and Electrically Forced Liquid Jets. *J. Am. Chem. Soc* 2003, 125, 1154–1155. [PubMed: 12553802]
- (35). Li D; Wang Y; Xia Y Electrospinning of Polymeric and Ceramic Nanofibers as Uniaxially Aligned Arrays. *Nano Lett* 2003, 3, 1167–1171.
- (36). Theron A; Zussman E; Yarin A Electrostatic Field–Assisted Alignment of Electrospun Nanofibres. *Nanotechnology* 2001, 12, 384–390.
- (37). Deitzel JM; Kleimeyer JD; Hirvonen JK; Beck Tan NC Controlled Deposition of Electrospun Poly(ethylene oxide) Fibers. *Polymer* 2001, 42, 8163–8170.
- (38). Dersch R; Liu T; Schaper A; Greiner A; Wendorff J Electrospun Nanofibers: Internal Structure and Intrinsic Orientation. *J. Polym. Sci., Part A: Polym. Chem* 2003, 41, 545–553.
- (39). Sun Z; Zussman E; Yarin AL; Wendorff JH; Greiner A Compound Core–Shell Polymer Nanofibers by Co-Electrospinning. *Adv. Mater* 2003, 15, 1929–1932.
- (40). Smit E; B ttner U; Sanderson RD Continuous Yarns from Electrospun Fibers. *Polymer* 2005, 46, 2419–2423.
- (41). Li D; Xia Y Electrospinning of Nanofibers: Reinventing the Wheel? *Adv. Mater* 2004, 16, 1151–1170.
- (42). Xue J; Xie J; Liu W; Xia Y Electrospun Nanofibers: New Concepts, Materials, and Applications. *Acc. Chem. Res* 2017, 50, 1976–1987. [PubMed: 28777535]
- (43). Sun B; Long YZ; Zhang HD; Li MM; Duvail JL; Jiang XY; Yin HL Advances in Three-Dimensional Nanofibrous Macrostructures via Electrospinning. *Prog. Polym. Sci* 2014, 39, 862–890.
- (44). Liao Y; Loh CH; Tian M; Wang R; Fane AG Progress in Electrospun Polymeric Nanofibrous Membranes for Water Treatment: Fabrication, Modification and Applications. *Prog. Polym. Sci* 2018, 77, 69–94.
- (45). Duft D; Achtzehn T; Müller R; Huber BA; Leisner T Rayleigh Jets from Levitated Microdroplets. *Nature* 2003, 421, 128. [PubMed: 12520291]
- (46). Li D; Marquez M; Xia Y Capturing Electrified Nanodroplets under Rayleigh Instability by Coupling Electrospray with a Sol–Gel Reaction. *Chem. Phys. Lett* 2007, 445, 271–275.
- (47). Reneker DH, Fong H, Eds. *Polymeric Nanofibers*; American Chemical Society: Washington, DC, USA, 2006; DOI: 10.1021/bk-2006-0918.
- (48). Finn R Capillary Surface Interfaces. *Notices AMS* 1999, 46, 770–781.
- (49). Young T III. An Essay on the Cohesion of Fluids. *Philos. Trans. R. Soc. London* 1805, 95, 65–87.
- (50). Reneker DH; Yarin AL Electrospinning Jets and Polymer Nanofibers. *Polymer* 2008, 49, 2387–2425.
- (51). Yarin AL; Koombhongse S; Reneker DH Taylor Cone and Jetting from Liquid Droplets in Electrospinning of Nanofibers. *J. Appl. Phys* 2001, 90, 4836–4846.
- (52). Collins RT; Jones JJ; Harris MT; Basaran OA Electrohydrodynamic Tip Streaming and Emission of Charged Drops from Liquid Cones. *Nat. Phys* 2008, 4, 149–154.
- (53). Fridrikh SV; Yu JH; Brenner MP; Rutledge GC Controlling the Fiber Diameter During Electrospinning. *Phys. Rev. Lett* 2003, 90, 144502. [PubMed: 12731920]
- (54). Feng J The Stretching of an Electrified Non–Newtonian Jet: A Model for Electrospinning. *Phys. Fluids* 2002, 14, 3912–3926.

- (55). Feng J Stretching of a Straight Electrically Charged Viscoelastic Jet. *J. Non-Newtonian Fluid Mech* 2003, 116, 55–70.
- (56). He JH; Wu Y; Zuo WW Critical Length of Straight Jet in Electrospinning. *Polymer* 2005, 46, 12637–12640.
- (57). Reneker DH; Kataphinan W; Theron A; Zussman E; Yarin AL Nanofiber Garlands of Polycaprolactone by Electrospinning. *Polymer* 2002, 43, 6785–6794.
- (58). Helgeson ME; Grammatikos KN; Deitzel JM; Wagner NJ Theory and Kinematic Measurements of the Mechanics of Stable Electrospun Polymer Jets. *Polymer* 2008, 49, 2924–2936.
- (59). Gañán-Calvo AM Cone–Jet Analytical Extension of Taylor’s Electrostatic Solution and the Asymptotic Universal Scaling Laws in Electrospraying. *Phys. Rev. Lett* 1997, 79, 217–220.
- (60). Xu H Formation and Characterization of Polymer Jets in Electrospinning Ph.D. Thesis; University of Akron, Akron, OH, USA, 2003.
- (61). Salem DR, Ed. Structure Formation in Polymeric Fibers; Hanser: Munich, 2001; Chapter 6.
- (62). Reneker DH; Yarin AL; Zussman E; Xu H Advances in Applied Mechanics; Elsevier, 2007; Vol. 41.
- (63). Liu F; Guo R; Shen M; Wang S; Shi X Effect of Processing Variables on the Morphology of Electrospun Poly[(lactic acid)-co-(glycolic acid)] Nanofibers. *Macromol. Mater. Eng* 2009, 294, 666–672.
- (64). Yarin A; Kataphinan W; Reneker DH Branching in Electrospinning of Nanofibers. *J. Appl. Phys* 2005, 98, 064501.
- (65). Collins G; Federici J; Imura Y; Catalani LH Charge Generation, Charge Transport, and Residual Charge in the Electrospinning of Polymers: A Review of Issues and Complications. *J. Appl. Phys* 2012, 111, 044701.
- (66). Catalani LH; Collins G; Jaffe M Evidence for Molecular Orientation and Residual Charge in the Electrospinning of Poly-(butylene terephthalate) Nanofibers. *Macromolecules* 2007, 40, 1693–1697.
- (67). Han T; Reneker DH; Yarin AL Pendulum–Like Motion of Straight Electrified Jets. *Polymer* 2008, 49, 2160–2169.
- (68). Filatov Y; Budyka A; Kirichenko V Electrospinning of Micro-and Nanofibers: Fundamentals in Separation and Filtration Processes; Begellhouse, 2007; Chapter 1.
- (69). Terada D; Kobayashi H; Zhang K; Tiwari A; Yoshikawa Ch.; Hanagata N Transient Charge-Masking Effect of Applied Voltage on Electrospinning of Pure Chitosan Nanofibers from Aqueous Solutions. *Sci. Technol. Adv. Mater* 2012, 13, 015003. [PubMed: 27877470]
- (70). Tong H-W; Wang M Negative Voltage Electrospinning and Positive Voltage Electrospinning of Tissue Engineering Scaffolds: A Comparative Study and Charge Retention on Scaffolds. *Nano LIFE* 2012, 2, 1250004.
- (71). Hu J; Wang X; Ding B; Lin J; Yu J; Sun G One-Step Electro-Spinning/Netting Technique for Controllably Preparing Polyurethane Nano-Fiber/Net. *Macromol. Rapid Commun* 2011, 32, 1729–1734. [PubMed: 21858891]
- (72). Demir MM; Yilgor I; Yilgor E; Erman B Electrospinning of Polyurethane Fibers. *Polymer* 2002, 43, 3303–3309.
- (73). Kessick R; Fenn J; Tepper G The Use of AC Potentials in Electrospraying and Electrospinning Processes. *Polymer* 2004, 45, 2981–2984.
- (74). Balogh A; Farkas B; Verreck G; Mensch J; Borbás E; Nagy B; Marosi G; Nagy ZK AC and DC Electrospinning of Hydroxypropylmethylcellulose with Polyethylene Oxides as Secondary Polymer for Improved Drug Dissolution. *Int. J. Pharm* 2016, 505, 159–166. [PubMed: 26997426]
- (75). Stanishevsky A; Brayer WA; Pokorný P; Kalouš T; Lukáš D Nanofibrous Alumina Structures Fabricated Using High-Yield Alternating Current Electrospinning. *Ceram. Int* 2016, 42, 17154–17161.
- (76). Sarkar S; Deevi S; Tepper G Biased AC Electrospinning of Aligned Polymer Nanofibers. *Macromol. Rapid Commun* 2007, 28, 1034–1039.
- (77). Maheshwari S; Chang H-C Assembly of Multi-Stranded Nanofiber Threads through AC Electrospinning. *Adv. Mater* 2009, 21, 349–354.

- (78). Zheng J-Y; Liu H-Y; Wang X; Zhao Y; Huang W-W; Zheng G-F; Sun D-H Electrohydrodynamic Direct-Write Orderly Micro/Nanofibrous Structure on Flexible Insulating Substrate. *J. Nanomater* 2014, 2014, 708186.
- (79). Luo CJ; Nangrejo M; Edirisinghe M A Novel Method of Selecting Solvents for Polymer Electrospinning. *Polymer* 2010, 51, 1654–1662.
- (80). Luo CJ; Stride E; Edirisinghe M Mapping the Influence of Solubility and Dielectric Constant on Electrospinning Polycaprolactone Solutions. *Macromolecules* 2012, 45, 4669–4680.
- (81). Husain O; Lau W; Edirisinghe M; Parhizkar M Investigating the Particle to Fibre Transition Threshold During Electrohydrodynamic Atomization of a Polymer Solution. *Mater. Sci. Eng., C* 2016, 65, 240–250.
- (82). Talwar S; Krishnan AS; Hinestroza JP; Pourdeyhimi B; Khan SA Electrospun Nanofibers with Associative Polymer–Surfactant Systems. *Macromolecules* 2010, 43, 7650–7656.
- (83). Angammana CJ; Jayaram SH A Modified Electrospinning Method for Conductive and Insulating Materials. *Proc. ESA Annu. Meet. Electrost* 2010, L3.
- (84). Angammana CJ; Jayaram SH Analysis of the Effects of Solution Conductivity on Electrospinning Process and Fiber Morphology. *IEEE Trans. Ind. Appl* 2011, 47, 1109–1117.
- (85). Haider A; Haider S; Kang I-K A Comprehensive Review Summarizing the Effect of Electrospinning Parameters and Potential Applications of Nanofibers in Biomedical and Biotechnology. *Arabian J. Chem* 2018, 11, 1165–1188.
- (86). Barakat NAM; Kanjwal MA; Sheikh FA; Kim HY Spider-Net within the N6, PVA and PU Electrospun Nanofiber Mats Using Salt Addition: Novel Strategy in the Electrospinning Process. *Polymer* 2009, 50, 4389–4396.
- (87). Wang X; Ding B; Yu J; Yang J Large-Scale Fabrication of Two-Dimensional Spider-Web-Like Gelatin Nano-Nets via Electro-Netting. *Colloids Surf., B* 2011, 86, 345–352.
- (88). Yang G-Z; Li H-P; Yang J-H; Wan J; Yu D-G Influence of Working Temperature on the Formation of Electrospun Polymer Nanofibers. *Nanoscale Res. Lett* 2017, 12, 55. [PubMed: 28105604]
- (89). González R; Pinto NJ Electrospun Poly(3-Hexylthiophene-2, 5-Diy) Fiber Field Effect Transistor. *Synth. Met* 2005, 151, 275–278.
- (90). Chronakis IS; Grapenson S; Jakob A Conductive Polypyrrole Nanofibers via Electrospinning: Electrical and Morphological Properties. *Polymer* 2006, 47, 1597–1603.
- (91). Huang Y-C; Lo T-Y; Chen C-H; Wu K-H; Lin C-M; Whang W-T Electrospinning of Magnesium-Ion Linked Binder-Less PEDOT:PSS Nanofibers for Sensing Organic Gases. *Sens. Actuators, B* 2015, 216, 603–607.
- (92). Okuzaki H; Takahashi T; Miyajima N; Suzuki Y; Kuwabara T Spontaneous Formation of Poly(p-phenylenevinylene) Nanofiber Yarns through Electrospinning of a Precursor. *Macromolecules* 2006, 39, 4276–4278.
- (93). Laforgue A; Robitaille L; Mokrini A; Ajji A Fabrication and Characterization of Ionic Conducting Nanofibers. *Macromol. Mater. Eng* 2007, 292, 1229–1236.
- (94). Bedford NM; Winget GD; Punnamaraju S; Steckl AJ Immobilization of Stable Thylakoid Vesicles in Conductive Nanofibers by Electrospinning. *Biomacromolecules* 2011, 12, 778–784. [PubMed: 21254765]
- (95). Bessaire B; Mathieu M; Salles V; Yeghoyan T; Celle C; Simonato J-P; Brioude A Synthesis of Continuous Conductive PEDOT:PSS Nanofibers by Electrospinning: A Conformal Coating for Optoelectronics. *ACS Appl. Mater. Interfaces* 2017, 9, 950–957. [PubMed: 27973763]
- (96). Cardenas JR; De Franca MGO; De Vasconcelos EA; De Azevedo WM; da Silva EF Jr Growth of Sub-micron Fibres of Pure Polyaniline Using the Electrospinning Technique. *J. Phys. D: Appl. Phys* 2007, 40, 1068–1071.
- (97). MacDiarmid A; Jones W; Norris I; Gao J; Johnson A; Pinto N; Hone J; Han B; Ko F; Okuzaki H; Llaguno M Electrostatically-Generated Nanofibers of Electronic Polymers. *Synth. Met* 2001, 119, 27–30.
- (98). Larrondo L; St. John Manley R Electrostatic Fiber Spinning from Polymer Melts. I. Experimental Observations on Fiber Formation and Properties. *J. Polym. Sci., Polym. Phys. Ed* 1981, 19, 909–920.

- (99). Brown TD; Dalton PD; Hutmacher DW Melt Electrospinning Today: An Opportune Time for an Emerging Polymer Process. *Prog. Polym. Sci.* 2016, 56, 116–166.
- (100). Hutmacher DW; Dalton PD Melt Electrospinning. *Chem.-Asian J.* 2011, 6, 44–56. [PubMed: 21080400]
- (101). Dalton PD; Klinkhammer K; Salber J; Klee D; Möller M Direct in Vitro Electrospinning with Polymer Melts. *Biomacromolecules* 2006, 7, 686–690. [PubMed: 16529400]
- (102). Molki M; Damronglerd P Electrohydrodynamic Enhancement of Heat Transfer for Developing Air Flow in Square Ducts. *Heat Transfer Eng.* 2006, 27, 35–45.
- (103). Zhmayev E; Cho D; Joo YL Electrohydrodynamic Quenching in Polymer Melt Electrospinning. *Phys. Fluids* 2011, 23, 073102.
- (104). Laohalertdecha S; Naphon P; Wongwises S A Review of Electrohydrodynamic Enhancement of Heat Transfer. *Renewable Sustainable Energy Rev.* 2007, 11, 858–876.
- (105). Zhmayev E; Zhou H; Joo YL Modeling of Non-Isothermal Polymer Jets in Melt Electrospinning. *J. Non-Newtonian Fluid Mech.* 2008, 153, 95–108.
- (106). Ould Ahmedou S; Havet M Effect of Process Parameters on the EHD Airflow. *J. Electrost.* 2009, 67, 222–227.
- (107). Dalton PD; Grafahrend D; Klinkhammer K; Klee D; Möller M Electrospinning of Polymer Melts: Phenomenological Observations. *Polymer* 2007, 48, 6823–6833.
- (108). Nayak R; Kyratzis IL; Truong YB; Padhye R; Arnold L Melt-Electrospinning of Polypropylene with Conductive Additives. *J. Mater. Sci.* 2012, 47, 6387–6396.
- (109). Brown TD; Dalton PD; Hutmacher DW Direct Writing by Way of Melt Electrospinning. *Adv. Mater.* 2011, 23, 5651–5657. [PubMed: 22095922]
- (110). Zhmayev E; Cho D; Joo YL Nanofibers from Gas-Assisted Polymer Melt Electrospinning. *Polymer* 2010, 51, 4140–4144.
- (111). Hochleitner G; Jüngst T; Brown TD; Hahn K; Moseke C; Jakob F; Dalton PD; Groll J Additive Manufacturing of Scaffolds with Sub-Micron Filaments via Melt Electrospinning Writing. *Biofabrication* 2015, 7, 035002. [PubMed: 26065373]
- (112). Zhu X; Niu Q; Xu Y; Wu G; Li G; Nie J; Ma G From Small Molecules to Polymer Fibers: Photopolymerization with Electrospinning on the Fly. *J. Photochem. Photobiol., A* 2018, 353, 101–107.
- (113). He H-W; Zhang B; Yan X; Dong R-H; Jia X-S; Yu GF; Ning X; Xia L-H; Long Y-Z Solvent-Free Thermocuring Electrospinning to Fabricate Ultrathin Polyurethane Fibers with High Conductivity by in Situ Polymerization of Polyaniline. *RSC Adv.* 2016, 6, 106945–106950.
- (114). Xu JF; Chen YZ; Wu D; Wu LZ; Tung CH; Yang QZ Photoresponsive Hydrogen-Bonded Supramolecular Polymers Based on a Stiff Stilbene Unit. *Angew. Chem., Int. Ed.* 2013, 52, 9738–9742.
- (115). Nuansing W; Georgilis E; de Oliveira TVAG; Charalambidis G; Eleta A; Coutsolelos AG; Mitraki A; Bittner AM Electrospinning of Tetraphenylporphyrin Compounds into Wires. Part. Part. Syst. Charact. 2014, 31, 88–93.
- (116). McKee MG; Layman JM; Cashion MP; Long TE Phospholipid Nonwoven Electrospun Membranes. *Science* 2006, 311, 353–355. [PubMed: 16424332]
- (117). Hunley MT; McKee MG; Long TE Submicron Functional Fibrous Scaffolds Based on Electrospun Phospholipids. *J. Mater. Chem.* 2007, 17, 605–608.
- (118). Jorgensen L; Qvortrup K; Chronakis IS Phospholipid Electrospun Nanofibers: Effect of Solvents and Co-Axial Processing on Morphology and Fiber Diameter. *RSC Adv.* 2015, 5, 53644–53652.
- (119). Cashion MP; Li X; Geng Y; Hunley MT; Long TE Gemini Surfactant Electrospun Membranes. *Langmuir* 2010, 26, 678–683. [PubMed: 19681628]
- (120). Hemp ST; Hudson AG; Allen MH; Pole SS; Moore RB; Long TE Solution Properties and Electrospinning of Phosphonium Gemini Surfactants. *Soft Matter* 2014, 10, 3970–3977. [PubMed: 24733359]
- (121). Singh G; Bittner AM; Loscher S; Malinowski N; Kern K Electrospinning of Diphenylalanine Nanotubes. *Adv. Mater.* 2008, 20, 2332–2336.

- (122). Nuansing W; Frauchiger D; Huth F; Rebollo A; Hillenbrand R; Bittner AM Electrospinning of Peptide and Protein Fibres: Approaching the Molecular Scale. *Faraday Discuss* 2013, 166, 209–221.
- (123). Tayi AS; Pashuck ET; Newcomb CJ; McClendon MT; Stupp SI Electrospinning Bioactive Supramolecular Polymers from Water. *Biomacromolecules* 2014, 15, 1323–1327. [PubMed: 24697625]
- (124). Celebioglu A; Uyar T Electrospinning of Nanofibers from Non-Polymeric Systems: Polymer -Free Nanofibers from Cyclodextrin Derivatives. *Nanoscale* 2012, 4, 621–631. [PubMed: 22159162]
- (125). Hunley MT; Karikari AS; McKee MG; Mather BD; Layman JM; Fornof AR; Long TE Taking Advantage of Tailored Electrostatics and Complementary Hydrogen Bonding in the Design of Nanostructures for Biomedical Applications. *Macromol. Symp* 2008, 270, 1–7.
- (126). Singer JC; Ringk A; Giesa R; Schmidt HW Melt Electrospinning of Small Molecules. *Macromol. Mater. Eng* 2015, 300, 259–276.
- (127). Choi S-S; Lee SG; Im SS; Kim SH; Joo YL Silica Nanofibers from Electrospinning/Sol-Gel Process. *J. Mater. Sci. Lett* 2003, 22, 891–893.
- (128). Geltmeyer J; De Roo J; Van den Broeck F; Martins JC; De Buysser K; De Clerck K The Influence of Tetraethoxysilane Sol Preparation on the Electrospinning of Silica Nanofibers. *J. Sol-Gel Sci. Technol* 2016, 77, 453–462.
- (129). Gu Y; Chen D; Jiao X Synthesis and Electrochemical Properties of Nanostructured LiCoO₂ Fibers as Cathode Materials for Lithium-Ion Batteries. *J. Phys. Chem. B* 2005, 109, 17901–17906. [PubMed: 16853296]
- (130). Li D; McCann JT; Xia Y; Marquez M Electrospinning: A Simple and Versatile Technique for Producing Ceramic Nanofibers and Nanotubes. *J. Am. Ceram. Soc* 2006, 89, 1861–1869.
- (131). Jang J; Hyun BG; Ji S; Cho E; An BW; Cheong WH; Park J-U Rapid Production of Large-Area, Transparent and Stretchable Electrodes Using Metal Nanofibers as Wirelessly Operated Wearable Heaters. *NPG Asia Mater* 2017, 9, e432.
- (132). Li D; Xia Y Fabrication of Titania Nanofibers by Electrospinning. *Nano Lett* 2003, 3, 555–560.
- (133). Dai Y; Liu W; Formo E; Sun Y; Xia Y Ceramic Nanofibers Fabricated by Electrospinning and Their Applications in Catalysis, Environmental Science, and Energy Technology. *Polym. Adv. Technol* 2011, 22, 326–338.
- (134). Saquing CD; Tang C; Monian B; Bonino CA; Manasco JL; Alsberg E; Khan SA Alginate –Polyethylene Oxide Blend Nanofibers and the Role of the Carrier Polymer in Electrospinning. *Ind. Eng. Chem. Res* 2013, 52, 8692–8704.
- (135). Malwal D; Gopinath P Fabrication and Characterization of Poly(ethylene oxide) Templated Nickel Oxide Nanofibers for Dye Degradation. *Environ. Sci.: Nano* 2015, 2, 78–85.
- (136). Viswanathamurthi P; Bhattacharai N; Kim H; Khil M; Lee D; Suh E-K GeO₂ Fibers: Preparation, Morphology and Photoluminescence Property. *J. Chem. Phys* 2004, 121, 441–445. [PubMed: 15260565]
- (137). Efome JE; Rana D; Matsuura T; Lan CQ Metal– Organic Frameworks Supported on Nanofibers to Remove Heavy Metals. *J. Mater. Chem. A* 2018, 6, 4550–4555.
- (138). Efome JE; Rana D; Matsuura T; Lan CQ Insight Studies on Metal-Organic Framework Nanofibrous Membrane Adsorption and Activation for Heavy Metal Ions Removal from Aqueous Solution. *ACS Appl. Mater. Interfaces* 2018, 10, 18619–18629. [PubMed: 29763287]
- (139). Zhang C-L; Yu S-H Nanoparticles Meet Electrospinning: Recent Advances and Future Prospects. *Chem. Soc. Rev* 2014, 43, 4423–4448. [PubMed: 24695773]
- (140). Lu XF; Wang C; Wei Y One-Dimensional Composite Nanomaterials: Synthesis by Electrospinning and Their Applications. *Small* 2009, 5, 2349–2370. [PubMed: 19771565]
- (141). He D; Hu B; Yao Q-F; Wang K; Yu S-H Large-Scale Synthesis of Flexible Free-Standing SERS Substrates with High Sensitivity: Electrospun PVA Nanofibers Embedded with Controlled Alignment of Silver Nanoparticles. *ACS Nano* 2009, 3, 3993–4002. [PubMed: 19928883]
- (142). Jin Y; Yang D; Kang D; Jiang X Fabrication of Necklace-Like Structures via Electrospinning. *Langmuir* 2010, 26, 1186–1190. [PubMed: 19689141]

- (143). Zhang CL; Lv KP; Hu NY; Yu L; Ren XF; Liu SL; Yu SH Macroscopic-Scale Alignment of Ultralong Ag Nanowires in Polymer Nanofiber Mat and Their Hierarchical Structures by Magnetic-Field-Assisted Electrospinning. *Small* 2012, 8, 2936–2940. [PubMed: 22821678]
- (144). Huang Y; Bu N; Duan Y; Pan Y; Liu H; Yin Z; Xiong Y Electrohydrodynamic Direct-Writing. *Nanoscale* 2013, 5, 12007–12017. [PubMed: 24057297]
- (145). He XX; Zheng J; Yu GF; You MH; Yu M; Ning X; Long YZ Near-Field Electrospinning: Progress and Applications. *J. Phys. Chem. C* 2017, 121, 8663–8678.
- (146). Lei TP; Lu XZ; Yang F Fabrication of Various Micro/Nano Structures by Modified Near-Field Electrospinning. *AIP Adv* 2015, 5, 041301.
- (147). Zheng G; Li W; Wang X; Wu D; Sun D; Lin L Precision Deposition of a Nanofibre by Near-Field Electrospinning. *J. Phys. D: Appl. Phys* 2010, 43, 415501.
- (148). Parajuli D; Koomsap P; Parkhi AA; Supaphol P Experimental Investigation on Process Parameters of Near-Field Deposition of Electrospinning-Based Rapid Prototyping. *Virtual. Phys. Prototyp* 2016, 11, 193–207.
- (149). Fattah P; Dover JT; Brown JL 3D Near-Field Electrospinning of Biomaterial Microfibers with Potential for Blended Microfiber-Cell-Loaded Gel Composite Structures. *Adv. Healthcare Mater* 2017, 6, 1700456.
- (150). Bisht GS; Canton G; Mirsepassi A; Kulinsky L; Oh S; Dunn-Rankin D; Madou MJ Controlled Continuous Patterning of Polymeric Nanofibers on Three-Dimensional Substrates Using Low-Voltage Near-Field Electrospinning. *Nano Lett* 2011, 11, 1831–1837. [PubMed: 21446719]
- (151). Xin Y; Reneker DH Hierarchical Polystyrene Patterns Produced by Electrospinning. *Polymer* 2012, 53, 4254–4261.
- (152). Luo GX; Teh KS; Liu YM; Zang XN; Wen ZY; Lin LW Direct-Write, Self-Aligned Electrospinning on Paper for Controllable Fabrication of Three-Dimensional Structures. *ACS Appl. Mater. Interfaces* 2015, 7, 27765–27770. [PubMed: 26592741]
- (153). Fuh YK; Wang BS Near Field Sequentially Electrospun Three-Dimensional Piezoelectric Fibers Arrays for Self-Powered Sensors of Human Gesture Recognition. *Nano Energy* 2016, 30, 677–683.
- (154). Fuh YK; Hsu HS Fabrication of Monolithic Polymer Nanofluidic Channels via Near-Field Electrospun Nanofibers as Sacrificial Templates. *J. Micro/Nanolithogr., MEMS, MOEMS* 2011, 10, 043004.
- (155). Wang X; Zheng G; Xu L; Cheng W; Xu B; Huang Y; Sun D Fabrication of Nanochannels via Near-Field Electrospinning. *Appl. Phys. A: Mater. Sci. Process* 2012, 108, 825–828.
- (156). Chang J; Liu YM; Heo K; Lee BY; Lee SW; Lin LW Direct-Write Complementary Graphene Field Effect Transistors and Junctions via Near-Field Electrospinning. *Small* 2014, 10, 1920–1925. [PubMed: 24599879]
- (157). Valipouri A Production Scale up of Nanofibers: A Review. *J. Text. Polym* 2017, 5, 8–16.
- (158). Liu Y; Zhang L; Sun X-F; Liu J; Fan J; Huang D-W Multi-Jet Electrospinning *via* Auxiliary Electrode. *Mater. Lett* 2015, 141, 153–156.
- (159). Zhou FL; Gong RH; Porat I Mass Production of Nanofibre Assemblies by Electrostatic Spinning. *Polym. Int* 2009, 58, 331–342.
- (160). SalehHudin HS; Mohamad EN; Mahadi WNL; Muhammad Afifi A Multiple-Jet Electrospinning Methods for Nanofiber Processing: A Review. *Mater. Manuf. Processes* 2018, 33, 479–498.
- (161). Park CH; Pant HR; Kim CS Novel Robot-Assisted Angled Multi-Nozzle Electrospinning Set-Up: Computer Simulation with Experimental Observation of Electric Field and Fiber Morphology. *Text. Res. J* 2014, 84, 1044–1058.
- (162). Tomaszewski W; Szadkowski M Investigation of Electro-spinning with the Use of a Multi-Jet Electrospinning Head. *Fibres Text. Eur* 2005, 13 (4), 22–26.
- (163). Yang Y; Jia ZD; Li QA; Hou L; Liu JN; Wang LM; Guan ZC; Zahn M A Shield Ring Enhanced Equilateral Hexagon Distributed Multi-Needle Electrospinning Spinneret. *IEEE Trans. Dielectr. Electr. Insul* 2010, 17, 1592–1601.
- (164). Theron SA; Yarin AL; Zussman E; Kroll E Multiple Jets in Electrospinning: Experiment and Modeling. *Polymer* 2005, 46, 2889–2899.

- (165). Kim IG; Lee J-H; Unnithan AR; Park C-H; Kim CS A Comprehensive Electric Field Analysis of Cylinder-Type MultiNozzle Electrospinning System for Mass Production of Nanofibers. *J. Ind. Eng. Chem* 2015, 31, 251–256.
- (166). Akampumuza O; Gao H; Zhang H; Wu D; Qin XH Raising Nanofiber Output: The Progress, Mechanisms, Challenges, and Reasons for the Pursuit. *Macromol. Mater. Eng* 2018, 303, 1700269.
- (167). Zheng Y; Gong RH; Zeng Y Multijet Motion and Deviation in Electrospinning. *RSC Adv* 2015, 5, 48533–48540.
- (168). Liu YB; Guo LL Homogeneous Field Intensity Control During Multi-Needle Electrospinning via Finite Element Analysis and Simulation. *J. Nanosci. Nanotechnol* 2013, 13, 843–847. [PubMed: 23646527]
- (169). Kim G; Cho Y-S; Kim WD Stability Analysis for MultiJets Electrospinning Process Modified with a Cylindrical Electrode. *Eur. Polym. J* 2006, 42, 2031–2038.
- (170). Varesano A; Carletto RA; Mazzuchetti G Experimental Investigations on the Multi-Jet Electrospinning Process. *J. Mater. Process. Technol* 2009, 209, 5178–5185.
- (171). Xie S; Zeng YC Effects of Electric Field on Multineedle Electrospinning: Experiment and Simulation Study. *Ind. Eng. Chem. Res* 2012, 51, 5336–5345.
- (172). Zhao Y; Jiang J; Li W; Wang X; Zhang K; Zhu P; Zheng G Electrospinning Jet Behaviors under the Constraints of a Sheath Gas. *AIP Adv* 2016, 6, 115022.
- (173). Wang B; Yao YY; Peng JR; Lin Y; Liu WL; Luo Y; Xiang RL; Li RX; Wu DC Preparation of Poly(ester imide) Ultrafine Fibers by Gas-Jet/Electrospinning. *J. Appl. Polym. Sci* 2009, 114, 883–891.
- (174). Wojasinski M; Golawski J; Ciach T Blow-Assisted Multi-jet Electrospinning of Poly-L-lactic acid Nanofibers. *J. Polym. Res* 2017, 24, 76–84.
- (175). Varabhas JS; Chase GG; Reneker DH Electrospun Nanofibers from a Porous Hollow Tube. *Polymer* 2008, 49, 4226–4229.
- (176). Zhou F-L; Gong R-H; Porat I Polymeric Nanofibers via Flat Spinneret Electrospinning. *Polym. Eng. Sci* 2009, 49, 2475–2481.
- (177). Zhou F-L; Gong R-H; Porat I Needle and Needleless Electrospinning for Nanofibers. *J. Appl. Polym. Sci* 2010, 115, 2591–2598.
- (178). Zheng YS; Liu XK; Zeng YC Electrospun Nanofibers from a Multihole Spinneret with Uniform Electric Field. *J. Appl. Polym. Sci* 2013, 130, 3221–3228.
- (179). Sun D; Chang C; Li S; Lin L Near-Field Electrospinning. *Nano Lett* 2006, 6, 839–842. [PubMed: 16608294]
- (180). Thoppey NM; Bochinski JR; Clarke LI; Gorga RE Unconfined Fluid Electrospun into High Quality Nanofibers from a Plate Edge. *Polymer* 2010, 51, 4928–4936.
- (181). Thoppey NM; Bochinski JR; Clarke LI; Gorga RE Edge Electrospinning for High Throughput Production of Quality Nanofibers. *Nanotechnology* 2011, 22, 345301. [PubMed: 21799242]
- (182). Thoppey NM; Gorga RE; Bochinski JR; Clarke LI Effect of Solution Parameters on Spontaneous Jet Formation and Throughput in Edge Electrospinning from a Fluid-Filled Bowl. *Macromolecules* 2012, 45, 6527–6537.
- (183). Wang X; Xu W Effect of Experimental Parameters on Needleless Electrospinning from a Conical Wire Coil. *J. Appl. Polym. Sci* 2012, 123, 3703–3709.
- (184). Lukas D; Sarkar A; Pokorny P Self–Organization of Jets in Electrospinning from Free Liquid Surface: A Generalized Approach. *J. Appl. Phys* 2008, 103 (7), 084309.
- (185). Jiang G; Zhang S; Qin X High Throughput of Quality Nanofibers via One Stepped Pyramid-Shaped Spinneret. *Mater. Lett* 2013, 106, 56–58.
- (186). Jiang G; Zhang S; Wang Y; Qin X An Improved Free Surface Electrospinning with Micro-Bubble Solution System for Massive Production of Nanofibers. *Mater. Lett* 2015, 144, 22–25.
- (187). Nanospider Electrospinning Technology; Elmarco, <http://www.elmarco.com/electrospinning/electrospinning-technology/>.
- (188). Niu HT; Lin T; Wang XG Needleless Electrospinning. I. A Comparison of Cylinder and Disk Nozzles. *J. Appl. Polym. Sci* 2009, 114, 3524–3530.

- (189). Niu H; Wang X; Lin T Needleless Electrospinning: Influences of Fibre Generator Geometry. *J. Text. Inst* 2012, 103, 787–794.
- (190). Bhattacharyya I; Molaro MC; Braatz RD; Rutledge GC Free Surface Electrospinning of Aqueous Polymer Solutions from a Wire Electrode. *Chem. Eng. J* 2016, 289, 203–211.
- (191). Wang X; Niu H; Wang X; Lin T Needleless Electrospinning of Uniform Nanofibers Using Spiral Coil Spinnerets. *J. Nanomater* 2012, 2012, 785920.
- (192). Han WL; Nurwaha D; Li CL; Wang XH Free Surface Electrospun Fibers: The Combined Effect of Processing Parameters. *Polym. Eng. Sci* 2014, 54, 189–197.
- (193). Liu Z; Chen RX; He JH Active Generation of Multiple Jets for Producing Nanofibres with High Quality and High Throughput. *Mater. Des* 2016, 94, 496–501.
- (194). Li D; Xia Y Direct Fabrication of Composite and Ceramic Hollow Nanofibers by Electrospinning. *Nano Lett* 2004, 4, 933–938.
- (195). Loscertales IG; Barrero A; Guerrero I; Cortijo R; Marquez M; Gañán-Calvo AM Micro/Nano Encapsulation via Electrified Coaxial Liquid Jets. *Science* 2002, 295, 1695–1698. [PubMed: 11872835]
- (196). Yu JH; Fridrikh SV; Rutledge GC Production of Submicrometer Diameter Fibers by Two-Fluid Electrospinning. *Adv. Mater* 2004, 16, 1562–1566.
- (197). Lee B-S; Jeon S-Y; Park H; Lee G; Yang H-S; Yu W-R New Electrospinning Nozzle to Reduce Jet Instability and Its Application to Manufacture of Multi-layered Nanofibers. *Sci. Rep* 2015, 4, 6758.
- (198). Moghe AK; Gupta BS Co-Axial Electrospinning for Nanofiber Structures: Preparation and Applications. *Polym. Rev* 2008, 48, 353–377.
- (199). Yu D-G; Li X-Y; Wang X; Yang J-H; Bligh SWA; Williams GR Nanofibers Fabricated Using Triaxial Electrospinning as Zero Order Drug Delivery Systems. *ACS Appl. Mater. Interfaces* 2015, 7, 18891–18897. [PubMed: 26244640]
- (200). Lee GH; Song J-C; Yoon K-B Controlled Wall Thickness and Porosity of Polymeric Hollow Nanofibers by Coaxial Electrospinning. *Macromol. Res* 2010, 18, 571–576.
- (201). Agarwal S; Greiner A; Wendorff JH Electrospinning of Manmade and Biopolymer Nanofibers —Progress in Techniques, Materials, and Applications. *Adv. Funct. Mater* 2009, 19, 2863–2879.
- (202). Dror Y; Kuhn J; Avrahami R; Zussman E Encapsulation of Enzymes in Biodegradable Tubular Structures. *Macromolecules* 2008, 41, 4187–4192.
- (203). Klein S; Kuhn J; Avrahami R; Tarre S; Beliavski M; Green M; Zussman E Encapsulation of Bacterial Cells in Electrospun Microtubes. *Biomacromolecules* 2009, 10, 1751–1756. [PubMed: 21197961]
- (204). Korehei R; Kadla JF Encapsulation of T4 Bacteriophage in Electrospun Poly(ethylene oxide)/Cellulose Diacetate Fibers. *Carbohydr. Polym* 2014, 100, 150–157. [PubMed: 24188849]
- (205). Lagerwall JPF; McCann JT; Formo E; Scalia G; Xia Y Coaxial Electrospinning of Microfibres with Liquid Crystal in the Core. *Chem. Commun* 2008, 42, 5420–5422.
- (206). Wang M; Yu JH; Kaplan DL; Rutledge GC Production of Submicron Diameter Silk Fibers under Benign Processing Conditions by Two-Fluid Electrospinning. *Macromolecules* 2006, 39, 1102–1107.
- (207). Reddy CS; Arinstein A; Avrahami R; Zussman E Fabrication of Thermoset Polymer Nanofibers by Co-Electrospinning of Uniform Core-Shell Structures. *J. Mater. Chem* 2009, 19, 7198–7201.
- (208). Lu S; Duan X; Han Y; Huang H Silicone Rubber/Polyvinylpyrrolidone Microfibers Produced by Coaxial Electrospinning. *J. Appl. Polym. Sci.* 2013, 128, 2273–2276.
- (209). Niu H; Wang H; Zhou H; Lin T Ultrafine PDMS Fibers: Preparation from in Situ Curing-Electrospinning and Mechanical Characterization. *RSC Adv* 2014, 4, 11782–11787.
- (210). Liu L; Zhang F; Hu S; Zhang L; Wen S Preparation of Ultrafine Ethylene/Propylene/Diene Terpolymer Rubber Fibers by Coaxial Electrospinning. *Macromol. Mater. Eng* 2012, 297, 298–302.
- (211). Wang X; Zhang W-J; Yu D-G; Li X-Y; Yang H Epoxy Resin Nanofibers Prepared Using Electrospun Core/Sheath Nanofibers as Templates. *Macromol. Mater. Eng* 2013, 298, 664–669.

- (212). Yang G-Z; Li J-J; Yu D-G; He M-F; Yang J-H; Williams GR Nanosized Sustained-Release Drug Depots Fabricated Using Modified Tri-Axial Electrospinning. *Acta Biomater* 2017, 53, 233–241. [PubMed: 28137657]
- (213). Yu D-G; Yu J-H; Chen L; Williams GR; Wang X Modified Coaxial Electrospinning for the Preparation of High-Quality Ketoprofen-Loaded Cellulose Acetate Nanofibers. *Carbohydr Polym* 2012, 90, 1016–1023. [PubMed: 22840034]
- (214). Wen H-F; Yang C; Yu D-G; Li X-Y; Zhang D-F Electrospun Zein Nanoribbons for Treatment of Lead-Contained Wastewater. *Chem. Eng. J* 2016, 290, 263–272.
- (215). Yu D-G; Branford-White C; Bligh SWA; White K; Chatterton NP; Zhu L-M Improving Polymer Nanofiber Quality Using a Modified Co-Axial Electrospinning Process. *Macromol. Rapid Commun* 2011, 32, 744–750. [PubMed: 21438063]
- (216). Yu D-G; Branford-White CJ; Chatterton NP; White K; Zhu L-M; Shen X-X; Nie W Electrospinning of Concentrated Polymer Solutions. *Macromolecules* 2010, 43, 10743–10746.
- (217). Loscertales IG; Barrero A; Márquez M; Spretz R; Velarde-Ortiz R; Larsen G Electrically Forced Coaxial Nanojets for One-Step Hollow Nanofiber Design. *J. Am. Chem. Soc* 2004, 126, 5376–5377. [PubMed: 15113206]
- (218). Kim C; Jeong YI; Ngoc BTN; Yang KS; Kojima M; Kim YA; Endo M; Lee JW Synthesis and Characterization of Porous Carbon Nanofibers with Hollow Cores through the Thermal Treatment of Electrospun Copolymeric Nanofiber Webs. *Small* 2007, 3, 91–95. [PubMed: 17294476]
- (219). Zhao Y; Cao X; Jiang L Bio-Mimic Multichannel Microtubes by a Facile Method. *J. Am. Chem. Soc* 2007, 129, 764–765. [PubMed: 17243804]
- (220). Liu W; Ni C; Chase DB; Rabolt JF Preparation of Multilayer Biodegradable Nanofibers by Triaxial Electrospinning. *ACS Macro Lett* 2013, 2, 466–468.
- (221). Shami Z; Sharifi-Sanjani N; Khoei S; Faridi-Majidi R Triple Axial Coelectrospun Multifunctional Double-Shell $TiO_2@ZnO$ Carbon Hollow Nanofibrous Mat Transformed to C-Attached TiO_2 Brush-Like Nanotube Arrays: An Mo^{6+} Adsorbent Nonwoven Mat. *Ind. Eng. Chem. Res* 2014, 53, 14963–14973.
- (222). Han D; Steckl AJ Triaxial Electrospun Nanofiber Membranes for Controlled Dual Release of Functional Molecules. *ACS Appl. Mater. Interfaces* 2013, 5, 8241–8245. [PubMed: 23924226]
- (223). Jiang S; Duan G; Zussman E; Greiner A; Agarwal S Highly Flexible and Tough Concentric Triaxial Polystyrene Fibers. *ACS Appl. Mater. Interfaces* 2014, 6, 5918–5923. [PubMed: 24684423]
- (224). Ding Z; Salim A; Ziaie B Selective Nanofiber Deposition through Field-Enhanced Electrospinning. *Langmuir* 2009, 25, 9648–9652. [PubMed: 19705879]
- (225). Zhao S; Zhou Q; Long Y-Z; Sun G-H; Zhang Y Nanofibrous Patterns by Direct Electrospinning of Nanofibers onto Topographically Structured Non-Conductive Substrates. *Nanoscale* 2013, 5, 4993–5000. [PubMed: 23636504]
- (226). Song W; An D; Kao D-I; Lu Y-C; Dai G; Chen S; Ma M Nanofibrous Microposts and Microwells of Controlled Shapes and Their Hybridization with Hydrogels for Cell Encapsulation. *ACS Appl. Mater. Interfaces* 2014, 6, 7038–7044. [PubMed: 24806031]
- (227). Kim JH; Jang J; Jeong YH; Ko TJ; Cho D-W Fabrication of a Nanofibrous Mat with a Human Skin Pattern. *Langmuir* 2015, 31, 424–431. [PubMed: 25479420]
- (228). Cai XM; Zhu P; Lu XZ; Liu YF; Lei TP; Sun DH Electrospinning of Very Long and Highly Aligned Fibers. *J. Mater. Sci* 2017, 52, 14004–14010.
- (229). Li D; Wang Y; Xia Y Electrospinning Nanofibers as Uniaxially Aligned Arrays and Layer-by-Layer Stacked Films. *Adv. Mater* 2004, 16, 361–366.
- (230). Xu H; Cui W; Chang J Fabrication of Patterned PDLLA/PCL Composite Scaffold by Electrospinning. *J. Appl. Polym. Sci* 2013, 127, 1550–1554.
- (231). Zhang D; Chang J Patterning of Electrospun Fibers Using Electroconductive Templates. *Adv. Mater* 2007, 19, 3664–3667
- (232). Xu H; Lv F; Zhang Y; Yi Z; Ke Q; Wu C; Liu M; Chang J Hierarchically Micro-Patterned Nanofibrous Scaffolds with a Nanosized Bio-Glass Surface for Accelerating Wound Healing. *Nanoscale* 2015, 7, 18446–18452. [PubMed: 26503372]

- (233). Wang X; Lv F; Li T; Han Y; Yi Z; Liu M; Chang J; Wu C Electrospun Micropatterned Nanocomposites Incorporated with Cu₂S Nanoflowers for Skin Tumor Therapy and Wound Healing. *ACS Nano* 2017, 11, 11337–11349. [PubMed: 29059516]
- (234). Pan C; Han YH; Dong L; Wang J; Gu ZZ Electrospinning of Continuous, Large Area, Latticework Fiber onto Two-Dimensional Pin-Array Collectors. *J. Macromol. Sci., Part B: Phys* 2008, 47, 735–742.
- (235). Xie J; MacEwan MR; Ray WZ; Liu W; Siewe DY; Xia Y Radially Aligned, Electrospun Nanofibers as Dural Substitutes for Wound Closure and Tissue Regeneration Applications. *ACS Nano* 2010, 4, 5027–5036. [PubMed: 20695478]
- (236). Xie J; Liu W; MacEwan MR; Yeh Y-C; Thomopoulos S; Xia Y Nanofiber Membranes with Controllable Microwells and Structural Cues and Their Use in Forming Cell Microarrays and Neuronal Networks. *Small* 2011, 7, 293–297. [PubMed: 21294253]
- (237). Vaquette C; Cooper-White JJ Increasing Electrospun Scaffold Pore Size with Tailored Collectors for Improved Cell Penetration. *Acta Biomater* 2011, 7, 2544–2557. [PubMed: 21371575]
- (238). Liu Y; Zhang L; Li H; Yan S; Yu J; Weng J; Li X Electrospun Fibrous Mats on Lithographically Micropatterned Collectors to Control Cellular Behaviors. *Langmuir* 2012, 28, 17134–17142. [PubMed: 23153038]
- (239). Ahirwal D; Hebraud A; Kadar R; Wilhelm M; Schlatter G From Self-Assembly of Electrospun Nanofibers to 3D cm Thick Hierarchical Foams. *Soft Matter* 2013, 9, 3164–3172.
- (240). Nedjari S; Eap S; Hébraud A; Wittmer CR; Benkirane-Jessel N; Schlatter G Electrospun Honeycomb as Nests for Controlled Osteoblast Spatial Organization. *Macromol. Biosci* 2014, 14, 1580–1589. [PubMed: 25138713]
- (241). Nedjari S; Schlatter G; Hebraud A Thick Electrospun Honeycomb Scaffolds with Controlled Pore Size. *Mater. Lett* 2015, 142, 180–183.
- (242). Zhang D; Chang J Electrospinning of Three-Dimensional Nanofibrous Tubes with Controllable Architectures. *Nano Lett* 2008, 8, 3283–3287. [PubMed: 18767890]
- (243). Xu H; Li H; Ke Q; Chang J An Anisotropically and Heterogeneously Aligned Patterned Electrospun Scaffold with Tailored Mechanical Property and Improved Bioactivity for Vascular Tissue Engineering. *ACS Appl. Mater. Interfaces* 2015, 7, 8706–8718. [PubMed: 25826222]
- (244). Dempsey DK; Schwartz CJ; Ward RS; Iyer AV; Parakka JP; Cosgriff-Hernandez EM Micropatterning of Electrospun Polyurethane Fibers through Control of Surface Topography. *Macromol. Mater. Eng* 2010, 295, 990–994.
- (245). Kakunuri M; Wanasekara ND; Sharma CS; Khandelwal M; Eichhorn SJ Three-Dimensional Electrospun Micropatterned Cellulose Acetate Nanofiber Surfaces with Tunable Wettability. *J. Appl. Polym. Sci* 2017, 134, 44709.
- (246). Persano L; Camposeo A; Tekmen C; Pisignano D Industrial Upscaling of Electrospinning and Applications of Polymer Nanofibers: A Review. *Macromol. Mater. Eng* 2013, 298, 504–520.
- (247). Matthews JA; Wnek GE; Simpson DG; Bowlin GL Electrospinning of Collagen Nanofibers. *Biomacromolecules* 2002, 3, 232–238. [PubMed: 11888306]
- (248). Alfaro De Pra MA; Ribeiro-do-Valle RM; Maraschin M; Veleirinho B Effect of Collector Design on the Morphological Properties of Polycaprolactone Electrospun Fibers. *Mater. Lett* 2017, 193, 154–157.
- (249). Producing Electrospun Artificial Blood Vessels; inovenso, <https://www.inovenso.com/producing-electrospun-artificial-blood-vessels/>.
- (250). Jose RR; Elia R; Firpo MA; Kaplan DL; Peattie RA Seamless, Axially Aligned, Fiber Tubes, Meshes, Microbundles and Gradient Biomaterial Constructs. *J. Mater. Sci.: Mater. Med* 2012, 23, 2679–2695. [PubMed: 22890517]
- (251). Dalton PD; Klee D; Möller M Electrospinning with Dual Collection Rings. *Polymer* 2005, 46, 611–614.
- (252). Joseph J; Nair SV; Menon D Integrating Substrate Less Electrospinning with Textile Technology for Creating Biodegradable Three-Dimensional Structures. *Nano Lett* 2015, 15, 5420–5426. [PubMed: 26214718]

- (253). Shuakat MN; Lin T Direct Electrospinning of Nanofibre Yarns Using a Rotating Ring Collector. *J. Text. Inst* 2016, 107, 791–799.
- (254). Lee JH; Gim Y; Bae S; Oh C; Ko HS; Baik S; Oh TS; Yoo JB Determination of Twisting Angle of Electrospun Nanofiber Bundle for Continuous Electrospinning System. *J. Appl. Polym. Sci* 2017, 134, 45528.
- (255). Ali U; Zhou Y; Wang X; Lin T Direct Electrospinning of Highly Twisted, Continuous Nanofiber Yarns. *J. Text. Inst* 2012, 103, 80–88.
- (256). Peng H; Liu Y; Ramakrishna S Recent Development of Centrifugal Electrospinning. *J. Appl. Polym. Sci* 2017, 134, 44578.
- (257). Holopainen J; Penttinen T; Santala E; Ritala M Needleless Electrospinning with Twisted Wire Spinneret. *Nanotechnology* 2015, 26, 025301. [PubMed: 25513842]
- (258). Li M; Long Y-Z; Yang D; Sun J; Yin H; Zhao Z; Kong W; Jiang X; Fan Z Fabrication of One Dimensional Superfine Polymer Fibers by Double-Spinning. *J. Mater. Chem* 2011, 21, 13159–13162.
- (259). Edmondson D; Cooper A; Jana S; Wood D; Zhang M Centrifugal Electrospinning of Highly Aligned Polymer Nanofibers over a Large Area. *J. Mater. Chem* 2012, 22, 18646–18652.
- (260). Kong L; Ziegler GR Rheological Aspects in Fabricating Pullulan Fibers by Electro-Wet-Spinning. *Food Hydrocolloids* 2014, 38, 220–226.
- (261). Wu J; Hong Y Enhancing Cell Infiltration of Electrospun Fibrous Scaffolds in Tissue Regeneration. *Bioact. Mater* 2016, 1, 56–64. [PubMed: 29744395]
- (262). Hong S; Kim G Fabrication of Size-Controlled Three-Dimensional Structures Consisting of Electrohydrodynamically Produced Polycaprolactone Micro/Nanofibers. *Appl. Phys. A: Mater. Sci. Process* 2011, 103, 1009–1014.
- (263). Teo W-E; Gopal R; Ramaseshan R; Fujihara K; Ramakrishna S A Dynamic Liquid Support System for Continuous Electrospun Yarn Fabrication. *Polymer* 2007, 48, 3400–3405.
- (264). Wang L; Wu Y; Guo B; Ma PX Nanofiber Yarn/Hydrogel Core–Shell Scaffolds Mimicking Native Skeletal Muscle Tissue for Guiding 3D Myoblast Alignment, Elongation, and Differentiation. *ACS Nano* 2015, 9, 9167–9179. [PubMed: 26280983]
- (265). Liu J; Chen G; Gao H; Zhang L; Ma S; Liang J; Fong H Structure and Thermo-Chemical Properties of Continuous Bundles of Aligned and Stretched Electrospun Polyacrylonitrile Precursor Nanofibers Collected in a Flowing Water Bath. *Carbon* 2012, 50, 1262–1270.
- (266). Park SM; Kim DS Electrolyte-Assisted Electrospinning for a Self-Assembled, Free-Standing Nanofiber Membrane on a Curved Surface. *Adv. Mater* 2015, 27, 1682–1687. [PubMed: 25594630]
- (267). Park SM; Eom S; Kim W; Kim DS Role of Grounded Liquid Collectors in Precise Patterning of Electrospun Nanofiber Mats. *Langmuir* 2018, 34, 284–290. [PubMed: 29215895]
- (268). Peng S; Li L; Kong Yoong Lee J; Tian L; Srinivasan M; Adams S; Ramakrishna S Electrospun Carbon Nanofibers and Their Hybrid Composites as Advanced Materials for Energy Conversion and Storage. *Nano Energy* 2016, 22, 361–395.
- (269). Rahaman MSA; Ismail AF; Mustafa A A Review of Heat Treatment on Polyacrylonitrile Fiber. *Polym. Degrad. Stab* 2007, 92, 1421–1432.
- (270). Wu M; Wang Q; Li K; Wu Y; Liu H Optimization of Stabilization Conditions for Electrospun Polyacrylonitrile Nanofibers. *Polym. Degrad. Stab* 2012, 97, 1511–1519.
- (271). Gergin ; Ismar E; Sarac AS Oxidative Stabilization of Polyacrylonitrile Nanofibers and Carbon Nanofibers Containing Graphene Oxide (GO): A Spectroscopic and Electrochemical Study. *Beilstein J. Nanotechnol* 2017, 8, 1616–1628. [PubMed: 28875098]
- (272). Zhang B; Yu Y; Xu ZL; Abouali S; Akbari M; He Y-B; Kang F; Kim J-K Correlation between Atomic Structure and Electrochemical Performance of Anodes Made from Electrospun Carbon Nanofiber Films. *Adv. Energy Mater* 2014, 4, 1301448.
- (273). Zhou Z; Lai C; Zhang L; Qian Y; Hou H; Reneker DH; Fong H Development of Carbon Nanofibers from Aligned Electrospun Polyacrylonitrile Nanofiber Bundles and Characterization of Their Microstructural, Electrical, and Mechanical Properties. *Polymer* 2009, 50, 2999–3006.
- (274). Yang KS; Edie DD; Lim DY; Kim YM; Choi YO Preparation of Carbon Fiber Web from Electrostatic Spinning of PMDA-ODA Poly(amic acid) Solution. *Carbon* 2003, 41, 2039–2046.

- (275). Kim C; Choi Y-O; Lee W-J; Yang K-S Supercapacitor Performances of Activated Carbon Fiber Webs Prepared by Electrospinning of PMDA-ODA Poly(amic acid) Solutions. *Electrochim. Acta* 2004, 50, 883–887.
- (276). Li X-F; Xu Q; Fu Y; Guo QX Preparation and Characterization of Activated Carbon from Kraft Lignin via KOH Activation. *Environ. Prog. Sustainable Energy* 2014, 33, 519–526.
- (277). Ruiz-Rosas R; Bedia J; Lallave M; Loscertales IG; Barrero A; Rodríguez-Mirasol J; Cordero T The Production of Submicron Diameter Carbon Fibers by the Electrospinning of Lignin. *Carbon* 2010, 48, 696–705.
- (278). Park SH; Kim C; Choi YO; Yang KS Preparations of Pitch-Based CF/ACF Webs by Electrospinning. *Carbon* 2003, 41, 2655–2657.
- (279). Yang Y; Centrone A; Chen L; Simeon F; Alan Hatton T; Rutledge G Highly Porous Electrospun Polyvinylidene Fluoride (PVDF)-Based Carbon Fiber. *Carbon* 2011, 49, 3395–3403.
- (280). Deng L; Young RJ; Kinloch IA; Zhu Y; Eichhorn SJ Carbon Nanofibres Produced from Electrospun Cellulose Nanofibres. *Carbon* 2013, 58, 66–5.
- (281). Salleh WNW; Ismail AF Fabrication and Characterization of PEI/PVP-Based Carbon Hollow Fiber Membranes for CO₂/CH₄ and CO₂/N₂ Separation. *AIChE J* 2012, 58, 3167–3175.
- (282). Chen Q; Zhang T; Qiao X; Li D; Yang J Li₃V₂(PO₄)₃/C Nanofibers Composite as a High Performance Cathode Material For lithium-Ion Battery. *J. Power Sources* 2013, 234, 197–200.
- (283). Zhang L; Hsieh Y-L Carbon Nanofibers with Nanoporosity and Hollow Channels from Binary Polyacrylonitrile Systems. *Eur. Polym. J* 2009, 45, 47–56.
- (284). Ko F; Gogotsi Y; Ali A; Naguib N; Ye H; Yang GL; Li C; Willis P Electrospinning of Continuous Carbon Nanotube-Filled Nanofiber Yarns. *Adv. Mater* 2003, 15, 1161–1165.
- (285). Liu J; Yue Z; Fong H Continuous Nanoscale Carbon Fibers with Superior Mechanical Strength. *Small* 2009, 5, 536–542. [PubMed: 19197971]
- (286). Sui G; Sun F; Yang X; Ji J; Zhong W Highly Aligned Polyacrylonitrile-Based Nano-Scale Carbon Fibres with Homogeneous Structure and Desirable Properties. *Compos. Sci. Technol* 2013, 87, 77–85.
- (287). Wu H; Hu L; Rowell MW; Kong D; Cha JJ; McDonough JR; Zhu J; Yang Y; McGehee MD; Cui Y Electrospun Metal Nanofiber Webs as High-Performance Transparent Electrode. *Nano Lett* 2010, 10, 4242–4248. [PubMed: 20738115]
- (288). Ludwig T; Bohr C; Queraltó A; Frohnoven R; Fischer T; Mathur S Semiconductors and Semimetals; Elsevier, 2018; Vol. 98, pp 1–70, DOI: 10.1016/bs.semsem.2018.04.003.
- (289). Wu H; Zhang R; Liu X; Lin D; Pan W Electrospinning of Fe, Co, and Ni Nanofibers: Synthesis, Assembly, and Magnetic Properties. *Chem. Mater* 2007, 19, 3506–3511.
- (290). Shui J; Li JCM Platinum Nanowires Produced by Electrospinning. *Nano Lett* 2009, 9, 1307–1314. [PubMed: 19260644]
- (291). Kim J; Kang J; Jeong U; Kim H; Lee H Catalytic, Conductive, and Transparent Platinum Nanofiber Webs for Fto-Free Dye-Sensitized Solar Cells. *ACS Appl. Mater. Interfaces* 2013, 5, 3176–3181. [PubMed: 23517275]
- (292). Pol VG; Koren E; Zaban A Fabrication of Continuous Conducting Gold Wires by Electrospinning. *Chem. Mater* 2008, 20, 3055–3062.
- (293). Chen H-T; Lin H-L; Kuo C; Chen I-G UV-Induced Synthesis of Silver Nanofiber Networks as Transparent Electrodes. *J. Mater. Chem. C* 2016, 4, 7675–7682.
- (294). Wu H; Kong D; Ruan Z; Hsu P-C; Wang S; Yu Z; Carney TJ; Hu L; Fan S; Cui Y A Transparent Electrode Based on a Metal Nanotrough Network. *Nat. Nanotechnol* 2013, 8, 421–425. [PubMed: 23685985]
- (295). Yang X; Hu X; Wang Q; Xiong J; Yang H; Meng X; Tan L; Chen L; Chen Y Large-Scale Stretchable Semiembedded Copper Nanowire Transparent Conductive Films by an Electrospinning Template. *ACS Appl. Mater. Interfaces* 2017, 9, 26468–26475. [PubMed: 28731322]
- (296). Subianto S; Donnadio A; Cavalieri S; Pica M; Casciola M; Jones DJ; Rozière J Reactive Coaxial Electrospinning of ZrP/ZrO₂ Nanofibres. *J. Mater. Chem. A* 2014, 2, 13359–13365.
- (297). Malwal D; Gopinath P Fabrication and Applications of Ceramic Nanofibers in Water Remediation: A Review. *Crit. Rev. Environ. Sci. Technol* 2016, 46, 500–534.

- (298). Chronakis IS Novel Nanocomposites and Nanoceramics Based on Polymer Nanofibers Using Electrospinning Process-A Review. *J. Mater. Process. Technol.* 2005, 167, 283–293.
- (299). Li W; Cao C-Y; Chen C-Q; Zhao Y; Song W-G; Jiang L Fabrication of Nanostructured Metal Nitrides with Tailored Composition and Morphology. *Chem. Commun.* 2011, 47, 3619–3621.
- (300). Zhou X; Qiu Y; Yu J; Yin J; Gao S Tungsten Carbide Nanofibers Prepared by Electrospinning with High Electrocatalytic Activity for Oxygen Reduction. *Int. J. Hydrogen Energy* 2011, 36, 7398–7404.
- (301). Song J; Wang X; Yan J; Yu J; Sun G; Ding B Soft Zr-Doped TiO₂ Nanofibrous Membranes with Enhanced Photocatalytic Activity for Water Purification. *Sci. Rep.* 2017, 7, 1636. [PubMed: 28487571]
- (302). Ostermann R; Li D; Yin Y; McCann JT; Xia Y V₂O₅ Nanorods on TiO₂ Nanofibers: A New Class of Hierarchical Nanostructures Enabled by Electrospinning and Calcination. *Nano Lett.* 2006, 6, 1297–1302. [PubMed: 16771598]
- (303). McCann JT; Chen JI; Li D; Ye Z-G; Xia Y Electrospinning of Polycrystalline Barium Titanate Nanofibers with Controllable Morphology and Alignment. *Chem. Phys. Lett.* 2006, 424, 162–166.
- (304). Formo E; Yavuz MS; Lee EP; Lane L; Xia Y Functionalization of Electrospun Ceramic Nanofibre Membranes with Noble-Metal Nanostructures for Catalytic Applications. *J. Mater. Chem.* 2009, 19, 3878–3882.
- (305). Zou Z; Ye J; Sayama K; Arakawa H Direct Splitting of Water under Visible Light Irradiation with an Oxide Semiconductor Photocatalyst. *Nature* 2001, 414, 625–627. [PubMed: 11740556]
- (306). Lu P; Qiao B; Lu N; Hyun DC; Wang J; Kim MJ; Liu J; Xia Y Photochemical Deposition of Highly Dispersed Pt Nanoparticles on Porous CeO₂ nanofibers for the Water-Gas Shift Reaction. *Adv. Funct. Mater.* 2015, 25, 4153–4162.
- (307). Liu Z; Miao Y-E; Liu M; Ding Q; Tjiu WW; Cui X; Liu T Flexible Polyaniline-Coated TiO₂/SiO₂ Nanofiber Membranes with Enhanced Visible-Light Photocatalytic Degradation Performance. *J. Colloid Interface Sci.* 2014, 424, 49–55. [PubMed: 24767497]
- (308). Li W; Wang Y; Ji B; Jiao X; Chen D Flexible Pd/CeO₂-TiO₂ Nanofibrous Membrane with High Efficiency Ultrafine Particulate Filtration and Improved CO Catalytic Oxidation Performance. *RSC Adv.* 2015, 5, 58120–58127.
- (309). Zhang R; Wang X; Song J; Si Y; Zhuang X; Yu J; Ding B In Situ Synthesis of Flexible Hierarchical TiO₂ Nanofibrous Membranes with Enhanced Photocatalytic Activity. *J. Mater. Chem. A* 2015, 3, 22136–22144.
- (310). Horzum N; Muñoz-Espí R; Glasser G; Demir MM; Landfester K; Crespy D Hierarchically Structured Metal Oxide/Silica Nanofibers by Colloid Electrospinning. *ACS Appl. Mater. Interfaces* 2012, 4, 6338–6345. [PubMed: 23092359]
- (311). Zhu P; Hong Y; Liu B; Zou G The Synthesis of Titanium Carbide-Reinforced Carbon Nanofibers. *Nanotechnology* 2009, 20, 255603. [PubMed: 19491464]
- (312). Li X; Chen Y; Zhou L; Mai Y-W; Huang H Exceptional Electrochemical Performance of Porous TiO₂-Carbon Nanofibers for Lithium Ion Battery Anodes. *J. Mater. Chem. A* 2014, 2, 3875–3880.
- (313). Liu Y; Xu J; Qin X; Xin H; Yuan X; Zhang J; Li D; Song C Electrode Activation via Vesiculation: Improved Reversible Capacity of γ -Fe₂O₃@C/MWNT Composite Anodes for Lithium-Ion Batteries. *J. Mater. Chem. A* 2015, 3, 9682–9688.
- (314). Park S-H; Lee W-J Coaxial Carbon Nanofiber/NiO Core-Shell Nanocables as Anodes for Lithium Ion Batteries. *RSC Adv.* 2015, 5, 23548–23555.
- (315). Sridhar R; Lakshminarayanan R; Madhaiyan K; Amutha Barathi V; Lim KHC; Ramakrishna S Electrosprayed Nanoparticles and Electrospun Nanofibers Based on Natural Materials: Applications in Tissue Regeneration, Drug Delivery and Pharmaceuticals. *Chem. Soc. Rev.* 2015, 44, 790–814. [PubMed: 25408245]
- (316). Nagase K; Nagumo Y; Kim M; Kim HJ; Kyung HW; Chung HJ; Sekine H; Shimizu T; Kanazawa H; Okano T; et al. Local Release of VEGF Using Fiber Mats Enables Effective Transplantation of Layered Cardiomyocyte Sheets. *Macromol. Biosci.* 2017, 17, 1700073.

- (317). Zhu Y; Han X; Xu Y; Liu Y; Zheng S; Xu K; Hu L; Wang C Electrospun Sb/C Fibers for a Stable and Fast Sodium-Ion Battery Anode. *ACS Nano* 2013, 7, 6378–6386. [PubMed: 23802576]
- (318). Xia G; Li D; Chen X; Tan Y; Tang Z; Guo Z; Liu H; Liu Z; Yu X Carbon-Coated Li₃N Nanofibers for Advanced Hydrogen Storage. *Adv. Mater* 2013, 25, 6238–6244. [PubMed: 23966063]
- (319). Huang J; Zhang B; Xie YY; Lye WWK; Xu Z-L; Abouali S; Akbari Garakani M; Huang J-Q; Zhang T-Y; Huang B; et al. Electrospun Graphitic Carbon Nanofibers with in-Situ Encapsulated Co–Ni Nanoparticles as Freestanding Electrodes for Li–O₂ Batteries. *Carbon* 2016, 100, 329–336.
- (320). Cavaliere S; Subianto S; Chevallier L; Jones DJ; Roziere J Single Step Elaboration of Size-Tuned Pt Loaded Titania Nanofibres. *Chem. Commun* 2011, 47, 6834–6836.
- (321). Zhang F; Yuan C; Zhu J; Wang J; Zhang X; Lou XW Flexible Films Derived from Electrospun Carbon Nanofibers Incorporated with Co₃O₄ Hollow Nanoparticles as Self-Supported Electrodes for Electrochemical Capacitors. *Adv. Funct. Mater* 2013, 23, 3909–3915.
- (322). Lu X; Zhao Y; Wang C Fabrication of PbS Nanoparticles in Polymer-Fiber Matrices by Electrospinning. *Adv. Mater* 2005, 17, 2485–2488.
- (323). Wang J; Yao H-B; He D; Zhang C-L; Yu S-H Facile Fabrication of Gold Nanoparticles-Poly(vinyl alcohol) Electrospun Water-Stable Nanofibrous Mats: Efficient Substrate Materials for Biosensors. *ACS Appl. Mater. Interfaces* 2012, 4, 1963–1971. [PubMed: 22409429]
- (324). Li D; McCann JT; Xia Y Use of Electrospinning to Directly Fabricate Hollow Nanofibers with Functionalized Inner and Outer Surfaces. *Small* 2005, 1, 83–86. [PubMed: 17193354]
- (325). Yun YJ; Hong WG; Kim WJ; Jun Y; Kim BH A Novel Method for Applying Reduced Graphene Oxide Directly to Electronic Textiles from Yarns to Fabrics. *Adv. Mater* 2013, 25, 5701–5705. [PubMed: 23946273]
- (326). Saetia K; Schnorr JM; Mannarino MM; Kim SY; Rutledge GC; Swager TM; Hammond PT Spray-Layer-by-Layer Carbon Nanotube/Electrospun Fiber Electrodes for Flexible Chemiresistive Sensor Applications. *Adv. Funct. Mater* 2014, 24, 492–502.
- (327). Zhou B; Li Y; Deng H; Hu Y; Li B Antibacterial Multilayer Films Fabricated by Layer-by-Layer Immobilizing Lysozyme and Gold Nanoparticles on Nanofibers. *Colloids Surf., B* 2014, 116, 432–438.
- (328). Drew C; Liu X; Ziegler D; Wang X; Bruno FF; Whitten J; Samuelson LA; Kumar J Metal Oxide-Coated Polymer Nanofibers. *Nano Lett* 2003, 3, 143–147.
- (329). Liu W; Yeh Y-C; Lipner J; Xie J; Sung H-W; Thomopoulos S; Xia Y Enhancing the Stiffness of Electrospun Nanofiber Scaffolds with a Controlled Surface Coating and Mineralization. *Langmuir* 2011, 27, 9088–9093. [PubMed: 21710996]
- (330). Li X; Xie J; Lipner J; Yuan X; Thomopoulos S; Xia Y Nanofiber Scaffolds with Gradations in Mineral Content for Mimicking the Tendon-to-Bone Insertion Site. *Nano Lett* 2009, 9, 2763–2768. [PubMed: 19537737]
- (331). Kolluru PV; Lipner J; Liu W; Xia Y; Thomopoulos S; Genin GM; Chasiotis I Strong and Tough Mineralized PLGA Nanofibers for Tendon-to-Bone Scaffolds. *Acta Biomater* 2013, 9, 9442–9450. [PubMed: 23933048]
- (332). Lin C-C; Fu S-J; Lin Y-C; Yang IK; Gu Y Chitosan-Coated Electrospun PLA Fibers for Rapid Mineralization of Calcium Phosphate. *Int. J. Biol. Macromol* 2014, 68, 39–47. [PubMed: 24768970]
- (333). Li D; McCann JT; Gratt M; Xia Y Photocatalytic Deposition of Gold Nanoparticles on Electrospun Nanofibers of Titania. *Chem. Phys. Lett* 2004, 394, 387–391.
- (334). GhavamiNejad A; Rajan Unnithan A; Ramachandra Kurup Sasikala A; Samarikhala M; Thomas RG; Jeong YY; Nasseri S; Murugesan P; Wu D; Hee Park C; et al. Mussel-Inspired Electrospun Nanofibers Functionalized with Size-Controlled Silver Nanoparticles for Wound Dressing Application. *ACS Appl. Mater. Interfaces* 2015, 7, 12176–12183. [PubMed: 25989513]
- (335). Formo E; Lee E; Campbell D; Xia Y Functionalization of Electrospun TiO₂ Nanofibers with Pt Nanoparticles and Nanowires for Catalytic Applications. *Nano Lett* 2008, 8, 668–672. [PubMed: 18205427]

- (336). Formo E; Camargo PH; Lim B; Jiang M; Xia Y Functionalization of ZrO_2 Nanofibers with Pt Nanostructures: The Effect of Surface Roughness on Nucleation Mechanism and Morphology Control. *Chem. Phys. Lett.* 2009, 476, 56–61.
- (337). Formo E; Peng Z; Lee E; Lu X; Yang H; Xia Y Direct Oxidation of Methanol on Pt Nanostructures Supported on Electrospun Nanofibers of Anatase. *J. Phys. Chem. C* 2008, 112, 9970–9975.
- (338). Dai Y; Lu X; McKiernan M; Lee EP; Sun Y; Xia Y Hierarchical Nanostructures of K-Birnessite Nanoplates on Anatase Nanofibers and Their Application for Decoloration of Dye Solution. *J. Mater. Chem.* 2010, 20, 3157–3162.
- (339). Lu P; Xia Y Novel Nanostructures of Rutile Fabricated by Templating Against Yarns of Polystyrene Nanofibrils and Their Catalytic Applications. *ACS Appl. Mater. Interfaces* 2013, 5, 6391–6399. [PubMed: 23763369]
- (340). Yoon K; Yang Y; Lu P; Wan D; Peng HC; Stamm Masias K; Fanson PT; Campbell CT; Xia Y A Highly Reactive and Sinter-Resistant Catalytic System Based on Platinum Nanoparticles Embedded in the Inner Surfaces of CeO_2 Hollow Fibers. *Angew. Chem., Int. Ed.* 2012, 51, 9543–9546.
- (341). Yao Y; Huang Z; Xie P; Lacey SD; Jacob RJ; Xie H; Chen F; Nie A; Pu T; Rehwoldt M; et al. Carbothermal Shock Synthesis of High-Entropy-Alloy Nanoparticles. *Science* 2018, 359, 1489–1494. [PubMed: 29599236]
- (342). Wang H; Ma D; Huang X; Huang Y; Zhang X General and Controllable Synthesis Strategy of Metal Oxide/ TiO_2 Hierarchical Heterostructures with Improved Lithium-Ion Battery Performance. *Sci. Rep.* 2012, 2, 701. [PubMed: 23050085]
- (343). Kong J; Liu Z; Yang Z; Tan HR; Xiong S; Wong SY; Li X; Lu X Carbon/ SnO_2 /Carbon Core/Shell/Shell Hybrid Nanofibers: Tailored Nanostructure for the Anode of Lithium Ion Batteries with High Reversibility and Rate Capacity. *Nanoscale* 2012, 4, 525–530. [PubMed: 22127410]
- (344). Mu J; Shao C; Guo Z; Zhang M; Zhang Z; Zhang P; Chen B; Liu Y In_2O_3 Nanocubes/Carbon Nanofibers Heterostructures with High Visible Light Photocatalytic Activity. *J. Mater. Chem.* 2012, 22, 1786–1793.
- (345). Zhao B; Jiang S; Su C; Cai R; Ran R; Tade MO; Shao ZA 3D Porous Architecture Composed of TiO_2 Nanotubes Connected with a Carbon Nanofiber Matrix for Fast Energy Storage. *J. Mater. Chem. A* 2013, 1, 12310–12320.
- (346). Xiao X; Yuan L; Zhong J; Ding T; Liu Y; Cai Z; Rong Y; Han H; Zhou J; Wang ZL High-Strain Sensors Based on ZnO Nanowire/Polystyrene Hybridized Flexible Films. *Adv. Mater.* 2011, 23, 5440–5444. [PubMed: 22002439]
- (347). Harrison RH; Steele JAM; Chapman R; Gormley AJ; Chow LW; Mahat MM; Podhorska L; Palgrave RG; Payne DJ; Hettiaratchy SP; et al. Modular and Versatile Spatial Functionalization of Tissue Engineering Scaffolds through Fiber-Initiated Controlled Radical Polymerization. *Adv. Funct. Mater.* 2015, 25, 5748–5757. [PubMed: 27134621]
- (348). Kowalczyk T; Nowicka A; Elbaum D; Kowalewski TA Electrospinning of Bovine Serum Albumin. Optimization and the Use for Production of Biosensors. *Biomacromolecules* 2008, 9, 2087–2090. [PubMed: 18576601]
- (349). Patra SN; Bhattacharyya D; Ray S; Easteal AJ Electrospun Poly(Lactic Acid) Based Conducting Nanofibrous Networks. *IOP Conf. Ser.: Mater. Sci. Eng.* 2009, 4, 012020.
- (350). Gilchrist SE; Lange D; Letchford K; Bach H; Fazli L; Burt HM Fusidic Acid and Rifampicin Co-Loaded PLGA Nanofibers for the Prevention of Orthopedic Implant Associated Infections. *J. Controlled Release* 2013, 170, 64–73.
- (351). Lee KH; Kim HY; La YM; Lee DR; Sung NH Influence of a Mixing Solvent with Tetrahydrofuran and N,N-Dimethylformamide on Electrospun Poly(Vinyl Chloride) Nonwoven Mats. *J. Polym. Sci., Part B: Polym. Phys.* 2002, 40, 2259–2268.
- (352). Rho KS; Jeong L; Lee G; Seo BM; Park YJ; Hong SD; Roh S; Cho JJ; Park WH; Min BM Electrospinning of Collagen Nanofibers: Effects on the Behavior of Normal Human Keratinocytes and Early-Stage Wound Healing. *Biomaterials* 2006, 27, 1452–1461. [PubMed: 16143390]

- (353). Huang ZM; Zhang YZ; Ramakrishna S; Lim CT Electrospinning and Mechanical Characterization of Gelatin Nano-fibers. *Polymer* 2004, 45, 5361–5368.
- (354). Ji Y; Ghosh K; Shu XZ; Li B; Sokolov JC; Prestwich GD; Clark RAF; Rafailovich MH Electrospun Three-Dimensional Hyaluronic Acid Nanofibrous Scaffolds. *Biomaterials* 2006, 27, 3782–3792. [PubMed: 16556462]
- (355). Hang Y; Zhang Y; Jin Y; Shao H; Hu X Preparation of Regenerated Silk Fibroin/Silk Sericin Fibers by Coaxial Electro-spinning. *Int. J. Biol. Macromol* 2012, 51, 980–986. [PubMed: 22935694]
- (356). Liu Y; Ding Y; Zhang Y; Lei Y Pt–Au Nanocorals, Pt Nanofibers and Au Microparticles Prepared by Electrospinning and Calcination for Nonenzymatic Glucose Sensing in Neutral and Alkaline Environment. *Sens. Actuators, B* 2012, 171–172, 954–961.
- (357). Azad A-M Fabrication of Transparent Alumina (Al_2O_3) Nanofibers by Electrospinning. *Mater. Sci. Eng., A* 2006, 435–436, 468–473.
- (358). Yang X; Shao C; Liu Y; Mu R; Guan H Nanofibers of CeO_2 via an Electrospinning Technique. *Thin Solid Films* 2005, 478, 228–231.
- (359). Cui Z; Wang S; Zhang Y; Cao M High-Performance Lithium Storage of Co_3O_4 Achieved by Constructing Porous Nanotube Structure. *Electrochim. Acta* 2015, 182, 507–515.
- (360). Zheng W; Li Z; Zhang H; Wang W; Wang Y; Wang C Electrospinning Route for $\alpha\text{-Fe}_2\text{O}_3$ Ceramic Nanofibers and Their Gas Sensing Properties. *Mater. Res. Bull* 2009, 44, 1432–1436.
- (361). Fan Q; Whittingham MS Electrospun Manganese Oxide Nanofibers as Anodes for Lithium-Ion Batteries. *Electrochem. Solid-State Lett* 2007, 10, A48–A51.
- (362). Yang A; Tao X; Pang GKH; Siu KGG Preparation of Porous Tin Oxide Nanobelts Using the Electrospinning Technique. *J. Am. Ceram. Soc* 2008, 91, 257–262.
- (363). Ban C; Chernova NA; Whittingham MS Electrospun Nano-Vanadium Pentoxide Cathode. *Electrochem. Commun* 2009, 11, 522–525.
- (364). Wang G; Ji Y; Huang XR; Yang XQ; Gouma PI; Dudley M Fabrication and Characterization of Polycrystalline WO_3 Nanofibers and Their Application for Ammonia Sensing. *J. Phys. Chem. B* 2006, 110, 23777–23782. [PubMed: 17125339]
- (365). Ju Y-W; Park J-H; Jung H-R; Cho S-J; Lee W-J Fabrication and Characterization of Cobalt Ferrite (CoFe_2O_4) Nanofibers by Electrospinning. *Mater. Sci. Eng., B* 2008, 147, 7–12.
- (366). Sahner K; Gouma P; Moos R Electrodeposited and Sol-Gel Precipitated P-Type $\text{SrTi}_{1-x}\text{Fe}_x\text{O}_{3-\delta}$ Semiconductors for Gas Sensing. *Sensors* 2007, 7, 1871–1886. [PubMed: 28903202]
- (367). Luo W; Hu X; Sun Y; Huang Y Electrospun Porous ZnCo_2O_4 Nanotubes as a High-Performance Anode Material for Lithium-Ion Batteries. *J. Mater. Chem* 2012, 22, 8916–8921.
- (368). Arun N; Aravindan V; Jayaraman S; Shubha N; Ling WC; Ramakrishna S; Madhavi S Exceptional Performance of a High Voltage Spinel $\text{LiNi}_{0.5}\text{Mn}_{1.5}\text{O}_4$ Cathode in All One Dimensional Architectures with an Anatase TiO_2 Anode by Electrospinning. *Nanoscale* 2014, 6, 8926–8934. [PubMed: 24965606]
- (369). Xia G; Li D; Chen X; Tan Y; Tang Z; Guo Z; Liu H; Liu Z; Yu X Carbon-Coated Li_3N Nanofibers for Advanced Hydrogen Storage. *Adv. Mater* 2013, 25, 6238–6244. [PubMed: 23966063]
- (370). Xu Y; Wang J; Shen L; Dou H; Zhang X One-Dimensional Vanadium Nitride Nanofibers Fabricated by Electro-spinning for Supercapacitors. *Electrochim. Acta* 2015, 173, 680–686.
- (371). Shi M; Zhao L; Song X; Liu J; Zhang P; Gao L Highly Conductive Mo_2C Nanofibers Encapsulated in Ultrathin MnO_2 Nanosheets as a Self-Supported Electrode for High-Performance Capacitive Energy Storage. *ACS Appl. Mater. Interfaces* 2016, 8, 32460–32467. [PubMed: 27808498]
- (372). Eick BM; Youngblood JP SiC Nanofibers by Pyrolysis of Electrospun Preceramic Polymers. *J. Mater. Sci* 2009, 44, 160–165.
- (373). Zhang L; Hu J; Voevodin AA; Fong H Synthesis of Continuous TiC Nanofibers and/or Nanoribbons through Electro-spinning Followed by Carbothermal Reduction. *Nanoscale* 2010, 2, 1670–1673. [PubMed: 20820698]

- (374). Tao X; Zhou S; Ma J; Xiang Z; Hou R; Wang J; Li X A Facile Method to Prepare ZrC Nanofibers by Electrospinning and Pyrolysis of Polymeric Precursors. *Ceram. Int.* 2017, 43, 3910–3914.
- (375). Liu D; Li W; Li L; Ling H; You T Facile Preparation of Ni Nanowire Embedded Nitrogen and Sulfur Dual-Doped Carbon Nanofibers and Its Superior Catalytic Activity toward Urea Oxidation. *J. Colloid Interface Sci.* 2018, 529, 337–344. [PubMed: 29940317]
- (376). Liu J; Liang J; Wang C; Ma J Electrospun CoSe@N-Doped Carbon Nanofibers with Highly Capacitive Li Storage. *J. Energy Chem.* 2019, 33, 160.
- (377). Guo L; Sun H; Qin C; Li W; Wang F; Song W; Du J; Zhong F; Ding Y Flexible Fe₃O₄ Nanoparticles/N-Doped Carbon Nanofibers Hybrid Film as Binder-Free Anode Materials for Lithium-Ion Batteries. *Appl. Surf. Sci.* 2018, 459, 263–270.
- (378). Xia J; Jiang K; Xie J; Guo S; Liu L; Zhang Y; Nie S; Yuan Y; Yan H; Wang X Tin Disulfide Embedded in N-, S-Doped Carbon Nanofibers as Anode Material for Sodium-Ion Batteries. *Chem. Eng. J.* 2019, 359, 1244–1251.
- (379). Yu X; Pei C; Chen W; Feng L 2 Dimensional WS₂ Tailored Nitrogen-Doped Carbon Nanofiber as a Highly Pseudocapacitive Anode Material for Lithium-Ion Battery. *Electrochim. Acta* 2018, 272, 119–126.
- (380). Cai N; Fu J; Chan V; Liu M; Chen W; Wang J; Zeng H; Yu F MnCo₂O₄@Nitrogen-Doped Carbon Nanofiber Composites with Meso-Microporous Structure for High-Performance Symmetric Supercapacitors. *J. Alloys Compd.* 2019, 782, 251–262.
- (381). Katsogiannis KAG; Vladisavljević GT; Georgiadou S; Rahmani R Assessing the Increase in Specific Surface Area for Electrospun Fibrous Network Due to Pore Induction. *ACS Appl. Mater. Interfaces* 2016, 8, 29148–29154. [PubMed: 27700029]
- (382). Megelski S; Stephens JS; Chase DB; Rabolt JF Micro-and Nanostructured Surface Morphology on Electrospun Polymer Fibers. *Macromolecules* 2002, 35, 8456–8466.
- (383). Rezabeigi E; Wood-Adams PM; Demarquette NR Complex Morphology Formation in Electrospinning of Binary and Ternary Poly(Lactic Acid) Solutions. *Macromolecules* 2018, 51, 4094–4107.
- (384). Dayal P; Liu J; Kumar S; Kyu T Experimental and Theoretical Investigations of Porous Structure Formation in Electro-spun Fibers. *Macromolecules* 2007, 40, 7689–7694.
- (385). Lin J; Ding B; Yu J Direct Fabrication of Highly Nanoporous Polystyrene Fibers via Electrospinning. *ACS Appl. Mater. Interfaces* 2010, 2, 521–528. [PubMed: 20356200]
- (386). Celebioglu A; Uyar T Electrospun Porous Cellulose Acetate Fibers from Volatile Solvent Mixture. *Mater. Lett.* 2011, 65, 2291–2294.
- (387). Lubasova D; Martinova L Controlled Morphology of Porous Polyvinyl Butyral Nanofibers. *J. Nanometer* 2011, 2011, 292516.
- (388). Li D; Wu T; He N; Wang J; Chen W; He L; Huang C; Ei-Hamshary HA; Al-Deyab SS; Ke Q; et al. Three-Dimensional Polycaprolactone Scaffold via Needleless Electrospinning Promotes Cell Proliferation and Infiltration. *Colloids Surf., B* 2014, 121, 432–443.
- (389). McCann JT; Marquez M; Xia Y Highly Porous Fibers by Electrospinning into a Cryogenic Liquid. *J. Am. Chem. Soc.* 2006, 128, 1436–1437. [PubMed: 16448099]
- (390). Casper CL; Stephens JS; Tassi NG; Chase DB; Rabolt JF Controlling Surface Morphology of Electrospun Polystyrene Fibers: Effect of Humidity and Molecular Weight in the Electrospinning Process. *Macromolecules* 2004, 37, 573–578.
- (391). Lu P; Xia Y Maneuvering the Internal Porosity and Surface Morphology of Electrospun Polystyrene Yarns by Controlling the Solvent and Relative Humidity. *Langmuir* 2013, 29, 7070–7078. [PubMed: 23530752]
- (392). Pai C-L; Boyce MC; Rutledge GC Morphology of Porous and Wrinkled Fibers of Polystyrene Electrospun from Dimethylformamide. *Macromolecules* 2009, 42, 2102–2114.
- (393). Fashandi H; Karimi M Characterization of Porosity of Polystyrene Fibers Electrospun at Humid Atmosphere. *Thermochim. Acta* 2012, 547, 38–46.
- (394). Fashandi H; Ghomi A Interplay of Phase Separation and Physical Gelation in Morphology Evolution within Nanoporous Fibers Electrospun at High Humidity Atmosphere. *Ind. Eng. Chem. Res.* 2015, 54, 240–253.

- (395). Fashandi H; Karimi M Comparative Studies on the Solvent Quality and Atmosphere Humidity for Electrospinning of Nano-porous Polyetherimide Fibers. *Ind. Eng. Chem. Res* 2014, 53, 235–245.
- (396). Shu D; Xi P; Li S; Li C; Wang X; Cheng B Morphologies and Properties of PET Nano Porous Luminescence Fiber: Oil Absorption and Fluorescence-Indicating Functions. *ACS Appl. Mater. Interfaces* 2018, 10, 2828–2836. [PubMed: 29294290]
- (397). Qi Z; Yu H; Chen Y; Zhu M Highly Porous Fibers Prepared by Electrospinning a Ternary System of Nonsolvent/Solvent/Poly(L-lactic acid). *Mater. Lett* 2009, 63, 415–418.
- (398). Yu X; Xiang H; Long Y; Zhao N; Zhang X; Xu J Preparation of Porous Polyacrylonitrile Fibers by Electrospinning a Ternary System of PAN/DMF/H₂O. *Mater. Lett* 2010, 64, 2407–2409.
- (399). Nayani K; Katepalli H; Sharma CS; Sharma A; Patil S; Venkataraghavan R Electrospinning Combined with Nonsolvent-Induced Phase Separation to Fabricate Highly Porous and Hollow Submicrometer Polymer Fibers. *Ind. Eng. Chem. Res* 2012, 51, 1761–1766.
- (400). Katsogiannis KAG; Vladisavljevi GT; Georgiadou S Porous Electrospun Polycaprolactone (PCL) Fibres by Phase Separation. *Eur. Polym. J* 2015, 69, 284–295.
- (401). Chen P-Y; Tung S-H One-Step Electrospinning to Produce Nonsolvent-Induced Macroporous Fibers with Ultrahigh Oil Adsorption Capability. *Macromolecules* 2017, 50, 2528–2534.
- (402). Seo Y-A; Pant HR; Nirmala R; Lee J-H; Song KG; Kim HY Fabrication of Highly Porous Poly(ϵ -caprolactone) Microfibers via Electrospinning. *J. Porous Mater* 2012, 19, 217–223.
- (403). Muñoz-Bonilla A; Fernández-García M; Rodríguez-Hernández J Towards Hierarchically Ordered Functional Porous Polymeric Surfaces Prepared by the Breath Figures Approach. *Prog. Polym. Sci* 2014, 39, 510–554.
- (404). Gupta A; Saquing CD; Afshari M; Tonelli AE; Khan SA; Kotek R Porous Nylon-6 Fibers via a Novel Salt-Induced Electrospinning Method. *Macromolecules* 2009, 42, 709–715.
- (405). Peng M; Li D; Shen L; Chen Y; Zheng Q; Wang H Nanoporous Structured Submicrometer Carbon Fibers Prepared via Solution Electrospinning of Polymer Blends. *Langmuir* 2006, 22, 9368–9374. [PubMed: 17042555]
- (406). Zhang L; Hsieh Y-L Nanoporous Ultrahigh Specific Surface Polyacrylonitrile Fibres. *Nanotechnology* 2006, 17, 4416–4423.
- (407). Zhang Z; Li X; Wang C; Fu S; Liu Y; Shao C Polyacrylonitrile and Carbon Nanofibers with Controllable Nanoporous Structures by Electrospinning. *Macromol. Mater. Eng* 2009, 294, 673–678.
- (408). Wang H; Yang X; Wu Q; Zhang Q; Chen H; Jing H; Wang J; Mi S-B; Rogach AL; Niu C Encapsulating Silica/Antimony into Porous Electrospun Carbon Nanofibers with Robust Structure Stability for High-Efficiency Lithium Storage. *ACS Nano* 2018, 12, 3406–3416. [PubMed: 29641178]
- (409). Han SO; Son WK; Cho D; Youk JH; Park WH Preparation of Porous Ultra-Fine Fibres via Selective Thermal Degradation of Electrospun Polyetherimide/Poly(3-hydroxybutyrate-*co*-3-hydroxyvalerate) Fibres. *Polym. Degrad. Stab* 2004, 86, 257–262.
- (410). Tran C; Kalra V Fabrication of Porous Carbon Nanofibers with Adjustable Pore Sizes as Electrodes for Supercapacitors. *J. Power Sources* 2013, 235, 289–296.
- (411). Zuo W; Zhu M; Yang W; Yu H; Chen Y; Zhang Y Experimental Study on Relationship Between Jet Instability and Formation of Beaded Fibers During Electrospinning. *Polym. Eng. Sci* 2005, 45, 704–709.
- (412). Luo C; Li L; Li J; Yang G; Ding S; Zhi W; Weng J; Zhou S Modulating Cellular Behaviors through Surface Nanoroughness. *J. Mater. Chem* 2012, 22, 15654–15664.
- (413). Ding S; Li J; Luo C; Li L; Yang G; Zhou S Synergistic Effect of Released Dexamethasone and Surface Nanoroughness on Mesenchymal Stem Cell Differentiation. *Biomater. Sci* 2013, 1, 1091–1100.
- (414). Tan SH; Inai R; Kotaki M; Ramakrishna S Systematic Parameter Study for Ultra-Fine Fiber Fabrication *via* Electrospinning Process. *Polymer* 2005, 46, 6128–6134.
- (415). Tian X; Bai H; Zheng Y; Jiang L Bio-Inspired Heterostructured Bead-on-String Fibers That Respond to Environmental Wetting. *Adv. Funct. Mater* 2011, 21, 1398–1402.

- (416). Qi H; Hu P; Xu J; Wang A Encapsulation of Drug Reservoirs in Fibers by Emulsion Electrospinning: Morphology Characterization and Preliminary Release Assessment. *Biomacromolecules* 2006, 7, 2327–2330. [PubMed: 16903678]
- (417). Crespy D; Friedemann K; Popa AM Colloid-Electrospinning: Fabrication of Multicompartment Nanofibers by the Electrospinning of Organic or/and Inorganic Dispersions and Emulsions. *Macromol. Rapid Commun.* 2012, 33, 1978–1995. [PubMed: 23129202]
- (418). Yuan W; Zhang K-Q Structural Evolution of Electrospun Composite Fibers from the Blend of Polyvinyl Alcohol and Polymer Nanoparticles. *Langmuir* 2012, 28, 15418–15424. [PubMed: 23039272]
- (419). Lim J-M; Moon JH; Yi G-R; Heo C-J; Yang S-M Fabrication of One-Dimensional Colloidal Assemblies from Electrospun Nanofibers. *Langmuir* 2006, 22, 3445–3449. [PubMed: 16584206]
- (420). Wei M; Kang B; Sung C; Mead J Core-Sheath Structure in Electrospun Nanofibers from Polymer Blends. *Macromol. Mater. Eng.* 2006, 291, 1307–1314.
- (421). Wang C; Hsiue T-T Core-Shell Fibers Electrospun from Phase-Separated Blend Solutions: Fiber Formation Mechanism and Unique Energy Dissipation for Synergistic Fiber Toughness. *Biomacromolecules* 2017, 18, 2906–2917. [PubMed: 28853864]
- (422). Yarin AL Coaxial Electrospinning and Emulsion Electro-spinning of Core-Shell Fibers. *Polym. Adv. Technol.* 2011, 22, 310–317.
- (423). Sun XY; Shankar R; Börner HG; Ghosh TK; Spontak RJ Field-Driven Biofunctionalization of Polymer Fiber Surfaces During Electrospinning. *Adv. Mater.* 2007, 19, 87–91.
- (424). Chiu YJ; Tseng HF; Lo YC; Wu BH; Chen JT Plateau-Rayleigh Instability Morphology Evolution (PRIME): From Electrospun Core-Shell Polymer Fibers to Polymer Microbowls. *Macromol. Rapid Commun.* 2017, 38, 1600689.
- (425). Zhang J-F; Yang D-Z; Xu F; Zhang Z-P; Yin R-X; Nie J Electrospun Core-Shell Structure Nanofibers from Homogeneous Solution of Poly(ethylene oxide)/Chitosan. *Macromolecules* 2009, 42, 5278–5284.
- (426). Chen M; Dong M; Havelund R; Regina VR; Meyer RL; Besenbacher F; Kingshott P Thermo-Responsive Core-Sheath Electrospun Nanofibers from Poly (N-isopropylacrylamide)/Poly-caprolactone Blends. *Chem. Mater.* 2010, 22, 4214–4221.
- (427). Jiang Y; Fang D; Song G; Nie J; Chen B; Ma G Fabrication of Core-Shell Nanofibers by Single Capillary Electro-spinning Combined with Vapor Induced Phase Separation. *New J. Chem.* 2013, 37, 2917–2924.
- (428). Xu X; Zhuang X; Chen X; Wang X; Yang L; Jing X Preparation of Core-Sheath Composite Nanofibers by Emulsion Electrospinning. *Macromol. Rapid Commun.* 2006, 27, 1637–1642.
- (429). Bazilevsky AV; Yarin AL; Megaridis CM Co-Electrospinning of Core-Shell Fibers Using a Single-Nozzle Technique. *Langmuir* 2007, 23, 2311–2314. [PubMed: 17266345]
- (430). Jo E; Lee S; Kim KT; Won YS; Kim HS; Cho EC; Jeong U Core-Sheath Nanofibers Containing Colloidal Arrays in the Core for Programmable Multi-Agent Delivery. *Adv. Mater.* 2009, 21, 968–972.
- (431). Yang Y; Li X; Cui W; Zhou S; Tan R; Wang C Structural Stability and Release Profiles of Proteins from Core-Shell Poly (DL-lactide) Ultrafine Fibers Prepared by Emulsion Electrospinning. *J. Biomed. Mater. Res., Part A* 2008, 86, 374–385.
- (432). Li X; Zhang H; Li H; Yuan X Encapsulation of Proteinase K in PELA Ultrafine Fibers by Emulsion Electrospinning: Preparation and *in Vitro* Evaluation. *Colloid Polym. Sci.* 2010, 288, 1113–1119.
- (433). Chen W; Li D; Ei-Shanshory A; El-Newehy M; Ei-Hamshary HA; Al-Deyab SS; He C; Mo X Dexamethasone Loaded Core-Shell SF/PEO Nanofibers *via* Green Electrospinning Reduced Endothelial Cells Inflammatory Damage. *Colloids Surf., B* 2015, 126, 561–568.
- (434). Li LL; Peng SJ; Lee JKY; Ji DX; Srinivasan M; Ramakrishna S Electrospun Hollow Nanofibers for Advanced Secondary Batteries. *Nano Energy* 2017, 39, 111–139.
- (435). McCann JT; Li D; Xia Y Electrospinning of Nanofibers with Core-Sheath, Hollow, or Porous Structures. *J. Mater. Chem.* 2005, 15, 735–738.

- (436). Chen H; Wang N; Di J; Zhao Y; Song Y; Jiang L Nanowire-in-Microtube Structured Core/Shell Fibers via Multifluidic Coaxial Electrospinning. *Langmuir* 2010, 26, 11291–11296. [PubMed: 20337483]
- (437). Hong Y; Chen X; Jing X; Fan H; Gu Z; Zhang X Fabrication and Drug Delivery of Ultrathin Mesoporous Bioactive Glass Hollow Fibers. *Adv. Funct. Mater* 2010, 20, 1503–1510.
- (438). Li Z; Zhang JT; Chen YM; Li J; Lou XW Pie-Like Electrode Design for High-Energy Density Lithium-Sulfur Batteries. *Nat. Commun* 2015, 6, 8850. [PubMed: 26608228]
- (439). Niu C; Meng J; Wang X; Han C; Yan M; Zhao K; Xu X; Ren W; Zhao Y; Xu L; et al. General Synthesis of Complex Nanotubes by Gradient Electrospinning and Controlled Pyrolysis. *Nat. Commun* 2015, 6, 7402. [PubMed: 26067281]
- (440). Yin Y-B; Xu J-J; Liu Q-C; Zhang X-B Macroporous Interconnected Hollow Carbon Nanofibers Inspired by Golden-Toad Eggs toward a Binder-Free, High-Rate, and Flexible Electrode. *Adv. Mater* 2016, 28, 7494–7500. [PubMed: 27348717]
- (441). Sun Y; Sills RB; Hu X; Seh ZW; Xiao X; Xu H; Luo W; Jin H; Xin Y; Li T; et al. A Bamboo-Inspired Nanostructure Design for Flexible, Foldable, and Twistable Energy Storage Devices. *Nano Lett* 2015, 15, 3899–3906. [PubMed: 26011653]
- (442). Cheng Y; Zou B; Wang C; Liu Y; Fan X; Zhu L; Wang Y; Ma H; Cao X Formation Mechanism of Fe₂O₃ Hollow Fibers by Direct Annealing of the Electrospun Composite Fibers and Their Magnetic, Electrochemical Properties. *CrystEngComm* 2011, 13, 2863–2870.
- (443). Hong YJ; Yoon J-W; Lee J-H; Kang YC A New Concept for Obtaining SnO₂ Fiber-in-Tube Nanostructures with Superior Electrochemical Properties. *Chem. -Eur. J* 2015, 21, 371–376. [PubMed: 25450513]
- (444). Lang L; Wu D; Xu Z Controllable Fabrication of TiO₂ 1D-Nano/Micro Structures: Solid, Hollow, and Tube-in-Tube Fibers by Electrospinning and the Photocatalytic Performance. *Chem. -Eur. J* 2012, 18, 10661–10668. [PubMed: 22806770]
- (445). Cho JS; Hong YJ; Kang YC Electrochemical Properties of Fiber-in-Tube-and Filled-Structured TiO₂ Nanofiber Anode Materials for Lithium-Ion Batteries. *Chem. -Eur. J* 2015, 21, 11082–11087. [PubMed: 26119328]
- (446). Peng S; Li L; Hu Y; Srinivasan M; Cheng F; Chen J; Ramakrishna S Fabrication of Spinel One-Dimensional Architectures by Single-Spinneret Electrospinning for Energy Storage Applications. *ACS Nano* 2015, 9, 1945–1954. [PubMed: 25602640]
- (447). Koombhongse S; Liu W; Reneker DH Flat Polymer Ribbons and Other Shapes by Electrospinning. *J. Polym. Sci., Part B: Polym. Phys* 2001, 39, 2598–2606.
- (448). Koski A; Yim K; Shivkumar S Effect of Molecular Weight on Fibrous PVA Produced by Electrospinning. *Mater. Lett* 2004, 58, 493–497.
- (449). Li S; Zhao Y; Wang C; Li D; Gao K Fabrication and Characterization Unique Ribbon-Like Porous Ag/LaFeO₃ Nanobelts Photocatalyst via Electrospinning. *Mater. Lett* 2016, 170, 122–125.
- (450). Ner Y; Stuart JA; Whited G; Sotzing GA Electrospinning Nanoribbons of a Bioengineered Silk-Elastin-Like Protein (SELP) from Water. *Polymer* 2009, 50, 5828–5836.
- (451). Hashimoto T; Murase H; Ohta Y A New Scenario of Flow-Induced Shish-Kebab Formation in Entangled Polymer Solutions. *Macromolecules* 2010, 43, 6542–6548.
- (452). Liu S; Zhang F; Zheng G; Dai K; Liu C; Shen C; Guo JZ Direct Microscopic Observation of Shish-Kebab Structure in High-Temperature Electrospun iPP Fibers. *Mater. Lett* 2016, 172, 149–152.
- (453). Cui K; Ma Z; Tian N; Su F; Liu D; Li L Multiscale and Multistep Ordering of Flow-Induced Nucleation of Polymers. *Chem. Rev* 2018, 118, 1840–1886. [PubMed: 29350931]
- (454). Wang B; Li B; Xiong J; Li CY Hierarchically Ordered Polymer Nanofibers via Electrospinning and Controlled Polymer Crystallization. *Macromolecules* 2008, 41, 9516–9521.
- (455). Chen X; Dong B; Wang B; Shah R; Li CY Crystalline Block Copolymer Decorated, Hierarchically Ordered Polymer Nanofibers. *Macromolecules* 2010, 43, 9918–9927.
- (456). Chen X; Wang W; Cheng S; Dong B; Li CY Mimicking Bone Nanostructure by Combining Block Copolymer Self-Assembly and 1D Crystal Nucleation. *ACS Nano* 2013, 7, 8251–8257. [PubMed: 23972012]

- (457). Holzmeister A; Greiner A; Wendorff JH Barbed Nanowires" from Polymers *via* Electrospinning. *Polym. Eng. Sci* 2009, 49, 148–153.
- (458). Beachley V; Katsanevakis E; Zhang N; Wen X A Novel Method to Precisely Assemble Loose Nanofiber Structures for Regenerative Medicine Applications. *Adv. Healthcare Mater* 2013, 2, 343–351.
- (459). Xie J; Li X; Lipner J; Manning CN; Schwartz AG; Thomopoulos S; Xia Y "Aligned-to-Random" Nanofiber Scaffolds for Mimicking the Structure of the Tendon-to-Bone Insertion Site. *Nanoscale* 2010, 2, 923–926. [PubMed: 20648290]
- (460). Yang D; Lu B; Zhao Y; Jiang X Fabrication of Aligned Fibrous Arrays by *Magnetic Electrospinning*. *Adv. Mater* 2007, 19, 3702–3706.
- (461). Liu Y; Zhang X; Xia Y; Yang H Magnetic-Field-Assisted Electrospinning of Aligned Straight and Wavy Polymeric Nanofibers. *Adv. Mater* 2010, 22, 2454–2457. [PubMed: 20376855]
- (462). Wang X; Ding B; Sun G; Wang M; Yu J Electro-Spinning/Netting: A Strategy for the Fabrication of Three-Dimensional Polymer Nano-Fiber/Nets. *Prog. Mater. Sci* 2013, 58, 1173–1243.
- (463). Pant HR; Bajgai MP; Nam KT; Chu KH; Park S-J; Kim HY Formation of Electrospun Nylon-6/Methoxy Poly-(ethylene glycol) Oligomer Spider-Wave Nanofibers. *Mater. Lett* 2010, 64, 2087–2090.
- (464). Wang N; Si Y; Yu J; Fong H; Ding B Nano-Fiber/Net Structured PVA Membrane: Effects of Formic Acid as Solvent and Crosslinking Agent on Solution Properties and Membrane Morphological Structures. *Mater. Des* 2017, 120, 135–143.
- (465). Ding B; Li C; Miyauchi Y; Kuwaki O; Shiratori S Formation of Novel 2D Polymer Nanowebs via Electrospinning. *Nanotechnology* 2006, 17, 3685–3691.
- (466). Ding B; Wang X; Yu J; Wang M Polyamide 6 Composite Nano-Fiber/Net Functionalized by Polyethyleneimine on Quartz Crystal Microbalance for Highly Sensitive Formaldehyde Sensors. *J. Mater. Chem* 2011, 21, 12784–12792.
- (467). Nirmala R; Nam KT; Park S-J; Shin Y-S; Navamathavan R; Kim HY Formation of High Aspect Ratio Polyamide-6 Nanofibers via Electrically Induced Double Layer During Electrospinning. *Appl. Surf. Sci* 2010, 256, 6318–6323.
- (468). Wang X; Ding B; Yu J; Si Y; Yang S; Sun G Electro-Netting: Fabrication of Two-Dimensional Nano-Nets for Highly Sensitive Trimethylamine Sensing. *Nanoscale* 2011, 3, 911–915. [PubMed: 21152536]
- (469). Yan G; Yu J; Qiu Y; Yi X; Lu J; Zhou X; Bai X Self-Assembly of Electrospun Polymer Nanofibers: A General Phenomenon Generating Honeycomb-Patterned Nanofibrous Structures. *Langmuir* 2011, 27, 4285–4289. [PubMed: 21425819]
- (470). Carlberg B; Wang T; Liu J Direct Photolithographic Patterning of Electrospun Films for Defined Nanofibrillar Microarchitectures. *Langmuir* 2010, 26, 2235–2239. [PubMed: 20092342]
- (471). Jun I; Chung Y-W; Heo Y-H; Han H-S; Park J; Jeong H; Lee H; Lee YB; Kim Y-C; Seok H-K; et al. Creating Hierarchical Topographies on Fibrous Platforms Using Femtosecond Laser Ablation for Directing Myoblasts Behavior. *ACS Appl. Mater. Interfaces* 2016, 8, 3407–3417. [PubMed: 26771693]
- (472). Sharma CS; Sharma A; Madou M Multiscale Carbon Structures Fabricated by Direct Micropatterning of Electrospun Mats of SU-8 Photoresist Nanofibers. *Langmuir* 2010, 26, 2218–2222. [PubMed: 20070083]
- (473). Jia C; Yu D; Lamarre M; Leopold PL; Teng YD; Wang H Patterned Electrospun Nanofiber Matrices via Localized Dissolution: Potential for Guided Tissue Formation. *Adv. Mater* 2014, 26, 8192–8197. [PubMed: 25352221]
- (474). Rebollar E; Cordero D; Martins A; Chiussi S; Reis RL; Neves NM; León B Improvement of Electrospun Polymer Fiber Meshes Pore Size by Femtosecond Laser Irradiation. *Appl. Surf. Sci* 2011, 257, 4091–4095.
- (475). Lee BL-P; Jeon H; Wang A; Yan Z; Yu J; Grigoropoulos C; Li S Femtosecond Laser Ablation Enhances Cell Infiltration into Three-Dimensional Electrospun Scaffolds. *Acta Biomater* 2012, 8, 2648–2658. [PubMed: 22522128]

- (476). Lee SJ; Oh SH; Liu J; Soker S; Atala A; Yoo JJ The Use of Thermal Treatments to Enhance the Mechanical Properties of Electrospun Poly(ϵ -Caprolactone) Scaffolds. *Biomaterials* 2008, 29, 1422–1430. [PubMed: 18096219]
- (477). Wang S-X; Yang L; Stubbs LP; Li X; He C Lignin-Derived Fused Electrospun Carbon Fibrous Mats as High Performance Anode Materials for Lithium Ion Batteries. *ACS Appl. Mater. Interfaces* 2013, 5, 12275–12282. [PubMed: 24256294]
- (478). Shi Z; Jin G; Wang J; Zhang J Free-Standing, Welded Mesoporous Carbon Nanofibers as Anode for High-Rate Performance Li-Ion Batteries. *J. Electroanal. Chem* 2017, 795, 26–31.
- (479). Zernetsch H; Kern A; Jäschke P; Glasmacher B Laser Processing of Electrospun PCL Fiber Mats for Tissue Engineering. *Int. J. Artif. Organs* 2015, 38, 607–614. [PubMed: 26728788]
- (480). Zillohu AU; Abdelaziz R; Hedayati MK; Emmler T; Homaeigohar S; Elbahri M Plasmon-Mediated Embedding of Nanoparticles in a Polymer Matrix: Nanocomposites Patterning, Writing, and Defect Healing. *J. Phys. Chem. C* 2012, 116, 17204–17209.
- (481). Zillohu AU; Alissawi N; Abdelaziz R; Elbahri M Thermo-Plasmonics for Localized Graphitization and Welding of Polymeric Nanofibers. *Materials* 2014, 7, 323–332. [PubMed: 28788459]
- (482). Huang L; Manickam SS; McCutcheon JR Increasing Strength of Electrospun Nanofiber Membranes for Water Filtration Using Solvent Vapor. *J. Membr. Sci* 2013, 436, 213–220.
- (483). Li H; Zhu C; Xue J; Ke Q; Xia Y Enhancing the Mechanical Properties of Electrospun Nanofiber Mats through Controllable Welding at the Cross Points. *Macromol. Rapid Commun* 2017, 38, 1600723.
- (484). Meng Y; Lou K; Qi R; Guo Z; Shin B; Liu G; Shan F Nature Inspired Capillary-Driven Welding Process for Boosting Metal-Oxide Nanofiber Electronics. *ACS Appl. Mater. Interfaces* 2018, 10, 20703–20711. [PubMed: 29799183]
- (485). Zhao J-H; Xu L; Liu Q Effect of Ethanol Post-Treatment on the Bubble-Electrospun Poly (Vinyl Alcohol) Nanofiber. *Therm. Sci* 2015, 19, 1353–1356.
- (486). Jang SY; Seshadri V; Khil MS; Kumar A; Marquez M; Mather PT; Sotzing GA Welded Electrochromic Conductive Polymer Nanofibers by Electrostatic Spinning. *Adv. Mater* 2005, 17, 2177–2180.
- (487). Wang W; Jin X; Zhu Y; Zhu C; Yang J; Wang H; Lin T Effect of Vapor-Phase Glutaraldehyde Crosslinking on Electrospun Starch Fibers. *Carbohydr. Polym* 2016, 140, 356–361. [PubMed: 26876862]
- (488). Zong X; Ran S; Fang D; Hsiao BS; Chu B Control of Structure, Morphology and Property in Electrospun Poly(glycolide-co-lactide) Non-Woven Membranes via Post-Draw Treatments. *Polymer* 2003, 44, 4959–4967.
- (489). Fan S; Zhang Y; Shao H; Hu X Electrospun Regenerated Silk Fibroin Mats with Enhanced Mechanical Properties. *Int. J. Biol. Macromol* 2013, 56, 83–88. [PubMed: 23403022]
- (490). Sun W; Cai Q; Li P; Deng X; Wei Y; Xu M; Yang X Post-Draw PAN-PMMA Nanofiber Reinforced and Toughened Bis-GMA Dental Restorative Composite. *Dent. Mater* 2010, 26, 873–880. [PubMed: 20579722]
- (491). Na H; Li Q; Sun H; Zhao C; Yuan X Anisotropic Mechanical Properties of Hot-Pressed PVDF Membranes with Higher Fiber Alignments via Electrospinning. *Polym. Eng. Sci* 2009, 49, 1291–1298.
- (492). Na H; Zhao Y; Zhao C; Yuan X Effect of Hot-Press on Electrospun Poly (vinylidene fluoride) Membranes. *Polym. Eng. Sci* 2008, 48, 934–940.
- (493). Gopal R; Kaur S; Ma Z; Chan C; Ramakrishna S; Matsuura T Electrospun Nanofibrous Filtration Membrane. *J. Membr. Sci* 2006, 281, 581–586.
- (494). Yang Y; Simeon F; Hatton TA; Rutledge GC Polyacrylonitrile-Based Electrospun Carbon Paper for Electrode Applications. *J. Appl. Polym. Sci* 2012, 124, 3861–3870.
- (495). Ali AA; Rutledge G Hot-Pressed Electrospun PAN Nano Fibers: An Idea for Flexible Carbon Mat. *J. Mater. Process. Technol* 2009, 209, 4617–4620.
- (496). Wang Z; Sahadevan R; Yeh CN; Menkhaus TJ; Huang J; Fong H Hot-Pressed Polymer Nanofiber Supported Graphene Membrane for High-Performance Nanofiltration. *Nanotechnology* 2017, 28, 31LT02.

- (497). Zhou T; Yao Y; Xiang R; Wu Y Formation and Characterization of Polytetrafluoroethylene Nanofiber Membranes for Vacuum Membrane Distillation. *J. Membr. Sci* 2014, 453, 402–408.
- (498). Peng Q; Sun X-Y; Spagnola JC; Hyde GK; Spontak RJ; Parsons GN Atomic Layer Deposition on Electrospun Polymer Fibers as a Direct Route to Al_2O_3 Microtubes with Precise Wall Thickness Control. *Nano Lett* 2007, 7, 719–722. [PubMed: 17279801]
- (499). De Villiers MM; Otto DP; Strydom SJ; Lvov YM Introduction to Nanocoatings Produced by Layer-by-Layer (LBL) Self-Assembly. *Adv. Drug Delivery Rev* 2011, 63, 701–715.
- (500). Deng H; Zhou X; Wang X; Zhang C; Ding B; Zhang Q; Du Y Layer-by-Layer Structured Polysaccharides Film-Coated Cellulose Nanofibrous Mats for Cell Culture. *Carbohydr. Polym* 2010, 80, 474–479.
- (501). Park JH; Kim BS; Yoo YC; Khil MS; Kim HY Enhanced Mechanical Properties of Multilayer Nano-Coated Electrospun Nylon 6 Fibers via a Layer-by-Layer Self-Assembly. *J. Appl. Polym. Sci* 2008, 107, 2211–2216.
- (502). Krogman KC; Lowery JL; Zacharia NS; Rutledge GC; Hammond PT Spraying Asymmetry into Functional Membranes Layer-by-Layer. *Nat. Mater* 2009, 8, 512. [PubMed: 19377464]
- (503). Dai Y; Formo E; Li H; Xue J; Xia Y Surface Functionalized Electrospun Titania Nanofibers for the Scavenging and Recycling of Precious Metal Ions. *ChemSusChem* 2016, 9, 2912–2916. [PubMed: 27658705]
- (504). Yan J; Huang Y; Miao Y-E; Tjiu WW; Liu T Polydopamine-Coated Electrospun Poly(vinyl alcohol)/Poly(acrylic acid) Membranes as Efficient Dye Adsorbent with Good Recyclability. *J. Hazard. Mater* 2015, 283, 730–739. [PubMed: 25464316]
- (505). Wu H; Kong J; Yao X; Zhao C; Dong Y; Lu X Polydopamine-Assisted Attachment of β -Cyclodextrin on Porous Electrospun Fibers for Water Purification under Highly Basic Condition. *Chem. Eng. J* 2015, 270, 101–109.
- (506). Kaur S; Ma Z; Gopal R; Singh G; Ramakrishna S; Matsuura T Plasma-Induced Graft Copolymerization of Poly (methacrylic acid) on Electrospun Poly (vinylidene fluoride) Nanofiber Membrane. *Langmuir* 2007, 23, 13085–13092. [PubMed: 18004889]
- (507). Martins A; Pinho ED; Faria S; Pashkuleva I; Marques AP; Reis RL; Neves NM Surface Modification of Electrospun Polycaprolactone Nanofiber Meshes by Plasma Treatment to Enhance Biological Performance. *Small* 2009, 5, 1195–1206. [PubMed: 19242938]
- (508). Yue M; Zhou B; Jiao K; Qian X; Xu Z; Teng K; Zhao L; Wang J; Jiao Y Switchable Hydrophobic/Hydrophilic Surface of Electrospun Poly (l-lactide) Membranes Obtained by CF_4 Microwave Plasma Treatment. *Appl. Surf. Sci* 2015, 327, 93–99.
- (509). Bhattacharya A; Misra B Grafting: A Versatile Means to Modify Polymers: Techniques, Factors and Applications. *Prog. Polym. Sci* 2004, 29, 767–814.
- (510). Fu G; Xu L; Yao F; Zhang K; Wang X; Zhu M; Nie S Smart Nanofibers from Combined Living Radical Polymerization, “Click Chemistry”, and Electrospinning. *ACS Appl. Mater. Interfaces* 2009, 1, 239–243. [PubMed: 20353208]
- (511). Dong Z-Q; Wang B-J; Ma X-H; Wei Y-M; Xu Z-L FAS Grafted Electrospun Poly (vinyl alcohol) Nanofiber Membranes with Robust Superhydrophobicity for Membrane Distillation. *ACS Appl. Mater. Interfaces* 2015, 7, 22652–22659. [PubMed: 26411526]
- (512). Blakeney BA; Tambralli A; Anderson JM; Andukuri A; Lim DJ; Dean DR; Jun H-W Cell Infiltration and Growth in a Low Density, Uncompressed Three-Dimensional Electrospun Nanofibrous Scaffold. *Biomaterials* 2011, 32, 1583–1590. [PubMed: 21112625]
- (513). Song J; Gao H; Zhu G; Cao X; Shi X; Wang Y The Construction of Three-Dimensional Composite Fibrous Macrostructures with Nanotextures for Biomedical Applications. *Biofabrication* 2016, 8, 035009. [PubMed: 27563025]
- (514). Si Y; Yu J; Tang X; Ge J; Ding B Ultralight Nanofibre-Assembled Cellular Aerogels with Superelasticity and Multifunctionality. *Nat. Commun* 2014, 5, 5802. [PubMed: 25512095]
- (515). Duan G; Jiang S; Jérôme V; Wendorff JH; Fathi A; Uhm J; Altstadt V; Herling M; Breu J; Freitag R; Agarwal S; Greiner A Ultralight, Soft Polymer Sponges by Self-Assembly of Short Electrospun Fibers in Colloidal Dispersions. *Adv. Funct. Mater* 2015, 25, 2850–2856.
- (516). Vaquette C; Cooper-White J A Simple Method for Fabricating 3-D Multilayered Composite Scaffolds. *Acta Biomater* 2013, 9, 4599–4608. [PubMed: 22902817]

- (517). Xu T; Miszuk JM; Zhao Y; Sun H; Fong H Electrospun Polycaprolactone 3D Nanofibrous Scaffold with Interconnected and Hierarchically Structured Pores for Bone Tissue Engineering. *Adv. Healthcare Mater* 2015, 4, 2238–2246.
- (518). Chen W; Ma J; Zhu L; Morsi Y; Al-Deyab SS; Mo X; El-Hamshary H Superelastic, Superabsorbent and 3D Nanofiber-Assembled Scaffold for Tissue Engineering. *Colloids Surf., B* 2016, 142, 165–172.
- (519). Chen W; Chen S; Morsi Y; El-Hamshary H; El-Newhy M; Fan C; Mo X Superabsorbent 3D Scaffold Based on Electrospun Nanofibers for Cartilage Tissue Engineering. *ACS Appl. Mater. Interfaces* 2016, 8, 24415–24425. [PubMed: 27559926]
- (520). Yao Q; Cosme JG; Xu T; Miszuk JM; Picciani PH; Fong H; Sun H Three Dimensional Electrospun PCL/PLA Blend Nanofibrous Scaffolds with Significantly Improved Stem Cells Osteogenic Differentiation and Cranial Bone Formation. *Biomaterials* 2017, 115, 115–127. [PubMed: 27886552]
- (521). Joshi MK; Pant HR; Tiwari AP; Park CH; Kim CS; Kim HJ Multi-Layered Macroporous Three-Dimensional Nanofibrous Scaffold via a Novel Gas Foaming Technique. *Chem. Eng. J* 2015, 275, 79–88.
- (522). Jiang S; Duan G; Kuhn U; Mörl M; Altstadt V; Yarin AL; Greiner A Spongy Gels by a Top-Down Approach from Polymer Fibrous Sponges. *Angew. Chem., Int. Ed* 2017, 56, 3285–3288.
- (523). Jiang J; Chen S; Wang H; Carlson MA; Gombart AF; Xie J CO₂-Expanded Nanofiber Scaffolds Maintain Activity of Encapsulated Bioactive Materials and Promote Cellular Infiltration and Positive Host Response. *Acta Biomater* 2018, 68, 237–248. [PubMed: 29269334]
- (524). Jiang J; Carlson MA; Teusink MJ; Wang H; MacEwan MR; Xie J Expanding Two-Dimensional Electrospun Nanofiber Membranes in the Third Dimension by a Modified Gas-Foaming Technique. *ACS Biomater. Sci. Eng* 2015, 1, 991–1001.
- (525). Jiang J; Li Z; Wang H; Wang Y; Carlson MA; Teusink MJ; MacEwan MR; Gu L; Xie J Expanded 3D Nanofiber Scaffolds: Cell Penetration, Neovascularization, and Host Response. *Adv. Healthcare Mater* 2016, 5, 2993–3003.
- (526). Stuart MAC; Huck WTS; Genzer J; Muller M; Ober C; Stamm M; Sukhorukov GB; Szleifer I; Tsukruk VV; Urban M; et al. Emerging Applications of Stimuli-Responsive Polymer Materials. *Nat. Mater* 2010, 9, 101–113. [PubMed: 20094081]
- (527). Huang C; Soenen SJ; Rejman J; Lucas B; Braeckmans K; Demeester J; De Smedt SC Stimuli-Responsive Electrospun Fibers and Their Applications. *Chem. Soc. Rev* 2011, 40, 2417–2434. [PubMed: 21390366]
- (528). Xie J; Li X; Xia Y Putting Electrospun Nanofibers to Work for Biomedical Research. *Macromol. Rapid Commun* 2008, 29, 1775–1792. [PubMed: 20011452]
- (529). Cao S; Hu B; Liu H Synthesis of Ph-Responsive Crosslinked Poly[styrene-co-(maleic sodium anhydride)] and Cellulose Composite Hydrogel Nanofibers by Electrospinning. *Polym. Int* 2009, 58, 545–551.
- (530). Wang Y; Lai C; Hu H; Liu Y; Fei B; Xin JH Temperature-Responsive Nanofibers for Controllable Oil/Water Separation. *RSC Adv* 2015, 5, 51078–51085.
- (531). Apsite I; Stoychev G; Zhang W; Jehnichen D; Xie J; Ionov L Porous Stimuli-Responsive Self-Folding Electrospun Mats for 4D Biofabrication. *Biomacromolecules* 2017, 18, 3178–3184. [PubMed: 28840711]
- (532). Zhang C-L; Cao F-H; Wang J-L; Yu Z-L; Ge J; Lu Y; Wang Z-H; Yu S-H Highly Stimuli-Responsive Au Nanorods/Poly(N-isopropylacrylamide) (PNIPAM) Composite Hydrogel for Smart Switch. *ACS Appl. Mater. Interfaces* 2017, 9, 24857–24863. [PubMed: 28635250]
- (533). Elashnikov R; Slepíkova P; Rimpelová S; Ulrich P; Švorík V; Lyutakov O Temperature-Responsive PLLA/PNIPAM Nanofibers for Switchable Release. *Mater. Sci. Eng., C* 2017, 72, 293–300.
- (534). Dang JM; Leong KW Myogenic Induction of Aligned Mesenchymal Stem Cell Sheets by Culture on Thermally Responsive Electrospun Nanofibers. *Adv. Mater* 2007, 19, 2775–2779. [PubMed: 18584057]

- (535). Webster M; Miao J; Lynch B; Green DS; Jones-Sawyer R; Linhardt RJ; Mendenhall J Tunable Thermo-Responsive Poly(N-vinylcaprolactam) Cellulose Nanofibers: Synthesis, Characterization, and Fabrication. *Macromol. Mater. Eng.* 2013, 298, 447–453.
- (536). Loh XJ; Peh P; Liao S; Sng C; Li J Controlled Drug Release from Biodegradable Thermoresponsive Physical Hydrogel Nanofibers. *J. Controlled Release* 2010, 143, 175–182.
- (537). Kim Y-J; Matsunaga YT Thermo-Responsive Polymers and Their Application as Smart Biomaterials. *J. Mater. Chem. B* 2017, 5, 4307–4321.
- (538). Maeda S; Kato T; Kogure H; Hosoya N Rapid Response of Thermo-Sensitive Hydrogels with Porous Structures. *Appl. Phys. Lett* 2015, 106, 171909.
- (539). Wang J; Sutti A; Wang X; Lin T Fast Responsive and Morphologically Robust Thermo-Responsive Hydrogel Nanofibres from Poly(N-isopropylacrylamide) and Poss Crosslinker. *Soft Matter* 2011, 7, 4364–4369.
- (540). Zhang J; Chen W; Yu L; Li M; Neumann F; Li W; Haag R Selective Endothelial Cell Adhesion via Mussel-Inspired Hybrid Microfibrous Scaffold. *ACS Appl. Nano Mater.* 2018, 1, 1513–1521.
- (541). Kim Y-J; Ebara M; Aoyagi T A Smart Nanofiber Web That Captures and Releases Cells. *Angew. Chem., Int. Ed* 2012, 51, 10537–10541.
- (542). Lin XL; Tang DY; Gu S; Du HF; Jiang EY Electrospun Poly(N-isopropylacrylamide)/Poly(caprolactone) – Based Polyurethane Nanofibers as Drug Carriers and Temperature-Controlled Release. *New J. Chem* 2013, 37, 2433–2439.
- (543). Kim Y-J; Ebara M; Aoyagi T A Smart Hyperthermia Nanofiber with Switchable Drug Release for Inducing Cancer Apoptosis. *Adv. Funct. Mater* 2013, 23, 5753–5761.
- (544). Chen M; Li Y-F; Besenbacher F Electrospun Nanofibers-Mediated on-Demand Drug Release. *Adv. Healthcare Mater* 2014, 3, 1721–1732.
- (545). Oh HH; Ko Y-G; Uyama H; Park WH; Cho D; Kwon OH Fabrication and Characterization of Thermoresponsive Polystyrene Nanofibrous Mats for Cultured Cell Recovery. *BioMed Res. Int* 2014, 2014, 480694. [PubMed: 24696851]
- (546). Ramanan VV; Hribar KC; Katz JS; Burdick JA Nanofiber-Nanorod Composites Exhibiting Light-Induced Reversible Lower Critical Solution Temperature Transitions. *Nanotechnology* 2011, 22, 494009. [PubMed: 22101516]
- (547). Kocak G; Tunçer C; Bütin V pH-Responsive Polymers. *Polym. Chem* 2017, 8, 144–176.
- (548). Chunder A; Sarkar S; Yu Y; Zhai L Fabrication of Ultrathin Polyelectrolyte Fibers and Their Controlled Release Properties. *Colloids Surf., B* 2007, 58, 172–179.
- (549). Demirci S; Celebioglu A; Aytac Z; Uyar T pH-Responsive Nanofibers with Controlled Drug Release Properties. *Polym. Chem* 2014, 5, 2050–2056.
- (550). Chen M; Gao S; Dong M; Song J; Yang C; Howard KA; Kjems J; Besenbacher F Chitosan/siRNA Nanoparticles Encapsulated in PLGA Nanofibers for siRNA Delivery. *ACS Nano* 2012, 6, 4835–4844. [PubMed: 22621383]
- (551). Jiang J; Xie J; Ma B; Bartlett DE; Xu A; Wang CH Mussel-Inspired Protein-Mediated Surface Functionalization of Electrospun Nanofibers for pH-Responsive Drug Delivery. *Acta Biomater* 2014, 10, 1324–1332. [PubMed: 24287161]
- (552). Di W; Czarny RS; Fletcher NA; Krebs MD; Clark HA Comparative Study of Poly (ϵ -caprolactone) and Poly (lactic-*co*-glycolic acid)-Based Nanofiber Scaffolds for pH-Sensing. *Pharm. Res* 2016, 33, 2433–2444. [PubMed: 27380188]
- (553). Jeevarajan AS; Vani S; Taylor TD; Anderson MM Continuous pH Monitoring in a Perfused Bioreactor System Using an Optical pH Sensor. *Biotechnol. Bioeng* 2002, 78, 467–472. [PubMed: 11948454]
- (554). Chen M; Besenbacher F Light-Driven Wettability Changes on a Photoresponsive Electrospun Mat. *ACS Nano* 2011, 5, 1549–1555. [PubMed: 21288000]
- (555). Akiyama H; Tamada K; Nagasawa J. i.; Abe K; Tamaki T Photoreactivity in Self-Assembled Monolayers Formed from Asymmetric Disulfides Having para-Substituted Azobenzenes. *J. Phys. Chem. B* 2003, 107, 130–135.
- (556). Wang Y; Ma N; Wang Z; Zhang X Photocontrolled Reversible Supramolecular Assemblies of an Azobenzene-Containing Surfactant with α -Cyclodextrin. *Angew. Chem., Int. Ed* 2007, 119, 2881–2884.

- (557). Fu G-D; Xu L-Q; Yao F; Li G-L; Kang E-T Smart Nanofibers with a Photoresponsive Surface for Controlled Release. *ACS Appl. Mater. Interfaces* 2009, 1, 2424–2427. [PubMed: 20356110]
- (558). Abidian MR; Kim D-H; Martin DC Conducting-Polymer Nanotubes for Controlled Drug Release. *Adv. Mater* 2006, 18, 405–409. [PubMed: 21552389]
- (559). Baughman RH; Cui C; Zakhidov AA; Iqbal Z; Barisci JN; Spinks GM; Wallace GG; Mazzoldi A; De Rossi D; Rinzler AG; et al. Carbon Nanotube Actuators. *Science* 1999, 284, 1340–1344. [PubMed: 10334985]
- (560). Yun J; Im JS; Lee Y-S; Kim H-I Electro-Responsive Transdermal Drug Delivery Behavior of PVA/PAA/MWCNT Nanofibers. *Eur. Polym. J* 2011, 47, 1893–1902.
- (561). Wang S; Sun Z; Yan E; Yuan J; Gao Y; Bai Y; Chen Y; Wang C; Zheng Y; Jing T Magnetic Composite Nanofibers Fabricated by Electrospinning of Fe₃O₄/Gelatin Aqueous Solutions. *Mater. Sci. Eng., B* 2014, 190, 126–132.
- (562). Graeser M; Bognitzki M; Massa W; Pietzonka C; Greiner A; Wendorff JH Magnetically Anisotropic Cobalt and Iron Nanofibers *via* Electrospinning. *Adv. Mater* 2007, 19, 4244–4247.
- (563). Wang M; Singh H; Hatton TA; Rutledge GC Field-Responsive Superparamagnetic Composite Nanofibers by Electrospinning. *Polymer* 2004, 45, 5505–5514.
- (564). Lendlein A; Kelch S Shape-Memory Polymers. *Angew. Chem., Int. Ed* 2002, 41, 2034–2057.
- (565). Zhao Q; Qi HJ; Xie T Recent Progress in Shape Memory Polymer: New Behavior, Enabling Materials, and Mechanistic Understanding. *Prog. Polym. Sci* 2015, 49, 79–120.
- (566). Yao YT; Xu YC; Wang B; Yin WL; Lu HB Recent Development in Electrospun Polymer Fiber and Their Composites with Shape Memory Property: A Review. *Pigm. Resin Technol.* 2018, 47, 47–54.
- (567). Zhuo H; Hu J; Chen S Coaxial Electrospun Polyurethane Core-Shell Nanofibers for Shape Memory and Antibacterial Nanomaterials. *eXPRESS Polym. Lett* 2011, 5, 182–187.
- (568). Chen H; Cao X; Zhang J; Zhang J; Ma Y; Shi G; Ke Y; Tong D; Jiang L Electrospun Shape Memory Film with Reversible Fibrous Structure. *J. Mater. Chem* 2012, 22, 22387–22391.
- (569). Yao YT; Wei HQ; Wang JJ; Lu HB; Leng JS; Hui D Fabrication of Hybrid Membrane of Electrospun Polycaprolactone and Polyethylene Oxide with Shape Memory Property. *Composites, Part B* 2015, 83, 264–269.
- (570). Zhuo HT; Hu JL; Chen SJ; Yeung LP Preparation of Polyurethane Nanofibers by Electrospinning. *J. Appl. Polym. Sci* 2008, 109, 406–411.
- (571). Chung SE; Park CH; Yu W-R; Kang TJ Thermoresponse Shape Memory Characteristics of Polyurethane Electrospun Web. *J. Appl. Polym. Sci* 2011, 120, 492–500.
- (572). Zhang F; Zhang Z; Liu Y; Lu H; Leng J The Quintuple-Shape Memory Effect in Electrospun Nanofiber Membranes. *Smart Mater. Struct* 2013, 22, 085020.
- (573). Gong T; Li WB; Chen HM; Wang L; Shao SJ; Zhou SB Remotely Actuated Shape Memory Effect of Electrospun Composite Nanofibers. *Acta Biomater* 2012, 8, 1248–1259. [PubMed: 22186162]
- (574). Lu HB; Yin JY; Xu B; Gou JH; Hui D; Fu YQ Synergistic Effects of Carboxylic Acid-Functionalized Carbon Nanotube and Nafion/Silica Nanofiber on Electrical Actuation Efficiency of Shape Memory Polymer Nanocomposite. *Composites, Part B* 2016, 100, 146–151.
- (575). Tseng LF; Mather PT; Henderson JH Shape-Memory-Actuated Change in Scaffold Fiber Alignment Directs Stem Cell Morphology. *Acta Biomater* 2013, 9, 8790–8801. [PubMed: 23851156]
- (576). Wang J; Quach A; Brasch ME; Turner CE; Henderson JH On-Command on/off Switching of Progenitor Cell and Cancer Cell Polarized Motility and Aligned Morphology *via* a Cytocompatible Shape Memory Polymer Scaffold. *Biomaterials* 2017, 140, 150–161. [PubMed: 28649015]
- (577). Bao M; Lou X; Zhou Q; Dong W; Yuan H; Zhang Y Electrospun Biomimetic Fibrous Scaffold from Shape Memory Polymer of PDLLA-*co*-TMC for Bone Tissue Engineering. *ACS Appl. Mater. Interfaces* 2014, 6, 2611–2621. [PubMed: 24476093]
- (578). Baker RM; Tseng L-F; Iannolo MT; Oest ME; Henderson JH Self-Deploying Shape Memory Polymer Scaffolds for Grafting and Stabilizing Complex Bone Defects: A Mouse Femoral Segmental Defect Study. *Biomaterials* 2016, 76, 388–398. [PubMed: 26561935]

- (579). Sonseca A; Menes O; Gimenez E A Comparative Study of the Mechanical, Shape-Memory, and Degradation Properties of Poly(lactic acid) Nanofiber and Cellulose Nanocrystal Reinforced Poly(mannitol sebacate) Nanocomposites. *RSC Adv* 2017, 7, 21869–21882.
- (580). Wang S; Liu K; Yao X; Jiang L Bioinspired Surfaces with Superwettability: New Insight on Theory, Design, and Applications. *Chem. Rev* 2015, 115, 8230–8293. [PubMed: 26244444]
- (581). Ge J; Zhao H-Y; Zhu H-W; Huang J; Shi L-A; Yu S-H Advanced Sorbents for Oil–Spill Cleanup: Recent Advances and Future Perspectives. *Adv. Mater* 2016, 28, 10459–10490. [PubMed: 27731513]
- (582). Sheng JL; Zhang M; Xu Y; Yu JY; Ding B Tailoring Water-Resistant and Breathable Performance of Polyacrylonitrile Nanofibrous Membranes Modified by Polydimethylsiloxane. *ACS Appl. Mater. Interfaces* 2016, 8, 27218–27226. [PubMed: 27661093]
- (583). Sheng JL; Zhang M; Luo WJ; Yu JY; Ding B Thermally Induced Chemical Cross-Linking Reinforced Fluorinated Polyurethane/Polyacrylonitrile/Polyvinyl Butyral Nanofibers for Waterproof-Breathable Application. *RSC Adv* 2016, 6, 29629–29637.
- (584). Sas I; Gorga RE; Joines JA; Thoney KA Literature Review on Superhydrophobic Self-Cleaning Surfaces Produced by Electrospinning. *J. Polym. Sci., Part B: Polym. Phys* 2012, 50, 824–845.
- (585). Self-Cleaning Surface; SESB (Smart Elements for Sustainable Building Envelopes), <http://www.sesbe.eu/achieved-results/materialfunctionalization/self-cleaning-surface/>.
- (586). Bedford NM; Steckl AJ Photocatalytic Self Cleaning Textile Fibers by Coaxial Electrospinning. *ACS Appl. Mater. Interfaces* 2010, 2, 2448–2455.
- (587). Blossey R Self-Cleaning Surfaces-Virtual Realities. *Nat. Mater* 2003, 2, 301–306. [PubMed: 12728235]
- (588). Li F; Li QM; Kim H Spray Deposition of Electrospun TiO₂ Nanoparticles with Self-Cleaning and Transparent Properties onto Glass. *Appl. Surf. Sci* 2013, 276, 390–396.
- (589). Virovska D; Paneva D; Manolova N; Rashkov I; Karashanova D Photocatalytic Self-Cleaning Poly(L-lactide) Materials Based on a Hybrid between Nanosized Zinc Oxide and Expanded Graphite or Fullerene. *Mater. Sci. Eng., C* 2016, 60, 184–194.
- (590). Ueda E; Levkin PA Emerging Applications of Superhydrophilic-Superhydrophobic Micropatterns. *Adv. Mater* 2013, 25, 1234–1247. [PubMed: 23345109]
- (591). Menini R; Farzaneh M Production of Superhydrophobic Polymer Fibers with Embedded Particles Using the Electrospinning Technique. *Polym. Int* 2008, 57, 77–84.
- (592). Ma M; Hill RM; Lowery JL; Fridrikh SV; Rutledge GC Electrospun Poly(styrene-block-dimethylsiloxane) Block Copolymer Fibers Exhibiting Superhydrophobicity. *Langmuir* 2005, 21, 5549–5554. [PubMed: 15924488]
- (593). Satilmis B; Uyar T Superhydrophobic Hexamethylene Diisocyanate Modified Hydrolyzed Polymers of Intrinsic Microporosity Electrospun Ultrafine Fibrous Membrane for the Adsorption of Organic Compounds and Oil/Water Separation. *ACS Appl. Nano Mater* 2018, 1, 1631–1640.
- (594). Han D; Steckl AJ Superhydrophobic and Oleophobic Fibers by Coaxial Electrospinning. *Langmuir* 2009, 25, 9454–9462. [PubMed: 19374456]
- (595). Jiang L; Zhao Y; Zhai J A Lotus-Leaf-Like Superhydrophobic Surface: A Porous Microsphere/Nanofiber Composite Film Prepared by Electrohydrodynamics. *Angew. Chem., Int. Ed* 2004, 43, 4338–4341.
- (596). Liu Z; Wang H; Wang E; Zhang X; Yuan R; Zhu Y Superhydrophobic Poly(vinylidene fluoride) Membranes with Controllable Structure and Tunable Wettability Prepared by One-Step Electrospinning. *Polymer* 2016, 82, 105–113.
- (597). Ma M; Gupta M; Li Z; Zhai L; Gleason KK; Cohen RE; Rubner MF; Rutledge GC Decorated Electrospun Fibers Exhibiting Superhydrophobicity. *Adv. Mater* 2007, 19, 255–259.
- (598). Toohey KS; Sottos NR; Lewis JA; Moore JS; White SR Self-Healing Materials with Microvascular Networks. *Nat. Mater* 2007, 6, 581–585. [PubMed: 17558429]
- (599). Wu XF; Yarin AL Recent Progress in Interfacial Toughening and Damage Self-Healing of Polymer Composites Based on Electrospun and Solution-Blown Nanofibers: An Overview. *J. Appl. Polym. Sci* 2013, 130, 2225–2237.

- (600). Lee MW; An S; Yoon SS; Yarin AL Advances in Self-Healing Materials Based on Vascular Networks with Mechanical Self-Repair Characteristics. *Adv. Colloid Interface Sci* 2018, 252, 21–37. [PubMed: 29329666]
- (601). Luo X; Mather PT Shape Memory Assisted Self-Healing Coating. *ACS Macro Lett* 2013, 2, 152–156.
- (602). Hansen CJ; Wu W; Toohey KS; Sottos NR; White SR; Lewis JA Self-Healing Materials with Interpenetrating Microvascular Networks. *Adv. Mater* 2009, 21, 4143–4147.
- (603). Wu XF; Rahman A; Zhou Z; Pelot DD; Sinha-Ray S; Chen B; Payne S; Yarin AL Electrospinning Core-Shell Nanofibers for Interfacial Toughening and Self-Healing of Carbon-Fiber/Epoxy Composites. *J. Appl. Polym. Sci* 2013, 129, 1383–1393.
- (604). Lee MW; An S; Jo HS; Yoon SS; Yarin AL Self-Healing Nanofiber-Reinforced Polymer Composites. 1. Tensile Testing and Recovery of Mechanical Properties. *ACS Appl. Mater. Interfaces* 2015, 7, 19546–19554. [PubMed: 26284888]
- (605). Alexander SLM; Matolyak LE; Korley LTJ Intelligent Nanofiber Composites: Dynamic Communication between Materials and Their Environment. *Macromol. Mater. Eng.* 2017, 302, 1700133.
- (606). Lee MW; An S; Lee C; Liou M; Yarin AL; Yoon SS Hybrid Self-Healing Matrix Using Core-Shell Nanofibers and Capsuleless Microdroplets. *ACS Appl. Mater. Interfaces* 2014, 6, 10461–10468. [PubMed: 24884204]
- (607). Park JH; Braun PV Coaxial Electrospinning of Self-Healing Coatings. *Adv. Mater* 2010, 22, 496–499. [PubMed: 20217741]
- (608). Lee MW; An S; Lee C; Liou M; Yarin AL; Yoon SS Self-Healing Transparent Core-Shell Nanofiber Coatings for Anti-Corrosive Protection. *J. Mater. Chem. A* 2014, 2, 7045–7053.
- (609). An S; Liou M; Song KY; Jo HS; Lee MW; Al-Deyab SS; Yarin AL; Yoon SS Highly Flexible Transparent Self-Healing Composite Based on Electrospun Core-Shell Nanofibers Produced by Coaxial Electrospinning for Anti-Corrosion and Electrical Insulation. *Nanoscale* 2015, 7, 17778–17785. [PubMed: 26456716]
- (610). Doan TQ; Leslie LS; Kim SY; Bhargava R; White SR; Sottos NR Characterization of Core-Shell Microstructure and Self-Healing Performance of Electrospun Fiber Coatings. *Polymer* 2016, 107, 263–272.
- (611). Zussman E Encapsulation of Cells within Electrospun Fibers. *Polym. Adv. Technol* 2011, 22, 366–371.
- (612). Murínová S; Dercová K Response Mechanisms of Bacterial Degraders to Environmental Contaminants on the Level of Cell Walls and Cytoplasmic Membrane. *Int. J. Microbiol.* 2014, 2014, 873081. [PubMed: 25057269]
- (613). Salalha W; Kuhn J; Dror Y; Zussman E Encapsulation of Bacteria and Viruses in Electrospun Nanofibres. *Nanotechnology* 2006, 17, 4675. [PubMed: 21727596]
- (614). Letnik I; Avrahami R; Rokem JS; Greiner A; Zussman E; Greenblatt C Living Composites of Electrospun Yeast Cells for Bioremediation and Ethanol Production. *Biomacromolecules* 2015, 16, 3322–3328. [PubMed: 26351729]
- (615). Lopez-Rubio A; Sanchez E; Sanz Y; Lagaron JM Encapsulation of Living Bifidobacteria in Ultrathin PVOH Electrospun Fibers. *Biomacromolecules* 2009, 10, 2823–2829. [PubMed: 19817490]
- (616). Damasceno R; Roggia I; Pereira C; de Sá E Rhizobia Survival in Seeds Coated with Polyvinyl Alcohol (PVA) Electrospun Nanofibres. *Can. J. Microbiol* 2013, 59, 716–719. [PubMed: 24206353]
- (617). De Gregorio PR; Michavila G; Ricciardi Muller L; de Souza Borges C; Pomares MF; Saccol de Sá EL; Pereira C; Vincent PA Beneficial Rhizobacteria Immobilized in Nanofibers for Potential Application as Soybean Seed Bioinoculants. *PLoS One* 2017, 12, e0176930. [PubMed: 28472087]
- (618). Zanatta G; Steffens D; Braghieri DI; Fernandes RA; Netto CA; Pranke P Viability of Mesenchymal Stem Cells During Electrospinning. *Braz. J. Med. Biol. Res.* 2012, 45, 125–130. [PubMed: 22183245]

- (619). Townsend-Nicholson A; Jayasinghe SN Cell Electrospinning: A Unique Biotechnology for Encapsulating Living Organisms for Generating Active Biological Microthreads/Scaffolds. *Biomacro-molecules* 2006, 7, 3364–3369.
- (620). Jayasinghe SN; Auguste J; Scotton CJ Platform Technologies for Directly Reconstructing 3D Living Biomaterials. *Adv. Mater* 2015, 27, 7794–7799. [PubMed: 26508202]
- (621). Ang HY; Irvine SA; Avrahami R; Sarig U; Bronstein T; Zussman E; Boey FYC; Machluf M; Venkatraman SS Characterization of a Bioactive Fiber Scaffold with Entrapped HUVECs in Coaxial Electrospun Core-Shell Fiber. *Biomatter* 2014, 4, e28238. [PubMed: 24553126]
- (622). Li Z; Zhang H; Zheng W; Wang W; Huang H; Wang C; MacDiarmid AG; Wei Y Highly Sensitive and Stable Humidity Nanosensors Based on LiCl Doped TiO₂ Electrospun Nanofibers. *J. Am. Chem. Soc* 2008, 130, 5036–5037. [PubMed: 18341281]
- (623). Yang G; Kampstra KL; Abidian MR High Performance Conducting Polymer Nanofiber Biosensors for Detection of Biomolecules. *Adv. Mater* 2014, 26, 4954–4960. [PubMed: 24719293]
- (624). Ji X; Su Z; Wang P; Ma G; Zhang S Ready-to-Use” Hollow Nanofiber Membrane-Based Glucose Testing Strips. *Analyst* 2014, 139, 6467–6473. [PubMed: 25343161]
- (625). Zhou C; Xu L; Song J; Xing R; Xu S; Liu D; Song H Ultrasensitive Non-enzymatic Glucose Sensor Based on Three-Dimensional Network of ZnO-CuO Hierarchical Nanocomposites by Electrospinning. *Sci. Rep* 2015, 4, 7382.
- (626). Senthamilan A; Balusamy B; Uyar T Glucose Sensors Based on Electrospun Nanofibers: A Review. *Anal. Bioanal. Chem* 2016, 408, 1285–1306. [PubMed: 26573168]
- (627). Yang D; Liu X; Jin Y; Zhu Y; Zeng D; Jiang X; Ma H Electrospinning of Poly(dimethylsiloxane)/Poly(methyl methacrylate) Nanofibrous Membrane: Fabrication and Application in Protein Microarrays. *Biomacromolecules* 2009, 10, 3335–3340. [PubMed: 19924999]
- (628). Tsou PH; Chou CK; Saldana SM; Hung MC; Kameoka J The Fabrication and Testing of Electrospun Silica Nanofiber Membranes for the Detection of Proteins. *Nanotechnology* 2008, 19, 445714. [PubMed: 19081800]
- (629). Li M; Zhang J; Zhang H; Liu Y; Wang C; Xu X; Tang Y; Yang B Electrospinning: A Facile Method to Disperse Fluorescent Quantum Dots in Nanofibers without Förster Resonance Energy Transfer. *Adv. Funct. Mater* 2007, 17, 3650–3656.
- (630). Wu H; Sun Y; Lin D; Zhang R; Zhang C; Pan W GaN Nanofibers Based on Electrospinning: Facile Synthesis, Controlled Assembly, Precise Doping, and Application as High Performance UV Photodetector. *Adv. Mater* 2009, 21, 227–231.
- (631). Jeong S; Cho H; Han S; Won P; Lee H; Hong S; Yeo J; Kwon J; Ko SH High Efficiency, Transparent, Reusable, and Active PM_{2.5} Filters by Hierarchical Ag Nanowire Percolation Network. *Nano Lett* 2017, 17, 4339–4346. [PubMed: 28609619]
- (632). Zhang R; Liu C; Zhou G; Sun J; Liu N; Hsu PC; Wang H; Qiu Y; Zhao J; Wu T; et al. Morphology and Property Investigation of Primary Particulate Matter Particles from Different Sources. *Nano Res* 2018, 11, 3182–3192.
- (633). Koo WT; Jang JS; Qiao S; Hwang W; Jha G; Penner RM; Kim ID Hierarchical Metal–Organic Framework-Assembled Membrane Filter for Efficient Removal of Particulate Matter. *ACS Appl. Mater. Interfaces* 2018, 10, 19957–19963. [PubMed: 29779365]
- (634). Zhao X; Wang S; Yin X; Yu J; Ding B Slip-Effect Functional Air Filter for Efficient Purification of PM_{2.5}. *Sci. Rep* 2016, 6, 35472. [PubMed: 27748419]
- (635). Nel A Air Pollution-Related Illness: Effects of Particles. *Science* 2005, 308, 804–806. [PubMed: 15879201]
- (636). Liu K; Liu C; Hsu PC; Xu J; Kong B; Wu T; Zhang R; Zhou G; Huang W; Sun J; et al. Core –Shell Nanofibrous Materials with High Particulate Matter Removal Efficiencies and Thermally Triggered Flame Retardant Properties. *ACS Cent. Sci.* 2018, 4, 894–898. [PubMed: 30062118]
- (637). Wang Y; Li W; Xia Y; Jiao X; Chen D Electrospun Flexible Self-Standing γ-Alumina Fibrous Membranes and Their Potential as High-Efficiency Fine Particulate Filtration Media. *J. Mater. Chem. A* 2014, 2, 15124–15131.

- (638). Greiner A; Wendorff WJ Electrospinning: A Fascinating Method for the Preparation of Ultrathin Fibers. *Angew. Chem., Int. Ed* 2007, 46, 5670–5703.
- (639). Wang C; Wu S; Jian M; Xie J; Xu L; Yang X; Zheng Q; Zhang Y Silk Nanofibers as High Efficient and Lightweight Air Filter. *Nano Res* 2016, 9, 2590–2597.
- (640). Liu B; Zhang S; Wang X; Yu J; Ding B Efficient and Reusable Polyamide-56 Nanofiber/Nets Membrane with Bimodal Structures for Air Filtration. *J. Colloid Interface Sci* 2015, 457, 203–211. [PubMed: 26188726]
- (641). Liu C; Hsu PC; Lee HW; Ye M; Zheng G; Liu N; Li W; Cui Y Transparent Air Filter for High-Efficiency PM_{2.5} Capture. *Nat. Commun* 2015, 6, 6205. [PubMed: 25683688]
- (642). Cho BM; Nam YS; Cheon JY; Park WH Residual Charge and Filtration Efficiency of Polycarbonate Fibrous Membranes Prepared by Electrospinning. *J. Appl. Polym. Sci* 2015, 132, 41340.
- (643). Wang S; Zhao X; Yin X; Yu J; Ding B Electret Polyvinylidene Fluoride Nanofibers Hybridized by Polytetrafluoroethylene Nanoparticles for High-Efficiency Air Filtration. *ACS Appl. Mater. Interfaces* 2016, 8, 23985–23994. [PubMed: 27552028]
- (644). Zhang S; Liu H; Zuo F; Yin X; Yu J; Ding B A Controlled Design of Ripple-Like Polyamide-6 Nanofiber/Nets Membrane for High-Efficiency Air Filter. *Small* 2017, 13, 1603151.
- (645). Yao L; Garmash O; Bianchi F; Zheng J; Yan C; Kontkanen J; Junninen H; Mazon SB; Ehn M; Paasonen P; et al. Atmospheric New Particle Formation from Sulfuric Acid and Amines in a Chinese Megacity. *Science* 2018, 361, 278–281. [PubMed: 30026225]
- (646). Zhang R; Liu B; Yang A; Zhu Y; Liu C; Zhou G; Sun J; Hsu PC; Zhao W; Lin D; et al. In Situ Investigation on the Nanoscale Capture and Evolution of Aerosols on Nanofibers. *Nano Lett* 2018, 18, 1130–1138. [PubMed: 29297691]
- (647). Zhang R; Liu C; Hsu PC; Zhang C; Liu N; Zhang J; Lee HR; Lu Y; Qiu Y; Chu S; et al. Nanofiber Air Filters with High-Temperature Stability for Efficient PM_{2.5} Removal from the Pollution Sources. *Nano Lett* 2016, 16, 3642–3649. [PubMed: 27167892]
- (648). Zhu M; Han J; Wang F; Shao W; Xiong R; Zhang Q; Pan H; Yang Y; Samal SK; Zhang F; et al. Electrospun Nanofibers Membranes for Effective Air Filtration. *Macromol. Mater. Eng* 2017, 302, 1600353.
- (649). Yang AK; Cai LL; Zhang RF; Wang JY; Hsu PC; Wang HX; Zhou GM; Xu JW; Cui Y Thermal Management in Nanofiber-Based Face Mask. *Nano Lett* 2017, 17, 3506–3510. [PubMed: 28505460]
- (650). Li X; Wang N; Fan G; Yu J; Gao J; Sun G; Ding B Electreted Polyetherimide-Silica Fibrous Membranes for Enhanced Filtration of Fine Particles. *J. Colloid Interface Sci* 2015, 439, 12–20. [PubMed: 25463170]
- (651). Zhao X; Li Y; Hua T; Jiang P; Yin X; Yu J; Ding B Low-Resistance Dual-Purpose Air Filter Releasing Negative Ions and Effectively Capturing PM_{2.5}. *ACS Appl. Mater. Interfaces* 2017, 9, 12054–12063. [PubMed: 28293955]
- (652). Ramakrishna S; Fujihara K; Teo WE; Yong T; Ma Z; Ramaseshan R Electrospun Nanofibers: Solving Global Issues. *Mater. Today* 2006, 9, 40–50.
- (653). Wen Q; Di J; Zhao Y; Wang Y; Jiang L; Yu J Flexible Inorganic Nanofibrous Membranes with Hierarchical Porosity for Efficient Water Purification. *Chem. Sci* 2013, 4, 4378–4382.
- (654). Wang X; Dou L; Yang L; Yu J; Ding B Hierarchical Structured MnO₂@SiO₂ Nanofibrous Membranes with Superb Flexibility and Enhanced Catalytic Performance. *J. Hazard. Mater* 2017, 324, 203–212. [PubMed: 28340992]
- (655). Tang X; Si Y; Ge J; Ding B; Liu L; Zheng G; Luo W; Yu J In Situ Polymerized Superhydrophobic and Superoleophilic Nanofibrous Membranes for Gravity Driven Oil-Water Separation. *Nanoscale* 2013, 5, 11657–11664. [PubMed: 24100352]
- (656). Wang Y; Huang H; Gao J; Lu G; Zhao Y; Xu Y; Jiang L TiO₂-SiO₂ Composite Fibers with Tunable Interconnected Porous Hierarchy Fabricated by Single-Spinneret Electrospinning toward Enhanced Photocatalytic Activity. *J. Mater. Chem. A* 2014, 2, 12442–12448.
- (657). Zhan S; Chen D; Jiao X; Song Y Mesoporous TiO₂/SiO₂ Composite Nanofibers with Selective Photocatalytic Properties. *Chem. Commun* 2007, 0, 2043–2045.

- (658). Wang N; Zhang XM; Wang Y; Yu WX; Chan HLW Microfluidic Reactors for Photocatalytic Water Purification. *Lab Chip* 2014, 14, 1074–1082. [PubMed: 24481005]
- (659). Meng ZX; Zhang X; Qin JH A High Efficiency Microfluidic-Based Photocatalytic Microreactor Using Electrospun Nanofibrous TiO₂ as a Photocatalyst. *Nanoscale* 2013, 5, 4687–4690. [PubMed: 23636609]
- (660). Ahmed FE; Lalia BS; Hashaikeh R A Review on Electrospinning for Membrane Fabrication: Challenges and Applications. *Desalination* 2015, 356, 15–30.
- (661). Wang C; Zheng T; Luo R; Liu C; Zhang M; Li J; Sun X; Shen J; Han W; Wang L In Situ Growth of ZIF-8 on PAN Fibrous Filter for Highly Efficient U (VI) Removal. *ACS Appl. Mater. Interfaces* 2018, 10, 24164–24171. [PubMed: 29938491]
- (662). Liang H; Yao A; Jiao X; Li C; Chen D Fast and Sustained Degradation of Chemical Warfare Agent Simulants Using Flexible Self-Supported Metal-Organic Framework Filters. *ACS Appl. Mater. Interfaces* 2018, 10, 20396–20403. [PubMed: 29806452]
- (663). Ye R; Hurlburt TJ; Sabirov K; Alayoglu S; Somorjai GA Molecular Catalysis Science: Perspective on Unifying the Fields of Catalysis. *Proc. Natl. Acad. Sci. U. S. A* 2016, 113, 5159–5166. [PubMed: 27114536]
- (664). Lancaster L; Abdallah W; Banta S; Wheeldon I Engineering Enzyme Microenvironments for Enhanced Biocatalysis. *Chem. Soc. Rev* 2018, 47, 5177–5186. [PubMed: 29796541]
- (665). Velasco-Lozano S; Benitez-Mateos AI; Lopez-Gallego F Co-immobilized Phosphorylated Cofactors and Enzymes as Self-Sufficient Heterogeneous Biocatalysts for Chemical Processes. *Angew. Chem., Int. Ed* 2017, 56, 771–775.
- (666). Britton J; Majumdar S; Weiss GA Continuous Flow Biocatalysis. *Chem. Soc. Rev* 2018, 47, 5891–5918. [PubMed: 29922795]
- (667). Zhang Y; Ge J; Liu Z Enhanced Activity of Immobilized or Chemically Modified Enzymes. *ACS Catal* 2015, 5, 4503–4513.
- (668). Ji X; Wang P; Su Z; Ma G; Zhang S Enabling Multi-Enzyme Biocatalysis Using Coaxial-Electrospun Hollow Nanofibers: Redesign of Artificial Cells. *J. Mater. Chem. B* 2014, 2, 181–190.
- (669). Herricks TE; Kim S-H; Kim J; Li D; Kwak JH; Grate JW; Kim SH; Xia Y Direct Fabrication of Enzyme-Carrying Polymer Nanofibers by Electrospinning. *J. Mater. Chem* 2005, 15, 3241–3245.
- (670). Klibanov AM Why Are Enzymes Less Active in Organic Solvents Than in Water? *Trends Biotechnol* 1997, 15, 97–101. [PubMed: 9080715]
- (671). Tang C; Saquing CD; Morton SW; Glatz BN; Kelly RM; Khan SA Cross-Linked Polymer Nanofibers for Hyper-thermophilic Enzyme Immobilization: Approaches to Improve Enzyme Performance. *ACS Appl. Mater. Interfaces* 2014, 6, 11899–11906. [PubMed: 25058141]
- (672). Mano N; de Pouliquet A O₂ Reduction in Enzymatic Biofuel Cells. *Chem. Rev* 2018, 118, 2392–2468. [PubMed: 28930449]
- (673). Both Engel A; Holade Y; Tingry S; Cherifi A; Cornu D; Servat K; Napporn TW; Kokoh KB Electrospun Carbon Fibers: Promising Electrode Material for Abiotic and Enzymatic Catalysis. *J. Phys. Chem. C* 2015, 119, 16724–16733.
- (674). Sun W; Lu X; Tong Y; Lei J; Nie G; Wang C A One-Pot Synthesis of a Highly Dispersed Palladium/Polypyrrole/Polyacrylonitrile Nanofiber Membrane and Its Recyclable Catalysis in Hydrogen Generation from Ammonia Borane. *J. Mater. Chem. A* 2014, 2, 6740–6746.
- (675). Ranjith KS; Celebioglu A; Eren H; Biyikli N; Uyar T Monodispersed, Highly Interactive Facet (111)-Oriented Pd Nano-grains by ALD onto Free-Standing and Flexible Electrospun Polymeric Nanofibrous Webs for Catalytic Application. *Adv. Mater. Interfaces* 2017, 4, 1700640.
- (676). Mitschang F; Schmalz H; Agarwal S; Greiner A Tea-Bag-Like Polymer Nanoreactors Filled with Gold Nanoparticles. *Angew. Chem., Int. Ed* 2014, 53, 4972–4975.
- (677). Wang M; Ye C; Liu H; Xu M; Bao S Nanosized Metal Phosphides Embedded in Nitrogen-Doped Porous Carbon Nanofibers for Enhanced Hydrogen Evolution at All pH Values. *Angew. Chem., Int. Ed* 2018, 57, 1963–1967.
- (678). Li T; Lv Y; Su J; Wang Y; Yang Q; Zhang Y; Zhou J; Xu L; Sun D; Tang Y Anchoring CoFe₂O₄ Nanoparticles on N-Doped Carbon Nanofibers for High-Performance Oxygen Evolution Reaction. *Adv. Sci* 2017, 4, 1700226.

- (679). Bauer A; Lee K; Song C; Xie Y; Zhang J; Hui R Pt Nanoparticles Deposited on TiO₂ Based Nanofibers: Electrochemical Stability and Oxygen Reduction Activity. *J. Power Sources* 2010, 195, 3105–3110.
- (680). Jiménez-Morales I; Cavaliere S; Jones D; Rozière J Strong Metal-Support Interaction Improves Activity and Stability of Pt Electrocatalysts on Doped Metal Oxides. *Phys. Chem. Chem. Phys* 2018, 20, 8765–8772. [PubMed: 29541731]
- (681). Ding Z; Cheng Q; Zou L; Fang J; Zou Z; Yang H Controllable Synthesis of Titanium Nitride Nanotubes by Coaxial Electrospinning and Their Application as a Durable Support for Oxygen Reduction Reaction Electrocatalysts. *Chem. Commun* 2017, 53, 13233–13236.
- (682). Dai Y; Lu P; Cao Z; Campbell CT; Xia Y The Physical Chemistry and Materials Science Behind Sinter-Resistant Catalysts. *Chem. Soc. Rev* 2018, 47, 4314–4331. [PubMed: 29745393]
- (683). Dai Y; Lim B; Yang Y; Cobley CM; Li W; Cho EC; Grayson B; Fanson PT; Campbell CT; Sun Y; et al. A Sinter-Resistant Catalytic System Based on Platinum Nanoparticles Supported on TiO₂ Nanofibers and Covered by Porous Silica. *Angew. Chem., Int. Ed* 2010, 49, 8165–8168.
- (684). Lu P; Campbell CT; Xia Y A Sinter-Resistant Catalytic System Fabricated by Maneuvering the Selectivity of SiO₂ Deposition onto the TiO₂ Surface Versus the Pt Nanoparticle Surface. *Nano Lett* 2013, 13, 4957–4962. [PubMed: 24000792]
- (685). Fu W; Dai Y; Li JPH; Liu ZB; Yang Y; Sun Y; Huang Y; Ma R; Zhang L; Sun Y Unusual Hollow Al₂O₃ Nanofibers with Loofah-Like Skins: Intriguing Catalyst Supports for Thermal Stabilization of Pt Nanocrystals. *ACS Appl. Mater. Interfaces* 2017, 9, 21258–21266. [PubMed: 28575576]
- (686). Li X; Zhi L Graphene Hybridization for Energy Storage Applications. *Chem. Soc. Rev* 2018, 47, 3189–3216. [PubMed: 29512678]
- (687). Shaikh JS; Shaikh NS; Mali SS; Patil JV; Pawar KK; Kanjanaboops P; Hong CK; Kim JH; Patil PS Nanoarchitectures in Dye-Sensitized Solar Cells: Metal Oxides, Oxide Perovskites and Carbon-Based Materials. *Nanoscale* 2018, 10, 4987–5034. [PubMed: 29488524]
- (688). Freitag M; Teuscher J; Saygili Y; Zhang X; Giordano F; Liska P; Hua J; Zakeeruddin SM; Moser JE; Grätzel M; et al. Dye-Sensitized Solar Cells for Efficient Power Generation under Ambient Lighting. *Nat. Photonics* 2017, 11, 372–378.
- (689). O'Regan B; Grätzel M A Low-Cost, High-Efficiency Solar Cell Based on Dye-Sensitized Colloidal TiO₂ Films. *Nature* 1991, 353, 737–740.
- (690). Ren Y; Sun D; Cao Y; Tsao HN; Yuan Y; Zakeeruddin SM; Wang P; Grätzel M A Stable Blue Photosensitizer for Color Palette of Dye-Sensitized Solar Cells Reaching 12.6% Efficiency. *J. Am. Chem. Soc* 2018, 140, 2405–2408. [PubMed: 29323883]
- (691). Wang G; Xiao W; Yu J High-Efficiency Dye-Sensitized Solar Cells Based on Electrospun TiO₂ Multi-Layered Composite Film Photoanodes. *Energy* 2015, 86, 196–203.
- (692). Wu J; Lan Z; Lin J; Huang M; Huang Y; Fan L; Luo G; Lin Y; Xie Y; Wei Y Counter Electrodes in Dye-Sensitized Solar Cells. *Chem. Soc. Rev* 2017, 46, 5975–6023. [PubMed: 28840218]
- (693). Cao Y; Dong YJ; Feng HL; Chen HY; Kuang DB Electrospun TiO₂ Nanofiber Based Hierarchical Photoanode for Efficient Dye-Sensitized Solar Cells. *Electrochim. Acta* 2016, 189, 259–264.
- (694). Kim J-H; Sung S-J; Kim K-P; Hwang D-K Effect of Hot-Pressing on an Electrospun TiO₂ Electrode for Dye-Sensitized Solar Cells. *Appl. Phys. Express* 2014, 7, 072301.
- (695). Joly D; Jung J; Kim I; Demadrille R Electrospun Materials for Solar Energy Conversion: Innovations and Trends. *J. Mater. Chem. C* 2016, 4, 10173–10197.
- (696). Krishnamoorthy T; Thavasi V; Subodh GM; Ramakrishna S A First Report on the Fabrication of Vertically Aligned Anatase TiO₂ Nanowires by Electrospinning: Preferred Architecture for Nanostructured Solar Cells. *Energy Environ. Sci* 2011, 4, 2807–2812.
- (697). Chen H; Xu Y; Kuang D; Su C Recent Advances in Hierarchical Macroporous Composite Structures for Photoelectric Conversion. *Energy Environ. Sci* 2014, 7, 3887–3901.
- (698). Zhang X; Thavasi V; Mhaisalkar SG; Ramakrishna S Novel Hollow Mesoporous 1D TiO₂ Nanofibers as Photovoltaic and Photocatalytic Materials. *Nanoscale* 2012, 4, 1707–1716. [PubMed: 22315140]

- (699). Joshi P; Zhang L; Chen Q; Galipeau D; Fong H; Qiao Q Electrospun Carbon Nanofibers as Low-Cost Counter Electrode for Dye-Sensitized Solar Cells. *ACS Appl. Mater. Interfaces* 2010, 2, 3572–3577. [PubMed: 21073177]
- (700). Zhou Z; Sigdel S; Gong J; Vaagensmith B; Elbohy H; Yang H; Krishnan S; Wu X; Qiao Q Graphene-Beaded Carbon Nanofibers with Incorporated Ni Nanoparticles as Efficient Counter-Electrode for Dye-Sensitized Solar Cells. *Nano Energy* 2016, 22, 558–563.
- (701). Priya ARS; Subramania A; Jung Y; Kim K High-Performance Quasi-Solid-State Dye-Sensitized Solar Cell Based on an Electrospun PVDF-HFP Membrane Electrolyte. *Langmuir* 2008, 24, 9816–9819. [PubMed: 18672916]
- (702). Li Y; Lee D; Kim JY; Kim B; Park N; Kim K; Shin J; Choi I; Ko M Highly Durable and Flexible Dye-Sensitized Solar Cells Fabricated on Plastic Substrates: PVDF-Nanofiber-Reinforced TiO₂ Photoelectrodes. *Energy Environ. Sci.* 2012, 5, 8950–8957.
- (703). Zhou R; Guo W; Yu R; Pan C Highly Flexible, Conductive and Catalytic Pt Networks as Transparent Counter Electrodes for Wearable Dye-Sensitized Solar Cells. *J. Mater. Chem. A* 2015, 3, 23028–23034.
- (704). Yang WS; Park BW; Jung EH; Jeon NJ; Kim YC; Lee DU; Shin SS; Seo J; Kim EK; Noh JH; et al. Iodide Management in Formamidinium-Lead-Halide-Based Perovskite Layers for Efficient Solar Cells. *Science* 2017, 356, 1376–1379. [PubMed: 28663498]
- (705). Niu GD; Guo XD; Wang LD Review of Recent Progress in Chemical Stability of Perovskite Solar Cells. *J. Mater. Chem. A* 2015, 3, 8970–8980.
- (706). Shalan AE; Barhoum A; Elseman AM; Rashad MM; Lira-Cantú M Handbook of Nanofibers; Springer: Cham, Switzerland, 2018; pp 1–33
- (707). Mali SS; Shim CS; Hong CK Highly Porous Zinc Stannate (Zn₂SnO₄) Nanofibers Scaffold Photoelectrodes for Efficient Methyl Ammonium Halide Perovskite Solar Cells. *Sci. Rep.* 2015, 5, 11424. [PubMed: 26094863]
- (708). Mali SS; Shim CS; Kim H; Hong CK Reduced Graphene Oxide (RGO) Grafted Zinc Stannate (Zn₂SnO₄) Nanofiber Scaffolds for Highly Efficient Mixed-Halide Perovskite Solar Cells. *J. Mater. Chem. A* 2016, 4, 12158–12169.
- (709). Mali SS; Patil JV; Kim H; Hong CK Synthesis of SnO₂ Nanofibers and Nanobelts Electron Transporting Layer for Efficient Perovskite Solar Cells. *Nanoscale* 2018, 10, 8275–8284. [PubMed: 29687121]
- (710). Mai L; Sheng J; Xu L; Tan S; Meng J One-Dimensional Hetero-Nanostructures for Rechargeable Batteries. *Acc. Chem. Res.* 2018, 51, 950–959. [PubMed: 29620351]
- (711). Hwang TH; Lee YM; Kong BS; Seo JS; Choi JW Electrosprun Core–Shell Fibers for Robust Silicon Nanoparticle-Based Lithium Ion Battery Anodes. *Nano Lett.* 2012, 12, 802–807. [PubMed: 22206272]
- (712). Dunn B; Kamath H; Tarascon JM Electrical Energy Storage for the Grid: A Battery of Choices. *Science* 2011, 334, 928–935. [PubMed: 22096188]
- (713). Liu K; Liu Y; Lin D; Pei A; Cui Y Materials for Lithium-Ion Battery Safety. *Sci. Adv.* 2018, 4, eaas9820. [PubMed: 29942858]
- (714). Wang H; Yuan S; Ma D; Zhang X; Yan J Electrospun Materials for Lithium and Sodium Rechargeable Batteries: From Structure Evolution to Electrochemical Performance. *Energy Environ. Sci.* 2015, 8, 1660–1681.
- (715). Miao X; Chen Z; Wang N; Nuli Y; Wang J; Yang J; Hirano S Electrospun V₂MoO₈ as a Cathode Material for Rechargeable Batteries with Mg Metal Anode. *Nano Energy* 2017, 34, 26–35.
- (716). Sun Y; Liu N; Cui Y Promises and Challenges of Nanomaterials for Lithium-Based Rechargeable Batteries. *Nat. Energy* 2016, 1, 16071.
- (717). Self EC; Naguib M; Ruther RE; McRen EC; Wycisk R; Liu G; Nanda J; Pintauro PN High Areal Capacity Si/LiCoO₂ Batteries from Electrospun Composite Fiber Mats. *ChemSusChem* 2017, 10, 1823–1831. [PubMed: 28276166]
- (718). Li N; Chen Z; Ren W; Li F; Cheng HM Flexible Graphene-Based Lithium Ion Batteries with Ultrafast Charge and Discharge Rates. *Proc. Natl. Acad. Sci. U. S. A.* 2012, 109, 17360–17365. [PubMed: 23045691]

- (719). Liu W; Song MS; Kong B; Cui Y Flexible and Stretchable Energy Storage: Recent Advances and Future Perspectives. *Adv. Mater* 2017, 29, 1603436.
- (720). Xu Y; Zhu Y; Han F; Luo C; Wang C 3D Si/C Fiber Paper Electrodes Fabricated Using a Combined Electrospray/Electrospinning Technique for Li-Ion Batteries. *Adv. Energy Mater* 2015, 5, 1400753.
- (721). Zhu J; Chen L; Xu Z; Lu B Electrospinning Preparation of Ultra-Long Aligned Nanofibers Thin Films for High Performance Fully Flexible Lithium-Ion Batteries. *Nano Energy* 2015, 12, 339–346.
- (722). Xiao Q; Zhang Q; Fan Y; Wang X; Susantyoko RA Soft Silicon Anodes for Lithium Ion Batteries. *Energy Environ. Sci* 2014, 7, 2261–2268.
- (723). Liu X; Ren D; Hsu H; Feng X; Xu GL; Zhuang M; Gao H; Lu L; Han X; Chu Z; Li J; He X; Amine K; Ouyang M; et al. Thermal Runaway of Lithium-Ion Batteries without Internal Short Circuit. *Joule* 2018, 2, 2047–2064.
- (724). Liang Z; Zheng G; Liu C; Liu N; Li W; Yan K; Yao H; Hsu PC; Chu S; Cui Y Polymer Nanofiber-Guided Uniform Lithium Deposition for Battery Electrodes. *Nano Lett* 2015, 15, 2910–2916. [PubMed: 25822282]
- (725). Liu K; Liu W; Qiu Y; Kong B; Sun Y; Chen Z; Zhuo D; Lin D; Cui Y Electrospun Core-Shell Microfiber Separator with Thermal-Triggered Flame-Retardant Properties for Lithium-Ion Batteries. *Sci. Adv* 2017, 3, e1601978. [PubMed: 28097221]
- (726). Aricò AS; Bruce P; Scrosati B; Tarascon J-M; van Schalkwijk W Nanostructured Materials for Advanced Energy Conversion and Storage Devices. *Nat. Mater* 2005, 4, 366–377. [PubMed: 15867920]
- (727). Liu W; Lee SW; Lin D; Shi F; Wang S; Sendek AD; Cui Y Enhancing Ionic Conductivity in Composite Polymer Electrolytes with Well-Aligned Ceramic Nanowires. *Nat. Energy* 2017, 2, 17035.
- (728). Zhao HP; Liu L; Vellacheri R; Lei Y Recent Advances in Designing and Fabricating Self-Supported Nanoelectrodes for Supercapacitors. *Adv. Sci* 2017, 4, 1700188.
- (729). Yu G; Hu L; Vosgueritchian M; Wang H; Xie X; McDonough JR; Cui X; Cui Y; Bao Z Solution-Processed Graphene/MnO₂ Nanostructured Textiles for High-Performance Electrochemical Capacitors. *Nano Lett* 2011, 11, 2905–2911. [PubMed: 21667923]
- (730). Wang FX; Wu XW; Yuan XH; Liu ZC; Zhang Y; Fu LJ; Zhu YS; Zhou QM; Wu YP; Huang W Latest Advances in Supercapacitors: From New Electrode Materials to Novel Device Designs. *Chem. Soc. Rev* 2017, 46, 6816–6854. [PubMed: 28868557]
- (731). Wang CH; Kaneti YV; Bando Y; Lin JJ; Liu C; Li JS; Yamauchi Y Metal-Organic Framework-Derived One-Dimensional Porous or Hollow Carbon-Based Nanofibers for Energy Storage and Conversion. *Mater. Horiz* 2018, 5, 394–407.
- (732). Lee G; Seo YD; Jang J ZnO Quantum Dot-Decorated Carbon Nanofibers Derived from Electrospun ZIF-8/PVA Nanofibers for High-Performance Energy Storage Electrodes. *Chem. Commun* 2017, 53, 11441–11444.
- (733). Tebyetekerwa M; Wang X; Wu Y; Yang S; Zhu M; Ramakrishna S Controlled Synergistic Strategy to Fabricate 3D-Skeletal Hetero-Nanosponges with High Performance for Flexible Energy Storage Applications. *J. Mater. Chem. A* 2017, 5, 21114–21121.
- (734). Huang Q; Liu L; Wang D; Liu J; Huang Z; Zheng Z One-Step Electrospinning of Carbon Nanowebs on Metallic Textiles for High-Capacitance Supercapacitor Fabrics. *J. Mater. Chem. A* 2016, 4, 6802–6808.
- (735). Kayarkatte MK; Delikaya Ö, Roth C Freestanding Catalyst Layers: A Novel Electrode Fabrication Technique for PEM Fuel Cells via Electrospinning. *ChemElectroChem* 2017, 4, 404–411.
- (736). Ercolano G; Farina F; Cavaliere S; Jones DJ; Rozière J Towards Ultrathin Pt Films on Nanofibres by Surface-Limited Electrodeposition for Electrocatalytic Applications. *J. Mater. Chem. A* 2017, 5, 3974–3980.
- (737). Zhang W; Pintauro PN High-Performance Nanofiber Fuel Cell Electrodes. *ChemSusChem* 2011, 4, 1753–1757. [PubMed: 22110012]

- (738). Brodt M; Wycisk R; Dale NV; Pintauro P Power Output and Durability of Electrospun Fuel Cell Fiber Cathodes with PVDF and Nafion/PVDF Binders. *J. Electrochem. Soc* 2016, 163, F401–F410.
- (739). Aruna ST; Balaji LS; Kumar SS; Prakash BS Electrospinning in Solid Oxide Fuel Cells—A Review. *Renewable Sustainable Energy Rev* 2017, 67, 673–682.
- (740). Agarwal S; Greiner A; Wendorff JH Functional Materials by Electrospinning of Polymers. *Prog. Polym. Sci* 2013, 38, 963–991.
- (741). Shin DW; Guiver MD; Lee YM Hydrocarbon-Based Polymer Electrolyte Membranes: Importance of Morphology on Ion Transport and Membrane Stability. *Chem. Rev* 2017, 117, 4759–4805. [PubMed: 28257183]
- (742). Boaretti C; Pasquini L; Sood R; Giancola S; Donnadio A; Roso M; Modesti M; Cavaliere S Mechanically Stable Nanofibrous sPEEK/Aquivion® Composite Membranes for Fuel Cell Applications. *J. Membr. Sci* 2018, 545, 66–74.
- (743). Mollá S; Compañ V Polyvinyl Alcohol Nanofiber Reinforced Nafion Membranes for Fuel Cell Applications. *J. Membr. Sci* 2011, 372, 191–200.
- (744). Choi J; Lee KM; Wycisk R; Pintauro PN; Mather PT Nanofiber Network Ion-Exchange Membranes. *Macromolecules* 2008, 41, 4569–4572.
- (745). Park JW; Wycisk R; Lin G; Chong PY; Powers D; Van Nguyen T; Dowd RP, Jr; Pintauro, P. N. Electrospun Nafion/PVDF Single-Fiber Blended Membranes for Regenerative H₂/Br₂ Fuel Cells. *J. Membr. Sci* 2017, 541, 85–92.
- (746). Shui J; Chen C; Li JCM Evolution of Nanoporous Pt-Fe Alloy Nanowires by Dealloying and Their Catalytic Property for Oxygen Reduction Reaction. *Adv. Funct. Mater* 2011, 21, 3357–3362.
- (747). Chen D; Zhang R; Wang R; Negro LD; Minteer SD Gold Nanofiber-Based Electrodes for Plasmon-Enhanced Electro-catalysis. *J. Electrochem. Soc* 2016, 163, H1132–H1135.
- (748). Lai Q; Zhao Y; Liang Y; He J; Chen J In Situ Confinement Pyrolysis Transformation of ZIF-8 to Nitrogen-Enriched Meso-Microporous Carbon Frameworks for Oxygen Reduction. *Adv. Funct. Mater* 2016, 26, 8334–8344.
- (749). Liu D; Zhang X; Sun Z; You T Free-Standing Nitrogen-Doped Carbon Nanofiber Films as Highly Efficient Electrocatalysts for Oxygen Reduction. *Nanoscale* 2013, 5, 9528–9531. [PubMed: 23986349]
- (750). Huang P; Li H; Huang X; Chen D Multiheteroatom-Doped Porous Carbon Catalyst for Oxygen Reduction Reaction Prepared Using 3D Network of ZIF-8/Polymeric Nanofiber as a Facile-Doping Template. *ACS Appl. Mater. Interfaces* 2017, 9, 21083–21088. [PubMed: 28616964]
- (751). Suzuki T; Hasan Z; Funahashi Y; Yamaguchi T; Fujishiro Y; Awano M Impact of Anode Microstructure on Solid Oxide Fuel Cells. *Science* 2009, 325, 852–855. [PubMed: 19679808]
- (752). Wachsman ED; Lee KT Lowering the Temperature of Solid Oxide Fuel Cells. *Science* 2011, 334, 935–939. [PubMed: 22096189]
- (753). Jeon Y; Myung J; Hyun S; Shul Y; Irvine JTS Corn-Cob Like Nanofibres as Cathode Catalysts for an Effective Microstructure Design in Solid Oxide Fuel Cells. *J. Mater. Chem. A* 2017, 5, 3966–3973.
- (754). Zhi M; Mariani N; Gemmen R; Gerdes K; Wu N Nanofiber Scaffold for Cathode of Solid Oxide Fuel Cell. *Energy Environ. Sci* 2011, 4, 417–420.
- (755). Zhi M; Lee S; Miller N; Menzler NH; Wu N An Intermediate-Temperature Solid Oxide Fuel Cell with Electrospun Nanofiber Cathode. *Energy Environ. Sci* 2012, 5, 7066–7071.
- (756). Chen Y; Bu Y; Zhang Y; Yan R; Ding D; Zhao B; Yoo S; Dang D; Hu R; Yang C; Liu M A Highly Efficient and Robust Nanofiber Cathode for Solid Oxide Fuel Cells. *Adv. Energy Mater* 2017, 7, 1601890.
- (757). Chen Y; Bu Y; Zhao B; Zhang Y; Ding D; Hu R; Wei T; Rainwater B; Ding Y; Chen F; Yang C; Liu J; Liu M A Durable, High-Performance Hollow-Nanofiber Cathode for Intermediate-Temperature Fuel Cells. *Nano Energy* 2016, 26, 90–99.
- (758). Avouris P; Chen J Nanotube Electronics and Optoelectronics. *Mater. Today* 2006, 9, 46–54.
- (759). Persano L; Camposeo A; Pisignano D Active Polymer Nanofibers for Photonics, Electronics, Energy Generation and Micromechanics. *Prog. Polym. Sci* 2015, 43, 48–95.

- (760). Lin CC; Jiang DH; Kuo CC; Cho CJ; Tsai YH; Satoh T; Su C Water-Resistant Efficient Stretchable Perovskite-Embedded Fiber Membranes for Light-Emitting Diodes. *ACS Appl. Mater. Interfaces* 2018, 10, 2210–2215. [PubMed: 29308867]
- (761). Vohra V; Giovanella U; Tubino R; Murata H; Botta C Electroluminescence from Conjugated Polymer Electrospun Nanofibers in Solution Processable Organic Light-Emitting Diodes. *ACS Nano* 2011, 5, 5572–5578. [PubMed: 21634431]
- (762). Di Camillo D; Fasano V; Ruggieri F; Santucci S; Lozzi L; Camposeo A; Pisignano D Near-Field Electrospinning of Light-Emitting Conjugated Polymer Nanofibers. *Nanoscale* 2013, 5, 11637–11642. [PubMed: 24114142]
- (763). Liao H; Guo S; Cao S; Wang L; Gao F; Yang Z; Zheng J; Yang W A General Strategy for in Situ Growth of All-Inorganic CsPbX_3 ($X = \text{Br}, \text{I}$, and Cl) Perovskite Nanocrystals in Polymer Fibers toward Significantly Enhanced Water/Thermal Stabilities. *Adv. Opt. Mater* 2018, 6, 1800346.
- (764). Choi J; Shim YS; Park CH; Hwang H; Kwack JH; Lee DJ; Park YW; Ju B Junction-Free Electrospun Ag Fiber Electrodes for Flexible Organic Light-Emitting Diodes. *Small* 2018, 14, 1702567.
- (765). Yang H; Lightner CR; Dong L Light-Emitting Coaxial Nanofibers. *ACS Nano* 2012, 6, 622–628. [PubMed: 22196130]
- (766). Cui Y; Zhong Z; Wang D; Wang WU; Lieber CM High Performance Silicon Nanowire Field Effect Transistors. *Nano Lett* 2003, 3, 149–152.
- (767). Peng L; Zhang Z; Wang S Carbon Nanotube Electronics: Recent Advances. *Mater. Today* 2014, 17, 433–442.
- (768). Cho H; Min SY; Lee TW Electrospun Organic Nanofiber Electronics and Photonics. *Macromol. Mater. Eng* 2013, 298, 475–486.
- (769). Ye D; Ding Y; Duan Y; Su J; Yin Z; Huang YA Large-Scale Direct-Writing of Aligned Nanofibers for Flexible Electronics. *Small* 2018, 14, 1703521.
- (770). Chen JY; Kuo CC; Lai CS; Chen WC; Chen HL Manipulation on the Morphology and Electrical Properties of Aligned Electrospun Nanofibers of Poly(3-hexylthiophene) for Field-Effect Transistor Applications. *Macromolecules* 2011, 44, 2883–2892.
- (771). Wang C; Meng Y; Guo ZD; Shin B; Liu GX; Shan FK High-Performance Field-Effect Transistors Based on Gadolinium Doped Indium Oxide Nanofibers and Their Application in Logic Gate. *Appl. Phys. Lett* 2018, 112, 213501.
- (772). Meng Y; Lou K; Qi R; Guo Z; Shin B; Liu G; Shan F Nature-Inspired Capillary-Driven Welding Process for Boosting Metal-Oxide Nanofiber Electronics. *ACS Appl. Mater. Interfaces* 2018, 10, 20703–20711. [PubMed: 29799183]
- (773). Lee SW; Lee HJ; Choi JH; Koh WG; Myoung JM; Hur JH; Park JJ; Cho JH; Jeong U Periodic Array of Polyelectrolyte-Gated Organic Transistors from Electrospun Poly(3-hexylthiophene) Nanofibers. *Nano Lett* 2010, 10, 347–351. [PubMed: 19994870]
- (774). Aamodt JM; Grainger DW Extracellular Matrix-Based Biomaterial Scaffolds and the Host Response. *Biomaterials* 2016, 86, 68–82. [PubMed: 26890039]
- (775). Zhang YS; Xia Y Multiple Facets for Extracellular Matrix Mimicking in Regenerative Medicine. *Nanomedicine* 2015, 10, 689–692. [PubMed: 25816873]
- (776). Hussey GS; Dziki JL; Badylak SF Extracellular Matrix-Based Materials for Regenerative Medicine. *Nat. Rev. Mater* 2018, 3, 159–173.
- (777). Bancelin S; Aimé C; Gusachenko I; Kowalcuk L; Latour G; Coradin T; Schanne-Klein MC Determination of Collagen Fibril Size via Absolute Measurements of Second-Harmonic Generation Signals. *Nat. Commun* 2014, 5, 4920. [PubMed: 25223385]
- (778). Wang X; Ding B; Li B Biomimetic Electrospun Nanofibrous Structures for Tissue Engineering. *Mater. Today* 2013, 16, 229–241.
- (779). Cheng J; Jun Y; Qin J; Lee SH Electrospinning Versus Microfluidic Spinning of Functional Fibers for Biomedical Applications. *Biomaterials* 2017, 114, 121–143. [PubMed: 27880892]
- (780). Wise SG; Byrom MJ; Waterhouse A; Bannon PG; Weiss AS; Ng MK A Multilayered Synthetic Human Elastin/Polycaprolactone Hybrid Vascular Graft with Tailored Mechanical Properties. *Acta Biomater* 2011, 7, 295–303. [PubMed: 20656079]

- (781). Xu C; Huang Y; Wu J; Tang L; Hong Y Triggerable Degradation of Polyurethanes for Tissue Engineering Applications. *ACS Appl. Mater. Interfaces* 2015, 7, 20377–20388. [PubMed: 26312436]
- (782). Braghieri DI; Steffens D; Pranke P Electrospinning for Regenerative Medicine: A Review of the Main Topics. *Drug Discovery Today* 2014, 19, 743–753. [PubMed: 24704459]
- (783). Lauffenburger DA; Horwitz AF Cell Migration: A Physically Integrated Molecular Process. *Cell* 1996, 84, 359–369. [PubMed: 8608589]
- (784). Tracy LE; Minasian RA; Caterson EJ Extracellular Matrix and Dermal Fibroblast Function in the Healing Wound. *Adv. Wound Care* 2016, 5, 119–136.
- (785). Horwitz R; Webb D Cell Migration. *Curr. Biol* 2003, 13, R756–R759. [PubMed: 14521851]
- (786). Schwartz MA; Horwitz AR Integrating Adhesion, Protrusion, and Contraction During Cell Migration. *Cell* 2006, 125, 1223–1225. [PubMed: 16814706]
- (787). Mayor R; Etienne-Manneville S The Front and Rear of Collective Cell Migration. *Nat. Rev. Mol. Cell Biol* 2016, 17, 97–109. [PubMed: 26726037]
- (788). Sundararaghavan HG; Saunders RL; Hammer DA; Burdick JA Fiber Alignment Directs Cell Motility over Chemotactic Gradients. *Biotechnol. Bioeng* 2013, 110, 1249–1254. [PubMed: 23172355]
- (789). Liu Y; Franco A; Huang L; Gersappe D; Clark RA; Rafailovich MH Control of Cell Migration in Two and Three Dimensions Using Substrate Morphology. *Exp. Cell Res* 2009, 315, 2544–2557. [PubMed: 19464288]
- (790). Mi HY; Salick MR; Jing X; Crone WC; Peng XF; Turng LS Electrospinning of Unidirectionally and Orthogonally Aligned Thermoplastic Polyurethane Nanofibers: Fiber Orientation and Cell Migration. *J. Biomed. Mater. Res., Part A* 2015, 103, 593–603.
- (791). Ottosson M; Jakobsson A; Johansson F Accelerated Wound Closure-Differently Organized Nanofibers Affect Cell Migration and Hence the Closure of Artificial Wounds in a Cell Based in Vitro Model. *PLoS One* 2017, 12, e0169419. [PubMed: 28060880]
- (792). Hurtado A; Cregg JM; Wang HB; Wendell DF; Oudega M; Gilbert RJ; McDonald JW Robust CNS Regeneration after Complete Spinal Cord Transection Using Aligned Poly-L-lactic acid Microfibers. *Biomaterials* 2011, 32, 6068–6079. [PubMed: 21636129]
- (793). Qu J; Zhou D; Xu X; Zhang F; He L; Ye R; Zhu Z; Zuo B; Zhang H Optimization of Electrospun TSF Nanofiber Alignment and Diameter to Promote Growth and Migration of Mesenchymal Stem Cells. *Appl. Surf. Sci* 2012, 261, 320–326.
- (794). Englund-Johansson U; Netanyah E; Johansson F Tailor-Made Electrospun Culture Scaffolds Control Human Neural Progenitor Cell Behavior-Studies on Cellular Migration and Phenotypic Differentiation. *J. Biomater. Nanobiotechnol* 2017, 8, 72746.
- (795). Wang HB; Mullins ME; Cregg JM; McCarthy CW; Gilbert RJ Varying the Diameter of Aligned Electrospun Fibers Alters Neurite Outgrowth and Schwann Cell Migration. *Acta Biomater* 2010, 6, 2970–2978. [PubMed: 20167292]
- (796). Shi J; Wang L; Zhang F; Li H; Lei L; Liu L; Chen Y Incorporating Protein Gradient into Electrospun Nanofibers as Scaffolds for Tissue Engineering. *ACS Appl. Mater. Interfaces* 2010, 2, 1025–1030. [PubMed: 20423122]
- (797). Tanes ML; Xue J; Xia Y General Strategy for Generating Gradients of Bioactive Proteins on Electrospun Nanofiber Mats by Masking with Bovine Serum Albumin. *J. Mater. Chem. B* 2017, 5, 5580–5587. [PubMed: 28848651]
- (798). Wu T; Xue J; Li H; Zhu C; Mo X; Xia Y General Method for Generating Circular Gradients of Active Proteins on Nanofiber Scaffolds Sought for Wound Closure and Related Applications. *ACS Appl. Mater. Interfaces* 2018, 10, 8536–8545. [PubMed: 29420008]
- (799). Li X; Li M; Sun J; Zhuang Y; Shi J; Guan D; Chen Y; Dai J Radially Aligned Electrospun Fibers with Continuous Gradient of SDF1 α for the Guidance of Neural Stem Cells. *Small* 2016, 12, 5009–5018. [PubMed: 27442189]
- (800). Rao SS; Nelson MT; Xue R; DeJesus JK; Viapiano MS; Lannutti JJ; Sarkar A; Winter JO Mimicking White Matter Tract Topography Using Core-Shell Electrospun Nanofibers to Examine Migration of Malignant Brain Tumors. *Biomaterials* 2013, 34, 5181–5190. [PubMed: 23601662]

- (801). Reya T; Morrison SJ; Clarke MF; Weissman IL Stem Cells, Cancer, and Cancer Stem Cells. *Nature* 2001, 414, 105–111. [PubMed: 11689955]
- (802). Morrison SJ; Spradling AC Stem Cells and Niches: Mechanisms That Promote Stem Cell Maintenance Throughout Life. *Cell* 2008, 132, 598–611. [PubMed: 18295578]
- (803). Bruggeman KF; Williams RJ; Nisbet DR Dynamic and Responsive Growth Factor Delivery from Electrospun and Hydrogel Tissue Engineering Materials. *Adv. Healthcare Mater* 2018, 7, 1700836.
- (804). Kilian KA; Bugarija B; Lahn BT; Mrksich M Geometric Cues for Directing the Differentiation of Mesenchymal Stem Cells. *Proc. Natl. Acad. Sci. U. S. A* 2010, 107, 4872–4877. [PubMed: 20194780]
- (805). Sankar S; Sharma CS; Rath SN; Ramakrishna S Electrospun Nanofibres to Mimic Natural Hierarchical Structure of Tissues: Application in Musculoskeletal Regeneration. *J. Tissue Eng. Regener. Med* 2018, 12, e604–e619.
- (806). Zhang C; Yuan H; Liu H; Chen X; Lu P; Zhu T; Yang L; Yin Z; Heng BC; Zhang Y; et al. Well-Aligned Chitosan-Based Ultrafine Fibers Committed Teno-Lineage Differentiation of Human Induced Pluripotent Stem Cells for Achilles Tendon Regeneration. *Biomaterials* 2015, 53, 716–730. [PubMed: 25890767]
- (807). Wu S; Peng H; Li X; Streubel PN; Liu Y; Duan B Effect of Scaffold Morphology and Cell Co-Culture on Tenogenic Differentiation of HADMSC on Centrifugal Melt Electrospun Poly(L-lactic acid) Fibrous Meshes. *Biofabrication* 2017, 9, 044106. [PubMed: 29134948]
- (808). Shao W; He J; Wang Q; Cui S; Ding B Biominerized Poly(L-lactic-*co*-glycolic acid)/Graphene Oxide/Tussah Silk Fibroin Nanofiber Scaffolds with Multiple Orthogonal Layers Enhance Osteoblastic Differentiation of Mesenchymal Stem Cells. *ACS Biomater. Sci. Eng* 2017, 3, 1370–1380.
- (809). Taskin MB; Xu R; Gregersen H; Nygaard JV; Besenbacher F; Chen M Three-Dimensional Polydopamine Functionalized Coiled Microfibrous Scaffolds Enhance Human Mesenchymal Stem Cells Colonization and Mild Myofibroblastic Differentiation. *ACS Appl. Mater. Interfaces* 2016, 8, 15864–15873. [PubMed: 27265317]
- (810). Wu S; Duan B; Liu P; Zhang C; Qin X; Butcher JT Fabrication of Aligned Nanofiber Polymer Yarn Networks for Anisotropic Soft Tissue Scaffolds. *ACS Appl. Mater. Interfaces* 2016, 8, 16950–16960. [PubMed: 27304080]
- (811). Chen H; Huang X; Zhang M; Damanik F; Baker MB; Leferink A; Yuan H; Truckenmuller R; Van Blitterswijk C; Moroni L Tailoring Surface Nanoroughness of Electrospun Scaffolds for Skeletal Tissue Engineering. *Acta Biomater* 2017, 59, 82–93. [PubMed: 28690010]
- (812). Xu T; Yang H; Yang D; Yu ZZ Polylactic Acid Nanofiber Scaffold Decorated with Chitosan Islandlike Topography for Bone Tissue Engineering. *ACS Appl. Mater. Interfaces* 2017, 9, 21094–21104. [PubMed: 28537074]
- (813). Tang Y; Liu L; Li J; Yu L; Wang L; Shi J; Chen Y Induction and Differentiation of Human Induced Pluripotent Stem Cells into Functional Cardiomyocytes on a Compartmented Monolayer of Gelatin Nanofibers. *Nanoscale* 2016, 8, 14530–14540. [PubMed: 27412150]
- (814). Ren Z; Ma S; Jin L; Liu Z; Liu D; Zhang X; Cai Q; Yang X Repairing a Bone Defect with a Three-Dimensional Cellular Construct Composed of a Multi-Layered Cell Sheet on Electrospun Mesh. *Biofabrication* 2017, 9, 025036. [PubMed: 28631613]
- (815). Song J; Zhu G; Wang L; An G; Shi X; Wang Y Assembling of Electrospun Meshes into Three-Dimensional Porous Scaffolds for Bone Repair. *Biofabrication* 2017, 9, 015018. [PubMed: 28140360]
- (816). Chen H; Malheiro ABFB; Van Blitterswijk C; Mota C; Wieringa PA; Moroni L Direct Writing Electrospinning of Scaffolds with Multidimensional Fiber Architecture for Hierarchical Tissue Engineering. *ACS Appl. Mater. Interfaces* 2017, 9, 38187–38200. [PubMed: 29043781]
- (817). Kennedy KM; Bhaw-Luximon A; Jhurry D Cell-Matrix Mechanical Interaction in Electrospun Polymeric Scaffolds for Tissue Engineering: Implications for Scaffold Design and Performance. *Acta Biomater* 2017, 50, 41–55. [PubMed: 28011142]
- (818). Vatankhah E; Prabhakaran MP; Semnani D; Razavi S; Zamani M; Ramakrishna S Phenotypic Modulation of Smooth Muscle Cells by Chemical and Mechanical Cues of Electrospun

- Tecophilic/Gelatin Nanofibers. *ACS Appl. Mater. Interfaces* 2014, 6, 4089–4101. [PubMed: 24588215]
- (819). Mohammadi Amirabad L; Massumi M; Shamsara M; Shabani I; Amari A; Mossahebi Mohammadi M; Hosseinzadeh S; Vakilian S; Steinbach SK; Khorramizadeh MR; Soleimani M; Barzin J; et al. Enhanced Cardiac Differentiation of Human Cardiovascular Disease Patient-Specific Induced Pluripotent Stem Cells by Applying Unidirectional Electrical Pulses Using Aligned Electroactive Nanofibrous Scaffolds. *ACS Appl. Mater. Interfaces* 2017, 9, 6849–6864. [PubMed: 28116894]
- (820). Damaraju SM; Shen Y; Elele E; Khusid B; Eshghinejad A; Li J; Jaffe M; Arinze TL Three-Dimensional Piezoelectric Fibrous Scaffolds Selectively Promote Mesenchymal Stem Cell Differentiation. *Biomaterials* 2017, 149, 51–62. [PubMed: 28992510]
- (821). Deng Y; Yang Y; Wei S Peptide-Decorated Nanofibrous Niche Augments in Vitro Directed Osteogenic Conversion of Human Pluripotent Stem Cells. *Biomacromolecules* 2017, 18, 587–598. [PubMed: 28068081]
- (822). Jia C; Luo B; Wang H; Bian Y; Li X; Li S; Wang H Precise and Arbitrary Deposition of Biomolecules onto Biomimetic Fibrous Matrices for Spatially Controlled Cell Distribution and Functions. *Adv. Mater* 2017, 29, 1701154.
- (823). Zhang C; Wang X; Zhang E; Yang L; Yuan H; Tu W; Zhang H; Yin Z; Shen W; Chen X; et al. An Epigenetic Bioactive Composite Scaffold with Well-Aligned Nanofibers for Functional Tendon Tissue Engineering. *Acta Biomater* 2018, 66, 141–156. [PubMed: 28963019]
- (824). Wu S; Wang Y; Streubel PN; Duan B Living Nanofiber Yarn-Based Woven Bioteextiles for Tendon Tissue Engineering Using Cell Tri-Culture and Mechanical Stimulation. *Acta Biomater* 2017, 62, 102–115. [PubMed: 28864251]
- (825). Hsu CC; Serio A; Amdursky N; Besnard C; Stevens MM Fabrication of Hemin-Doped Serum Albumin-Based Fibrous Scaffolds for Neural Tissue Engineering Applications. *ACS Appl. Mater. Interfaces* 2018, 10, 5305–5317. [PubMed: 29381329]
- (826). Dinis TM; Elia R; Vidal G; Dermigny Q; Denoeud C; Kaplan DL; Egles C; Marin F 3D Multi-Channel Bi-Function-alized Silk Electrospun Conduits for Peripheral Nerve Regeneration. *J. Mech. Behav. Biomed. Mater* 2015, 41, 43–55. [PubMed: 25460402]
- (827). Stewart JD Peripheral Nerve Fascicles: Anatomy and Clinical Relevance. *Muscle Nerve* 2003, 28, 525–541. [PubMed: 14571454]
- (828). Gu X; Ding F; Williams DF Neural Tissue Engineering Options for Peripheral Nerve Regeneration. *Biomaterials* 2014, 35, 6143–6156. [PubMed: 24818883]
- (829). Tian L; Prabhakaran MP; Ramakrishna S Strategies for Regeneration of Components of Nervous System: Scaffolds, Cells and Biomolecules. *Regener. Biomater* 2015, 2, 31–45.
- (830). Angius D; Wang H; Spinner RJ; Gutierrez-Cotto Y; Yaszemski MJ; Windebank AJ A Systematic Review of Animal Models Used to Study Nerve Regeneration in Tissue-Engineered Scaffolds. *Biomaterials* 2012, 33, 8034–8039. [PubMed: 22889485]
- (831). Xie J; MacEwan MR; Schwartz AG; Xia Y Electrospun Nanofibers for Neural Tissue Engineering. *Nanoscale* 2010, 2, 35–44. [PubMed: 20648362]
- (832). Simitzi C; Ranella A; Stratakis E Controlling the Morphology and Outgrowth of Nerve and Neuroglial Cells: The Effect of Surface Topography. *Acta Biomater* 2017, 51, 21–52. [PubMed: 28069509]
- (833). Jin L; Xu Q; Li C; Huang J; Zhang Y; Wu D; Wang Z Engineering 3D Aligned Nanofibers for Regulation of Cell Growth Behavior. *Macromol. Mater. Eng* 2017, 302, 1600448.
- (834). Xie J; MacEwan MR; Li X; Sakiyama-Elbert SE; Xia Y Neurite Outgrowth on Nanofiber Scaffolds with Different Orders, Structures, and Surface Properties. *ACS Nano* 2009, 3, 1151–1159. [PubMed: 19397333]
- (835). Huang C; Ouyang Y; Niu H; He N; Ke Q; Jin X; Li D; Fang J; Liu W; Fan C; et al. Nerve Guidance Conduits from Aligned Nanofibers: Improvement of Nerve Regeneration through Longitudinal Nanogrooves on a Fiber Surface. *ACS Appl. Mater. Interfaces* 2015, 7, 7189–7196. [PubMed: 25786058]

- (836). Huang C; Tang Y; Liu X; Sutti A; Ke Q; Mo X; Wang X; Morsi Y; Lin T Electrospinning of Nanofibres with Parallel Line Surface Texture for Improvement of Nerve Cell Growth. *Soft Matter* 2011, 7, 10812–10817.
- (837). Zhang K; Zheng H; Liang S; Gao C Aligned PLLA Nanofibrous Scaffolds Coated with Graphene Oxide for Promoting Neural Cell Growth. *Acta Biomater* 2016, 37, 131–142. [PubMed: 27063493]
- (838). Li X; Macewan MR; Xie JD; Siewe D; Yuan X; Xia Y Fabrication of Density Gradients of Biodegradable Polymer Micro-particles and Their Use in Guiding Neurite Outgrowth. *Adv. Funct. Mater* 2010, 20, 1632–1637. [PubMed: 21687818]
- (839). Balint R; Cassidy NJ; Cartmell SH Conductive Polymers: Towards a Smart Biomaterial for Tissue Engineering. *Acta Biomater* 2014, 10, 2341–2353. [PubMed: 24556448]
- (840). Rivers TJ; Hudson TW; Schmidt CE Synthesis of a Novel, Biodegradable Electrically Conducting Polymer for Biomedical Applications. *Adv. Funct. Mater* 2002, 12, 33–37.
- (841). Lee YS; Collins G; Livingston Arinze T Neurite Extension of Primary Neurons on Electrospun Piezoelectric Scaffolds. *Acta Biomater* 2011, 7, 3877–3886. [PubMed: 21810489]
- (842). Wu Y; Wang L; Guo B; Shao Y; Ma PX Electroactive Biodegradable Polyurethane Significantly Enhanced Schwann Cells Myelin Gene Expression and Neurotrophin Secretion for Peripheral Nerve Tissue Engineering. *Biomaterials* 2016, 87, 18–31. [PubMed: 26897537]
- (843). Liu W; Thomopoulos S; Xia Y Electrospun Nanofibers for Regenerative Medicine. *Adv. Healthcare Mater* 2012, 1, 10–25.
- (844). Xie J; Macewan MR; Willerth SM; Li X; Moran DW; Sakiyama-Elbert SE; Xia Y Conductive Core-Sheath Nanofibers and Their Potential Application in Neural Tissue Engineering. *Adv. Funct. Mater* 2009, 19, 2312–2318. [PubMed: 19830261]
- (845). Sun B; Wu T; Wang J; Li D; Wang J; Gao Q; Bhutto MA; El-Hamshary H; Al-Deyab SS; Mo X Polypyrrole-Coated Poly(L-lactic acid-*co*- ϵ -caprolactone)/Silk Fibroin Nanofibrous Membranes Promoting Neural Cell Proliferation and Differentiation with Electrical Stimulation. *J. Mater. Chem. B* 2016, 4, 6670–6679.
- (846). Zhang J; Qiu K; Sun B; Fang J; Zhang K; El-Hamshary H; Al-Deyab SS; Mo X The Aligned Core-Sheath Nanofibers with Electrical Conductivity for Neural Tissue Engineering. *J. Mater. Chem. B* 2014, 2, 7945–7954.
- (847). Xie J; Liu W; MacEwan MR; Bridgman PC; Xia Y Neurite Outgrowth on Electrospun Nanofibers with Uniaxial Alignment: The Effects of Fiber Density, Surface Coating, and Supporting Substrate. *ACS Nano* 2014, 8, 1878–1885. [PubMed: 24444076]
- (848). Xue J; Yang J; O'Connor DM; Zhu C; Huo D; Boulis NM; Xia Y Differentiation of Bone Marrow Stem Cells into Schwann Cells for the Promotion of Neurite Outgrowth on Electrospun Fibers. *ACS Appl. Mater. Interfaces* 2017, 9, 12299–12310. [PubMed: 28322042]
- (849). Hadlock T; Sundback C; Hunter D; Cheney M; Vacanti JP A Polymer Foam Conduit Seeded with Schwann Cells Promotes Guided Peripheral Nerve Regeneration. *Tissue Eng* 2000, 6, 119–127. [PubMed: 10941207]
- (850). Chiono V; Tonda-Turo C Trends in the Design of Nerve Guidance Channels in Peripheral Nerve Tissue Engineering. *Prog. Neurobiol* 2015, 131, 87–104. [PubMed: 26093353]
- (851). Jeffries EM; Wang Y Incorporation of Parallel Electrospun Fibers for Improved Topographical Guidance in 3D Nerve Guides. *Biofabrication* 2013, 5, 035015. [PubMed: 23945055]
- (852). Yao L; Billiar KL; Windebank AJ; Pandit A Multichanneled Collagen Conduits for Peripheral Nerve Regeneration: Design, Fabrication, and Characterization. *Tissue Eng., Part C* 2010, 16, 1585–1596.
- (853). Hu X; Huang J; Ye Z; Xia L; Li M; Lv B; Shen X; Luo Z A Novel Scaffold with Longitudinally Oriented Microchannels Promotes Peripheral Nerve Regeneration. *Tissue Eng., Part A* 2009, 15, 3297–3308. [PubMed: 19382873]
- (854). Chang YC; Chen MH; Liao SY; Wu HC; Kuan CH; Sun JS; Wang TW Multichanneled Nerve Guidance Conduit with Spatial Gradients of Neurotrophic Factors and Oriented Nanotopography for Repairing the Peripheral Nervous System. *ACS Appl. Mater. Interfaces* 2017, 9, 37623–37636. [PubMed: 28990762]

- (855). Lee DJ; Fontaine A; Meng X; Park D Biomimetic Nerve Guidance Conduit Containing Intraluminal Microchannels with Aligned Nanofibers Markedly Facilitates in Nerve Regeneration. *ACS Biomater. Sci. Eng* 2016, 2, 1403–1410.
- (856). Cai J; Peng X; Nelson KD; Eberhart R; Smith GM Permeable Guidance Channels Containing Microfilament Scaffolds Enhance Axon Growth and Maturation. *J. Biomed. Mater. Res., Part A* 2005, 75, 374–386.
- (857). Sun B; Zhou Z; Wu T; Chen W; Li D; Zheng H; El-Hamshary H; Al-Deyab SS; Mo X; Yu Y Development of Nanofiber Sponges-Containing Nerve Guidance Conduit for Peripheral Nerve Regeneration in Vivo. *ACS Appl. Mater. Interfaces* 2017, 9, 26684–26696. [PubMed: 28718615]
- (858). Huang L; Zhu L; Shi X; Xia B; Liu Z; Zhu S; Yang Y; Ma T; Cheng P; Luo K; et al. A Compound Scaffold with Uniform Longitudinally Oriented Guidance Cues and a Porous Sheath Promotes Peripheral Nerve Regeneration in Vivo. *Acta Biomater* 2018, 68, 223–236. [PubMed: 29274478]
- (859). Wu T; Li D; Wang Y; Sun B; Li D; Morsi Y; El-Hamshary H; Al-Deyab SS; Mo X Laminin-Coated Nerve Guidance Conduits Based on Poly(L-lactide-co-glycolide) Fibers and Yarns for Promoting Schwann Cells' Proliferation and Migration. *J. Mater. Chem. B* 2017, 5, 3186–3194.
- (860). Li D; Pan X; Sun B; Wu T; Chen W; Huang C; Ke Q; El-Hamshary HA; Al-Deyab SS; Mo X Nerve Conduits Constructed by Electrospun P(LLA-CL) Nanofibers and PLLA Nanofiber Yarns. *J. Mater. Chem. B* 2015, 3, 8823–8831.
- (861). Wang J; Windbergs M Functional Electrospun Fibers for the Treatment of Human Skin Wounds. *Eur. J. Pharm. Biopharm* 2017, 119, 283–299. [PubMed: 28690200]
- (862). Dias JR; Granja PL; Bartolo PJ Advances in Electrospun Skin Substitutes. *Prog. Mater. Sci* 2016, 84, 314–334.
- (863). Sundaramurthi D; Krishnan UM; Sethuraman S Electrospun Nanofibers as Scaffolds for Skin Tissue Engineering. *Polym. Rev* 2014, 54, 348–376.
- (864). Qin S; Clark RAF; Rafailovich MH Establishing Correlations in the En-Mass Migration of Dermal Fibroblasts on Oriented Fibrillar Scaffolds. *Acta Biomater* 2015, 25, 230–239. [PubMed: 26117312]
- (865). Sun L; Gao W; Fu X; Shi M; Xie W; Zhang W; Zhao F; Chen X Enhanced Wound Healing in Diabetic Rats by Nanofibrous Scaffolds Mimicking the Basketweave Pattern of Collagen Fibrils in Native Skin. *Biomater. Sci* 2018, 6, 340–349. [PubMed: 29265119]
- (866). Pal P; Srivas PK; Dadhich P; Das B; Maulik D; Dhara S Nano-/Microfibrous Cotton-Wool-Like 3D Scaffold with Core-Shell Architecture by Emulsion Electrospinning for Skin Tissue Regeneration. *ACS Biomater. Sci. Eng* 2017, 3, 3563–3575.
- (867). Ma B; Xie J; Jiang J; Wu J Sandwich-Type Fiber Scaffolds with Square Arrayed Microwells and Nanostructured Cues as Microskin Grafts for Skin Regeneration. *Biomaterials* 2014, 35, 630–641. [PubMed: 24144904]
- (868). Lee JM; Chae T; Sheikh FA; Ju HW; Moon BM; Park HJ; Park YR; Park CH Three Dimensional poly(ϵ -caprolactone) and Silk Fibroin Nanocomposite Fibrous Matrix for Artificial Dermis. *Mater. Sci. Eng., C* 2016, 68, 758–767.
- (869). Norouzi M; Boroujeni SM; Omidvarkordshouli N; Soleimani M Advances in Skin Regeneration: Application of Electrospun Scaffolds. *Adv. Healthcare Mater* 2015, 4, 1114–1133.
- (870). Xie Z; Paras CB; Weng H; Punnaikitashem P; Su LC; Vu K; Tang L; Yang J; Nguyen KT Dual Growth Factor Releasing Multi-Functional Nanofibers for Wound Healing. *Acta Biomater* 2013, 9, 9351–9359. [PubMed: 23917148]
- (871). Pal P; Dadhich P; Srivas PK; Das B; Maulik D; Dhara S Bilayered Nanofibrous 3D Hierarchy as Skin Rudiment by Emulsion Electrospinning for Burn Wound Management. *Biomater. Sci* 2017, 5, 1786–1799.
- (872). Lai HJ; Kuan CH; Wu HC; Tsai JC; Chen TM; Hsieh DJ; Wang TW Tailored Design of Electrospun Composite Nanofibers with Staged Release of Multiple Angiogenic Growth Factors for Chronic Wound Healing. *Acta Biomater* 2014, 10, 4156–4166. [PubMed: 24814882]
- (873). Lee EJ; Huh BK; Kim SN; Lee JY; Park CG; Mikos AG; Choy YB Application of Materials as Medical Devices with Localized Drug Delivery Capabilities for Enhanced Wound Repair. *Prog. Mater. Sci* 2017, 89, 392–410. [PubMed: 29129946]

- (874). Lu Y; Huang J; Yu G; Cardenas R; Wei S; Wujcik EK; Guo Z Coaxial Electrospun Fibers: Applications in Drug Delivery and Tissue Engineering. Wiley Interdiscip. Rev. Nanomed. Nanobiotechnol 2016, 8, 654–677. [PubMed: 26848106]
- (875). Dhand C; Venkatesh M; Barathi VA; Harini S; Bairagi S; Goh Tze Leng E; Muruganandham N; Low KZW; Fazil MHUT; Loh XJ; Srinivasan DK; Liu SP; Beuerman RW; Verma NK; Ramakrishna S; Lakshminarayanan R; et al. Bioinspired Crosslinking and Matrix-Drug Interactions for Advanced Wound Dressings with Long-Term Antimicrobial Activity. Biomaterials 2017, 138, 153–168. [PubMed: 28578293]
- (876). Son WK; Youk JH; Lee TS; Park WH Preparation of Antimicrobial Ultrafine Cellulose Acetate Fibers with Silver Nanoparticles. Macromol. Rapid Commun 2004, 25, 1632–1637.
- (877). Yang X; Yang J; Wang L; Ran B; Jia Y; Zhang L; Yang G; Shao H; Jiang X Pharmaceutical Intermediate-Modified Gold Nanoparticles: Against Multidrug-Resistant Bacteria and Wound-Healing Application via an Electrospun Scaffold. ACS Nano 2017, 11, 5737–5745. [PubMed: 28531351]
- (878). Wang L; Yang J; Ran B; Yang X; Zheng W; Long Y; Jiang X Small Molecular TGF- β 1-Inhibitor-Loaded Electrospun Fibrous Scaffolds for Preventing Hypertrophic Scars. ACS Appl. Mater. Interfaces 2017, 9, 32545–32553. [PubMed: 28875694]
- (879). Cheng L; Sun X; Zhao X; Wang L; Yu J; Pan G; Li B; Yang H; Zhang Y; Cui W Surface Biofunctional Drug-Loaded Electrospun Fibrous Scaffolds for Comprehensive Repairing Hypertrophic Scars. Biomaterials 2016, 83, 169–181. [PubMed: 26774564]
- (880). Zhang Q; Oh JH; Park CH; Baek JH; Ryoo HM; Woo KM Effects of Dimethyloxalylglycine-Embedded Poly(ϵ -caprolactone) Fiber Meshes on Wound Healing in Diabetic Rats. ACS Appl. Mater. Interfaces 2017, 9, 7950–7963. [PubMed: 28211272]
- (881). Lv F; Wang J; Xu P; Han Y; Ma H; Xu H; Chen S; Chang J; Ke Q; Liu M; et al. A Conducive Bioceramic/Polymer Composite Biomaterial for Diabetic Wound Healing. Acta Biomater 2017, 60, 128–143. [PubMed: 28713016]
- (882). Li J; Lv F; Xu H; Zhang Y; Wang J; Yi Z; Yin J; Chang J; Wu C A Patterned Nanocomposite Membrane for High-Efficiency Healing of Diabetic Wound. J. Mater. Chem. B 2017, 5, 1926–1934.
- (883). Ren X; Han Y; Wang J; Jiang Y; Yi Z; Xu H; Ke Q An Aligned Porous Electrospun Fibrous Membrane with Controlled Drug Delivery—An Efficient Strategy to Accelerate Diabetic Wound Healing with Improved Angiogenesis. Acta Biomater 2018, 70, 140–153. [PubMed: 29454159]
- (884). Wu Y; Wang L; Guo B; Ma PX Interwoven Aligned Conductive Nanofiber Yarn/Hydrogel Composite Scaffolds for Engineered 3D Cardiac Anisotropy. ACS Nano 2017, 11, 5646–5659. [PubMed: 28590127]
- (885). Fleischer S; Shevach M; Feiner R; Dvir T Coiled Fiber Scaffolds Embedded with Gold Nanoparticles Improve the Performance of Engineered Cardiac Tissues. Nanoscale 2014, 6, 9410–9414. [PubMed: 24744098]
- (886). Zhao G; Zhang X; Lu TJ; Xu F Recent Advances in Electrospun Nanofibrous Scaffolds for Cardiac Tissue Engineering. Adv. Funct. Mater 2015, 25, 5726–5738.
- (887). Castilho M; Feyen D; Flandes-Iparraguirre M; Hochleitner G; Groll J; Doevedans PAF; Vermonden T; Ito K; Sluijter JPG; Malda J Melt Electrospinning Writing of Poly-hydroxymethylglycolide-co- ϵ -caprolactone-Based Scaffolds for Cardiac Tissue Engineering. Adv. Healthcare Mater 2017, 6, 1700311.
- (888). Schoen B; Avrahami R; Baruch L; Efraim Y; Goldfracht I; Elul O; Davidov T; Gepstein L; Zussman E; Machluf M Electrospun Extracellular Matrix: Paving the Way to Tailor-Made Natural Scaffolds for Cardiac Tissue Regeneration. Adv. Funct. Mater 2017, 27, 1700427.
- (889). Kitsara M; Agbulut O; Kontziamasis D; Chen Y; Menasche P Fibers for Hearts: A Critical Review on Electrospinning for Cardiac Tissue Engineering. Acta Biomater 2017, 48, 20–40. [PubMed: 27826001]
- (890). Wanjare M; Hou L; Nakayama KH; Kim JJ; Mezak NP; Abilez OJ; Tzatzalos E; Wu JC; Huang NF Anisotropic Microfibrous Scaffolds Enhance the Organization and Function of Cardiomyocytes Derived from Induced Pluripotent Stem Cells. Biomater. Sci 2017, 5, 1567–1578. [PubMed: 28715029]

- (891). Liu Y; Xu G; Wei J; Wu Q; Li X Cardiomyocyte Coculture on Layered Fibrous Scaffolds Assembled from Micropatterned Electrospun Mats. *Mater. Sci. Eng., C* 2017, 81, 500–510.
- (892). Fleischer S; Feiner R; Shapira A; Ji J; Sui X; Daniel Wagner H; Dvir T Spring-Like Fibers for Cardiac Tissue Engineering. *Biomaterials* 2013, 34, 8599–8606. [PubMed: 23953840]
- (893). Han J; Wu Q; Xia Y; Wagner MB; Xu C Cell Alignment Induced by Anisotropic Electrospun Fibrous Scaffolds Alone Has Limited Effect on Cardiomyocyte Maturation. *Stem Cell Res* 2016, 16, 740–750. [PubMed: 27131761]
- (894). Senel Ayaz HG; Perets A; Ayaz H; Gilroy KD; Govindaraj M; Brookstein D; Lelkes PI Textile-Templated Electrospun Anisotropic Scaffolds for Regenerative Cardiac Tissue Engineering. *Biomaterials* 2014, 35, 8540–8552. [PubMed: 25017096]
- (895). Wang L; Wu Y; Hu T; Guo B; Ma PX Electrospun Conductive Nanofibrous Scaffolds for Engineering Cardiac Tissue and 3D Bioactuators. *Acta Biomater* 2017, 59, 68–81. [PubMed: 28663141]
- (896). Fleischer S; Shapira A; Feiner R; Dvir T Modular Assembly of Thick Multifunctional Cardiac Patches. *Proc. Natl. Acad. Sci. U. S. A* 2017, 114, 1898–1903. [PubMed: 28167795]
- (897). Sarkar S; Schmitz-Rixen T; Hamilton G; Seifalian AM Achieving the Ideal Properties for Vascular Bypass Grafts Using a Tissue Engineered Approach: A Review. *Med. Biol. Eng. Comput* 2007, 45, 327–336. [PubMed: 17340153]
- (898). Zhang Y; Li XS; Guex AG; Liu SS; Müller E; Malini RI; Zhao HJ; Rottmar M; Maniura-Weber K; Rossi RM; et al. A Compliant and Biomimetic Three-Layered Vascular Graft for Small Blood Vessels. *Biofabrication* 2017, 9, 025010. [PubMed: 28382923]
- (899). Shojaee M; Bashur CA Compositions Including Synthetic and Natural Blends for Integration and Structural Integrity: Engineered for Different Vascular Graft Applications. *Adv. Healthcare Mater* 2017, 6, 1700001.
- (900). Wu T; Zhang J; Wang Y; Li D; Sun B; El-Hamshary H; Yin M; Mo X Fabrication and Preliminary Study of a Biomimetic Tri-Layer Tubular Graft Based on Fibers and Fiber Yarns for Vascular Tissue Engineering. *Mater. Sci. Eng., C* 2018, 82, 121–129.
- (901). Hasan A; Memic A; Annabi N; Hossain M; Paul A; Dokmeci MR; Dehghani F; Khademhosseini A Electrospun Scaffolds for Tissue Engineering of Vascular Grafts. *Acta Biomater* 2014, 10, 11–25. [PubMed: 23973391]
- (902). Wu T; Zhang J; Wang Y; Sun B; Yin M; Bowlin GL; Mo X Design and Fabrication of a Biomimetic Vascular Scaffold Promoting *in Situ* Endothelialization and Tunica Media Regeneration. *ACS Appl. Bio Mater* 2018, 1, 833–844.
- (903). Zhou F; Jia X; Yang Y; Yang Q; Gao C; Hu S; Zhao Y; Fan Y; Yuan X Nanofiber-Mediated MicroRNA-126 Delivery to Vascular Endothelial Cells for Blood Vessel Regeneration. *Acta Biomater* 2016, 43, 303–313. [PubMed: 27477849]
- (904). de Valence S; Tille JC; Gilberto JP; Mrowczynski W; Gurny R; Walporth BH; Moller M Advantages of Bilayered Vascular Grafts for Surgical Applicability and Tissue Regeneration. *Acta Biomater* 2012, 8, 3914–3920. [PubMed: 22771455]
- (905). Wang T; Ji X; Jin L; Feng Z; Wu J; Zheng J; Wang H; Xu ZW; Guo L; He N Fabrication and Characterization of Heparin-Grafted Poly-L-lactic acid-Chitosan Core-Shell Nanofibers Scaffold for Vascular Gasket. *ACS Appl. Mater. Interfaces* 2013, 5, 3757–3763. [PubMed: 23586670]
- (906). Qiu X; Lee BLP; Ning X; Murthy N; Dong N; Li S End-Point Immobilization of Heparin on Plasma-Treated Surface of Electrospun Polycarbonate-Urethane Vascular Graft. *Acta Biomater* 2017, 51, 138–147. [PubMed: 28069505]
- (907). Zhu T; Yu K; Bhutto MA; Guo X; Shen W; Wang J; Chen W; El-Hamshary H; Al-Deyab SS; Mo X Synthesis of RGD-Peptide Modified Poly(ester-urethane) Urea Electrospun Nanofibers as a Potential Application for Vascular Tissue Engineering. *Chem. Eng. J* 2017, 315, 177–190.
- (908). Zheng W; Wang Z; Song L; Zhao Q; Zhang J; Li D; Wang S; Han J; Zheng XL; Yang Z; et al. Endothelialization and Patency of RGD-Functionalized Vascular Grafts in a Rabbit Carotid Artery Model. *Biomaterials* 2012, 33, 2880–2891 [PubMed: 22244694]
- (909). Wu T; Jiang B; Wang Y; Yin A; Huang C; Wang S; Mo X Electrospun Poly(L-lactide-*co*-caprolactone)-Collagen-Chitosan Vascular Graft in a Canine Femoral Artery Model. *J. Mater. Chem. B* 2015, 3, 5760–5768.

- (910). Yao Y; Wang J; Cui Y; Xu R; Wang Z; Zhang J; Wang K; Li Y; Zhao Q; Kong D Effect of Sustained Heparin Release from PCL/Chitosan Hybrid Small-Diameter Vascular Grafts on Anti-Thrombogenic Property and Endothelialization. *Acta Biomater* 2014, 10, 2739–2749. [PubMed: 24602806]
- (911). Lee KW; Johnson NR; Gao J; Wang Y Human Progenitor Cell Recruitment via SDF1 α Coacervate-Laden PGS Vascular Grafts. *Biomaterials* 2013, 34, 9877–9885. [PubMed: 24060423]
- (912). Seyednejad H; Ji W; Yang F; Van Nostrum CF; Vermonden T; Van den Beucken JJ; Dhert WJ; Hennink WE; Jansen JA Coaxially Electrospun Scaffolds Based on Hydroxyl-Functionalized Poly(ϵ -caprolactone) and Loaded with VEGF for Tissue Engineering Applications. *Biomacromolecules* 2012, 13, 3650–3660. [PubMed: 23039047]
- (913). Rujitanaroj PO; Aid-Launais R; Chew SY; Le Visage C Polysaccharide Electrospun Fibers with Sulfated Poly(fucose) Promote Endothelial Cell Migration and VEGF-Mediated Angiogenesis. *Biomater. Sci* 2014, 2, 843–852.
- (914). Yu J; Wang A; Tang Z; Henry J; Li-Ping Lee B; Zhu Y; Yuan F; Huang F; Li S The Effect of Stromal Cell-Derived Factor-1 α /Heparin Coating of Biodegradable Vascular Grafts on the Recruitment of Both Endothelial and Smooth Muscle Progenitor Cells for Accelerated Regeneration. *Biomaterials* 2012, 33, 8062–8074. [PubMed: 22884813]
- (915). Avci-Adali M; Ziemer G; Wendel HP Induction of EPC Homing on Biofunctionalized Vascular Grafts for Rapid *in Vivo* Self-Endothelialization-A Review of Current Strategies. *Biotechnol. Adv* 2010, 28, 119–129. [PubMed: 19879347]
- (916). Wang Y; Shi H; Qiao J; Tian Y; Wu M; Zhang W; Lin Y; Niu Z; Huang Y Electrospun Tubular Scaffold with Circumferentially Aligned Nanofibers for Regulating Smooth Muscle Cell Growth. *ACS Appl. Mater. Interfaces* 2014, 6, 2958–2962. [PubMed: 24417638]
- (917). Wu T; Zhang J; Wang Y; Sun B; Guo X; Morsi Y; El-Hamshary H; El-Newehy M; Mo X Development of Dynamic Liquid and Conjugated Electrospun Poly(L-lactide-*co*-caprolactone)/Collagen Nanoyarns for Regulating Vascular Smooth Muscle Cells Growth. *J. Biomed. Nanotechnol* 2017, 13, 303–312. [PubMed: 29381285]
- (918). Yuan H; Qin J; Xie J; Li B; Yu Z; Peng Z; Yi B; Lou X; Lu X; Zhang Y Highly Aligned Core-Shell Structured Nanofibers for Promoting Phenotypic Expression of Vsmcs for Vascular Regeneration. *Nanoscale* 2016, 8, 16307–16322. [PubMed: 27714091]
- (919). Zhou P; Zhou F; Liu B; Zhao Y; Yuan X Functional Electrospun Fibrous Scaffolds with Dextran-*g*-Poly(L-lysine)-VAPG/MicroRNA-145 to Specially Modulate Vascular SMCs. *J. Mater. Chem. B* 2017, 5, 9312–9325.
- (920). Zhang H; Jia X; Han F; Zhao J; Zhao Y; Fan Y; Yuan X Dual-Delivery of VEGF and PDGF by Double-Layered Electrospun Membranes for Blood Vessel Regeneration. *Biomaterials* 2013, 34, 2202–2212. [PubMed: 23290468]
- (921). Han F; Jia X; Dai D; Yang X; Zhao J; Zhao Y; Fan Y; Yuan X Performance of a Multilayered Small-Diameter Vascular Scaffold Dual-Loaded with VEGF and PDGF. *Biomaterials* 2013, 34, 7302–7313. [PubMed: 23830580]
- (922). Pan Y; Zhou X; Wei Y; Zhang Q; Wang T; Zhu M; Li W; Huang R; Liu R; Chen J; Fan G; Wang K; Kong D; Zhao Q; et al. Small-Diameter Hybrid Vascular Grafts Composed of Polycaprolactone and Polydioxanone Fibers. *Sci. Rep* 2017, 7, 3615. [PubMed: 28620160]
- (923). Wu W; Allen RA; Wang Y Fast-Degrading Elastomer Enables Rapid Remodeling of a Cell-Free Synthetic Graft into a Neoartery. *Nat. Med* 2012, 18, 1148–1153. [PubMed: 22729285]
- (924). Bergmeister H; Seyidova N; Schreiber C; Strobl M; Grasl C; Walter I; Messner B; Baudis S; Frohlich S; Marchetti-Deschmann M; et al. Biodegradable, Thermoplastic Polyurethane Grafts for Small Diameter Vascular Replacements. *Acta Biomater* 2015, 11, 104–113. [PubMed: 25218664]
- (925). Mooar P. Muscles. The Merck Manuals Online Medical Library; Merck: Kenilworth, NJ, USA, 2007.
- (926). Ju YM; Atala A; Yoo JJ; Lee SJ *In Situ* Regeneration of Skeletal Muscle Tissue through Host Cell Recruitment. *Acta Biomater* 2014, 10, 4332–4339. [PubMed: 24954910]

- (927). Hajiali F; Tajbakhsh S; Shojaei A Fabrication and Properties of Polycaprolactone Composites Containing Calcium Phosphate-Based Ceramics and Bioactive Glasses in Bone Tissue Engineering: A Review. *Polym. Rev* 2018, 58, 164–207.
- (928). Ko E; Lee JS; Kim H; Yang SY; Yang D; Yang K; Lee J; Shin J; Yang HS; Ryu W; et al. Electrospun Silk Fibroin Nanofibrous Scaffolds with Two-Stage Hydroxyapatite Functionalization for Enhancing the Osteogenic Differentiation of Human Adipose-Derived Mesenchymal Stem Cells. *ACS Appl. Mater. Interfaces* 2018, 10, 7614–7625. [PubMed: 28475306]
- (929). Singh BN; Pramanik K Development of Novel Silk Fibroin/Polyvinyl Alcohol/Sol-Gel Bioactive Glass Composite Matrix by Modified Layer by Layer Electrospinning Method for Bone Tissue Construct Generation. *Biofabrication* 2017, 9, 015028. [PubMed: 28332482]
- (930). Nasajpour A; Ansari S; Rinoldi C; Rad AS; Aghaloo T; Shin SR; Mishra YK; Adelung R; Swieszkowski W; Annabi N; et al. A Multifunctional Polymeric Periodontal Membrane with Osteogenic and Antibacterial Characteristics. *Adv. Funct. Mater* 2018, 28, 1703437.
- (931). Zhou P; Cheng X; Xia Y; Wang P; Zou K; Xu S; Du J Organic/Inorganic Composite Membranes Based on Poly(L-lactic-co-glycolic acid) and Mesoporous Silica for Effective Bone Tissue Engineering. *ACS Appl. Mater. Interfaces* 2014, 6, 20895–20903. [PubMed: 25394879]
- (932). Luo J; Zhang H; Zhu J; Cui X; Gao J; Wang X; Xiong J 3-D Mineralized Silk Fibroin/Polycaprolactone Composite Scaffold Modified with Polyglutamate conjugated with BMP-2 Peptide for Bone Tissue Engineering. *Colloids Surf., B* 2018, 163, 369–378.
- (933). Chamundeswari VN; Siang LY; Chuah YJ; Tan JS; Wang D-A; Loo SCJ Sustained Releasing Sponge-Like 3D Scaffolds for Bone Tissue Engineering Applications. *Biomed. Mater* 2018, 13, 015019.
- (934). Sophia Fox AJ; Bedi A; Rodeo SA The Basic Science of Articular Cartilage: Structure, Composition, and Function. *Sports Health* 2009, 1, 461–468. [PubMed: 23015907]
- (935). Jiang T; Carbone EJ; Lo KWH; Laurencin CT Electrospinning of Polymer Nanofibers for Tissue Regeneration. *Prog. Polym. Sci* 2015, 46, 1–24.
- (936). Garrigues NW; Little D; Sanchez-Adams J; Ruch DS; Guilak F Electrospun Cartilage-Derived Matrix Scaffolds for Cartilage Tissue Engineering. *J. Biomed. Mater. Res., Part A* 2014, 102, 3998–4008.
- (937). Weinreb JH; Sheth C; Apostolakos J; McCarthy M-B; Barden B; Cote MP; Mazzocca AD Tendon Structure, Disease, and Imaging. *Muscles Ligaments Tendons J* 2014, 4, 66–73. [PubMed: 24932450]
- (938). Yang G; Lin H; Rothrauff BB; Yu S; Tuan RS Multilayered Polycaprolactone/Gelatin Fiber-Hydrogel Composite for Tendon Tissue Engineering. *Acta Biomater* 2016, 35, 68–76. [PubMed: 26945631]
- (939). Evrova O; Houska J; Welti M; Bonavoglia E; Calcagni M; Giovanoli P; Vogel V; Buschmann J Bioactive, Elastic, and Biodegradable Emulsion Electrospun Degrapol Tube Delivering PDGF-BB for Tendon Rupture Repair. *Macromol. Biosci* 2016, 16, 1048–1063. [PubMed: 27071839]
- (940). Mouthuy PA; Zargar N; Hakimi O; Lostis E; Carr A Fabrication of Continuous Electrospun Filaments with Potential for Use as Medical Fibres. *Biofabrication* 2015, 7, 025006. [PubMed: 25987265]
- (941). Thayer PS; Dimling AF; Plessl DS; Hahn MR; Guelcher SA; Dahlgren LA; Goldstein AS Cellularized Cylindrical Fiber/Hydrogel Composites for Ligament Tissue Engineering. *Biomacromolecules* 2014, 15, 75–83. [PubMed: 24266805]
- (942). Deepthi S; Jeevitha K; Nivedhitha Sundaram M; Chennazhi KP; Jayakumar R Chitosan-Hyaluronic Acid Hydrogel Coated Poly(caprolactone) Multiscale Bilayer Scaffold for Ligament Regeneration. *Chem. Eng. J* 2015, 260, 478–485.
- (943). Jana S; Levengood SK; Zhang M Anisotropic Materials for Skeletal-Muscle-Tissue Engineering. *Adv. Mater* 2016, 28, 10588–10612. [PubMed: 27865007]
- (944). Jana S; Cooper A; Zhang M Chitosan Scaffolds with Unidirectional Microtubular Pores for Large Skeletal Myotube Generation. *Adv. Healthcare Mater* 2013, 2, 557–561.

- (945). Severt SY; Maxwell SL; Bontrager JS; Leger JM; Murphy AR Mimicking Muscle Fiber Structure and Function through Electromechanical Actuation of Electrospun Silk Fiber Bundles. *J. Mater. Chem. B* 2017, 5, 8105–8114.
- (946). Armitage OE; Oyen ML Indentation across Interfaces between Stiff and Compliant Tissues. *Acta Biomater* 2017, 56, 36–43. [PubMed: 28062353]
- (947). Seidi A; Ramalingam M; Elloumi-Hannachi I; Ostrovidov S; Khademhosseini A Gradient Biomaterials for Soft-to-Hard Interface Tissue Engineering. *Acta Biomater* 2011, 7, 1441–1451. [PubMed: 21232635]
- (948). Xu K; Kuntz LA; Foehr P; Kuempel K; Wagner A; Tuebel J; Deimling CV; Burgkart RH Efficient Decellularization for Tissue Engineering of the Tendon-Bone Interface with Preservation of Biomechanics. *PLoS One* 2017, 12, e0171577. [PubMed: 28170430]
- (949). Font Tellado S; Bonani W; Balmayor ER; Foehr P; Motta A; Migliaresi C; Van Griensven M Fabrication and Characterization of Biphasic Silk Fibroin Scaffolds for Tendon/Ligament-to-Bone Tissue Engineering. *Tissue Eng., Part A* 2017, 23, 859–872. [PubMed: 28330431]
- (950). Banik BL; Bowers DT; Fattahi P; Brown JL Bio-Instructive Scaffolds for Musculoskeletal Tissue Engineering and Regenerative Medicine; Elsevier, 2017; Chapter 9, pp 203–233.
- (951). Qu D; Subramony SD; Boskey AL; Pleshko N; Doty SB; Lu HH Compositional Mapping of the Mature Anterior Cruciate Ligament-to-Bone Insertion. *J. Orthop. Res* 2017, 35, 2513–2523. [PubMed: 28176356]
- (952). Yang PJ; Temenoff JS Engineering Orthopedic Tissue Interfaces. *Tissue Eng., Part B* 2009, 15, 127–141.
- (953). Kishan AP; Robbins AB; Mohiuddin SF; Jiang M; Moreno MR; Cosgriff-Hernandez EM Fabrication of Macromolecular Gradients in Aligned Fiber Scaffolds Using a Combination of in-Line Blending and Air-Gap Electrospinning. *Acta Biomater* 2017, 56, 118–128. [PubMed: 28017867]
- (954). Li X; Cheng R; Sun Z; Su W; Pan G; Zhao S; Zhao J; Cui W Flexible Bipolar Nanofibrous Membranes for Improving Gradient Microstructure in Tendon-to-Bone Healing. *Acta Biomater* 2017, 61, 204–216. [PubMed: 28778532]
- (955). Khorshidi S; Karkhaneh A A Review on Gradient Hydrogel/Fiber Scaffolds for Osteochondral Regeneration. *J. Tissue Eng. Regener. Med* 2018, 12, e1974–e1990.
- (956). Boushell MK; Hung CT; Hunziker EB; Strauss EJ; Lu HH Current Strategies for Integrative Cartilage Repair. *Connect. Tissue Res* 2017, 58, 393–406. [PubMed: 27599801]
- (957). Mohan N; Wilson J; Joseph D; Vaikkath D; Nair PD Biomimetic Fiber Assembled Gradient Hydrogel to Engineer Glycosaminoglycan Enriched and Mineralized Cartilage: An in Vitro Study. *J. Biomed. Mater. Res., Part A* 2015, 103, 3896–3906.
- (958). Ladd MR; Lee SJ; Stitzel JD; Atala A; Yoo JJ Co-Electrospun Dual Scaffolding System with Potential for Muscle-Tendon Junction Tissue Engineering. *Biomaterials* 2011, 32, 1549–1559. [PubMed: 21093046]
- (959). Taetzsch T; Tenga MJ; Valdez G Muscle Fibers Secrete FGFBP1 to Slow Degeneration of Neuromuscular Synapses During Aging and Progression of ALS. *J. Neurosci* 2017, 37, 70–82. [PubMed: 28053031]
- (960). Martin NR; Passey SL; Player DJ; Mudera V; Baar K; Greensmith L; Lewis MP Neuromuscular Junction Formation in Tissue-Engineered Skeletal Muscle Augments Contractile Function and Improves Cytoskeletal Organization. *Tissue Eng., Part A* 2015, 21, 2595–2604. [PubMed: 26166548]
- (961). Lee BK; Ju YM; Cho JG; Jackson JD; Lee SJ; Atala A; Yoo JJ End-to-Side Neurorrhaphy Using an Electrospun PCL/Collagen Nerve Conduit for Complex Peripheral Motor Nerve Regeneration. *Biomaterials* 2012, 33, 9027–9036. [PubMed: 22998812]
- (962). Zong C; Wang M; Yang F; Chen G; Chen J; Tang Z; Liu Q; Gao C; Ma L; Wang J A Novel Therapy Strategy for Bile Duct Repair Using Tissue Engineering Technique: PCL/PLGA Bilayered Scaffold with hMSCs. *J. Tissue Eng. Regener. Med* 2017, 11, 966–976.
- (963). Gao Q; Huang C; Sun B; Aqeel BM; Wang J; Chen W; Mo X; Wan X Fabrication and Characterization of Metal Stent Coating with Drug-Loaded Nanofiber Film for Gallstone Dissolution. *J. Biomater. Appl* 2016, 31, 784–796. [PubMed: 27698255]

- (964). Moazeni N; Vadood M; Semnani D; Hasani H Modeling the Compliance of Polyurethane Nanofiber Tubes for Artificial Common Bile Duct. *Mater. Res. Express* 2018, 5, 025004.
- (965). Wang X; Shan H; Wang J; Hou Y; Ding J; Chen Q; Guan J; Wang C; Chen X Characterization of Nanostructured Ureteral Stent with Gradient Degradation in a Porcine Model. *Int. J. Nanomed* 2015, 10, 3055–3064.
- (966). Ajalloueian F; Lemon G; Hilborn J; Chronakis IS; Fossum M Bladder Biomechanics and the Use of Scaffolds for Regenerative Medicine in the Urinary Bladder. *Nat. Rev. Urol* 2018, 15, 155. [PubMed: 29434369]
- (967). Horst M; Milleret V; Noetzli S; Gobet R; Sulser T; Eberli D Polyesterurethane and Acellular Matrix Based Hybrid Biomaterial for Bladder Engineering. *J. Biomed. Mater. Res., Part B* 2017, 105, 658–667.
- (968). Ajalloueian F; Zeiai S; Fossum M; Hilborn JG Constructs of Electrospun PLGA, Compressed Collagen and Minced Urothelium for Minimally Manipulated Autologous Bladder Tissue Expansion. *Biomaterials* 2014, 35, 5741–5748. [PubMed: 24768046]
- (969). Wu T; Zheng H; Chen J; Wang Y; Sun B; Morsi Y; El-Hamshary H; Al-Deyab SS; Chen C; Mo X Application of a Bilayer Tubular Scaffold Based on Electrospun Poly(L-lactide-*co*-caprolactone)/Collagen Fibers and Yarns for Tracheal Tissue Engineering. *J. Mater. Chem. B* 2017, 5, 139–150.
- (970). Yang G; Li X; He Y; Ma J; Ni G; Zhou S From Nano to Micro to Macro: Electrospun Hierarchically Structured Polymeric Fibers for Biomedical Applications. *Prog. Polym. Sci* 2018, 81, 80–113.
- (971). Chen Z; Chen Z; Zhang A; Hu J; Wang X; Yang Z Electrospun Nanofibers for Cancer Diagnosis and Therapy. *Biomater. Sci* 2016, 4, 922–932. [PubMed: 27048889]
- (972). Paul KB; Singh V; Vanjari SRK; Singh SG One Step Biofunctionalized Electrospun Multiwalled Carbon Nanotubes Embedded Zinc Oxide Nanowire Interface for Highly Sensitive Detection of Carcinoma Antigen-125. *Biosens. Bioelectron* 2017, 88, 144–152. [PubMed: 27520500]
- (973). Ali MA; Mondal K; Jiao Y; Oren S; Xu Z; Sharma A; Dong L Microfluidic Immuno-Biochip for Detection of Breast Cancer Biomarkers Using Hierarchical Composite of Porous Graphene and Titanium Dioxide Nanofibers. *ACS Appl. Mater. Interfaces* 2016, 8, 20570–20582. [PubMed: 27442623]
- (974). Xue R; Behera P; Viapiano MS; Lannutti JJ Rapid Response Oxygen-Sensing Nanofibers. *Mater. Sci. Eng., C* 2013, 33, 3450–3457.
- (975). Xue R; Ge C; Richardson K; Palmer A; Viapiano M; Lannutti JJ Microscale Sensing of Oxygen via Encapsulated Porphyrin Nanofibers: Effect of Indicator and Polymer "Core" Permeability. *ACS Appl. Mater. Interfaces* 2015, 7, 8606–8614. [PubMed: 25850567]
- (976). Zhao Y; Fan Z; Shen M; Shi X Hyaluronic Acid-Functionalized Electrospun Polyvinyl Alcohol/Polyethyleneimine Nanofibers for Cancer Cell Capture Applications. *Adv. Mater. Interfaces* 2015, 2, 1500256.
- (977). Chen S; Boda SK; Batra SK; Li X; Xie J Emerging Roles of Electrospun Nanofibers in Cancer Research. *Adv. Healthcare Mater* 2018, 7, 1701024.
- (978). Ma L; Yang G; Wang N; Zhang P; Guo F; Meng J; Zhang F; Hu Z; Wang S; Zhao Y Trap Effect of Three-Dimensional Fibers Network for High Efficient Cancer-Cell Capture. *Adv. Healthcare Mater* 2015, 4, 838–843.
- (979). Xu G; Tan Y; Xu T; Yin D; Wang M; Shen M; Chen X; Shi X; Zhu X Hyaluronic Acid-Functionalized Electrospun PLGA Nanofibers Embedded in a Microfluidic Chip for Cancer Cell Capture and Culture. *Biomater. Sci* 2017, 5, 752–761. [PubMed: 28256649]
- (980). Zhao L; Lu YT; Li F; Wu K; Hou S; Yu J; Shen Q; Wu D; Song M; OuYang WH; et al. High-Purity Prostate Circulating Tumor Cell Isolation by a Polymer Nanofiber-Embedded Microchip for Whole Exome Sequencing. *Adv. Mater* 2013, 25, 2897–2902. [PubMed: 23529932]
- (981). Hou S; Zhao L; Shen Q; Yu J; Ng C; Kong X; Wu D; Song M; Shi X; Xu X; et al. Polymer Nanofiber-Embedded Microchips for Detection, Isolation, and Molecular Analysis of Single Circulating Melanoma Cells. *Angew. Chem., Int. Ed* 2013, 52, 3379–3383.

- (982). Yu CC; Ho BC; Juang RS; Hsiao YS; Naidu RVR; Kuo CW; You YW; Shyue JJ; Fang JT; Chen P Poly(3,4-ethylenedioxythiophene)-Based Nanofiber Mats as an Organic Bioelectronic Platform for Programming Multiple Capture/Release Cycles of Circulating Tumor Cells. *ACS Appl. Mater. Interfaces* 2017, 9, 30329–30342. [PubMed: 28825302]
- (983). Chen S; Li R; Li X; Xie J Electrospinning: An Enabling Nanotechnology Platform for Drug Delivery and Regenerative Medicine. *Adv. Drug Delivery Rev* 2018, 132, 188–213.
- (984). Janani G; Pillai MM; Selvakumar R; Bhattacharyya A; Sabarinath C An in Vitro 3D Model Using Collagen Coated Gelatin Nanofibers for Studying Breast Cancer Metastasis. *Biofabrication* 2017, 9, 015016. [PubMed: 28000609]
- (985). Ma NK; Lim JK; Leong MF; Sandanaraj E; Ang BT; Tang C; Wan AC Collaboration of 3D Context and Extracellular Matrix in the Development of Glioma Stemness in a 3D Model. *Biomaterials* 2016, 78, 62–73. [PubMed: 26684838]
- (986). Domura R; Sasaki R; Okamoto M; Hirano M; Kohda K; Napiwocki B; Turng L-S Comprehensive Study on Cellular Morphologies, Proliferation, Motility, and Epithelial-Mesenchymal Transition of Breast Cancer Cells Incubated on Electrospun Polymeric Fiber Substrates. *J. Mater. Chem. B* 2017, 5, 2588–2600.
- (987). Jain A; Betancur M; Patel GD; Valmikinathan CM; Mukhatyar VJ; Vakharia A; Pai SB; Brahma B; MacDonald TJ; Bellamkonda RV Guiding Intracortical Brain Tumour Cells to an Extracortical Cytotoxic Hydrogel Using Aligned Polymeric Nano-fibres. *Nat. Mater* 2014, 13, 308–316. [PubMed: 24531400]
- (988). Acevedo F; Hermosilla J; Sanhueza C; Mora-Lagos B; Fuentes I; Rubilar M; Concheiro A; Alvarez-Lorenzo C Gallic Acid Loaded PEO-Core/Zein-Shell Nanofibers for Chemopreventive Action on Gallbladder Cancer Cells. *Eur. J. Pharm. Sci* 2018, 119, 49–61.
- (989). Yohe ST; Herrera VL; Colson YL; Grinstaff MW 3D Superhydrophobic Electrospun Meshes as Reinforcement Materials for Sustained Local Drug Delivery against Colorectal Cancer Cells. *J. Controlled Release* 2012, 162, 92–101.
- (990). Chen Z; Liu W; Zhao L; Xie S; Chen M; Wang T; Li X Acid-Labile Degradation of Injectable Fiber Fragments to Release Bioreducible Micelles for Targeted Cancer Therapy. *Biomacromolecules* 2018, 19, 1100–1110.
- (991). Zhao X; Yuan Z; Yildirimer L; Zhao J; Lin ZY; Cao Z; Pan G; Cui W Tumor-Triggered Controlled Drug Release from Electrospun Fibers Using Inorganic Caps for Inhibiting Cancer Relapse. *Small* 2015, 11, 4284–4291. [PubMed: 26034038]
- (992). Lei C; Cui Y; Zheng L; Kah-Hoe Chow P; Wang CH Development of a Gene/Drug Dual Delivery System for Brain Tumor Therapy: Potent Inhibition via RNA Interference and Synergistic Effects. *Biomaterials* 2013, 34, 7483–7494. [PubMed: 23820014]
- (993). PK Papyrus: Coronary Balloon-Expandable Stent Systems; Biotronik, <https://www.biotronik.com/en-us/products/vi/coronary/pk-papyrus>.
- (994). Wang J; An Q; Li D; Wu T; Chen W; Sun B; Ei-Hamshary H; Al-Deyab SS; Zhu W; Mo X Heparin and Vascular Endothelial Growth Factor Loaded Poly (L-lactide-*co*-caprolactone) Nanofiber Covered Stent-Graft for Aneurysm Treatment. *J. Biomed. Nanotechnol* 2015, 11, 1947–1960. [PubMed: 26554154]
- (995). ReDura: Biomimetic-Synthetic-Absorbable Dural Substitute; Medprin, <http://www.medprin.cn/vancheerfile/files/2017/2/2017022011042808.pdf>.
- (996). NeoDura: Absorbable Dural Repair Patch; Medprin, <http://www.medprin.cn/en/product/show.aspx?m=123007001&i=100000020466455>.
- (997). Shalumon KT; Sheu C; Chen CH; Chen SH; Jose G; Kuo CY; Chen JP Multi-Functional Electrospun Antibacterial Core-Shell Nanofibrous Membranes for Prolonged Prevention of Post-Surgical Tendon Adhesion and Inflammation. *Acta Biomater* 2018, 72, 121–136. [PubMed: 29626695]
- (998). Selvam AK; Nallathambi G Polyacrylonitrile/Silver Nanoparticle Electrospun Nanocomposite Matrix for Bacterial Filtration. *Fibers Polym* 2015, 16, 1327–1335.
- (999). Guo S; Ke Q; Wang H; Jin X; Li Y Poly(butylene terephthalate) Electrospun/Melt-Blown Composite Mats for White Blood Cell Filtration. *J. Appl. Polym. Sci* 2013, 128, 3652–3659.

- (1000). Wang Z; Zheng W; Wu Y; Wang J; Zhang X; Wang K; Zhao Q; Kong D; Ke T; Li C Differences in the Performance of PCL-Based Vascular Grafts as Abdominal Aorta Substitutes in Healthy and Diabetic Rats. *Biomater. Sci* 2016, 4, 1485–1492. [PubMed: 27537499]
- (1001). Motamed AS; Mirzadeh H; Hajiesmaeilbaigi F; Bagheri-Khoulenjani S; Shokrgozar MA Piezoelectric Electrospun Nanocomposite Comprising Au NPs/PVDF for Nerve Tissue Engineering. *J. Biomed. Mater. Res., Part A* 2017, 105, 1984–1993.
- (1002). Li H; Wu T; Xie M; Shi Y; Shen S; Zhao M; Yang X; Figueroa-Cosme LM; Ke Q; Xia Y Enhancing the Tactile and Near-Infrared Sensing Capabilities of Electrospun PVDF Nanofibers with the Use of Gold Nanocages. *J. Mater. Chem. C* 2018, 6, 10263–10269.
- (1003). Wu T; Li H; Xie M; Shen S; Wang W; Zhao M; Mo X; Xia Y Incorporation of Gold Nanocages into Electrospun Nanofibers for Efficient Water Evaporation through Photothermal Heating. *Mater. Today Energy* 2019, 12, 129–135.
- (1004). Global Nanofibers Market: Trends Analysis & Forecasts to 2021; Research and Markets, https://www.researchandmarkets.com/research/5psrpd/global_nanofibers.
- (1005). Nanospinner 416 Industrial Electrospinning Line; inovenso, <https://www.inovenso.com/portfolio-view/nanospinner416>.
- (1006). Technology page; Elmarco, <http://www.elmarco.com>.
- (1007). Elmarco, http://www.elmarco.com/upload/obrazky/galerie_obrazku/production-line-ns-8s1600u-3-43.jpg.
- (1008). Li H; Chen H; Zhong X; Wu W; Ding Y; Yang W Interjet Distance in Needleless Melt Differential Electrospinning with Umbellate Nozzles. *J. Appl. Polym. Sci* 2014, 131, 40515.
- (1009). Zander NE; Sweetser D; Cole DP; Gillan M Formation of Nanofibers from Pure and Mixed Waste Streams Using Electrospinning. *Ind. Eng. Chem. Res* 2015, 54, 9057–9063.
- (1010). Strain IN; Wu Q; Pourrahimi AM; Hedenqvist MS; Olsson RT; Andersson RL Electrospinning of Recycled PET to Generate Tough Mesomorphic Fibre Membranes for Smoke Filtration. *J. Mater. Chem. A* 2015, 3, 1632–1640.
- (1011). Schinwald A; Murphy FA; Prina-Mello A; Poland CA; Byrne F; Movia D; Glass JR; Dickerson JC; Schultz DA; Jeffree CE; et al. The Threshold Length for Fiber-Induced Acute Pleural Inflammation: Shedding Light on the Early Events in Asbestos-Induced Mesothelioma. *Toxicol. Sci* 2012, 128, 461–470. [PubMed: 22584686]
- (1012). Maynard AD; Aitken RJ; Butz T; Colvin V; Donaldson K; Oberdörster G; Philbert MA; Ryan J; Seaton A; Stone V; Tinkle SS; Tran L; Walker NJ; Warheit DB Safe Handling of Nanotechnology. *Nature* 2006, 444, 267–269. [PubMed: 17108940]
- (1013). Donaldson K; Tran CL An Introduction to the Short-Term Toxicology of Respirable Industrial Fibres. *Mutat. Res., Fundam. Mol. Mech. Mutagen* 2004, 553, 5–9.
- (1014). Asbestos Exposure and Cancer Risk; National Cancer Institute, <https://www.cancer.gov/about-cancer/causes-prevention/risk/substances/asbestos/asbestos-fact-sheet>.
- (1015). Li W-C; Fu N-F; Wu J-C; Li X-J; Pan R-H; Zheng Y-Y; Gan Y-J; Ling J-A; Liang H-Q; Liang D-Y Inhalation of Bacterial Cellulose Nanofibers Facilitates Silica Particle Clearance in a Rat Silicosis Model. *Am. J. Clin. Exp. Med* 2016, 4, 204–211.
- (1016). Kenry; Lim CT Nanofiber Technology: Current Status and Emerging Developments. *Prog. Polym. Sci* 2017, 70, 1–17.
- (1017). Weitz RT; Harnau L; Rauschenbach S; Burghard M; Kern K Polymer Nanofibers via Nozzle-Free Centrifugal Spinning. *Nano Lett* 2008, 8, 1187–1191. [PubMed: 18307320]
- (1018). Badrossamay MR; McIlwee HA; Goss JA; Parker KK Nanofiber Assembly by Rotary Jet-Spinning. *Nano Lett* 2010, 10, 2257–2261. [PubMed: 20491499]
- (1019). Ren L; Pandit V; Elkin J; Denman T; Cooper JA; Kotha SP Large-Scale and Highly Efficient Synthesis of Micro-and Nano-Fibers with Controlled Fiber Morphology by Centrifugal Jet Spinning for Tissue Regeneration. *Nanoscale* 2013, 5, 2337–2345. [PubMed: 23392606]
- (1020). Sarkar K; Gomez C; Zambrano S; Ramirez M; de Hoyos E; Vasquez H; Lozano K Electrospinning to Forcespinning. *Mater. Today* 2010, 13, 12–14.
- (1021). Smoukov SK; Tian T; Vitchuli N; Gangwal S; Geisen P; Wright M; Shim E; Marquez M; Fowler J; Velev OD Scalable Liquid Shear-Driven Fabrication of Polymer Nanofibers. *Adv. Mater* 2015, 27, 2642–2647. [PubMed: 25788298]

- (1022). Tokarev A; Trotsenko O; Griffiths IM; Stone HA; Minko S Magnetospinning of Nano-and Microfibers. *Adv. Mater* 2015, 27, 3560–3565. [PubMed: 25953082]
- (1023). Tokarev A; Asheghali D; Griffiths IM; Trotsenko O; Gruzd A; Lin X; Stone HA; Minko S Touch-and Brush-Spinning of Nanofibers. *Adv. Mater* 2015, 27, 6526–6532. [PubMed: 26395284]
- (1024). Mahalingam S; Edirisinghe M Forming of Polymer Nanofibers by a Pressurised Gyration Process. *Macromol. Rapid Commun* 2013, 34, 1134–1139. [PubMed: 23749758]
- (1025). Heseltine PL; Ahmed J; Edirisinghe M Developments in Pressurized Gyration for the Mass Production of Polymeric Fibers. *Macromol. Mater. Eng* 2018, 303, 1800218.

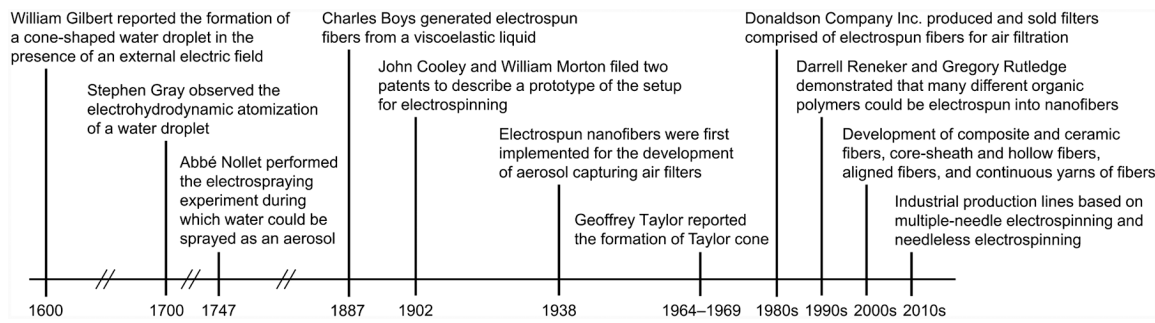


Figure 1.
Brief summary of the development history of electrospinning.

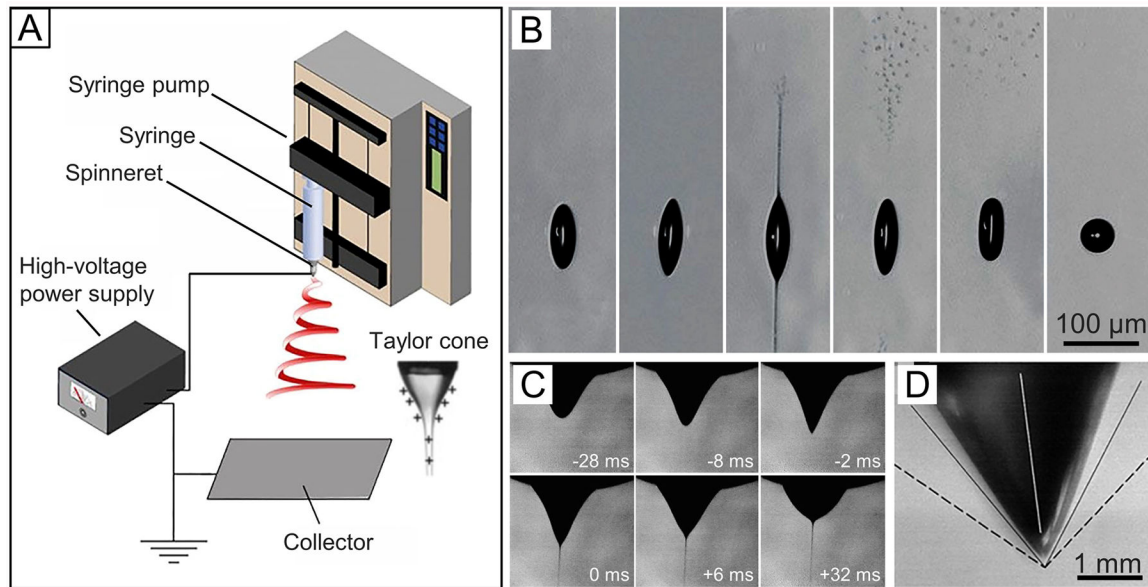
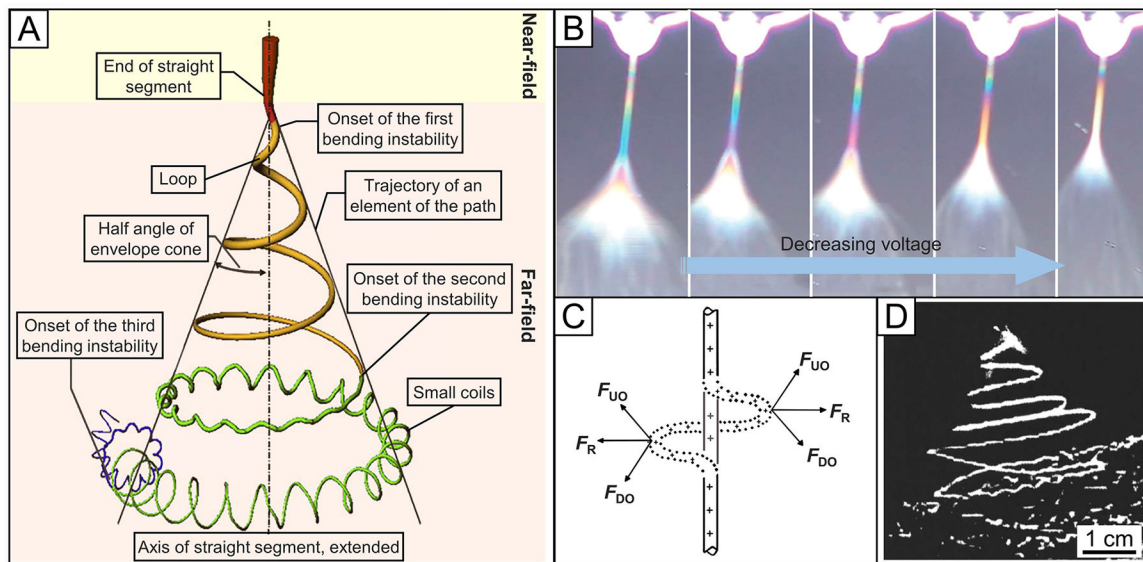


Figure 2.

(A) Basic setup for electrospinning. (B) High-speed photographs showing the disintegration of a levitated droplet of ethylene glycol charged to the Rayleigh limit for the ejection of two jets. (C) Photographs showing the evolution of a pendant drop of PEO in water from a spherical to a conical shape, followed by the ejection of a jet. (D) Photograph of the droplet at the critical point. (A) Reprinted with permission from ref 42. Copyright 2017 American Chemical Society. (B) Reprinted with permission from ref 45. Copyright 2003 Springer Nature. (C) Reprinted with permission from ref 50. Copyright 2008 Elsevier. (D) Reprinted with permission from ref 51. Copyright 2001 AIP Publishing.

**Figure 3.**

(A) Diagram showing the path of an electrospun jet. (B) Characteristic interference colors observed in the straight segment of a jet comprised of aqueous PEO, providing live information about the jet diameter and length of straight segment as a function of the applied voltage. (C) Schematic illustration of the forces acting on a charged jet. The perturbed segment is forced by F_{DO} downward and outward by the charges above the perturbed region. At the same time, the perturbed segment is forced by F_{UO} upward and outward by the charges below the perturbation. The net force, F_R (the lateral electrostatic force), is along a radial direction with respect to the straight jet, and it grows exponentially with time as the radial displacement of the segment increases. F_R is responsible for the bending of the jet. (D) Stereographic image showing the instantaneous position of the bending jet during the different stages of bending instabilities. (A, B, and D) Adapted with permission from ref 47. Copyright 2006 American Chemical Society. (C) Reprinted with permission from ref 50. Copyright 2008 Elsevier.

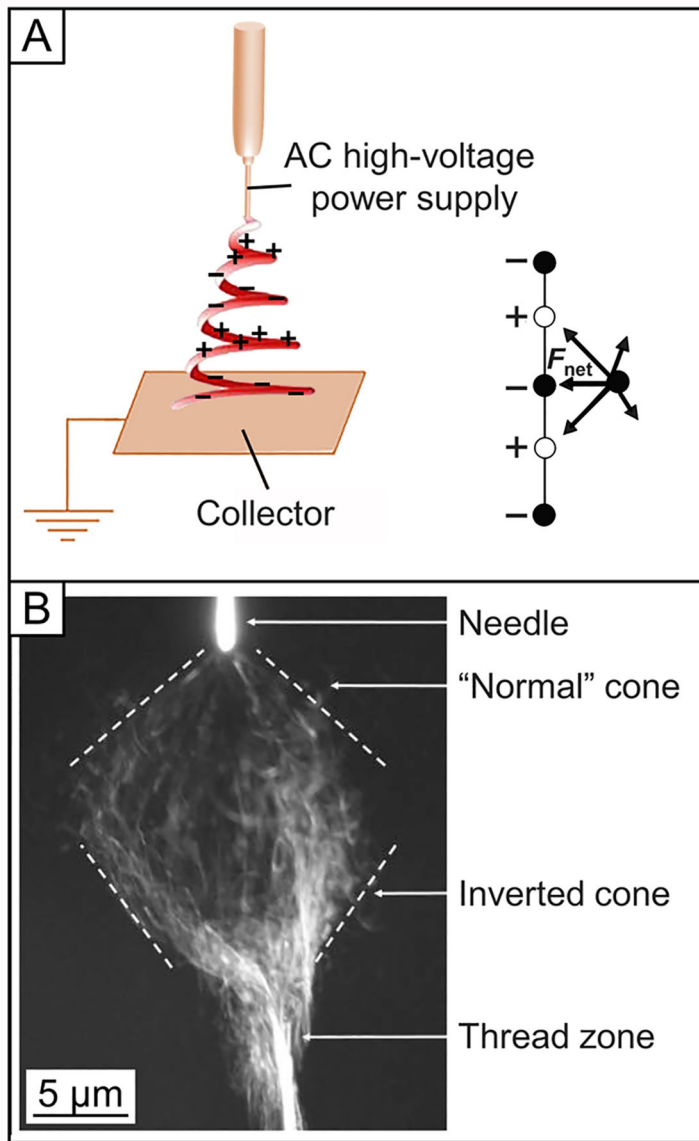


Figure 4.

(A) Illustration of AC electrospinning, and the forces acting on a displaced segment of an electrically charged jet. (B) Photograph of the jet during AC electrospinning, which was taken at an exposure time of 0.02 s. The whipping envelope can be seen as a combination of a normal, upright cone and an inverted cone. A distinct thread zone is seen below the apex of the inverted cone. Reprinted with permission from refs 76 and 77. Copyright 2007 and 2009 Wiley-VCH, respectively.

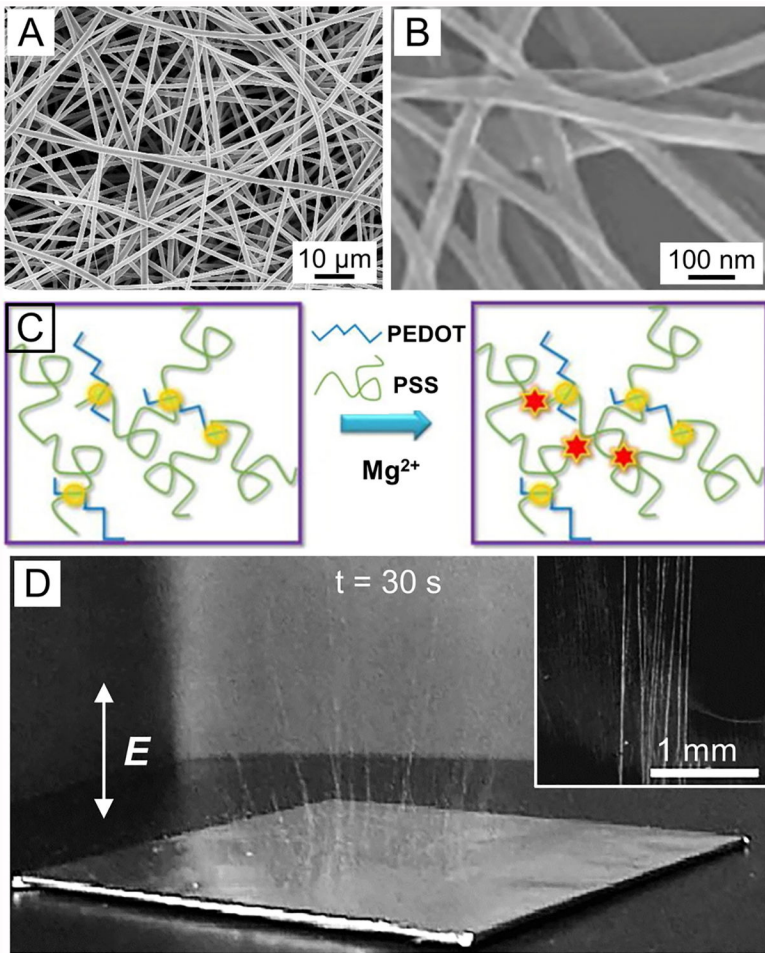
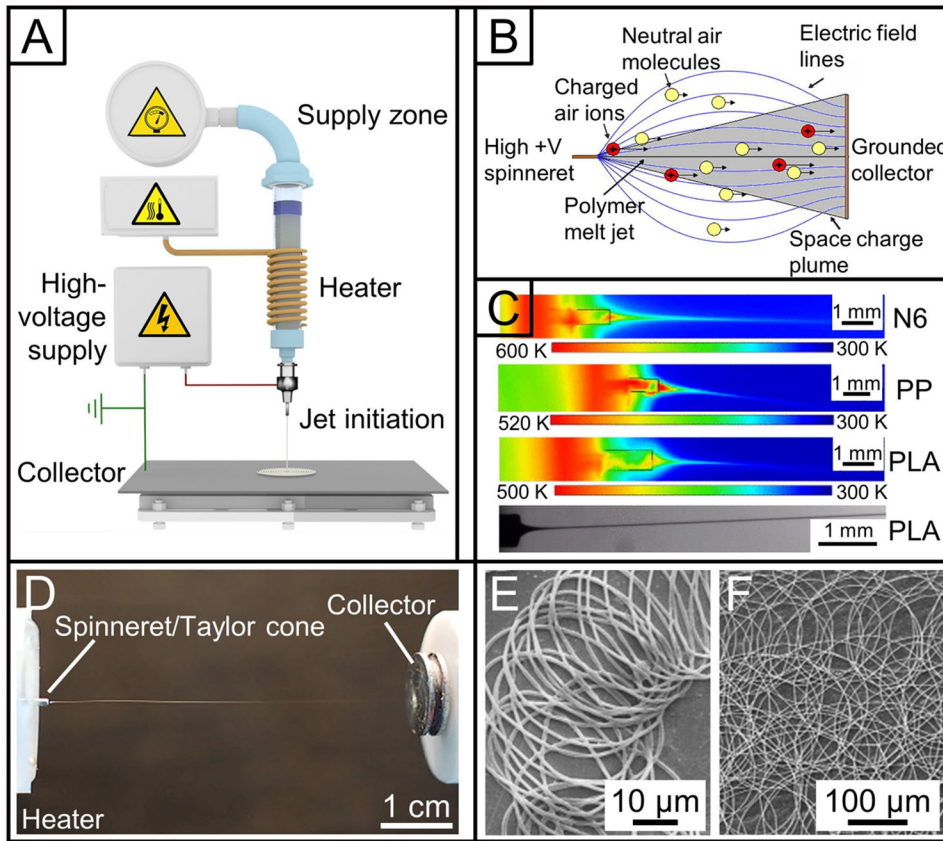
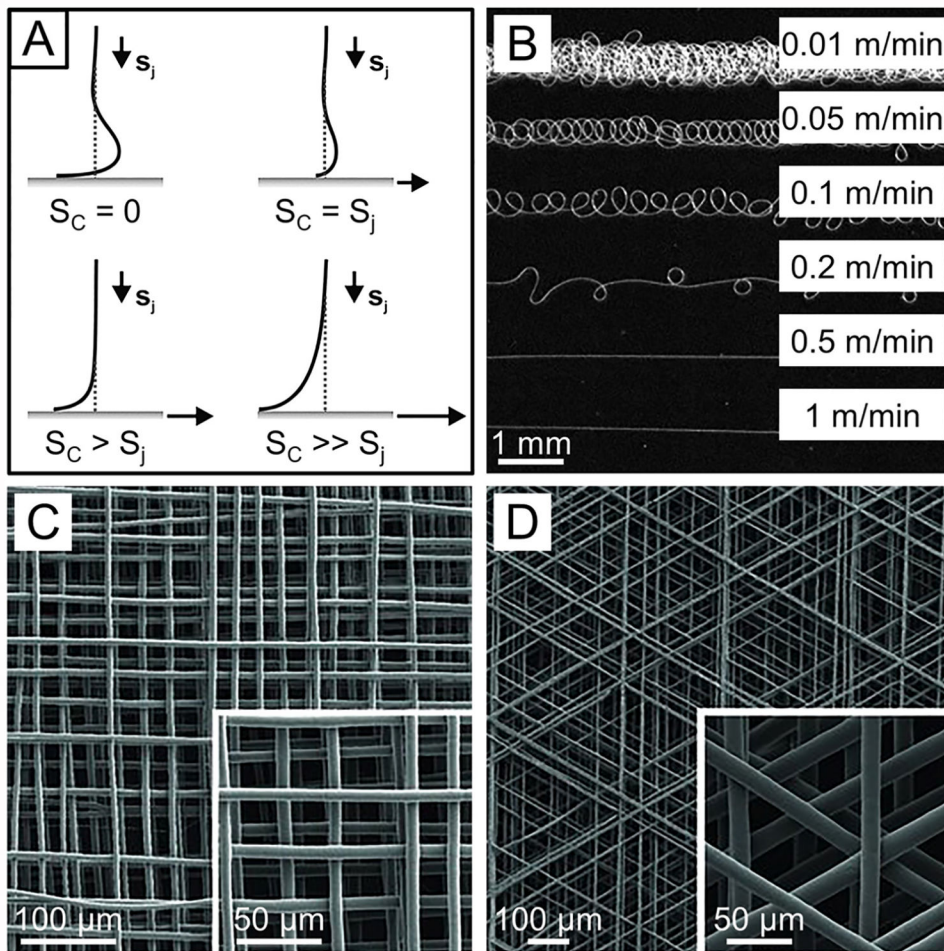


Figure 5.

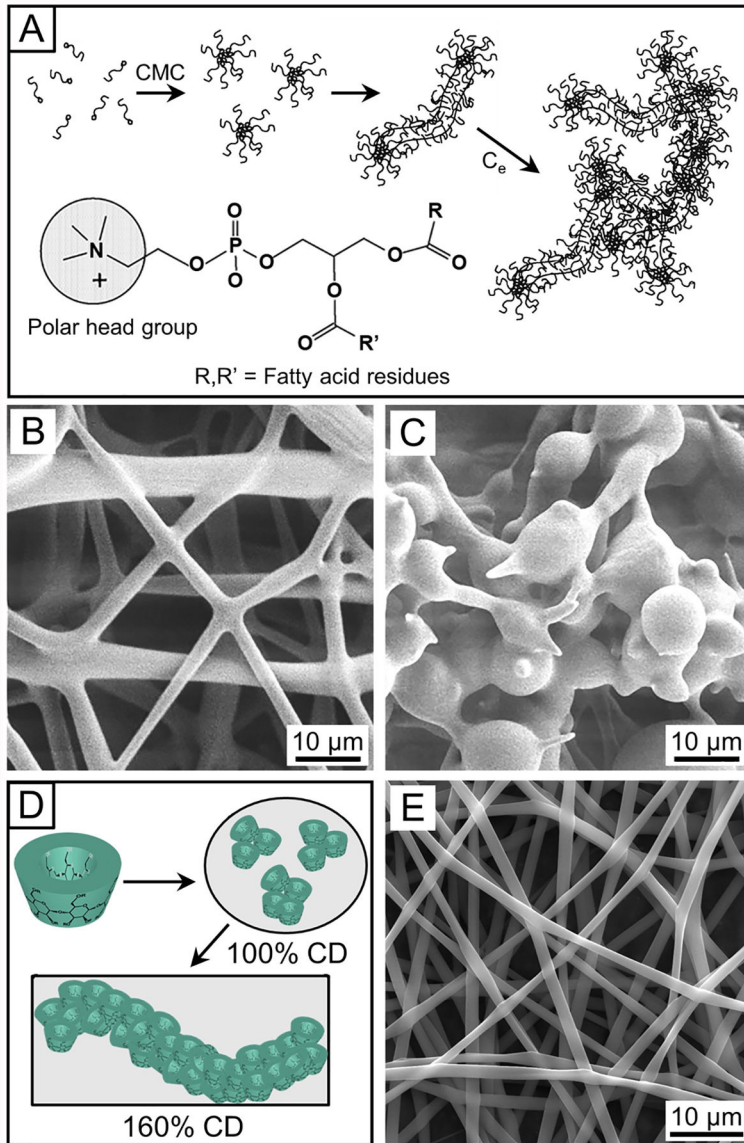
(A) SEM image of a typical example of electrospun PVP nanofibers, indicating the formation of a nonwoven mat. (B) SEM image of nanofibers made of a blend of PEDOT and PSS electrospun from an aqueous mixture containing Mg(NO₃)₂. (C) Schematic diagram showing the physical cross-linking of PEDOT and PSS by Mg²⁺ ions for the improvement of viscoelasticity. (D) Photograph showing the formation of “standing fibers” during the electrospinning of conductive polymers. The inset shows a magnified view. (B and C) Reprinted with permission from ref 91. Copyright 2015 Elsevier. (D) Reprinted with permission from ref 92. Copyright 2006 American Chemical Society.

**Figure 6.**

(A) Schematic illustration of a setup for electrospinning a polymer melt onto a static collector. (B) Illustration of electrohydrodynamically driven air flow for melt electrospinning, which is capable of enhancing the heat transfer between the jet and the surrounding medium (typically, air) by 1 order of magnitude. (C) Temperature profiles showing rapid cooling of electrospun nylon-6 (N6), PP, and PLA molten jets, as well as a photograph of the PLA molten jet. (D) Photograph of a molten jet during melt electrospinning. The molten pendant droplet has one single Taylor cone that is elongated while the jet is particularly long and is visible over almost the entire distance to the collector. (E and F) SEM images showing typical examples of coiled fibers commonly observed during melt electrospinning. The coiled fibers were formed from molten jets of (E) PP and (F) a blend of poly(ethylene glycol) (PEG)-b-PCL and PCL, respectively. (A) Reprinted with permission from ref 99. Copyright 2016 Elsevier. (B and C) Reprinted with permission from ref 103. Copyright 2011 AIP Publishing. (D–F) Reprinted with permission from ref 107. Copyright 2007 Elsevier.

**Figure 7.**

(A) Correlation between the shape of the jet and the speed of the collector (S_C) relative to the speed of the jet (S_j) during melt electrospinning. (B) Photograph of PCL fibers produced by melt electrospinning. The collector was moving at constant horizontal speeds that increase from the top to the bottom as indicated on the images. (C and D) SEM images showing the assembly of PCL fibers into multilayered stacks with the orientation of fibers in adjacent layers rotated by 90° and 60°, respectively. Reprinted with permission from ref 109. Copyright 2011 Wiley-VCH.

**Figure 8.**

(A) Schematic showing the worm-like micelles of phospholipids entangled in a concentrated solution. (B and C) SEM images showing the morphologies of (B) lecithin fibers and (C) lecithin droplets obtained by electrospinning a lecithin solution in a 70:30 (wt %) mixture of chloroform and DMF at concentrations of 43 and 35 wt %, respectively. (D) Chemical structure of β -cyclodextrin (CD), and schematic illustration of the truncated, cone-shaped, molecular structure of CD. (E) SEM image of nanofibers produced by electrospinning a 120% (w/v) hydroxypropyl- β -CD solution in dimethylacetamide. (A–C) Reprinted with permission from ref 116. Copyright 2006 The American Association for the Advancement of Science. (D and E) Reprinted with permission from ref 124. Copyright 2012 Royal Society of Chemistry.

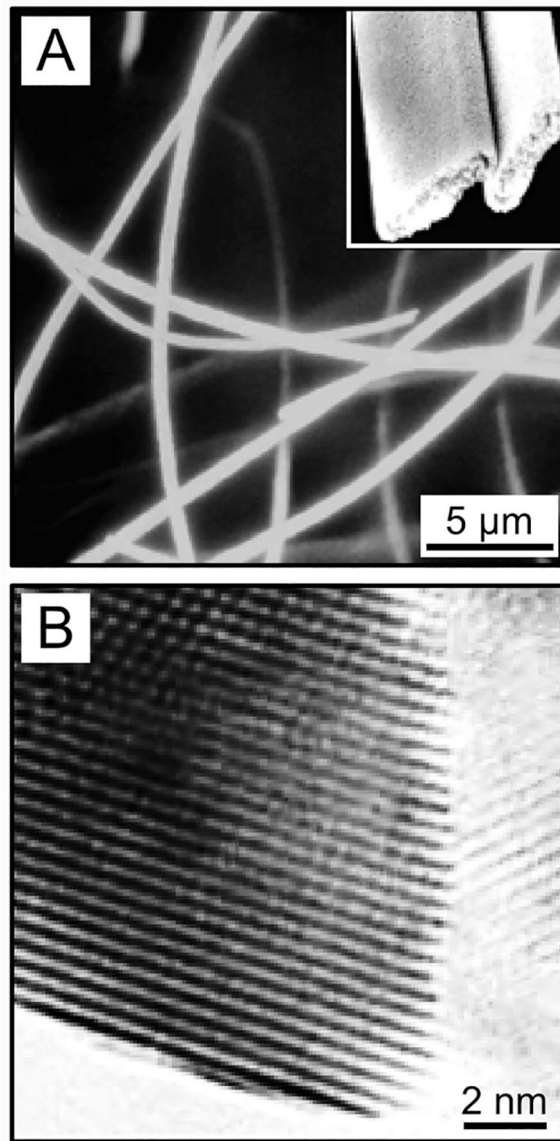
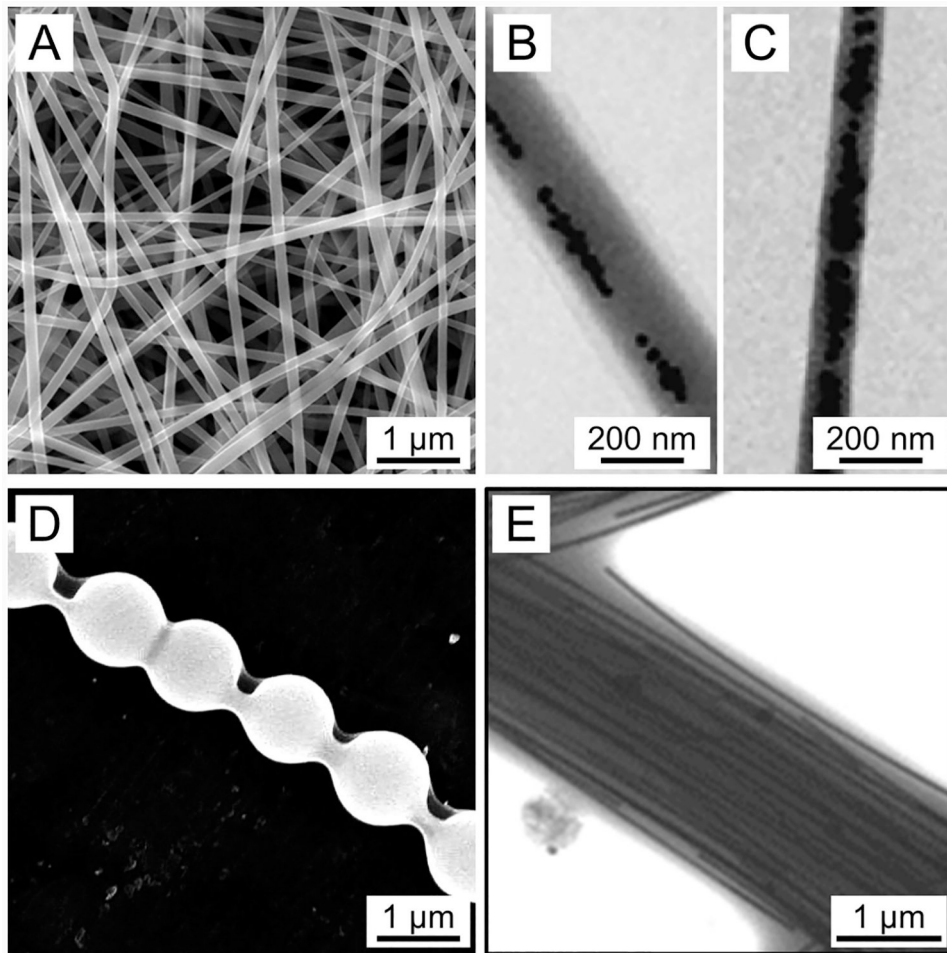
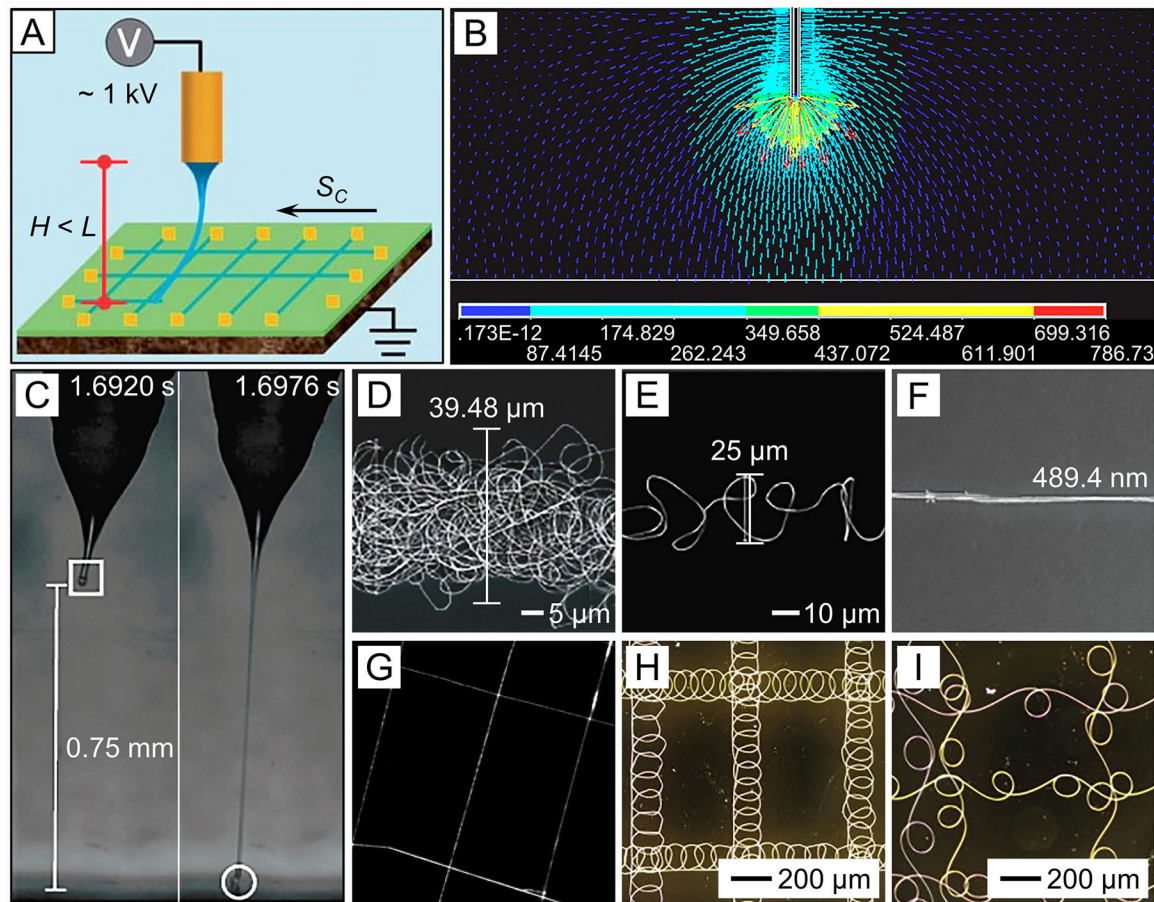


Figure 9.

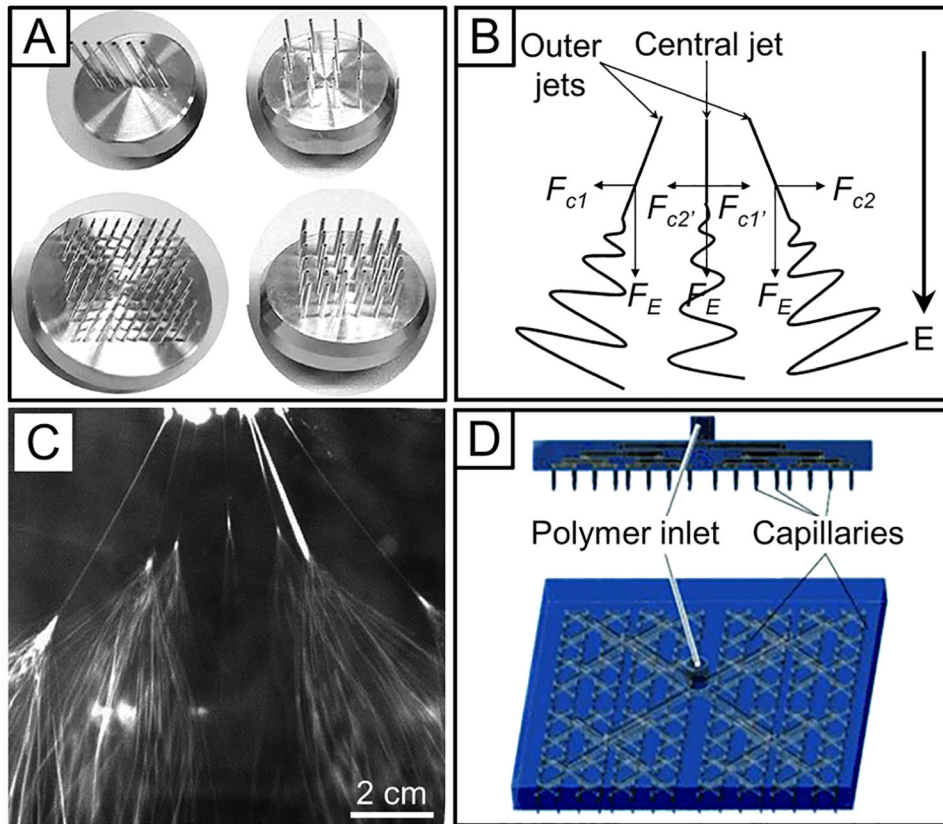
(A) SEM and (B) high-resolution TEM images of LiCoO_2 fibers with diameters in the range of $0.5\text{--}2 \mu\text{m}$, which were obtained by electrospinning an inorganic sol–gel solution prepared from lithium acetate, cobalt acetate, distilled water, and citric acid. The inset in panel A shows an enlarged view of the fibers. Reprinted with permission from ref 129. Copyright 2005 American Chemical Society.

**Figure 10.**

(A) SEM image of composite nanofibers comprised of PVP and amorphous TiO₂ electrospun from a PVP solution containing Ti(O*i*Pr)₄. (B and C) TEM images of representative composite nanofibers containing well-dispersed Ag nanoparticles fabricated by electrospinning an aqueous PVA solution containing Ag nanoparticles at Ag to PVA molar ratios of (B) 2:530 and (C) 4:530, respectively. (D) SEM image showing the necklace-like structure of a composite fiber comprised of PVA and 0.91 μm SiO₂ particles. (E) TEM image of a composite fiber comprised of PVP and Ag nanowires. More than 10 Ag nanowires could be assembled within and aligned along a single fiber. (A) Reprinted with permission from ref 132. Copyright 2003 American Chemical Society. (B and C) Reprinted with permission from ref 141. Copyright 2009 American Chemical Society. (D) Reprinted with permission from ref 142. Copyright 2010 American Chemical Society. (E) Reprinted with permission from ref 143. Copyright 2012 Wiley-VCH.

**Figure 11.**

(A) Schematic illustration of the setup for near-field electrospinning to directly write fibers on a moveable collector (at a moving speed of S_C) when the distance (H) between the tip of the spinneret and the collector is kept within the straight region (the critical length is L). (B) Electric field distribution around a needle tip in the near-field electrospinning process. (C) Photographs of a straight, charged PEO jet recorded using a high-speed camera during near-field electrospinning, and (D–F) SEM images of the PEO fibers deposited on a silicon substrate when the collector moved at speeds of (D) 0.03, (E) 0.20, and (F) 0.36 m/s, respectively. (G) SEM image of PEO fibers deposited in a pattern by controlling the motion of the collector along both X and Y directions during near-field electrospinning. (H and I) Optical micrographs of patterned arrays of coiled PS fibers obtained through near-field electrospinning. (A) Reprinted with permission from ref 144. Copyright 2013 Royal Society of Chemistry. (B) Reprinted with permission from ref 146. Copyright 2015 AIP Publishing. (C–F) Reprinted with permission from ref 147. Copyright 2010 IOP Publishing. (G) Reprinted with permission from ref 150. Copyright 2011 American Chemical Society. (H and I) Reprinted with permission from ref 151. Copyright 2012 Elsevier.

**Figure 12.**

(A) Examples of needle arrangement for multiple-needle electrospinning: 1D versus 2D array (e.g., square or rectangular pattern). (B) Path and force analyses of the central and outer jets during multiple-needle electrospinning. Besides electric field force (F_E), Coulombic force (F_C) is also exerted on each jet by their neighbors. (C) Photograph recorded using a high-speed camera, showing the behaviors of the jets in the multiple-needle electro-spinning process at an applied voltage of 20 kV with the use of seven hexagonally distributed needles. (D) Multiple-needle melt electro-spinning device produced by ITA-Aachen, Germany, with the use of 64 needles in an 8×8 array. (A) Reprinted with permission from ref 166. Copyright 2018 Wiley-VCH. (B and C) Reprinted with permission from ref 167. Copyright 2015 Royal Society of Chemistry.(D) Reprinted with permission from ref 100 Copyright 2011 Wiley-VCH.

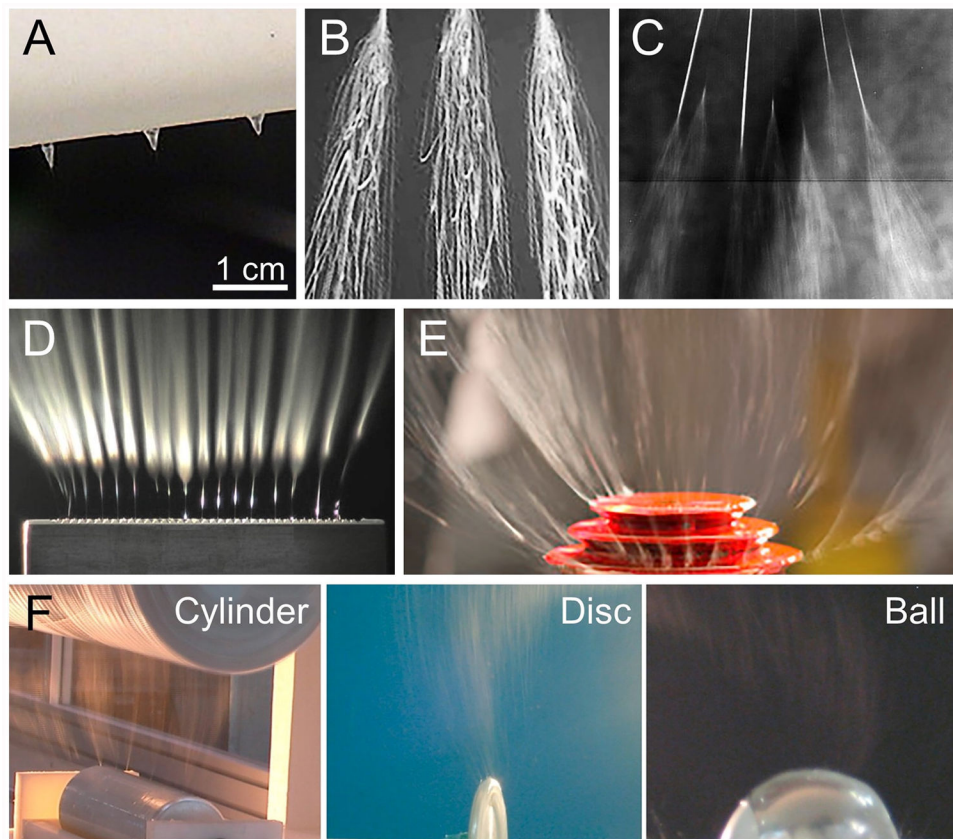
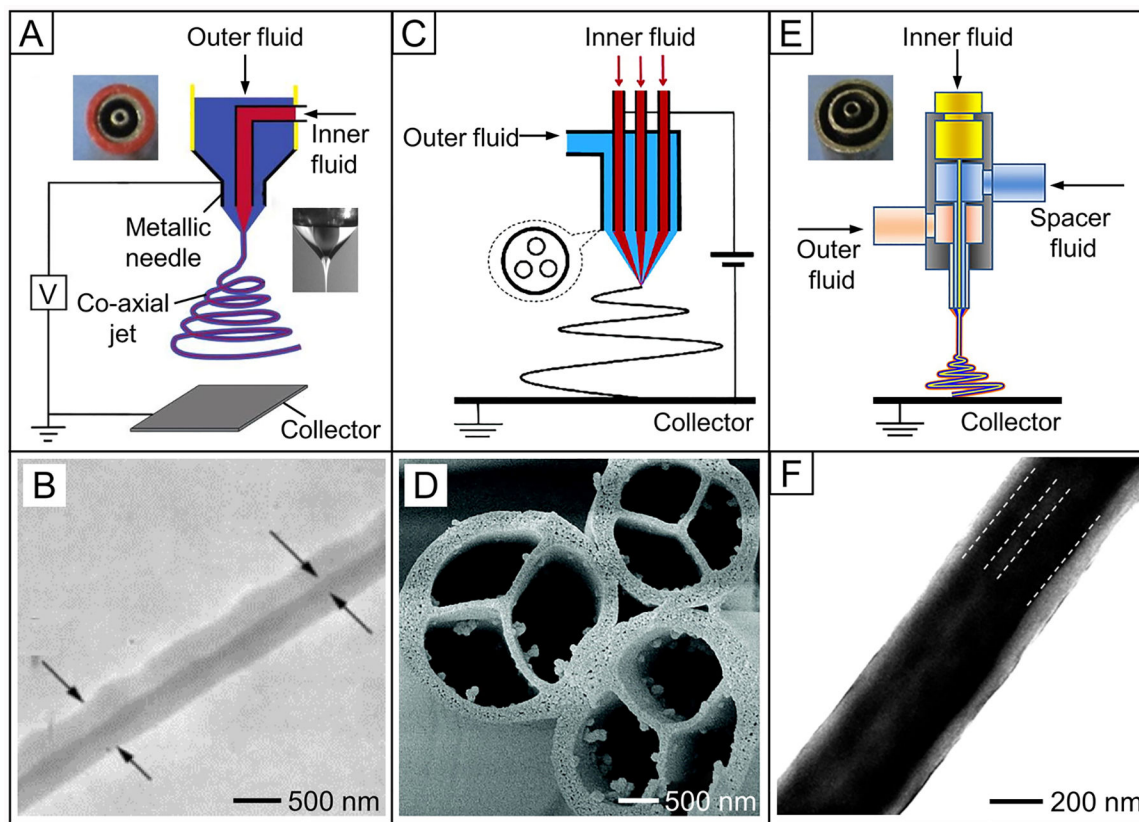
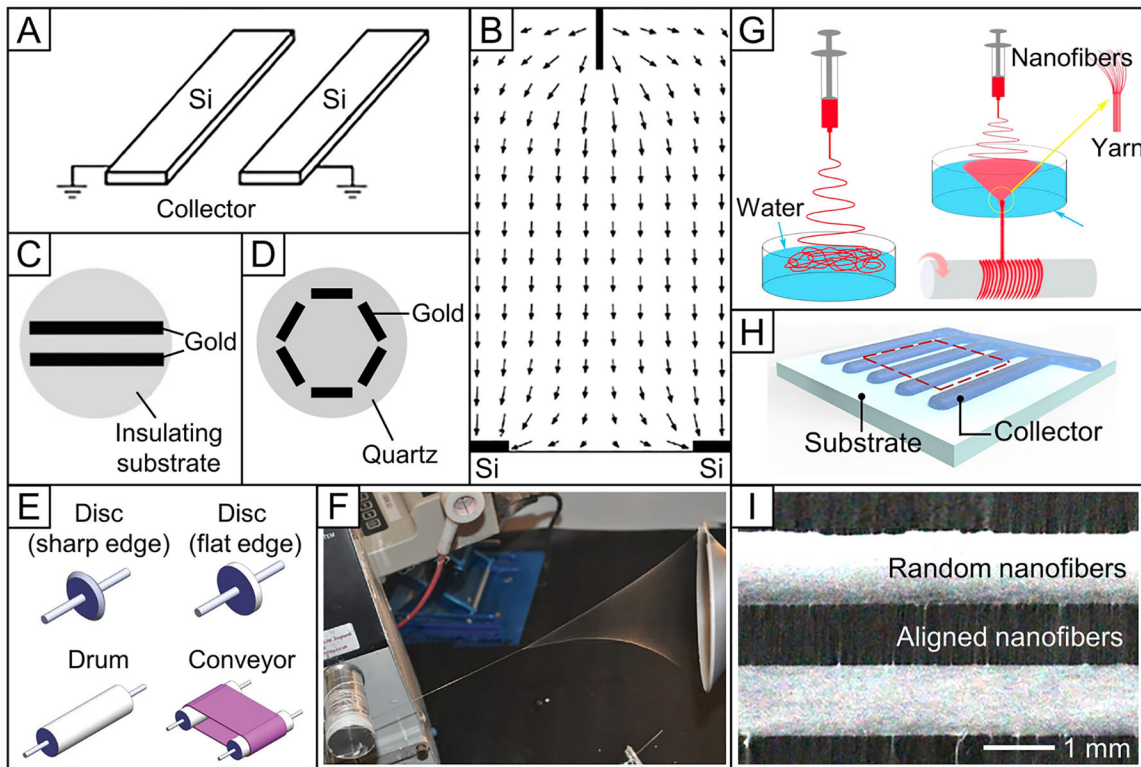


Figure 13.

(A) Photograph showing the conical drops of a polymer solution hanging from the bottom of a PTFE tube from the drilled holes, and (B) photograph of the multiple jets ejected from the holes. (C) Photograph of an electrospinning process that uses a metallic substrate containing seven holes as the spinneret, from which seven jets were simultaneously ejected. (D and E) Photographs of electrospinning processes that use (D) a jagged metallic plate and (E) a stepped pyramid as the solid spinnerets, respectively. (F) Photographs of electrospinning processes involving various rotatory solid spinnerets to eject multiple jets simultaneously. (A and B) Reprinted with permission from ref 175. Copyright 2008 Elsevier. (C) Reprinted with permission from ref 178. Copyright 2013 Wiley-VCH. (D) Reprinted with permission from ref 184. Copyright 2008 AIP Publishing. (E) Reprinted with permission from ref 186. Copyright 2015 Elsevier. (F) Reprinted with permission from ref 189. Copyright 2012 Taylor & Francis.

**Figure 14.**

(A) Schematic illustration of a coaxial electrospinning process. The inset to the left of the drawing shows a photograph of the concentric spinneret. The inset to the right of the drawing shows a photograph of the structured Taylor cone emerging from the vertexes of the two menisci, which involves water coated by a thin shell of olive oil. (B) TEM image of the PANi@PVA core–sheath nanofibers. The arrows indicate the outer edges of the sheath and core, respectively. (C) Schematic illustration of the electrospinning process with the use of a spinneret comprised of three metallic needles inserted in an outer needle in the pattern of an equilateral triangle, and (D) SEM image of the fibers in which the channels were divided into three independent flabellate parts by a Y-shaped inner ridge. (E) Triaxial electrospinning with the use of a concentric spinneret. The inset shows a photograph of the concentric spinneret. (F) TEM image of the fibers comprised of a trilayered structure made of DNA core, PCL intermediate layer, and nylon-6 outer sheath. (A) Adapted with permission from refs 194 and 195. Copyright 2004 and 2002 American Chemical Society and The American Association for the Advancement of Science, respectively. (B) Reprinted with permission from ref 196. Copyright 2004 Wiley-VCH. (C and D) Reprinted with permission from ref 219. Copyright 2007 American Chemical Society. (E and F) Reprinted with permission from ref 222. Copyright 2013 American Chemical Society.

**Figure 15.**

(A) Schematic illustration of a collector comprising two conductive substrates separated by a void gap and (B) calculated electric field strength vectors in the region between the needle and the collector. The arrows denote the directions of the electrostatic field lines. (C and D) Schematic illustrations of patterned collectors comprised of (C) two and (D) six gold electrodes deposited on a highly insulating substrate (such as quartz wafer). (E) Schematic illustrations of rotatory solid collectors (e.g., drum, disc, and conveyor). (F) Formation of a nanofiber yarn using rotary metal funnel as the collector, followed by continuously withdrawing and twisting the newly formed yarn with a winder. (G) Schematic illustrations of the setups that use a liquid bath to collect nanofibers or a liquid vortex to form a nanofiber yarn. (H) Schematic illustration showing the use of conductive liquid as the collector that is selectively deposited on a substrate, and (I) SEM image of a patterned mat obtained using a 3 M KCl solution as the collector. (A and B) Reprinted with permission from ref 35. Copyright 2003 American Chemical Society. (C and D) Reprinted with permission from ref 229. Copyright 2004 Wiley-VCH. (E) Reprinted with permission from ref 246. Copyright 2013 Wiley-VCH. (F) Reprinted with permission from ref 255. Copyright 2012 Taylor & Francis. (G) Reprinted with permission from ref 261. Copyright 2016 Elsevier. (H and I) Reprinted with permission from ref 267. Copyright 2018 American Chemical Society.

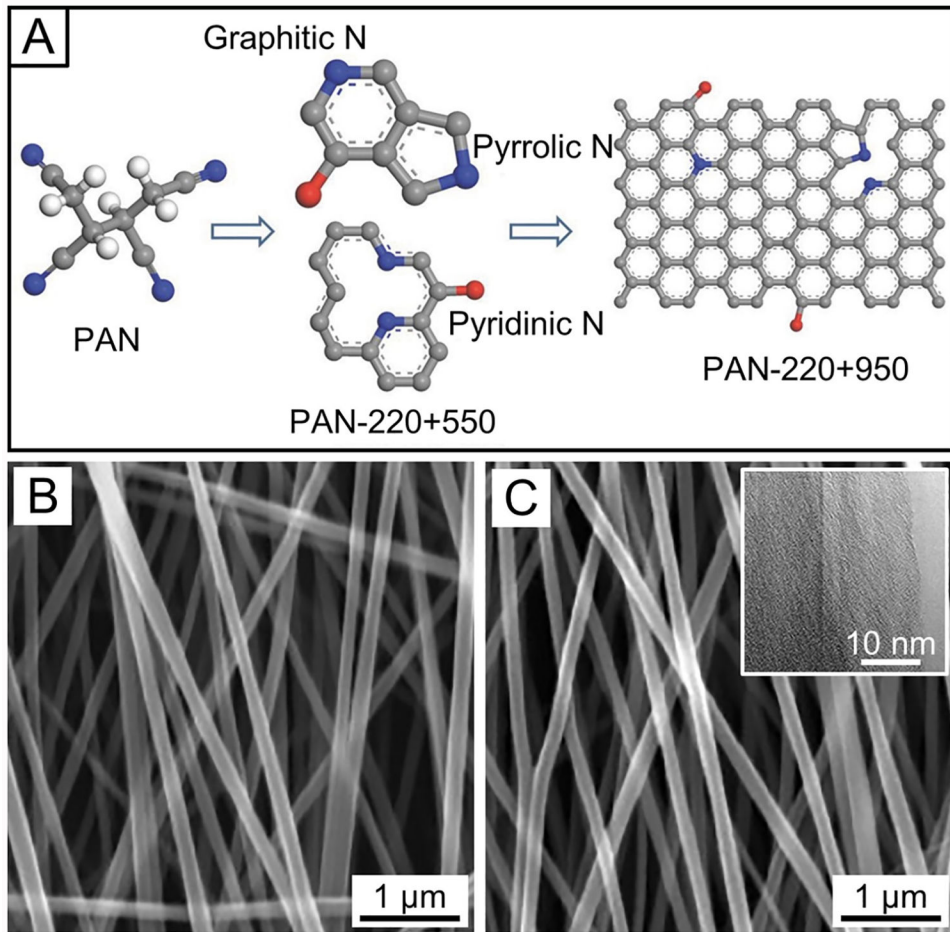
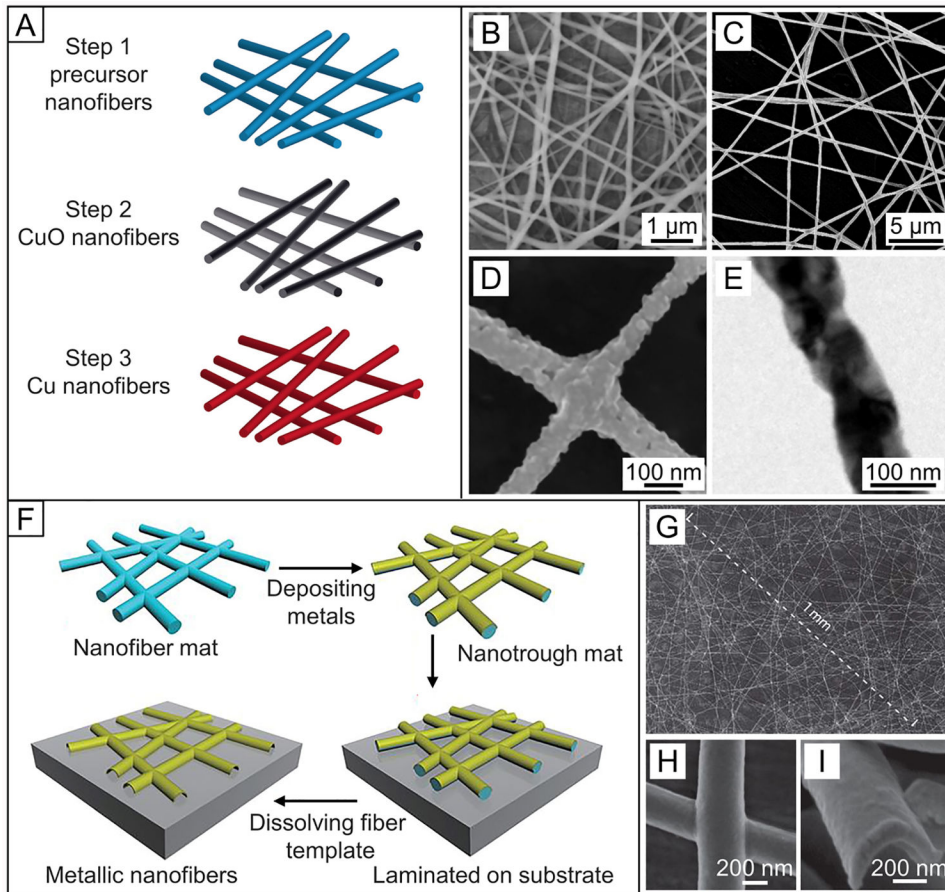


Figure 16.

(A) Schematic showing the structural evolution of PAN during thermal treatment (white = H atoms; gray = C atoms; blue = N atoms; and red = O atoms). SEM images of (B) the as-spun PAN nanofibers and (C) carbon nanofibers produced after carbonization at 1000 °C. The inset in panel C shows a TEM image of the carbon nanofibers. (A) Reprinted with permission from ref 272. Copyright 2014 Wiley-VCH. (B and C) Reprinted with permission from ref 273. Copyright 2009 Elsevier.

**Figure 17.**

(A) Schematic of an indirect method for the fabrication of metallic nanofibers. (B) SEM image of composite nanofibers comprising of PVA and copper acetate. (C and D) SEM image of Cu nanofibers at (C) low and (D) high magnifications produced after calcination of the composite nanofibers in air at 500 °C, showing fusion at the cross-points. (E) TEM image of the Cu nanofibers. (F) Schematic of an indirect, template-assisted method for the fabrication of metallic nanofibers by depositing metals on the surface of as-spun polymer nanofibers, followed by selective removal of the polymer template. (G and H) Top-view SEM images of a network of intertwined Au nanofibers at (G) low and (H) high magnifications, showing fusion at the cross-points. (I) SEM image of the cross-section of a single Au nanofiber, revealing its hollow shape. (A–E) Reprinted with permission from ref 287. Copyright 2010 American Chemical Society. (F–I) Reprinted with permission from ref 294. Copyright 2013 Springer Nature.

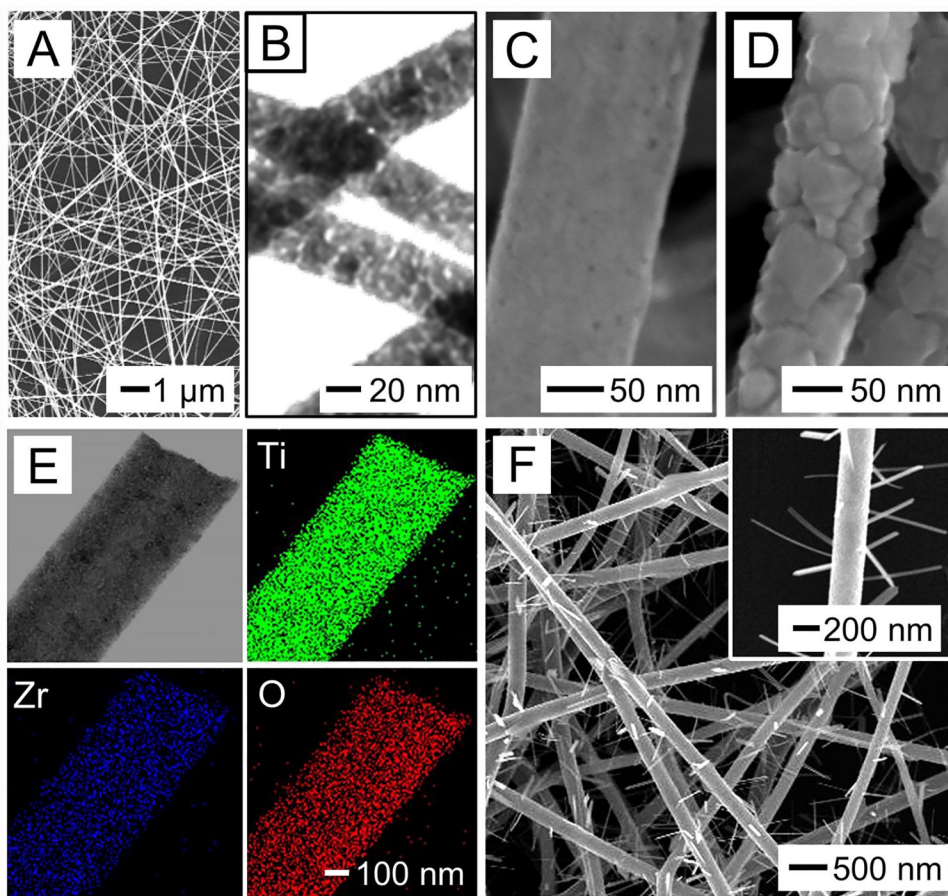
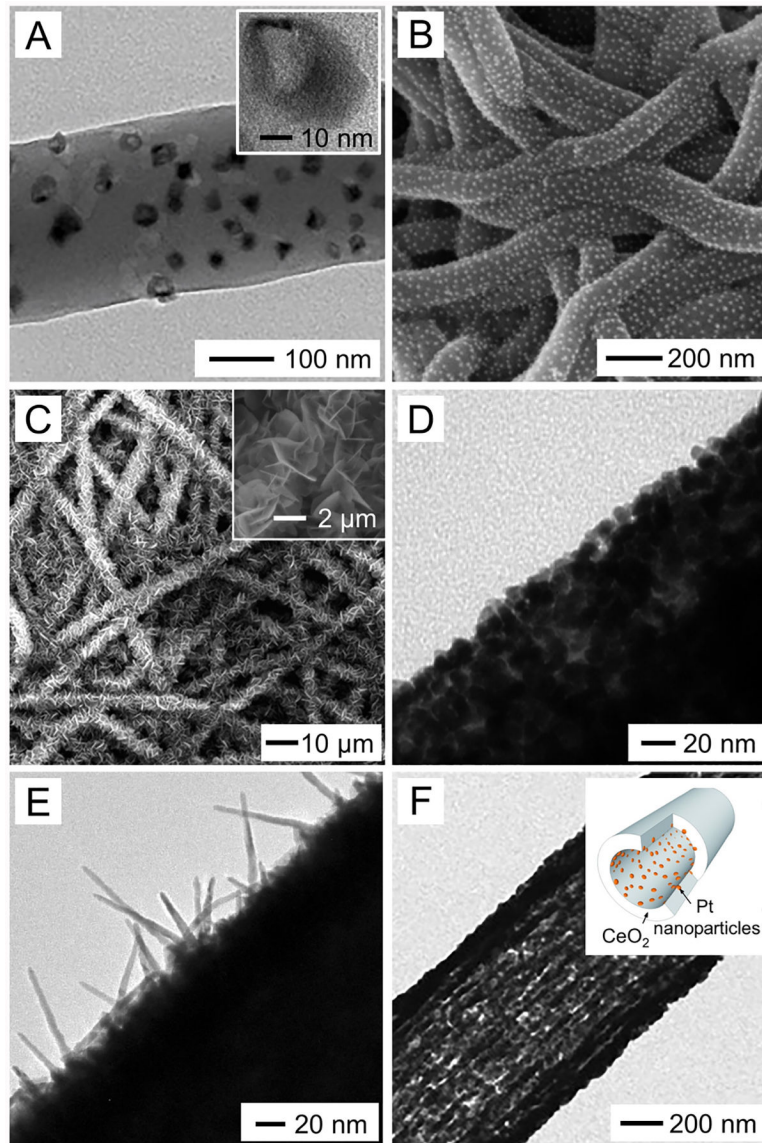


Figure 18.

(A and B) SEM and TEM images of the anatase nanofibers obtained by calcination of the composite nanofibers comprised of PVP and amorphous TiO₂ in air at 500 °C for 3 h. (C and D) High-magnification SEM images of anatase and rutile nanofibers, respectively, obtained by calcinating amorphous TiO₂ in air at 500 and 1000 °C. (E) TEM image of one representative Zr-doped TiO₂ nanofiber and the elemental maps of Ti, Zr, and O in the nanofiber. (F) SEM images at low and high (the inset) magnifications show the nanorod-on-nanofiber hierarchical nanostructure consisting of V₂O₅ nanorods grown on the surfaces of TiO₂ nanofibers. (A and B) Reprinted with permission from ref 132. Copyright 2003 American Chemical Society. (C and D) Reprinted with permission from ref 42. Copyright 2017 American Chemical Society. (E) Reprinted with permission from ref 301. Copyright 2017 Springer Nature. (F) Reprinted with permission from ref 302. Copyright 2006 American Chemical Society.

**Figure 19.**

(A) TEM image of a single carbon nanofiber containing Co_3O_4 hollow nanoparticles with nonuniform shell thicknesses. The inset gives TEM at a higher magnification, showing the structure of the Co_3O_4 hollow nanoparticle. (B) SEM image of PVA nanofibers with Au nanoparticles attached to the surface. (C) SEM image of PLGA nanofibers with nanoparticles of $\text{Ca}_3(\text{PO}_4)_2$ grown on the surface. The inset shows a magnified SEM image. (D and E) TEM images of anatase nanofiber with (D) Pt nanoparticles and (E) Pt nanorods grown on the surface. (F) TEM image and schematic illustration (inset) of a representative CeO_2 hollow nanofiber with Pt nanoparticles embedded in the inner surface. (A) Reprinted with permission from ref 321. Copyright 2013 Wiley-VCH. (B) Reprinted with permission from ref 323. Copyright 2012 American Chemical Society. (C) Reprinted with permission from ref 330. Copyright 2009 American Chemical Society. (D and E) Reprinted with

permission from ref 335. Copyright 2008 American Chemical Society. (F) Reprinted with permission from ref 340. Copyright 2012 Wiley-VCH.

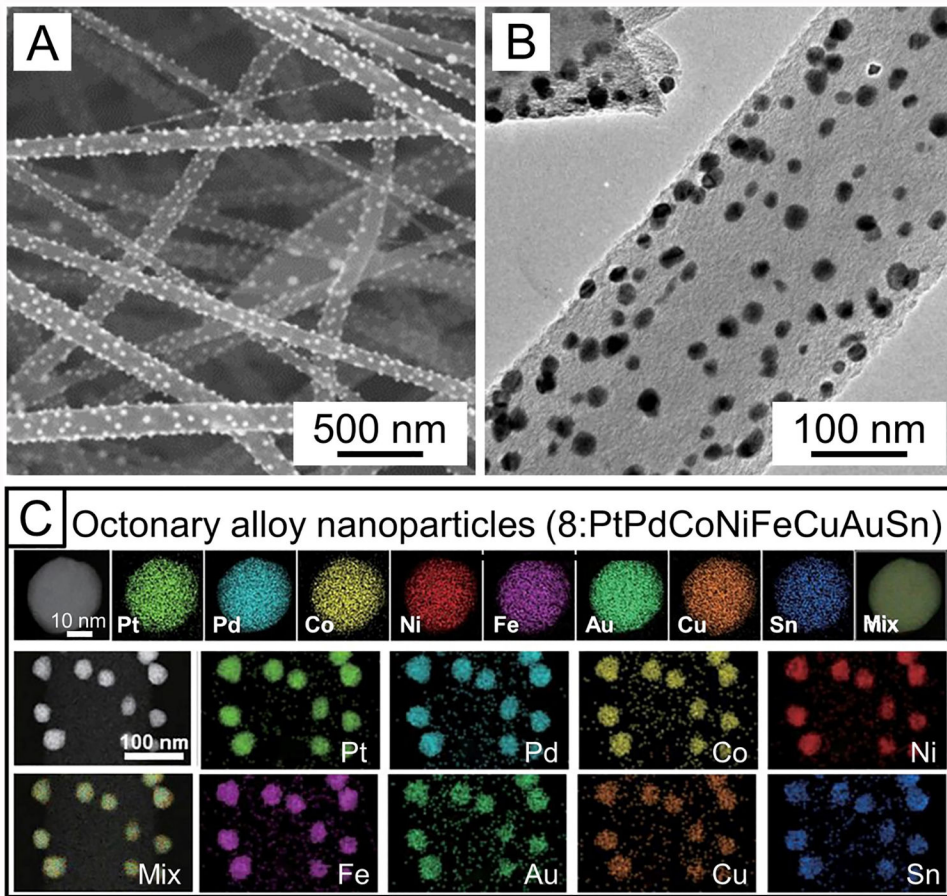


Figure 20.

(A) SEM and (B) TEM images of octonary alloy nanoparticles immobilized on carbon nanofibers that were derived from electrospun PAN nanofibers. (C) The high-angle annular dark-field images and scanning transmission electron microscopy elemental maps of octonary (PtPdCoNiFeCuAuSn) nanoparticle(s), verifying the compositional uniformity. Reprinted with permission from ref 341. Copyright 2018 The American Association for the Advancement of Science.

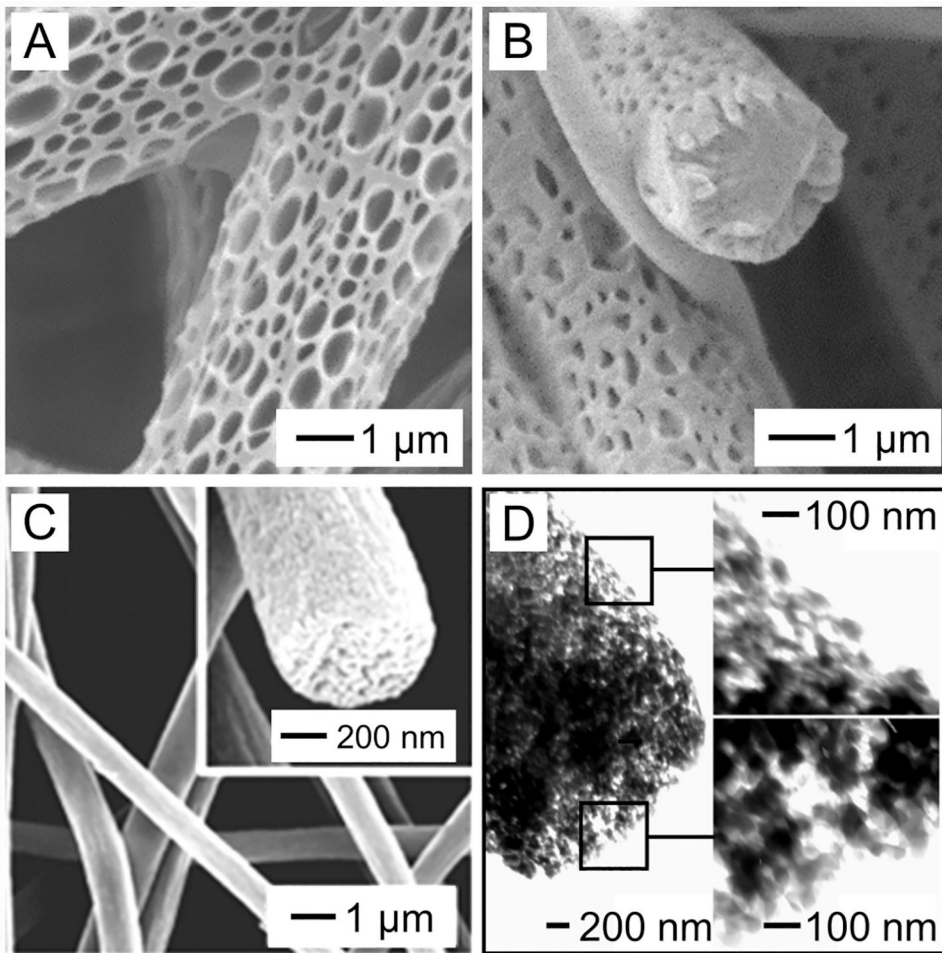


Figure 21.

SEM images of the (A) surface and (B) core of highly porous PLA nanofibers which were produced by electrospinning a 12.1 wt % PLA solution in dichloromethane. (C) SEM image of porous PS nanofibers prepared by electrospinning the jet into liquid nitrogen, followed by drying in vacuum. The inset gives an SEM image of the broken end of a nanofiber at a higher magnification, confirming that the fiber was porous throughout. (D) TEM image of the porous PS nanofiber with the insets at a higher magnification. (A and B) Reprinted with permission from ref 383. Copyright 2018 American Chemical Society. (C and D) Reprinted with permission from ref 389. Copyright 2006 American Chemical Society.

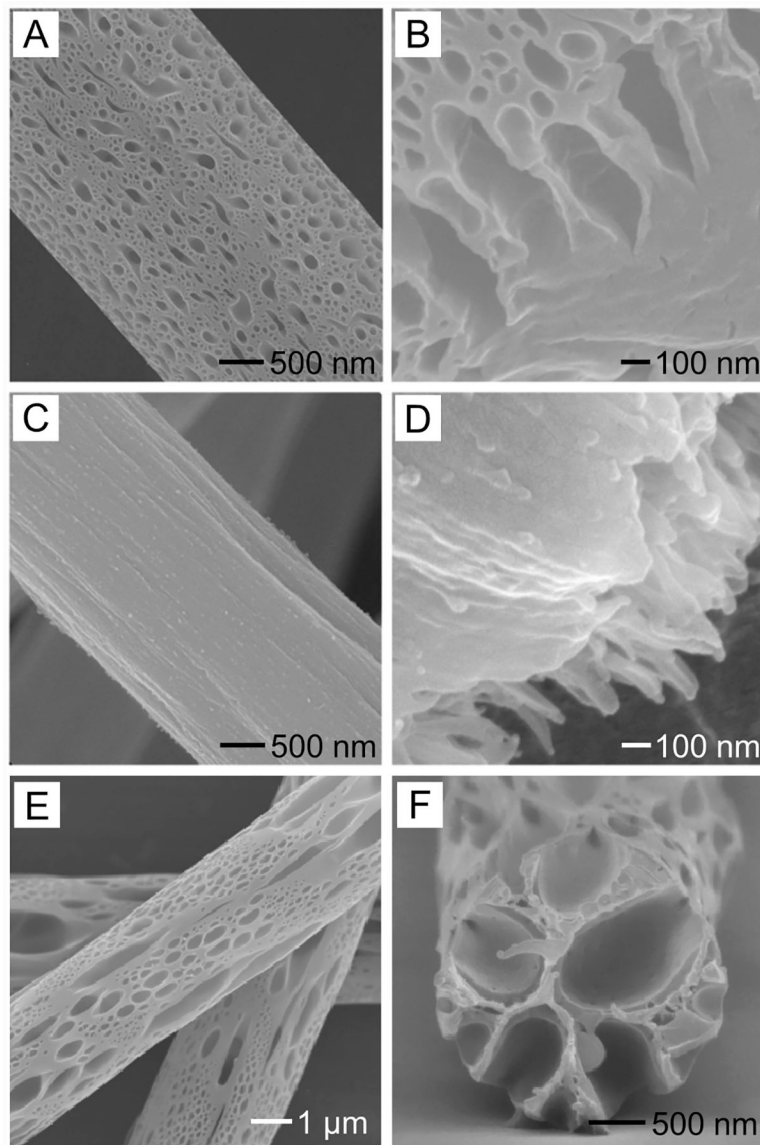


Figure 22.

(A–D) SEM images of the surface and cross-section of porous PS fibers fabricated by electrospinning a 20 wt % PS solution in (A and B) THF and (C and D) a mixture of DMF and THF at a weight ratio of 1:1 under a relative humidity of 62%. (E and F) SEM images of the surface and cross-section of porous PS fibers produced by electrospinning a 30 wt % PS solution in a mixture of chlorobenzene (solvent) and DMSO (nonsolvent) at a volume ratio of 70:3 under a relative humidity of 50–70%. (A–D) Reprinted with permission from ref 391. Copyright 2013 American Chemical Society. (E and F) Reprinted with permission from ref 401. Copyright 2017 American Chemical Society.

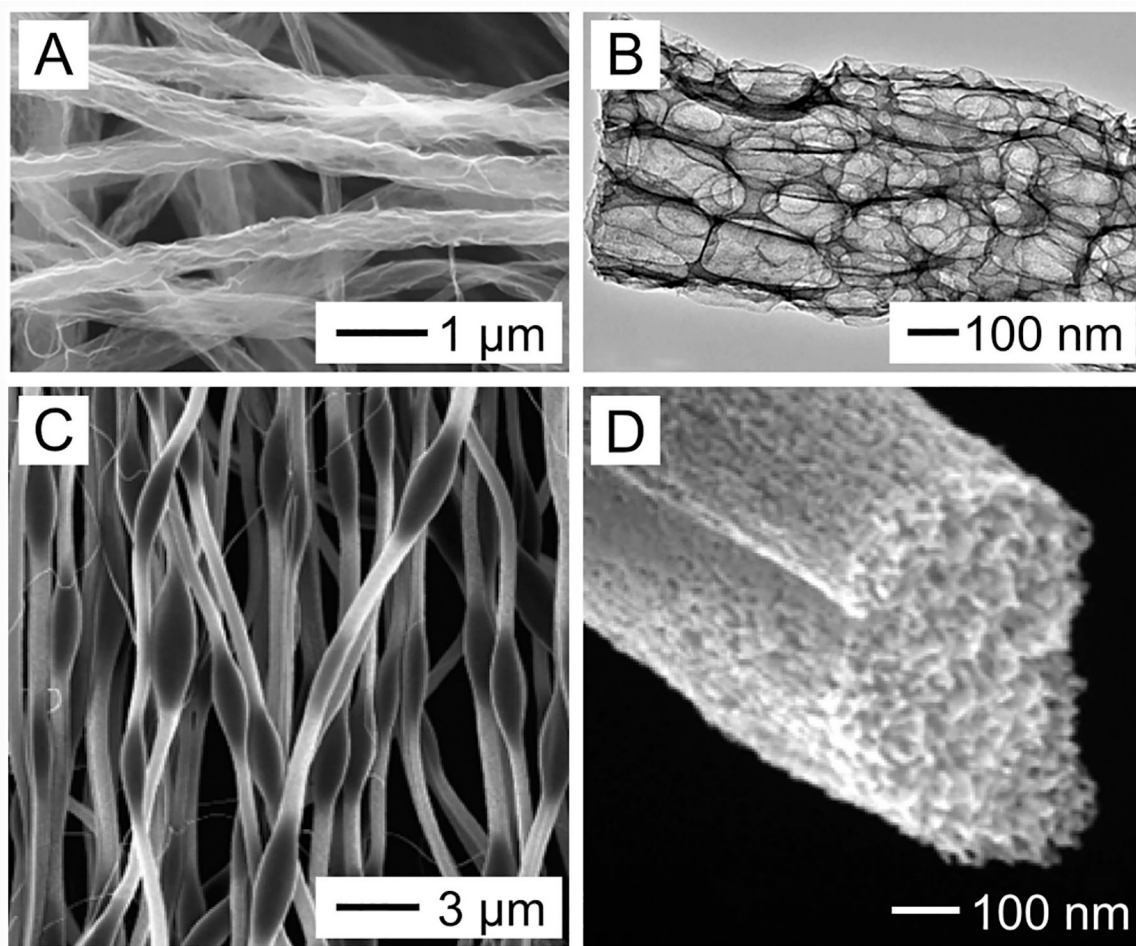
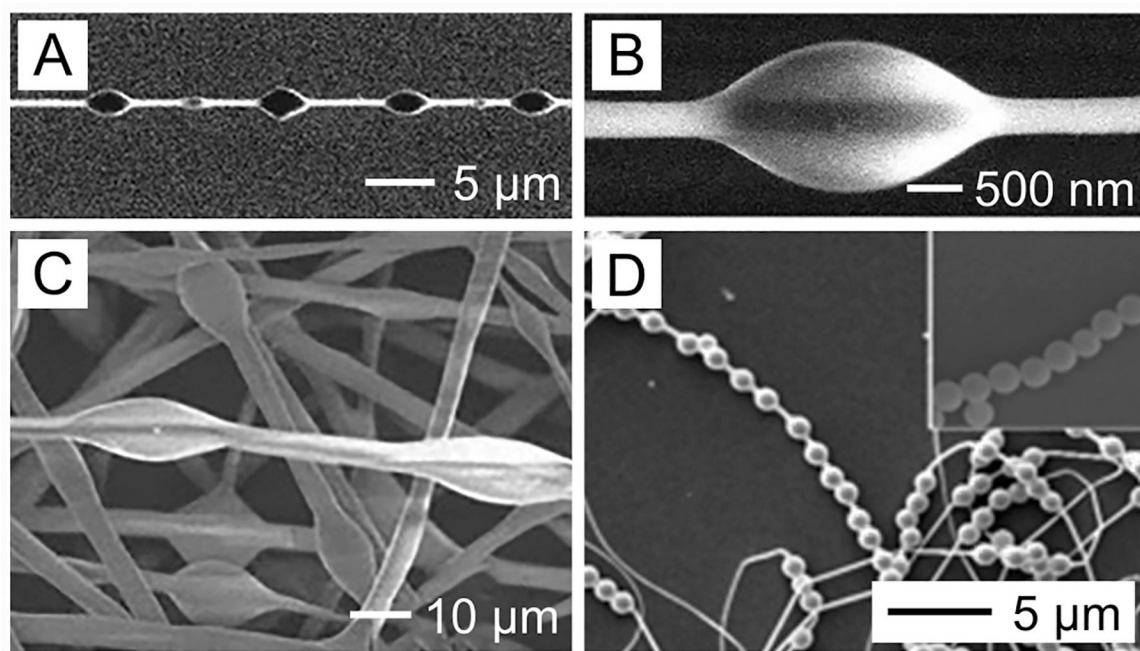
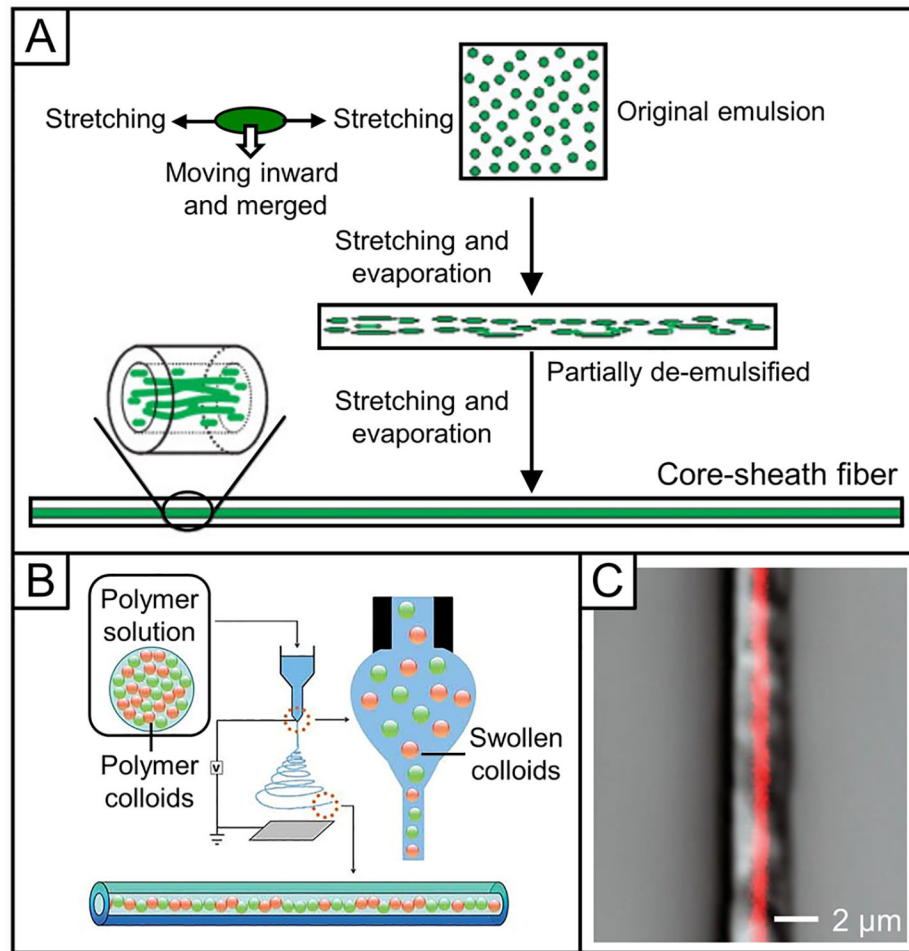


Figure 23.

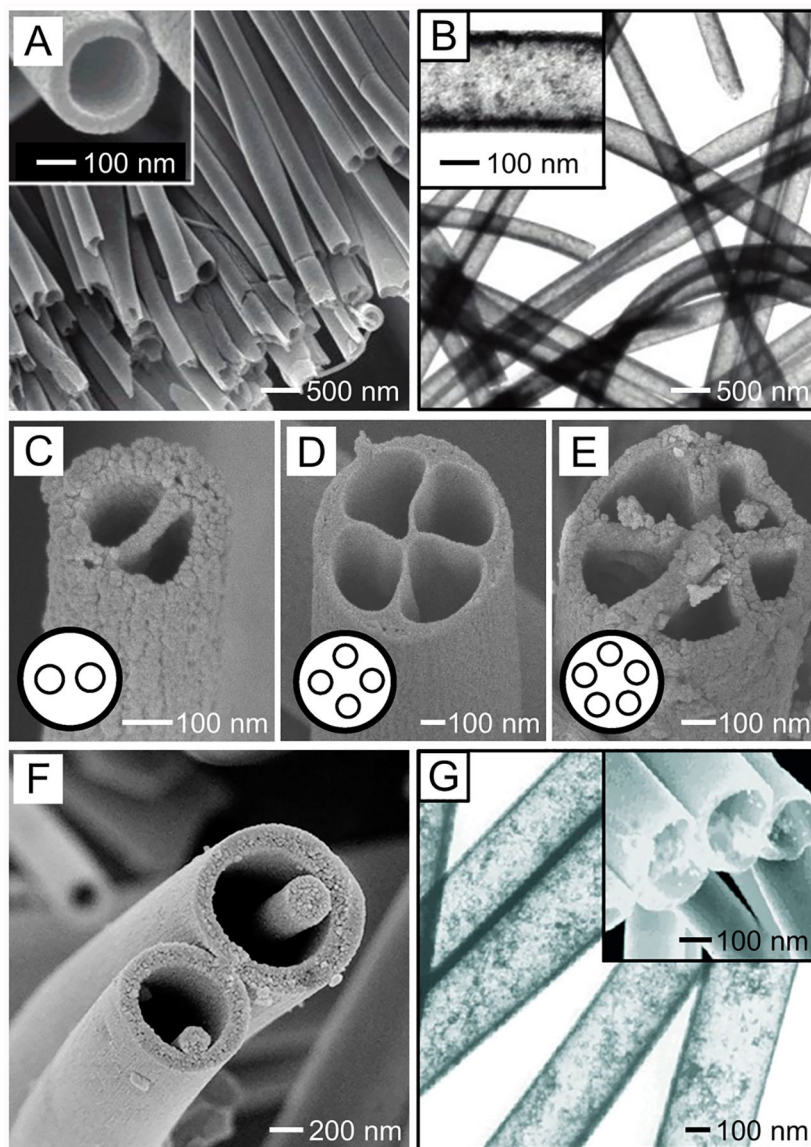
(A) SEM and (B) TEM images of macroporous carbon fibers fabricated by etching the hybrid fibers made of carbon, SiO_2 , and Sb in an aqueous HF solution to remove the SiO_2 and Sb nanoparticles. (C and D) SEM images of the (C) surface and (D) cross-section of porous TiO_2 nanofibers obtained by calcining electrospun core–sheath nanofibers to remove both PS and PVP. (A and B) Reprinted with permission from ref 408. Copyright 2018 American Chemical Society. (C and D) Reprinted with permission from ref 194. Copyright 2004 American Chemical Society.

**Figure 24.**

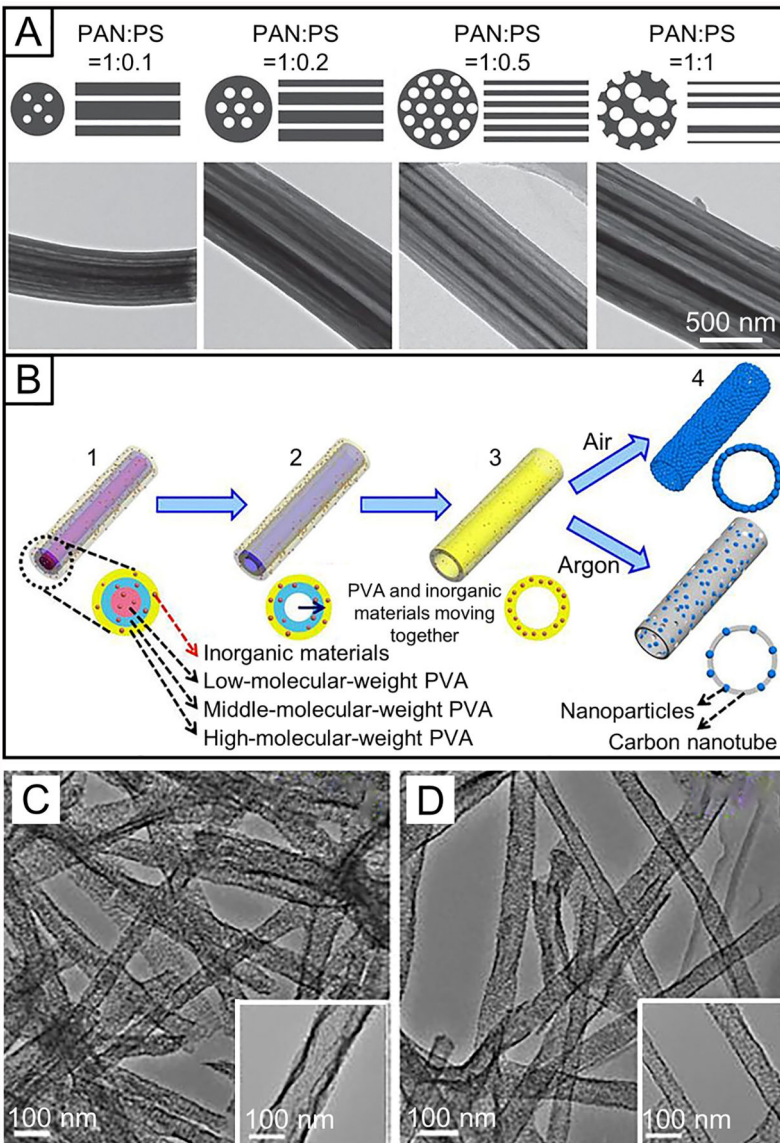
(A) SEM image of the natural capture silk of a cribellate spider with regularly distributed glue droplets on it, and (B) the magnified SEM image of a glue droplet on the capture silk. (C) SEM image of the bead-on-string heterostructured fibers in which hydrophilic PEG beads are distributed on a hydrophobic string of PS. (D) SEM image of electrospun polyacrylamide fibers on which $1\text{ }\mu\text{m}$ SiO_2 beads are strung together. The inset shows a magnified SEM image. (A–C) Reprinted with permission from ref 415. Copyright 2011 Wiley-VCH. (D) Reprinted with permission from ref 419. Copyright 2006 American Chemical Society.

**Figure 25.**

(A) Schematic illustration showing the formation of core–sheath nanofibers by emulsion electrospinning. (B) Schematic illustration showing the formation of core–sheath nanofibers that contain an array of colloids in the core by electrospinning a polymer solution containing cross-linked and swollen polymer colloids. (C) Confocal laser scanning microscopy image of a typical core–sheath fiber consisting of a PCL sheath and PNIPAAm microgel particles in the core. (A) Reprinted with permission from ref 428. Copyright 2006 Wiley-VCH. (B and C) Reprinted with permission from ref 430. Copyright 2009 Wiley-VCH.

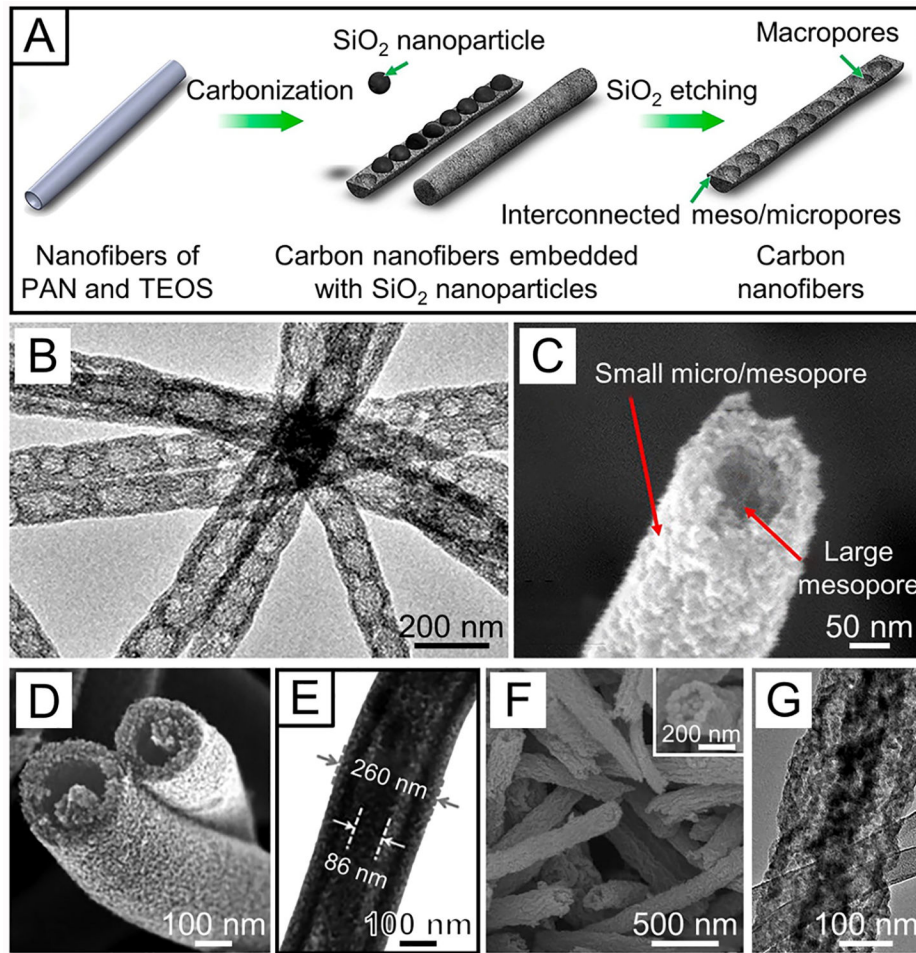
**Figure 26.**

(A and B) SEM and TEM images of anatase hollow nanofibers obtained by removing the heavy mineral oil in the core of core–sheath nanofibers comprised of PVP-TiO₂ sheath, followed by calcination in air. (C–E) SEM images of hollow nanofibers with two, four, and five channels, respectively, fabricated by adjusting the number of the inner capillaries for the coaxial electrospinning. The inset in each figure shows a cross-sectional illustration of the spinneret used to generate the hollow fibers. (F) SEM image of the cross-section of anatase nanofibers with nanowire-in-microtube structure. (G) TEM and SEM (inset) images of hollow TiO₂ nanofibers with SnO₂ nanoparticles coated on their inner surfaces. (A and B) Reprinted with permission from ref 194. Copyright 2004 American Chemical Society. (C–E) Reprinted with permission from ref 219. Copyright 2007 American Chemical Society. (F) Reprinted with permission from ref 436. Copyright 2010 American Chemical Society. (G) Reprinted with permission from ref 324. Copyright 2005 Wiley-VCH.

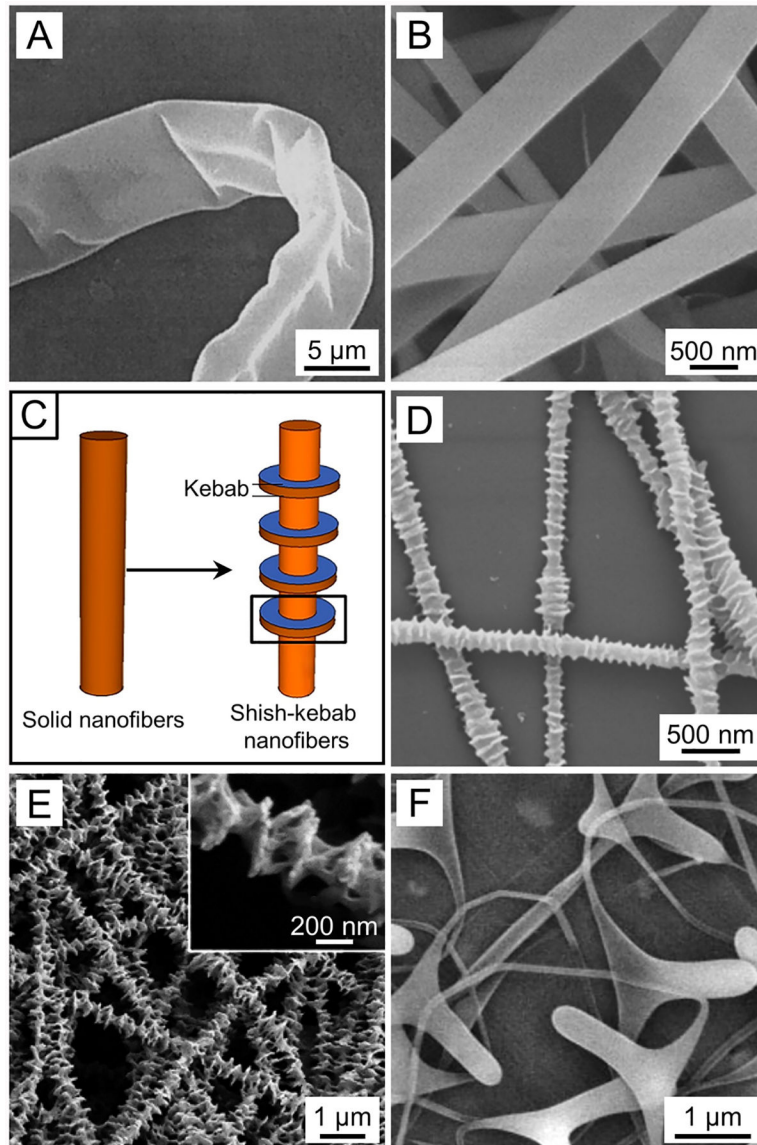
**Figure 27.**

(A) Schematic diagrams and TEM images of the hollow nanofibers with different numbers of channels produced by varying the ratio of PS to PAN in the range of 1:10 to 1:1. (B) Schematic of the “gradient” electrospinning and controlled pyrolysis method for the preparation of mesoporous hollow nanofibers: (1) electrospinning of a solution containing PVA with different molecular weights (low-, middle-, and high-molecular-weight PVA in a weight ratio of 3:2:1) and metal salt precursors; (2) pyrolyzed inner low-and middle-molecular-weight PVA, moving toward the high-molecular-weight PVA; (3) convergence of all of the pyrolyzed PVA and inorganic materials together in the tube’s wall; and (4) pyrolysis of all the PVA after sintering in air with uniform mesoporous hollow nanofibers being obtained. When sintering in Ar, hollow carbon nanofibers embedded with tiny inorganic nanoparticles are obtained. (C and D) TEM images of (C) LiV₃O₈ and (D) MnO₂ mesoporous hollow nanofibers, respectively, fabricated using this method. (A) Reprinted

with permission from ref 438. Copyright 2015 Springer Nature. (B–D) Reprinted with permission from ref 439. Copyright 2015 Springer Nature.

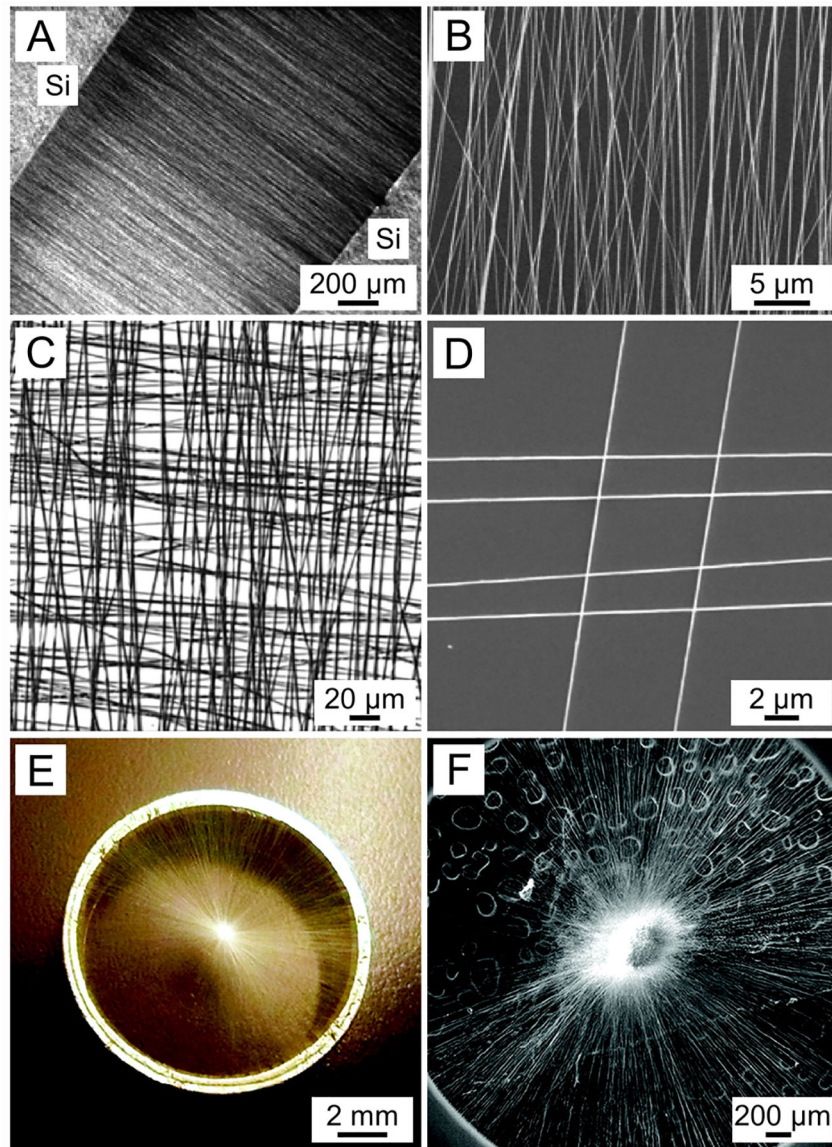
**Figure 28.**

(A) Schematic showing the fabrication of hollow carbon nanofibers with a bamboo-like structure using SiO_2 particles as hard templates. The electrospun nanofibers made of a blend of PAN and TEOS were carbonized at 1200 °C in an atmosphere of H_2 and Ar (5:95 in volume). The ultrafine SiO_2 clusters were transferred into much larger SiO_2 particles through aggregation and further lined up in the core of the nanofiber. After removing the hard templates through chemical etching, hollow carbon nanofibers were produced. (B and C) TEM and SEM images of the as-obtained bamboo-like carbon nanofibers that had hollow interior together with an interconnected pore structure. (D and E) SEM and TEM images of SnO_2 nanotubes with a fiber-in-tube structure. (F and G) SEM and TEM images of CoMn_2O_4 nanotubes with a tube-in-tube nanostructure with the inset in panel F showing a magnified SEM image. (A–C) Reprinted with permission from ref 441. Copyright 2015 American Chemical Society. (D and E) Reprinted with permission from ref 443. Copyright 2015 Wiley-VCH. (F and G) Reprinted with permission from ref 446. Copyright 2015 American Chemical Society.

**Figure 29.**

(A) SEM image of a ribbon-like fiber produced by electrospinning a 30 wt % PS solution in DMF. (B) SEM image of ribbon-like fibers produced by electrospinning an 18 wt % aqueous solution of silk-elastin-like protein. (C) Schematic illustration comparing the morphology of a solid nanofiber and a nanofiber with a shish-kebab structure. (D) SEM image of PEO nanofibers with a shish-kebab structure by depositing PEO crystals along the PEO nanofibers. (E) SEM image of nanofibers with a shish-kebab structure, in which PCL-b-poly(acrylic acid) kebabs are deposited on PCL nanofibers. The inset shows the magnified SEM image. (F) SEM image of nanofibers with a high frequency of short branches produced by electrospinning a 3 wt % aqueous PVA solution. (A) Reprinted with permission from ref 447. Copyright 2001 Wiley-VCH. (B) Reprinted with permission from ref 450. Copyright 2009 Elsevier. (C and E) Reprinted with permission from ref 456. Copyright 2013 American

Chemical Society. (D) Reprinted with permission from ref 454. Copyright 2008 American Chemical Society. (F) Reprinted with permission from ref 457. Copyright 2009 Wiley-VCH.

**Figure 30.**

(A) Dark-field optical micrograph and (B) SEM image of uniaxially aligned PVP nanofibers collected on top of the gap formed between two silicon stripes. (C) Optical micrograph of a grid formed by stacking two layers of uniaxially aligned PVP nanofibers (with their long axes rotated by 90°). (D) SEM image of a simple device structure that was directly fabricated by transferring SnO₂ nanofibers onto the same substrate to form a 2 × 4 array of crossbar junctions. (E) Photograph of a scaffold comprised of radially aligned PCL nanofibers deposited on a ring, and (F) SEM image of the radially aligned nanofibers in the scaffold. (A–D) Reprinted with permission from ref 35. Copyright 2003 American Chemical Society. (E and F) Reprinted with permission from ref 235. Copyright 2010 American Chemical Society.

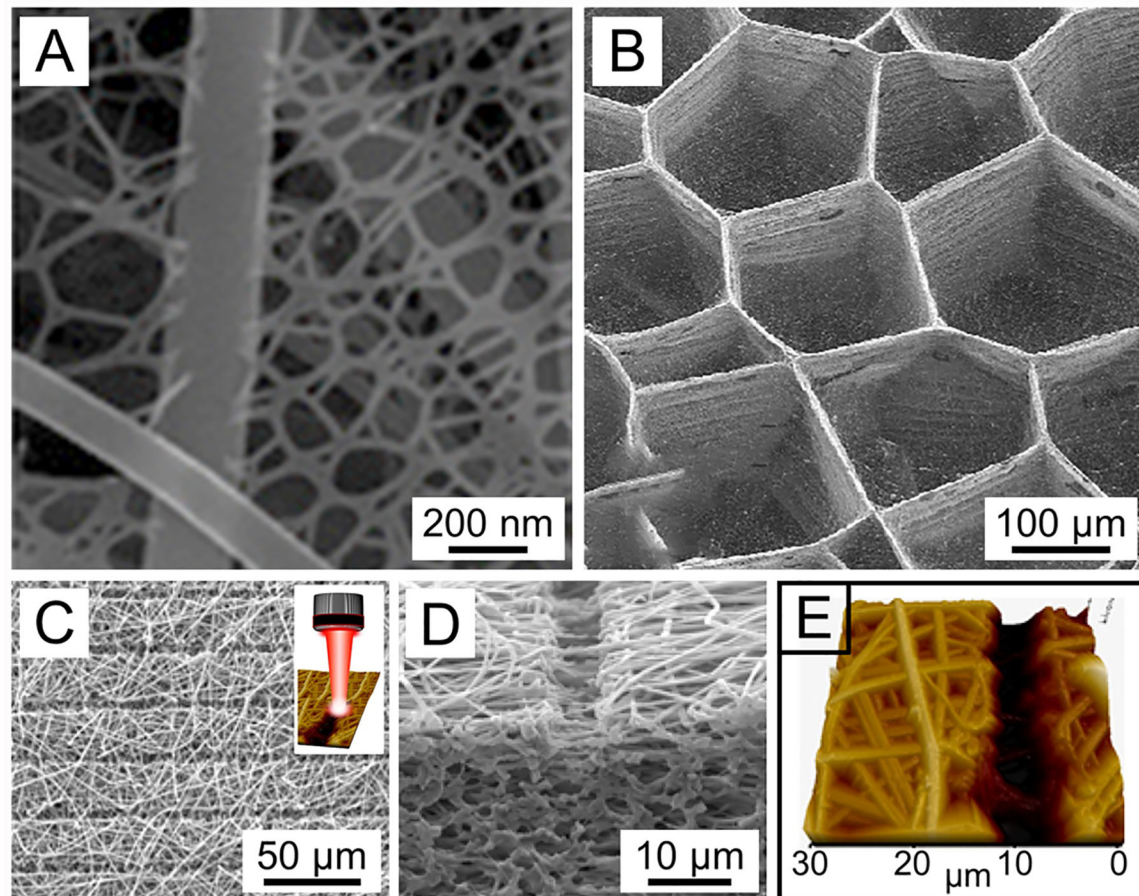


Figure 31.

(A) SEM image of a mat of poly(acrylic acid) nanofibers containing nanonets made of ultrathin nanowires (ca. 30 nm in diameter). (B) SEM image of a mat of PVA nanofibers with a honeycomb-patterned architecture. (C–E) Surface and cross-sectional SEM images and the atomic force microscopy (AFM) image showing the morphology of a nanofiber-based mat with grooves that were ablated by a femtosecond laser, as the schematic shown in the inset in panel C. (A) Reprinted with permission from ref 466. Copyright 2011 Royal Society of Chemistry. (B) Reprinted with permission from ref 469. Copyright 2011 American Chemical Society. (C–E) Reprinted with permission from ref 471. Copyright 2016 American Chemical Society.

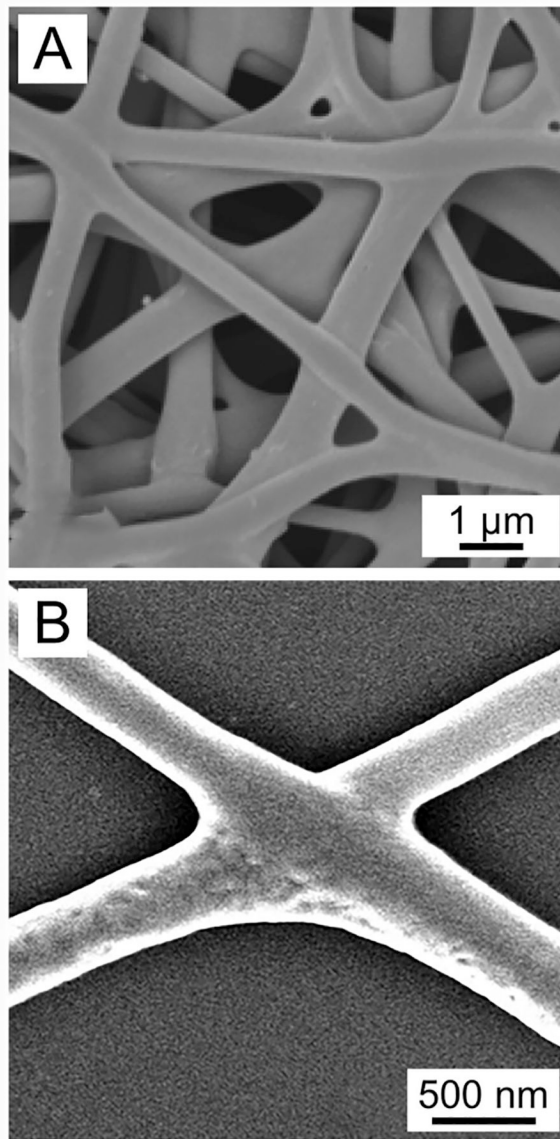
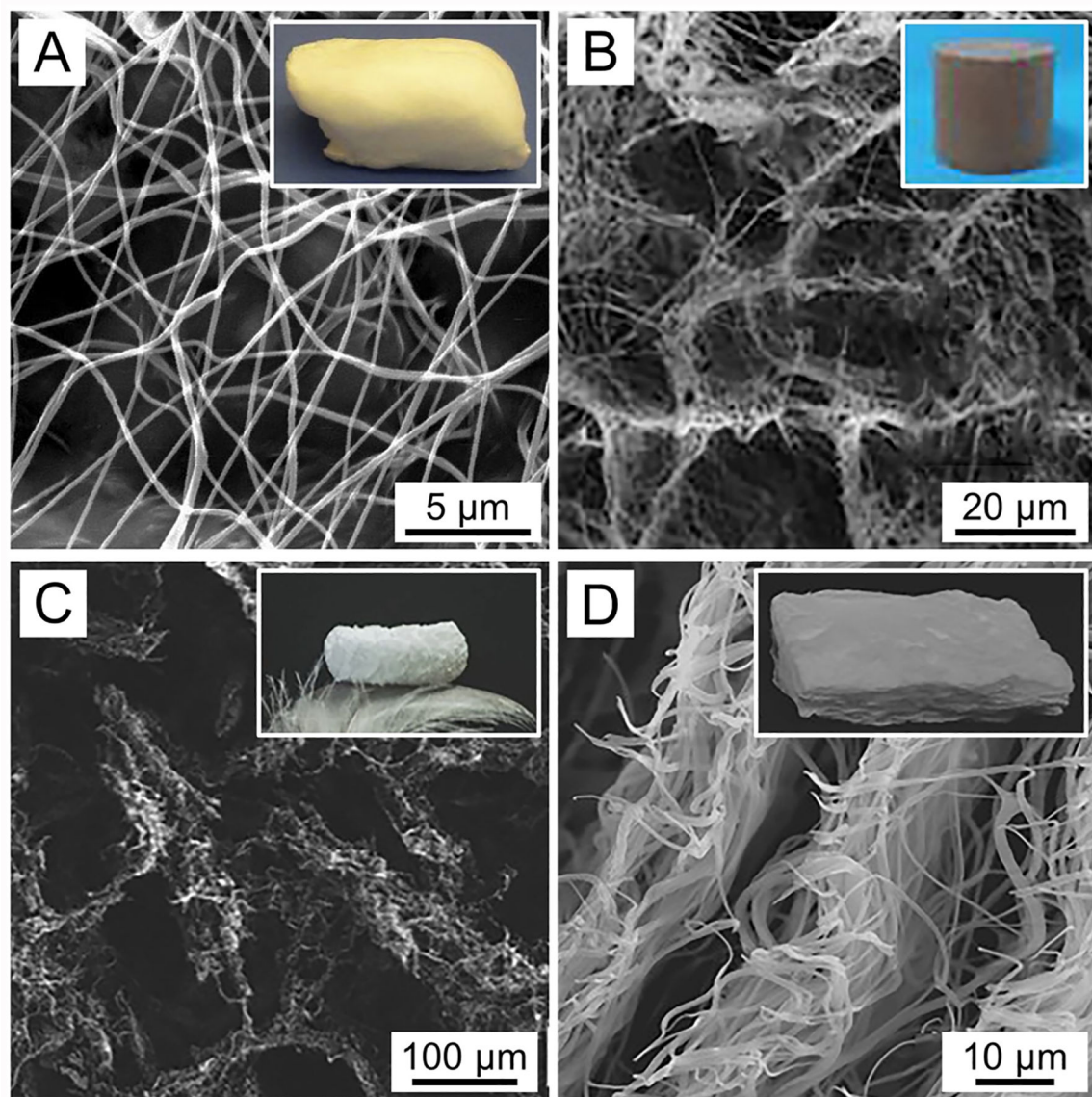
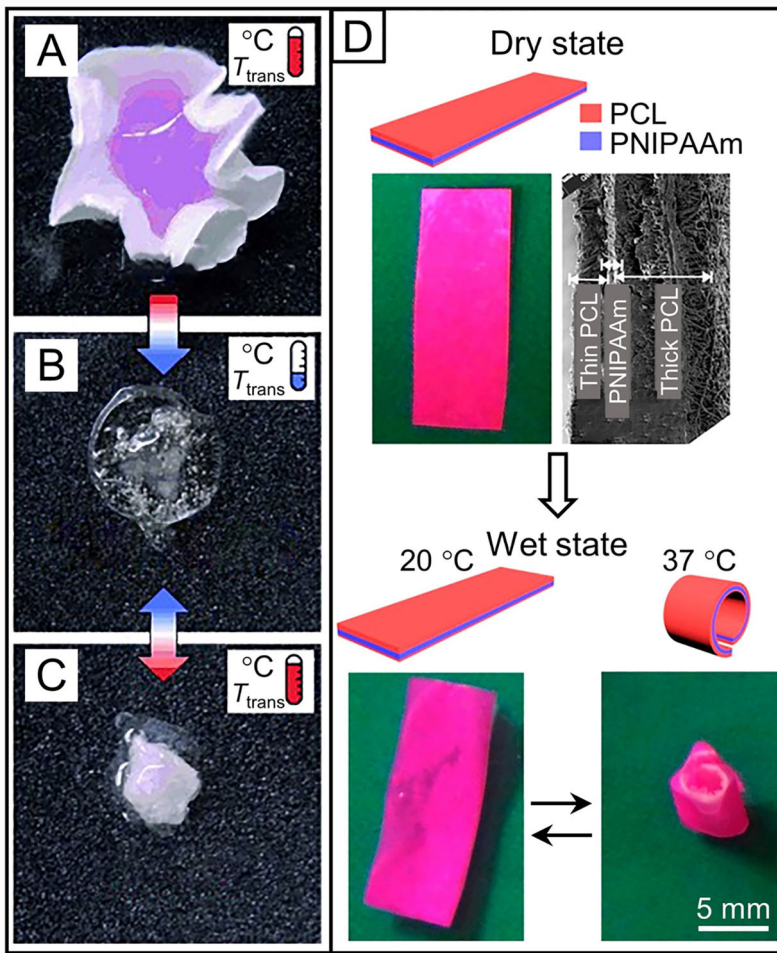


Figure 32.

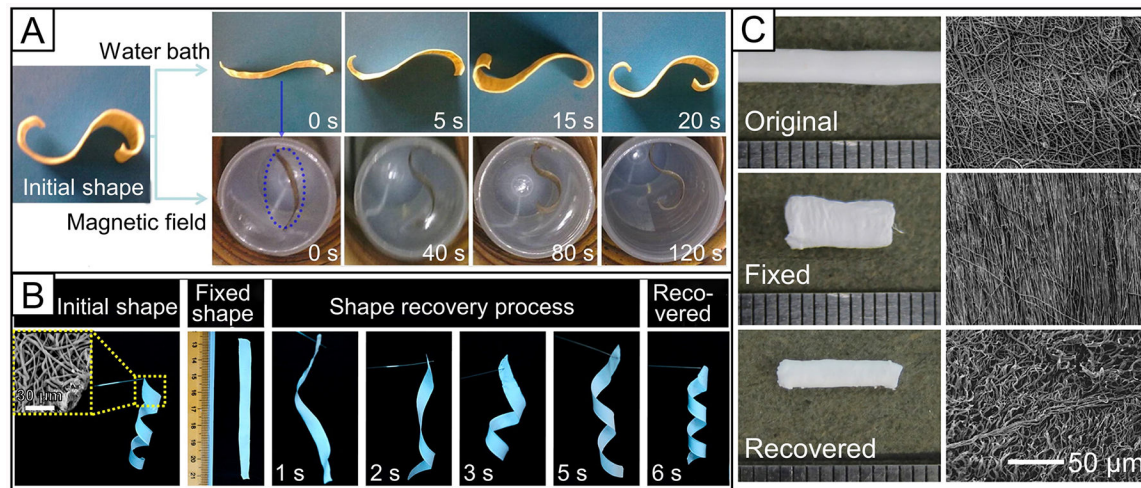
(A) SEM image of carbon nanofibers with welding at cross-points by carbonizing the nanofibers made of a blend of lignin and PEO at a lignin to PEO weight ratio of 90:10. (B) SEM image of two electrospun PCL nanofibers after exposure to the vapor of DMF for 60 min, showing welding of the two nanofibers at the cross-point. (A) Reprinted with permission from ref 477. Copyright 2013 American Chemical Society. (B) Reprinted with permission from ref 483. Copyright 2017 Wiley-VCH.

**Figure 33.**

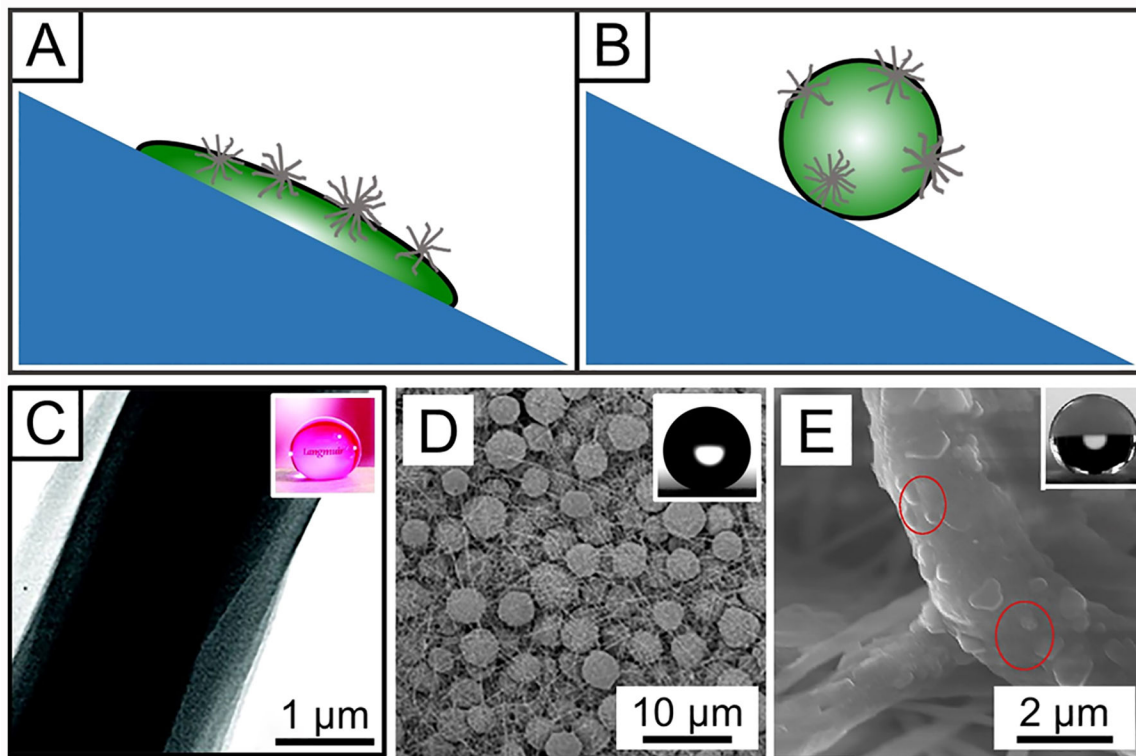
(A) SEM image of a 3D cotton-ball-like foam with a highly porous structure obtained by collecting PCL nanofibers in a nonconductive spherical dish embedded with an array of metal probes. (B) SEM image of a 3D foam comprised of nanofibers made of a blend of PAN and SiO₂ fabricated by homogenizing short nanofibers, followed by freeze-drying. (C) SEM image of a 3D foam comprised of PCL nanofibers fabricated through thermally induced agglomeration of short PCL nanofibers, followed by freeze-drying. (D) SEM image of a 3D foam with a highly ordered structure fabricated by expanding a mat of random PCL nanofibers. Photographs of the corresponding 3D foams are shown in the insets. (A) Reprinted with permission from ref 512. Copyright 2011 Elsevier. (B) Reprinted with permission from ref 514. Copyright 2014 Springer Nature. (C) Reprinted with permission from ref 517. Copyright 2015 Wiley-VCH. (D) Reprinted with permission from ref 525. Copyright 2016 Wiley-VCH.

**Figure 34.**

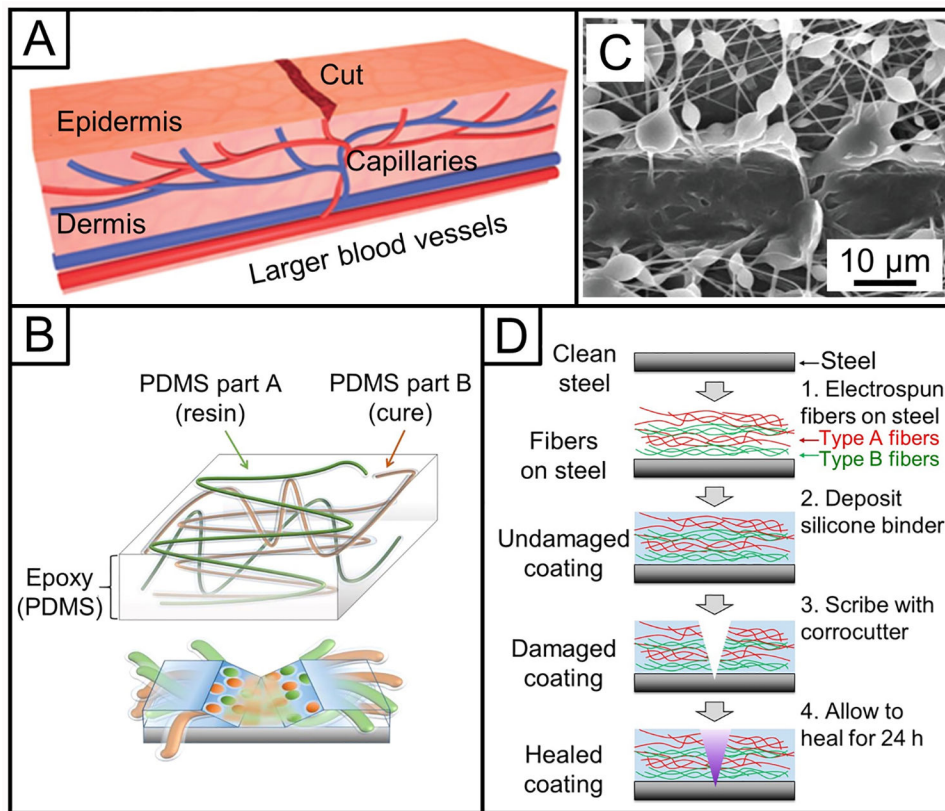
(A–C) Capture and release of cells using a thermoresponsive nanofiber-based mat that transforms from a fibrous to a hydrogel-like structure through a wrapping, swelling, and shrinking process in response to temperature changes. (D) Thermoresponsive property of a trilayer mat comprising a thick layer of PNIPAAm nanofibers sandwiched between two layers of PCL nanofibers with different thicknesses (<100 and 400 μm , respectively) for actuating. The trilayer mat in the dry state in air at room temperature shows no folding (right, SEM image of a cross-section of the trilayer mat), and the trilayer mat in water shows no folding at 20 °C, while short-side rolling at 37 °C. (A–C) Reprinted with permission from ref 541. Copyright 2012 Wiley-VCH. (D) Reprinted with permission from ref 531. Copyright 2017 American Chemical Society.

**Figure 35.**

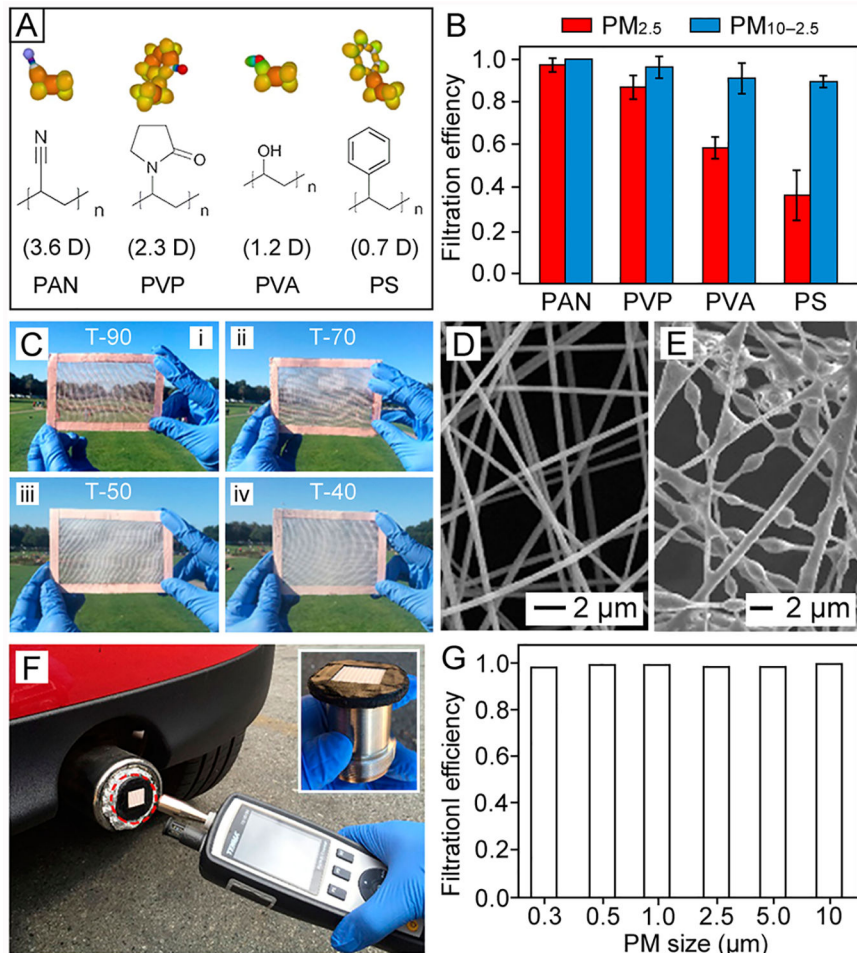
(A) Series of photographs showing the shape-memory recovery process of the composite nanofibers containing PCL and multiwalled carbon nanotubes coated with Fe_3O_4 nanoparticles in a water bath at 46 °C and in an alternating magnetic field with a frequency of 20 kHz and a field strength of 6.8 kA/m. (B) Demonstration of the shape-memory effect of poly(D,L-lactide-*co*-trimethylene carbonate) nanofibers recovering from a temporary shape of straight strip to take the permanent spiral shape within about 6 s upon heating to 39 °C in a water bath. The inset gives an SEM image showing the morphology of the nanofibers. (C) Shape-memory behavior of a sleeve constructed from shape-memory nanofibers as revealed by photographs and SEM images of the sleeves before fixing, after fixing, and after recovery (ruled markings on the images: mm). (A) Reprinted with permission from ref 573. Copyright 2012 Elsevier. (B) Reprinted with permission from ref 577. Copyright 2014 American Chemical Society. (C) Reprinted with permission from ref 578. Copyright 2016 Elsevier.

**Figure 36.**

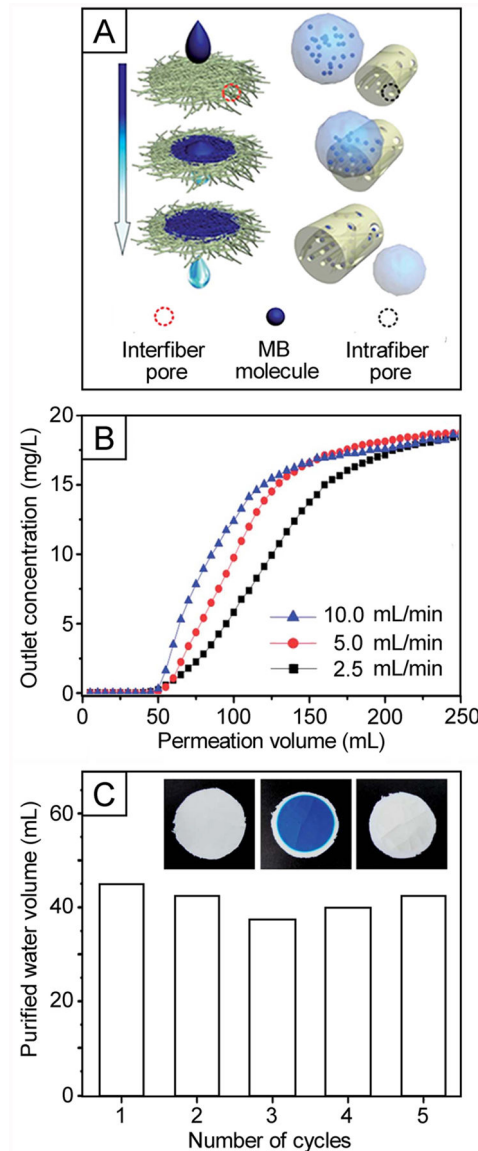
Transport mechanisms of water with dirt particles on (A) superhydrophilic and (B) superhydrophobic surfaces to form a droplet flow and a film flow, respectively. (C) SEM image of a PCL@ PTFE core–sheath nanofiber, and the resultant mat showing a static WCA of 158°. (D) SEM image of a nanofiber mat prepared by electrospinning a 7 wt % PS solution in DMF, and the resultant mat showing a static WCA of 162°. (E) SEM image of PVDF nanofibers integrated with ZnO nanoparticles on the surface by directly electrospinning a PVDF solution containing 10 wt % ZnO nanoparticles, and the resultant mat showing a static WCA of 171°. The insets in panels C–E show photographs of water droplets on the surface of the corresponding mats. (C) Reprinted with permission from ref 594. Copyright 2009 American Chemical Society. (D) Reprinted with permission from ref 595. Copyright 2004 Wiley-VCH. (E) Reprinted with permission from ref 596. Copyright 2016 Elsevier.

**Figure 37.**

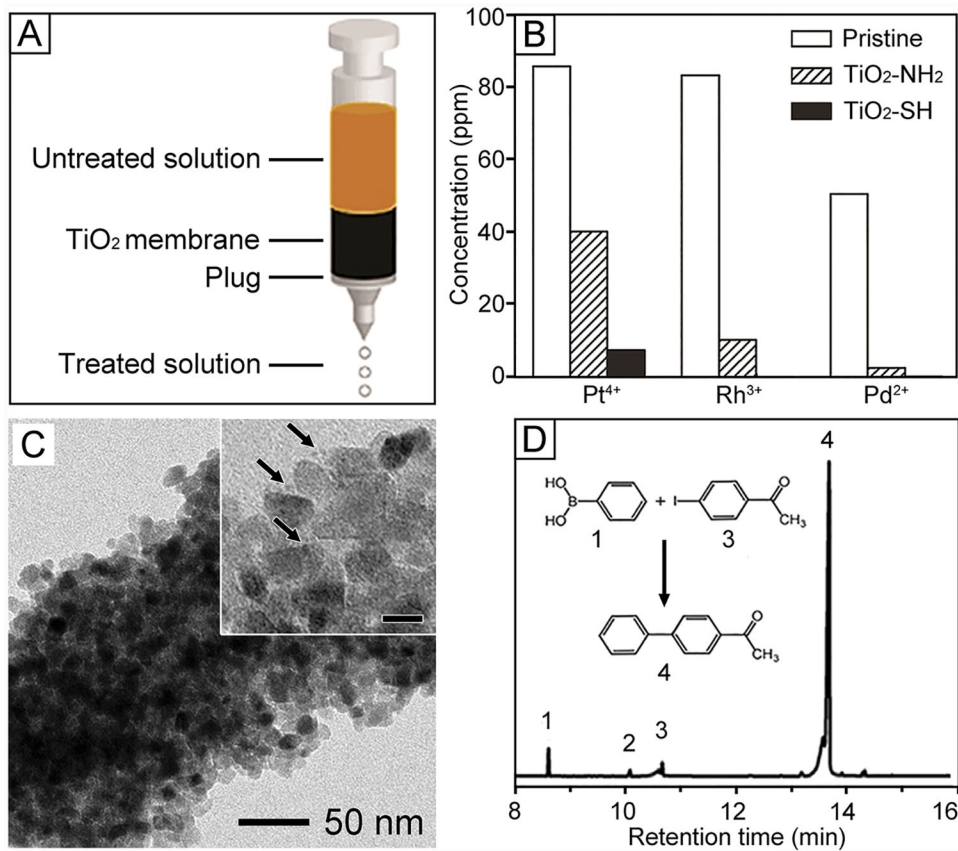
(A) Schematic diagram of the capillary network in the dermis layer of skin, with a cut in the epidermis layer. (B) Structure of self-healing, fiber-reinforced composite. Core–sheath nanofibers with resin monomer and curing agent in the core are mutually entangled and embedded in a PDMS matrix. When damage occurs, the resin monomer and curing agent will be released and polymerization reaction results in PDMS-reinforced healing. (C) SEM image of healing agent released from the capsules of bead-on-string core–sheath nanofibers when ruptured by mechanical scribing. (D) Illustration of a self-healing composite containing the nanofibers to be utilized as the coating for protecting the steel surface from corrosion. (A) Reprinted with permission from ref 598. Copyright 2007 Springer Nature. (B) Reprinted with permission from ref 604. Copyright 2015 American Chemical Society. (C) Reprinted with permission from ref 607. Copyright 2010 Wiley-VCH. (D) Reprinted with permission from ref 610. Copyright 2016 Elsevier.

**Figure 38.**

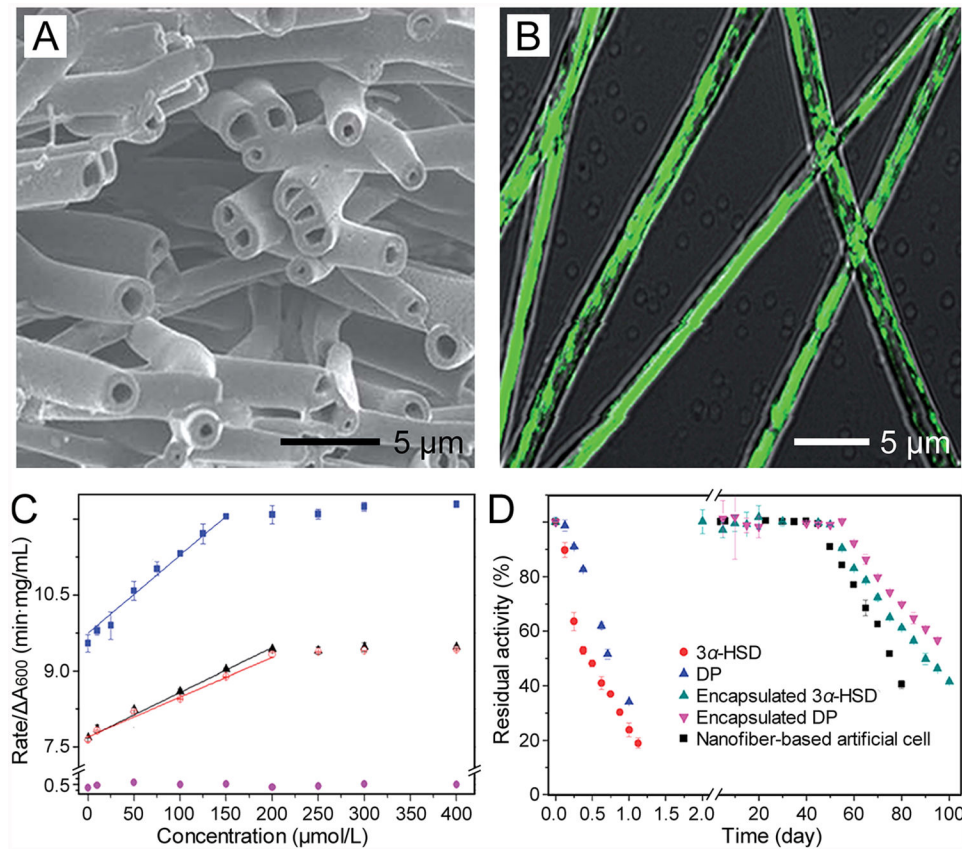
(A) Molecular models and formulas of different polymers (i.e., PAN, PVP, PVA, and PS) with calculated dipole moments for the repeating units of each polymer. (B) Filtration efficiencies to PMs for the different types of membranes based on PAN, PVP, PVA, and PS. (C) Photographs of polyimide-based air filters with transmittances at 90% (T-90), 70% (T-70), 50% (T-50), and 40% (T-40), and SEM images of the air filter (D) before and (E) after capturing PMs. (F) The PM number concentration measurement of car exhaust with an air filter. The inset shows a stainless-steel pipe coated with a polyimide filter with transmittance at 50% shown by the red circle. (G) Filtration efficiency of PMs from car exhaust gas. (A and B) Reprinted with permission from ref 641. Copyright 2015 Springer Nature. (C–G) Reprinted with permission from ref 647. Copyright 2016 American Chemical Society.

**Figure 39.**

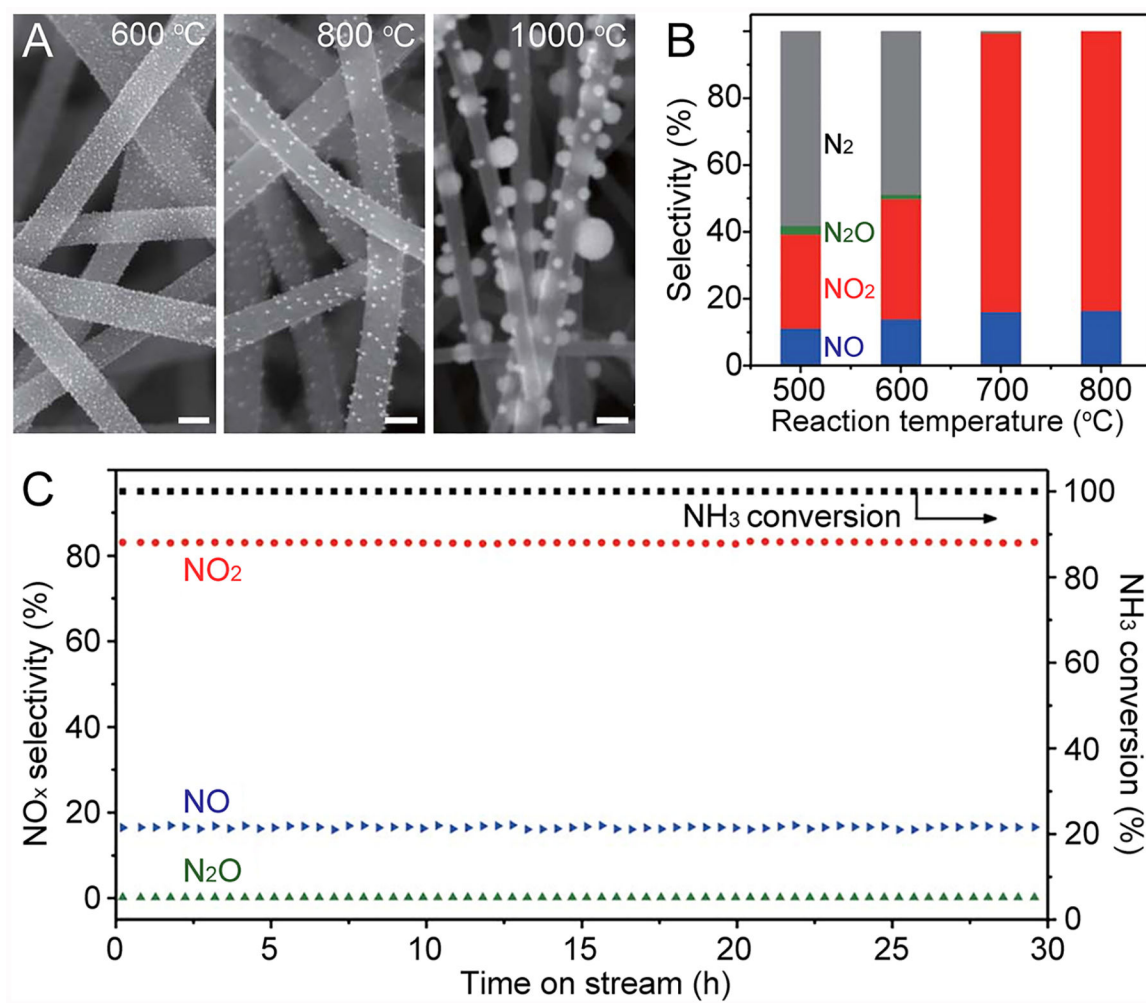
(A) Illustration of the permeation and adsorption processes. The methylene blue solution spreads rapidly on the surface of a mat made of a blend of SiO₂ and TiO₂ and permeates through the void space between the nanofibers. Meanwhile, methylene blue molecules are predominantly captured by intrafiber pores to generate purified water. (B) Breakthrough curves for the permeation of a methylene blue solution through the porous mats at various fluxes. (C) Cyclic test at a flux of 5 mL/h. The insets are the optical images of porous mat before use (left), used (middle), and after calcination (right), respectively. Reprinted with permission from ref 653. Copyright 2013 Royal Society of Chemistry.

**Figure 40.**

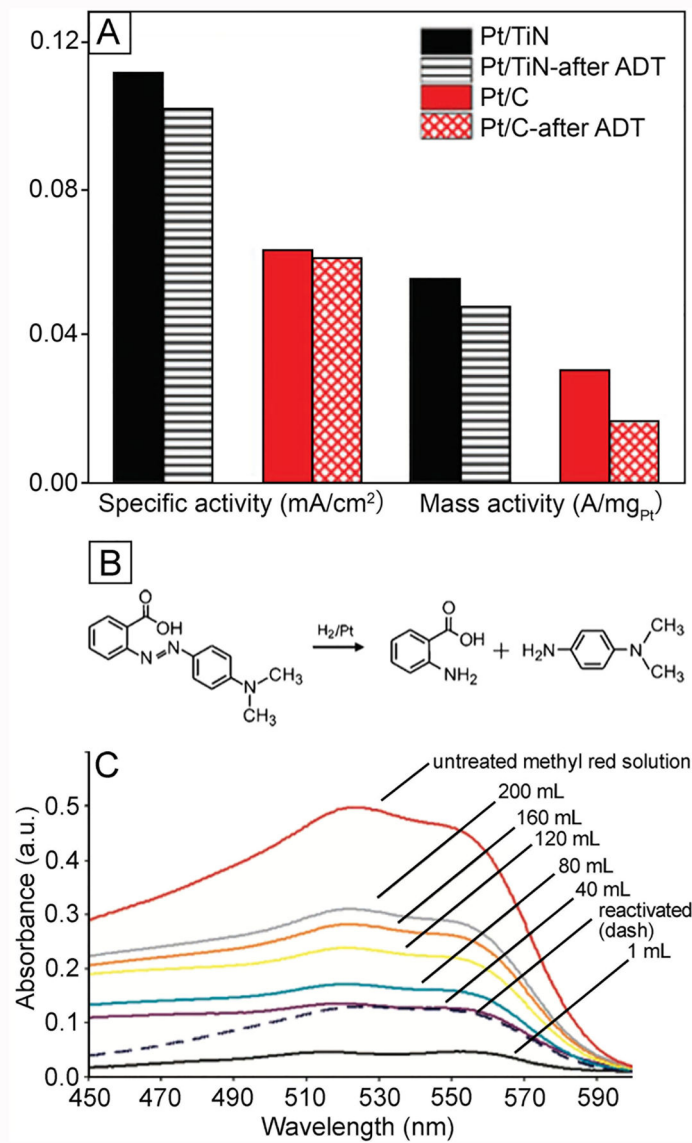
(A) Illustration of a continuous-flow system used for removing precious metal ions. (B) Comparison of the capabilities of the pristine, amino- TiO_2 , and thiol- TiO_2 nanofiber-based mats for scavenging Pt^{4+} , Rh^{3+} , and Pd^{2+} ions. (C) TEM images of a TiO_2 nanofiber decorated with Pd nanoparticles (indicated by arrows in the inset), which were formed by reducing the scavenged Pd^{2+} ions with NaBH_4 . The scale bar in the inset is 10 nm. (D) Chromatography-mass spectrometry chromatogram taken from the first 0.5 mL of the product solution of a Suzuki coupling reaction. The four peaks can be assigned as follows: (1) phenylboronic acid, (2) biphenyl, (3) 4'-iodoacetophenone, and (4) 4-acetylphenylbiphenyl. In addition to the reactants (1 and 3) and product (4), a small amount of biphenyl (2) was observed as a byproduct, corresponding to a selectivity of 99.2%. Reprinted with permission from ref 503. Copyright 2016 Wiley-VCH.

**Figure 41.**

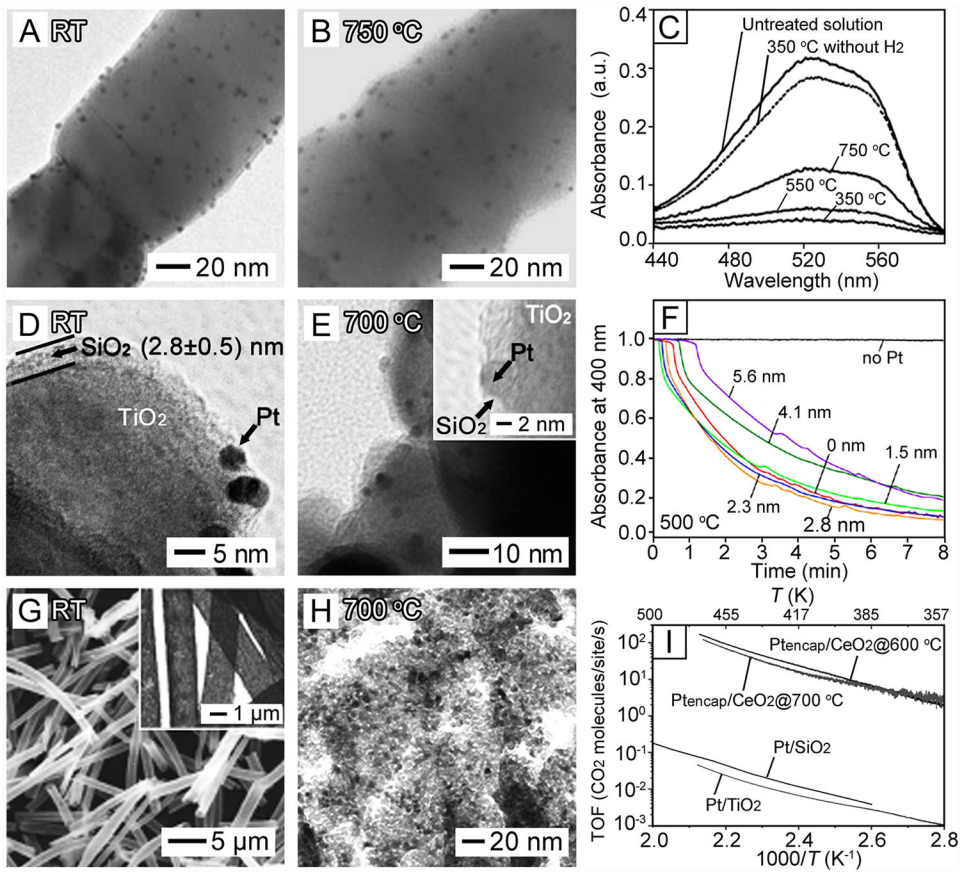
(A) SEM image of hollow polyurethane nanofibers prepared through coaxial electrospinning. (B) Confocal laser scanning microscopy image showing hollow nanofibers loaded with 3 α -hydroxysteroid dehydrogenase (3 α -HSD; labeled with fluorescein isothiocyanate). (C) Calibration curves for the bile acid assay obtained using multienzyme systems consisting of 3 α -HSD, diaphorase (DP), and nicotinamide adenine dinucleotide in different forms. (■) Free multienzymes and co-factor, (▲) nanofiber-based artificial cell, (○) co-immobilized 3 α -HSD and DP with added free nicotinamide adenine dinucleotide, and (●) blank hollow nanofibers. (D) Stability of the free and individually encapsulated 3 α -HSD and DP, as well as the stability of nanofiber-based multienzyme artificial cells involving co-encapsulated 3 α -HSD, DP, and nicotinamide adenine dinucleotide for bile acid assay at 25 °C. Reprinted with permission from ref 668. Copyright 2014 Royal Society of Chemistry.

**Figure 42.**

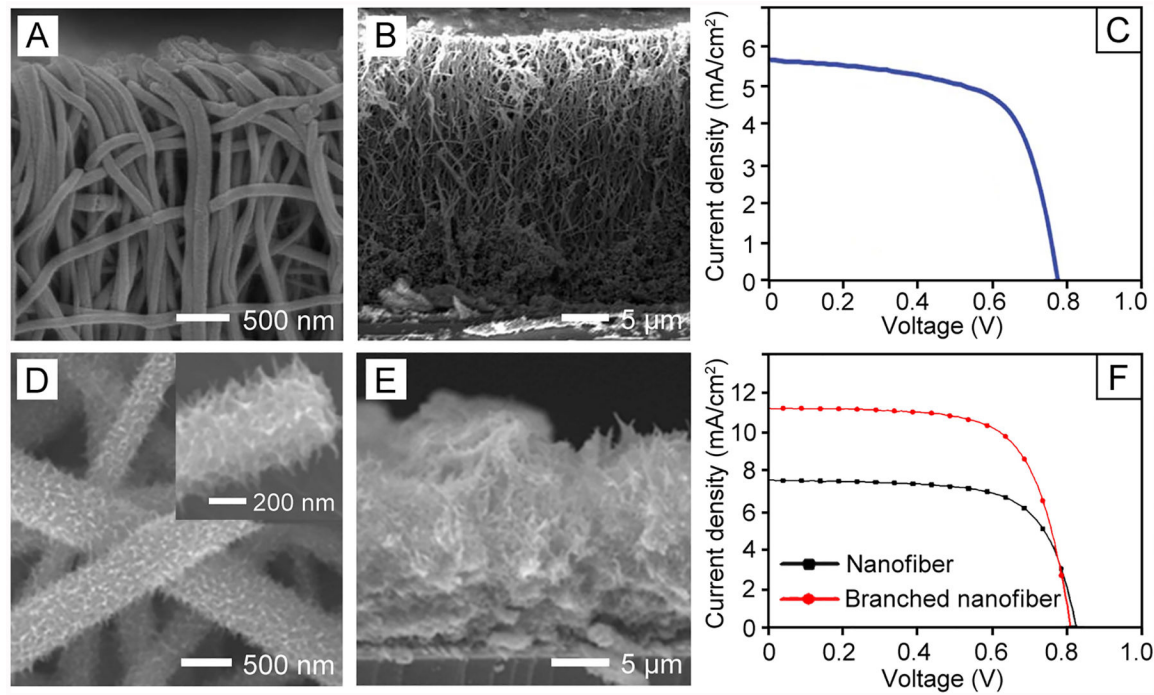
(A) SEM images of AuNi nanoparticles supported on carbon nanofibers obtained through carbonization at different temperatures. The scale bars are 200 nm. A higher carbonization temperature leads to higher crystallinity and lower defect concentrations within the carbon nanofibers, affecting the size and dispersion of the alloy nanoparticles. (B) Temperature-dependent product distribution and conversion of NH_3 by PtPdRhRuCe nanoparticles. (C) Time-dependent catalytic performance of PtPdRhRuCe nanoparticles at 700 °C. Reprinted with permission from ref 341. Copyright 2018 American Association for the Advancement of Science.

**Figure 43.**

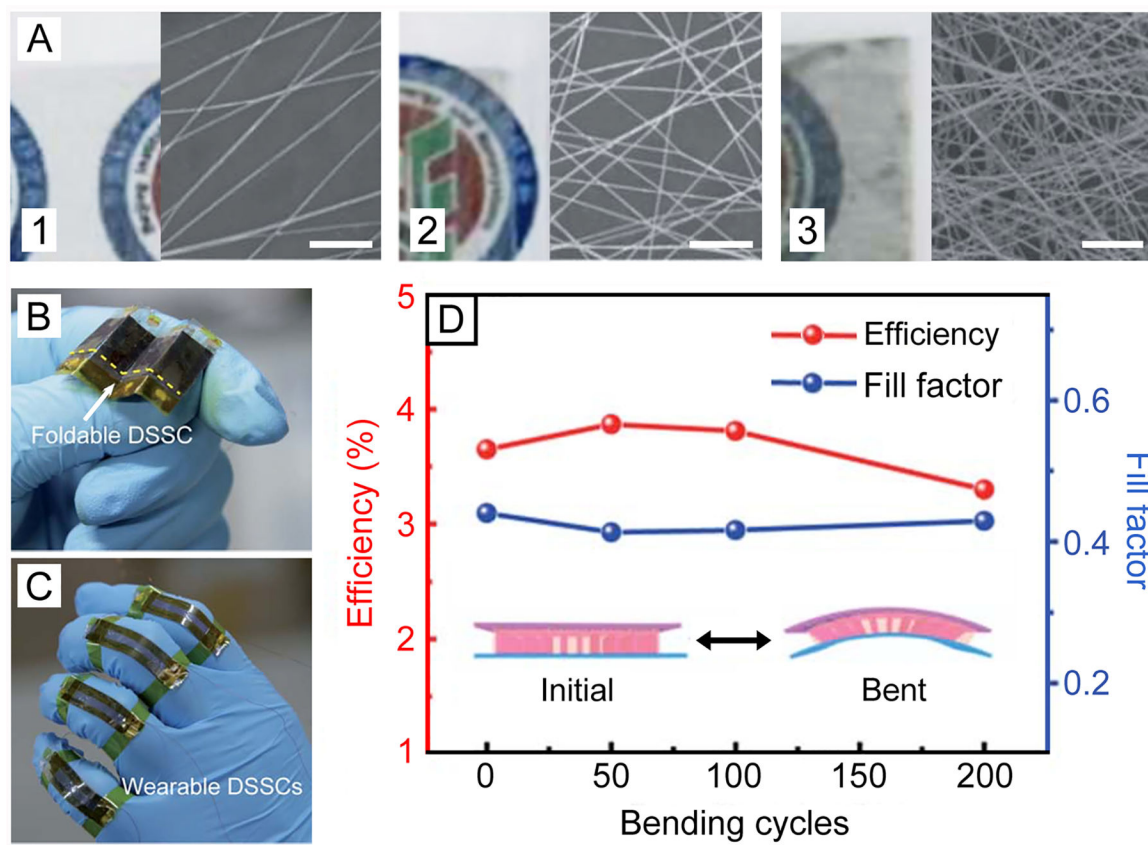
(A) Comparison of the stability for an electrocatalyst involving Pt nanoparticles on TiN hollow nanofibers and a commercial Pt/C catalyst before and after ADT. (B) Hydrogenation of methyl red. (C) UV-vis spectra of the methyl red solution, after different volumes of it have passed through the mat of TiO_2 nanofibers immobilized with Pt nanoparticle that could serve as a catalyst to cleave the azo bond in methyl red by hydrogenation. (A) Reprinted with permission from ref 681. Copyright 2017 Royal Society of Chemistry. (B) Reprinted with permission from ref 42. Copyright 2017 American Chemical Society. (C) Reprinted with permission from ref 335. Copyright 2008 American Chemical Society.

**Figure 44.**

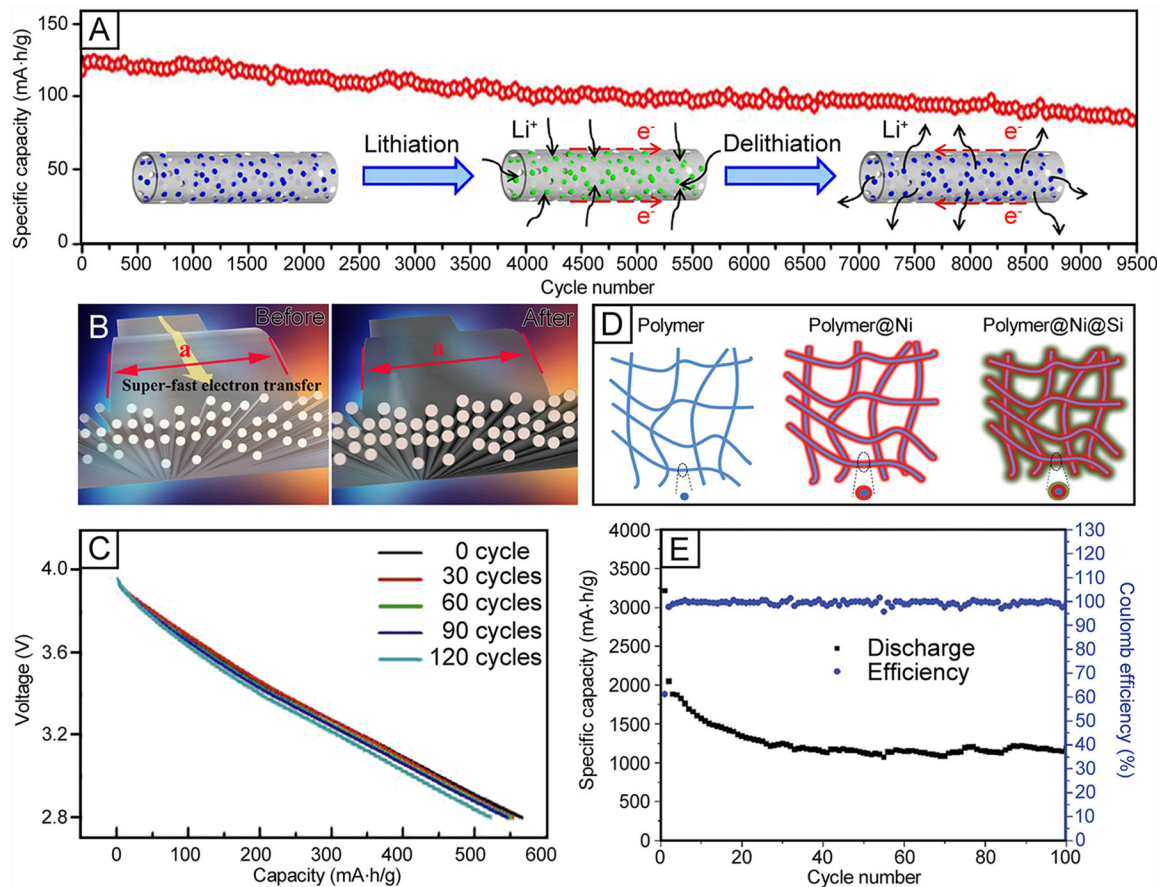
TEM images of Pt nanoparticles immobilized on a TiO₂ nanofiber and then coated by a porous sheath of SiO₂ (A) before and (B) after calcination at 750 °C for 2 h, and (C) UV-vis spectra of a methyl red solution before and after hydrogenation in the presence of the nanofibers calcined at different temperatures. (D and E) TEM images showing the selective deposition of SiO₂ onto the surface of TiO₂ nanofibers while exposing the surface of Pt nanoparticles, with an “island-in-the-sea” configuration (D) before and (E) after calcination at 700 °C for 2 h, and (F) the normalized absorbance at 400 nm for the reaction solution (p-nitrophenol and NaBH₄) versus reaction time after the addition of Pt/TiO₂-SiO₂ catalysts (with the SiO₂ thicknesses being 1.5, 2.3, 2.8, 4.1, and 5.6 nm, respectively) and after calcination at 500 °C for 2 h. (G) SEM and TEM (inset) images of Pt nanoparticles immobilized on the inner surfaces of hollow CeO₂ nanofibers (Pt_{encap}/CeO₂). (H) TEM image of the hollow Pt_{encap}/CeO₂ nanofibers after calcination at 700 °C. (I) Turnover frequencies (TOFs) at an O₂/CO ratio of 1:2 versus temperature for the hollow Pt_{encap}/CeO₂ nanofibers calcined at 600 and 700 °C, respectively, for 2 h, compared with the cases of Pt-immobilized SiO₂ or TiO₂ nanofibers. (A–C) Reprinted with permission from ref 683. Copyright 2010 Wiley-VCH. (D–F) Reprinted with permission from ref 684. Copyright 2013 American Chemical Society. (G–I) Reprinted with permission from ref 340. Copyright 2012 Wiley-VCH.

**Figure 45.**

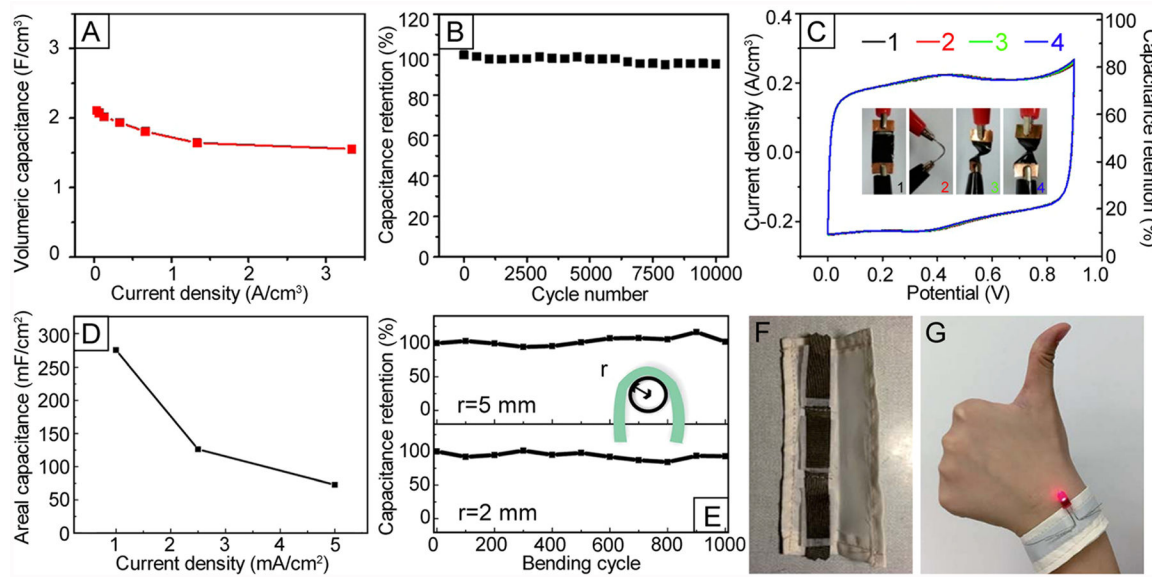
SEM images of an array of vertically aligned TiO₂ nanofibers (A) before and (B) after being attached on a fluorine-doped tin oxide glass.(C) Current density–voltage curve of a DSSC based on the TiO₂ nanofiber arrays in panel B. (D) Top-view and (E) cross-sectional view of nanorod-decorated TiO₂ nanofibers. The inset in panel D is a magnified image of one nanofiber. (F) Current density–voltage curves of DSSCs based on conventional TiO₂ nanofibers and nanorod-decorated TiO₂ nanofibers, respectively. (A–C) Reprinted with permission from ref 696. Copyright 2011 Royal Society of Chemistry. (D–F) Reprinted with permission from ref 693. Copyright 2016 Elsevier.

**Figure 46.**

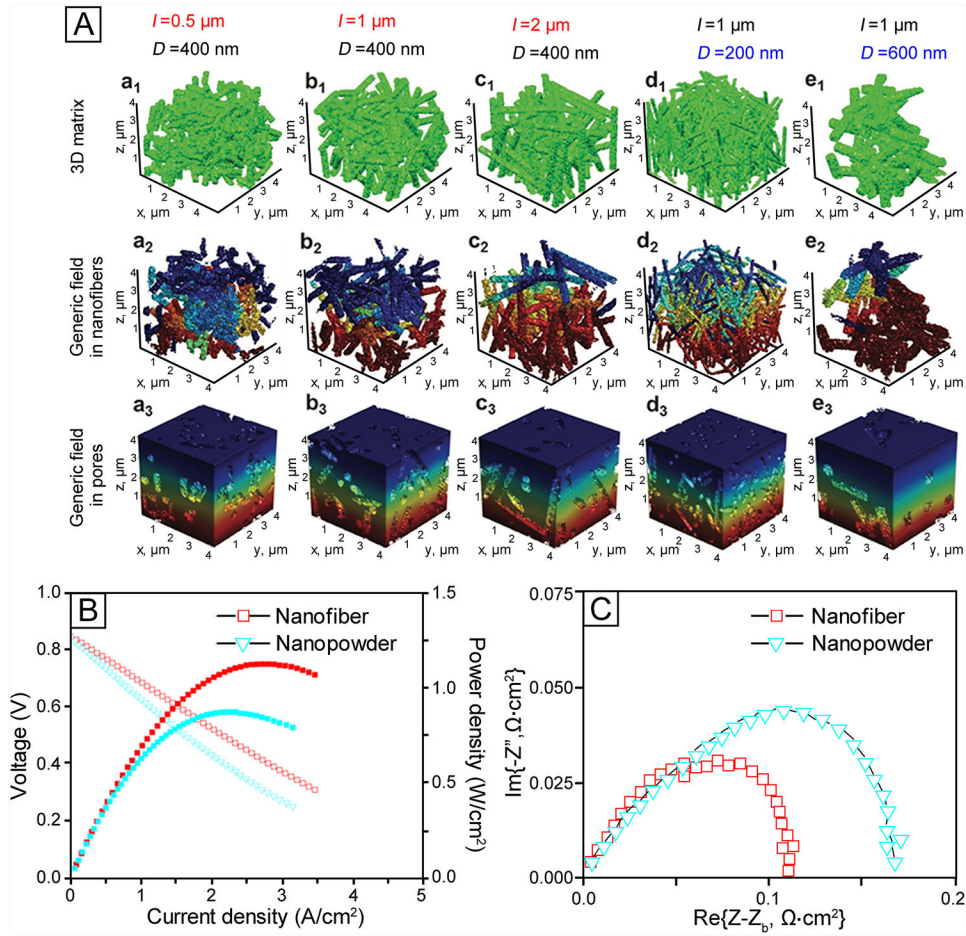
(A) Photographs of Pt networks with different transmittances and their corresponding SEM images. In the first image, the fiber network has a transmittance of 90%. The scale bars are 20 μm . Photographs of (B) foldable DSSC and (C) wearable DSSCs affixed to human fingers. (D) Stability measurements of one flexible DSSC after periodic bending. Reprinted with permission from ref 703. Copyright 2015 Royal Society of Chemistry.

**Figure 47.**

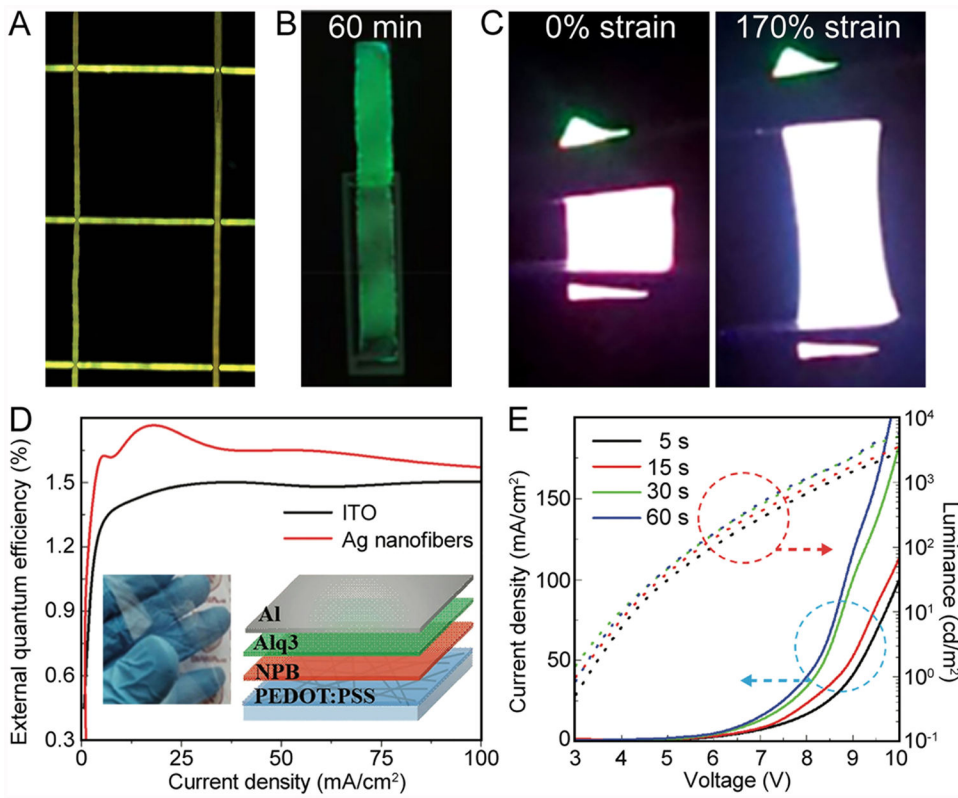
(A) Long cycling performance of $\text{Li}_3\text{V}_2(\text{PO}_4)_3$ mesoporous hollow nanofibers for a large number of 9500 cycles in a lithium half-cell. The inset shows a schematic of the lithiation and delithiation processes of mesoporous hollow nanofibers. (B) Three-dimensional view of the mat comprised of aligned carbon nanofibers containing In_2O_3 nanoparticles before and after electrochemical cycling. (C) The voltage versus specific capacity profiles of fully flexible LIB before and after 30, 60, 90, and 120 cycles of bending. (D) Schematic illustration of the stretchable PVDF@Ni@Si core–sheath nanofiber-based mat, and (E) the bending cycle performance of the LIB with the use of the mat as the negative electrode. (A) Reprinted with permission from ref 439. Copyright 2015 Springer Nature. (B and C) Adapted with permission from ref 721. Copyright 2015 Elsevier. (D and E) Adapted with permission from ref 722. Copyright 2014 Royal Society of Chemistry.

**Figure 48.**

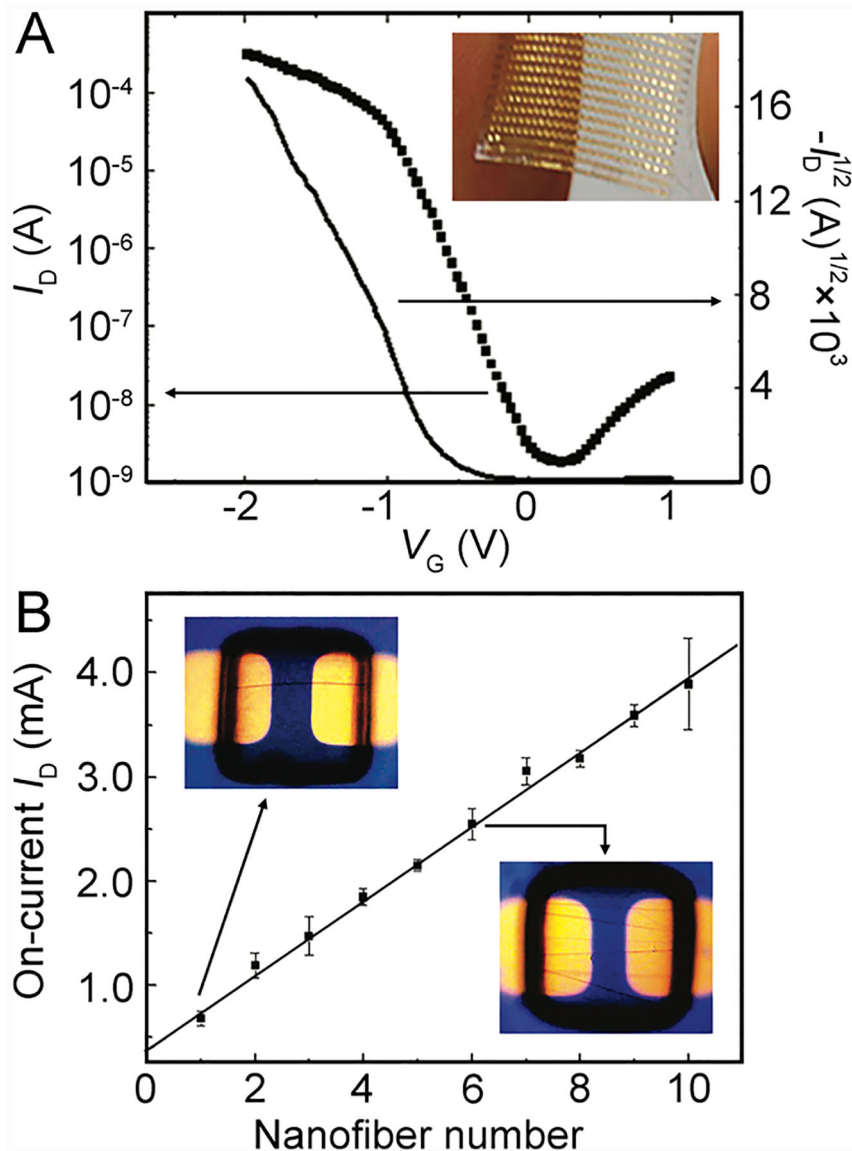
(A) Volumetric capacitance with respect to current density and (B) cycle life of flexible supercapacitor based on bamboo-like carbon nanofibers. (C) Current density–voltage curves and capacitance retention tested at 100 mV/s of the flexible supercapacitor under different mechanical deformation conditions. The insets are digital images of the flexible device bended by (1) 0° and (2) 90° and twisted by (3) 90° and (4) 180°. (D) The areal capacitance of the supercapacitor in a textile format at different current densities. (E) Capacitance retention of the supercapacitor fabric under different bending radii. (F and G) Photographs showing (F) structural diagram of three pieces of supercapacitor fabrics integrated into a wristband (G) that powers a LED with 1.6 V turn-on voltage. (A–C) Adapted with permission from ref 441. Copyright 2015 American Chemical Society. (D–G) Adapted with permission from ref 734. Copyright 2016 Royal Society of Chemistry.

**Figure 49.**

(A) Visualization of (a₁–e₁) a 3D nanofiber matrix as well as generic field within (a₂–e₂) nanofibers and (a₃–e₃) pores. The fibers in panels a–c) had different lengths (0.5, 1, and 2 μm , respectively) at a fixed diameter of 400 nm. The fibers in panels b, d, and e had different diameters (400, 200, and 600 nm, respectively) at a fixed length of 1 μm . (B) Current density –voltage and current density–power curves and (C) impedance spectra of a fuel cell with the cathode made of hollow nanofibers and powders, respectively. (A) Adapted with permission from ref 756. Copyright 2017 Wiley-VCH. (B and C) Adapted with permission from ref 757. Copyright 2016 Elsevier.

**Figure 50.**

(A) Confocal fluorescence micrograph of an array of poly[2-methoxy-5-(2-ethyl-hexyloxy)-1,4-phenylenevinylene] nanofibers. (B) Photograph of the CsPb(Br_{0.8}I_{0.2})₃ nanocrystals-encapsulated poly(styrene-butadiene-styrene) nanofibers under UV excitation for 1 h when immersed in an aqueous solution, and (C) the strain test for the mat of light-emitting nanofibers under UV excitation. (D) External quantum efficiency of organic LEDs based on Ag nanofibers and ITO as a function of current density, respectively. The insets of panel D give a photograph of the flexible substrate with Ag nanofibers and schematic illustration showing the structure of a typical organic LED (NPB, N,N'-di(1-naphthyl)-N,N'-diphenyl-(1,1'-biphenyl)-4,4'-diamine; Alq₃, tris(8-hydroxyquinolinato)aluminum). (E) Current density–voltage and luminance–voltage characteristics of the flexible organic LEDs based on Ag nanofibers that were deposited on the substrates for 5, 15, 30, and 60 s, respectively. (A) Reprinted with permission from ref 762. Copyright 2013 Royal Society of Chemistry. (B and C) Reprinted with permission from ref 760. Copyright 2018 American Chemical Society. (D and E) Reprinted with permission from ref 764. Copyright 2018 Wiley-VCH.

**Figure 51.**

(A) Transfer characteristic and a photograph (inset) of an array of flexible FETs. (B) Plot of the maximum on-current drain current (I_D) versus number of nanofibers bridging the source and drain electrodes. The insets show two typical optical micrographs of the FETs containing one and six poly(3-hexylthiophene) nanofibers, respectively. Reprinted with permission from ref 773. Copyright 2010 American Chemical Society.

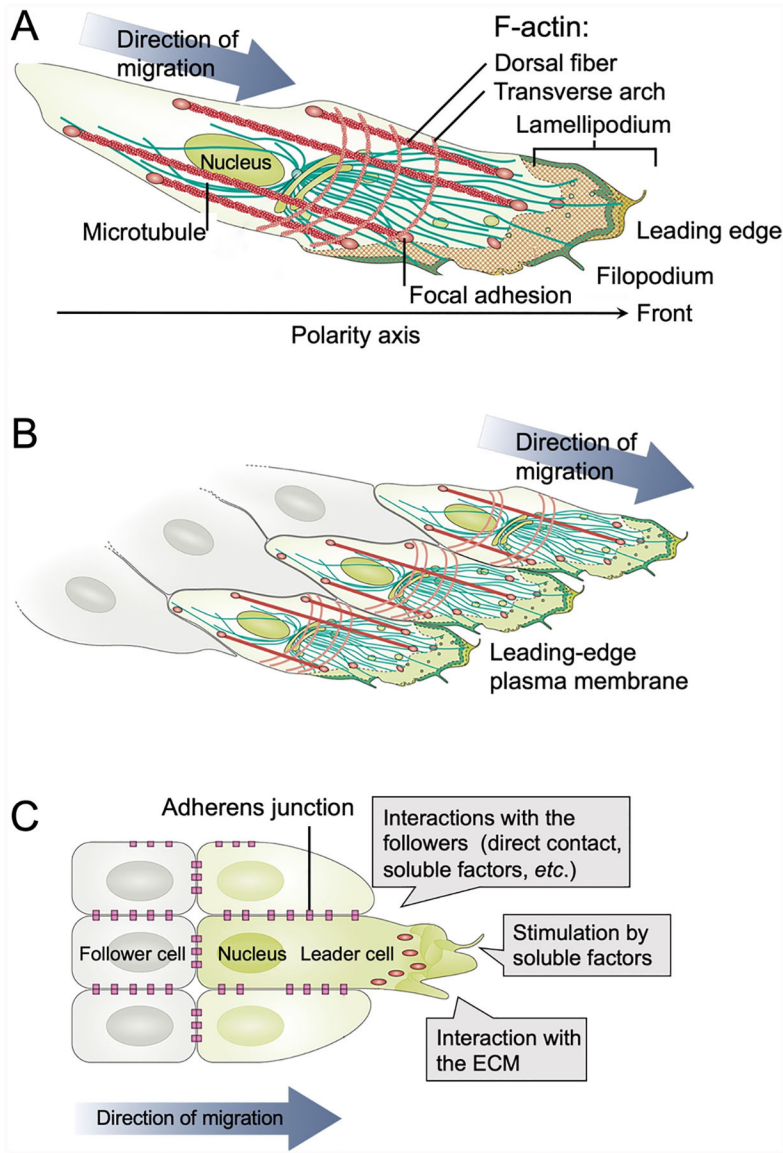


Figure 52.

Migration mechanism of (A) an individual cell and (B and C) a collection of cells. Reprinted with permission from ref 787. Copyright 2016 Springer Nature.

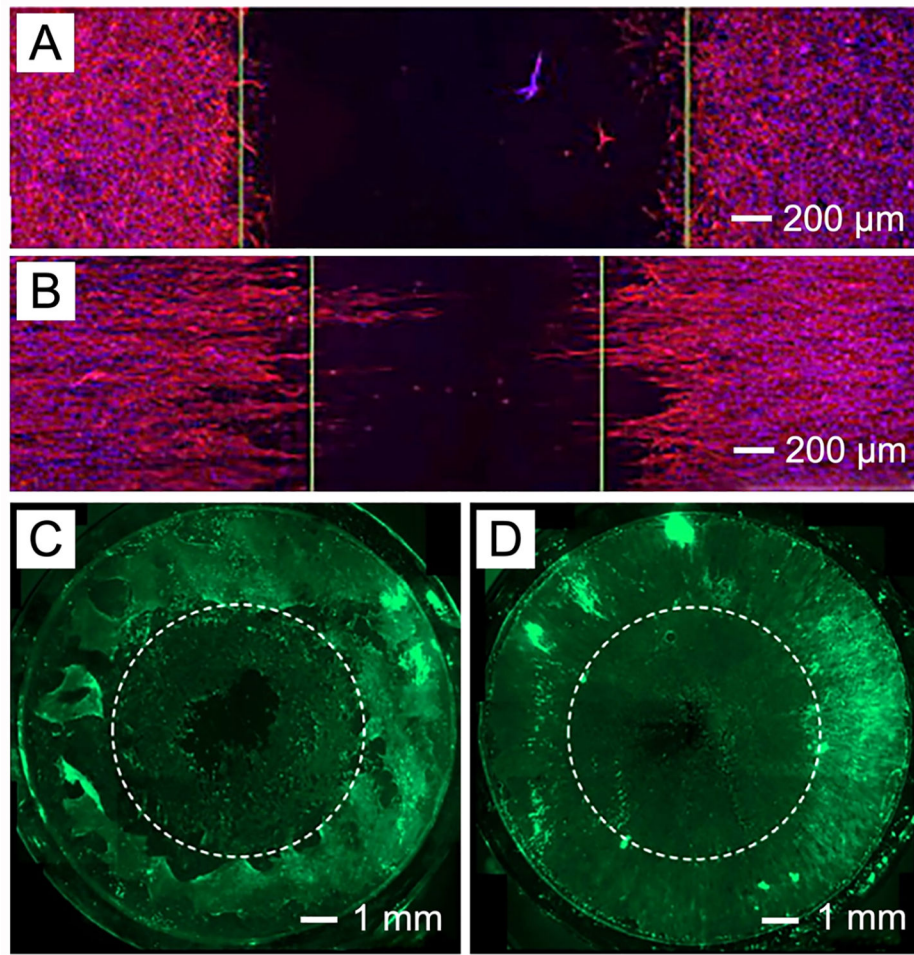
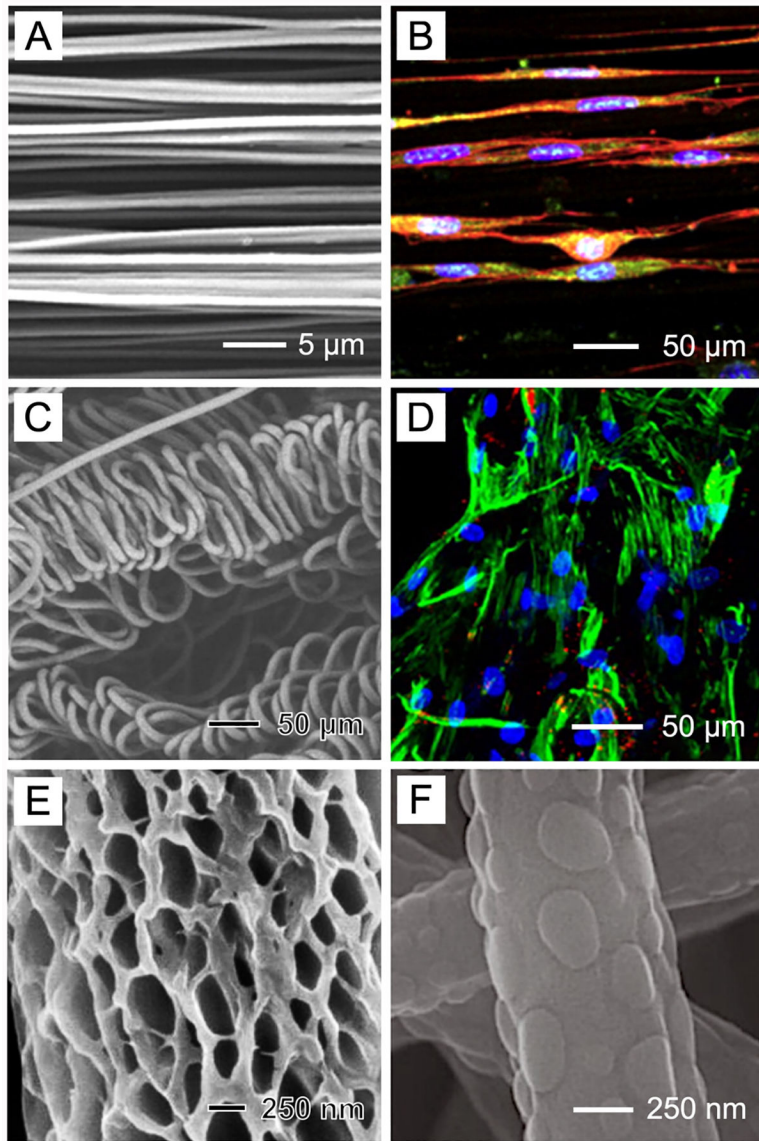


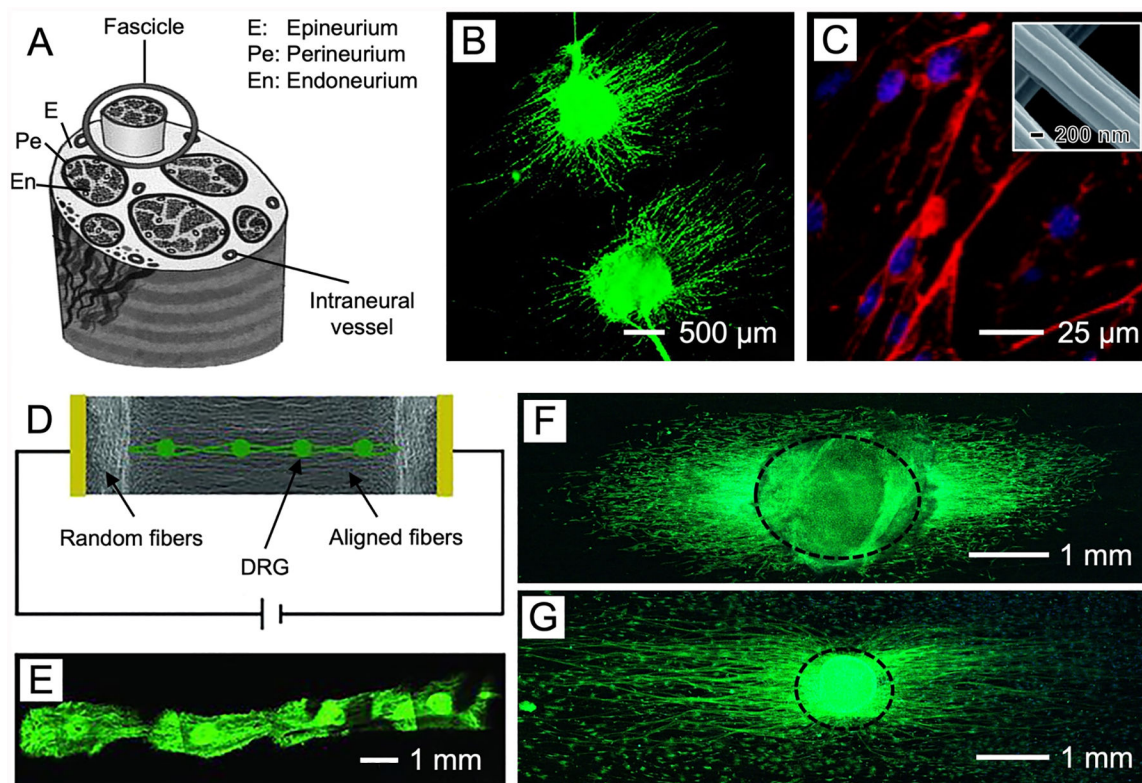
Figure 53.

(A and B) Fluorescence micrographs showing the migration of astrocytes on (A) random and (B) uniaxially aligned PLA fibers, respectively, after culturing for 5 days. (C and D) Fluorescence micrographs comparing the migration of cells when dural tissues were cultured on scaffolds made of (C) random and (D) radially aligned PCL nanofibers, respectively, for 4 days. The dashed circle indicates the border of dural cells after seeding at day 0. (A and B) Reprinted with permission from ref 792. Copyright 2011 Elsevier. (C and D) Reprinted with permission from ref 235. Copyright 2010 American Chemical Society.

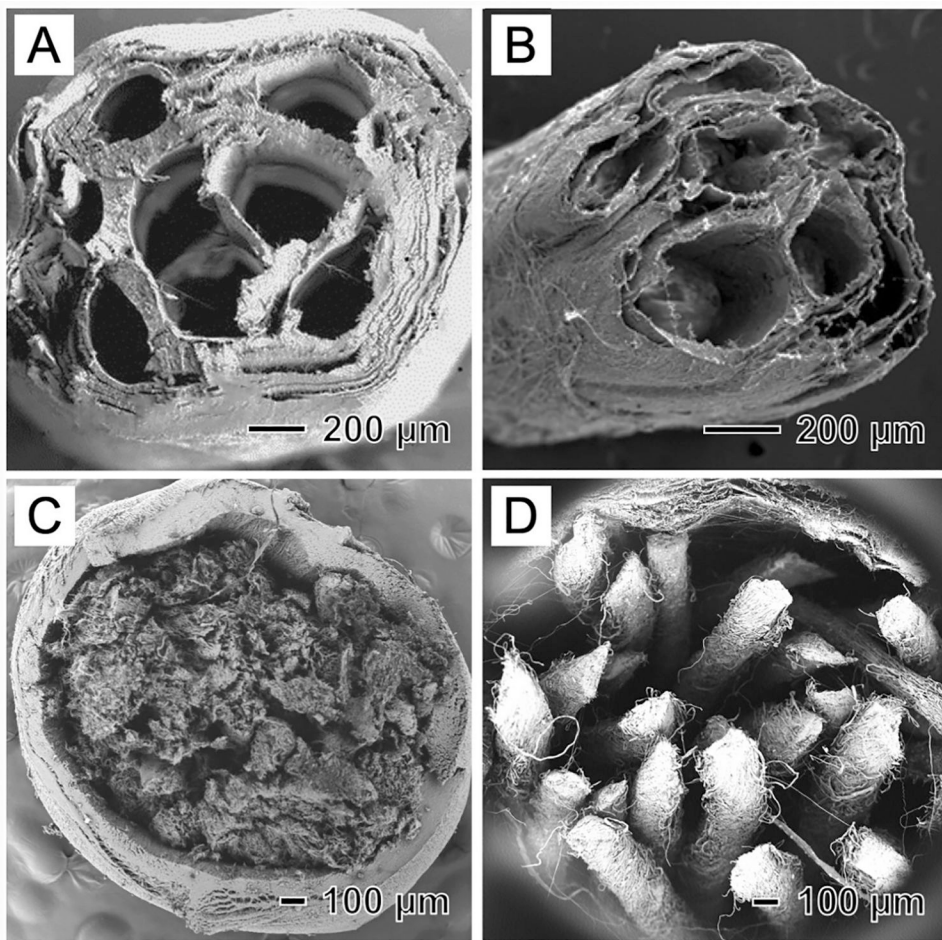
**Figure 54.**

(A) SEM image showing the uniaxially aligned nanofibers made of a blend of chitosan, gelatin, PLA, and PEO. (B) Immunofluorescence micrograph showing tenogenic differentiation of human iPSCs-derived MSCs on the nanofibers in panel A. Cells were stained with MKX antibody for monitoring tenogenic phenotype. Cytoskeletons were stained by tetraethyl rhodamine isothiocyanate-conjugated phalloidin, while cell nuclei were stained by 4',6-diamidino-2-phenylindole. (C) SEM image showing the morphology of coiled PCL fibers. (D) Immunofluorescence micrograph showing the differentiation of bone marrow-derived MSCs into fibroblasts and proto-myofibroblasts after incubation on the fibers in panel C for 5 weeks. Cells were stained with FSP1 antibody to reveal fibroblastic phenotype and α -SMA antibody to reveal myofibroblastic phenotype. Cell nuclei were stained with Hoechst. (E) SEM image showing porous fibers made of a blend of poly(ethylene oxide terephthalate) and poly(butylene terephthalate) fabricated by electro-

spinning under a relative humidity of 70%. (F) SEM image showing the generation of island-like chitosan protrusions on PLA nanofibers. (A and B) Reprinted with permission from ref 806. Copyright 2015 Elsevier. (C and D) Reprinted with permission from ref 809. Copyright 2016 American Chemical Society. (E) Reproduced with permission from ref 811. Copyright 2017 Elsevier. (F) Reprinted with permission from ref 812. Copyright 2017 American Chemical Society.

**Figure 55.**

(A) Schematic of the native structure of a peripheral nerve. (B) Fluorescence micrograph showing the typical morphology of DRG cultured on uniaxially aligned PCL nanofibers. (C) Fluorescence micrograph of Schwann cells cultured on the nanofibers made of cellulose acetate butyrate, with the inset showing the SEM image of a single nanofiber with parallel lines on the textured surface. (D) Schematic illustration of neurites extending from DRG cultured on uniaxially aligned PCL@PPy core–sheath nanofibers in the presence of electrical stimulation. (E) Fluorescence micrograph showing that the nanofibers in panel D led to the extension and potential connection of neurites from several DRG bodies after culturing under electrical stimulation. (F and G) Fluorescence micrographs showing neurites extending from DRG cultured on uniaxially aligned PCL fibers (F) coated with laminin and (G) then seeded with Schwann cells that were differentiated from bone marrow-derived MSCs. (A) Reprinted with permission from ref 826. Copyright 2015 Elsevier. (B) Reprinted with permission from ref 834. Copyright 2009 American Chemical Society. (C) Reprinted with permission from ref 836. Copyright 2011 Royal Society of Chemistry. (D and E) Reprinted with permission from ref 843. Copyright 2012 Wiley-VCH. (F and G) Reprinted with permission from ref 848. Copyright 2017 American Chemical Society.

**Figure 56.**

SEM images showing the structures of different NGCs. (A) Multichannel NGC made of silk fibroin fibers. (B) NGC consisting of intraluminal microchannels with aligned nanofibers made of a blend of RGD-conjugated polyurea and PCL. (C) NGC made of a blend of PLCL and silk fibroin, with nanofibers as the wall and nanofiber sponges in the lumen. (D) NGC made of PLGA, with nanofibers as the wall and arrays of nanofiber yarns in the lumen and coated with laminin. (A) Reprinted with permission from ref 826. Copyright 2015 Elsevier. (B) Reprinted with permission from ref 855. Copyright 2016 American Chemical Society. (C) Reprinted with permission from ref 857. Copyright 2017 American Chemical Society. (D) Reprinted with permission from ref 859. Copyright 2017 Royal Society of Chemistry.

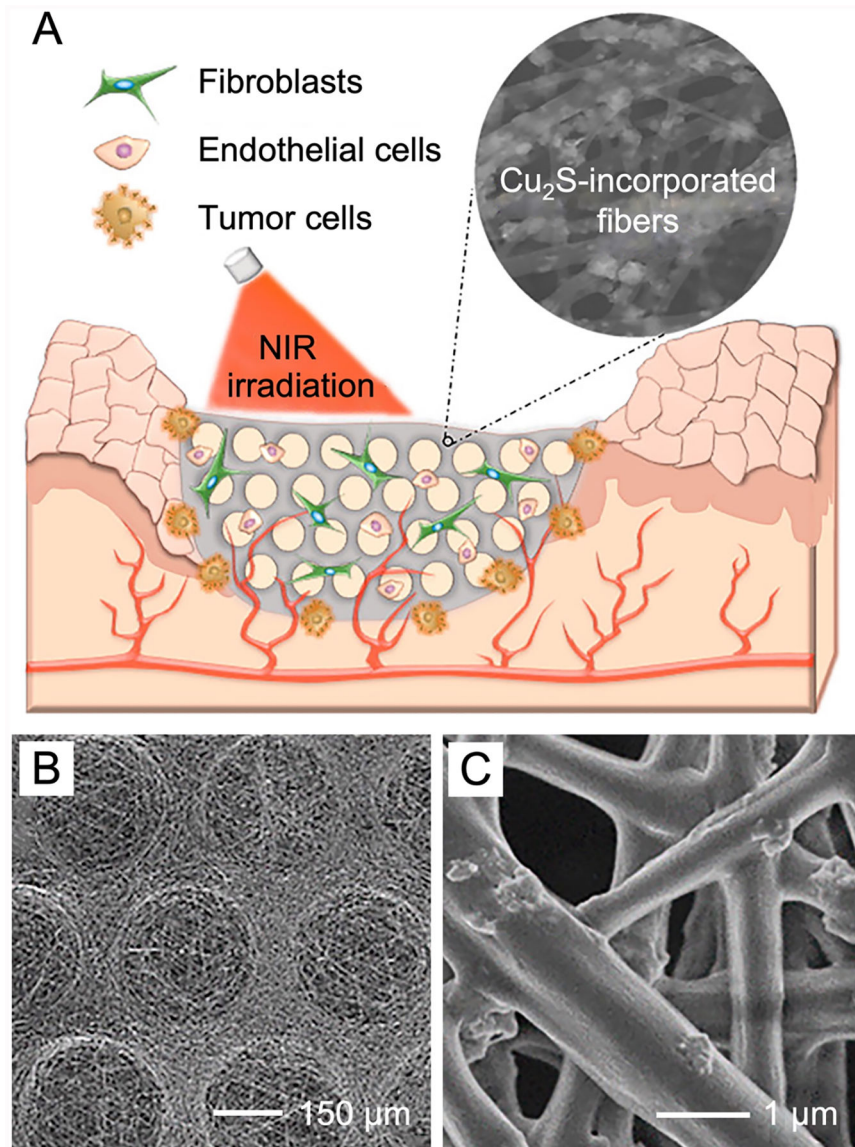


Figure 57.

(A) Schematic showing the localized treatment of skin tumor and wound healing with the use of a micropatterned scaffold made of a blend of PLA and PCL nanofibers and doped with Cu₂S nanoscale flowers. (B) SEM image showing the morphology of the micropatterned scaffold. (C) Representative SEM image showing the Cu₂S-incorporated nanofibers in panel B. Reprinted with permission from ref 233. Copyright 2017 American Chemical Society.

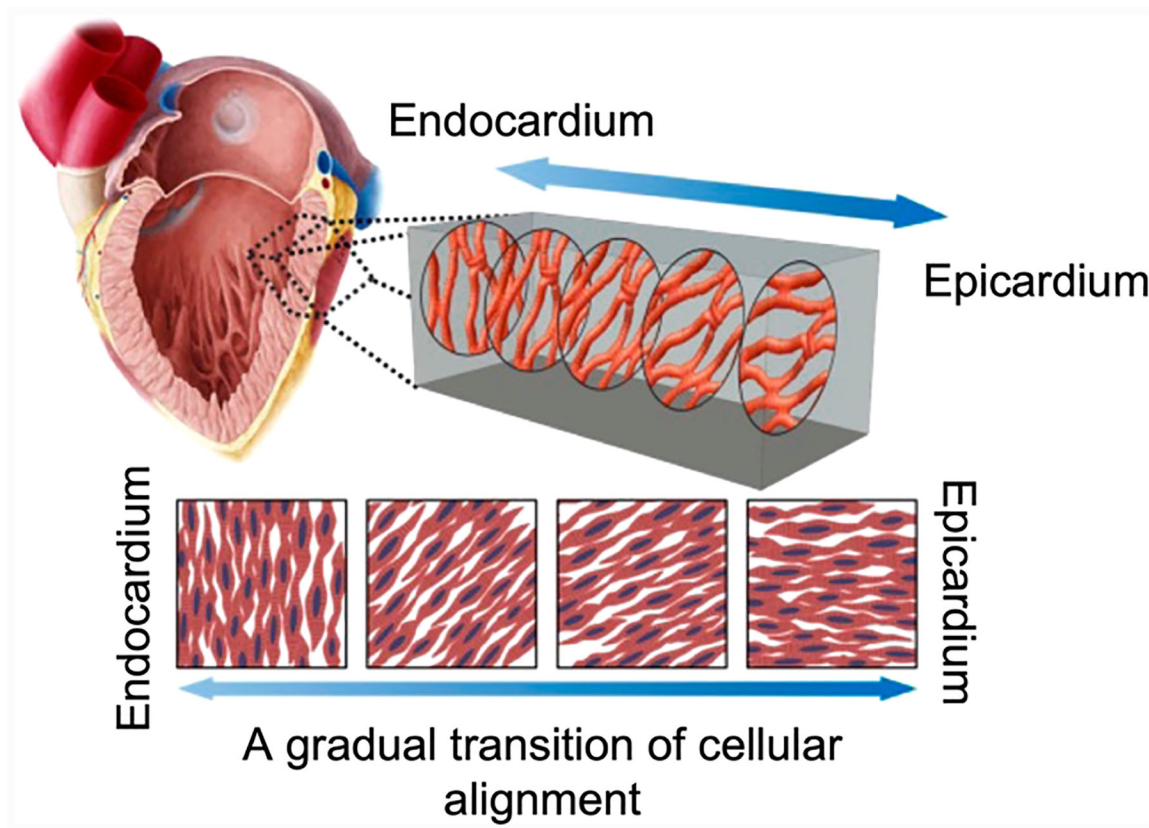


Figure 58.

Schematic of the cardiac microstructure. A transmural block cut from the ventricular wall showing a gradual transition of aligned cell layers from endocardium to epicardium matrix. Reprinted with permission from ref 884. Copyright 2017 American Chemical Society.

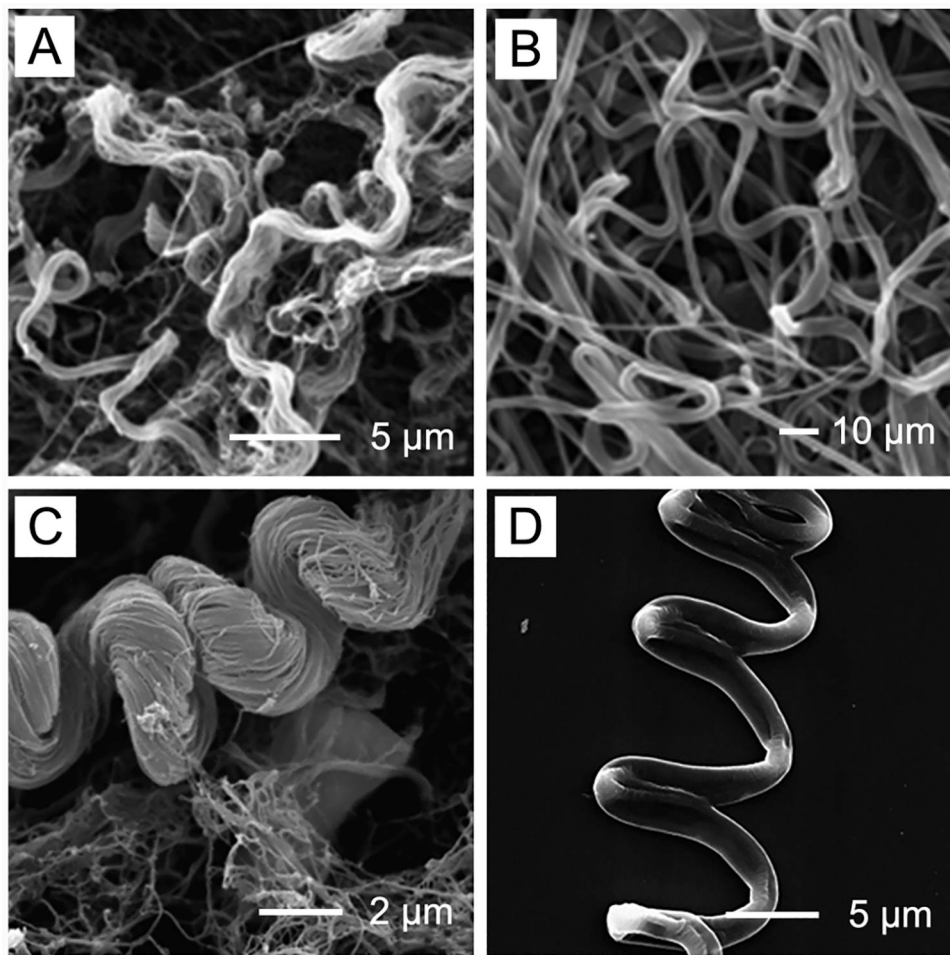


Figure 59.

SEM images showing (A, C) coiled morphology of the perimysial fibers in the native heart matrix and (B, D) coiled PCL fibers produced by electrospinning. Reprinted with permission from ref 892. Copyright 2013 Elsevier.

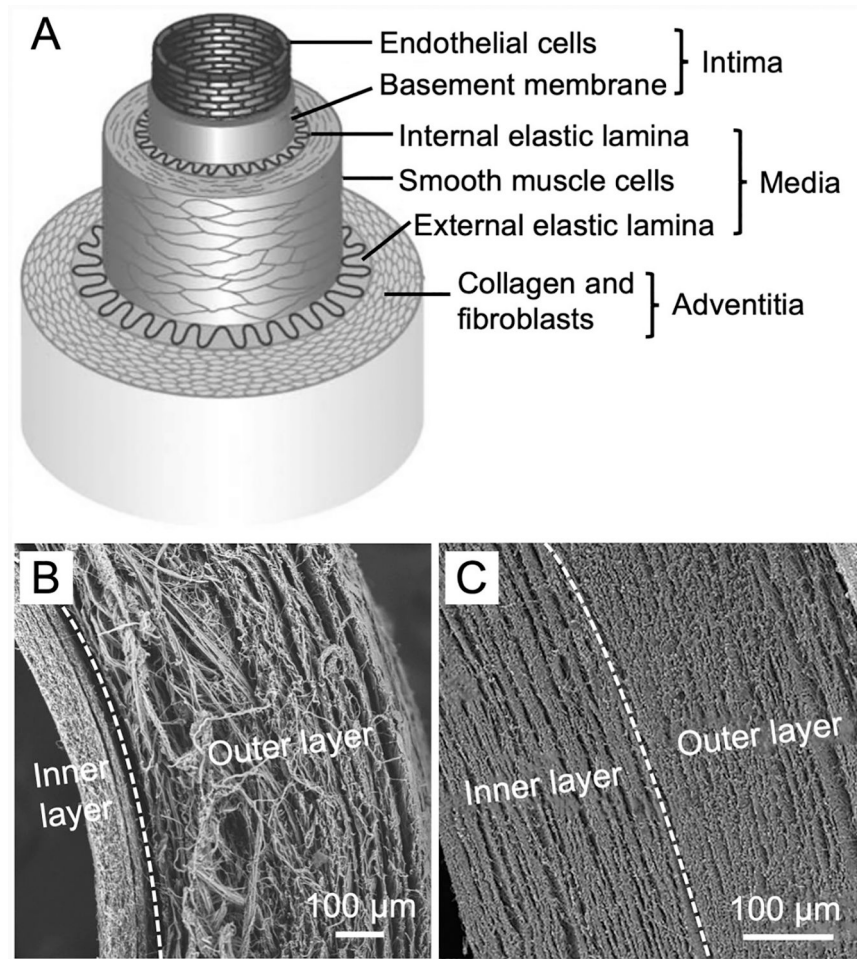
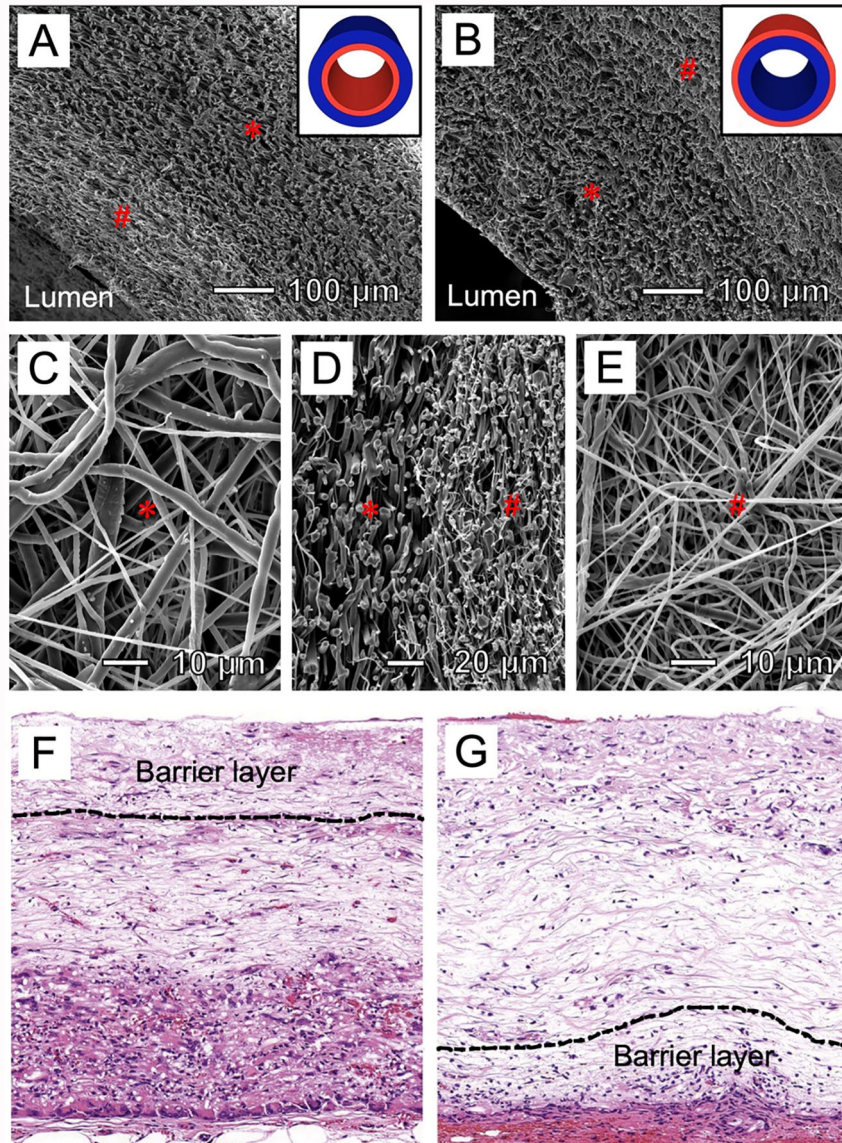


Figure 60.

(A) Schematic showing the structure of a native blood vessel. (B) SEM image of the cross-section of a multilayered vascular conduit made of a blend of PLCL and collagen, with dense nanofibers incorporated with heparin and an anti-CD133 antibody as the inner layer and porous nanofibers yarns as the outer layer. (C) SEM image showing the cross-section of a multilayered vascular conduit with microRNA 126-incorporated PEG-b-PLCL fibers as the inner layer and a blend of PCL and gelatin fibers as the outer layer. (A) Reprinted with permission from ref 897. Copyright 2007 Springer Nature. (B) Reprinted with permission from ref 902. Copyright 2018 American Chemical Society. (C) Reprinted with permission from ref 903. Copyright 2016 Elsevier.

**Figure 61.**

Sequential deposition of two layers of nanofibers with different porosities to generate bilayer vascular scaffolds. (A–E) SEM images showing the vascular scaffold (A) that has (C) a high-porosity nanofiber layer (as indicated by *) on the adventitial side and (E) a low-porosity nanofiber layer (as indicated by #) on the luminal side, and (B) that has a high-porosity nanofiber layer on the luminal side and a low-porosity nanofiber layer on the adventitial side, respectively. The insets in (A) and (B) show schematic illustration of the vascular scaffolds, respectively. (D) SEM image showing the transition between the two layers. (F and G) Hematoxylin & eosin images showing the cross-section of the vascular scaffolds after implantation for 12 weeks in rat abdominal aorta replacement models. The barrier layer refers to the nanofiber layer with a low porosity. Reprinted with permission from ref 904. Copyright 2012 Elsevier.

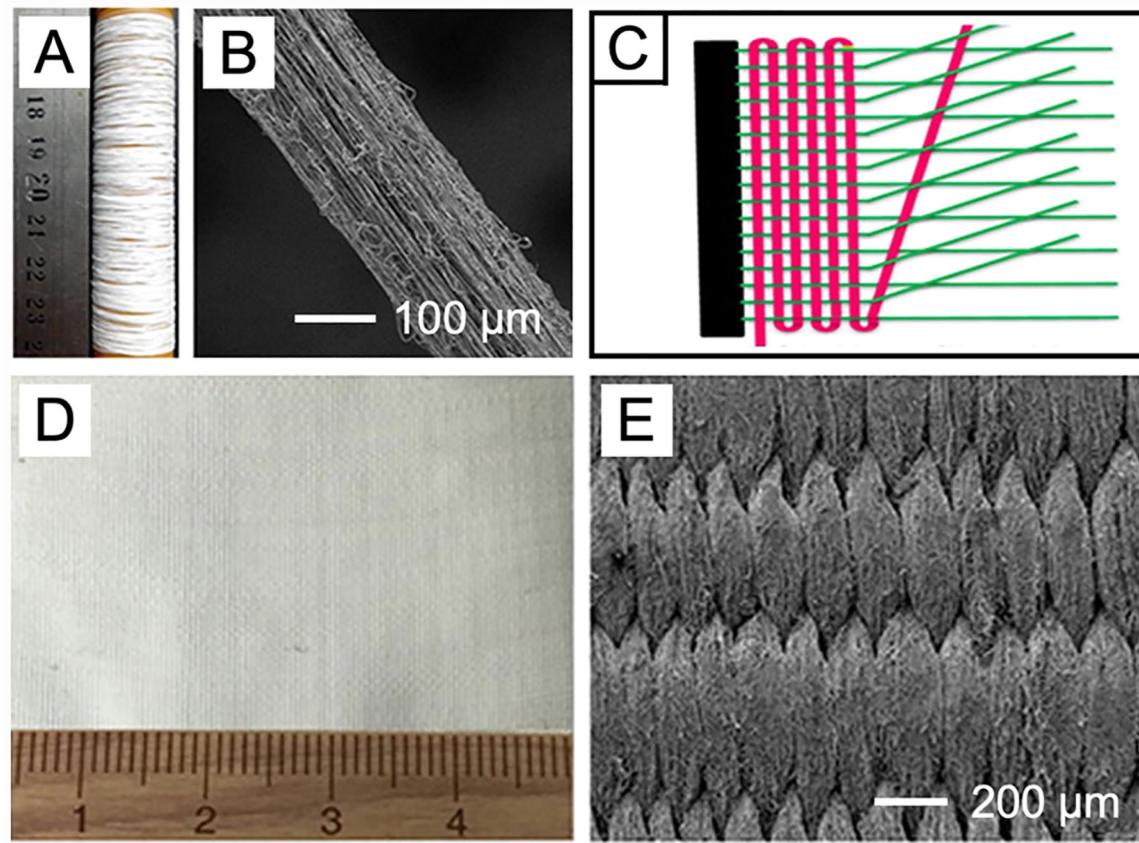
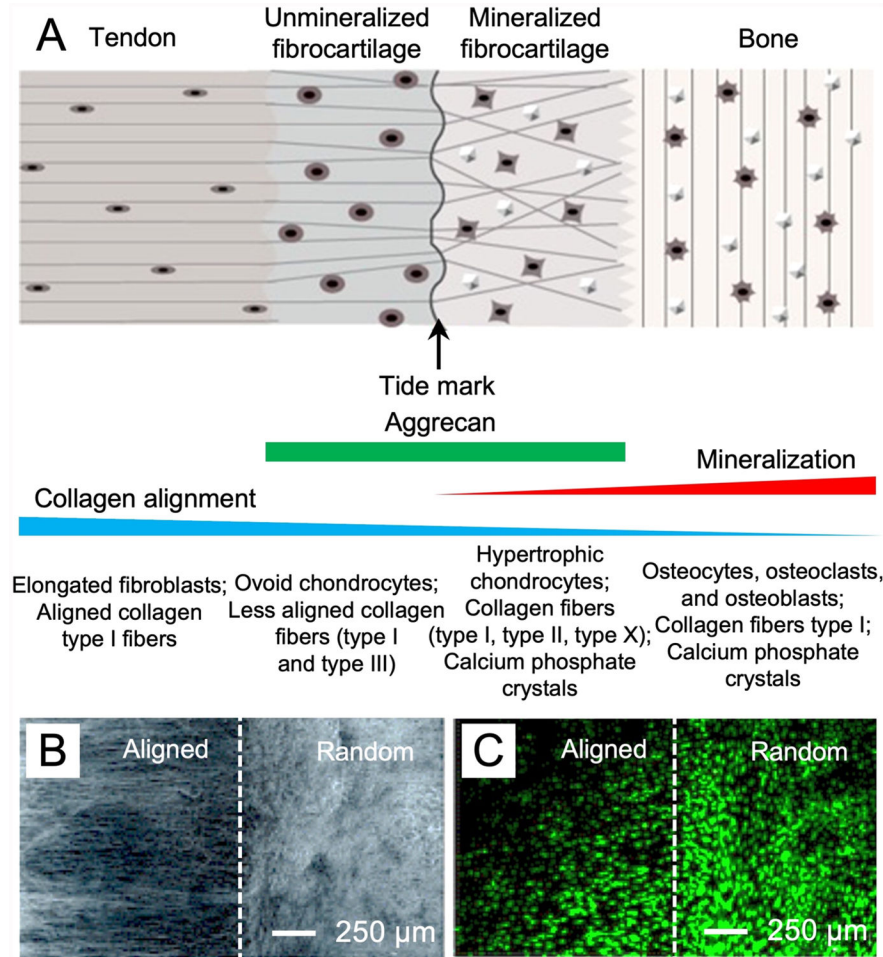


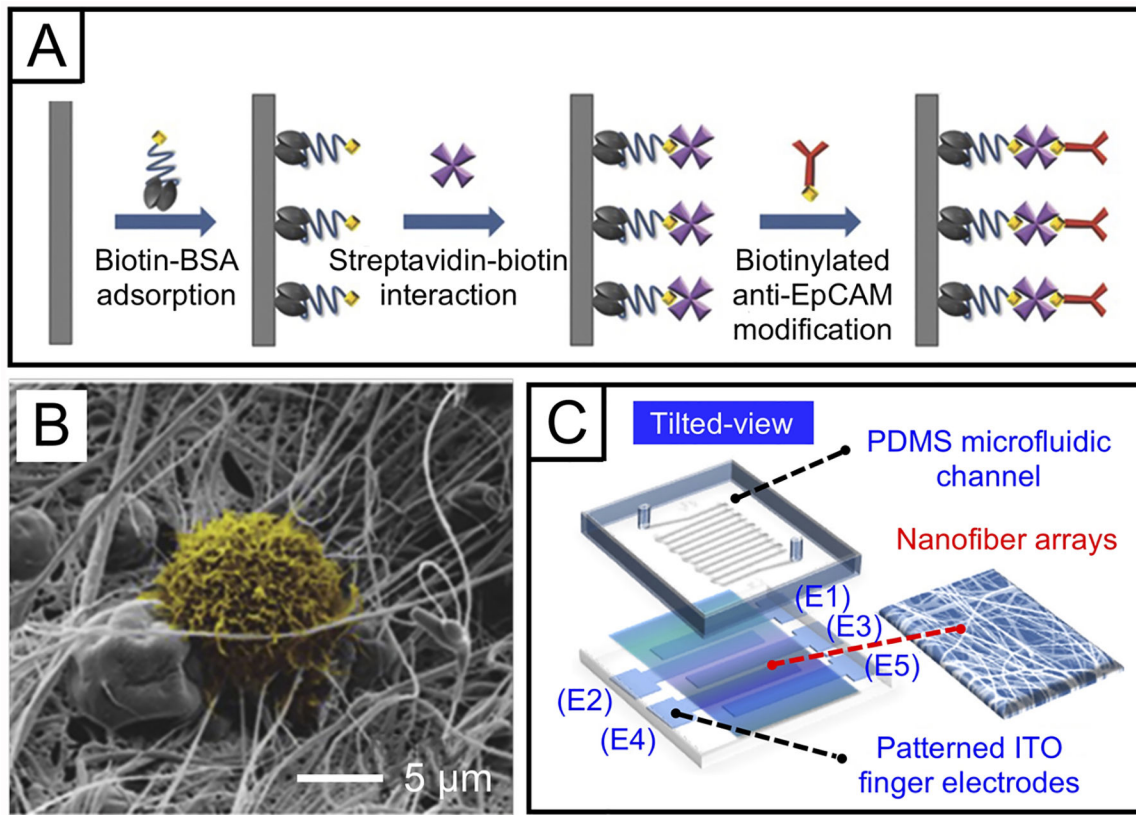
Figure 62.

(A) Photograph and (B) SEM image of a PCL nanofiber yarn. (C) Schematic of the textile-weaving process. (D) Photograph and (E) SEM image of the plain-weaving fabric made of PCL nanofiber yarns (with a high weaving density, as the weft) and multiple PLA filaments (with a low weaving density, as the warp). Reprinted with permission from ref 824.

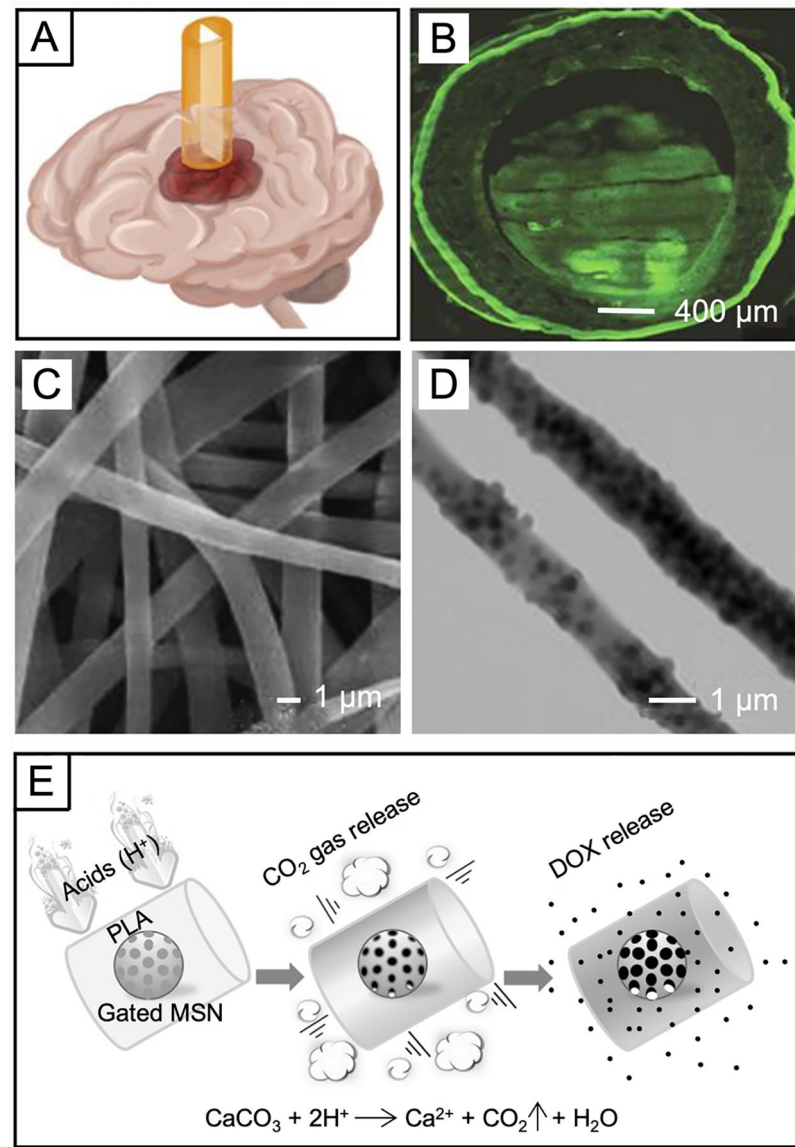
Copyright 2017 Elsevier.

**Figure 63.**

(A) Diagram showing the tendon-to-bone interface insertion site. (B) SEM image of scaffold consisting of uniaxially aligned-to-random PLGA nanofibers. (C) Fluorescence micrograph showing the morphologies of tendon fibroblasts on the aligned-to-random nanofibers after incubation for 7 days. (A) Reprinted with permission from ref 950. Copyright 2017 Elsevier. (B and C) Reprinted with permission from ref 459. Copyright 2010 Royal Society of Chemistry.

**Figure 64.**

(A) Schematic illustration of a procedure for modifying the surface of nanofibers (EpCAM, epithelial-cell adhesion molecule antibody). (B) SEM image showing the capture of MCF7 cancer cells using the PS nanofibers with a beaded morphology after modifying the surface using the procedure shown in panel A. (C) Bioelectronic device fabricated by depositing the functionalized PEO-PEDOT@PSS core-sheath nanofibers on an array of individually addressable electrodes of ITO and integrated with a PDMS chamber containing microfluidic channels. (A and B) Reprinted with permission from ref 978. Copyright 2015 Wiley-VCH. (C) Reprinted with permission from ref 982. Copyright 2017 American Chemical Society.

**Figure 65.**

(A) Schematic illustration of a conduit containing a mat of uniaxially aligned PCL nanofibers inserted into a rat brain to guide the migration of glioblastoma cells from the primary tumor site to the apoptotic sink. (B) Fluorescence micrograph showing the tumor cells being directed into the cyclopamine-conjugated collagen hydrogel for apoptosis. (C) SEM and (D) TEM images of the PLA fibers containing mesoporous silica nanoparticles loaded with doxorubicin (DOX) and then capped with CaCO₃. (E) Schematic illustration of the release mechanism for the pH-responsive controlled release system shown in panels C and D to kill cancer cells in the acidic environment of cancerous tissue by leveraging the reaction between CaCO₃ and an acid. (A and B) Reprinted with permission from ref 987. Copyright 2014 Springer Nature. (C–E) Reprinted with permission from ref 991. Copyright 2015 Wiley-VCH.

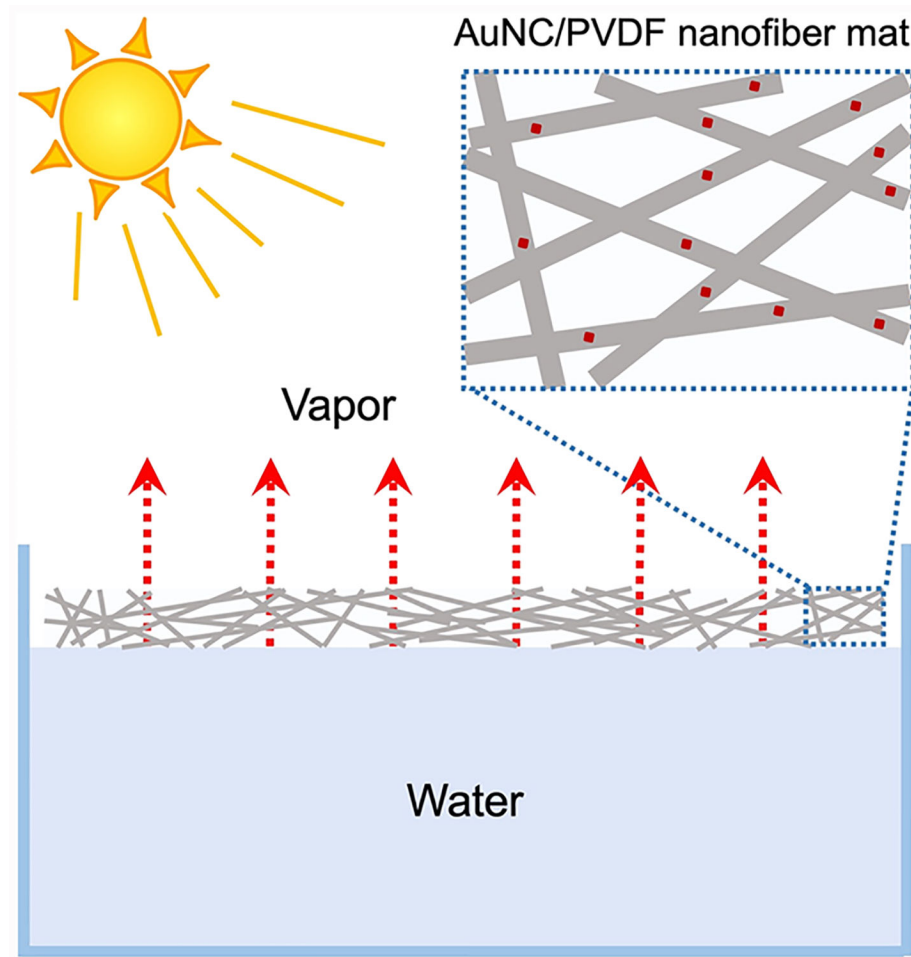


Figure 66.

Schematic illustration showing the evaporation of water from the surface of a pool when a nonwoven mat of PVDF nanofibers containing Au nanocages (AuNC/PVDF) is placed on the surface and irradiated with light. Reprinted with permission from ref 1003. Copyright 2019 Elsevier.

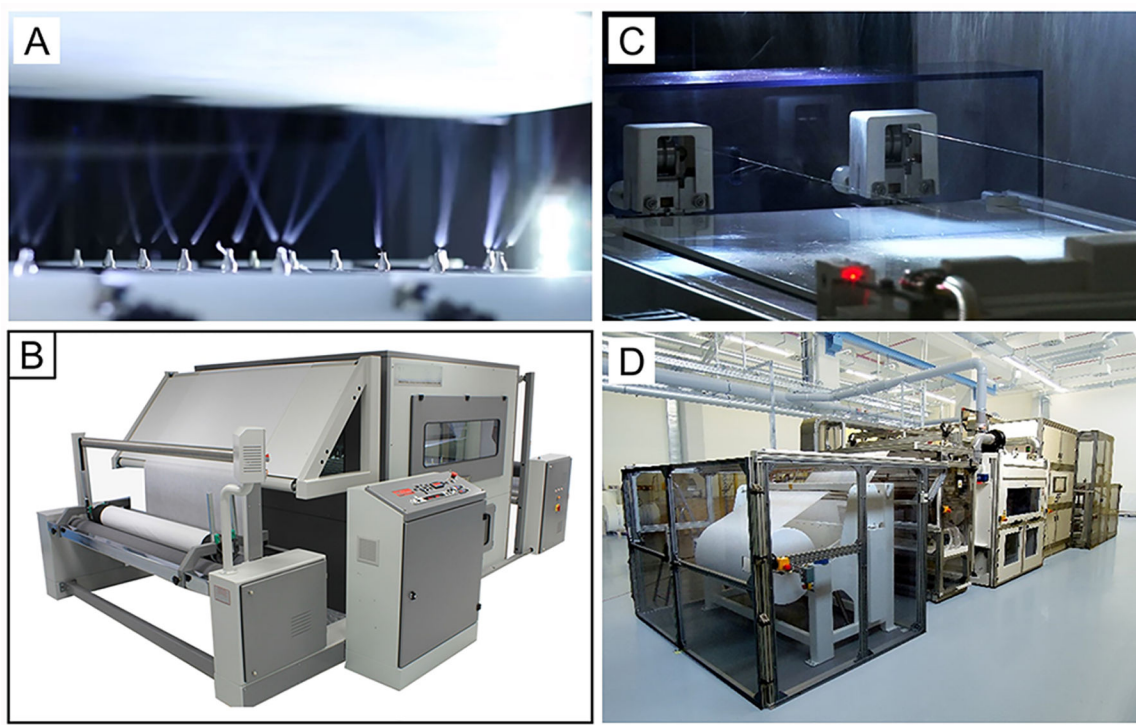


Figure 67.

(A) Multiple-needle electrospinning developed by Inovenso Inc., which involves 110 needles and (B) a photograph of the industrial machine, which is able to produce nonwoven mats of 1.0 m in width. (C) Needleless electrospinning with the Nanospider Production Line developed by Elmarco Inc., which uses a metal wire electrode to eject multiple jets and (D) a photograph of the Nanospider NS 8S1600U industrial machine, which is capable of producing nonwoven mats with a maximum width of 1.6 m. (A and B) Reprinted with permission from ref 1005. Copyright Inovenso Inc. (C and D) Reprinted with permission from refs 1006 and 1007, respectively. Copyright Elmarco Inc.

Table 1.
Different Types of Materials That Have Been Prepared as Fibers via Electrospinning^a

material	solvent	carrier polymer	ref
thermoplastic polymer			
Nylon-6	formic acid and acetic acid		86
PAN	DMSO and trifluoroacetic acid		272
PCL	HFIP		347
PEO	water		348
PLA	DMF and chloroform		349
PLGA	THF and DMF		350
PP			103
PS	DMF and toluene		346
PVC	THF and DMF		351
PVP	ethanol and water		35
thermoset polymer			
bisphenol A ethoxylate dimethacrylate	PCL		207
epoxy resin	ethanol and acetone	PVP	211
ethylene-propylene/diene terpolymer rubber			210
PDMS	THF	PVP	209
conjugated polymer			
PANi	formic acid		97
PPy	DMF		90
PEDOT and PSS	water		91
natural polymer			
chitosan	trifluoroacetic acid		247
collagen	HFIP		352
gelatin	trifluoroethanol and HFIP		353
hyaluronic acid	DMF and water		354
silk fibroin	formic acid		355
metal	ethylene glycol		131
Ag			

material	solvent	carrier polymer	ref
Ag	water	PVA	141
Co	isopropyl alcohol and water	Polyvinyl butyral	289
Cu	water	PVA	287
Fe	isopropyl alcohol and water	poly(vinyl butyral)	289
Pt	DMF and water	PVP	356
Pt-Au	DMF and water	PVP	356
metal oxides			
Al ₂ O ₃	ethanol	PVP	357
CeO ₂	water	PVA	358
Co ₃ O ₄	DMF	PVP	359
CuO	water	PVA	287
Fe ₂ O ₃	water	PVA	360
Mn ₃ O ₄	DMF and chloroform	PMMA	361
SiO ₂	water and ethanol	PVA	127
SnO ₂	water, propanol, and isopropanol	PVA	362
TiO ₂	ethanol	PVP	132
V ₂ O ₅	DMF and chloroform	PMMA	363
WO ₃	propanol and DMF	poly(vinyl acetate)	364
ZrO ₂	ethanol	PVP	336
BaTiO ₃	isopropanol	PVP	292
CoFe ₂ O ₄	DMF and THF	poly(vinyl acetate)	365
LiCoO ₂	water		129
NiFe ₂ O ₄	isopropanol	PVP	366
ZnCo ₂ O ₄	ethanol	PVP	367
LiNi _{0.5} Mn _{1.5} O ₄	ethanol	PVP	368
metal nitrides			
Li ₃ N	water	PVA	369
NbN	ethanol	PVP	299
TiN	ethanol and acetic acid	PVP	299
VN	DMF	PVP	370

material	solvent	carrier polymer	ref
Ti _x V ₂ N	2-propanol	PVP	299
metal carbides			
Mo ₂ C	water	PVA	371
SiC	DMF	PS	372
TiC	DMF	PVP	373
WC	water	PVP	300
ZrC	ethanol	PVP	374
doped-carbon			
Ni/N,S-doped carbon	DMF	PAN	375
CoSe/N-doped carbon	DMF	PAN	376
Fe ₃ O ₄ /N-doped carbon	DMF	PAN	377
SnS ₂ /N,S-doped carbon	DMF	PVP	378
WS _x /N-doped carbon	DMF	PAN	379
MnCo ₂ O ₄ @N-doped carbon	DMF	PAN	380

^aNote that essentially all the inorganic materials were derived from precursor compounds post-electrospinning.

Commercial Products Based on Electrospun Nanofibers

Table 2.

product	company	application	description	company Web site
SETA diffuser filters	HRV	air filtration	biodegradable and antibacterial filters for capturing microscopic particles	https://www.hrv.co.nz
Exceed	eSpin Technologies	air filtration	residential or commercial building filters	http://www.espinetechnologies.com
micrograde NF filter	MANN-HUMMEL	air filtration	air filters comprised of a medium carrier and an extremely thin coating of ultrafine polymer fibers for commercial vehicles	https://www.mann-hummel.com
ProTura nanofiber	United Air Specialists	air filtration	cellulose-based filters with a surface layer composed of nanofibers	http://www.clarcorindustrialair.com
Smart Mask	NASK	facemasking	nanofibers for facemask	http://nask.hk
ZN 8848 facemask	CHnano	facemasking	nanofibers for filtering water and killing bacteria	http://www.zhongnakaiji.com
naked filter	Liquidity Corp.	household/bottled water filtration	water filters comprised of nanofibers for reducing cell debris, bacteria, and viruses, etc.	http://liquico.com
nanotrap filter	Coway	household water filtration	self-cleaning nanofibers	http://www.coway.com/
filter nanofiber	AstraPool	filtration system for residential pools	nanofiber-based filtering unit used in super clean zone	https://www.astralpool.com
FERENA	Koken	filtering unit for clean room furniture	thousands of layers of Phonix nanofibers in a composite for serving as an acoustic substrate fabrics comprised of nanofibers for making pillows	http://www.koken-ltd.co.jp
return focus pod	IQ Commercial	furniture	nanofiber-based mats made of PLLA, PLA, PCL, polyurethane, and carbon or activated carbon nanofibers, for biomedical applications	http://www.iqcommercial.co.nz
Nanodream, nanofiber pillow lining	RevolutionFibres Ltd.	fabrics	medical grade polycarbonate urethane nanofibers as the vascular access graft	https://www.revolutionfibres.com
Cytoweb sheets	eSpin Technologies	biomedical area	nanofibers made of PLLA as a dural substitute for repairing defective dura and avoiding adhesion with the surrounding tissues	http://www.espinetechnologies.com
AVfio vascular access graft	Nicast	biomedical area	composite nanofibers made of a mixture of synthetic materials and gelatin as an absorbable dural repair patch for avoiding adhesion between brain tissue and the skull	http://nicast.com
ReDura	MEDPRIN	biomedical area	wound dressing produced <i>in situ</i> for repairing any wound shape	http://www.medprin.cn
NeoDura	MEDPRIN	biomedical area	wound dressing produced <i>in situ</i> for repairing any wound shape	http://nicast.com
SpinCare	Nicast	biomedical area		

product	company	application	description	company Web site
Papyrus, coronary balloon-expandable stent systems	BIOTRONIK	biomedical area	electrospun polyurethane nanofibers for covering the surface of a single stent	https://www.biotronik.com
silk fibroin tubular scaffold, flat sheet scaffold, disc	SKE Advanced Therapies	laboratory tissue culture	electrospun tubular, flat sheet, and disc scaffolds made of silk fibroin for 3D cell culture and tissue engineering	http://leonardino.eu/index.php/ske-research-equipment/
Mimetix scaffold	Electrospinning Company	laboratory tissue culture	scaffolds comprised of random or aligned nanofibers for cell culture in 384-, 96-, or 12-well plates, as well as crown cell inserts in 6-, 12-, or 24-well plates	https://www.electrospinning.co.uk
nanofiber solutions	Nanofiber Solutions	laboratory tissue culture	aligned (NanoAligned) or randomly oriented (NanoECM) degradable or nondegradable polymer nanofibers integrated into standard multiwell plates for high-throughput cell culture, cancer research, stem cell, and regenerative medicine	http://www.nanofbersolutions.com
3D insert	3D Bioteck	laboratory tissue culture	3D scaffolds made of PS, PCL, or PLGA for cell culture	http://www.3dbiotekstore.com